Bettina Albers · Mieczysław Kuczma
Editors

Continuous Media with Microstructure 2

Springer

Continuous Media with Microstructure 2

Bettina Albers · Mieczysław Kuczma
Editors

Continuous Media with Microstructure 2

Springer

Editors
Bettina Albers
Faculty of Engineering
University of Duisburg-Essen
Essen
Germany

Mieczysław Kuczma
Faculty of Civil and Environmental Engineering
Poznań University of Technology
Poznań
Poland

ISBN 978-3-319-28239-8 ISBN 978-3-319-28241-1 (eBook)
DOI 10.1007/978-3-319-28241-1

Library of Congress Control Number: 2009943376

Printed on acid-free paper

This Springer imprint is published by SpringerNature
The registered company is Springer International Publishing AG Switzerland

The 2nd conference on Continuous Media with Microstructure (CMwM2015) *was held on March 2–5, 2015 in Łagów, Poland, in memory of*

Professor Krzysztof Wilmański

who regrettably passed away on 26/08/2012.

We dedicate this book of CMwM2015 *contributions to him.*

Preface

This book is a collection of papers dedicated to the memory of Prof. Dr. Krzysztof Wilmański. It contains the written form of many contributions to the 2nd International Conference on *Continuous Media with Microstructure* held in Łagów, Poland, March 2–5, 2015 (Fig. 1).

CMwM2015, also announced as an ECCOMAS Special Interest Conference, was organized by the Polish Academy of Sciences, Poznan University of Technology, Berlin University of Technology, and the Polish Association for Computational Mechanics. Many friends and colleagues of Prof. Krzysztof Wilmański eagerly accepted the invitation of the conference chairpersons Bettina Albers (at that time: TU Berlin) and Mieczysław Kuczma (Poznan UT). Professor Krzysztof Wilmański regrettably passed away on August 26, 2012 but would have celebrated his 75th birthday on March 1, 2015. The 1st conference CMwM took place in Zielona Góra, Poland, in 2010 to celebrate the 70th birthday of Prof. Wilmański. At this occasion he received the first part of the book *Continuous Media with Microstructure*. That book contains further information about him, especially a photo, his curriculum, and his publication list (Reference: Albers, B. (ed.):

Fig. 1 Participants of the 2nd International Conference on Continuous Media with Microstructure

Continuous Media with Microstructure. Collection in Honor of Krzysztof Wilmanski, Springer, Berlin, Heidelberg, 2010, ISBN 978-3-642-11444-1).

CMwM2015 was a conference with an intimate atmosphere, attended by nearly 40 scientists from Brazil, Czech Republic, Estonia, Georgia, Germany, Italy, Poland, Russia, and the USA, who gave 35 presentations.

The general lectures were delivered by

- Tadeusz Burczyński on *Intelligent optimization of media with microstructure*,
- Carlo Giovanni Lai on *Measurement of damping ratio spectra in soils from the exact solution of Kramers-Krönig equations of linear viscoelasticity*,
- I-Shih Liu on *A mixture theory of porous media and some problems of poroelasticity*,
- Martin Ostoja-Starzewski on *Continuum mechanics beyond the second law of thermodynamics*,
- Jörg Schröder on *A FE^2-homogenization scheme for the analysis of product properties of two-phase magnetoelectric composites*, and
- David M.J. Smeulders on *Electrokinetic experiments in porous media for energy applications*.

The contributions to the book concern various aspects of extension of classical continuum models and of engineering applications of continuum theories. In particular, the contributions deal with the following subjects:

- continuum mechanics,
- thermodynamics,
- porous and granular media,
- engineering applications.

We would like to kindly thank both the participants of *CMwM2015* and the contributors to the current book for the nice cooperation and for their commitment. Furthermore, we are grateful for technical work, especially the transformation of some contributions into LaTeX, by Benedikt Preugschat. Last but not least we appreciate very much the pleasant collaboration with Springer, especially with Christoph Baumann who accepted the publication of this book.

Essen — Bettina Albers
Poznań — Mieczysław Kuczma
October 2015

Contents

Part IV Engineering Applications

Contributors

Hans-Dieter Alber Fachbereich Mathematik, Technische Universität Darmstadt, Darmstadt, Germany

Bettina Albers Geotechnical Engineering, Universität Duisburg-Essen, Essen, Germany

Erich Bauer Institute of Applied Mechanics, Graz University of Technology, Graz, Austria

Włodzimierz Andrzej Bednarek Division of Bridge Building and Railway Tracks, Institute of Civil Engineering, Poznan University of Technology, Poznan, Poland

Arkadi Berezovski Institute of Cybernetics at Tallinn University of Technology, Tallinn, Estonia

Mihhail Berezovski Embry-Riddle Aeronautical University, Daytona Beach, FL, USA

Nikolay G. Burago Ishlinski Institute for Problems in Mechanics RAS, Moscow, Russia

Gianfranco Capriz Dipartimento di Matematica, Università degli Studi di Pisa, Pisa, and Accademia dei Lincei, Rome, Italy

Oscar Castro-Orgaz University of Córdoba, Córdoba, Spain

Monika Chuda-Kowalska Poznan University of Technology, Institute of Structural Engineering, Poznan, Poland

Gianpietro Del Piero Dipartimento di Ingegneria, Universitá di Ferrara, Ferrara, Italy; International Research Center M&MoCS, Cisterna di Latina, Italy

Arkadiusz Denisiewicz Division of Structural Mechanics, University of Zielona Góra, Zielona Góra, Poland

Petia Dineva Institute of Mechanics, BAS, Sofia, Bulgaria

Ioanna-Kleoniki Fontara Chair of Geomechanics and Geotechnics, Christian-Albrechts University, Kiel, Germany

Mohammadreza Gaeini Eindhoven University of Technology, Eindhoven, The Netherlands

Pasquale Giovine DICEAM, Università Mediterranea di Reggio Calabria, Reggio Calabria, Italy

Kolumban Hutter ETH Zürich, Zuerich, Switzerland

Pavel Krejčí Institute of Mathematics, Czech Academy of Sciences, Praha 1, Czech Republic

Mieczysław Kuczma Division of Structural Mechanics, Poznan University of Technology, Poznań, Poland

Miroslav Kureš Institute of Mathematics, Brno University of Technology, Brno, Czech Republic

Carlo G. Lai Department of Civil Engineering and Architecture, University of Pavia, Pavia, Italy

Shuiquan Lan Eindhoven University of Technology, Eindhoven, The Netherlands

I-Shih Liu Instituto de Matemática, Universidade Federal do Rio de Janeiro, Rio de Janeiro, Brazil

Paolo Maria Mariano DICeA, University of Florence, Firenze, Italy

Bogdan T. Maruszewski Institute of Applied Mechanics, Poznan University of Technology, Poznan, Poland

Bohdan Michalak Department of Structural Mechanics, Lodz University of Technology, Łódź, Poland

Ingo Müller Technische Universität Berlin, Berlin, Germany

Silvia Nedea Eindhoven University of Technology, Eindhoven, The Netherlands

Ilia S. Nikitin Institute for Computer Aided Design, Moscow, Russia

Martin Ostoja-Starzewski Department of Mechanical Science and Engineering, Institute for Condensed Matter Theory and Beckman Institute, University of Illinois at Urbana-Champaign, Urbana, IL, USA

Ali G. Özcebe Department of Civil and Environmental Engineering, Politecnico di Milano, Milan, Italy

Martyna Rabenda Department of Structural Mechanics, Lodz University of Technology, Łódź, Poland

Camilo Rindt Eindhoven University of Technology, Eindhoven, The Netherlands

Marek Romanowicz Department of Mechanical Engineering, Bialystok University of Technology, Bialystok, Poland

Ewa Eliza Rożko Institute of Fundamental Technological Research Polish Academy of Sciences, Warsaw, Poland

Jan Jerzy Sławianowski Polish–Japanese Academy of Information Technology, Warsaw, Poland; Institute of Fundamental Technological Research Polish Academy of Sciences, Warsaw, Poland

David M.J. Smeulders Eindhoven University of Technology, Eindhoven, The Netherlands

Merab Svanadze Ilia State University, Tbilisi, Georgia

Olga Szlachetka Faculty of Civil and Environmental Engineering, Warsaw University of Life Sciences-SGGW, Warsaw, Poland

Mariusz Urbaniak Department of Strength of Materials, Lodz University of Technology, Lodz, Poland

Monika Wągrowska Faculty of Civil and Environmental Engineering, Warsaw University of Life Sciences-SGGW, Warsaw, Poland

Artur Wirowski Department of Structural Mechanics, Lodz University of Technology, Łódź, Poland

Frank Wuttke Chair of Geomechanics and Geotechnics, Christian-Albrechts University, Kiel, Germany

Huaichen Zhang Eindhoven University of Technology, Eindhoven, The Netherlands

Krzysztof Wilmanski (1940–2012)

Ingo Müller

When I first met Krzysztof Wilmanski in 1977 he was one of the bright young scientists in the Institute of Fundamental Technological Research of the Polish Academy of Sciences. This was the time of the cold war and it was not altogether easy for us westerners to meet colleagues from beyond the iron curtain. But among all people from the east it was still easiest to meet Polish scientists. Because, indeed, the wise elder scientists at the helm of the Polish Academy—among them Professors Nowacki, Olszak, Fiszdon, and Sawczuk—held some influence in political circles. And they knew that good science requires free and easy communication between scientists. Also they believed in mechanics as an essential part of the natural sciences.

Therefore they sent their young mechanicians abroad, to the east and to the west. Still, it was easier for them go east. Thus, long before I met him, Krzyszt of Wilmanski had been in Moscow, where he tried to join Professor Sedov's research group. Somehow that did not work out well. He was disappointed and left after a few months. Next he went to Baltimore where at the time—in the late 1960s—Professors Truesdell and Ericksen conducted a lively group of graduate student and post-doctoral fellows at the Johns Hopkins University. He was well received there and worked successfully. Thus in a manner of speaking he finished his scientific education there, an education which had started in civil engineering.

Strangely, although I had been at Johns Hopkins before Krzysztof and again after he had left, we never met there. However, we had been exposed to the same unique scientific atmosphere, created by professors Ericksen and Truesdell at the height of Rational thermodynamics; and so, —even without actually meeting—, we became members of a loosely knit group which, much later, some unfriendly person dubbed the "Johns Hopkins gang".

I. Müller (✉)
Technische Universität Berlin, Straße des 17. Juni, 10623 Berlin, Germany
e-mail: ingo.mueller@alumni.tu-berlin.de

B. Albers and M. Kuczma (eds.), *Continuous Media with Microstructure 2*,
DOI 10.1007/978-3-319-28241-1_1

After Johns Hopkins Krzysztof went to Iraq. There was a program, haggled out between the Polish government and some oil-rich left-leaning Arabian states in the near east, by which Polish professors could obtain a well-paid teaching job—in Iraq, or Syria, or Libya—for 1 or 2 years. So, Krzysztof went to Iraq for 2 years. Scientifically that stay was little fruitful, later he would complain that he met a mix of ignorance and arrogance in his host faculty. But the job was profitable money-wise. And so on a side trip to Saudi Arabia Krzysztof acquired a nice new red BMW.

All of this was before Krzysztof and I met.

When we did meet I was a young professor in Paderborn, Germany, recently returned from the United States. The occasion was the founding of ISIMM, the International Society for the Interaction of Mechanics and Mathematics which took place in Kozubnik in the south of Poland. That society was to further facilitate scientific relations between the East and the West and many of the grand old men of mechanics were there. Well, with the exception of the Russians; they feared a conflict of interest with IUTAM, the International Union of Theoretical and Applied Mechanics which was the forum for east-west interaction officially recognized by the Soviet government. But everybody else who was somebody in mechanics and applied mathematics was present in Kozubnik: Sneddon, Chadwick and Spencer from Great Britain, Fichera, Graffi and Grioli from Italy, Kirchgässner and Kröner from Germany, i.e. West Germany. And of course all the Polish tycoons of science were there. Krzysztof Wilmanski and myself were in the junior crowd, along with Robin Knops, Costas Dafermos, Carlo Cercignani and many others. Little did we think at the time that we should in the future become officers of the Society; and yet that happened: Between the years 2000 and 2004 Krzysztof and I were president and secretary of ISIMM.

On the last day of the meeting, a Saturday morning, a decrepit Russian-built bus was to carry the participants back to Warsaw airport. However, the technological decline of the East was already far advanced and so the bus wouldn't start; an essential part of the ignition system was broken. Henryk Zorski, Krzysztof Wilmanski and I myself were watching when the driver gave up his efforts and announced a 3-h delay, because he had to send to Kattowitz for a spare part. Naively I asked Zorski whether he thought that the needed part would be available in Kattowitz. "Oh, no", said Henryk, always the cynic, "nowhere in Poland but there will be a spare bus."

I myself was spared the bus ride, because Krzysztof offered to take me in his BMW. Looking back I now realize that the long ride in close companionship was to soften me up, so that I should support Krzysztof's application for a Humboldt scholarship which he was preparing. Really that effort on his part was quite unneccessary. I would have supported that application anyhow, after all: One member of the Johns Hopkins gang and the other. But the trip as such was not uneventful. Indeed, the pot holes of Southern Poland yanked a shock absorber clean out of the body of the BMW. There was a tremendous noise in the back and when we reached Krakow it became

imperative to find a workshop—at noon on a Saturday in a socialist economy! I considered that hopeless. However, Krzysztof was unfazed and thus he proved not only a keen scientist but also an ingenious organizer of an everyday calamity. He developed a train of thought by which the dairies of the town of necessity are on a 24 h schedule, —including Saturdays—, that they need lorries for the collection and distribution of milk and that the lorries, given their state of repair, need a dairy-owned workshop for repairs. So, we inquired about dairies, found the appertaining workshop and there was a young mechanic who welded the shock absorber back into the place where it belonged.

Time had been lost, though, and so Krzysztof regretted that he could not show me the tomb of Marshall Pilsudski whom he admired very much for having chased out the Russians from some small eastern part of Poland in 1918, or so, and for a short while. Krzysztof was a fervent Polish patriot and remained that throughout his life, even after—much later—he became a German citizen. In fact sometimes he surprised me with his Polish view of events in German history. Actually, if the truth were known there seem to be few events in the histories of the two countries which are viewed in the same light from the two sides of the Polish-German border; excepting only, of course, Russian attempts for domination.

Anyway, the application for the Humboldt scholarship was successful and so, early in 1979, Krzysztof showed up in Paderborn. This started a year of intensive and successful collaboration between the two of us, mostly on shape memory alloys. And that was before anybody else in continuum mechanics recognized the importance of these materials for the understanding of large deformations in solids. So, when I moved to Berlin in that same year, Krzysztof came with me and we continued our work. For me and, I believe, for Krzysztof as well this was a highly satisfactory period of joint learning and research, which we would have liked to continue. But politics intervened, cold war politics.

As some of you may know, the Humboldt foundation gives stipends for no more than 1 year. But, upon application this period can be extended for up to another year. So, naturally Krzysztof and I applied and we got the extension. But cold war tactics was against us. Krzysztof was in trouble with the Polish authorities when he applied for keeping his passport. At that time the official communist doctrine about Germany, dictated by the Russians, was that there were three Germanies: West Germany, DDR and Westberlin. So Krzysztof in joining me in Berlin had violated the rules laid down in his passport which allowed him to visit West Germany only. He had to be punished and he was not allowed to stay on in Berlin. Friends back in Paderborn offered him an office but, although they meant well, they worked on different subjects. So our collaboration suffered; all of this was in the days before e-mail which might have helped us a lot.

And so began Krzysztof's veritable scientific odyssey in Germany and between Germany and Poland: Paderborn, Berlin, Warsaw, Berlin, Hamburg, Berlin, Essen. This odyssey lasted 14 years instead of the requisite ten. During his Warsaw period

the two of us organized a Euromech conference on shape memory in Jabłonna near Warsaw. In Hamburg Krzysztof became an expert on plasticity, in Essen he developed an improved theory of porous and granular media and in the end in Berlin, at the Weierstrass Institute, he concentrated his research efforts on wave propagation in soils, in close collaboration with civil engineers: Wet soils for off-shore wind turbines and dry soils for tunneling.

A high point in his itinerant life, perhaps, was Krzysztof's invitation to a year's stay at the Wissenschaftskolleg Berlin. That august institution—the Institute of Advanced Studies—had heretofore never invited natural scientists—it thrives on political and social "sciences". However, in 1984 I got the unexpected possibility to invite two persons from the natural sciences and they were Ronald Rivlin and Krzysztof Wilmanski. The three of us spent at least 1 day a week together in intensive discussion.

This was the time when a disaster concerning the stability of rheological fluids had overwhelmed Rational Thermodynamics, the theory of Coleman and Noll: According to that theory the free energy should have a maximum in equilibrium when everybody in thermodynamics knew for a century that it has to have a minimum. Rivlin was overjoyed, because he disliked Coleman and Noll for their close association with Truesdell. I myself did not care much, since I worked on Extended Thermodynamics which was untouched by the disaster. And Krzysztof suggested that we look into the problem and perhaps understand its reason. So we studied the papers by Dunn and Fosdick and by Joseph on fluids of nth grade and we came to the conclusion that it is not legitimate to approximate the constitutive functional of the history of some field by a few time derivatives of the field at the present time. The procedure leads to instability. Rivlin did not appreciate the result since it cast doubt on the usefulness of the Rivlin-Ericksen tensors, with which he was strongly associated. And Fosdick—when asked—was also unenthusiastic, because he maintained that stability would miraculously reappear far from equilibrium; a clear case of wishful thinking. So Krzysztof and I were frustrated; we did write a paper and published it in Rheologica Acta to show that the free energy indeed has a minimum in equilibrium as it should be. And there was some interest, —at least we received a lot of reprint requests. But the paper did not really catch on. And, if the truth were known, our arguments lacked the systematic clarity necessary to be convincing. Indeed the problem of a proper thermodynamic theory of non-Newtonian fluids remains unsolved to this day.

Years later, when Roger Fosdick celebrated his 60th birthday, Krzysztof and I addressed the problem again from the point of view of the kinetic theory of rheological fluids. Somewhat maliciously we offered that study for Roger's Festschrift. But then it turned out that neither of us could attend the anniversary meeting and so our paper remained unpublished except as a preprint report of the Weierstrass Institute.

So let me pull our main conclusion out of oblivion in this present eulogy for Krzysztof: Considering a solution of Hookean dumbells—a standard model of

rheology—we derived a differential equation between the deviatoric stress and the deviatoric velocity gradient, viz.[1]

$$\left(1+\frac{1}{2}\frac{\zeta}{\lambda}\frac{\delta}{\delta t}\right)t_{<pq>}=\eta_0\left(1+\frac{\eta_s}{\eta_0}\frac{1}{2}\frac{\zeta}{\lambda}\frac{\delta}{\delta t}\right)\frac{\partial u_{<p}}{\partial x_{q>}} \tag{1}$$

λ is the elastic constant of the dumbell spring. ζ is the Stokes friction coefficient of a dumbell mass in the solvent and η_s is the viscosity of the solvent. η_0 is defined as $\eta_s+\frac{5}{6}nkT\frac{\zeta}{\lambda}$ with n as the number density of dumbells. The equation is known as the Giesekus equation in rheology, but our derivation was marginally more systematic than Giesekus's so that there was a tiny little bit of originality.

All the coefficients are positive so that in regard to stability the equation is fine: If the velocity gradient vanishes, the stress will exponentially approach zero and if the stress vanishes, the velocity gradient relaxes to zero.

So far so good. The argument, —based on reliable molecular considerations—, shows us what the constitutive relation between the stress and the velocity gradient should look like in a rheological fluid. And this does not have the form assumed by Rational thermodynamics. Indeed, in Rational Thermodynamics the stress should be alone on the left-hand-side and it should be given by the velocity gradient and its time derivatives. Such a form may be obtained by shifting the operator $1+\frac{1}{2}\frac{\zeta}{\lambda}\frac{\delta}{\delta t}$ from the numerator on the left-hand-side to the denominator of the right-hand-side and then approximating it—rather daringly—as follows

$$\frac{1}{1+\frac{1}{2}\frac{\zeta}{\lambda}\frac{\delta}{\delta t}}\approx 1-\frac{1}{2}\frac{\zeta}{\lambda}\frac{\delta}{\delta t}. \tag{2}$$

In this manner we obtain

$$t_{<ij>}\approx\eta_0\left(1+\left(\frac{\eta_s}{\eta_0}-1\right)\frac{1}{2}\frac{\zeta}{\lambda}\frac{\delta}{\delta t}\right)\frac{\partial u_{<i}}{\partial x_{j>}}. \tag{3}$$

Now, however, this equation leads to instability. Indeed, if the stress vanishes, the velocity gradient grows exponentially (!) which makes no sense. Thus Krzysztof and I showed in our paper where the instability comes from and how it should be avoided. The fallacy lies in the daring approximation which is inherent in the a priori assumption that the stress should be determined by the velocity gradient and its rate of change.

[1]The complicated time derivatives are Oldroyt derivatives. But for the present brief review we may consider it as just an ordinary time derivative.

Weierstraß-Institut
für Angewandte Analysis und Stochastik

im Forschungsverbund Berlin e.V.

Elementary thermodynamic and stochastic arguments on a non-Newtonian fluid

Ingo Müller [1], Krzysztof Wilmanski [2]

submitted April 28th 1999

[1] Technische Universität Berlin
Institut für Verfahrenstechnik
Fachbereich 6
Fasanenstr. 90
10623 Berlin
Germany
E-Mail: im@thermo08.pi.tu-berlin.de

[2] Weierstraß-Institut
für Angewandte Analysis
und Stochastik
Mohrenstraße 39
D-10117 Berlin
Germany
E-Mail:wilmansk@wias-berlin.de

Preprint No. 485
Berlin 1999

1991 Mathematics Subject Classification
Key words and phrases. Non-Newtonian fluids

Later, —due to the demands of subsequent jobs—Krzysztof left that interesting field and turned to more practical tasks, primarily in wave propagation in porous media as mentioned before. The primary objective was diagnostic, viz. the diagnosis of hidden irregularities in soils. For this work he finally found a secure and stimulating environment in the Weierstrass Institute in Berlin, where he spent the 10 years before his retirement in 2005.

But that was by no means the end of his scientific career. Krzysztof's passion for science and academia did not allow him to stay idle. So he accepted an appointment at the newly founded University of Zielona Góra in Poland where he spent the last years of his life in scientific research, teaching and administration. The faculty in Zielona Góra was lucky to have him, a man of vast experience gathered in many countries in a lifetime devoted to science.

At the end—still working and publishing and full of enthusiasm and energy—he had to succumb to the perfidious sudden attack of the disease that threatens all of us.

I have mourned him, and I am sure we all did, those of us who knew him.

Berlin, 05.05.2015 Ingo Müller

Part I
Continuum Mechanics

Virtual Power and Pseudobalance Equations for Generalized Continua

Gianpietro Del Piero

Abstract In this paper the balance equations of linear and angular momentum are deduced from some regularity properties of the system of contact actions and from the law of action and reaction. This approach provides a simple and unifying formulation of the theories of non polar and polar continua. It also allows for a direct deduction of the classical plate and beam theories as special Cosserat continua, obtained by dimensional reduction induced by appropriate geometrical constraints.

Deduction of Balance Equations

1. The traditional, generally accepted approach to Continuum Mechanics is based on Euler's balance laws of linear and angular momentum. During the second half of the past century, this approach was revisited a number of times. In 1963, W. Noll showed that the Euler laws are in fact a consequence of the postulate of the indifference of power [12]. Later, Gurtin and Martins [9] and Šilhavý [14, 15] came to the conclusion that the same laws, until then regarded as balance equations between distance and contact actions, are in fact regularity assumptions on the system of the contact actions alone.
   This conclusion also originated from an idea of Noll. In [13] he showed that, if a system of contact actions is skew-symmetric,[1] it is also additive on the boundaries of disjoint sets.[2] If this is the case, the contact action over the boundary of a part Π of the body, which may also be seen as a volume action,

[1] This assumption corresponds to Newton's law of action and reaction.
[2] That is, if Π and Π' are disjoint sets with a portion S of boundary in common and if $Q(S) = -Q(-S)$ is the contact action interchanged across S, the contact action on $\partial(\Pi \cup \Pi')$ is the sum of the contact actions on $\partial\Pi$ and on $\partial\Pi'$.

G. Del Piero (✉)
Dipartimento di Ingegneria, Universitá di Ferrara, 44100 Ferrara, Italy
e-mail: dlpgpt@unife.it

G. Del Piero
International Research Center M&MoCS, 04012 Cisterna di Latina, Italy

B. Albers and M. Kuczma (eds.), *Continuous Media with Microstructure 2*,
DOI 10.1007/978-3-319-28241-1_2

$$F(\Pi) = -Q(\partial\Pi), \tag{1}$$

is additive on disjoint sets.[3] In the presence of sufficient regularity, a *surface density* s can be associated with Q and a *volume density* $b^\dagger$ can be associated with F, and the preceding equation can be given the form

$$\int_\Pi b^\dagger(x)\,\mathrm{d}V = -\int_{\partial\Pi} s(x,\partial\Pi)\,\mathrm{d}A. \tag{2}$$

A system of contact actions which admits both surface and volume densities is called a *Cauchy flux*, and Eq. (2) is called a *pseudobalance equation*. The reason for the name is that, though it looks like a balance equation, *this is not a balance equation, but only an identity between two different representations of the same contact action*.

The pseudobalance equation is all what is needed to prove the dependence of $s(x,\partial\Pi)$ on the normal n to $\partial\Pi$ at x,[4] and the linearity of this dependence.[5] That is, to prove that there is a linear transformation on the vectors, the *Cauchy stress tensor* T, such that

$$s = Tn. \tag{3}$$

Thus, rather than a consequence of the balance of linear momentum, the existence of the Cauchy tensor is a property enjoyed by all sufficiently regular skew-symmetric systems of contact actions. This reduces the importance of the role played by the Euler balance laws, which are usually considered as a fundamental postulate of mechanics. Indeed, to define a *classical continuum* it becomes convenient to take as primitive the concept of *external power*, which is an integral involving the inner products of the *external actions* of contact s and at distance b by a field v of *virtual velocities*[6]

$$P_{ext}(\Pi, v) = \int_\Pi b\cdot v\,\mathrm{d}V + \int_{\partial\Pi} s\cdot v\,\mathrm{d}A. \tag{4}$$

In particular, a *rigid virtual velocity field* is a vector field of the form

$$v(x) = a + \varpi\times x, \tag{5}$$

[3] The minus sign on the right is just matter of convenience.

[4] The dependence of s on the normal was conjectured by Cauchy, and was currently called the *Cauchy postulate*. Only in 1959 Noll proved that this conjecture is true, under the assumption that the internal actions have a local character [11]. Since then, the Cauchy postulate has become the *Noll theorem*.

[5] This is the *tetrahedron theorem* of Cauchy.

[6] Alternatively, one can take as primitives the concept of virtual velocity and the existence of two types of actions, distance and contact.

with a and ϖ arbitrary constant vector fields. Assuming the *indifference of power* under rigid virtual velocity fields,

$$P_{ext}(\Pi, a) = 0, \qquad P_{ext}(\Pi, \varpi \times x) = 0, \tag{6}$$

the balance laws of Euler

$$\int_{\Pi} b \, \mathrm{d}V + \int_{\partial\Pi} s \, \mathrm{d}A = 0, \quad \int_{\Pi} x \times b \, \mathrm{d}V + \int_{\partial\Pi} x \times s \, \mathrm{d}A = 0, \tag{7}$$

easily follow. With the aid of the relation (3) and of the divergence theorem, the surface integral in (4) can be transformed into a volume integral, called the *internal power*

$$P_{int}(\Pi, v) = \int_{\Pi} \left((b + \operatorname{div} T) \cdot v + T \cdot \nabla v \right) \mathrm{d}V. \tag{8}$$

The indifference conditions (6) applied to this integral yield the *local forms* of the balance equations

$$\operatorname{div} T + b = 0, \qquad T = T^T. \tag{9}$$

Equating the two expressions (4), (8) of the power, the *equation of virtual power*

$$P_{ext}(\Pi, v) = P_{int}(\Pi, v) \tag{10}$$

is obtained. This is not an equation between two different powers, as it is frequently asserted,[7] but only an identity between two different expressions of the same power.
Substituting the local forms (9) into the internal power (8), a *reduced form* for the power is obtained

$$P_{red}(\Pi, v) = \int_{\Pi} T \cdot \nabla v^S \, \mathrm{d}V. \tag{11}$$

This reduced form characterizes T as the unique *active internal action* present in a classical continuum, and ∇v^S as the corresponding *generalized deformation velocity*.

2. The framework introduced above is easily extended to the generalized continua. A *generalized continuum* is a continuum whose description involves a finite array $\{\xi^\alpha\}$ of primary variables (*state variables*), which can be scalar, vectorial, or tensorial. Coupled with dual variables β^α, σ^α of the same tensorial nature (*bulk and surface external actions*), they determine the external power[8]

[7] In fact, on this assumption is based of the "method of virtual power" developed by Germain [7, 8] and others.

[8] Here and in the following, repeated indices are summed.

$$P_{ext}(\Pi, v, v^\alpha) = \int_\Pi (b \cdot v + \beta^\alpha \cdot v^\alpha)\, \mathrm{d}V + \int_{\partial\Pi} (s \cdot v + \sigma^\alpha \cdot v^\alpha)\, \mathrm{d}A, \quad (12)$$

in which the v^α are the *virtual velocities* of the state variables. If the contact actions σ^α are Cauchy fluxes, each of them has its own pseudobalance equation

$$\int_{\partial\Pi} \sigma^\alpha(x, \partial\Pi)\, \mathrm{d}A = -\int_\Omega \beta^{\alpha\dagger}(x)\, \mathrm{d}V, \quad (13)$$

and from it, with the aid of Noll's and Cauchy's theorems, follows the existence of a linear transformation Σ^α such that

$$\sigma^\alpha = \Sigma^\alpha n. \quad (14)$$

The divergence theorem then allows the passage from the external to the internal power

$$P_{int}(\Pi, v, v^\alpha) = \int_\Pi \left((b + \operatorname{div} T) \cdot v + T \cdot \nabla v + (\beta^\alpha + \operatorname{div} \Sigma^\alpha) \cdot v^\alpha + \Sigma^\alpha \cdot \nabla v^\alpha\right) \mathrm{d}V, \quad (15)$$

from which the balance equations are deduced imposing the indifference to rigid virtual velocity fields. But, unlike in classical continua, the *rigid virtual velocities* are not uniquely defined, since their definition depends on the physical nature of the state variables. In what follows, we consider two classes of generalized continua, *polar* and *non-polar*, with different definitions of rigid virtual velocities. In a non-polar continuum, the state variables describe rearrangements of matter at the microscopic level. A rigid virtual velocity involves no rearrangements, that is, the corresponding virtual velocities v^α are zero. Therefore, the indifference conditions are

$$P_{ext}(\Pi, a, 0) = 0, \qquad P_{ext}(\Pi, Wx, 0) = 0, \quad (16)$$

where W is the skew-symmetric tensor associated with the rotation vector ϖ, defined by the relation

$$Wa = \varpi \times a, \quad (17)$$

for all vectors a. In a polar continuum, the state variables introduce further degrees of freedom for the deformation. Then a rigid rotation is a simultaneous rotation of the macroscopic deformation and of the state variable. In the case of tensorial variables,[9] the virtual velocities v^α are tensor fields, and the appropriate indifference conditions are

$$P_{ext}(\Pi, a, 0) = 0, \qquad P_{ext}(\Pi, Wx, W) = 0. \quad (18)$$

[9] This case includes the *micromorphic continua* [6] and, in particular, the *micropolar continua*, also called *Cosserat continua*.

Thus, the polar and non-polar continua have the same translational indifference condition, but different rotational indifference conditions.

3. An example of a non-polar continuum is met in the theory of *gradient plasticity*. This theory is based on the Kröner-Lee decomposition

$$\nabla f = F^e F^p, \tag{19}$$

according to which the macroscopic deformation gradient ∇f is supposed to be the composition of a microscopic rearrangement F^p and of the local deformation F^e necessary to restore the macroscopic deformation ∇f. This decomposition defines a generalized continuum described by a single state variable, the tensor F^p. For it, the relation (14) has the form

$$S = \mathbb{T} n, \tag{20}$$

where the second-order tensor S is the contact action associated with F^p and the third-order tensor $\mathbb{T}$ is the corresponding internal action. Denoting by L^p the virtual velocity of F^p, the external and internal powers take the form

$$\begin{aligned} P_{ext}(\Pi, v, L^p) &= \int_{\Pi} (b \cdot v + B \cdot L^p)\, \mathrm{d}V + \int_{\partial\Pi} (s \cdot v + S \cdot L^p)\, \mathrm{d}A, \\ P_{int}(\Pi, v, L^p) &= \int_{\Pi} \big((b + \mathrm{div} T) \cdot v + T \cdot \nabla v \\ &\qquad + (B + \mathrm{div}\mathbb{T}) \cdot L^p + \mathbb{T} \cdot \nabla L^p\big)\, \mathrm{d}V. \end{aligned} \tag{21}$$

The indifference conditions (16) yield the same restrictions (9) of the classical continuum, and therefore the reduced form of the internal power is

$$P_{red}(\Pi, v, L^p) = \int_{\Pi} \big(T \cdot \nabla v^S + (B + \mathrm{div}\mathbb{T}) \cdot L^p + \mathbb{T} \cdot \nabla L^p\big)\, \mathrm{d}V. \tag{22}$$

In plasticity it assumed that the Cauchy stress T is a function of the elastic part F^e of the decomposition (19). From this decomposition follows the relation

$$\nabla v = L^e + L^p \tag{23}$$

between the corresponding virtual velocities. Thus, the reduced power takes the form

$$P_{red}(\Pi, v, L^p) = \int_{\Pi} \big(T \cdot D^e + T^p \cdot L^p + \mathbb{T} \cdot \nabla L^p\big)\, \mathrm{d}V, \tag{24}$$

where D^e is the symmetric part of L^e and T^p is the *plastic stress*

$$T^p = T + B + \mathrm{div}\mathbb{T}. \tag{25}$$

The last equation and the balance equation $(9)_1$ are the differential equations of the equilibrium problem of gradient plasticity.[10] The formulation of the problem is completed by a set of constitutive equations between the internal actions T, T^p, $\mathbb{T}$ and the corresponding generalized deformations, and by appropriate boundary conditions.

4. In a polar continuum, quite frequently the state variables are supposed to be vectorial, and in this case they are called the *directors*. The number of the directors depends on the nature of the continuum. For example, the *liquid crystals* have just one director, in *crystal plasticity* the number of the directors coincides with the number of the slip planes, and a *micromorphic continuuum* is characterized by a triple of linearly independent directors. Just as the macroscopic deformation of the body is described locally by the deformation gradient ∇f, the microscopic deformation of a micromorphic continuuum is described by a second-order tensor F^m, the *microscopic deformation gradient*. Thus, at each point of the continuum the microdeformation has the same geometric structure of the macrodeformation undergone by the whole body.[11]
In the microdeformation, the directors d^α are mapped into the vectors $F^m d^\alpha$. Denoting by

$$v^\alpha = L^m d^\alpha \tag{26}$$

the corresponding virtual velocity, substituting into (12), and setting

$$B = \beta^\alpha \otimes d^\alpha, \qquad S = \sigma^\alpha \otimes d^\alpha, \tag{27}$$

the external and internal powers (21) are re-obtained, with L^m in place of L^p. With the indifference conditions (18), the balance laws are

$$\mathrm{div} T + b = 0, \qquad T + T^m = (T + T^m)^T, \qquad T^m = B + \mathrm{div}\mathbb{T}. \tag{28}$$

That is, the symmetry of the Cauchy stress T required by the balance laws (9) of the non-polar continua is now replaced by the symmetry of the tensor $T + T^m$. As a consequence, in the integrand function of $(21)_2$ one has

$$\begin{aligned} T \cdot \nabla v + (B + \mathrm{div}\mathbb{T}) \cdot L^m &= T^S \cdot \nabla v^S + T^W \cdot \nabla v^W + T^m \cdot L^m \\ &= T^S \cdot \nabla v^S - T^{mW} \cdot \nabla v^W + T^m \cdot L^m = T^S \cdot \nabla v^S + T^m \cdot \mathcal{L}^m, \end{aligned} \tag{29}$$

[10] We emphasize that (25) is a consequence of the pseudobalance equation (13) and not a new balance equation. In the literature, it is named *balance of micromomentum, microforce balance, equilibrium equation for the macrostress tensor*, and is presented, at least tacitly, as a new axiom of mechanics.

[11] Ericksen and Truesdell [5], Mindlin [10] and Eringen [6].

where

$$\mathcal{L}^m = L^m - \nabla v^W \tag{30}$$

is the virtual velocity of the directors with respect to the body already deformed by the macroscopic deformation. The reduced power then takes the form

$$P_{red}(\Pi, v, L^m) = \int_\Pi \left(T^S \cdot \nabla v^S + T^m \cdot \mathcal{L}^m + \mathbb{T} \cdot \nabla L^m\right) \mathrm{d}V. \tag{31}$$

For a micromorphic continuum, the differential equations of the equilibrium problem are $(9)_1$ and $(28)_3$, and the constitutive equations are relations between the internal actions T^S, T^m, $\mathbb{T}$ and the generalized deformations ∇v^S, $\mathcal{L}^m$, ∇L^m. The Cauchy stress is not symmetric, and its skew-symmetric part T^W does not appear in the expression of the power. It plays the role of a reaction, determined by the relation $(28)_2$, $T^W = -T^{mW}$.

5. [12]In a micromorphic continuum, the deformation of the directors may be subject to geometrical constraints. For example, the *micropolar continua* are micromorphic continua for which the only deformation allowed to the orthonormal triple of directors is a rigid rotation, variable from point to point. Thus, if $R^m U^m$ is the polar decomposition of F^m, the constraint acting on a micropolar continuum is

$$F^m = R^m, \qquad U^m = I. \tag{32}$$

In this case the virtual velocity L^m reduces to its skew-symmetric part W^m, and in the external power we have

$$B \cdot L^m = B^W \cdot W^m = c \cdot \omega, \qquad S \cdot L^m = S^W \cdot W^m = m \cdot \omega, \tag{33}$$

with ω, $c/2$ and $m/2$ the vectors associated with W^m, B^W and S^W by the relation (17)

$$W^m a = \omega \times a, \qquad B^W a = \frac{1}{2} c \times a, \quad S^W a = \frac{1}{2} m \times a. \tag{34}$$

The external power then takes the form

$$\mathcal{P}_{ext}(\Pi, v, \omega) = \int_\Pi \left(b \cdot v + c \cdot \omega\right) \mathrm{d}V + \int_{\partial\Pi} \left(s \cdot v + m \cdot \omega\right) \mathrm{d}A, \tag{35}$$

with ω the vectorial measure of the virtual rotation of the directors, and c and m the *volume couple* and the *surface couple*. If s and m are Cauchy fluxes, they have the representations

[12]For reasons of brevity, from here on most of the statements are given without comments and proofs. More detailed treatments can be found in the paper [2] and in the forthcoming lecture notes [4]. For plate and beam theories, see [3].

$$s = Tn, \qquad m = Mn, \tag{36}$$

with T the Cauchy stress and M the *couple stress tensor*. With the aid of the divergence theorem one obtains the internal power

$$\mathcal{P}_{int}(\Pi, v, \omega) = \int_{\Pi} \left((b + \mathrm{div} T) \cdot v + T \cdot \nabla v + (c + \mathrm{div} M) \cdot \omega + M \cdot \nabla \omega\right) \mathrm{d}V. \tag{37}$$

The indifference conditions now give

$$\mathrm{div} T + b = 0, \qquad \mathrm{div} M + c + 2t = 0, \tag{38}$$

with t the vector associated with the skew-symmetric part of T. Substitution into Eq. (37) yields the reduced form

$$\mathcal{P}_{red}(\Pi, v, \omega) = \int_{\Pi} \left(T^S \cdot \nabla v^S - 2\, t \cdot \varphi + M \cdot \nabla \omega\right) \mathrm{d}V, \tag{39}$$

where

$$\varphi = \omega - \frac{1}{2} \mathrm{curl}\, v \tag{40}$$

is the vector measure of the relative rotation $W^m - \nabla v^W$. The equilibrium problem now consists of the differential equations (38), of constitutive equations relating the internal actions T^S, t and M with the generalized deformations ∇v^S, φ and $\nabla \omega$, and of a set of boundary conditions.

The *constrained Cosserat continua* are obtained by imposing the supplementary constraint

$$\omega = \frac{1}{2} \mathrm{curl}\, v, \tag{41}$$

which requires that the relative rotation φ be zero.[13] For such continua the indifference conditions still have the form (38), and the reduced power is

$$\mathcal{P}_{red}(\Pi, v) = \int_{\Pi} \left(T^S \cdot \nabla v^S + \frac{1}{2} M \cdot \nabla \mathrm{curl}\, v\right) \mathrm{d}V. \tag{42}$$

Here, T^S and M are the only active internal actions. The rotation ω formally disappears from the list of the geometric variables, though its effects are still present in the product $M \cdot \nabla \mathrm{curl}\, v$.[14] As a consequence, t is not anymore an active internal action, and therefore it is not anymore determined by a constitutive equation. In

[13] This constraint corresponds to the *Cauchy-Born hypothesis*, according to which the directors follow the macroscopic deformation.

[14] The presence of a microstructure which does not appear explicitly in the expression of the power characterizes this continuum as a *continuum with latent microstructure* [1].

the equilibrium problem, t is eliminated from the differential equations (38) with the aid of the identity

$$\mathrm{div} T^W = -\mathrm{curl}\, t, \tag{43}$$

thanks to which the two equations merge in the single, higher-order equation

$$\mathrm{div} T^S + \frac{1}{2}\mathrm{curl}\,(\mathrm{div} M + c) + b = 0. \tag{44}$$

Of course, the boundary conditions must be re-formulated accordingly.

6. Other geometrical constraints lead to *dimensional reduction*, providing thereby the classical theories of plates and beams, viewed as two- and one-dimensional Cosserat continua. Assume that the body in its reference configuration has a cylindrical shape, and let $\{e, e^\alpha\}$ be an orthonormal triple of vectors, with e directed as the axis of the cylinder. The constraint

$$v(x) = v_3(x_1, x_2)\, e, \qquad \omega(x) = \omega_\alpha(x_1, x_2)\, e^\alpha, \qquad \alpha \in \{1, 2\}, \tag{45}$$

allows for a virtual velocity v parallel to e and for a virtual rotation ω about an axis orthogonal to e. It also requires that both v and ω be constant in the direction e. Under these constraints, the external power (35) reduces to

$$P_{ext}(\Gamma, v_3, \omega_\alpha) = \int_\Gamma (b_3 v_3 + c_\alpha \omega_\alpha)\, \mathrm{d}A + \int_{\partial\Gamma} (s_3 v_3 + m_\alpha \omega_\alpha)\, \mathrm{d}\ell, \tag{46}$$

where the volume element Π is replaced by its perpendicular projection Γ in the direction e, and $\mathrm{d}\ell$ is the line element on the boundary line $\partial\Gamma$.
In the relations (36), by effect of the constraints, the stress tensor T_{ij} degenerates into the vector of the *internal shearing forces* Q_α, and the couple-stress tensor M_{ij} degenerates into the 2×2 tensor of the *internal moments* $M_{\alpha\beta}$

$$s_3 = Q_\alpha n_\alpha, \qquad m_\alpha = M_{\alpha\beta} n_\beta. \tag{47}$$

Then the internal power becomes

$$\mathcal{P}_{int}(\Gamma, v_3, \omega_\alpha) = \int_\Gamma \big((q + Q_{\alpha,\alpha})v_3 + Q_\alpha v_{3,\alpha} + (c_\alpha + M_{\alpha\beta,\beta})\omega_\alpha + M_{\alpha\beta}\omega_{\alpha,\beta}\big)\, \mathrm{d}A, \tag{48}$$

with the component b_3 of the body force now viewed as a transverse load q. The indifference conditions (18) provide the balance equations

$$Q_{\alpha,\alpha} + q = 0, \qquad M_{\alpha\beta,\beta} + c_\alpha + e_{\alpha\beta} Q_\beta = 0, \tag{49}$$

which, in turn, lead to the reduced power

$$P_{red}(\Gamma, v, \omega) = \int_{\Gamma} (Q_\alpha \varphi_\alpha + M_{\alpha\beta}\omega_{\alpha,\beta})\, \mathrm{d}A, \tag{50}$$

where

$$\varphi_\alpha = v_{3,\alpha} + e_{\alpha\beta}\omega_\beta \tag{51}$$

are the rotations of the directors relative to the deformed surface Γ. Thus, the active internal actions are Q_α and $M_{\alpha\beta}$, and φ_α and $\omega_{\alpha,\beta}$ are the corresponding generalized deformations. The equations (49) are the equilibrium equations of the *Reissner-Mindlin plate theory*. Here, this theory has been deduced from that of the three-dimensional micropolar continuum, simply by imposing the constraint (45).
Moreover, the *Kirchhoff-Love plate theory* is obtained by imposing the additional constraint

$$\varphi_\alpha = 0. \tag{52}$$

Indeed, with this constraint, in the reduced power (50) the first term cancels, and $\omega_{\alpha,\beta}$ is replaced by $e_{\alpha\gamma}v_{3,\gamma\beta}$. Introducing the *modified moment tensor*

$$M^*_{\gamma\beta} = e_{\gamma\alpha}M_{\alpha\beta}, \tag{53}$$

which is the one currently used in the constrained plate theory, the reduced power takes the form

$$P_{red}(\Gamma, v) = -\int_{\Gamma} M^*_{\gamma\beta} v_{3,\gamma\beta}\, \mathrm{d}A. \tag{54}$$

The active internal forces are reduced to the tensor $M^*_{\gamma\beta}$, and the associated generalized deformation is the *curvature tensor* $-v_{3,\gamma\beta}$. As a consequence, the vector Q_α must be eliminated from the balance equations (49). This gives rise to the unique, higher order equation

$$M^*_{\gamma\beta,\gamma\beta} + c^*_{\gamma,\gamma} + q = 0, \tag{55}$$

where $c^*_\gamma = e_{\gamma\alpha}c_\alpha$ is the modified external couple. This is the equilibrium equation of the Kirchhoff-Love plate theory.

7. In a quite similar way, it can be shown that the constraints

$$v(x) = v(x_3), \qquad \omega(x) = \omega(x_3) \tag{56}$$

provide the *Timoshenko beam theory*, and that the additional constraint

$$\omega_\alpha = -e_{\alpha\beta}v'_\beta \tag{57}$$

leads to the *Euler-Bernoulli beam theory*. For a detailed treatment, the interested reader is addressed to the paper [3].

References

1. Capriz, G.: Continua with Microstructure. Springer, Berlin (1989)
2. Del Piero, G.: Non-classical continua, pseudobalance, and the law of action and reaction. Math. Mech. Complex Syst. **2**, 71–107 (2014)
3. Del Piero, G.: A rational approach to Cosserat continua, with application to plate and beam theories. Mech. Res. Commun. **58**, 97–104 (2014)
4. Del Piero, G.: Une approche rationnelle des milieux continus avec microstructure, in: Mécanique des milieux continus généralisés. Collection Mécanique théorique, Cépaduès, Toulouse (forthcoming)
5. Ericksen, J.L., Truesdell, C.: Exact theory of stress and strain in rods and shells. Arch. Ration. Mech. Anal. **1**, 295–323 (1958)
6. Eringen, A.C.: Mechanics of micromorphic continua. In: Kröner, E. (ed.) Mechanics of Generalized Continua. Proceedings of IUTAM Symposium, Freundenstadt & Stuttgart, pp. 18–35. Springer, Berlin (1967)
7. Germain, P.: La méthode des puissances virtuelles en mécanique des milieux continus. Première partie: théorie du second gradient. J. de Mécanique **12**, 235–274 (1973)
8. Germain, P.: The method of virtual powers in continuum mechanics. Part 2: microstructure. SIAM J. Appl. Math. **25**, 556–575 (1973)
9. Gurtin, M.E., Martins, L.C.: Cauchy's theorem in classical physics. Arch. Ration. Mech. Anal. **60**, 305–324 (1976)
10. Mindlin, R.D.: Micro-structure in linear elasticity. Arch. Ration. Mech. Anal. **16**, 51–78 (1964)
11. Noll, W.: The foundations of classical mechanics in the light of recent advances in continuum mechanics. In: The Axiomatic Method, with Special Reference to Geometry and Physics. North-Holland, Amsterdam, pp. 266–281 (1959). Reprinted. In: The Foundations of Continuum Mechanics and Thermodynamics, Selected Papers of W. Noll. Springer, Berlin (1974)
12. Noll, W.: La mécanique classique, basée sur un axiome d'objectivité. In: La Méthode Axiomatique dans les Mécaniques Classiques et Nouvelles, pp. 47–56. Gauthier-Villars, Paris (1963). Reprinted In: The Foundations of Continuum Mechanics and Thermodynamics, Selected Papers of W. Noll. Springer, Berlin (1974)
13. Noll, W.: Lectures on the foundations of continuum mechanics and thermodynamics. Arch. Ration. Mech. Anal. **52**, 62–92 (1973)
14. Šilhavý, M.: The existence of the flux vector and the divergence theorem for general Cauchy fluxes. Arch. Ration. Mech. Anal. **90**, 195–212 (1985)
15. Šilhavý, M.: Cauchy's stress theorem and tensor fields with divergences in L^p. Arch. Ration. Mech. Anal. **116**, 223–255 (1991)

Hypocontinua

Gianfranco Capriz and Pasquale Giovine

Abstract Earlier proposals for a theory of continuous bodies for which the tacit axiom of enduring permanence of material elements fails to apply (continua called appropriately ephemeral) are briefly reviewed and, in some detail, corrected. The consequent derivation of a simpler class echoing that of hypoelastic bodies introduced by Truesdell is preened and put on surer footing for possible progress.

1 Preamble

We pursue here the same topics of a paper with selfsame title [6], but the emphasis is on some critical issues within the theory of ephemeral continua [5, 8] (issues of relevance for the derivation of balance equations here) and on consequences of the latter on energy balances. For the reader who did not chance on those earlier papers meant to pacify some acid controversies [11, 12, 14, 24, 25] their essential traits are briefly recalled below.

The term 'ephemeral continua' was proposed by one of us to designate sparsely granular or molecular bodies (such as are gases) for which, when they are modelled as continua, the tacit axiom of permanence of material elements fails to apply. Of course, the scales involved in the two instances, referred to above, are hugely different; nevertheless, the same mathematical structures are convenient in the analysis of some issues when dealing with either. Consequently we happen to use some words (for instance, the term molecule) ambiguously. Then, more fields are needed to report events, as occurs when dealing with non-simple bodies; the peculiarity here is the

G. Capriz
Dipartimento di Matematica, Università degli Studi di Pisa,
Pisa, and Accademia dei Lincei, Rome, Italy
e-mail: gianfranco.capriz@mac.com

P. Giovine (✉)
DICEAM, Università Mediterranea di Reggio Calabria,
via Graziella 1, località Feo di Vito, 89122 Reggio Calabria, Italy
e-mail: giovine@unirc.it

B. Albers and M. Kuczma (eds.), *Continuous Media with Microstructure 2*,
DOI 10.1007/978-3-319-28241-1_3

involvement of a symmetric non-negative definite tensor, the Reynolds' tensor, which could be interpreted as a density of rebounds due to molecular collisions.

Hypocontinua are a very special class of ephemera, for which the evolution equations have formal analogy with those of Truesdell's hypoelastic media (to which one chapter is dedicated in each of two treatises of the Encyclopedia of Physics, volumes III/1 and III/3 [22, 23]), hence the name. True, the sources of the two proposals may seem to be foreign rather than akin, as we remark more clearly in the following Sect. 3. Hypocontinua may even seem to imply a repudiation of the main inducement for the introduction of ephemerality, as a decisive constraint seems to restore obligations ensuing from the tacit axiom, in the standard theory, of perpetuity of material elements, an axiom refuted at the outset in that introduction. However, the collateral structure implied by the Reynolds' tensor is safeguarded, so that, in the end, links are found to be stricter than expected.

We start by recalling the essential introductory moves one takes when staging ephemerality. Actually this preamble contains also, by the way, a number of clarifying remarks for a better understanding of some details of the proposal; so its length exceeds that required by a bare summary.

The space where bodies are modeled coarsely is still the three-dimensional Euclidean space $\mathscr{E}$ of places x; the coarse image of a body at an instant τ is still a fit region $\mathscr{B}_\tau$ in $\mathscr{E}$ [19]. But, when aspiring to a more circumstantial local view, one imagines the whole physical space split into minute cubic boxes $\mathfrak{c}$, briefly called loculi, of edge δ (conventionally as in molecular dynamics) and asserts to be able to explore with an appropriate enlarging device the matter in each box. The partition is irrelevant at the coarse scale; fading sight narrows each loculus to a pinpoint so that any $\mathfrak{c}$ can be designated by the image x in $\mathscr{E}$ of the latter: $\mathfrak{c}(x)$. The imagined magnification of any $\mathfrak{c}$ must be, in principle, so great as to trace granules or even molecules in it. At the same time δ must be large enough for the loculus to contain a sufficiently populous cluster of molecules: meaning and avail must be ensured for statistical estimates beyond averages; in fact, the cluster in each box and at each instant τ, is declared to form a grand canonical ensemble.

A heavy restriction is accepted here: molecules are, under all magnifications, modeled as points, not otherwise marked but for their instantaneous placement within each $\mathfrak{c}(x)$ and for the velocity of each. That restriction, unfortunately but for initial simplicity, excludes the use of the model for important physical objects such as mixtures, even only binary when they must be separated into two different clusters.

The coarse view of events is modeled within $\mathscr{E}$ and is narrated via the geometric and analytical tools adopted in the standard theory of simple continua. Loculi do not find leeway within $\mathscr{E}$; each one is asserted to expand within its own local euclidean space $\mathscr{E}_x$, occupying there the cubic box of edge δ. Any sub-place in $\mathfrak{c}(x)$ is identified by a vector y issued from the center of mass of the cluster, center mirrored by x within $\mathscr{E}$.

Finally, the context which the model inhabits is the Cartesian product of Euclidean spaces: $\mathscr{E} \times \mathscr{E}_x$. Of course, one must always have in mind that the whole physical space

is one, though mathematical convenience leads us to imagine it split into separate minute fragments placed into distinct spaces. Thus also the viewer of the two scenes is the same: when independence of the observer is rightly imposed on some quantity, be it macro or micro or nano, the rotation tensor entering the requirement is unique.

Some delicate issues must still be sorted out. Molecules may exit or enter a loculus not to disappear into or appear from the exterior of the box within its local space. They must, somehow, be pictured to enter in or emigrate from boxes placed in adjoining spaces. To bypass such hurdle, one avoids to pursue cross-boundary paths; rather, one restricts oneself to measuring rates of trespass, a process which may be performed remaining within the box.

As we have mentioned already, a sharp view is presumed to allow us to distinguish sub-places y within $\mathfrak{c}(x)$. We may then imagine further that, by an even sharper view, we could explore a neighborhood of each y, as one does in standard kinetic theory, but now at one remove down. That exploration should let us measure the velocities w of all molecules in each neighborhood and determine their distribution $\Theta(\tau, x; y, w)$ within the vectorial space $\mathscr{V}$ of velocities; i.e., the number of molecules per unit volume $\Theta\, d\mathscr{V}$, having velocities within the infinitesimal ball $(w + dw)$ around w.

Remark that, as in the kinetic theory but now within the neighborhood of y, we disregard knowledge of the sub-place of each molecule, but keep note of its velocity w, to decide finally about the frequency Θ.

Actually, reference to Θ is mainly of introductory value here and would only be relevant to establish eventually later possible links with thermodynamics via an adapted Boltzmann equation. Here, one needs only refer to number density θ at y:

$$\theta(\tau, x; y) = \int_{\mathscr{V}} \Theta(\tau, x; y, w)\, d\mathscr{V} \tag{1}$$

and to the average velocity w_* at y

$$w_*(\tau, x; y) = \theta^{-1} \int_{\mathscr{V}} w\, \Theta(\tau, x; y, w)\, d\mathscr{V}; \tag{2}$$

we may assume that our exploration around y has given us them directly.

Thus, in particular, the numerosity $\omega(\tau, x)$ of all molecules in $\mathfrak{c}(x)$ at time τ would be

$$\omega(\tau, x) = \int_{\mathfrak{c}(x)} \theta(\tau, x; y)\, dvol \tag{3}$$

and we are led to the first step in the invention of a continuum to be associated with the molecular (or the minutely and sparsely granular) cluster of specks, each of mass μ. The continuum would have a density

$$\rho(\tau, x) = \mu\, \delta^{-3}\, \omega(\tau, x). \tag{4}$$

For the same time and place, the obvious choice for a gross velocity v is the filtered velocity:

$$v(\tau, x) = \delta^{-3} \int_{\mathfrak{c}(x)} w_* dvol. \tag{5}$$

Such artificially created fields were called *aeolian,* i.e. of the wind produced by the molecular flow, because they could, eventually, be read experimentally by an appropriate anemometer.

The support of the field $v(\tau, x)$ belongs to the four dimensional space-time $\mathscr{T} \times \mathscr{E}$ ($\mathscr{T}$ the axis of time), say, and it is a cylinder with $\mathscr{B}_\tau$ an instantaneous cross-section at time τ, within the interval of interest, say $[0, \bar{\tau}]$. For any $\bar{x} \in \mathscr{B}_{\bar{\tau}}$, we can feign a streak line $x = \hat{x}(\tau, \bar{x})$ within the cylinder by integration backwards (i.e., by a retrogression similar to one described in Chap. 3 (iv) of [10], but here in space-time) from $\tau = \bar{\tau}$ to $\tau = 0$ of the differential equation

$$\frac{\partial \hat{x}(\tau, \bar{x})}{\partial \tau} = v(\tau, \hat{x}), \qquad \hat{x}(\tau, \bar{x}) = \bar{x}; \tag{6}$$

where we have used the sign of partial derivation (although $\bar{x}$ has only the rôle of a parameter here) to avoid confusion with later total derivatives.

Thus we have achieved the description of a gross motion of a 'fictitious' continuous body, non material but based nevertheless on the collective properties of the motion of the molecules. It is not preposterous to assume that the field v be so smooth as to lead to smooth streak lines and to a one-to-one, also smooth, correspondence between the present place $\hat{x}(\tau)$ along one of those lines and the initial place $x_o = \hat{x}(0, \bar{x})$ on it. Finally, we have created the premises for the adoption of the axiom of permanence (here of 'fictitious' rather than 'material' elements) quoted in the beginning paragraph of this section. Hence, we are allowed (within obvious provisos) to import concepts and results from the standard theory; such as the placement gradient F:

$$F(\tau, x) = \frac{\partial x(\tau, x_o)}{\partial x_o}, \tag{7}$$

(where, from now on, $x(\tau, x_o) := \hat{x}(\tau, \hat{x}(0, \bar{x}))$) and the equation valid for it

$$\dot{F}(\tau, x) := \frac{\partial F}{\partial \tau} + \left(\frac{\partial F}{\partial x}\right) v = LF, \tag{8}$$

where

$$L = \frac{\partial v}{\partial x}, \tag{9}$$

and the superimposed dot signifies total time derivation along the streak-lines.

The availability of the field of filtered velocities v allows us to introduce the peculiar velocities c_* of agitation within each loculus

$$c_*(\tau, x; y) := w_*(\tau, x; y) - v(\tau, x). \tag{10}$$

It has the disadvantage of being observer dependent: for two observers rotating one with reference to the other at a rotational velocity q, the peculiar velocities would differ by $(\mathbf{e}q)y$ ($\mathbf{e}$ being the third order Ricci's tensor). True, here $|y|$ is extremely small, being of an order just above that of molecular distances; thus, $|q|$ should be extremely large to cause trouble. Biscari and Cercignani have studied the apparent effect of observer rotation on Fourier law of heat flow [2].

Nevertheless, we strive here to avoid the blight. Success is assured because, contrary to the restricted presumptions in the kinetic theory, we are supposed here to know, by (1), the number density θ at any sub-place y in each loculus. Therefore we can calculate:

(i) the instantaneous *Euler's inertia tensor* for unit mass Y for all molecules in $\mathfrak{c}(x)$:

$$Y(\tau, x) := \omega^{-1} \int_{\mathfrak{c}(x)} \theta\, y \otimes y\, dvol, \tag{11}$$

(ii) the instantaneous *tensor moment of momentum* for unit mass K again for all molecules in $\mathfrak{c}(x)$:

$$K(\tau, x) := \omega^{-1} \int_{\mathfrak{c}(x)} \theta\, y \otimes c_*\, dvol. \tag{12}$$

We have already chosen to issue the vectors y from the center of mass of molecules in $\mathfrak{c}(x)$ and their total momentum per unit mass is simply ωv so that:

$$\int_{\mathfrak{c}(x)} \theta\, y\, dvol = 0, \quad \int_{\mathfrak{c}(x)} \theta c_*\, dvol = 0. \tag{13}$$

Now, with an effort of fantasy, let us imagine a fictitious element of a continuum, not strictly material but nonetheless characterized by the concrete behavior of local molecules. An element which: (i) occupies, at time τ, the place x; (ii) has density ρ as per (4); (iii) translates with velocity $v(\tau, x)$; (iv) moves along the streak-lines obtained via integration of (6); (v) has a distribution of mass leading to a tensor moment of inertia $Y(\tau, x)$ with positive determinant; (vi) suffers a rate of change of that distribution conditioned by a tensor moment of momentum per unit mass $K(\tau, x)$.

In our analysis we do not ask finally for information deeper than the one deriving from the list above, except for a last quantity summarizing consequences of local agitation. That agitation apart, the local motion of molecules are intended as described, at a middle scale, by a distortion of affine type at a rate B (a kinetic tensor) as familiar from the theory of pseudo-rigid bodies [10], a rate which links Y and K:

$$K = YB^T \tag{14}$$

(a superimposed T meaning transposed).

As Y is supposed to be invertible, $B(\tau, x)$ becomes also available. Then one may split w_* into three addenda by the introduction of a new peculiar velocity c:

$$c(\tau, x; y) := w_*(\tau, x; y) - v(\tau, x) - [B(\tau, x)]y, \tag{15}$$

which, contrary to c_*, is observer independent.

At first, we do not pursue a detailed knowledge of the fields c; but, rather, as announced, we introduce a new tensor H based on c:

$$H(\tau, x) := \omega^{-1} \int_{\mathfrak{c}(x)} \theta\, c \otimes c\, dvol, \tag{16}$$

which, multiplied by ρ, leads to Reynolds' tensor measuring, as declared in [10], 'the apparent stress due to change of moment of momentum'; in fact ρH has the physical dimension of a stress (also of an energy density, of course), but, in our opinion and in accordance with the declaration just mentioned, it is a kinetic quantity gauging a contribution to the time-rate of change of K. Hence we are led later to suggest for it an evolution equation to replace, in a sense, one proposed in the theory of hypoelasticity for the tensor of Cauchy's stress [21].

Because c may be interpreted as the average relative velocity of the molecules belonging to the bunch in the immediate neighbourhood of y within $\mathfrak{c}(x)$, it could be imagined also to be the relative velocity of a fictitious sub-element presently at y. Consequently, one must account for a sub-local relative momentum and an associated kinetic energy not yet accounted for at the mesolevel. The adjective 'relative' is there to insist that the value is measured by an observer translating at the rate v and deforming at the rate B or, rather, by an observer who has already discounted those kinetic circumstances. So, the instantaneous total relative momentum over $\mathfrak{c}(x)$ and the associated tensor moment vanish:

$$\int_{\mathfrak{c}(x)} \theta\, c\, dvol = 0, \quad \int_{\mathfrak{c}(x)} \theta\, y \otimes c\, dvol = 0. \tag{17}$$

In contrast to (17), the relative kinetic energy tensor per unit mass (16) vanishes only exceptionally. Our efforts above assure us that such energy, often transmogrified as of thermal gender, be observer independent.

As our aim, at the moment, is only the simplest continuum model of partly disorderly flow, all we need, essentially, from the deeper analysis, is the evaluation of the so far hidden contribution of the inertia associated with irregular motions inside each $\mathfrak{c}(x)$, inertia which needs to be added to the time-rate of change of K yet to be measured mesoscopically as mentioned above. To achieve that aim, the variable y under integral sign in (12), must not be simply taken as the mark of a free place in $\mathfrak{c}(x)$, but, rather, as the mark of a place occupied instantaneously by a fictitious sub-element,

hence, as such, subject to time change. Its time-derivative equals the relative velocity c of the sub-element. The result is that the term to be added is exactly H.

It is worth to evidence the independence repeatedly quoted in an even more explicit guise by mimicking, for the affine middle picture, results already recalled, for the gross view. Precisely, we may seek a double vector $G(\tau, x)$ having the rôle which the placement gradient F has; i.e., by compounding an orthogonal double vector and a symmetric positive definite tensor (for F, they would be an orthogonal tensor Q, say, and the square root of the left Cauchy-Green tensor $\tilde{C}$ such that $F = \tilde{C}^{1/2}\, Q$).

The principal axes of Y could offer the middle scale ghost reference, the eigenvalues could be measure the main changes in length and the orthogonal double vector R could specify the rotation of axes from an initial frame:

$$Y = \delta^2 G G^T, \qquad G = \delta^{-1} Y^{1/2} R. \tag{18}$$

The velocities c are measured by an observer sitting on a frame moving as specified by R; hence unrelated with other observers moving or otherwise.

A final remark should have been inserted even earlier, really: the analogy with well-known gross results is so strict than an equivalent form of (8), i.e. $L = \dot{F} F^{-1}$, is mirrored at the middle scale by a direct relationship between B and $\dot{G}$; but for detail we refer to [3] and remarks within the next section.

2 Balances

We continue our digest of essential traits of earlier essays, adding some clarifying remarks. The proposed model is an apparently standard continuum with additional or alternative entities: (i) streak lines, rather than trajectories of material elements; (ii) aeolian, or wind, velocity v, tracing those lines; (iii) corresponding displacements and displacement gradient F, strictly akin to standard but differently significant; (iv) time-dependent fields of distinct local affine deformation embodied by the field of the double vector G, in a vague analogy of those required in theories of elastic-plastic behavior; (v) fields of moment of inertia Y and moment of momentum K, as in many theories of multi-polar or pseudo-rigid bodies; (vi) fields of a kinetic tensor H, analogous to one representing anisotropic kinetic energy within theories of granular bodies and in certain theories of turbulent flows; (vii) the field $c(\tau, x; y)$ describing a sort of sub-locally averaged agitation of molecules within each loculus.

One point needs to be evidenced: the fields Y and K (leading to consequent fields B and G) are defined at each instant τ through totals over loculi of fixed location and size. The time-derivatives used to measure inertia must be evaluated following the contrived aeolian motion. Moreover, the molecules which instantaneously occupy one loculus tend to invade, in reality, an irregular, ill-defined set which, in approximation, we take to be obtained from the original loculus by deforming it at the rate B, with a volume change rate $\operatorname{tr} B$. At the same time, the fictitious wind elements change shape at the rate L, hence change volume at the rate $\operatorname{tr} L$, with an incongruence

$$\sigma = \operatorname{tr} L - \operatorname{tr} B. \tag{19}$$

To meet the two challenges one must:

(i) involve tensors of Piola type Y^P, K^P instead of Y, K; for instance

$$Y^P = (\det\tilde{X})G^{-1}YG^{-T}, \tag{20}$$

with

$$\tilde{X} = FG^{-1}, \text{ so that } (\det\tilde{X})^{\cdot}(\det\tilde{X})^{-1} = \sigma; \tag{21}$$

(ii) take over an adapted Oldroyd derivative [20], marked here by a superimposed little circle:

$$\mathring{Y} := (\det\tilde{X})^{-1}G\dot{Y}^PG^T, \text{ where } \dot{Y}^P = \frac{\partial Y^P}{\partial\tau} + (\mathrm{grad}_x Y^P)v. \tag{22}$$

Explicitly

$$\mathring{Y} = \dot{Y} - BY - YB^T + \sigma Y. \tag{23}$$

Such rate could be called retrovected, in contrast to the convected rate used by Truesdell in [22] (see (99.10)).

To come to the effective time-rate of change of K, the decisive remarks preceding and following (17), regarding the influence of deep irregular motions inside $\mathfrak{c}(x)$, must be brought to bear: we must add to $\mathring{K}$ the tensor H. This presence of H, modeling, as already remarked, deeper effects on the value of inertia, is critical when deriving corollaries; for instance in a new approach to the theory of α-β Navier-Stokes fluids [7]. Because preconditions and aims are different, the addendum is absent in all theories of continua with affine microstructure; that absence makes those theories inadequate, in our opinion, to cover aspects of turbulence [13].

There is a crucial difference from formal analogy in the expression of the time-rate of H. Strictly, as in the reasoning above that led us to add H to the Oldroyd derivative of K, we should have conceived the velocities c appearing in the definition of H as the sub-velocities of fictitious sub-elements and, consequently, we should add terms containing the time-derivatives of c. Arbitrarily we evade the consequences of these circumstances and thus achieve closure of an otherwise infinite set of fields and corresponding balances. The problem and its gratuitous evasion is common with the very successful theory of extended thermodynamics and we recommend to accept the evasion, pending a check on how plausible appear, nevertheless, corollaries.

A finer point, in the time-derivation of H, which escaped our earlier analysis, must be brought to bear. The rate of change of the bunch of molecules belonging at an instant to a loculus influences the rate of change H only in sofar its expanse changes not its shape. So that rate reduces to

$$(\det\tilde{X})^{-1}[(\det\tilde{X})H]^{\cdot} = \dot{H} + \sigma H. \tag{24}$$

Actually a surprising circumstance is met later when evaluating the density of kinetic energy rate associated with the motion of our complex body: the terms involving H in the expression of tensorial moment of inertia contribute exactly the addenda missing above to complete the full Oldroyd derivative of H:

$$\mathring{H} = \dot{H} + \sigma H - BH - HB^T, \tag{25}$$

as we shall see.

There remains the question of which time-derivative is appropriate for the vector v and the scalar ρ, also originally defined via totals over loculi, hence affected by volume changes but not by meso-affine distortion. If we substitute $v \otimes v$ for Y in (23) and cancel terms containing B, as G is now effective only through its determinant, the cogent conclusion is that

$$\mathring{v} = \dot{v} + \frac{1}{2}\sigma v \tag{26}$$

(contrary to $\mathring{v} = \dot{v} + \sigma v$ adopted in earlier papers [5, 6] by a forced analogy with the simplest theory of bodies with variable mass, but wrongly).

The same rule applies to the bivector G, for which, in an indicial notation, only the first index connects with the aeolian referral:

$$\mathring{G} = \dot{G} + \frac{1}{2}\sigma\, G. \tag{27}$$

The result is transferred to the affillation between B and the time-rate of G announced at the end of Sect. 1:

$$\mathring{B} = \mathring{G}G^{-1} = \dot{G}G^{-1} + \frac{1}{2}\sigma I, \tag{28}$$

where I is the identity tensor.

An important corollary is the identity which is usually named balance of moment of inertia:

$$\mathring{Y} = 0 \quad \text{or} \quad \dot{Y} - BY - YB^T + \sigma Y = 0, \tag{29}$$

because

$$\mathring{Y} = \overline{\mathring{(GG^T)}} = 2\mathrm{sym}\left[\left(\dot{G}G^{-1} + \frac{1}{2}\sigma I - B\right) GG^T\right] = 0. \tag{30}$$

Similarly, if we substitute ρI for Y in (23), cancel again terms containing B, but substitute $(\det G)$ for $(\det \tilde{X})$, we obtain

$$\mathring{\rho} = \dot{\rho} + \rho\, \mathrm{tr}B. \tag{31}$$

The balance equations require now fundamental decisions on the general mathematical structure which is adeguate to express totals and densities of molecular

compulsions (both internal and at a frontier). The details of such decisions (i.e., the expression of constitutive laws for volume densities and stress and compulsive hyperstresses) are, justly, deferred to later specific studies; the generalities (e.g., the choice of volume and area densities only and the dependence of the latter on geometric properties of the frontier) will, however, open the ground for, and condition radically, each successive particular theory.

For momentum, the formal validity of Cauchy's structural proposal is accepted here. To an ample extent that proposal was proved right, in the present context, by Noll in [18], when he was seeking, as we are here, a continuum theory on the basis of a statistical approach.

An extension of Noll's analysis to cover, at least largely, the requirements for the balance of tensor moments was provided in [3].

The balance equation for H is written in formal analogy with the previous two. But the choice of terms expressing production is delicate and risky. We are groping here in the no-man's land near the border between mechanics and thermodynamics and there hazards abound: there may be the need, disregarded here, to involve energy distributions directly, not buried within averages and variances.

In conclusion the set of proposed balance equations reads:

- conservation of mass:
$$\frac{\partial \rho}{\partial \tau} + \operatorname{div}(\rho v) - \sigma \rho = 0; \tag{32}$$

- balance of momentum
$$\rho \left(\frac{\partial v}{\partial \tau} + (\operatorname{grad} v)\, v + \frac{1}{2} \sigma v \right) = \rho b + \operatorname{div} T; \tag{33}$$

- balance of moment of momentum
$$\rho \left[\left(\frac{\partial K}{\partial \tau} + (\operatorname{grad} K) v \right) - BK - KB^T + \sigma K + H \right] = \rho M - A + \operatorname{div} \mathbf{m} \tag{34}$$

or
$$\rho \left[\delta^2 G G^T \left(\frac{\partial B}{\partial \tau} + (\operatorname{grad} B) v \right)^T + H \right] = \rho M - A + \operatorname{div} \mathbf{m}; \tag{35}$$

- balance of agitation
$$\rho \left[\frac{\partial H}{\partial \tau} + (\operatorname{grad} H) v + \sigma H \right] = \rho J - Z + \operatorname{div} \mathbf{j}. \tag{36}$$

The equation of conservation of moment of inertia (29), sometimes added to the set, is not listed above because, in our context, it is an identity, as mentioned already.

As we have remarked before (24), there was a misconception in earlier papers in the choice of the time-rate of H. The strict analogy pursued then with the option

appropriate for K does not seem to fit physical circumstances and would lead, anyway, to unacceptable corollaries (for instance when deriving the kinetic energy theorem). So (36) above must substitute the lame laws earlier proposed (5.7) of [8] and (17) of [3].

As for the right-hand sides, the meaning of b and T in (33) is the standard one. ρM and the third-order tensor $\mathbf{m}$ express, in (34), respectively, bulk and contact external compulsions, whereas A is intimate bulk self compulsion. Formally, the right hand side of (34) is identical to one accepted for bodies with affine microstructure and for multipolar continua [15].

The right hand side of (36) is suggested in analogy of the former right-hand sides without specific justification, temporarily, with obvious presumptions regarding $\rho J, Z$ and third-order tensor $\mathbf{j}$ to account, respectively, for external or intimate bulk compulsions and contact compulsion. However, the suggestion would merit reservations or, at least, qualifications; perhaps even downright changes with the involvement of the distribution Θ.

The sign affecting A and Z is formally irrelevant; it is a conventional choice that gives them here the stamp of pressures rather than tractions. The choice must be borne in mind when explicit constitutive laws need be set forth.

It is not straightforward to compare the set of 19 balance equations above with anyone of the numerous suggestions promoted to bridge the gap existing between standard continuum mechanics and the dynamics (eventually thermodynamics) of granular media, including the theories inspired by the kinetic theory of gases. Some differences are easily discounted: for instance, a number of Authors adopt a so-called 14 moment set where only the trace of H appears and (36) is substituted by its scalar version.

The main obstacles are found in:

- our separation of macro and meso motions with the consequent crucial role assigned to the tensor meso moment of momentum;
- the entry of H as an essential ingredient in the associated inertia plus the possible effects of suffusion;
- our favouring the interpretation of Reynolds' tensor as a kinetic rather than dynamic field and our exclusion of temperature in view of its uncertain status in an approach based fundamentally on densities rather than distributions.

The contrast is obvious with extended thermodynamics (see [17], for instance); its 20 moment set contains, besides a set of 10 equations mirroring our (32), (33), (36), constitutive choices apart, an evolution equation for temperature, while the remaining nine equations are moments, but foreign to K.

Vice versa, the strictest link for (36) is with the so-called Reynolds' stress equation, where explicit constitutive rules for Z and $\mathbf{j}$ are also displayed. They involve, however, beyond variance H, also third-order moments (or skewness) which we declared explicitly to exclude, as to insure full closure. Finally, the entrainment inertia is ruled by $-L$, rather than B as in (36), the meso-scopic motions asseverated by us being ignored.

In any case some useful notions introduced over the years by many Authors for the closure problem in turbulence modeling (essential references are in the tract [9] available on the web) could be borrowed here to specify, more readily, constitutive casts, in particular for our Z.

Actually the main attention, at first, was addressed in the literature to special steady incompressible streams and hence to a direct link of H with the gross wind motion; for instance, Boussinesq already recommended that the deviator of H be taken proportional to $D = \operatorname{sym} L$ by a constant eddy (kinematical) viscosity. A vaguely similar outcome would arise in a skeletal version of (36) canceling some terms (including J and $\mathbf{j}$) and assuming Z linear in D.

A prompting by Truesdell (see (99.11) of [22]) involving, if brashly interpreted, a time-rate of H and therefore nearer to our (36), could be construed, in our present parlance, for the eddy viscosity to be, rather then a constant scalar, a fourth-order tensor operating on D.

A significant outcome of the set of balance equations is the associated kinetic energy theorem. But, before we proceed to recall that theorem, we must muse upon a remark in Sect. 3 of [5] which evidences the fact that the kinetic energy W of the cluster of molecules in each $\mathfrak{c}(x)$,

$$W = \frac{1}{2\omega}\int_{\mathfrak{c}(x)} dvol \int_{\mathscr{V}} w \otimes w\, \Theta\, d\mathscr{V} = \frac{1}{2\omega}\int_{\mathscr{V}} w \otimes w\, \hat{\theta}\, d\mathscr{V}, \qquad (37)$$

$$\text{with} \quad \hat{\theta} = \int_{\mathfrak{c}(x)} \Theta\, dvol,$$

cannot be determined in terms of filtered variables based on number densities alone: the distribution Θ has a direct rôle. Besides, the enormous body of results from the kinetic theory, stemming from the Boltzmann equation, proves, by implication, that Θ might be essential also to specify compulsion densities, be they volumetric or tactile.

Roughly, a parting of the ways occurs: either one restricts ambitions to what a sort of extended mechanics can offer by widening the range of descriptive parameters (as, here, where G and H are added) or one faces thermodynamic complexities, where the account of each local setting involves distribution functions directly not only through their filtered versions.

We take here the first way out and hence refer to (32)–(36); the consequent reduced kinetic energy tensor $\widetilde{W}$ per unit mass (already mentioned in [5]) is introduced as follows:

$$\widetilde{W} = \frac{1}{2\omega}\int_{\mathfrak{c}(x)} \tilde{\theta}\, \tilde{w} \otimes \tilde{w}\, dvol, \qquad (38)$$

and found to be equal to

$$\widetilde{W} = \frac{1}{2}(v \otimes v + BYB^T + H) \qquad (39)$$

whereas its Oldroyd derivative is equal to

$$\overset{\circ}{W} = \frac{1}{2}\overline{(v \otimes v + H)}^{\cdot} + \frac{1}{2}\overline{(BYB^T)}^{\circ} + \frac{1}{2}\sigma\,(v \otimes v + H). \tag{40}$$

By multiplying both members of (33) on the left by v and taking the symmetric component of the resulting tensors. Acting with B on both sides of (35) and again taking the symmetric component. Adding term by term the two results plus (36) multiplied on each side by $1/2$ and integrating the result over any fit region $\mathfrak{b}$ belonging to $\mathscr{B}_\tau$, the theorem of tensor kinetic energy follows

$$\begin{aligned}\int_{\mathfrak{b}} \rho \overset{\circ}{W}\, dvol \;&= \int_{\mathfrak{b}} \rho \left[\mathrm{sym}(v \otimes b + BM + \frac{1}{2}J\right] dvol \\ &+ \int_{\partial\mathfrak{b}} \left\{\mathrm{sym}[v \otimes Tn + \mathbf{m}(Bn)] + \frac{1}{2}\mathbf{j}\, n\right\} darea \\ &- \int_{\mathfrak{b}} \left[\mathrm{sym}(LT^T + BA + \mathbf{b}\mathbf{m}^t) + \frac{1}{2}Z\right] dvol,\end{aligned} \tag{41}$$

where n is the unit vector normal to $\partial\mathfrak{b}$, the exponent t means minor right transposition (for a third-order tensor) and $\mathbf{b} := \mathrm{grad}B$ (see Eq. (11) of [6]).

The usual interpretation applies of the three terms of the right-hand side; external bodily compulsions, the first; external compulsions across the boundary, the second. Finally the last term is figured to measure the tensor power of internal compulsions; its density is then

$$-\,\mathrm{sym}(LT^T + BA + \mathbf{b}\mathbf{m}^t + 2^{-1}Z). \tag{42}$$

Now, our mathematical model of events must mirror rigorously the physical fact that, per se, any kinetic behavior of the frame, on which the observers sit, must have no influence whatsoever on their evaluation of the power density expressed either by its tensorial form (42) or, at least, by the trace of (42)

$$-\,(L \cdot T + B \cdot A^T + \mathbf{b} \cdot {}^t\mathbf{m} + 2^{-1}\mathrm{tr}Z). \tag{43}$$

But their reading of L and B are both changed by the addition of the same skew tensor as a consequence of a rigid rotation of their frame, a rotation which leaves, instead, $\mathbf{b}$ unscathed. Additional effects may ensue from certain choices of constitutive laws for T, A, $\mathbf{m}$, Z and $\mathbf{j}$. Vice versa a cute constitutive rule might correct other unwanted influences. Thus, we must delimit somehow the choices open to the mathematical modeller of constitutive laws for T, A, $\mathbf{m}$ and Z, specifically regarding the variables involved in these laws.

For instance, if $\mathbf{U}(U)$ and $\mathbf{H}(H)$ are fourth-order tensor functions only of the variables indicated with $U := \mathbf{e}[(F^T\mathrm{grad}G)^T]$ a density of dislocations (see Sect. 4 of [5]); then both

$$Z = [\mathbf{U}(U)]\,U \quad \text{and} \quad Z = [\mathbf{H}(H)]\,D \tag{44}$$

are acceptable constitutive laws for Z as they are both indifferent to observer motion. The first was suggested in Sect. 8 of [5]; the second is an interpretation of Truesdell's proposal for hypo elastic bodies. There is a radical difference between the two choices (44), of relevance later: if $\mathbf{H}$ does not reduce to a constant tensor (i.e., if its dependence on H is excluded), the power may end up by depending non-linearly on time rates. Of course such event may occur also, for instance, if Cauchy's stress contains a viscous term (i.e., a term proportional to D by a constant viscosity). Another remark regarding $\mathbf{H}$ must be premised. It has the physical dimensions of a stress. Its semitrace str $\mathbf{H}$ (i.e., the second order tensor obtained from $\mathbf{H}$ by contracting the first two indices) acts in the way that T and A do. We may expect it to show up similar behaviour throughout.

To simplify discussions we will deal below only to conditions where the following axiom applies:

Constitutive Axiom C1. Constitutive laws are each, separately, observer independent. The variables involved may only be F and G, L, B, $\mathbf{b}$ and H and their gradients, in appropriate groupings, each observer independent such as F^TF, G^TG, F^TG, $D = \mathrm{sym}L$, $\mathrm{sym}B$, $\mathrm{skw}(L - B)$, $F^T\mathrm{grad}G$.

Such axiom is insufficient to make the power (43) observer independent due to separate presence of L and B. The decisive additional axiom which ensures the desired property is

Axiom A1. The constitutive laws for T and A satisfy identically the condition

$$\mathrm{skw}T = \mathrm{skw}A, \quad \text{or} \quad (T^T + A) \in \mathrm{Sym}. \tag{45}$$

Artificial counterexamples would assert for T, A and $\mathbf{m}$ the properties above, but would relax the constitutive law for Z to read

$$Z = [\mathbf{H}(H)]\,L \quad \text{or} \quad Z = [\mathbf{H}(H)]\,B. \tag{46}$$

Then it would still be possible to achieve the asked for property of (43) by requiring, instead of (45)

$$\left(T^T + A + \frac{1}{2}\mathrm{str}\,\mathbf{H}\right) \in \mathrm{Sym}. \tag{47}$$

No restriction ever ensues for the semi-deviator tensor,

$$\mathrm{sdev}\,\mathbf{H} := \mathbf{H} - \frac{1}{3}\,I \otimes \mathrm{str}\,\mathbf{H}, \tag{48}$$

neither here nor later when, within the next section, we introduce a specific constraint with the consequence, then, that no reactive component arise.

Because of the importance, for ephemeral continua, of tensor powers, one is led to propose, more severely, that independence from the observer be asserted even for the full tensorial version, though always accepting constitutive Axiom C1. As already remarked, definition implies that a rigid rotation would not affect $\mathbf{b}$. Also

the sought tensorial property would necessarily imply the restricted scalar one and hence (43) which may be then presumed. Then the only obligation which remains to be satisfied is

$$\mathrm{sym}[W(T^T + A)] = 0, \quad \forall\ W \in \mathrm{Skw}. \tag{49}$$

Acceptance of (49) implies, as already remarked, that of (43); therefore $T^T + A$ is symmetric. Then (49) can be rewritten as

$$W(T^T + A) + (T + A^T)W^T = 0 \tag{50}$$

or

$$W(T^T + A) - (T^T + A)W = 0. \tag{51}$$

The definition itself of skew matrix assures us that the only symmetric tensor which commutes with a skew tensor is a spherical tensor, say αI. We conclude with

Axiom A2: the constitutive laws for T and A satisfy identically the condition

$$T + A^T = \alpha I, \tag{52}$$

with α a scalar function. The requisite advanced sometimes that T coincides with $-A^T$ is a sufficient, but not necessary, condition to satisfy (49).

3 Hypocontinua

The matter we comment on in this section was already treated specifically in [6] and, by the way, in Sect. 9 of [5]. Briefly the term hypocontinuum was introduced for bodies the evolution of which is ruled by balance equations obtained from (32)–(36) when a perfect constraint is introduced to force B to coincide with L. The adjective 'perfect' meaning, as customary, that the internal compulsions $T, A, \mathbf{m}, \mathbf{H}$ are each the sum of an active addendum ($T^a, A^a, \mathbf{m}^a, \mathrm{str}\,\mathbf{H}^a$) and of one reactive to the constraint ($T^r, A^r, \mathbf{m}^r, \mathrm{str}\,\mathbf{H}^r$) and the latter satisfy (45) separately; furthermore their power is identically null for any motion allowed by the constraint:

$$D \cdot \left[T^r + (A^r)^T + \frac{1}{2}\mathrm{str}\,\mathbf{H}^r \right] + \mathrm{grad}\,L \cdot {}^t\mathbf{m}^r = 0, \quad \forall D, H, \mathrm{grad}\,L. \tag{53}$$

The constraint cancels the primary freedom attributed to ephemeral continua as the wind streak lines end up by coinciding with paths of material elements; however, a 'tensorial pressure' ρH due to agitation within each element remains and it is this latter phenomenon embedded in the model which allows the link with hypoelasticity.

The detais are given in the papers quoted above presuming, we repeat, that condition (45) be transferred separately to active and reactive stresses under an axiom stronger than Axiom C1:

Constitutive Axiom C2. The second choice (44) is excluded. The variables involved may be F and G and their gradients (thus L, B and H are disallowed).

Consequently, in particular, conspicuous viscous effects are left out. The resulting system is as follows:

$$\frac{\partial \rho}{\partial \tau} + \operatorname{div}(\rho v) = 0, \tag{54}$$

$$\rho\left(\frac{\partial v}{\partial \tau} + Lv\right) - \operatorname{div}\left\{\rho\delta^2\left[\frac{\partial L}{\partial \tau} + (\operatorname{grad} L)v\right]FF^T\right\} \tag{55}$$

$$= \rho b - \operatorname{div}\left(\rho M^T\right) + \operatorname{div}\left[\operatorname{sym}(T^a + A^a) + \rho H - (\operatorname{div}\mathbf{m}^a)^T\right],$$

$$\rho\left[\frac{\partial H}{\partial \tau} + (\operatorname{grad} H)\, v\right] = \rho J - Z + \operatorname{div}\mathbf{j}. \tag{56}$$

A comment on (55) is weighty: the term ρH is placed in it on the right-hand side within the square brackets as though it were an addendum to stress, whereas, in our delivery, physical dimensions apart, it is of kinetic origin and essence. The reason for the choice of placing is later uniformity with Truesdell proposal; however, the choice evidences, in our opinion, an ambiguity inherent in that proposal.

The complexity of this system, even if largely reduced when compared with the general one, is staggering: (55) involves up to third-order mixed derivatives of v, together with the left strain tensor FF^T. We have also already remarked in [6] that boundary conditions associated with (55) are outlandish as inertial effects may be expected to be relevant at the frontier. However, most terms added to the standard equation of Cauchy are forced, by the constraint, to be, generally, very small: $|y|$ is of the order of δ, whereas $|c|$ may be of order of $|v|$. Thus terms containing Y, those relating to moment of momentum and the corresponding compulsions may be disregarded; they would become significant only if $|c|$ were of the order of δ^{-1}. Thus, one may be content with the much simpler equation:

$$\rho\left(\frac{\partial v}{\partial \tau} + Lv\right) - \operatorname{div}(\rho H) = \rho b + \operatorname{div}\left[\operatorname{sym}(T^a + A^a)\right]. \tag{57}$$

If Axiom A2 is allowed instead of A1 and hence the condition (52) ensues and is transferred to the active stresses, then $(T^a + A^a)$ recedes to a spherical tensor αI and (57), (56) become formally similar to the set valid for hypo elastic materials (see (99.11) of [22]), except that here the kinetic quantity $\rho H + \alpha I$ takes, more agreeably in our opinion, the place that straight stress has in (55); in fact, the significance attributed to the field ruled by the second balance equation is the fundamental discrepancy between the two approaches.

Thus, the partial formal concurrence appears to be more incidental than essential. Truesdell's goal could be interpreted as an attempt to model a self-mutant simple continuum (i.e., a body constitutively mutant via the history of its own deformations as specified by the first placement gradient). Instead our results issues of a non-simple

continuum the behaviour of which is influenced to a large extent, (in the end, here, exclusively, through constraints) by a tensor $-\rho H$ with the dimension of a stress but generated by a deeper disorderly behaviour of a cluster of specks.

However, Truesdell constitutive choice conflicts with the acceptance of Axiom C2, an assumption which is imperative to obtain (55). The contrast might be framed within a, so far, sidestepped issue: how do we configure the cogency to induce a mutated response; does it imply a contribution to intimate power, additional to that generated by microstress (and, possibly, by meso-iperstress), thus appearing in the kinetic energy theorem or is it due to a powerless kinetic urgency.

In our presentation of hypocontinua the answer is affirmative for the first choice in the dilemma and one may wonder how much different our results would be, having accepted a linear dependence of Z on D (our interpretation of Truesdell proposal rendered explicit by the second of (44)) with the fourth-order tensor $\mathbf{H}$ symmetric in the first two indices and in the last two, that is: $\mathbf{H}_{ijlm} = \mathbf{H}_{jilm} = \mathbf{H}_{ijml}$ (so that $\mathbf{H}$ is an operator of anisotropic eddy viscosity).

The scalar internal power density of compulsion can be easily obtained from (42) introducing the constitutive law $(44)_2$ together with the constraint $L = B$:

$$-\left(\frac{1}{2}\mathrm{tr}\,(\mathbf{H}D) + L\cdot(T + A^T) + \mathrm{grad}\,L\cdot {}^t\mathbf{m}\right). \tag{58}$$

The sums of active and reactive compulsions are introduced in the system (33), (34), (36) and an appropriate combination is sought (but, as we shall see, without success) to achieve again a format where only active compulsions appear. Because $\mathbf{j}$ and the semideviator sdev $\mathbf{H}$ of $\mathbf{H}$ do not enter (43), we exclude that they may react to constraints, so they are fully active. Finally, the arbitrariness of D requires

$$T^r + A^r + \frac{1}{2}\,\mathrm{str}\,\mathbf{H}^r = 0. \tag{59}$$

By substituting these results in balances (33), (35) and (36) the resulting field equations are:

$$\begin{aligned}\rho\left(\frac{\partial v}{\partial \tau} + Lv\right) - \mathrm{div}\left\{\rho\delta^2\left[\frac{\partial L}{\partial \tau} + (\mathrm{grad}L)v\right]FF^T\right\} \\ = \rho b - \mathrm{div}\left(\rho M^T\right) + \mathrm{div}\left[\mathrm{sym}(T^a + A^a) + \rho H - (\mathrm{div}\,\mathbf{m}^a)^T - \mathrm{str}\,\mathbf{H}^r\right],\end{aligned} \tag{60}$$

$$\rho\left[\frac{\partial H}{\partial \tau} + (\mathrm{grad}H)\,v\right] = \rho J + \mathrm{div}\,\mathbf{j}^a - \mathbf{H}^a D - \frac{1}{3}\,(I\otimes \mathrm{str}\mathbf{H}^r)\,D. \tag{61}$$

Thus it is not possible, under the circumstances, to obtain a set of balance equations which are 'pure', in the sense that no reactive compulsion appears in them. Such failure should not surprise as it was already met when incompressibility was imposed on a linearly viscous fluid (see Sect. 4.6.2 of [16]).

Such obnoxious analytical conclusion could be understood as the consequence of some shortcomings of the mathematical model. Each model requires qualifications, obviously, and we have already remarked above that our evaluation of kinetic energy of the cluster of molecules within a loculus in terms of filtered variables alone is deficient; also the closure of the set of statistical entities beyond H is an arbitrary restriction. However, the main obstacle here appears to be, in both cases quoted, the presence, in the expression of power of internal compulsions, of a term quadratic in the disfigurement rates (D and H). Compounded with the constraint, that available power must imply deeper physical effects which might escape chronicle via the fields directly involved here so far. For instance, the distribution Θ is supplanted here by less specific number densities and the surrender may be prejudicial.

4 Extended Mechanics

We list, in this concluding section, a number of advances which we attribute to the field of continuum mechanics (with the canon: geometric setting and consequent kinetics; dynamic balances; constitutive laws with attendant analytic discipline of initial and boundary conditions) in the territory of thermodynamics still afflicted by doubts and disputes (see, typically, [1]) even if, nevertheless, vastly successful. The list is open-ended and merely suggestive of topics which seem to us to merit attention, as already predicated, for instance, in [4].

A significant outcome of the set of balance equations (33), (35) and (36) is the associated kinetic energy theorem (41). It could be imagined as due to the conjoining of two theorems, one merely issuing from (33) and formally involving only standard quantities

$$\frac{1}{2}\int_{\mathfrak{l}}[\rho(v\otimes v)^{\cdot}+\sigma\, v\otimes v]\,dvol=\int_{\mathfrak{l}}\rho\,\mathrm{sym}(v\otimes b)\,dvol \\ +\int_{\partial\mathfrak{l}}\mathrm{sym}(v\otimes Tn)\,darea-\int_{\mathfrak{l}}\mathrm{sym}(LT^{T})\,dvol \tag{62}$$

and the other counting contributions due to the new fields entering our extended mechanics

$$\frac{1}{2}\int_{\mathfrak{b}}\rho\,\overset{\circ}{\overline{(BYB^{T}+H)}}\,dvol=\int_{\mathfrak{b}}\rho\left\{\mathrm{sym}[B(M-H)]+\frac{1}{2}J\right\}\,dvol \\ +\int_{\partial\mathfrak{b}}\left\{\mathrm{sym}[\mathbf{m}(Bn)]+\frac{1}{2}\mathbf{j}\,n\right\}\,darea-\int_{\mathfrak{b}}\left[\mathrm{sym}(BA+\mathbf{b}\mathbf{m}^{t})+\frac{1}{2}Z\right]\,dvol, \tag{63}$$

both valid separately.

Under becoming assumptions of smoothness and in view of its validity for any choice of $\mathfrak{b}$, (63) may be replaced by a prerequisite on densities

$$\rho\,\overset{\circ}{\overline{\left(BYB^T+H\right)}}+2\,\mathrm{sym}(BA+\mathbf{b}\mathbf{m}^t)+Z \qquad (64)$$
$$=\rho\,\{2\,\mathrm{sym}[B(M-H)]+J\}+\mathrm{div}\left[(\mathbf{m}+{}^t\mathbf{m})\oslash B+\mathbf{j}\right],$$

where the tensor product $\oslash$ between tensors of the third and the second order is so defined: $(\mathbf{m}\oslash B)_{ijl}:=\mathbf{m}_{ijk}B_{kl}$.

Then we could interpret (64) as the balance equation for the whole meso energy: i.e., comprising also the affine (in particular the vorticose) contribution beyond the sole energy of agitation H. In fact, nominally, (64) could substitute (36) within the set of balance equations.

Such perspective would become particularly suggestive if the medium were perfect in the sense that a potential energy exists from which all compulsions can be derived so that the whole left-hand side of (64) may be written as the time-rate of an internal meso energy. The matter is discussed in some detail in [5], see especially the final part of Sect. 8. There are already precise hints in the literature regarding A and $\mathbf{m}$; a suggestion for Z advanced in [5], Sect. 8, was already quoted; clearly the presence of viscous effects as specified by $(44)_2$ must instead be excluded. Finally (64) would mimic outwardly the first principle of thermodynamics, and a class of 'thermal' phenomena could be dealt with within our extended mechanics.

The mimicry would become much more striking if one descends to the special case of hypocontinua and simplifies (64) accordingly or starts again but from (55), (56) rather than the general set:

$$\int_{\mathfrak{b}}\rho\overset{\circ}{\hat{W}}\,dvol=\int_{\mathfrak{b}}\rho\left[\mathrm{sym}(v\otimes b+BM)+\frac{1}{2}J\right]dvol+\int_{\partial\mathfrak{b}}\left\{\frac{1}{2}\mathbf{j}\,n \qquad (65)$$
$$+\,\mathrm{sym}\left\{v\otimes\left[\mathrm{sym}(T^a+A^a)+\rho(H+\delta^2\dot{L}FF^T)-(\mathrm{div}\,\mathbf{m}^a)^T\right]n\right\}\right\}\,darea$$
$$-\int_{\mathfrak{b}}\left\{\frac{1}{2}Z+\mathrm{sym}\left[L\,(\mathrm{sym}(T^a+A^a)-\mathrm{div}\,\mathbf{m}^a)\right]\right\}dvol.$$

Then, receding to traces of all tensors involved and again assuming perfection of the material involved, the equation would appear strikingly similar to that expressing the first principle of thermodynamics. The kinship should not surprise: we caused meso energies to emerge beyond those measured along the gross flow, though still in terms of explicit additional geometric and kinetic parameters.

Of course the power of hyperstress would involve the introduction of hyperstrains and their time rates. Precisely:

- the third-order tensor of wryness $\mathscr{W}$

$$\mathscr{W}_{ijk}:=G_{iK,J}\,F^{-1}_{Ji}\,G^{-1}_{Kk} \qquad (66)$$

and of torsion $\mathfrak{h}$

$$\langle := \frac{1}{2}(\mathscr{W} - \mathscr{W}^t); \tag{67}$$

- plus the second-order tensor of density of dislocations $\mathfrak{u}$

$$\mathfrak{u}_{AB} := \mathbf{e}_{ACD}\, F_{iB}\, G_{iD,C} \tag{68}$$

(see Sect. 4 of [5]).

These variables, together with the standard choice $C = F^T F$ and some kindred ones such as $G^T G$ and $G^T F$, would be invoked to construct a promising extended hyperelasticity via an internal energy specified in terms of them in elaborate analogy of Chap. 2 and, in particular, of paragraph 82 of [22]. The last integrand in (65) expresses the rate of change of internal energy density.

Within the latter, some kinetic quantities have an important role, such as

- the deranging $(L - B)$, the symmetric part of which measures the slippage of Eckart-Truesdell, whereas the skew part gives the difference between vorticities
- an intensity of microvorticity,

both observer-independent. For details we refer again to Sect. 5 of [5].

The most critical handicap in the proposals above is the acceptance of Constitutive Axiom C2 and consequent endorsement of balance laws (54), (55), (56). For instance, even the alternative laws (60), (61) involve the sofar unspecified reactive term $\mathbf{H}^r$; we might guess that the escape from the dilemma will impose the introduction of new fields necessarily exiting from the field of mechanics proper.

We attempt below a, perhaps whimsical, route which seems to lead us near to a scale measuring intensity of deeper energies.

To begin we must promote the acceptance of a pseudo distribution α^* based on the field, within $\mathfrak{c}(x)$, of meso kinetic energy

$$\theta_* = \frac{1}{\kappa_*}\mathrm{tr}(BYB^T + H), \quad \text{with} \quad \kappa_* = \int_{\mathfrak{c}(x)} \mathrm{tr}\,(BYB^T + H)\, dvol, \tag{69}$$

the integral of which over $\mathfrak{c}(x)$ is unity.

Then, proceed to find the subset $\mathfrak{c}_\xi$ of $\mathfrak{c}$ where the quantity (69) above is less than ξ $(0 < \xi < 1)$. The derivative $\alpha^*(\xi)$ of $\left(\kappa_*^{-1}\int_{\mathfrak{c}_\xi} \theta_*\, dvol\right)$ is such that $\alpha^*(\xi)d\xi$ gives the value of the fraction of molecules with energy within the interval $[\xi\kappa_*, (\xi + d\xi)\kappa_*]$; thus a connection is established with standard developments and with the challenges on the road to a definition of temperature.

These matters touch on many hotly debated controversies and are left for a lengthier future essay.

Acknowledgments This research is part of the activities of the Project PON 04a2-F: "BE&SAVE AQUASYSTEM SIGLOD-Programma operativo nazionale di Ricerca e competitività 2007–2013". The support of GNFM-INDAM is also acknowledged.

References

1. Biró, T.S.: Is There a Temperature? Conceptual Challenges at High Energy, Acceleration and Complexity, Fundamental Theories of Physics 171. Springer, New York (2011)
2. Biscari, P., Cercignani, C.: Stress and heat flux in non-inertial reference frames. Contin. Mech. Thermodyn. **9**, 1–11 (1997)
3. Brocato, M., Capriz, G.: Clockwork, ephemeral and hybrid continua. Phys. Mesomech. **14**, 124–144 (2011)
4. Capriz, G.: A quest for an 'extended' continuum mechanics. Note Matemat. **27**, 27–41 (2007)
5. Capriz, G.: On ephemeral continua. Phys. Mesomech. **11**, 285–298 (2008)
6. Capriz, G.: Hypocontinua. In: Albers, B. (ed.) Continuous Media with Microstructure, pp. 61–70. Springer, Berlin (2010)
7. Capriz, G., Fried, E.: The ephemeral nature of Navier-Stokes-$\alpha\beta$ continua. Rendiconti Lincei **22**, 73–87 (2011)
8. Capriz, G., Mariano, P.M.: Objective fluxes in a multi-scale continuum description of sparse medium dynamics. Physica A **415**, 354–365 (2014)
9. Celik, I.B.: Introductory Turbulence Modeling. West Virginia University (1999)
10. Cohen, H., Muncaster, R.G.: The Theory of Pseudo-Rigid Bodies. Springer, New York (1988)
11. Dunwoody, J.: Comment: The bogus axioms of continuum mechanics [Bull. Inst. Math. Appl. **17**, 98–102 (1981)] by Woods, L. C, with a reply by Woods, L. C. Bull. Inst. Math. Appl. **17**, 219–220 (1981)
12. Edelen, D.G.B., McLennan, J.A.: Material indifference: a principle or a convenience. Int. J. Eng. Sci. **11**, 813–817 (1973)
13. Eringen, A.C.: Micromorphic theory of turbulence. ZAMP **61**, 119–132 (2009)
14. Green, A.E.: A note on axioms of continuum mechanics: The bogus axioms of continuum mechanics [Bull. Inst. Math. Appl. **17**, 98–102 (1981)] by Woods, L. C. Bull. Inst. Math. Appl. **18**, 7–9 (1982)
15. Green, A.E., Rivlin, R.S.: Multipolar continuum mechanics. Arch. Ration. Mech. Anal. **17**, 113–147 (1964)
16. Mariano, P.M., Galano, L.: Fundamentals of the Mechanics of Solids. Birkhauser, Boston (2015)
17. Mueller, I.: Extended Thermodynamics. A multifield theory for excellence. In: Capriz, G., Mariano, P.M. (eds.) Advances in Multifield Theories for Continuua with Substructure, pp. 115–126. Birkhauser, Basel (2004)
18. Noll, W.: Die Herleitung der Grundgleichungen der Thermomechanik der Kontinua aus der statistichen Mechanik. J. Ration. Mech. Anal. **4**, 627–646 (1955)
19. Noll, W., Virga, E.G.: Fit regions and functions with bounded variation. Arch. Ration. Mech. Anal. **102**, 1–21 (1988)
20. Oldroyd, J.G.: Non-Newtonian flow of liquids and solids. Rheology, Theory and Applications 1, Ch. 16. Academic Press, New York (1956)
21. Truesdell, C.A.: Hypoelasticity. J. Ration. Mech. Anal. **4**, 83–133 (1955)
22. Truesdell, C.A., Noll, W.: The Non-Linear Field Theories of Mechanics. In: Flügge, S. (ed.) Encyclopedia of Physics III/3, pp. 1–602. Springer, Berlin (1965)
23. Truesdell, C.A., Toupin, R.A.: The Classical Field Theories. In: Flügge, S. (ed.) Encyclopedia of Physics III/1, pp. 226–858. Springer, Berlin (1960)
24. Woods, L.C.: The bogus axioms of continuum mechanics. Bull. Inst. Math. Appl. **17**, 98–102 (1981)
25. Woods, L.C.: More on the bogus axioms of continuum mechanics. Bull. Inst. Math. Appl. **18**, 64–66 (1982)

Some Remarks to Higher Order Frames Occurring in Continuum Mechanics

Miroslav Kureš

Abstract Frame bundles are described with respect to their role in continuum mechanics, the structure jet groups are studied and some expressions in local coordinates are derived. It is introduced the general (r-th order) microstructure configuration and it is suggested what needs to be investigated in subsequent research.

1 Introduction

Samuel Forest published in [4] the following nice table representing a hierarchy of higher order continua.

Name	No. of d.o.f.	d.o.f.	References
Cauchy	3	$\mathbf{u}$	Cauchy (1822)
Microdilatation	4	$\mathbf{u}$, χ	Goodman and Cowin (1972); Steeb and Diebels (2003)
Cosserat	6	$\mathbf{u}$, $\mathbf{R}$	Kafadar and Eringen (1971)
Microstretch	7	$\mathbf{u}$, χ, $\mathbf{R}$	Eringen (1990)
Microstrain	9	$\mathbf{u}$, $\mathbf{C}^\sharp$	Forest and Sievert (2006)
Micromorphic	12	$\mathbf{u}$, χ	Eringen and Suhubi (1964); Mindlin (1964)

The meaning of the symbols is as follows: $\mathbf{u}$ is the displacement field, χ is the microdeformation tensor field, $\mathbf{C}^\sharp$ is the right Cauchy-Green tensor, $\mathbf{R}$ is the special microdeformation, namely the rotation.

Certainly, it would be beneficial to have a unified and effective theoretical description of all such cases. In this paper, we show that a very elegant way is to use differential geometry. Using it, a lot of successful and understandable interpretations have already been created, for an example in the book *Material Inhomogeneities and their Evolution: A Geometric Approach* [3] of authors Marcelo Epstein and Marek

M. Kureš (✉)
Institute of Mathematics, Brno University of Technology, Technická 2,
61669 Brno, Czech Republic
e-mail: kures@fme.vutbr.cz

B. Albers and M. Kuczma (eds.), *Continuous Media with Microstructure 2*,
DOI 10.1007/978-3-319-28241-1_4

Elżanowski, in the lecture notes *Introduction to Continuum Mechanics* [7] of Panayiotis Papadopoulos or a number of scientific papers as e.g. *Continuum dynamics on a vector bundle for a directed medium* [8] by Yamaoka and Adachi. Here, we are trying to unify the geometric approach and use a truly modern language of fibered bundles which is systematically developed in the monograph *Natural Operations in Differential Geometry* [6] of Kolář et al.

Besides this unifying language there are also some of our calculations (principal morphisms between frame bundles with different structure groups, the form of elements of Toupin subgroups) completely new in terms of the explicit expression. We are convinced that local coordinate expressions are necessary to be truly effective in applications. Nevertheless, the paper is much more something else: an outline of the program. The program of an investigation in special higher order principal bundle morphisms—it is shown here that it is a powerful theoretical background.

2 The Configuration

Let B and S be two smooth manifolds ($\dim B = b$, $\dim S = s$, $b \leq s$) and

$$\kappa : B \to S$$

a smooth embedding (i.e. an injective smooth mapping such that $\kappa(B)$ is a submanifold of S and the (co)restricted mapping $B \to \kappa(B)$ is a diffeomorphism, see [6]). We will call B the *body*, S the *space* and κ the *configuration*. As B and S are manifolds, they are endowed with local maps $\varphi^B_\iota : U_\iota \to \mathbb{R}^b$ ($U_\iota \subseteq B$, $\iota \in I$) and $\varphi^S_{\bar\iota} : V_{\bar\iota} \to \mathbb{R}^s$ ($V_{\bar\iota} \subseteq S$, $\bar\iota \in \bar I$).[1] The maps provide local coordinates: let points $P \in B$ have coordinates (ξ^j), $j = 1, \ldots, b$ and points $p \in S$ have coordinates (x^i), $i = 1, \ldots, s$. The *local coordinate expression of the configuration* κ is a map

$$\bar\kappa : \mathbb{R}^b \to \mathbb{R}^s$$

such that

$$\bar\kappa \circ \varphi^B_\iota = \varphi^S_{\bar\iota} \circ \kappa$$

and it is expressed by

$$x^i = \kappa^i(\xi^j).$$

[1] In classical situations, we meet the case $\dim B \leq 3$ and $S = \mathbb{R}^3$ where B can be covered by a single map, so both index set I and $\bar I$ are singleton. Let us mention as a curiosity that some authors, cf. [5], consider local maps inversely—as mappings from the real space to a manifold, which is not a problem.

Of course, it is an infinite number of configurations in general. One of them is labeled as significant, so called *reference configuration*

$$\kappa_0 : B \to S.$$

We will now assume that different configurations are smoothly parameterized. Let us consider one-dimensional manifold T (with local maps $\varphi^T_{\tilde{\imath}} : W_{\tilde{\imath}} \to \mathbb{R}$, $W_{\tilde{\imath}} \subseteq T$, $\tilde{\imath} \in \tilde{I}$ giving a local coordinate t to a point of T) and a smooth map

$$\chi : B \times T \to S$$

endowed with the property that its restrictions to specific t are configurations, in particular

$$\chi_{|t=t_0} = \kappa_0.$$

Usually, t is interpreted as *time* and the map χ is called the *motion*. Its local coordinate expression is

$$x^i = \chi^i(\xi^j, t).$$

The velocity and acceleration vectors are expressed by

$$v^i = \frac{\mathrm{d}\chi^i}{\mathrm{d}t} \quad \text{and} \quad a^i = \frac{\mathrm{d}^2\chi^i}{\mathrm{d}t^2}.$$

Let us consider the position vector r with respect to the reference configuration κ_0, as $r : B \times T \to S$,

$$r^i(X^j, t) = \chi^i(\xi^j, t) - X^i \quad \text{where} \quad X^i = \chi^i(\xi^j, t_0);$$

such a position vector is called the *deformation of B with respect to the reference configuration κ_0 in time t*. Then the *deformation gradient of B* is

$$F^i_{\bar{\imath}} = \frac{\mathrm{d}r^i}{\mathrm{d}X^{\bar{\imath}}}.$$

Now we will add to the body its microstructure. Classically, the *microstructure* is expressed by k linearly independent vectors, $k \leq s$, called *directors* (cf. e.g. [8]) assigned to points $p \in \kappa(B) \subseteq S$. Thus, we consider frames over points of $\kappa(B) \subseteq S$, in particular we do not exclude the case $k > b$. It seems well-reasoned, because, for example, two-dimensional plate materials are placed in three-dimensional space, their thickness is neglected, but a rotation of their particles is required three-dimensional. This is illustrated in the Fig. 1. In this situation, we introduce frames by a strictly geometric way in Sect. 2.

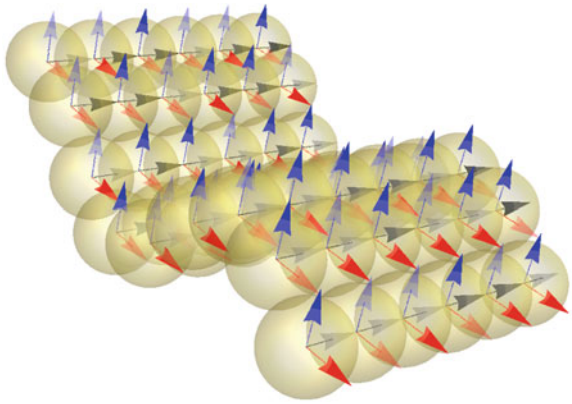

Fig. 1 Three directors (*blue*, *red* and *black*) determining rotations of particles of a two-dimensional body in the three-dimensional space

3 Frame Bundles (of the First Order)

Let us consider smooth mappings from $\mathbb{R}^b$ ($b = \dim B$) to B such that the rank of their tangent maps in $\mathbf{0} = (0, \ldots, 0)$ equals b, i.e. we consider immersions. We define the *first order frame bundle* P^1B over B as the space of 1-jets of such immersions from $\mathbb{R}^b$ into B, i.e.

$$P^1B = \operatorname{imm} J^1_0\left(\mathbb{R}^b, B\right).$$

1-jets in question, i.e. elements of P^1B, form a principal bundle over the base manifold B. Analogously, we have the bundle P^1S over S. These bundles disposes of right actions by general linear groups $\mathrm{GL}(b, \mathbb{R})$ and $\mathrm{GL}(s, \mathbb{R})$, respectively. Now, we take principal bundle morphism (a fiber bundle morphism which interwines with group actions)

$$K : P^1B \to P^1S$$

over the base map κ. This morphism will be called the *Cosserat configuration*. In local coordinates, P^1B has induced local coordinates $\xi^j, \xi^{\bar{j}}_j, j, \bar{j} = 1, \ldots, b$, P^1S has induced local coordinates $x^i, x^{\bar{i}}_i, i, \bar{i} = 1, \ldots, s$ and the morphism K is expressed by

$$\begin{aligned} x^i &= \kappa^i(\xi^j) \\ x^{\bar{i}}_i &= K^{\bar{i}}_i(\xi^j, \xi^{\bar{j}}_j). \end{aligned}$$

Let us express K. First, we take a fixed homomorphism $H_\varphi : \mathrm{GL}(b, \mathbb{R}) \to \mathrm{GL}(s, \mathbb{R})$ by the following way. The element $\beta \in \mathrm{GL}(b, \mathbb{R})$ will be embedded to $\mathrm{GL}(s, \mathbb{R})$ and multiplied by a fixed $\varphi \in \mathrm{GL}(s, \mathbb{R})$ from right. The result will be denoted by $\sigma \in \mathrm{GL}(s, \mathbb{R})$. It means $\sigma^{\bar{i}}_i = H_{\varphi^{\bar{i}}_i}(\beta) = \beta^i_k \varphi^k_{\bar{i}}$ for $i \leq b$ and $\sigma^{\bar{i}}_i = H_{\varphi^{\bar{i}}_i}(\beta) = \varphi^{\bar{i}}_i$ for $b < i \leq s$.

Hence K needs to satisfy

$$K^i_{\bar{i}}(\xi^j, \xi^j_k\beta^k_{\bar{j}}) = K^i_k(\xi^j, \xi^j_{\bar{j}})\sigma^k_{\bar{i}} = K^i_p(\xi^j, \xi^j_{\bar{j}})\beta^p_l\varphi^l_{\bar{i}} + K^i_q(\xi^j, \xi^j_{\bar{j}})\varphi^q_{\bar{i}}$$
$$(p \le b, b < q \le s).$$

If φ is the identity, we have $\varphi^k_{\bar{i}} = \delta^k_{\bar{i}}$ (Kronecker delta) and the formula transforms into

$$K^i_{\bar{i}}(\xi^j, \xi^j_k\beta^k_{\bar{j}}) = K^i_p(\xi^j, \xi^j_{\bar{j}})\beta^p_{\bar{i}} \qquad (\bar{i} \le b)$$
$$K^i_{\bar{i}}(\xi^j, \xi^j_k\beta^k_{\bar{j}}) = K^i_{\bar{i}}(\xi^j, \xi^j_{\bar{j}}) \qquad (b < \bar{i} \le s).$$

We recognize $K^i_{\bar{i}}$ as linear in $\xi^j_{\bar{j}}$ for $\bar{i} \le b$ and as constant in $\xi^j_{\bar{j}}$ for $b < \bar{i} \le s$.[2]

4 Jet Groups: Toupin Subgroups

A group G is called a *split extension* of a group N by a group $\bar{H}$ 1if N is a normal subgroup of G and G contains a subgroup H such that $H \cong \bar{H}$, $N \cap H = \{e\}$ and $NH = G$. Alternatively one says that G is a *semidirect product* of N by $\bar{H}$. The notation is $G = N \times | \bar{H}$ [2].

Alternatively, given any two arbitrary groups $\bar{N}$ and $\bar{H}$ and a group homomorphism[3] $\tau : \bar{H} \to \text{Aut } \bar{N}$, we can construct a new group $G = \bar{N} \times |_\tau \bar{H}$ through its operation $*$ defined by

$$(\bar{n}_1, \bar{H}_1) * (\bar{n}_2, \bar{H}_2) = \left(\bar{n}_1\tau(\bar{H}_1)(\bar{n}_2), \bar{H}_1\bar{H}_2\right)$$

Then pairs $(\bar{n}, e_{\bar{H}})$ form a normal subgroup N of G isomorphic to $\bar{N}$, while pairs $(e_{\bar{N}}, \bar{H})$ form a subgroup H of G isomorphic to $\bar{H}$. This semidirect product is consistent with the definition above, namely $\bar{N} \times |_\tau \bar{H} = N \times | \bar{H}$.

r-jets of smooth maps $\mathbb{R}^n \to \mathbb{R}^n$ with non-zero Jacobian determinant in $\mathbf{0} = (0, \ldots, 0)$ and sending $\mathbf{0}$ to $\mathbf{0}$ together with the jet composition form a group which is called the *r-th jet group* and denoted by G^r_n, for details see [6]. Moreover, for $0 \le s < r$, we have a canonical epimorphism $\pi^{r\to s}_n : G^r_n \to G^s_n$. (We consider G^0_n as the trivial group.) Let us write $B^{r\to s}_n = \ker \pi^{r\to s}$. Groups $B^{r\to s}_n$ are normal subgroups of G^r_n, see [6], Proposition 13.11.

Thus, in the sense discussed above, we have $G^r_n = B^{r\to 1}_n \times | G^1_n$.

---

[2] thus not depending on $\xi^j_{\bar{j}}$.

[3] such a group homomorphisms can be induced by an action (left or right) of $\bar{H}$ on $\bar{N}$, for details see [6].

We remark that G_n^1 is nothing but the general linear group GL $(n, \mathbb{R})$ for which a structure of subgroups is extensively studied for many years and includes i.a. triangular and diagonal subgroups, orthogonal and symplectic subgroups, etc. So, let M be a subgroup of $(e_{B_n^{r\to 1}}, G_n^1)$ (e.g. induced from classical groups just mentioned), $m \in M$ and let $b \in B_n^{r\to 1}$. Then elements bmb^{-1} generates the conjugate subgroup $T = bMb^{-1}$ of G_n^r which is called the *Toupin subgroup* of G_n^r associated with M and b.

For a subgroup K of G_n^r, let $\pi_K^{r\to 1}$ denote the restriction of $\pi^{r\to 1}$ to K. Then, for $a \in G_n^1$, we will examine the fiber $\left(\pi_K^{r\to 1}\right)^{-1}(a)$.

First, for a Toupin subgroup T, we observe $\left(\pi_T^{r\to 1}\right)^{-1}(\mathrm{id}_{G_n^1}) = \mathrm{id}_T$. This leads to the following definition. We say that a subgroup K of G_n^r is the *generalized Toupin subgroup* of G_n^r if it has the property that $\left(\pi_K^{r\to 1}\right)^{-1}(\mathrm{id}_{G_n^1})$ is singleton.

In [3], authors proved for $r = 2$ that exist

- generalized Toupin subgroups of G_n^r which are not Toupin subgroup;
- one-parameter subgroups in G_n^r which are not generalized Toupin subgroup.

Now, we present the form of Toupin subgroup in local coordinates. First, we recall that for $a = (a_j^i, a_{jk}^i)$, $b = (b_j^i, b_{jk}^i) \in G_n^2$, the composition $c = ba = b \circ a$ is given by $c = (c_j^i, c_{jk}^i) = (b_k^i a_j^k, b_{lm}^i a_j^l a_k^m + b_l^i a_{jk}^l)$. We easily find that for $b = (\delta_j^i, b_{jk}^i) \in B_n^{2\to 1}$ its inverse $b^{-1} = (\delta_j^i, -b_{jk}^i)$. Then for $h = (h_j^i, 0)$, where (h_j^i) represents a subgroup of G_n^1,

$$bhb^{-1} = (h_j^i, b_{lm}^i h_j^l h_k^m - h_l^i b_{jk}^l).$$

We immediately see that for $h_j^i = \delta_j^i$ we obtain the identity as required.

5 Frame Bundles (of a General Order)

We define the *r-th order frame bundle* $P^r B$ over B as the space of r-jets of immersions from $\mathbb{R}^b$ into B, i.e.

$$P^r B = \mathrm{imm}\, J_0^r\left(\mathbb{R}^b, B\right).$$

1-jets in question, i.e. elements of $P^1 B$, form a principal bundle over the base manifold B. The structure group of $P^r B$ is G_b^r which acts smoothly on $P^r B$ on the right by the jet composition, i.e. $P^r B$ is a principal G_b^r-bundle. We generalize the Cosserat configuration by the following way. A principal bundle morphism

$$\mathscr{K} : P^r B \to P^r S$$

over the base map κ will be called the *general (r-th order) microstructure configuration*.

We note that P^rB has induced local coordinates ξ^j, $\xi^j_{\bar{j}_1}$, ..., $\xi^j_{\bar{j}_1\ldots\bar{j}_r}$, $j, \bar{j}_1, \ldots, \bar{j}_r = 1, \ldots, b$ and P^1S has induced local coordinates x^i, $x^i_{\bar{i}_1}$, ..., $x^i_{\bar{i}_1\ldots\bar{i}_r}$ $i, \bar{i}_1, \ldots, \bar{i}_r = 1, \ldots, s$.

For the expression of $\mathscr{K}$, we take (analogously as for the Cosserat configuration), a fixed homomorphism $\mathscr{H}_\varphi : G^r_b \to G^r_s$, again, first by the embedding of the element of G^r_b to G^r_s and then by the right multiplying by an element φ form G^r_s. We are leaving to readers to calculate the coordinate expression of $\mathscr{K}$ now.

6 Higher Order Deformation Bundles and Reductions of Jet Groups—Interesting Challenges

In the Sect. 1, we introduce the deformation gradient for the configuration κ. Evidently, deformation gradients are 1-jets.

Analogously, deformation gradients for the case of the Cosserat configuration K are represented by nonholonomic 2-jets and the question whether these jets are semiholonomic or even holonomic can be (and is) discussed. In general, deformation gradients of the general microstructure configuration $\mathscr{K}$ form certain nonholonomic $(r+1)$-jets and emerging challenges are similar: what represent jets of special types (semiholonomic, holonomic, but not only), in particular, due to the constitutive equations of the material?

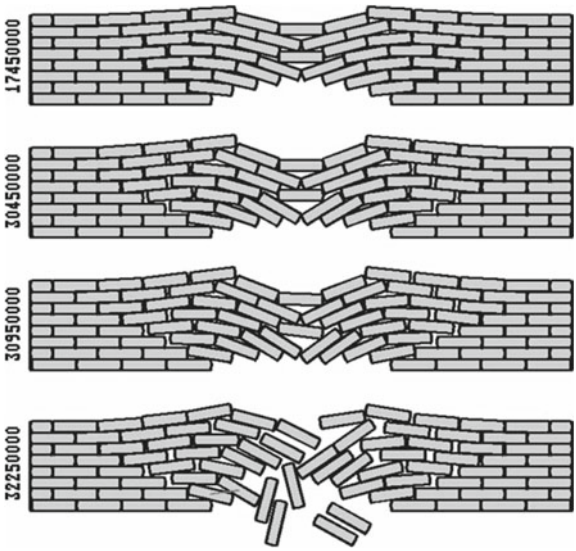

Fig. 2 There are numerous applications of Cosserat theory concerning rectangular structure of blocks; this figure is taken from the paper [1] of Dieter Besdo

Different, but no less important issue is a research of subgroups of jet groups G_n^r, similarly as it has been done in the case of Toupin subgroups. Of course, it leads to the phenomenon of material symmetry. Even an uninformed layman anticipates, when he had looked at Fig. 2, that there are situations when a total freedom in all possible ways of the motion is not the best to study; when the whole linear or jet group does not act, but operates only some suitable subgroup. We recall that if we have a principal G-bundle Y and an inclusion of a subgroup H into G, a *reduction of the structure group* (from G to H) is a principal H-bundle Z such that the pushout $Z \times_H G$ is isomorphic to Y. Note that these do not always exist, nor if they exist are they unique. Despite the complexity of the problem of reductions of jet groups, it is hopeful that it will not just pure mathematics, but also interesting results for continuum mechanics.

Acknowledgments The research is supported by Brno University of Technology, the specific research plan No. FSI-S-14-2290.

References

1. Besdo, D.: Towards a Cosserat-theory describing motion of an originally rectangular structure of blocks. Arch. Appl. Mech. **80**(1), 25–45 (2010)
2. Bogopolski, O.: Introduction to group theory, European Mathematical Society (2008)
3. Epstein, M., Elżanowski, M.: Material Inhomogeneities and their Evolution: A Geometric Approach. Springer (2007)
4. Forest, S.: Micromorphic media. In: Altenbach, H., Eremeyev, V.A. (eds.) Generalized Continua—from the Theory to Engineering Applications, pp. 249–300. Springer, Wien (2013)
5. Gamkrelidze, R.V. (ed.): Geometry I (Basic Ideas and Concepts of Differential Geometry). Springer, Berlin (1991)
6. Kolář, I., Michor, P.W., Slovák, J.: Natural Operations in Differential Geometry. Springer, Berlin (1993)
7. Papadopoulos, P.: Introduction to Continuum Mechanics, Lecture notes, Department of Mechanical Engineering, University of California, Berkeley, 2008. http://www.me.berkeley.edu/ME280B/notes.pdf
8. Yamaoka, H., Adachi, T.: Continuum Dynamics on a Vector Bundle for a Directed Medium. J. Phys. A. **43**(32), 15 p. (2010)

On the Origin of Balance Equations in Simple and Complex Continua: Unified View

Paolo Maria Mariano

Abstract Here I discuss the way we can derive balance equations for continua with active microstructure, furnishing a unified view on available models and a tool for constructing new ones. I indicate how the requirement of invariance under isometry-based changes in observers of *the power of the external actions* alone over a generic part of the body is a tool to derive standard and non-standard action-reaction principles, the representation of contact actions in terms of stresses, the possibility of nonzero microstructural self-actions, the balance equations, demanding a very limited number of assumptions. In presence of material mutations, which suggest to take into account multiple reference shapes for a body, we need to extend the procedure by introducing the notion of *relative power*. Its invariance under isometry-based changes in observers furnishes once again the results listed above and in addition the balances of configurational actions. Finally, I indicate how we can consider the covariance of the second law of thermodynamics and summarize what we can derive from this concept, and how.

1 Preamble

Here I copy down (changing the title) the talk I delivered in the 2015 meeting dedicated to Krzysztof Wilmanski in Łagów, Poland. The occasion notwithstanding, however, I do not have significant personal recollections of him, for I met him just once in Hungary. The contribution of his memory is then just cultural, for I discuss topics in continuum mechanics, the field of his interest, and is free of anecdotal and emotional issues. Independently of these aspects, however, I think that a concrete way of remembering a scholar several researchers in his field considered as a reference is to continue seriously our work, having as a guide a positive and constructive ethics, an ethics of respect for people, ourselves, the work itself.

P.M. Mariano (✉)
DICeA, University of Florence, via Santa Marta 3, I-50139 Firenze, Italy
e-mail: paolo.mariano@unifi.it

B. Albers and M. Kuczma (eds.), *Continuous Media with Microstructure 2*,
DOI 10.1007/978-3-319-28241-1_5

2 Reasons for Thinking of the Origins of the Balance Equations

A conceptual hierarchy in the skeleton of models in continuum mechanics emerges from fundamental treatises on the matter and is perhaps the primary legacy of the Truesdellian school (see [1, 36, 42, 44–46]). Such a hierarchy involves the description of the (geometric) shape of a body and its changes as a first step, followed by the representation of the actions and the pertinent balance equations, with the final assignment of the constitutive structures, restricted a priori by the need of not violating an expression of the second law of thermodynamics, which we commonly call Clausius-Duhem inequality, although neither Clausius nor Duhem never wrote it in the way we shape it nowadays, at least as far as I know. Each step in the hierarchy is independent of what follows it, while it depends on what preceeds it. The second part of such a statement requires some specifications, above all when we refer it to the balance equations. At a first glance the declared need of clarification would appear even superfluous for one could think instinctively just of reproducing directly in terms of fields the balances of momentum and moment of momentum met in the mechanics of discrete mass points, imagining this way to exhaust the problem. The choice is related to the way we describe the shape of a body and is successful in the traditional setting where we just indicate the place in space the body occupies. We can justify such a statement by thinking of the notion of force that we have in mechanics. A **force** is a *model* of what alters the state of a body motion (this way we include the rest state). Its action is measured by the power needed to generate such an alteration. Consider a mass point. Its shape is described by a point in space and the variation of its shape by the velocity. We measure the velocity and the power needed to move the mass point. The power evaluated over a specific velocity is a number. As a functional, it is linear in the velocity, which is a vector. In this setting a natural model of a force is something that gives us a number, once evaluated on the velocity, and is linear in the velocity itself: a covector, indeed, that we identify commonly with a vector when we refer to Cartesian frames. When we represent the shape of a continuous body only through the region in space it occupies, each point–now a material point–is endowed with three degrees of freedom only. Then the velocity field alone describes the instantaneous (incoming) changes in shape. At each point the velocity is a vector: the related interaction between a mass point and a "neighboring" one, along a prescribed direction, is then naturally described by a force: what we call *tension*. This is a way of understanding Cauchy's hypothesis of absence of local couples exchanged between neighboring material points of a continuous body. In other words, we are thinking of a body as a cluster of infinitely many indistinct material points, connected by bonds not transmitting couples. And this is the traditional approach to the continuum mechanics of deformable bodies.

To describe adequately–the adverb referring to the level of accuracy in our modelling activity we want to reach–some mechanical phenomena, however, we need to go beyond (even far away) the traditional format of continuum mechanics. An example is that of liquid crystals. Consider the nematic phase: we have a material

composed by stick molecules endowed with end-to-tail symmetry. Describing the shape of the body just in terms of the place in space it occupies does not allow us to account for the way such molecules are organized from place to place. We can consider the local molecular arrangement by attributing to every point the prevalent direction of molecules in a small neighborhood of it (see [11, 12]). In this way we endow every point of the region in space occupied by the body with additional degrees of freedom (those describing the local arrangement of the molecules), which are collected at each point in an element of the projective plane, a direction indeed. We can opt for considering a second-rank tensor, precisely a dyad between two unit vectors, instead of a direction alone, to give a more refined approximation of the local distribution of molecular orientations (see [9]). And the list of possibilities for the sole nematic phase does not end here [13]. The examples also are not limited to the realm of liquid crystals: vectors may describe the local polarization in ferroelectrics o magnetoelastic crystals (see, e.g., [3]), or collect the degrees of freedom exploited by the atoms in quasicrystals to assure the intrinsic long-range quasi-periodicity of the atomic clusters (see [20, 41]); the structure of the normal superfluid Helium requires the introduction of a complex field, while its isotope can be described by using elements of a manifold with dimension five; second-rank tensors are useful to depict the independent micro-deformations in polymers [10]; triads of unit vectors can be used in the dimension-reduced models of rods–here I use the word rod in a wide sense also for beam, shaft, column, etc.—and shells, as shown first by J. L. Ericksen and C. A. Truesdell [14]. The list can be extended but the present examples suffice to illustrate the scenario, which finds a unified format when we affirm that we describe the shape of a body by selecting the place it occupies in space and adding to each point descriptors of its microstructure selected in a differentiable manifold $\mathscr{M}$ (chosen without boundary as a matter of convenience), which we call *the manifold of microstructural shapes*. This view has been proposed first in solid-state physics to account for structural material complexity [27, 28]. First, G. Capriz coupled it with finite strains [4].

The rate of change in shape of the body is then given by the velocity field and the rates of the material morphology descriptors (a section of the tangent bundle of $\mathscr{M}$, if we think in geometrical terms). Standard tensions appear as entities developing power in the velocity, i.e. the rate of relative change of place between neighboring material elements, while other actions are power-conjugated (in the sense explained for tensions) with the time rates of the material morphology descriptors and their spatial variations. In other words, when we affirm that a material element of a continuous body is placed at x and its microstructure is described by $\nu \in \mathscr{M}$, we are impliciting considering the material element as a system, a sort of box with an inner structure described coarsely by ν. This is a step forward the traditional approach in continuum mechanics: there the use of the sole placement x as a descriptor of a material element implies considering it as an indistinct mass point, the simplest possible structure for a system. It is in energetic contact with its neighbors, and the circumstance generates the standard tension. In the extended view, we include additional mechanisms. Consider two material elements at x and $x + dx$ along a certain direction. If we freeze the microstructure and move far away the material

elements (two in this view) one another, we generate the common tension as in the standard format–this is the sole mechanism appearing there. However, we can imagine (1) to vary the microstructure of each material element in the *same* way or (2) to determine its inhomogeneous changes in space. In the first case a local inner action (*microstructural self-action*) appears within each material element; when evaluated over the rate of ν it furnishes the power needed to develop the relevant mechanism. Its geometric nature depends on the nature of ν. In the second case an additional contact action appears: it is of first-neighbor-type.

In all special cases, so in the unified theory, we face the problem of establishing appropriate balance equations, which involves all the actions just mentioned. Not always we find evident how the balance equations should be. Or better, we are not sure that acting by analogy with well-established practice in the traditional format of continuum mechanics or the mechanics of mass points could lead us to correct results. Correctness refers to the way we are able to describe the interaction mechanisms implied in our initial choices in the description of phenomena pertaining a given class of bodies. For these reasons it appears useful to discuss in terms of a model of models about the origin of the balance equations in continuum schemes, for we would like to have some first principle to derive such equations, according to Ockham's razor, i.e. with the best economy of hypotheses.

This is what I discuss in this article. What I essentially claim appears in the list below.

(a) When a body does not undergo structural mutations that alter the one-to-one correspondence between any current configuration and the reference one (an alteration occurring when fractures appear along a motion, e.g.) the requirement of invariance of the *external power* alone with respect to changes in observers that are isometric in the three-dimensional point space and with a certain general form specified later on $\mathscr{M}$ is a way of deducing balance equations with a restricted number of assumptions. The result is not new: it dates back 2002 [21], it has been anticipated in [6], with a restricted view on changes in observers on $\mathscr{M}$, and is an extension of what has been proposed in 1959/1963 [35] in the traditional format of continuum mechanics.

(b) In presence of structural mutations such as fractures or evolution of volumetric defects, imagining possible multiple reference shapes (differing each other by the defect pattern) and introducing the pertinent notion of *relative power* (as defined in general in [23] and proposed in conservative setting first in [8]), we find that the requirement of invariance of such a power under changes in observers of the type occurring in item 1 above furnishes the balance equations of standard and microstructural actions, supplemented by the configurational balances. Such a procedure requires a restricted number of assumptions and can be adequately–the adverb intended in Ockham's sense–accepted as a first principle.

(c) For stronger requirements of invariance, involving a larger class of changes in observers (those not necessarily based on rotations and translations of the frames in the ambient space), another way applies for a first principle to derive from a unique source all the ingredients of a continuum model. In fact, the mechanical

dissipation inequality (the isothermal version of the Clausius-Duhem inequality, a way of expressing the second law of thermodynamics) is *not only* a direct source of a priori constitutive restrictions and the expression of the mechanical dissipation, *but also* it can furnish *from a unique invariance requirement*

(i) the existence of the stress (and that of the microstress describing the microstructural contact interactions),
(ii) the existence (and the need, indeed) of bulk inner microstructural self-actions,
(iii) pointwise standard, microstructural, and configurational balance equations.

3 Remarks on the Geometric Language

If we choose $\mathscr{M}$ to be a differentiable manifold with finite dimension, we may construct a model of models unifying all special proposals we know, with the exception of the varifold-based description of crack nucleation proposed first in [18], in which at each point we add through measures information on the possible defect pattern crossing the point itself. In this last case, in fact, we select descriptors of the material morphology belonging to infinite-dimensional spaces. In contrast, once we accept the finite-dimensional choice (it suffices in the majority of cases and can be also coupled with the infinite-dimensional choice, as in [17], although we can't do much in the latter case), we could *naively* think of embedding $\mathscr{M}$ into a linear space, as Whitney's theorem [47] permits to do for all finite-dimensional manifolds. We could even select $\mathscr{M}$ to be a linear space, adding geometric constraints when they are suggested by the physics at hands. This choice is the one pursued by P. Germain in proposing the principle of virtual powers as a primary source for deriving balance equations [16]. We could comply with it for it does not require knowledge in geometry more extended that the elementary tensor calculus in Cartesian (or Euclidean if you want) frames, identifying this way covariant and contravariant tensor components, so not distinguishing from vectors and covectors as I do here. In this way we would reduce the effort just to the replica of standard integral balances, dressing slyly them with new names such as pseudobalances or something similar, and affirming that what distinguishes one case from another is just the algebraic choice of the descriptor of the material morphology, besides the assignment of constitutive structures, and forgetting that the *geometric* structure of $\mathscr{M}$ plays a non-trivial role in both the unified theory and its special cases.

Such a choice offers itself to immediate criticisms:

- Although a finite-dimensional differentiable manifold $\mathscr{M}$ can be always embedded into a linear space by Whitney's theorem, already mentioned, *the embedding is not unique*. If $\mathscr{M}$ is Riemannian, its embedding can be even isometric but it remains not unique. Moreover, the dimension of the target space depends on the regularity of the emebbedding itself (the pertinent theorems are in [31, 32]). Consequently, the resulting model would depend on the embedding, which is not

addressed by stringent physical instances. Also, if we would choose the manifold of microstructural shapes itself as a linear space, we would exclude from the tentative of constructing a unified scheme the cases in which the descriptor of the microstructural morphology belongs naturally to a non-linear manifold (examples are among those mentioned above and we can add the case of continua with distributed spins, when we describe them by resorting to unit vectors, for the unit sphere is a nonlinear manifold).

- As we shall see in the subsequent sections, even in the case in which $\mathscr{M}$ is a linear space, the assignment a priori of an integral balance of microstructural actions, although possible, is superfluous, as we shall see in the first theorem below.

Mechanics is geometry (see, e.g., [39, 43]). Mechanics is also analysis on the geometric structures (see, e.g., [19]). We have not to be afraid of the mathematical formalism for it is just a language both qualitative and quantitative, the sole language of this type, which may light up the inmost aspects of the mechanical behavior of materials, provided we have the appropriate care in clearly linking mathematical objects to the image we have of the physical phenomena. In fact, the only thing we have to be afraid of is a feeble attention to the conceptual connection between the physical significance and the mathematical tools used. This is matter of intuition level and deepmess of analysis, and we cannot buy such aspects if we do not have them by instinct and do not cultivate them. The rest we can learn having at disposal time and appropriate treatises.

4 Balance Equations: Ways to Get Them

4.1 A Summary of Possibilities

We list here various manners at our disposal to get balance equations in continuum models of the material behavior. They are divided in two groups.

In the *first group* no list of state variables comes into play.

1. We can assign directly **pointwise balances**.
2. We can assume the form of **integral balances**, deriving by localization–i.e. by presuming that they hold for any subset of the body with non-vanishing volume and appropriate regularity (it is the Euler principle)–their pointwise counterparts.
3. We can presume the validity of the **principle of the virtual power**, after the assumption of the structure of external and internal (or inner) powers.
4. We can presume the expression of the **external power** alone and require its **invariance** under rigid-body-type changes in observers.
5. In presence of material mutations–in the sense mentioned above–the notion of external power requires an extension to that of **relative power** for which we require the invariance with respect to a class of rigid-body-type changes in observers, including alteration of the reference space.

6. We can get balance equations from discrete schemes through homogenization procedures (see, e.g., [37, 38])–a fruitful and challenging sector here is the evaluation of the continuum limit of the Boltzmann equation (see [40]).

The *second group* of possible paths involves the choice of the list of state variables, so that we put on the same conceptual level the derivation of the balance equations and the (at least preliminary) assignment of the constitutive equations.

7. We can evaluate, in fact, the **first variation** of some **energy**, even including dissipation potentials.
8. We can impose a **balance of energy** and require its **covariance** in the case bulk forces can be dissipative.
9. We can assume an appropriate version of the **Poisson brackets**, even including **dissipative brackets** (they are connected with a dissipation potential).
10. We can decide a version of the **second law of thermodynamics** (even including the relative power) and require its **covariance.**

4.2 Remarks on the List Above

When we choose to follow one path, among those listed above, to determine balance equations in a setting extended with respect to the traditional format of continuum mechanics, we should not forget some aspects related with the nature of the procedures in the list.

#1 Pointwise balances are the final target of the discussion about balance equations. Prescribing them in analogy with the standard instances is a direct jump to the end. In doing it, beyond the structure of the equations, we presume also the representation of the microstructural contact actions in terms of microstresses and self-actions, without having proven the analogous of Cauchy's theorem for the standard tension, a theorem based also on the boundedness of the bulk actions, the knowledge of the integral balance of forces, the action-reaction principle. In some cases it is hard to do better–meaning with less assumptions–but if we choose this way, we have to remind that we are not sure about the effectiveness of the result: analogy, in fact, is not always a secure path.

#2 The assignment of integral balances demands less assumptions, indeed, and allows to try to prove Cauchy's type theorems. If we consider $\mathscr{M}$ as a non-linear manifold–the general unifying choice, indeed–prescribing an independent integral balance of microactions would be highly questionable mathematically. We would write, in fact, integrals involving integrands taking values on the cotangent bundle of $\mathscr{M}$, which is a non-linear space (unless $\mathscr{M}$ coincides with a linear space) and is the target space of the integrand, so the definition of the integral itself would be questionable. Moreover, if we consider $\mathscr{M}$ to be coincident with a linear space, we can see that such a balance would be essentially superfluous, as I show in the first theorem below.

#3 When we adopt the principle of virtual power, we are prescribing the *weak form* of the pointwise balance equations, the form used in computational procedures. The choice implies also the presumption of the expression of the contact actions in terms of stress. The proof of a Cauchy's type theorem would require the use of the integral balances, rendering superfluous the virtual power principle. In other words, in the principle of virtual power we presume a priori all the ingredients appearing in the balance equations without proving the existence of the standard and microstructural stresses and the possible self-actions. There is also a subtle connection between integral balances and the principle of virtual power, or virtual work, depending on whether we use the velocity or the displacement, as shown in 1979 by Antman and Osborn [2].

#4 In 1963, W. Noll suggested to impose the invariance of the power of all external actions (the external power then) on a generic part of a body with respect to rigid-body changes in observers in the ambient space as a natural source of the balance equations [35], promoting to the level of principle a previous result by G. Piola. Among the possibilities in the first group of the list above, this one demands least assumptions and can be used when the reference place is fixed once and for all. Such a procedure can be extended to the multi-field setting sketched above and is a tool for deriving clearly balance equations in both integral and pointwise form, as I explain below. The extension of such a procedure to complex continua, which requires to think non-trivially of the notion of observer and its changes, has been proposed first by G. Capriz and G. Mazzini in 1998 [6] considering, however, the sole case in which the special orthogonal group $SO(3)$ acts on $\mathscr{M}$. In tackling later the question and discussing further the notion of observer in such a setting, in 2002 P.M. Mariano has overcame that restriction [21]. A significant special case is the application of such a procedure to the dimension reduced models (i.e. the direct models) of rods and shells (see for details the pertinent long chapter in [24]).

#5 The idea of the relative power is an extension of the previous procedure when macroscopic structural changes in the body suggest to adopt multiple reference shapes (see [23] and for its introduction in conservative setting [8]).

#6 In the second set of possibilities listed above, the word *covariance* appears repeatedly. It is structure invariance with respect to diffeomorphism-based changes in observers.[1] In *conservative setting*, covariance appears in the Nöther theorem. Consider *finite-strain elastodynamics of simple bodies*. The Nöther theorem is based on the *invariance* of the Lagrangian density with respect to the action of families of diffeomorphisms on both spatial and referential coordinates. In the last case, the one involving the referential shape, the diffeomorphisms considered must be isocoric: two different observers **must** perceive the same **type** of material. To satisfy such a requirement, transformations of the reference shape must be *material isomorphisms* and as such, according to Noll's definition

[1] A diffeomorphism is a one-to-one differentiable map with differentiable inverse. A rotation followed or preceded by a translation is a special diffeomorphism. A homogeneous deformation is another special diffeomorphism. And so on ...

[34], they have to preserve locally the mass, i.e. they must be isocoric. And this aspect does not depend on whether we are thinking of solids or fluids. Classes of changes in observers and those of admissible motions are not necessarily coincident, in fact, as it is well known from elementary courses. The result of the Nöther theorem in finite-strain elastodynamics of simple bodies is that the required invariance of the Lagrangian density implies an equation involving the energy-momentum tensor and including standard and configurational balances as special cases. Standard balances are associated with the actions of diffeomorphisms over the ambient space where we place the current configurations. Configurational balances are determined by the changes of the reference shape (the material manifold, precisely) induced by diffeomorphisms, which have to be also material isomorphisms.

#7 In conservative setting, we can describe motions in terms of the Hamiltonian, either through the Hamilton equations or to their weak form represented by the Poisson brackets, which can be supplemented by appropriate dissipative brackets where there are effects that can be associated with a dissipation potential (see [29]).

#8 In presence of dissipative bulk external actions, not necessarily associated with a dissipation potential, covariance appears in the Marsden-Hughes theorem [26]. In its original version it is referred to the finite-strain elastodynamics of simple bodies. The attention focuses on the expression of the first principle of thermodynamics in isothermal conditions: the balance of mechanical energy. A requirement of covariance for it–here intended as structural invariance of the principle with respect to diffeomorphisms acting on the ambient space–implies the representation of the standard tension in terms of the stress tensor (i.e. Cauchy's theorem), the pointwise balances, the a priori constitutive restrictions on the stress.

#9 A immediate question arises: What about the presence of dissipative parts of the contact actions? In other words, since the Marsden-Hughes theorem is a variation of the Nöther theorem and a step toward the presence of dissipative structures, what should we imagine for phenomena involving irreversible strain (as in plasticity) or dissipative stress components (as in viscoelasticity)? For finite-strain plasticity, a 2013 theorem furnishes the answer (see [22]). Versions of it apt for traditional viscoelasticity and the multi-field setting for materials with complex microstructure, sketched above, are possible and I summarize at the end of these pages the essential steps leading to the expression pertaining to the multi-field setting discussed here.

5 Multi-field Setting for Continua with *Active* Microstructure

In the title of this section, I use the word *active* to underline a distinction. Every material, in fact, has its microstructure, which is the way molecules are entangled or atoms are arranged in some ordered clusters. When in traditional linear elasticity we

specify the symmetries of the constitutive elastic tensor, we are furnishing information on the material microstructure, in fact. Homogenization procedures allow us to account for even complicated arrangements of the matter, without going far beyond the traditional setting of continuum mechanics [30]. I have already mentioned, however, examples in which microstructural events have macroscopic influence in a way that we can barely or about nothing describe in the terms of the traditional format of continuum mechanics. These bodies are those that we can consider *with active microstructure*, and we can call them *complex bodies* in short. I have also described in words the way we can tackle the problem of representing their mechanics in a way that unifies, among other things, existing models. Some (standard) formal structures render more concrete the ideas presented so far.

The geometric environments we need to introduce are a differentiable manifold[2] $\mathscr{M}$, which we consider finite-dimensional and without boundary, and two isomorphic copies of the three-dimensional Euclidean point space, namely $\mathscr{E}^3$ and $\tilde{\mathscr{E}}^3$. These two last spaces differ at most by a translation and a rotation. We select in $\mathscr{E}^3$ a fit

[2]Consider a set $\mathscr{M}$ endowed with a topology, which is Hausdorff, i.e. for any pair of distinct elements of $\mathscr{M}$, say ν_1 and ν_2, we may find non-intersecting open neighborhoods $\mathscr{I}(\nu_1)$ and $\mathscr{I}(\nu_2)$ containing ν_1 and ν_2, respectively. We affirm that $\mathscr{M}$ is a *topological manifold* when it is *locally Euclidean*, i.e. every $\nu \in \mathscr{M}$ has an open subset of $\mathscr{M}$, $\mathscr{U}(\nu)$, containing it, which is homeomorphic to an open subset $\mathscr{V}$ of $\mathbb{R}^n$, meaning that it is possible to define a one-to-one mapping $\varphi : \mathscr{U} \longrightarrow \mathscr{V}$ of $\mathscr{U}$ onto $\mathscr{V}$. We call *coordinate chart* (simply *chart*) the pair $(\mathscr{U}, \varphi)$ and *atlas* the set $\mathfrak{F} := \{(\mathscr{U}_i, \varphi_i)\}$ of charts such that $\cup_i \mathscr{U}_i = \mathscr{M}$, for $i \in \tilde{I}$, with $\tilde{I}$ some index set. In other words, $\mathfrak{F}$ determines a covering of coordinate systems over the whole $\mathscr{M}$. In particular, we affirm that $\mathscr{M}$ has dimension n when all $\mathscr{U}_i$ are mapped onto sets $\mathscr{V} \subseteq \mathbb{R}^n$ with dimension n. If for *all* $i, j \in \bar{I}$, the change of coordinates between charts is of class C^k, i.e. $\varphi_i \circ \varphi_j^{-1} : \mathscr{U}_i \cap \mathscr{U}_j \longrightarrow \mathscr{V}_i \cap \mathscr{V}_j \subseteq \mathbb{R}^n$, with $\circ$ indicating map composition, is C^k with $1 \leq k \leq +\infty$, and for any chart $(\mathscr{U}, \varphi)$ such that $\varphi \circ \varphi_i^{-1}$ and $\varphi_i \circ \varphi^{-1}$ are C^k, for all $i \in \bar{I}$, we get $(\mathscr{U}, \varphi) \in \mathfrak{F}$, we affirm that $\mathscr{M}$ is a *differentiable manifold of class* C^k, simply a *differentiable manifold* when $k = +\infty$. A function $f : \mathfrak{I} \longrightarrow \mathscr{M}$, with $\mathfrak{I}$ some interval in $\mathbb{R}$, defines a curve over $\mathscr{M}$. We affirm that it is differentiable near $s \in \mathfrak{I}$ when, with $(\mathscr{U}, \varphi)$ a chart around $\nu(s)$, the map $\varphi \circ f$ is differentiable in the common sense. The derivative of the function f at s is what is called the *tangent vector* to ν at $\mathscr{M}$. Infinitely many smooth curves crossing ν can be defined over $\mathscr{M}$. The derivative of each of them defines a tangent vector to $\mathscr{M}$ at ν. Infinitely many smooth curves may have the same tangent vector at ν. If so, they agree near ν. The circumstance allows us to think of tangent vectors in terms of equivalence classes of functions. More precisely, we affirm that functions h and $\tilde{h}$, smooth curves on open sets containing ν, have the same *germ* when they agree in some neighborhood of ν. In particular, if h and $\tilde{h}$ are smooth, the set $\mathbb{H}_\nu$ of the equivalence classes $\mathbf{h}_\nu$, defined by the condition *to have the same germ*, and called themselves germs in short, is naturally endowed with the structure of an algebra over $\mathbb{R}$ by the operations of addition, scalar multiplication and multiplication of functions. In this setting a tangent vector υ at $\nu \in \mathscr{M}$ can be defined to be a linear derivation of the algebra $\mathbb{H}_\nu$, i.e., for all $h, \tilde{h} \in \mathbb{H}_\nu$ and $\alpha \in \mathbb{R}$, we have $\upsilon(h + \alpha\tilde{h}) = \upsilon(h) + \lambda\upsilon(\tilde{h})$ and $\upsilon(h \cdot \tilde{h}) = h(\nu)\upsilon(\tilde{h}) + \tilde{h}(\nu)\upsilon(h)$. Such properties point out that the set of all tangent vectors to $\mathscr{M}$ at ν, indicated by $T_\nu\mathscr{M}$, and called the *tangent space* of $\mathscr{M}$ at ν, is a linear space. The union, varying ν in $\mathscr{M}$, of all tangent spaces of $\mathscr{M}$ is called the *tangent bundle* of $\mathscr{M}$ and in general is not a linear space. For any $T_\nu\mathscr{M}$, the set of all linear functions over it, a set indicated by $T_\nu^*\mathscr{M}$ is called the *cotangent space* of $\mathscr{M}$ at ν (its elements are commonly called *covectors*). The union of all cotangent spaces of $\mathscr{M}$ is the so-called *cotangent bundle* of such a manifold and in general is not a linear space.

region $\mathscr{B}$ (itself a connected manifold in $\mathscr{E}^3$) as a macroscopic reference shape for a body. From $\mathscr{B}$ we define macroscopic body shapes that we consider deformed with respect to $\mathscr{B}$ by means of differentiable orientation preserving maps (**deformations**) $x \longmapsto y := u(x) \in \tilde{\mathscr{E}}^3$, with x a generic point in $\mathscr{B}$. The distinction between $\mathscr{E}^3$ and $\tilde{\mathscr{E}}^3$ renders significant the standard requirement that isometric changes in observers in the ambient space leave invariant the reference place $\mathscr{B}$, although they alter the frames assigned to the whole space. It can be also accepted for $\mathscr{B}$ is just a geometric environment where we measure how lengths, volumes and surfaces change under deformations, and we use it to make the comparisons defining what we can call defects, at least at macroscopic scale. Consequently, physics does not force us to consider $\mathscr{B}$ occupied by the body at any instant of any motion. We have just to require that it *could* be occupied by the body; no more. This choice renders more precise–for the reasons just discussed–the traditional distinction between Lagrangian (referential) and Eulerian (actual) representations of fields–adjectives attributed to maps defined over $\mathscr{B}$ and $u(\mathscr{B})$, respectively–because in the standard format referential and actual places of the body are included in the same space, although they are endowed with different coordinate systems. My insistence on such an aspect aims to prepare the ground to the discussion on the notion of observer in the next section. We commonly indicate by F the spatial derivative $Du(x)$ of u, evaluated at $x \in \mathscr{B}$, and call it **deformation gradient**, according to the traditional jargon. Consider three linearly independent vectors $\{\mathbf{e}_1, \mathbf{e}_2, \mathbf{e}_3\}$ at x. They constitute a vector basis in the tangent space (see footnote 2 for the definition) of $\mathscr{B}$ at x. The dual counterpart of such a basis is made of other three vectors $\{\mathbf{e}^1, \mathbf{e}^2, \mathbf{e}^3\}$ defined to be such that $\mathbf{e}^H \cdot \mathbf{e}_K = \delta^H_K$, with δ^H_K the Kronecker symbol. At $y = u(x)$ consider other three linearly independent vectors $\{\tilde{\mathbf{e}}_1, \tilde{\mathbf{e}}_2, \tilde{\mathbf{e}}_3\}$. They constitute a vector basis in the tangent space of $u(\mathscr{B})$ at $y = u(x)$. With respect to these bases, we have $F = F^i_A \tilde{\mathbf{e}}_i \otimes \mathbf{e}^A = \frac{\partial u^i(x)}{\partial x^A} \tilde{\mathbf{e}}_i \otimes \mathbf{e}^A$. Lower case indexes refer to coordinates on $u(\mathscr{B})$, while capital indexes label coordinates over $\mathscr{B}$. From a geometric viewpoint, F maps tangent vectors to $\mathscr{B}$ at x onto tangent vectors to $u(\mathscr{B})$ at $y = u(x)$. To summarize this standard statement we write $F \in \mathrm{Hom}(T_x\mathscr{B}, T_y u(\mathscr{B}))$. The proof is elementary. Consider a curve on $\mathscr{B}$ given by a smooth map $s \longmapsto x(s) \in \mathscr{B}$, with s a parameter ranging in $[-\bar{s}, \bar{s}]$, $\bar{s} > 0$. The tangent vector at $s = 0$ is $\mathsf{t} := \frac{dx(s)}{ds}|_{s=0}$. The deformation determines another curve $s \longmapsto u(x(s)) \in u(\mathscr{B})$ over the deformed shape of the body. The tangent vector to the deformed curve at $s = 0$ is given by $\mathsf{l} := \frac{du(x(s))}{ds}|_{s=0} = Du(x(0))\frac{dx}{ds}|_{s=0} = F\mathsf{t}$. Notice that $Du(x)$ is in principle different from the gradient $\nabla u(x) = (\frac{\partial y^i}{\partial x})^A \tilde{\mathbf{e}}_i \otimes \mathbf{e}_A$. The relation between the two is established by the metric in $\mathscr{B}$, once we assign it. Let g be such a metric. We have $\nabla u(x) = Du(x)g^{-1}$. $\nabla u(x)$ and $Du(x)$ can be identified when we refer to Cartesian frames so that the metric is the second-rank unit tensor. By F^* we indicate the *formal adjoint* of F. By definition F^* belongs to $\mathrm{Hom}(T^*_y u(\mathscr{B}), T^*_x \mathscr{B})$. Its relation with the *transpose* of F, namely F^T, is defined by the metric g in the reference place $\mathscr{B}$ and the one, call it $\tilde{g}$, in the ambient space. Formally, we have $F^T = g^{-1}F^* g$ (see [24] for the proof).

A differentiable field $x \longmapsto \nu := \tilde{\nu}(x) \in \mathscr{M}$ furnishes geometric information on the structure of the matter at finer spatial scales, translating them at macroscopic

scale. We call it **morphological descriptor map**. We write N for its spatial derivative $D\tilde{\nu}(x)$, so we have $N \in \mathrm{Hom}(T_x\mathscr{B}, T_\nu\mathscr{M})$. N^* indicates the formal adjoint of N and it is $N^* \in \mathrm{Hom}(T^*_\nu\mathscr{M}, T^*_x\mathscr{B})$.

In this setting, **motions** are *pairs* of time parameterized families of deformations and morphological descriptor maps:

$$(x,t) \longmapsto y := u(x,t),$$
$$(x,t) \longmapsto \nu := \tilde{\nu}(x,t),$$

with t the time, ranging in some interval of the real line. We assume that such maps are differentiable in time, at least with piecewise differentiable first time derivative (the assumption can be relaxed for the morphological descriptor map if we do not consider the possibility of microstructural inertia). We write then

$$\dot{y} := \frac{du(x,t)}{dt}$$

and

$$\dot{\nu} := \frac{d\tilde{\nu}(x,t)}{dt}$$

for the pertinent time rates in Lagrangian representation. $\dot{y}$ is the macroscopic velocity, while $\dot{\nu}$ indicates the time rate of the microscopic features represented by ν. We presume time differentiability for the first spatial derivatives of u and $\tilde{\nu}$ and write $\dot{F}$ and $\dot{N}$ for the pertinent rates.

6 Observers and Their Changes

Definition 1 An **observer** is a collection of coordinate systems (*atlas*, in short) over *all* the geometrical environments necessary to describe the morphology of a body and its motion.

In the multi-field setting considered here an observer is then the collection of (*i*) an atlas in the physical space, (*ii*) an atlas on the manifold of microstructural shapes, (*iii*) an atlas in the reference space, (*iv*) a time scale. Changes in observers are then transformations of one or more among these coordinate systems. The physics at hands addresses choices.

An axiom implicitly adopted in standard treatments is that *two different observers must perceive the same type of material*. Consequently, changes of the atlas in the reference space must be also material isomorphisms–the traditional notion introduced by Noll in [34] requires to be extended to such a setting but, in any case, the condition requiring the conservation of the referential mass density persists, so that, according

to the axiom just mentioned, changes of frames in the reference space must be isocoric, independently of the circumstance that we analyze solids or fluids, as I have already recalled. Commonly, such an axiom of *permanence of the material typology* under changes in observers is not rendered explicit but it is implicitly used in the Nöther theorem, the Marsden-Hughes theorem and, above all, when we compute the horizontal variation of the elastic energy in finite-strain elasticity.

6.1 Synchronous Isometry-Based Changes of Observers in Multi-field Setting

Consider smooth maps $t \longmapsto a(t) \in \mathbb{R}^3$ and $t \longmapsto Q(t) \in SO(3)$ and define a change in observer in the physical ambient space $\tilde{\mathscr{E}}^3$ by

$$y \longmapsto y' := a(t) + Q(t)(y - y_0),$$

where y_0 is an arbitrary fixed point. Then y and y' are the places of the same material point evaluated respectively by the two observers, say $\mathscr{O}$ and $\mathscr{O}'$, differing one another by rigid-body changes of place defined, at the instant t, by the translation $a(t)$ and the rotation $Q(t)$. Being an element of $SO(3)$, in fact, Q is orthogonal and with determinant equal to $+1$; it describes finite rotations in the three-dimensional point space. By computing the time derivative of y' and pulling back from $\mathscr{O}'$ to $\mathscr{O}$ the velocity $\dot{y}'$, we define a new velocity $\dot{y}^*$ to be

$$\dot{y}^* := Q^T \dot{y}' = c(t) + q(t) \times (y - y_0) + \dot{y}, \tag{1}$$

a standard relation in which $c := Q^T \dot{a}$ and q is the axial vector of the skew-symmetric tensor $Q^T \dot{Q}$.

Changing coordinates in the physical space alters also the perception of the microstructures. They are, in fact, *in* the physical space. Their separate representation on the manifold $\mathscr{M}$ is just a model choice, a matter of convenience. To account for such a circumstance, in order to establish classes of changes in observers compatible with the physics at hands, we define a *link* between changes in observers in the physical space, determined in general by elements of $\mathrm{Diff}(\tilde{\mathscr{E}}^3, \tilde{\mathscr{E}}^3)$, the space of diffeomorphisms of $\tilde{\mathscr{E}}^3$ onto itself–rotations and translations are special cases (see footnote 1)–and transformations of the atlas on the manifold $\mathscr{M}$, given by elements of $\mathrm{Diff}(\mathscr{M}, \mathscr{M})$, the group of diffeomorphism mapping $\mathscr{M}$ onto itself. Formally, we introduce a family of differentiable homomorphisms

$$\left\{ \lambda : \mathrm{Diff}(\tilde{\mathscr{E}}^3, \tilde{\mathscr{E}}^3) \longrightarrow \mathrm{Diff}(\mathscr{M}, \mathscr{M}) \right\}.$$

When the change in observer in the physical ambient space is of rigid-body type, as above, the set just defined reduces to

$$\{\lambda : SO(3) \longrightarrow \text{Diff}(\mathscr{M}, \mathscr{M})\}.$$

In this case, the counterpart of $\dot{y}^*$ is given by

$$\dot{\nu}^* = \dot{\nu} + \mathscr{A}(\nu)\, q, \tag{2}$$

with $\mathscr{A}(\nu) \in \text{Hom}\left(\mathbb{R}^3, T_\nu \mathscr{M}\right)$. When $SO(3)$ is not included in $\text{Diff}(\mathscr{M}, \mathscr{M})$ and the set $\{\lambda\}$ is not empty, by indicating by $\nu_{\lambda(Q)}$ the value of ν after the action of $\lambda(Q) \in \text{Diff}(\mathscr{M}, \mathscr{M})$ (once again the explicit expression of $\nu_{\lambda(Q)}$ depends on the tensorial nature of ν and $\lambda(Q)$), $\mathscr{A}(\nu)$ is given by

$$\mathscr{A}(\nu) = \frac{d\nu_{\lambda(Q)}}{d\lambda} \frac{d\lambda(Q)}{d\mathrm{q}} \Big|_{\mathrm{q}=0},$$

with $\mathrm{q}(t) \in \mathbb{R}^3$ the value of a smooth map $t \longmapsto \mathrm{q}(t)$ such that $Q(t) = \exp(-\mathbf{e}\mathrm{q}(t))$, $\mathbf{e}$ Ricci's symbol. Otherwise we get

$$\mathscr{A}(\nu) = \frac{d\nu_{\mathrm{q}}}{d\mathrm{q}} \Big|_{\mathrm{q}=0}.$$

For example, when $\mathscr{M}$ coincides with $\mathbb{R}^3$, we find $\mathscr{A} = \nu\times$. The choice of the relation (2) points out that the microstructural descriptor is *insensitive* to rigid translations in space of the whole body. In fact, ν at a point describes what is *inside* the material element placed there: it brings information about the inner structure, which translates with the point and changes independently of the translation itself. The relation (2) is also compatible with the basic structure of the unifying scheme for the models of continua with microstructure, which requires to maintain $\mathscr{M}$ as general as possible, i.e. not necessarily coinciding with a linear space and being endowed with a metric structure.

Isometry-based changes in observers pertain also to the space where we select the reference configuration. Let w the value at x and t of a vector field over the reference space. An observer in this space is a frame of reference. When we rotate and translate such a frame (remind: it pertains to the whole space), in the new frame we evaluate a new field with values w'. The pull-back of w' in the first frame (the first observer) gives a transformation rule analogous to (1), a rule defining w^*, namely

$$w^* := \bar{c}(t) + \bar{q}(t) \times (x - x_0) + w, \tag{3}$$

where x_0 is another arbitrary fixed point and the translation $\bar{c}$ and $\bar{q}$ do not coincide with c and q selected in the ambient physical space.

We do not consider here changes in the time scale.

6.2 *Extending the Setting: Diffeomorphism-Based Changes in Observers*

Time invariance is maintained even in the subsequent more general class of changes in observers: the one based on diffeomorphisms, which alter the ambient space, the reference one and the manifold.

- Over the ambient space we may consider the action of a time-parameterized class of elements of Diff$(\tilde{\mathscr{E}}^3, \tilde{\mathscr{E}}^3)$. Precisely we define smooth maps $t \longmapsto h_t : \tilde{\mathscr{E}}^3 \longrightarrow \tilde{\mathscr{E}}^3$, with $h_t \in \text{Diff}(\tilde{\mathscr{E}}^3, \tilde{\mathscr{E}}^3)$ and $h_0 = \textit{identity}$. The smoothness of h_t in time defines a velocity field $y \longmapsto \bar{v} := \frac{d}{dt} h_t \mid_{t=0}$ and the relation (1), i.e. the change $\dot{y} \longrightarrow \dot{y}^*$, becomes

$$\dot{y} \longrightarrow \dot{y}^{\#} := \dot{y} + \bar{v}.$$

- The class of differentiable homomorphisms λ generate over $\mathscr{M}$ maps $\lambda(h_t) : \mathscr{M} \longrightarrow \mathscr{M}$. However, nothing excludes in such a general setting the additional action of a time-parameterized family of elements of Diff $(\mathscr{M}, \mathscr{M})$, say $t \longmapsto \tilde{h}_t : \mathscr{M} \longrightarrow \mathscr{M}$, with $\tilde{h}_0 = \textit{identity}$, smooth with respect to time, an action excluded by definition in the class of changes in observers discussed in the previous section. Let us write υ for the velocity $\frac{d}{dt} \tilde{h}_t \mid_{t=0}$. The relation (2), i.e. the change $\dot{\upsilon} \longrightarrow \dot{\upsilon}^*$, becomes

$$\dot{\upsilon} \longrightarrow \dot{\upsilon}^{\#} := \dot{\upsilon} + \upsilon + \frac{1}{2} \mathscr{A}(\upsilon)\, \text{curl}\bar{v},$$

  where $\frac{1}{2}\text{curl}\bar{v}$ is the spin of the velocity $\bar{v}$; it plays the role of q in (2).
- Finally, over the reference space we may consider the action of a time-parameterized class of elements of Diff$(\mathscr{E}^3, \mathscr{E}^3)$. Then we define smooth maps $t \longmapsto \hat{h}_t : \mathscr{E}^3 \longrightarrow \mathscr{E}^3$, with $\hat{h}_t \in \text{Diff}(\mathscr{E}^3, \mathscr{E}^3)$ and $h_0 = \textit{identity}$ and write $\bar{w}$ for the velocity $\frac{d}{dt} \hat{h}_t \mid_{t=0}$. The relation (3), i.e. the change $w \longrightarrow w^*$, becomes

$$w \longrightarrow w^{\#} := w + \bar{w}.$$

7 External Power: Consequence of the Invariance Under Isometry-Based Changes in Observers

According to standard instances, even in the generalized setting discussed here we can assume that actions determined by microstructural changes are subdivided into bulk and contact families as it happens for the standard macroscopic ones.

Let us call **part** of the body in its reference place any subset of $\mathscr{B}$ with non-vanishing volume and the same (geometric) regularity of $\mathscr{B}$ itself.

We define the **power of external actions on a generic part** of $\mathscr{B}$ (**external power** in short) as the functional $\mathscr{P}^{ext}_{\mathfrak{b}}$, linear on the rates $\dot{y}$ and $\dot{\upsilon}$ and additive over disjoint

parts, given by

$$\mathscr{P}^{ext}_{\mathfrak{b}}(\dot{y},\dot{\nu}) := \int_{\mathfrak{b}} \left(b^{\ddagger}\cdot\dot{y}+\beta^{\ddagger}\cdot\dot{\nu}\right) dx + \int_{\partial\mathfrak{b}} (\mathfrak{t}\cdot\dot{y}+\tau\cdot\dot{\nu})\, d\mathscr{H}^2,$$

where $b^{\ddagger}(x) \in T^*_{u(x)}\mathscr{B}_a$ represents body forces (the sum of inertial and non-inertial components) and $\mathfrak{t}(x) \in T^*_{u(x)}\mathscr{B}_a$ is the traction through the boundary of $\mathfrak{b}$; $\tau(x) \in T^*_{\tilde{\nu}(x)}\mathscr{M}$ indicates microstructural contact actions, while $\beta^{\ddagger}(x) \in T^*_{\tilde{\nu}(x)}\mathscr{M}$ their external bulk counterparts over the microstructure alone. $d\mathscr{H}^2$ is the "surface" measure over $\partial\mathfrak{b}$.

By assumption $\mathfrak{t}$ and τ depend on both x and n at every instant t.

When we write such an expression of the power, we presume that the reference shape is fixed once and for all. We then subordinate $\mathscr{P}^{ext}_{\mathfrak{b}}$ to an axiom of invariance.

Axiom of power invariance [21]: The external power on a generic part $\mathfrak{b}$ or the whole $\mathscr{B}$ is invariant under isometry-based changes in observers, i.e.

$$\mathscr{P}^{ext}_{\mathfrak{b}}(\dot{y},\dot{\nu}) = \mathscr{P}^{ext}_{\mathfrak{b}}\left(\dot{y}^*,\dot{\nu}^*\right)$$

for any choice of c and q.

The axiom has stringent consequences.

Theorem 1 *The invariance of the external power under isometry-based changes in observers implies the following statements:*

1. *The integral balances*

$$\int_{\mathfrak{b}} b^{\ddagger} dx + \int_{\partial\mathfrak{b}} \mathfrak{t}\, d\mathscr{H}^2 = 0,$$
$$\int_{\mathfrak{b}} \left((y-y_0)\times b^{\ddagger} + \mathscr{A}^*\beta^{\ddagger}\right) dx + \int_{\partial\mathfrak{b}} \left((y-y_0)\times\mathfrak{t}+\mathscr{A}^*\tau\right) d\mathscr{H}^2 = 0,$$

   where $\mathscr{A}^*$ is the formal adjoint of $\mathscr{A}$, i.e. $\mathscr{A}^*(\nu) \in \mathrm{Hom}\left(T_{\nu}\mathscr{M}, \mathbb{R}^3\right)$, hold [21].
2. *The standard traction (here expressed in Lagrangian representation) satisfies the action-reaction principle:*

$$\mathfrak{t}(x,n) = -\mathfrak{t}(x,-n).$$

3. *The microstructural contact actions satisfy a non-standard action-reaction principle [23]:*

$$\mathscr{A}^*(\tau(x,n)+\tau(x,-n)) = 0.$$

4. *If $\mathfrak{t}(\cdot,n)$ is a continuous function of x and the standard bulk actions are bounded over the body $\mathfrak{t}(x,\cdot)$, a function of n, is homogeneous and additive, i.e. there exists a second-rank tensor field $x \longmapsto P(x)$ such that (Cauchy's theorem in referential*

form)

$$\mathfrak{t}(x, n) = P(x)\, n(x),$$

where

$$P(x) = \sum_{K=1}^{3} \mathfrak{t}(x, e_K) \otimes e_K \in \mathrm{Hom}(T_x^*\mathscr{B}, T_{u(x)}^* u(\mathscr{B}))$$

is the ***first Piola-Kirchhoff stress*** *and e_K is the kth vector of a basis in a neighborhood of x.*

5. *If $\tau(\cdot, n)$ is a continuous function of x and $\mathscr{A}^*\beta^{\ddagger}$ is bounded over $\mathscr{B}$, together with the standard bulk actions, $\tau(x, \cdot)$, a function of n, is homogeneous and additive, i.e. there exists a second-rank tensor field $x \longmapsto \mathscr{S}(x)$ such that*

$$\tau(x, n) = \mathscr{S}(x)\, n(x),$$

where

$$\mathscr{S}(x) = \sum_{K=1}^{3} \tau(x, e_K) \otimes e_K \in \mathrm{Hom}(T_x^*\mathscr{B}, T_v^*\mathscr{M})$$

is the so-called ***microstress*** *[23].*

6. *If the fields $x \longmapsto P$ and $x \longmapsto \mathscr{S}$ are in $C^1(\mathscr{B}) \cap C\left(\bar{\mathscr{B}}\right)$ and the fields $x \longmapsto b$, $x \longmapsto \beta^{\ddagger}$ are continuous over $\mathscr{B}$, the pointwise balance of forces*

$$\mathrm{Div}P + b^{\ddagger} = 0$$

holds and there exists a field $x \longmapsto z(x) \in T_v^*\mathscr{M}$ such that

$$\mathrm{Div}\mathscr{S} + \beta^{\ddagger} - z = 0$$

and

$$\mathrm{Skw}PF^* = \frac{1}{2}\mathsf{e}\left(\mathscr{A}^* z + \left(D\mathscr{A}^*\right)\mathscr{S}\right)$$

[21].

7. *The equation*

$$\mathscr{P}_{\mathfrak{b}}^{ext}(\dot{y}, \dot{v}) = \int_{\mathfrak{b}} \left(P \cdot \dot{F} + z \cdot \dot{v} + \mathscr{S} \cdot \dot{N}\right) dx$$

holds and we call ***internal*** *(or* ***inner****)* ***power*** *the right-hand side term.*

- z is a local action, the one of the microstructure "inside" the material element at x over itself. $\mathscr{S}$ measures the first-neighbor interactions due to inhomogeneous microstructural changes among neighboring material elements.
- If we would start from the relation in the item 7 of the theorem as a first principle–it would correspond to a principle of virtual power, when we allow the rates to be even virtual–we would impose the existence of the self-action and the stresses, in other words, we would presume a priori the structure of the balance equations.
- Item 1 in the theorem indicates that the assumption a priori of the existence of an independent *integral* balance of microstructural actions is superfluous. The circumstance that such actions appear in the (generalized) balance of torques does not imply at all that they are couples for the presence of the linear operator $\mathscr{A}^*$. In other words, per se the microstructural actions are not necessarily couples, while their projection through $\mathscr{A}^*$ into the ambient physical space generates couples.
- In the local balance of microstructural actions there is an intrinsic indetermination. In fact, the balance can be augmented by an arbitrary element of the kernel of $\mathscr{A}^*$. Such an ambiguity disappears when we impose covariance, along any path summarized in the second part of the list already discussed.
- In the finite-strain elastic case and in statics there are existence theorems in the unified theory. A general existence result appears in [25]; its proof requires the embedding of the manifold $\mathscr{M}$ into a linear space. However, notwithstanding the lack of uniqueness of the embedding already remarked, we find existence for any embedding. A previous result is in [33] and deals with the micromorphic case in which $\mathscr{M}$ is identified with a linear space. The coercivity assumption is weaker then the one adopted in [25]. However, the energy considered in reference [33] has just a decomposed structure (it is less general than the energy analyzed in [25]), which allows the weaker coercivity assumption. A more general existence result, obtained **without** embedding $\mathscr{M}$ in any linear space, but taking it as a complete Riemannian manifold and considering **multi-valued** microstructural descriptor maps (values defined to within a permutation), included in Ginzburg-Landau-type energies, appears in [15]. When we include inertia effects, existence theorems are available for special theories, such as liquid crystals (see, e.g., [7]).
- We may extend the traditional assumption that the bulk action $b^{\ddagger}$ admits an additive decomposition into inertial, b^{in}, and noninertial, b, components to the bulk microstructural actions, presuming an analogous decomposition $\beta^{\ddagger} = \beta + \beta^{in}$, identifying then the inertial components b^{in} and β^{in} by postulating that their power equals the negative of the kinetic energy time derivative for any choice of the rates involved. In the present multi-field setting, we commonly assume that the kinetic energy is the sum of standard and microstructural contributions (see results and discussions in [4, 5, 21]). I do not add here further details.

8 Presence of Macroscopic Material Mutations: The Relative Power

Let us relax the idea that the reference place is fixed once and for all. This choice becomes physically weighty when we consider structural irreversible changes in the material structure, which frustrate even partially the one-to-one correspondence between the reference shape and the actual one at each instant. Examples are nucleation and/or evolution relative to the rest of the body of fractures or bulk inhomogeneities along a motion. At a given instant the actual shape of a body is not in one-to-one correspondence with the initially chosen reference shape but with a copy of it differing by the (virtual) pre-image of the defect.

A way of describing such circumstances is to make use of **multiple reference shapes**. However, instead of considering a family of infinitely many possible reference shapes for the body under scrutiny, it suffices to introduce a sort of **infinitesimal generator** of the family itself: a (not necessarily integrable) vector field

$$x \longmapsto w := \tilde{w}(x) \in \mathbb{R}^3$$

over the reference shape. Then we define a power relative to the virtual rate w. The definition considers three key aspects: (1) the velocities $\dot{y}$ and w are not in the same space so we have to push forward w in the ambient space or to pull back $\dot{y}$ into the reference space to compare them; (2) an effect of the mutation is the rupture and reformation of the material bonds so that we may include configurational forces and couples, the latter ones determined also by possible changes in the material symmetry; (3) a mutation alters the energetic landscape.

To define what I call **relative power** [23] we need then to consider the following ingredients:

(a) the *free energy* ψ that we presume to be a differentiable function of x, t, and a list ς of state variables that we leave here *undetermined*–no constitutive equations enter into play–and
(b) bulk configurational forces f with dissipative nature and couples μ, which have, in contrast, both dissipative and conservative components.

We then define **relative power** the functional $\mathscr{P}^{rel}_{\mathfrak{b}}$ defined by

$$\mathscr{P}^{rel}_{\mathfrak{b}}(\dot{y}, \dot{\nu}, w) := \mathscr{P}^{rel-a}_{\mathfrak{b}}(\dot{y}, \dot{\nu}, w) + \mathscr{P}^{dis}_{\mathfrak{b}}(w)$$

with

$$\begin{aligned}\mathscr{P}^{rel}_{\mathfrak{b}}(\dot{y}, \dot{\nu}, w) := &\int_{\mathfrak{b}} b^{\ddagger} \cdot (\dot{y} - Fw)\, dx + \int_{\partial\mathfrak{b}} \mathfrak{t} \cdot (\dot{y} - Fw)\, d\mathscr{H}^2 \\ &+ \int_{\mathfrak{b}} \beta^{\ddagger} \cdot (\dot{\nu} - Nw)\, dx + \int_{\partial\mathfrak{b}} \tau \cdot (\dot{\nu} - Nw)\, d\mathscr{H}^2,\end{aligned}$$

and

$$\mathscr{P}_{\mathfrak{b}}^{dis}(w) := \int_{\partial\mathfrak{b}} (n\cdot w)\,\psi\, d\mathscr{H}^2 - \int_{\mathfrak{b}} (\partial_x\psi + f)\cdot w\, dx + \int_{\mathfrak{b}} \mu\cdot \mathrm{curl} w\, dx.$$

Above, $\partial_x\psi$ is the *explicit derivative* of $\psi = \tilde{\psi}(x,t,\varsigma)$ with respect to x, holding fixed ς. It accounts for the inhomogeneity in the energy landscape, altered by the mutation. The term $(n\cdot w)\,\psi$ is the flux energy density across the boundary $\partial\mathfrak{b}$, due to the mutation itself.

As for the external power, we subordinate $\mathscr{P}_{\mathfrak{b}}^{rel}$ to an axiom of invariance.

Axiom of invariance for the relative power [23]: *The relative power is invariant under isometry-based changes in observers, i.e.*

$$\mathscr{P}_{\mathfrak{b}}^{rel}(\dot{y},\dot{v},w) = \mathscr{P}_{\mathfrak{b}}^{rel}\left(\dot{y}^*,\dot{v}^*,w^*\right)$$

for any choice of $c, q, \bar{c}, \bar{q}$, *and any part* $\mathfrak{b}$

Even in this case we have stringent consequences.

Theorem 2 *The assumed invariance of the relative power under isometry-based changes in observers implies the validity of* ***the results 1-to-6 in Theorem*** *1 and the following* ***additional*** *statements [23]:*

(i) The integral configurational balances

$$\begin{aligned}
&\int_{\partial\mathfrak{b}} \mathbb{P} n\, d\mathscr{H}^2 - \int_{\mathfrak{b}} \left(F^* b^{\ddagger} + N^*\beta^{\ddagger}\right) dx - \int_{\mathfrak{b}} (\partial_x\psi + f)\, dx = 0,\\
&\int_{\partial\mathfrak{b}} (x-x_0)\times \mathbb{P} n\, d\mathscr{H}^2 - \int_{\mathfrak{b}} (x-x_0)\times \left(F^* b^{\ddagger} + N^*\beta^{\ddagger}\right) dx\\
&\quad - \int_{\mathfrak{b}} (x-x_0)\times(\partial_x\psi + f)\, dx + \int_{\mathfrak{b}} 2\mu dx = 0,
\end{aligned}$$

where $\mathbb{P} := \psi I - F^*P - N^*\mathscr{S}$, *with* I *the second-rank unit tensor, hold.*

(ii) If the field $x \longmapsto \mathbb{P}$ *is in* $C^1(\mathscr{B}) \cap C\left(\bar{\mathscr{B}}\right)$ *and* $x \longmapsto F^* b$, $x \longmapsto f$, $x \longmapsto \partial_x\psi$ *are continuous over* $\mathscr{B}$, *the pointwise configurational balances*

$$\begin{aligned}
\mathrm{Div}\mathbb{P} - F^* b^{\ddagger} - N^*\beta^{\ddagger} + \partial_x\psi &= f,\\
\mathrm{Skw}(g^{-1}\mathbb{P}) &= -2\bar{\mathrm{e}}\mu,
\end{aligned}$$

with $\bar{\mathrm{e}}$ *Ricci's symbol with all contravariant components, namely* $\bar{\mathrm{e}}^{ABC}$, *hold.*

(iii) The equation

$$\mathscr{P}_{\mathfrak{b}}^{rel}(\dot{y},\dot{v},w) = \int_{\mathfrak{b}} \left(P\cdot\dot{F} + z\cdot\dot{v} + \mathscr{S}\cdot\dot{N} + \mathbb{P}\cdot Dw + \mu\cdot\mathrm{curl} w\right) dx$$

holds and we call ***extended internal*** *(or* ***inner****)* ***power*** *the right-hand side term.*

9 Covariance of the Second Law

We have already discussed the notion of covariance and the way we can use it to derive balance equations. Traditionally it is called upon in conservative setting. First time it has been adopted in dissipative setting in a 2013 theorem [22], which deals with multiplicative finite-strain plasticity. That theorem can be extended to the multi-field setting discussed here. I show below in short the path to be followed. Details are yet unpublished.

9.1 Covariance Principle in Dissipative Setting

Let $B \leq 0$ be in short an expression of the second law for a given observer $\mathscr{O}$. Another observer, $\mathscr{O}'$, evaluate an inequality of the type $B' \leq 0$, with $B \neq B'$ in general. By pulling back or pushing forward the expression of one observer into the frame(s) of the other, we get inequalities like $B + B^{\dagger} \leq 0$ or $B + B^{\ddagger} \leq 0$.

The principle: *In any diffeomorphism-based change in observer, when we project the mechanical dissipation inequality evaluated by an observer into the frame defining the other, the additional term arising along the process is* **always non-positive**.

9.2 An Extended Expression of the Mechanical Dissipation Inequality

A key point is the explicit expression of the inequality $B \leq 0$. What I suggest here is restricted to the isothermal setting and is an extended expression of the mechanical dissipation inequality. It reads

$$B\left(\dot{y}, \dot{v}, w; \psi, \mathfrak{b}\right) := \frac{d}{dt}\int_{\mathfrak{b}} \psi \, dx - \mathscr{P}^{rel}_{\mathfrak{b}}\left(\dot{y}, \dot{v}, w\right) \leq 0. \tag{4}$$

The procedure to evaluate its structural covariance follows the steps below.

- Select the list of state variables appearing as entries of the energy–so far they have been left not specified in the expression of the relative power–restricting them by the help of objectivity assumptions (see [26, 42, 44–46] for the pertinent techniques). In particular, besides the presence of the spatial and material metrics, in the list of state variables the metric on $\mathscr{M}$ may appear when we consider $\mathscr{M}$ endowed with a metric structure as in the case it is Riemannian.
- Assume **covariance** (tensoriality) **of the free energy**. Formally, it means that we impose at every instant t the identity

$$\psi = \psi \circ \left(\hat{h}_t \times h_t \times \left(\lambda\left(h_t\right) \times \tilde{h}_t\right)\right),$$

where the symbol $\circ$ indicates as above standard map composition and $(\hat{h}_t \times h_t \times (\lambda\,(h_t) \times \tilde{h}_t))$ summarizes the combined action of $\hat{h}_t$, h_t, $(\lambda\,(h_t)\,, \tilde{h}_t)$, those of diffeomorphism-based changes in observers over reference and ambient spaces, and the manifold $\mathscr{M}$ of microstructural shapes, respectively. In particular, it is useful to express in terms of the time derivative of ψ, adapting to the setting discussed here the pertinent expression introduced in [22].

- Impose the covariance principle in dissipative setting to the mechanical dissipation inequality (4), written in terms of relative power.

The results that we find are

(1) the existence of the stress and the microstress, the latter one obtained without embedding the manifold of microstructural shapes into a linear space;
(2) the need of a bulk inner microstructural self-action to assure local balances;
(3) pointwise balances of standard, microstructural and configurational balance equations;
(4) a priori constitutive restrictions.

They all emerge from a unique invariance requirement.

Notice that, in general, under diffeomorphism-based changes of frames, as described above, since ψ is a density with respect to the volume measure, we should have

$$\psi = \det(D\hat{h}_t)\psi \circ (\hat{h}_t \times h_t \times (\lambda\,(h_t) \times \tilde{h}_t)).$$

The assumed covariance implies

$$\det(D\hat{h}_t) = 1,$$

i.e. that $\hat{h}_t$ must be isocoric, *independently of the material nature of the body*. Such a restriction on the changes in observers, that is exactly the one adopted in computing the horizontal variation of the energy in calculus of variations (see results in finite-strain elasticity in the treatise [19]), agrees also with the axiom of permanence of the material typology under changes in observers.

Acknowledgments This research is part of the activities of the research group in 'Theoretical Mechanics' of the 'Centro di Ricerca Matematica Ennio De Giorgi' of the Scuola Normale Superiore in Pisa. The support of GNFM-INDAM is acknowledged.

References

1. Antman, S.S.: Nonlinear Problems of Elasticity. Springer, Berlin (1995)
2. Antman, S.S., Osborn, J.E.: The principle of virtual work and integral laws of motion. Arch. Ration. Mech. Anal. **69**, 231–262 (1979)
3. Brown Jr, W.F.: Micromagnetics. Wiley (1963)

4. Capriz, G.: Continua with Microstructure. Springer, Berlin (1989)
5. Capriz, G., Giovine, P.: On microstructural inertia. Math. Mod. Meth. Appl. Sci. **7**, 211–216 (1997)
6. Capriz, G., Mazzini, G.: Invariance and balance in continuum mechanics. In: Nonlinear Analysis and Continuum Mechanics, pp. 27–35. Springer, New York (1998)
7. Coutaud, D., Shkoller, S.: Well-posedness of the full Ericksen-Leslie model of nematic liquid crystals. CRAS Mat. **333**, 919–934 (2001)
8. de Fabritiis, C., Mariano, P.M.: Geometry of interactions in complex bodies. J. Geom. Phys. **54**, 301–323 (2005)
9. De Gennes, P.-G., Prost, J.: The Physics of Liquid Crystals. Oxford University Press, Oxford (1993)
10. Doi, M., Edwards, S.F.: The Theory of Polymer Dynamics. Oxford University Press, Oxford (1986)
11. Ericksen, J.L.: Theory of anisotropic fluids. Trans. Soc. Rheol. **4**, 29–39 (1960)
12. Ericksen, J.L.: Conservation laws for liquid crystals. Trans. Soc. Rheol. **5**, 23–34 (1961)
13. Ericksen, J.L.: Liquid crystals with variable degree of orientation. Arch. Ration. Mech. Anal. **113**, 97–120 (1991)
14. Ericksen, J.L., Truesdell, C.A.: Exact theory of stress and strain in rods and shells. Arch. Ration. Mech. Anal. **1**, 295–323 (1958)
15. Focardi, M., Mariano, P.M., Spadaro, E.N.: Multi-value microstructural descriptors for complex materials: analysis of ground states. Arch. Ration. Mech. Anal. **215**, 899–933 (2015)
16. Germain, P.: The method of virtual power in continuum mechanics, Part 2: microstructure. SIAM J. Appl. Math. **25**, 556–575 (1973)
17. Giaquinta, M., Mariano, P.M., Modica, G.: A variational problem in the mechanics of complex materials. Dis. Cont. Dyn. Sys.—A **28**, 519–537 (2010)
18. Giaquinta, M., Mariano, P.M., Modica, G., Mucci, D.: Ground states of simple bodies that may undergo brittle fracture. Phys. D **239**, 1485–1502 (2010)
19. Giaquinta, M., Modica, G., Souček, J.: Cartesian currents in the calculus of variations, voll I and II. Springer, Berlin (1998)
20. Levine, D., Steinhardt, P.J.: Quasicrystals: a new class of ordered structures. Phys. Rev. Lett. **53**, 2477–2480 (1984)
21. Mariano, P.M.: Multifield theories in mechanics of solids. Adv. Appl. Mech. **38**, 1–93 (2002)
22. Mariano, P.M.: Covariance in plasticity. Proc. R. Soc. Lond. A **469**, 20130073 (1–17) (2013)
23. Mariano, P.M.: Mechanics of material mutations. Adv. Appl. Mech. **XX**, 1–92 (2014)
24. Mariano, P.M., Galano, L.: Fundamentals of the Mechanics of Solids. Birkhäuser Verlag, Boston (2015)
25. Mariano, P.M., Modica, G.: Ground states in complex bodies. ESAIM—Control, Optim. Calc. Var. **15**, 377–402 (2009)
26. Marsden, J.E., Hughes, T.R.J.: Mathematical Foundations of Elasticity. Prentice Hall Inc., Englewood Cliffs (1983)
27. Mermin, N.D.: The topological theory of defects in ordered media. Rev. Mod. Phys. **51**, 591–648 (1979)
28. Michel, L.: Symmetry defects and broken symmetry. Configurations. Hidden symmetry. Rev. Mod. Phys. **52**, 617–651 (1980)
29. Mielke, A.: On thermodynamically consistent models and gradient structures for thermoplasticity. GAMM-Mitt. **34**, 51–58 (2011)
30. Milton, G.W.: The Theory of Composites. Cambridge University Press, Cambridge (2002)
31. Nash, J.F.: C^1 isometric imbeddings. Ann. Math. **60**, 383–396 (1954)
32. Nash, J.F.: The imbedding problem for Riemannian manifold. Ann. Math. **63**, 20–63 (1956)
33. Neff, P.: Existence of minimizers for a finite-strain micromorphic elastic solid. Proc. R. Soc. Edinb. **136A**, 997–1012 (2006)
34. Noll, W.: A mathematical theory of the mechanical behavior of continuous media. Arch. Ration. Mech. Anal. **2**, 197–226 (1958)

35. Noll, W.: La Mécanique classique, basée sur une axiome d'objectivité, pp. 47-56 of La Méthode Axiomatique dans les Mécaniques Classiques et Nouvelles (Colloque International, Paris, 1959), Gauthier-Villars, Paris (1963)
36. Noll, W.: The Foundations of Mechanics and Thermodynamics. Springer, Berlin (1974)
37. Noll, W.: Translation of Walter Noll's "Derivation of the fundamental equations of continuum thermodynamics from statistical mechanics", translated by Richard B. Lehoucq and Anatole Von Lilienfeld-Toal. J. Elast. **100**, 5–24 (2010)
38. Pitteri, M.: On a statistical-kinetic model for generalized continua. Arch. Ration. Mech. Anal. **111**, 99–120 (1990)
39. Rożko, E.E., Sławianowski, J.J.: Essential nonlinearity in field theory and continuum mechanics. Second- and first-order generally-covariant models. J. Geom. Symmetry Phys. **34**, 51–76 (2014)
40. Saint-Raymond, L.: Hydrodynamic limits of the Boltzmann equation, Lecture Notes in Mathematics. Springer, Berlin (2009)
41. Shechtman, D., Blech, I., Gratias, D., Cahn, J.W.: Metallic phase with long-range orientational order and no translational symmetry. Phys. Rev. Lett. **53**, 1951–1954 (1984)
42. Šilhavý, M.: The Mechanics and Thermodynamics of Continuous Media. Springer, Berlin (1997)
43. Sławianowski, J.: Geometry of Phase Spaces. PWN-Polish Scientific Publishers, Warszawa, and Wiley, Chichester (1991)
44. Truesdell, C.A.: A First Course in Rational Continuum Mechanics. Academic Press, New York (1977)
45. Truesdell, C.A., Noll, W.: The Non-Linear Field Theories of Mechanics, 3rd edn. Springer, Berlin (2004)
46. Truesdell, C.A., Toupin, R.A.: Classical field theories of mechanics. In: Handbuch der Physics, pp. 226–793. Springer, Berlin (1960)
47. Whitney, H.: Differentiable manifolds. Ann. Math. **37**, 645–680 (1936)

A Refined Theory of the Layered Medium with the Slip at the Interface

Ilia S. Nikitin and Nikolay G. Burago

Abstract The equations for layered medium with slippage are obtained using the asymptotic method of homogenisation. The terms of second order respectively the small parameter of layer thickness are taken into account. The linear slip condition defines the dependence between the tangential jumps of displacements at the contact boundary and the shear stresses. The derived equations introduce asymptotically complete generalization of some models of layered media, which are based on the engineering approach or approximate hypotheses about the nature of the inter-layer deformation. Such generalized models are needed in the study of static and dynamic deformations of layered rock media. The wave properties of the resulting system of equations and dispersion relations for harmonic waves are described. The propagation of Rayleigh surface waves along the elastic layered half-plane boundary is investigated.

1 Introduction

The interest to the problem of propagation and transformation of waves in layered media is initiated by the seismology and engineering geophysics. As a rule the seismicity is observed in rock regions. Often these rocks contain regular grid of cracks which can be considered as layered structures. Classical studies of wave fields in such media usually are based on assumption of continuity of displacement fields. But for rather strong seismic actions the possibility of tangential displacement jumps at the inter-layer boundaries should be taken in to account. For long time actions it needs to

I.S. Nikitin (✉)
Institute for Computer Aided Design, 2nd Brestskaya street, 19/18,
Moscow, Russia
e-mail: i_nikitin@list.ru

N.G. Burago
Ishlinski Institute for Problems in Mechanics RAS, Vernadskogo 101-1,
Moscow, Russia
e-mail: burago@ipmnet.ru

B. Albers and M. Kuczma (eds.), *Continuous Media with Microstructure 2*,
DOI 10.1007/978-3-319-28241-1_6

use the "averaged" models of structured continuum media because of impossibility to trace deformations of each structural layer.

In our study by using asymptotic method [1, 6] the refined equations of layered medium with slippage are derived. The second order terms relatively small parameter of layer thickness are taken in to account. The linear slip relation between tangential displacement jumps at inter-layer boundaries and shear stresses is used. The zero order approximate equations for such media has been derived earlier in [3, 4]. The proposed here new equations represent complete generalization of layered media models [5, 7], which are based on engineering approaches or on approximate hypothesizes about layer deformations. Such generalized models are required for static and dynamic problems of rock media deformations and for dynamic wave propagation problems in geophysics. It should be noted also that the theory of layered media is suitable for description of composite materials with soft (rubber) sublayers between major more rigid (metallic) layers.

The properties of proposed refined system of equations are studied. The propagation of longitudinal, transversal and surface Rayleigh waves in layered media is investigated in refined settings.

2 Refined Equations

Consider infinite layered medium using Cartesian rectangular coordinate system (x_1, x_2, x_3). The axis x_3 is perpendicular to the planes of parallel flat boundaries between layers. Let the inter-layer boundaries have coordinates $x_3 = x^{(s)} = s\varepsilon$ $(s = 0, \pm 1, \pm 2, ...)$, where constant layer thickness $\varepsilon \ll 1$ is a small parameter. To say more exactly, the relation $\varepsilon / l \ll 1$ should be valid, here l is the size of distributed load application range, for instance, wave length in the processes under consideration. In such case all spatial values should be made dimensionless using this value l.

Assume that layer boundaries are always compressed and the following conditions are valid

$$\sigma_{33} < 0, \ [u_3] = [\sigma_{\gamma 3}] = [\sigma_{33}] = 0$$

Here $\sigma_{\gamma 3} = k_*[u_\gamma]$ is linear slippage of Winkler type, $k_*\varepsilon = k = O(1)$. Square brackets $[f] = f|_{x^{(s)}+0} - f|_{x^{(s)}-0}$ designate the jump of a value f at inter-layer boundary. Such conditions are valid approximately if the soft sublayers of thickness δ $(\delta/\varepsilon \ll 1)$ with small shear modulus μ_δ are present between layers. In this case we have

$$\sigma_{\gamma 3} = k[u_\gamma]/\varepsilon = \frac{k\delta}{\varepsilon}\frac{[u_\gamma]}{\delta} = \mu_\delta \frac{[u_\gamma]}{\delta}$$

Here $[u_\gamma]/\delta$ is shear deformation of soft sublayer. In this case $\mu_\delta = k\delta/\varepsilon$ or vise versa $k = \mu_\delta \varepsilon/\delta$. It is possible to say that is inter-layer shear connection coefficient. The layers themselves are elastic isotropic and subjected to Hooke's law

$$x_3 \neq x^{(s)} : \ \sigma_{ij,j} - \rho u_{i,tt} = 0, \ \sigma_{ij} = C_{ijkl} u_{k,l}$$

Here the elastic moduli tensor is

$$C_{ijkl} = \lambda \delta_{ij}\delta_{kl} + \mu(\delta_{ik}\delta_{jl} + \delta_{il}\delta_{jk})$$

According to the method of asymptotic homogenisation [1] let's introduce fast variable $\xi = x_3/\varepsilon$. According to [1] assume that $u_k = u_k(x_l, \xi, t)$ is a function, which is smooth regarding slow variables x_l and continuous regarding fast variable ξ, excluding points $\xi^{(s)} = x^{(s)}/\varepsilon$, where it may have jumps of first kind. Besides, along ξ the displacement is 1-periodic $[[u_i]] = u_i|_{\xi^{(s)}+1/2} - u_i|_{\xi^{(s)}-1/2} = 0$. Accounting such choice of variables and the differentiation rule for complex functions, the system of equations for cell of periodicity $x^{(s)} - 1/2 \le x_3 \le x^{(s)} + 1/2$, $-1/2 \le \xi \le 1/2$ may be rewritten as

$$\varepsilon^{-2} C_{i3k3} u_{k,\xi\xi} + \varepsilon^{-1}(C_{ijk3} u_{k,j\xi} + C_{i3kl} u_{k,l\xi}) + C_{ijkl} u_{k,lj} - \rho u_{i,tt} = 0$$

where $x_3 \neq x^{(s)}, \ \xi \neq 0$. At $x_3 = x^{(s)}, \ \xi = 0$ we use the contact conditions

$$\varepsilon^{-1} C_{33k3} u_{k,\xi} + C_{33kl} u_{k,l} < 0$$

$$[u_3] = 0, [\varepsilon^{-1} C_{i3k3} u_{k,\xi} + C_{i3kl} u_{k,l}] = 0, \ \ \varepsilon^{-1} C_{\gamma 3k3} u_{k,\xi} + C_{\gamma 3kl} u_{k,l} = k_* [u_\gamma]$$

The conditions of 1-periodicity are

$$[[u_i]] = u_i|_{\xi+1/2} - u_i|_{\xi-1/2} = 0$$

Here and farther greek indices (β,γ) take values 1 and 2, latine indices take values 1, 2, 3. The displacements are represented as asymptotic series regarding small parameter ε:

$$u_i = u_i^{(0)}(x_k, \xi, t) + \varepsilon u_i^{(1)}(x_k, \xi, t) + \varepsilon^2 u_i^{(2)}(x_k, \xi, t) + \varepsilon^3 u_i^{(3)}(x_k, \xi, t) + \cdots$$

Introduce the operation of averaging $\langle f \rangle$ for the function of fast variable ξ, which will be often used farther: $\langle f \rangle = \int_{-1/2}^{1/2} f d\xi$. Displacement approximations should satisfy the additional condition $\left\langle u_k^{(n)} \right\rangle = 0$ [1].

Substitute this representation into the theory of elasticity equations. Equating to zero the term with negative power ε^{-2} we get that zero approximation $u_i^{(0)}$ is independent on the fast variable ξ and $u_i^{(0)} = w_i(x_k, t)$. Equating to zero the term

with negative power ε^{-1} we get that first approximation $u_i^{(1)}$ satisfies the equation $C_{i3k3}u^{(1)}_{k,\xi\xi} = 0$. The resulting system of differential equations is:

$$\begin{aligned} &C_{ijkl}w_{k,jl} + C_{ijk3}u^{(1)}_{k,j\xi} + (C_{i3kl}u^{(1)}_{k,l} + C_{i3k3}u^{(2)}_{k,\xi})_{,\xi} \\ &\quad + \varepsilon\left[C_{ijkl}u^{(1)}_{k,jl} + C_{ijk3}u^{(2)}_{k,j\xi} + (C_{i3kl}u^{(2)}_{k,l} + C_{i3k3}u^{(3)}_{k,\xi})_{,\xi}\right] \\ &\quad + \varepsilon^2\left[C_{ijkl}u^{(2)}_{k,jl} + C_{ijk3}u^{(3)}_{k,j\xi} + (C_{i3kl}u^{(3)}_{k,l} + C_{i3k3}u^{(4)}_{k,\xi})_{,\xi}\right] + \cdots \\ &= \rho w_{i,tt} + \varepsilon\rho u^{(1)}_{i,tt} + \varepsilon^2\rho u^{(2)}_{i,tt} + \cdots \end{aligned}$$

A similar representation for stress tensor components is:

$$\sigma_{ij} = \sigma^{(0)}_{ij} + \varepsilon\sigma^{(1)}_{ij} + \varepsilon^2\sigma^{(2)}_{ij} + \cdots$$

where $\sigma^{(n)}_{ij} = C_{ijkl}u^{(n)}_{k,l} + C_{ijk3}u^{(n+1)}_{k,\xi}$.

All approximations for stresses are 1-periodic functions of ξ. In particular, the relation $\sigma^{(n)}_{i3} = C_{i3kl}u^{(n)}_{k,l} + C_{i3k3}u^{(n+1)}_{k,\xi}$ and conditions $[\sigma^{(n)}_{i3}] = 0$, $[[\sigma^{(n)}_{i3}]] = 0$ are valid. It is easy to see that $\left\langle \sigma^{(n),\xi}_{i3} \right\rangle = 0$.

Accounting the terms of definite order of ε, applying the averaging operation $\langle f \rangle$ and excluding the dependence on fast variable ξ, we get the model of a homogenised layered medium with slippage of Winkler type.

Let's derive the refined theory of second order. For this in the system of equations we keep the terms of order ε^2. Applying averaging operation $\langle\rangle$ for periodicity cell to the system of equations we get the following:

$$C_{ijkl}w_{k,jl} + C_{ijk3}\left\langle u^{(1)}_{k,\xi}\right\rangle_{,j} + \varepsilon C_{ijk3}\left\langle u^{(2)}_{k,\xi}\right\rangle_{,j} + \varepsilon^2 C_{ijk3}\left\langle u^{(3)}_{k,\xi}\right\rangle_{,j} = \rho w_{i,tt}$$

It is the final refined system of equations for layered medium with slippage. For complete formulations it needs to find the functions $\left\langle u^{(n)}_{k,\xi}\right\rangle$ (*n = 1, 2, 3*), which participate in the system. Every function $u_i^{(n)}(x_k, \xi, t)$ (*n = 1, 2, 3*) is found from the appropriate task in periodicity cell $(-1/2 \le \xi \le 1/2)$ [1], which is formulated by equating to zero the sum of terms of definite order ε^{n-1} in asymptotic system of equations. Additional conditions for these functions can be received by reformulating the contact inter-layer conditions for each function: conditions of 1-periodicity $[[u_i^{(n)}]] = 0$ and conditions $\left\langle u_i^{(n)}\right\rangle = 0$. Let's formulate these three tasks for the cell $(-1/2 \le \xi \le 1/2)$.

2.1 Task in Cell for n = 1

At $|\xi| < 1/2$: $C_{i3k3}u^{(1)}_{k,\xi\xi} = 0$.

At $\xi = 0$: $[C_{i3k3}u^{(1)}_{k,\xi}] = 0$, $[u^{(1)}_3] = 0$, $k[u^{(1)}_\gamma] = C_{\gamma 3kl}w_{k,l} + C_{\gamma 3k3}u^{(1)}_{k,\xi}$.

Additional conditions are: $[[u^{(1)}_i]] = 0$, $\left\langle u^{(1)}_i \right\rangle = 0$.

Dropping details, published in [2], write the solution of task 1 on the periodicity cell:

$u^{(1)}_\gamma = \phi_\gamma(\xi - sign\xi/2), u^{(1)}_3 = 0$, where $\phi_\gamma = -\tau_\gamma/(k+\mu)$, $\tau_\gamma = \mu(w_{\gamma,3}+w_{3,\gamma})$.

The derivatives needed for averaging are:

$$u^{(1)}_{3,\xi} = 0,\ u^{(1)}_{\gamma,\xi} = \phi_\gamma,$$
$$\left\langle u^{(1)}_{3,\xi} \right\rangle = 0,\ \left\langle u^{(1)}_{\gamma,\xi} \right\rangle = \phi_\gamma$$

2.2 Task in Cell for n = 2

At $|\xi| < 1/2$ have

$$C_{ijkl}w_{k,jl} + C_{ijk3}u^{(1)}_{k,j\xi} + (C_{i3kl}u^{(1)}_{k,l} + C_{i3k3}u^{(2)}_{k,\xi})_{,\xi} = \rho w_{i,tt}$$

Averaging this differential equation and accounting that

$$\left\langle (C_{i3kl}u^{(1)}_{k,l} + C_{i3k3}u^{(2)}_{k,\xi})_{,\xi} \right\rangle = 0$$

and that the rest terms of this equation do not depend on ξ, we get its simple consequence:

$$C_{i3k3}u^{(2)}_{k,\xi\xi} = -C_{i3kl}u^{(1)}_{k,\xi l}$$

At $\xi = 0$ have

$$[C_{i3k3}u^{(2)}_{k,\xi}] = -[C_{i3kl}u^{(1)}_{k,l}],\ [u^{(2)}_3] = 0,\ k[u^{(2)}_\gamma] = C_{\gamma 3kl}u^{(1)}_{k,l} + C_{\gamma 3k3}u^{(2)}_{k,\xi}$$

Additional conditions are $[[u^{(2)}_i]] = 0$, $\left\langle u^{(2)}_i \right\rangle = 0$.

Dropping details (see in [2]), write the solution of task 2 on periodicity cell

$$u^{(2)}_\gamma = -\psi_\gamma(\xi^2 - \xi sign\xi + 1/6)/2, u^{(2)}_3 = -\psi_3(\xi^2 - \xi sign\xi + 1/6)/2$$

where $\psi_\gamma = \phi_{\gamma,3}$, $\psi_3 = \lambda\phi_{\beta,\beta}/(\lambda + 2\mu)$

Derivatives needed for averaging are

$$u^{(2)}_{\gamma,\xi} = -\psi_\gamma(\xi - sign\xi/2),\ u^{(2)}_{3,\xi} = -\psi_3(\xi - sign\xi/2),\ \left\langle u^{(2)}_{3,\xi}\right\rangle = 0,\ \left\langle u^{(2)}_{\gamma,\xi}\right\rangle = 0$$

Hence second approximations for displacements are absent in refined system of equations.

2.3 Task in Cell for $n = 3$

At $|\xi| < 1/2$ have

$$C_{i3k3}u^{(3)}_{k,\xi\xi} = -C_{ijkl}u^{(1)}_{k,jl} - C_{i3kl}u^{(2)}_{k,\xi l} - C_{ijk3}u^{(2)}_{k,\xi j} + \rho u^{(1)}_{i,tt}$$

At $\xi = 0$ have

$$[C_{i3k3}u^{(3)}_{k,\xi}] = -[C_{i3kl}u^{(2)}_{k,l}],\ [u^{(3)}_3] = 0,\ k[u^{(3)}_\gamma] = C_{\gamma 3kl}u^{(2)}_{k,l} + C_{\gamma 3k3}u^{(3)}_{k,\xi}.$$

Additional conditions are $[[u^{(3)}_i]] = 0, \left\langle u^{(3)}_i\right\rangle = 0$

Consider solution for cases $i = \gamma$. The elasticity moduli tensor is

$$C_{ijkl}u^{(1)}_{k,jl} = C_{\gamma j\beta l}u^{(1)}_{\beta,jl}$$

$$= (\lambda\delta_{\gamma j}\delta_{\beta l} + \mu\delta_{\gamma\beta}\delta_{jl} + \mu\delta_{\gamma l}\delta_{j\beta})u^{(1)}_{\beta,jl} = (\lambda+\mu)u^{(1)}_{\beta,\beta\gamma} + \mu u^{(1)}_{\gamma,ll}$$

$$(C_{\gamma 3kl} + C_{\gamma lk3})u^{(2)}_{k,\xi l} = \left((\lambda+\mu)\delta_{\gamma l}\delta_{3k} + 2\mu\delta_{\gamma k}\delta_{3l}\right)u^{(2)}_{k,\xi l} = (\lambda+\mu)u^{(2)}_{3,\xi\gamma} + 2\mu u^{(2)}_{\gamma,\xi 3}$$

Task equation for $|\xi| < 1/2$ is

$$u^{(3)}_{\gamma,\xi\xi} = u^{(1)}_{\gamma,ll} - (\lambda+\mu)u^{(1)}_{\beta,\beta\gamma}/\mu - 2u^{(2)}_{\gamma,\xi 3} - (\lambda+\mu)u^{(2)}_{3,\xi\gamma}/\mu + \rho u^{(1)}_{i,tt}/\mu$$

At $\xi = 0$ have following conditions

$$[u^{(3)}_{\gamma,\xi}] = -[u^{(2)}_{\gamma,3} + u^{(2)}_{3,\gamma}] = 0$$
$$k[u^{(3)}_\gamma] = \mu(u^{(2)}_{\gamma,3} + u^{(2)}_{3,\gamma} + u^{(3)}_{\gamma,\xi})$$
$$[[u^{(3)}_\gamma]] = 0, \left\langle u^{(3)}_\gamma\right\rangle = 0$$

The equation may be rewritten as

$$u^{(3)}_{\gamma,\xi\xi} = \chi_\gamma\,(\xi - sign\xi/2)$$

where $\chi_\gamma = -\phi_{\gamma,ll} - (\lambda+\mu)\phi_{\beta,\beta\gamma}/\mu + 2\psi_{\gamma,3} + (\lambda+\mu)\psi_{3,\gamma}/\mu + \rho\phi_{\gamma,tt}/\mu$.
Integrating and accounting conditions for $\xi = 0$, we get [2]

$$u^{(3)}_{\gamma,\xi} = \chi_\gamma\left(\xi^2 - \xi sign\xi\right)/2 + \left(k\chi_\gamma + \mu\psi_{\gamma,3} + \mu\psi_{3,\gamma}\right)/(k+\mu)/12$$

Finally the expression for refined derivative is

$$\left\langle u^{(3)}_{\gamma,\xi}\right\rangle = \mu\left(\phi_{\gamma,\beta\beta} + (3\lambda+2\mu)\phi_{\beta,\beta\gamma}/(\lambda+2\mu) - \rho\phi_{\gamma,tt}/\mu\right)/(k+\mu)/12$$

Now consider solution for case $i = 3$. The elasticity moduli tensor is

$$C_{3jkl}u^{(1)}_{k,jl} = C_{3j\beta l}u^{(1)}_{\beta,jl} = (\lambda\delta_{3j}\delta_{\beta l} + \mu\delta_{3\beta}\delta_{jl} + \mu\delta_{3l}\delta_{j\beta})u^{(1)}_{\beta,jl} = (\lambda+\mu)u^{(1)}_{\beta,\beta 3}$$

$$(C_{33kl} + C_{3lk3})u^{(2)}_{k,\xi l} = ((\lambda+3\mu)\delta_{3l}\delta_{3k} + (\lambda+\mu)\delta_{kl})\,u^{(2)}_{k,\xi l}$$

$$= 2(\lambda+2\mu)u^{(2)}_{3,\xi 3} + (\lambda+\mu)u^{(2)}_{\beta,\xi\beta}$$

Task equation for $|\xi| < 1/2$ is

$$u^{(3)}_{3,\xi\xi} = -(\lambda+\mu)u^{(1)}_{\beta,\beta 3}/(\lambda+2\mu) - 2u^{(2)}_{3,\xi 3} - (\lambda+\mu)u^{(2)}_{\beta,\xi\beta}/(\lambda+2\mu)$$

$\xi = 0$: $[u^{(3)}_{3,\xi}] = -[u^{(2)}_{3,3}] - \lambda[u^{(2)}_{\beta,\beta}]/(\lambda+2\mu) = 0$
$u^{(2)}_3 = 0$, $[[u^{(3)}_3]] = 0$, $\left\langle u^{(3)}_3\right\rangle = 0$.
The equation may be rewritten as:

$$u^{(3)}_{3,\xi\xi} = \chi_3\,(\xi - sign\xi/2)$$

Here $\chi_3 = (\lambda+\mu)\psi_{\beta,\beta}/(\lambda+2\mu) + 2\psi_{3,3} - (\lambda+\mu)\phi_{\beta,\beta 3}/(\lambda+2\mu)$.
Integrating and accounting conditions for $\xi = 0$ we get [2]

$$u^{(3)}_{3,\xi} = \chi_3(\xi^2 - \xi sign\xi + 1/6)/2, \left\langle u^{(3)}_{3,\xi}\right\rangle = 0.$$

Finally the expressions for refined derivatives are

$$\left\langle u^{(3)}_{\gamma,\xi}\right\rangle = \frac{1}{12}\frac{\mu}{(k+\mu)}\left(\phi_{\gamma,\beta\beta} + \frac{3\lambda+2\mu}{\lambda+2\mu}\phi_{\beta,\beta\gamma} - \frac{\rho}{\mu}\phi_{\gamma,tt}\right), \left\langle u^{(3)}_{3,\xi}\right\rangle = 0.$$

3 Variants of Averaged System of Equations

Now we can formulate the refined system of equations for layered medium with slippage (latine indices *i, j, k, l* = 1, 2, 3; greek indices $\beta,\ \gamma$ = 1, 2):

$$C_{\gamma jkl}w_{k,jl} + C_{\gamma jk3}\left\langle u^{(1)}_{k,\xi}\right\rangle_{,j} + \varepsilon^2 C_{\gamma jk3}\left\langle u^{(3)}_{k,\xi}\right\rangle_{,j} = \rho w_{\gamma,tt}$$
$$C_{3jkl}w_{k,jl} + C_{3jk3}\left\langle u^{(1)}_{k,\xi}\right\rangle_{,j} + \varepsilon^2 C_{3jk3}\left\langle u^{(3)}_{k,\xi}\right\rangle_{,j} = \rho w_{3,tt}$$

Accounting the elastic moduli tensor the terms of this system of equations are written as

$$C_{\gamma jkl}w_{k,jl} = (\lambda+\mu)w_{k,k\gamma} + \mu w_{\gamma,kk}, \quad C_{3jkl}w_{k,jl} = (\lambda+\mu)w_{k,k3} + \mu w_{3,kk}$$

$$C_{\gamma jk3}\left\langle u^{(1)}_{k,\xi}\right\rangle_{,j} = C_{\gamma j\beta 3}\left\langle u^{(1)}_{\beta,\xi}\right\rangle_{,j} = \mu\phi_{\gamma,3}$$

$$C_{3jk3}\left\langle u^{(1)}_{k,\xi}\right\rangle_{,j} = C_{3j\beta 3}\left\langle u^{(1)}_{\beta,\xi}\right\rangle_{,j} = \mu\phi_{\beta,\beta}$$

$$C_{\gamma jk3}\left\langle u^{(3)}_{k,\xi}\right\rangle_{,j} = \mu\left\langle u^{(3)}_{\gamma,\xi}\right\rangle_{,3}$$

$$= \mu^2\left(\phi_{\gamma,\beta\beta 3} + (3\lambda+2\mu)\phi_{\beta,\beta\gamma 3}/(\lambda+2\mu) - \rho\phi_{\gamma,tt3}/\mu\right)/(k+\mu)/12$$

$$C_{3jk3}\left\langle u^{(3)}_{k,\xi}\right\rangle_{,j} = \left\langle u^{(3)}_{\beta,\xi}\right\rangle_{,\beta}$$

$$= \mu^2\left(4(\lambda+\mu)\phi_{\beta,\beta\alpha\alpha}/(\lambda+2\mu) - \rho\phi_{\beta,\beta tt}/\mu\right)/(k+\mu)/12$$

Finally refined system of equations is

$$\begin{aligned}
&(\lambda+\mu)w_{k,k\gamma} + \mu w_{\gamma,kk} + \mu\phi_{\gamma,3}\\
&\quad + \varepsilon^2\mu^2\left(\phi_{\gamma,\beta\beta 3} + (3\lambda+2\mu)\phi_{\beta,\beta\gamma 3}/(\lambda+2\mu) - \rho\phi_{\gamma,tt3}/\mu\right)/(k+\mu)/12 = \rho w_{\gamma,tt}\\
&(\lambda+\mu)w_{k,k3} + \mu w_{3,kk} + \mu\phi_{\beta,\beta}\\
&\quad + \varepsilon^2\mu^2\left(4(\lambda+\mu)\phi_{\beta,\beta\alpha\alpha}/(\lambda+2\mu) - \rho\phi_{\beta,\beta tt}/\mu\right)/(k+\mu)/12 = \rho w_{3,tt}
\end{aligned}$$

Remind that $\phi_\gamma = -\mu(w_{\gamma,3}+w_{3,\gamma})/(k+\mu)$. In general equations the expressions for ϕ_γ are not substituted to avoid the unnecessary complexity of formulas. It is seen that regarding spatial variables this is the system of forth order for the displacements w_k and it contains mixed time derivatives.

The system of equations is simplified for the case of ideal slipping contact between layers $k = 0$.

$$\begin{aligned}
&(\lambda+\mu)w_{k,k\gamma} + \mu w_{\gamma,kk} + \mu\phi_{\gamma,3}\\
&\quad + \varepsilon^2\mu\left(\phi_{\gamma,\beta\beta 3} + (3\lambda+2\mu)\phi_{\beta,\beta\gamma 3}/(\lambda+2\mu) - \rho\phi_{\gamma,tt3}/\mu\right)/12 = \rho w_{\gamma,tt}\\
&(\lambda+\mu)w_{k,k3} + \mu w_{3,kk} + \mu\phi_{\beta,\beta}\\
&\quad + \varepsilon^2\mu\left(4(\lambda+\mu)\phi_{\beta,\beta\alpha\alpha}/(\lambda+2\mu) - \rho\phi_{\beta,\beta tt}/\mu\right)/12 = \rho w_{3,tt}\\
&\phi_\gamma = -(w_{\gamma,3} + w_{3,\gamma})
\end{aligned}$$

Separately we formulate plane (2D) dynamic system of equations

$$
\begin{aligned}
&(\lambda+2\mu)w_{1,11}+\left(\lambda+\frac{k\mu}{k+\mu}\right)w_{3,13}+\frac{k\mu}{k+\mu}w_{1,33}\\
&-\frac{\varepsilon^2\mu^3}{3(k+\mu)^2}\frac{(\lambda+\mu)}{(\lambda+2\mu)}\left(w_{1,1133}+w_{3,3111}\right)\\
&+\frac{\rho\varepsilon^2\mu^2}{12(k+\mu)^2}\left(w_{1,33tt}+w_{3,31tt}\right)=\rho w_{1,tt}\\
&(\lambda+2\mu)w_{3,33}+\left(\lambda+\frac{k\mu}{k+\mu}\right)w_{1,13}+\frac{k\mu}{k+\mu}w_{3,11}\\
&-\frac{\varepsilon^2\mu^3}{3(k+\mu)^2}\frac{(\lambda+\mu)}{(\lambda+2\mu)}\left(w_{1,1113}+w_{3,1111}\right)\\
&+\rho\frac{\varepsilon^2\mu^2}{12(k+\mu)^2}\left(w_{1,13tt}+w_{3,11tt}\right)=\rho w_{3,tt}
\end{aligned}
$$

and quasi-static 2D system of equations

$$
\begin{aligned}
&(\lambda+2\mu)w_{1,11}+\left(\lambda+\frac{k\mu}{k+\mu}\right)w_{3,13}+\frac{k\mu}{k+\mu}w_{1,33}\\
&-\frac{\varepsilon^2\mu^3}{3(k+\mu)^2}\frac{(\lambda+\mu)}{(\lambda+2\mu)}\left(w_{1,1133}+w_{3,3111}\right)=0\\
&(\lambda+2\mu)w_{3,33}+\left(\lambda+\frac{k\mu}{k+\mu}\right)w_{1,13}+\frac{k\mu}{k+\mu}w_{3,11}\\
&-\frac{\varepsilon^2\mu^3}{3(k+\mu)^2}\frac{(\lambda+\mu)}{(\lambda+2\mu)}\left(w_{1,1113}+w_{3,1111}\right)=0
\end{aligned}
$$

Finally 1D dynamic or quasi-static system of equations for bending of layered massive (case $w_1=0$,$w_3=w_3(x_1,t)$) takes the view

$$
\frac{\varepsilon^2\mu^3}{3(k+\mu)^2}\frac{(\lambda+\mu)}{(\lambda+2\mu)}w_{3,1111}-\frac{k\mu}{k+\mu}w_{3,11}-\rho\frac{\varepsilon^2\mu^2}{12(k+\mu)^2}w_{3,11tt}+\rho w_{3,tt}=0
$$

for dynamics, and

$$
\frac{\varepsilon^2\mu^3}{3(k+\mu)^2}\frac{(\lambda+\mu)}{(\lambda+2\mu)}w_{3,1111}-\frac{k\mu}{k+\mu}w_{3,11}=0
$$

for quasi-statics. Formulas for stress tensor components are

$$
\begin{aligned}
&\sigma_{ij}^{(0)}=C_{ijkl}w_{k,l}+C_{ijk3}u_{k,\xi}^{(1)}\\
&\sigma_{ij}^{(0)}=\lambda\delta_{ij}w_{k,k}+\mu(w_{i,j}+w_{j,i})+\mu(\phi_i\delta_{j3}+\phi_j\delta_{i3})
\end{aligned}
$$

$$\sigma_{ij}^{(1)} = C_{ijkl}u_{k,l}^{(1)} + C_{ijk3}u_{k,\xi}^{(2)}$$
$$\sigma_{ij}^{(1)} = \left(\lambda\delta_{ij}\phi_{k,k} + \mu(\phi_{i,j} + \phi_{j,i}) - \lambda\delta_{ij}\psi_3 - \mu(\psi_i\delta_{j3} + \psi_j\delta_{i3})\right)(\xi - sign\xi/2)$$

where $\phi_3 = 0$, $\phi_\gamma = -\mu(w_{\gamma,3} + w_{3,\gamma})/(k+\mu)$, $\psi_\gamma = \phi_{\gamma,3}$, $\psi_3 = \lambda\phi_{\beta,\beta}/(\lambda+2\mu)$.

Boundary conditions for loaded surface are

$$\sigma_{ij}^{(0)} \cdot n_j = P_i, \quad \sigma_{ij}^{(1)} \cdot n_j = 0$$

In some problems for definite orientations of boundary normal vector the boundary condition of first order converts into identity. In such cases the boundary condition of second order should be used: $\sigma_{ij}^{(2)} \cdot n_j = 0$.

4 Wave Properties of Layered Medium with Slippage at Inter-layer Boundaries

Below the propagation of plane harmonic and surface Rayleigh waves in layered media is considered.

4.1 Plane Harmonic Waves

Let's define the properties of harmonic waves propagating in arbitrary direction regarding layer orientation at arbitrary inter-layer connection coefficient k. 2D dynamic system of equations for the medium under consideration is

$$\begin{aligned}
&(\lambda+2\mu)w_{1,11} + \left(\lambda + \frac{k\mu}{k+\mu}\right)w_{3,13} + \frac{k\mu}{k+\mu}w_{1,33} \\
&\quad - \frac{\varepsilon^2\mu^3}{3(k+\mu)^2}\frac{(\lambda+\mu)}{(\lambda+2\mu)}\left(w_{1,1133} + w_{3,3111}\right) \\
&\quad + \rho\frac{\varepsilon^2\mu^2}{12(k+\mu)^2}\left(w_{1,33tt} + w_{3,31tt}\right) = \rho w_{1,tt} \\
&(\lambda+2\mu)w_{3,33} + \left(\lambda + \frac{k\mu}{k+\mu}\right)w_{1,13} + \frac{k\mu}{k+\mu}w_{3,11} \\
&\quad - \frac{\varepsilon^2\mu^3}{3(k+\mu)^2}\frac{(\lambda+\mu)}{(\lambda+2\mu)}\left(w_{1,1113} + w_{3,1111}\right) \\
&\quad + \rho\frac{\varepsilon^2\mu^2}{12(k+\mu)^2}\left(w_{1,13tt} + w_{3,11tt}\right) = \rho w_{3,tt}
\end{aligned}$$

These equations may be rewritten as

$$(\lambda+2\mu)w_{1,11}+\lambda w_{3,13}+\tilde{\mu}(w_{1,3}+w_{3,1})_{,3}-\varepsilon^2\mu\beta_1\left(w_{1,3}+w_{3,1}\right)_{,113}$$
$$+\rho\varepsilon^2\beta_2\left(w_{1,3}+w_{3,1}\right)_{,3tt}=\rho w_{1,tt}$$
$$(\lambda+2\mu)w_{3,33}+\lambda w_{1,13}+\tilde{\mu}(w_{1,3}+w_{3,1})_{,1}-\varepsilon^2\mu\beta_1\left(w_{1,3}+w_{3,1}\right)_{,111}$$
$$+\rho\varepsilon^2\beta_2\left(w_{1,3}+w_{3,1}\right)_{,1tt}=\rho w_{3,tt}$$

Introduce the additional variables

$$U=w_{1,3}+w_{3,1}$$
$$V=\tilde{\mu}U-\varepsilon^2\mu\beta_1U_{,11}+\rho\varepsilon^2\beta_2U_{,tt}$$

The system of equations takes the following view

$$\left((\lambda+2\mu)w_{1,11}-\rho w_{1,tt}\right)+\lambda w_{3,13}+V_{,3}=0$$
$$\lambda w_{1,13}+\left((\lambda+2\mu)w_{3,33}-\rho w_{3,tt}\right)+V_{,1}=0$$
$$w_{1,3}+w_{3,1}-U=0$$
$$\tilde{\mu}u-\varepsilon^2\beta_2(\mu_*u_{,11}+\rho u_{,tt})-V=0$$

Here the following designations are introduced

$$\tilde{\mu}=\mu\frac{k}{k+\mu},\ \beta=\frac{\mu}{k+\mu},\ \beta_1=\frac{\lambda+\mu}{\lambda+2\mu}\beta^2/3,\ \beta_2=\beta^2/12,\ \mu_*=\mu\beta_1/\beta_2$$

We seek the solution of this system of equations as harmonic waves propagating in the direction $n=(n_1,n_3)$ with frequency ω and wave number $\kappa=\kappa n=(\kappa_1,\kappa_3)$

$$w_1=Ae^{i(\kappa_1x_1+\kappa_3x_3-\omega t)},\ w_3=Be^{i(\kappa_1x_1+\kappa_3x_3-\omega t)}$$
$$U=Ce^{i(\kappa_1x_1+\kappa_3x_3-\omega t)},\ V=De^{i(\kappa_1x_1+\kappa_3x_3-\omega t)}$$

where $\kappa_1=\kappa n_1$, $\kappa_3=\kappa n_3$, $|\kappa|=\kappa$, $|n|=1$, $k=2\pi/l$ is the wave number, l is harmonic wave length, $\varepsilon k=2\pi\varepsilon/l$, $\varepsilon^2k^2=4\pi^2(\varepsilon/l)^2$. The value $\varepsilon/l\ll1$ is a small parameter. In result we get the system of homogeneous algebraic equations

$$\left((\lambda+2\mu)\kappa_1^2+\mu_\varepsilon\kappa_3^2-\rho\omega^2\right)A+(\lambda+\mu_\varepsilon)\kappa_1\kappa_3B=0$$
$$(\lambda+\mu_\varepsilon)\kappa_1\kappa_3A+\left((\lambda+2\mu)\kappa_3^2+\mu_\varepsilon\kappa_1^2-\rho\omega^2\right)B=0$$

Here $\mu_\varepsilon=\tilde{\mu}+\varepsilon^2\beta_2(\mu_*\kappa_1^2-\rho\omega^2)$. Condition of the solvability for this algebraic system gives the equation for propagation velocities of harmonic waves in the medium under consideration:

$$\zeta^4-\left(1+\frac{\mu_\varepsilon}{(\lambda+2\mu)}\right)\zeta^2+\frac{\mu_\varepsilon}{(\lambda+2\mu)}+4\frac{(\lambda+\mu)}{(\lambda+2\mu)}\frac{(\mu-\mu_\varepsilon)}{(\lambda+2\mu)}n_1^2n_3^2=0$$

Here $\zeta^2 = \rho c^2/(\lambda + 2\mu) = c^2/c_1^2$, $c = \omega/\kappa$ is the phase velocity of wave propagation in layered medium, $c_1 = \sqrt{(\lambda + 2\mu)/\rho}$ and $c_2 = \sqrt{\mu/\rho}$ are velocities of elastic longitudinal and transverse waves in a homogeneous elastic medium.

Let α ($n_1 = \sin\alpha$) is the angle of wave propagation direction. For some values of α the biquadratic equation has exact solution.

At $\alpha = 0$ have $\zeta_1 = 1$ and $\zeta_2 = \sqrt{\tilde{\mu}}\Big/\sqrt{(\lambda + 2\mu)(1 + \varepsilon^2\kappa^2\beta_2)}$ for quasi-longitudinal wave and for quasi-transversal wave respectively.

At $\alpha = \pi/4$ have $\zeta_1 = \sqrt{(\lambda + \mu + \tilde{\mu} + \varepsilon^2\kappa^2\beta_2\mu_*/2)}\Big/\sqrt{(\lambda + 2\mu)(1 + \varepsilon^2\kappa^2\beta_2)}$ and $\zeta_2 = \sqrt{\mu}\Big/\sqrt{(\lambda + 2\mu)}$ for quasi-longitudinal wave and for quasi-transversal wave respectively.

At $\alpha = \pi/2$ have $\zeta_1 = 1$ and $\zeta_2 = \sqrt{(\tilde{\mu} + \varepsilon^2\kappa^2\beta_2\mu_*)}\Big/\sqrt{(\lambda + 2\mu)(1 + \varepsilon^2\kappa^2\beta_2)}$ for quasi-longitudinal wave and for quasi-transversal wave respectively.

At arbitrary α the solution of this equation may be sought in assumed approximation $\sim \varepsilon^2$ as $\zeta^2 = \zeta_0^2 + \zeta_*^2\varepsilon^2 + o(\varepsilon^2)$.

Zero approximation $\zeta = \zeta_0^2$ is found from equation:

$$\zeta_0^4 - \left(1 + \frac{\tilde{\mu}}{(\lambda + 2\mu)}\right)\zeta_0^2 + \frac{\tilde{\mu}}{(\lambda + 2\mu)} + \frac{(\lambda + \mu)}{(\lambda + 2\mu)}\frac{(\mu - \tilde{\mu})}{(\lambda + 2\mu)}\sin^2 2\alpha = 0$$

Values ζ_0^2 which correspond to quasi-longitudinal and quasi-transversal waves in layered medium are:

$$\zeta_0^2 = 0.5\,(1 + \tilde{\mu}/(\lambda + 2\mu) \pm D_0)$$

where

$$D_0 = \sqrt{\frac{(\lambda + \mu)^2}{(\lambda + 2\mu)^2} + 2\frac{(\lambda + \mu)}{(\lambda + 2\mu)}\frac{(\mu - \tilde{\mu})}{(\lambda + 2\mu)}\cos 4\alpha + \frac{(\mu - \tilde{\mu})^2}{(\lambda + 2\mu)^2}}$$

The correction coefficient ζ_*^2 is:

$$\zeta_*^2 = \beta_2\kappa^2(\zeta_0^2 - \cos^2 2\alpha)\left(\frac{\mu_*}{(\lambda + 2\mu)}\sin^2\alpha - \zeta_0^2\right)\left(2\zeta_0^2 - \left(1 + \frac{\tilde{\mu}}{(\lambda + 2\mu)}\right)\right)^{-1}$$

Approximate values of phase velocities with accuracy ε^2 are

$$\zeta \approx \zeta_0\left(1 + \kappa^2\varepsilon^2\beta_2(\zeta_0^2 - \cos^2 2\alpha)\left(\zeta_0^2 - \frac{\mu_*}{(\lambda + 2\mu)}\sin^2\alpha\right)/2\zeta_0^2 D_0\right)$$

From these formulas it is seen that the velocities of harmonic waves have small dispersion ($\sim \kappa^2\varepsilon^2$) and depend on the wave direction parameter α.

Now investigate the limit cases of these formulas at $\varepsilon \to 0$ ($\mu_\varepsilon \to \tilde{\mu}$). Firstly it is the limit case of ideal inter-layer contact (case of homogeneous elastic medium): $k \to \infty$ ($\tilde{\mu} \to \mu$), and secondly it is the limit case of ideal inter-layer slipping $k \to 0$ ($\tilde{\mu} \to 0$).

Quasi-longitudinal waves (sign plus in formulas for ζ_0 and ζ).

In this case for $\varepsilon \to 0$: $\zeta \to \zeta_0$.

For $k \to \infty$: $\zeta_0 \to 1$ ($c \to c_1$), (elastic longitudinal wave in isotropic medium).

For $k \to 0$: $\zeta_0^2 \to 0.5\,(1 + D_1)$

Here

$$D_1 = \sqrt{\frac{(\lambda+\mu)^2}{(\lambda+2\mu)^2} + \frac{2(\lambda+\mu)\mu}{(\lambda+2\mu)^2}\cos 4\alpha + \frac{\mu^2}{(\lambda+2\mu)^2}}$$

For $\alpha = 0, \pi/2$: $\zeta_0 \to 1$,$c \to c_1$, (waves along and cross layers).

For $\alpha = \pi/4$:$\zeta_0 \to \sqrt{(\lambda+\mu)/(\lambda+2\mu)}$ (waves propagated under an angle to the layer boundary direction, minimal propagation velocity).

Quasi-transversal waves (sign minus in formulas for ζ_0 and ζ).

In this case for $\varepsilon \to 0$: $\zeta \to \zeta_0$.

For $k \to \infty$: $\zeta \to c_2/c_1$ ($c \to c_2$), (elastic transversal wave in isotropic medium).

For $k \to 0$: $\zeta_0^2 \to 0.5\,(1 - D_1)$.

For $\alpha = 0, \pi/2$: $\zeta_0 \to 0$, $c \to 0$, (waves along and cross layers).

For $\alpha = \pi/4$: $\zeta_0 \to c_2/c_1$, $c \to c_2$, (waves propagated under an angle to the layer boundary direction, maximal propagation velocity).

The dependence of propagation velocities for quasi-longitudinal and quasi-transversal waves on coefficients of inter-layer connection k are shown in Fig. 1. Upper graphs correspond to quasi-longitudinal waves, lower graphs correspond to quasi-transversal waves at various values of small parameter $\varepsilon/l = 0.5, 0.3, 0.1$. Dimensionless elastic moduli are defined as $\lambda/(\lambda + 2\mu) = \mu/(\lambda + 2\mu) = 1/3$.

Above each graph the value of wave direction angle $= 0, 30°, 60°, 90°$ is shown. For $= 0, 90°$ the solutions are described by exact formulas given above and shown in Fig. 1a, d. For other values of the solution of biquadratic equation for $\zeta = c/c_1$ is calculated numerically and shown in Fig. 1b, c.

From these graphs the level of plane wave dispersion can be seen (for small values of the coefficient of inter-layer connection) for various wave directions. The dependence of dispersion on the layer thickness parameter ε/l can also be seen there. It is possible to conclude that the dispersion plays role only for dimensionless coefficients of inter-layer connection $k/(\lambda + 2\mu) < 0.7$. It is mostly significant for directions $= 90°$ (along layers) of quasi-transversal waves (see Fig. 1d, lower graphs).

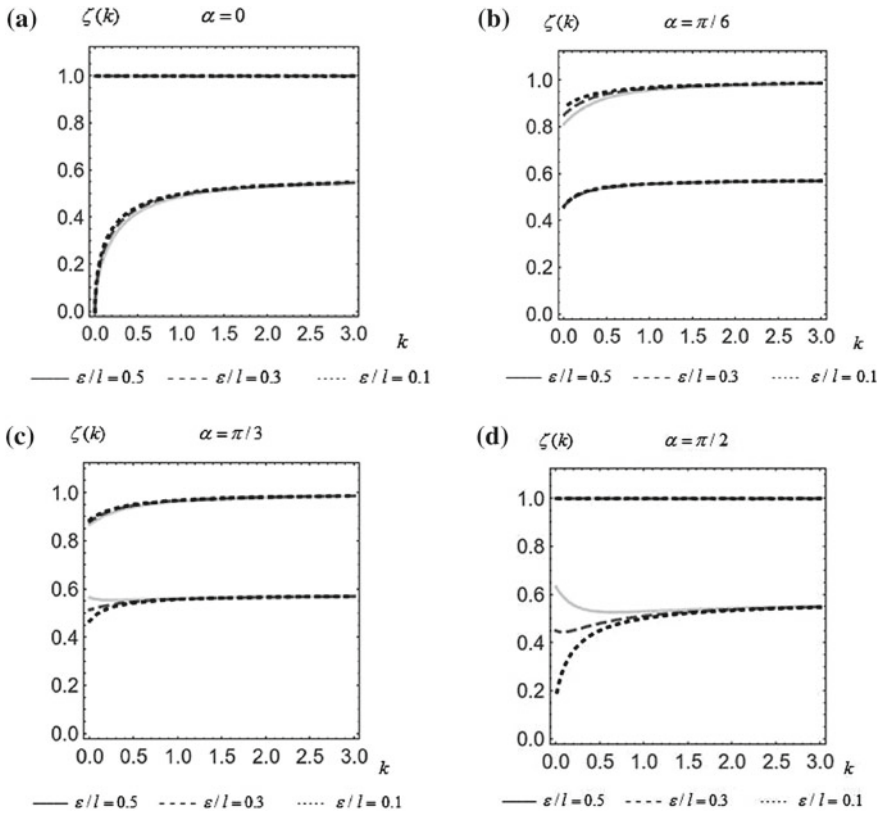

Fig. 1 The dependence of dimensionless velocities for quasi-longitudinal and quasi-transversal waves on coefficients of inter-layer connection k

4.2 Surface Rayleigh Waves

Consider surface waves on the boundary of layered half-plane $-\infty < x_3 \leq 0$, $-\infty < x_1 < \infty$ (plane task). The system of equations for displacements of layered medium with slippage at inter-layer boundaries is written earlier

$$\begin{aligned}
&\big((\lambda + 2\mu)w_{1,11} - \rho w_{1,tt}\big) + \lambda w_{3,13} + V_{,3} = 0\\
&\lambda w_{1,13} + \big((\lambda + 2\mu)w_{3,33} - \rho w_{3,tt}\big) + V_{,1} = 0\\
&w_{1,3} + w_{3,1} - U = 0,\ \tilde{\mu}U - \varepsilon^2\beta_2(\mu_* U_{,11} + \rho U_{,tt}) - V = 0
\end{aligned}$$

Boundary conditions at $x_3 = 0$

$$\sigma_{33} = (\lambda + 2\mu)w_{3,3} + \lambda w_{1,1} = 0,\ \sigma_{13} = \mu(w_{1,3} + w_{3,1}) = 0$$

At $x_3 \to -\infty$ have $w_1 \to 0$, $w_3 \to 0$.

Represent the solutions of this task as surface wave ($\gamma > 0$)

$$w_1 = Ae^{\gamma x_3} e^{i(\kappa_1 x_1 - \omega t)}, \; w_3 = Be^{\gamma x_3} e^{i(\kappa_1 x_1 - \omega t)}$$

Substituting this representation in to the system of differential equations we get the algebraic homogeneous system of equations

$$\begin{aligned} &\left(\mu_\varepsilon \gamma^2 - \kappa_1^2 \Delta_1\right) A + (\lambda + \mu_\varepsilon)\gamma i \kappa_1 B = 0 \\ &-\kappa_1^2 (\lambda + \mu_\varepsilon)\gamma A + \left((\lambda + 2\mu)\gamma^2 - \kappa_1^2 \Delta_{2\varepsilon}\right) i\kappa_1 B = 0 \end{aligned}$$

Here the following designations are used: $\mu_\varepsilon = \tilde{\mu} + \varepsilon^2 \beta_2 \kappa_1^2 \Delta_*$, $\Delta_* = \mu_* - \rho c^2$, $\Delta_1 = \lambda + 2\mu - \rho c^2$, $\Delta_{2\varepsilon} = \Delta_2 + \varepsilon^2 \beta_2 \kappa_1^2 \Delta_*$, $\Delta_2 = \tilde{\mu} - \rho c^2$.

Phase velocity of surface wave is $c = \omega/\kappa_1$. The solvability condition gives the biquadratic equation for γ

$$(\lambda + 2\mu)\mu_\varepsilon \gamma^4 - \kappa_1^2 \gamma^2 D_2 + \kappa_1^4 \Delta_1 \Delta_{2\varepsilon} = 0$$

where $D_2 = \mu_\varepsilon \Delta_{2\varepsilon} + (\lambda + 2\mu)\Delta_1 - (\lambda + \mu_\varepsilon)^2$.

From this equation we find two positive solutions$\gamma_{1,2} > 0$

$$\gamma_{1,2}^2 = \frac{\kappa_1^2 \left\{ D_2 \pm \sqrt{D_2^2 - 4(\lambda + 2\mu)\mu_\varepsilon \Delta_1 \Delta_{2\varepsilon}} \right\}}{2(\lambda + 2\mu)\mu_\varepsilon}$$

Then the solutions of task are

$$\begin{aligned} w_1 &= A_1 e^{\gamma_1 x_3} e^{i(\kappa_1 x_1 - \omega t)} + A_2 e^{\gamma_2 x_3} e^{i(\kappa_1 x_1 - \omega t)} \\ w_3 &= B_1 e^{\gamma_1 x_3} e^{i(\kappa_1 x_1 - \omega t)} + B_2 e^{\gamma_2 x_3} e^{i(\kappa_1 x_1 - \omega t)} \end{aligned}$$

where $i\kappa_1 B_{1,2} = \kappa_1^2 (\lambda + \mu_\varepsilon)\gamma_{1,2} A_{1,2} \left((\lambda + 2\mu)\gamma_{1,2}^2 - \kappa_1^2 \Delta_{2\varepsilon}\right)^{-1}$

Substituting these solutions into boundary conditions at $x_3 = 0$ get the system of equations

$$\begin{aligned} &\gamma_1 A_1 + \gamma_2 A_2 + i\kappa_1 B_1 + i\kappa_1 B_2 = 0 \\ &-\lambda \kappa_1^2 A_1 - \lambda \kappa_1^2 A_2 + (\lambda + 2\mu)\gamma_1 i\kappa_1 B_1 + (\lambda + 2\mu)\gamma_2 i\kappa_1 B_2 = 0 \end{aligned}$$

From this system of equations the amplitudes B_1 and B_2 may be excluded. Then we have two homogeneous equations regarding amplitudes A_1 and A_2. For simplification of expressions instead of $\gamma_{1,2} > 0$ introduce values $\eta_{1,2}$ from relations $\eta_{1,2} = \gamma_{1,2}/\kappa_1$. These values are defined by formulas

$$\eta_{1,2}^2 = \frac{D_2 \pm \sqrt{D_2^2 - 4(\lambda + 2\mu)\mu_\varepsilon \Delta_1 \Delta_{2\varepsilon}}}{2(\lambda + 2\mu)\mu_\varepsilon}$$

Homogeneous system of equations for amplitudes A_1 and A_2 is

$$\eta_1\left(1+\frac{(\lambda+\mu_\varepsilon)}{\left((\lambda+2\mu)\eta_1^2-\Delta_{2\varepsilon}\right)}\right)A_1+\eta_2\left(1+\frac{(\lambda+\mu_\varepsilon)}{\left((\lambda+2\mu)\eta_2^2-\Delta_{2\varepsilon}\right)}\right)A_2=0$$
$$\left(\frac{(\lambda+2\mu)(\lambda+\mu_\varepsilon)\eta_1^2}{\left((\lambda+2\mu)\eta_1^2-\Delta_{2\varepsilon}\right)}-\lambda\right)A_1+\left(\frac{(\lambda+2\mu)(\lambda+\mu_\varepsilon)\eta_2^2}{\left((\lambda+2\mu)\eta_2^2-\Delta_{2\varepsilon}\right)}-\lambda\right)A_2=0$$

For solvability the determinant of this system should be equal to zero. It gives the equation for unknown phase velocity of surface wave $c=\omega/\kappa_1$

$$4(\lambda+\mu)\eta_1\eta_2^2-\eta_2(1+\eta_2^2)\left((\lambda+2\mu)\eta_1^2+\lambda\eta_2^2\right)$$
$$-\frac{\Delta\mu_\varepsilon}{\mu}\left\{\eta_1\left((\lambda+2\mu)\eta_2^2+\lambda\right)+\eta_2(1+\eta_2^2)\left((\lambda+2\mu)\eta_1^2+\lambda\right)\right\}=0$$

Here we denote $\Delta\mu_\varepsilon=\mu-\mu_\varepsilon$. Again investigate the limit cases of this formula at $\varepsilon\to 0$ ($\mu_\varepsilon\to\tilde{\mu}$). In these cases

$$\eta_{1,2}^2=\frac{\tilde{D}_3\pm\sqrt{\tilde{D}_3^2-4(\lambda+2\mu)\tilde{\mu}\Delta_1\Delta_2}}{2(\lambda+2\mu)\tilde{\mu}}$$

where $\tilde{D}_3=\tilde{\mu}\Delta_2+(\lambda+2\mu)\Delta_1-(\lambda+\tilde{\mu})^2$.

The equation for surface wave propagation velocity is

$$4(\lambda+\mu)\eta_1\eta_2^2-\eta_2(1+\eta_2^2)\left((\lambda+2\mu)\eta_1^2+\lambda\eta_2^2\right)$$
$$-\frac{\mu}{(k+\mu)}\left\{\eta_1\left((\lambda+2\mu)\eta_2^2+\lambda\right)+\eta_2(1+\eta_2^2)\left((\lambda+2\mu)\eta_1^2+\lambda\right)\right\}=0$$

Case of ideal contact (ideal elastic medium)

In this case at $k\to\infty$ ($\tilde{\mu}\to\mu$):

$$\eta_1^2=1-c^2/c_1^2,\ \eta_2^2=1-c^2/c_2^2,\ \ 4(\lambda+\mu)\eta_1\eta_2-(1+\eta_2^2)\left((\lambda+2\mu)\eta_1^2+\lambda\eta_2^2\right)=0$$

After short transformation we come to classic Rayleigh wave:

$$4\sqrt{1-c^2/c_1^2}\sqrt{1-c^2/c_2^2}-(2-c^2/c_2^2)^2=0$$

Case of ideal inter-layer slipping

In this case at $k\to 0$ ($\tilde{\mu}\to 0$) treating μ_ε as small parameter we get:

$$\eta_1^2\sim\frac{4\mu(\lambda+\mu)-(\lambda+2\mu)\rho c^2}{(\lambda+2\mu)\mu_\varepsilon},\ \eta_2^2\sim\frac{(\lambda+2\mu-\rho c^2)(\mu_\varepsilon-\rho c^2)}{4\mu(\lambda+\mu)-(\lambda+2\mu)\rho c^2}$$
$$(3\lambda+2\mu)\eta_1\eta_2^2-2(\lambda+2\mu)\eta_1^2\eta_2(1+\eta_2^2)-\lambda\eta_2(1+\eta_2^2)^2-\lambda\eta_1=0$$

The graphs for dependence of dimensionless surface wave velocity c/c_1 on inter-layer connection coefficient k is shown in Fig. 2 for various values of layer thickness parameter $\varepsilon/l = 0.5, 0.3, 0.1$. As in previous case the wave number is $\kappa_1 = 2\pi/l$, where l is the length of harmonic surface wave. The asymptotic of classic Rayleigh root takes place for $k/(\lambda + 2\mu) > 1.5 \div 2$. These graphs are very similar to the lower graphs in Fig. 1d (quasi-transversal waves) for waves propagating along layers ($= 90°$) and very close to them. For classic Rayleigh waves, as it is known, $c_R/c_2 \approx 0.9$, the same relation is valid and in the case under consideration for ratio of velocity of surface waves to the velocity of quasi-transversal waves.

Remark that the applicability boundary of proposed asymptotic theory is not defined exactly. The upper boundary for small parameter $\varepsilon/l = 0.5$ is assumed quite approximately. Nevertheless, for inter-layer connection coefficients starting from values $k/(\lambda + 2\mu) > 0.7$, the calculations give very close meanings for propagation velocity of quasi-longitudinal, quasi-transversal and surface waves for the whole range of wave lengths $\varepsilon/l < 0.5$.

It should be noted that proposed refined theory may be used for investigation of transformation seismic waves exiting to the day surface in rock massifs with regular parallel crack grids accounting slippage at contact boundaries. Also this theory may be useful for description of composite materials with additional soft sublayers between more rigid layers.

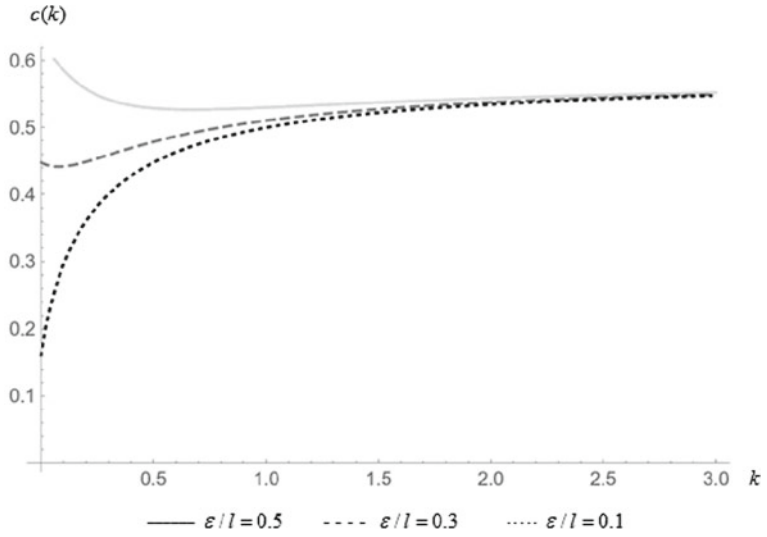

Fig. 2 The dependence of dimensionless surface wave velocity on inter-layer connection coefficient k

5 Conclusion

Using the asymptotic method of homogenisation the continuum theory of layered medium is built taking into account terms of second order accuracy regarding the small parameter of layer thickness. The linear slip contact condition is used to describe the relation between tangential displacement jumps and shear stresses. The wave properties of the proposed refined equations are studied, the dispersion relations are derived and the propagation of harmonic waves is investigated. The problem of surface Rayleigh like waves is solved.

Acknowledgments Authors are grateful to P.A. Yushkovsky and A.V. Ganshin for help in calculations. The work is supported by the Russian Foundation of Basic Research (project No. 15-08-02392).

References

1. Bakhvalov, N.S., Panasenko, G.P.: Averaging of Processes in Periodic Media. Nauka, Moscow (1984)
2. Burago, N.G., Nikitin, I.S., Yushkovsky, P.A.: Refined continuum model of layered medium with slippage at inter-layer boundaries. Preprint 1096. Ishlinsky Institute for Problems in Mechanics of Russian Academy of Sciences, Moscow (2015)
3. Nikitin, I.S.: Averaged equations of layered medium with nonlinear contact conditions of interlayer interaction. Izvestia AN SSSR. Solid Mech. **5**, 80–86 (1987)
4. Nikitin, I.S.: Dynamic models of layered and block media with slippage, friction and detachment. Izvestia RAN. Solid Mech. **4**, 154–165 (2008)
5. Salganik, R.L.: Approximation of continuum medium for description of layered massif deformation. Izvestia AN SSSR. Solid Mech. **3**, 48–56 (1987)
6. Sanchez-Palencia, E.: Nonhomogeneous Media and Vibration Theory. Springer, Berlin (1980)
7. Zvolinsky, N.V., Shkhinek, K.N.: Continuum model of layered medium. Izvestia AN SSSR. Solid Mech. **1**, 5–14 (1984)

Affinely Rigid Body and Affine Invariance in Physics

Jan Jerzy Sławianowski and Ewa Eliza Rożko

Abstract Discussed is the dynamics of affinely rigid body, i.e. of a mechanical system the configuration space of which is, roughly speaking, identical with the affine group. So, it is a system placed between two kinds of Euler equations: the rigid body and the ideal incompressible fluids. An essential novelty is our stress on models with the affinely-invariant kinetic energy. It turns out, it may be a toy model towards discussing the problem of affine, non-metrical invariance in fundamental physics, quantum theory and gravitation, and even the nuclear and cosmic physics. Quite independently of that, it may be shown that the affine geodetic model is able to describe the bounded vibrations of classical continua without any help of the external potential energy.

1 Introduction

It is well-known that very often some important and new mathematical and physical concepts and solutions appear in a consequence of unification of even quite different and mutually remote mathematical theories. Let us mention, e.g., the ergodic theory or probabilistic theories on algebraic structures [2–4, 16, 21]. Another example is the theory of dynamical systems defined on Lie groups or their homogeneous spaces. The algebraic structure of groups gives rise to the theory and classification of left-invariant and right-invariant dynamical systems. Let us mention, e.g., two important historical examples known as Euler equations [2, 3]. There are two kinds of them: the ordinary Euler equations of the rigid body motion, and the partial Euler equations for the ideal incompressible fluid. It is interesting that both of them were created

J.J. Sławianowski (✉)
Polish–Japanese Academy of Information Technology, Koszykowa str. 86,
02-008 Warsaw, Poland
e-mail: jslawian@pjwstk.edu.pl; jslawian@ippt.pan.pl

J.J. Sławianowski · E.E. Rożko
Institute of Fundamental Technological Research Polish Academy of Sciences,
Pawińskiego str. 5B, 02-106 Warsaw, Poland
e-mail: erozko@ippt.pan.pl

B. Albers and M. Kuczma (eds.), *Continuous Media with Microstructure 2*,
DOI 10.1007/978-3-319-28241-1_7

by the same person, just the famous mathematician Leonhard Euler. The rigid body kinetic energy and the corresponding equations of geodetic motion are invariant under the rotation group acting on itself through the left regular translations. When the rigid body is spherical then they are also right-invariant. And similarly, the Euler equations of the ideal incompressible fluid are right-invariant under the group of volume-preserving diffeomorphisms. Although this group is not a Lie group because of its infinite dimension, the general procedures of invariant systems on Lie groups may be at least formally used. This enabled one to guess some general expressions and hypotheses concerning the general solution and its properties. Once guessed in this way, they were later proved on an independent basis.

2 Lie Groups as Configuration Spaces

Let us now review some general principles of analytical mechanics on Lie groups. So, we assume that the configuration space Q is not any longer a general differential manifold, but rather a Lie group G, or perhaps some its infinite-dimensional analogue [3]. For simplicity we assume that it is linear, i.e., that it does possess a faithful finite-dimensional matrix representation. Let us mention, this restriction is not so academic as it might seem. Namely, for any $n > 2$, the universal covering groups $\overline{\mathrm{SL}}(n, \mathbb{R})$, $\overline{\mathrm{GL}}(n, \mathbb{R})$ fail to be linear. This has some influence on the concept of spinors, or rather on the attempts of affine generalization of the usual concept of spinors [34–38]. Being linear, G is a subgroup of some finite-dimensional matrix group, so $G \subset \mathrm{GL}(N, \mathbb{R})$ or $G \subset \mathrm{GL}(N, \mathbb{C})$, $N < \infty$. From now on, we restrict ourselves to the linear groups. This is sufficient and in any case simplifies the notation. Lie algebra of G and its dual are denoted respectively by $\mathfrak{g} = T_e G$ and $\mathfrak{g}^*$. The global or almost global relationship between G and $\mathfrak{g}$ is given by the exponential formula:

$$g(t^1, \ldots, t^k) = \exp\left(t^a e_a\right), \tag{1}$$

where $e_1, \ldots, e_k$ is a basis in $\mathfrak{g}$, the summation convention is used and obviously the matrix exponential is given by the power series:

$$\exp(A) = \sum_{r=0}^{\infty} \frac{1}{r!} A^r. \tag{2}$$

Lie algebra $\mathfrak{g}$ is closed under the commutator operation, so

$$[e_a, e_b] = C^c{}_{ab}\, e_c, \tag{3}$$

where $C^c{}_{ab}$ are structure constants in the base $e_1, \ldots, e_k$. The dual basis in $\mathfrak{g}^*$ is denoted by $e^1, \ldots, e^k$, where

$$e^a(e_b) = \langle e^a, e_b \rangle = \delta^a{}_b. \tag{4}$$

$G = \exp(\mathfrak{g})$ or at least it is finitely-generated by exponents $\exp(A)$. The dual $\mathfrak{g}^*$ consists of linear functions on $\mathfrak{g}$. However, very often it may be identified with $\mathfrak{g}$ itself via the trace formula:

$$\langle f, x \rangle = \mathrm{Tr}(fx). \tag{5}$$

When dealing with systems on Lie groups one uses the following Lie-algebraic velocities [32, 33]:

$$\Omega(t) = \dot{g}(t)g(t)^{-1}, \qquad \widehat{\Omega} = g(t)^{-1}\dot{g}(t). \tag{6}$$

They are non-holonomic when G is non-Abelian.

Tangent and cotangent bundles over G (i.e., bundles of contravariant and covariant vectors) are trivial [20]:

$$TG \simeq G \times \mathfrak{g}, \qquad T^*G \simeq G \times \mathfrak{g}^*. \tag{7}$$

Therefore, the mechanical states may be interpreted as pairs (g, Ω), or $(g, \widehat{\Omega})$. Let us observe that

$$\Omega = g\,\widehat{\Omega} g^{-1}, \qquad \widehat{\Omega} = g^{-1}\Omega g. \tag{8}$$

Using more sophisticated language we would write:

$$\Omega(t) = \mathrm{Ad}_{g(t)}\,\widehat{\Omega}, \qquad \mathrm{Ad}_g(u) = g\,u\,g^{-1}. \tag{9}$$

Similarly, in the canonical language of cotangent bundles mechanical states in T^*G are represented by pairs: (g, Σ), $(g, \widehat{\Sigma})$. In analytical terms we can write:

$$\Omega = \Omega^a\, e_a\ , \ \widehat{\Omega} = \widehat{\Omega}^a\, e_a \tag{10}$$

$$\Sigma = \Sigma_a\, e^a\ , \ \widehat{\Sigma} = \widehat{\Sigma}_a\, e^a, \tag{11}$$

where

$$\Omega^a = \Omega^a{}_i(q)\frac{\mathrm{d}q^i}{\mathrm{d}t}\ , \ \widehat{\Omega}^a = \widehat{\Omega}^a{}_i(q)\frac{\mathrm{d}q^i}{\mathrm{d}t} \tag{12}$$

$$\Sigma_a = p_i\,\Sigma^i{}_a(q)p_i\ , \ \widehat{\Sigma}_a = p_i\,\widehat{\Sigma}^i{}_a(q). \tag{13}$$

Obviously, the following equations are satisfied [36–38]:

$$\Sigma_a\Omega^a = \widehat{\Sigma}_a\widehat{\Omega}^a = p_i\dot{q}^i \tag{14}$$

$$\Sigma^i{}_a\Omega^a{}_j = \delta^i{}_j, \ \widehat{\Sigma}^i{}_a\widehat{\Omega}^a{}_j = \delta^i{}_j \tag{15}$$

$$\Omega^a{}_i\Sigma^i{}_b = \delta^a{}_b, \ \widehat{\Omega}^a{}_i\widehat{\Sigma}^i{}_b = \delta^a{}_b. \tag{16}$$

Left regular translations $L_g : x \mapsto gx$ act on those quantities as follows:

$$\Omega \mapsto g\Omega g^{-1} = \mathrm{Ad}_g\, \Omega, \qquad \widehat{\Omega} \mapsto \widehat{\Omega} \tag{17}$$

$$\Sigma \mapsto g\Sigma g^{-1} = \mathrm{Ad}^{*-1}_g \Sigma, \qquad \widehat{\Sigma} \mapsto \widehat{\Sigma}, \tag{18}$$

Let us notice that $\widehat{\Omega}$, $\widehat{\Sigma}$ are invariant. Similarly, the right regular translations $R_g : x \mapsto xg$ act in the following way:

$$\Omega \mapsto \Omega, \qquad \widehat{\Omega} \mapsto g^{-1}\widehat{\Omega} g = \mathrm{Ad}^{-1}_g\, \widehat{\Omega} \tag{19}$$

$$\Sigma \mapsto \Sigma, \qquad \widehat{\Sigma} \mapsto g^{-1}\widehat{\Sigma} g = \mathrm{Ad}^{*}_g \widehat{\Sigma}. \tag{20}$$

It is seen that the left and right transformation properties are completely opposite to each other.

The left- and right-invariant models of the kinetic energy are respectively given by:

$$T[\text{left}] = \frac{1}{2}\gamma_{ab}\Omega^a\Omega^b = \frac{1}{2}\gamma(\Omega, \Omega) \tag{21}$$

$$T[\text{right}] = \frac{1}{2}\gamma_{ab}\widehat{\Omega}^a\widehat{\Omega}^b = \frac{1}{2}\gamma(\widehat{\Omega}, \widehat{\Omega}) \tag{22}$$

where the coefficients γ_{ab} are constant.

Non-holonomic description of Legendre transformation is given by the formulas:

$$\Sigma_a = \frac{\partial T}{\partial \Omega^a}, \qquad \widehat{\Sigma}_a = \frac{\partial T}{\partial \widehat{\Omega}^a}. \tag{23}$$

The resulting canonical representation of the above left- and right-invariant kinetic energies is given by:

$$\mathscr{T}[\text{left}] = \frac{1}{2}\tilde{\gamma}^{ab}\Sigma_a\Sigma_b, \qquad \mathscr{T}[\text{right}] = \frac{1}{2}\tilde{\gamma}^{ab}\widehat{\Sigma}_a\widehat{\Sigma}_b. \tag{24}$$

Here the tilde—symbol $\tilde{\gamma}^{ab}$ denotes the inverse contravariant metric tensor, so that

$$\tilde{\gamma}^{ac}\gamma_{cb} = \delta^a{}_b. \tag{25}$$

The quantities Σ_a, $\widehat{\Sigma}_a$ are momentum mappings corresponding to the group of left and right acting regular translations in G. Their Poisson brackets may be expressed through the structure constants as follows [10]:

$$\left\{\Sigma_i, \Sigma_j\right\} = C^m{}_{ij}\Sigma_m, \quad \left\{\widehat{\Sigma}_i, \widehat{\Sigma}_j\right\} = -C^m{}_{ij}\widehat{\Sigma}_m, \quad \left\{\Sigma_i, \widehat{\Sigma}_j\right\} = 0. \tag{26}$$

Poisson brackets between "sigmas" and quantities f depending only on configuration variables q^i are given by:

$$\{\Sigma_a, f(q)\} = -\Sigma^i{}_a(q)\frac{\partial f}{\partial q^i}, \qquad \left\{\widehat{\Sigma}_a, f(q)\right\} = -\widehat{\Sigma}^i{}_a(q)\frac{\partial f}{\partial q^i}. \tag{27}$$

Obviously, any pair of functions depending only on configurations is Poisson-commuting:

$$\{g(q), f(q)\} = 0. \tag{28}$$

Any other Poisson brackets may be obtained from the above ones on the basis of the general structure properties of those operations.

For any interaction potential $\mathscr{V}(q)$ equations of motion have the form [2, 3, 21]:

$$\frac{\mathrm{d}f}{\mathrm{d}t} = \{f, H\}, \qquad H = \mathscr{T} + \mathscr{V}(q). \tag{29}$$

Therefore, for the left-invariant kinetic energy we obtain:

$$\frac{\mathrm{d}\widehat{\Sigma}_a}{\mathrm{d}t} = -\tilde{\gamma}^{cd}C^b{}_{ac}\widehat{\Sigma}_d\widehat{\Sigma}_b + \widehat{N}_a. \tag{30}$$

To be honest, this formula is generally valid for any, ever dissipative forces $\widehat{N}_a$. In the potential case we have obviously

$$\widehat{N}_a = -\widehat{\Sigma}^i{}_a(q)\frac{\partial \mathscr{V}}{\partial q^i}. \tag{31}$$

The above equations of motion may be written alternatively in terms of $\widehat{\Omega}$ or in mixed $\widehat{\Omega}$, $\widehat{\Sigma}$ -terms as follows:

$$\gamma_{ab}\frac{\mathrm{d}\widehat{\Omega}^b}{\mathrm{d}t} = -\gamma_{bd}C^b{}_{ac}\widehat{\Omega}^c\widehat{\Omega}^d + \widehat{N}_a \tag{32}$$

$$\frac{\mathrm{d}\widehat{\Sigma}_a}{\mathrm{d}t} = -C^b{}_{ac}\widehat{\Omega}^c\widehat{\Sigma}_b + \widehat{N}_a. \tag{33}$$

When we deal with geodetic system, i.e., when $\widehat{N}_a = 0$, these equations are explicitly solvable in terms of the time dependence of $\widehat{\Sigma}_a$ or $\widehat{\Omega}^a$. And finally, the motion in configuration space may be solved by integrating the defining equations:

$$\frac{\mathrm{d}q}{\mathrm{d}t} = q(t)\widehat{\Omega}, \tag{34}$$

after substituting the previously (in principle) found the time dependence of $\widehat{\Omega}$.

For the right-invariant models of T we obtain:

$$\frac{\mathrm{d}\Sigma_b}{\mathrm{d}t} = \tilde{\gamma}^{cd}C^b{}_{ac}\Sigma_d\Sigma_b + N_a. \tag{35}$$

When the system is moving under the influence of $\mathcal{V}$—potential forces, then N_a is linear in the differential of $\mathcal{V}$:

$$N_a = -\Sigma^i{}_a(q)\frac{\partial \mathcal{V}}{\partial q^i}. \tag{36}$$

It is interesting that for the geodetic left-invariant models the following conservation law holds:

$$\frac{\mathrm{d}\Sigma_a}{\mathrm{d}t} = 0. \tag{37}$$

For the general, i.e., not necessarily geodetic models with the left-invariant T the above conservation law is replaced by the balance law for Σ_a:

$$\frac{\mathrm{d}\Sigma_a}{\mathrm{d}t} = N_a. \tag{38}$$

Let us observe that the last two equations are free of the algebraic terms quadratic in "sigmas". They occur only in equations expressed in terms of $\widehat{\Sigma}_a$.

Of special interest are obviously doubly-invariant, i.e., left- and right-invariant models of the kinetic energy. On semi-simple groups they may be based on the Killing metric tensors

$$\gamma_{ab} = C^k{}_{la}C^l{}_{kb} = \gamma_{ba}. \tag{39}$$

If there is no potential energy or any kind of forces the general solution of equations of motion is then given simply by

$$q(t) = \exp(\Omega t)q(0) = q(0)\exp(\widehat{\Omega}t), \tag{40}$$

where obviously Ω, $\widehat{\Omega}$ are constant and related to each other as follows:

$$\widehat{\Omega} = q(0)^{-1}\Omega q(0). \tag{41}$$

When the metric γ_{ab} is not Killing, then something similar holds when G is the Cartesian product of simple groups G_K

$$G = \times_{K=1}^{N} G_K, \tag{42}$$

and the following combination of Killing metrics is used as γ:

$$\gamma = \oplus_{K=1}^{N} C_K \pi_K^* \gamma_K. \tag{43}$$

In this formula γ_K is the Killing metric on group G_K, C_K are constants and $\pi_K : G \to G_K$ is the natural projection of G onto the Kth factor G_K.

Let us summarize those remarks with the mentioned examples, i.e., rigid body and the ideal incompressible fluid.

When dealing with the rigid body in the three-dimensional Euclidean space, and neglecting the translational motion, the configuration space is identical with the three-dimensional rotation group $\mathrm{SO}(3,\mathbb{R})$. Non-holonomic velocities Ω, $\widehat{\Omega}$ are then simply the spatial and co-moving representations of angular velocity. They are skew-symmetric tensors, therefore in the three-dimensional space one can identify them with the spatial and material axial vectors with components Ω^a, $\widehat{\Omega}^A$ given respectively by:

$$\Omega^a{}_b = -\varepsilon^a{}_{bc}\Omega^c, \qquad \widehat{\Omega}^A{}_B = -\varepsilon^A{}_{BC}\widehat{\Omega}^C. \tag{44}$$

Here ε_{abc} is the totally antisymmetric symbol, $\varepsilon_{123} = 0$ and the shift of indices is meant in the sense of the Kronecker delta metrics δ_{ab}, δ_{AB}. Reciprocal relationships are given by:

$$\Omega^a = -\frac{1}{2}\,\varepsilon^a{}_b{}^c\Omega^b{}_c = \frac{1}{2}\,\varepsilon^a{}_b{}^c\Omega_c{}^b. \tag{45}$$

Similarly, for the relationship between $\Sigma^a{}_b$ and its pseudo-covector representation Σ_a we obtain the following two possible conventions:

1. If we assume in the rule for covector the summation over the skew-symmetric elements, then

$$\Sigma_a = \frac{1}{2}\,\varepsilon_{ae}{}^f\Sigma^e{}_f, \qquad \Sigma^e{}_f = \varepsilon^e{}_f{}^g\Sigma_g, \tag{46}$$

and

$$\langle\Sigma,\Omega\rangle = \Sigma_a\Omega^a = \frac{1}{2}\Sigma^a{}_b\Omega^b{}_a. \tag{47}$$

2. It we assume the summation over all possible elements, then obviously:

$$\Sigma_a\Omega^a = \Sigma^a{}_b\Omega^b{}_a, \tag{48}$$

and

$$\Sigma_a = \varepsilon_{ae}{}^f\Sigma^e{}_f, \qquad \Sigma^e{}_f = \frac{1}{2}\,\varepsilon^e{}_f{}^g\Sigma_g. \tag{49}$$

Rotational kinetic energy is given by the formula:

$$T = \frac{1}{2}\,I_{AB}\,\widehat{\Omega}^A\widehat{\Omega}^B = \sum_{A=1}^{3}\frac{I_A}{2}\,\left(\widehat{\Omega}^A\right)^2, \tag{50}$$

where I_{AB} is the tensor of inertia and I_A are its eigenvalues, i.e., solution of the equation

$$\det\left[I_{AB} - \lambda\eta_{AB}\right] = 0. \tag{51}$$

Obviously, I_{AB}, I_A are constants because they are referred to the material space. For any matrix $U \in \mathrm{SO}(3,\mathbb{R})$ T is left-invariant. It is right invariant when $I_1 = I_2 = I_3$.

When the problem is once degenerated, i.e., $I_a = I_b \neq I_c$, $a \neq b \neq c$, T is right invariant under $\mathrm{SO}(2, \mathbb{R})$—the group of rotations with respect to the c-axis.

Equation of motion have the following form:

$$I_1 \frac{\mathrm{d}\widehat{\Omega}_1}{\mathrm{d}t} = (I_2 - I_3)\,\widehat{\Omega}_2\widehat{\Omega}_3 + \widehat{N}_1 \tag{52}$$

$$I_2 \frac{\mathrm{d}\widehat{\Omega}_2}{\mathrm{d}t} = (I_3 - I_1)\,\widehat{\Omega}_3\widehat{\Omega}_1 + \widehat{N}_2 \tag{53}$$

$$I_3 \frac{\mathrm{d}\widehat{\Omega}_3}{\mathrm{d}t} = (I_1 - I_2)\,\widehat{\Omega}_1\widehat{\Omega}_2 + \widehat{N}_3 \tag{54}$$

where $\widehat{N}_a$ are co-moving components of torque. Let us observe that this form of equations is valid only in the physical three-dimensional case. These equations are autonomous in the geodetic case, when $\widehat{N}_a = 0$ (and $N = \varphi\widehat{N} = 0$), or when $\widehat{N}_a$ depend on mechanical state only through $\widehat{\Omega}$. They are so as well when $\widehat{N}_a$ depend only on $\widehat{\Omega}_a$. Geodetic equations are left-invariant.

Co-moving components of spin and its spatial components are respectively given by:

$$\widehat{\Omega}_A = \frac{\partial T}{\partial \widehat{\Sigma}^A} = I_{\underline{A}}\Omega^{\underline{A}} = I_{AB}\Omega^B \tag{55}$$

and kinetic Hamiltonian is then expressed as:

$$\mathscr{T} = \sum_{A=1}^{3} \frac{1}{2I_A}\widehat{\Sigma}_A^2 = \frac{1}{2}\, I^{AB}\widehat{\Sigma}_A\widehat{\Sigma}_B, \tag{56}$$

where, obviously, I^{AB} is reciprocal to I_{AB},

$$I^{AC}I_{CB} = \delta^A{}_B. \tag{57}$$

Poisson brackets are given by:

$$\{\Sigma_a, \Sigma_b\} = \varepsilon_{ab}{}^c\Sigma_c, \quad \left\{\widehat{\Sigma}_a, \widehat{\Sigma}_b\right\} = -\varepsilon_{ab}{}^c\widehat{\Sigma}_c, \quad \left\{\Sigma_a, \widehat{\Sigma}_b\right\} = 0. \tag{58}$$

Euler equations in spin terms are given by:

$$\frac{\mathrm{d}\widehat{\Sigma}_1}{\mathrm{d}t} = \left(\frac{1}{I_3} - \frac{1}{I_2}\right)\widehat{\Sigma}_2\widehat{\Sigma}_3 + \widehat{N}_1 \tag{59}$$

$$\frac{\mathrm{d}\widehat{\Sigma}_2}{\mathrm{d}t} = \left(\frac{1}{I_1} - \frac{1}{I_3}\right)\widehat{\Sigma}_3\widehat{\Sigma}_1 + \widehat{N}_2 \tag{60}$$

$$\frac{\mathrm{d}\widehat{\Sigma}_3}{\mathrm{d}t} = \left(\frac{1}{I_2} - \frac{1}{I_1}\right)\widehat{\Sigma}_1\widehat{\Sigma}_2 + \widehat{N}_3. \tag{61}$$

Please, be careful with the difference in sign in Poisson brackets for Σ_a and $\widehat{\Sigma}_a$.

When the rigid body is spherical ($I_1 = I_2 = I_3$), then the above balance laws become the usual balance law:

$$\frac{\mathrm{d}\widehat{\Sigma}_a}{\mathrm{d}t} = \widehat{N}_a, \tag{62}$$

in particular conservation laws for $\widehat{\Sigma}_a$ when $\widehat{N}_a = 0$.

In the spherical case the general solutions are given by exponents:

$$\varphi(t) = \exp(t\omega)\varphi(0) \tag{63}$$

with the skew-symmetric ω. Therefore, they are one-parameter groups or their cosets. In the anisotropic case the only exponent solutions are rotations about the main axes of inertia. Only rotations about the extreme axes are stable. We see that everything is but a simple special case of the above general group-theoretical systems.

Let us now review the Euler equations of the ideal incompressible fluids. The basic equation has the form:

$$\rho\frac{\mathrm{d}\mathbf{v}}{\mathrm{d}t} = \rho\left(\frac{\partial\mathbf{v}}{\partial t} + (\mathbf{v}\cdot\nabla)\mathbf{v}\right) = -\nabla p + \rho\mathbf{g}. \tag{64}$$

Iso-entropic motion has the form:

$$\frac{\mathrm{d}s}{\mathrm{d}t} = \frac{\partial s}{\partial t} + \mathbf{v}\mathrm{grad}s = 0 \tag{65}$$

$$\frac{\partial\rho s}{\partial t} + \mathrm{div}(\rho s\mathbf{v}) = 0 \tag{66}$$

$$\frac{\partial}{\partial t}\rho v^i = -\frac{\partial \Pi^{ik}}{\partial x^k}, \quad \Pi^{ik} = pg^{ik} + \rho v^i v^k \tag{67}$$

where obviously ρ is the density and $\mathbf{v}$ is the velocity field. The scalar product of two velocity fields is given by:

$$\langle\mathbf{v}_1, \mathbf{v}_1\rangle = \int_D \mathbf{v}_1\cdot\mathbf{v}_1 dx. \tag{68}$$

Here D is the region filled by fluid, incompressibility is described by:

$$\mathrm{div}\mathbf{v} = 0 \tag{69}$$

and $\mathbf{v}$ is assumed to be tangent to the boundary ∂D of the region. Kinetic energy is given by:

$$T = \frac{\rho}{2}\langle\mathbf{v}, \mathbf{v}\rangle = \frac{\rho}{2}\int_D g_{ij}v^i v^j dx, \tag{70}$$

where dx is the element of the Riemann volume.

At the time instant t the configuration is $g_t \in S\mathrm{Diff}\, D$, i.e., it belongs to the group of volume-preserving diffeomorphisms of D. At the instant $t + \tau$, the configuration is $\exp(\mathbf{v}\tau)g_t$, where τ is assumed to be small. Velocity field is obtained from $\dot{g}$ tangent at g to the group $S\mathrm{Diff}\, D$ of volume-preserving diffeomorphisms of D. As mentioned, being infinite-dimensional, $S\mathrm{Diff}\, D$ is not a Lie group, but the formal procedures of invariant systems are applicable to it and are very helpful in finding the solutions.

3 Affinely Rigid Body as a Mechanical System on the Homogeneous Space

Now we shall consider the deformable system with a finite number of degrees of freedom. This is the affinely-rigid body, i.e., roughly speaking, a system the configuration space of which is the affine or linear group. This is of course the natural generalization of the usual, i.e., metrically-rigid body. But deformations also occur, namely finite-dimensional homogeneous deformations. It turns out that even the usual, i.e., metrically rigid body becomes better described when one assumes it to be affinely-rigid, and only later one assumes the metrical constraints. The model may be also used in vibration of molecules, in micromorphic continuum, in nuclear models and even in the theory of cosmic bodies [8, 9, 11–15, 22–31, 33, 39].

It is more convenient to use the language of homogeneous spaces than that of Lie groups as configuration spaces. So, let $(N, U, \rightarrow, \eta)$ be the material affine space and $(M, V, \rightarrow, g)$—the physical space. U, V are linear translation spaces and $\eta \in U^* \otimes U^*$, $g \in V^* \otimes V^*$—the metric tensors [18]. Later on we shall see they are not necessary for the very formulation of affine degrees of freedom. The configuration space may be identified with

$$Q = M \times LI(U, V), \tag{71}$$

where $LI(U, V) \subset L(U, V)$ is the manifold of linear isomorphisms of U onto V. It describes internal (relative) degrees of freedom and M has to do with the translational motion of the center of mass. For any $\phi \in Q$ we have:

$$\Phi(t, a)^i = x^i(t) + \varphi^i{}_K(t)a^K. \tag{72}$$

In affine motion there are two measures of inertia: the total mass and the internal mas quadrupole [5–7, 32, 33],

$$m = \int_N d\mu(a), \qquad J^{KL} = \int a^K a^L d\mu(a). \tag{73}$$

Higher multipoles are non-essential and the dipole vanishes when a^K are material components of the radius vector with respect to the center of mass:

$$J^K = \int a^K d\mu(a) = 0. \tag{74}$$

Kinetic energy may be shown to be:

$$T = T_{\text{tr}} + T_{\text{int}} = \frac{m}{2} g_{ij} \frac{\mathrm{d}x^i}{\mathrm{d}t} \frac{\mathrm{d}x^j}{\mathrm{d}t} + \frac{1}{2} g_{ij} \frac{\mathrm{d}\varphi^i{}_A}{\mathrm{d}t} \frac{\mathrm{d}\varphi^j{}_B}{\mathrm{d}t} J^{AB}. \tag{75}$$

Legendre transformation is given by:

$$p_i = m g_{ij} \frac{\mathrm{d}x^j}{\mathrm{d}t}, \qquad p^A{}_i = g_{ij} \frac{\mathrm{d}\varphi^j{}_B}{\mathrm{d}t} J^{BA}. \tag{76}$$

Cauchy and Green deformation tensors are given by:

$$C_{ij} = \eta_{AB} (\varphi^{-1})^A{}_i (\varphi^{-1})^B{}_j, \qquad C^{ij} = \varphi^i{}_A \varphi^j{}_B \eta^{AB} \tag{77}$$

$$G_{AB} = g_{ij} \varphi^i{}_A \varphi^j{}_B, \qquad G^{AB} = (\varphi^{-1})^A{}_i (\varphi^{-1})^B{}_j g^{ij} \tag{78}$$

The kinetic Hamiltonian is given by:

$$\mathscr{T} = \mathscr{T}_{\text{tr}} + \mathscr{T}_{\text{int}} = \frac{1}{2m} g^{ij} p_i p_j + \frac{1}{2} \widetilde{J}_{AB} p^A{}_i p^B{}_j g^{ij}. \tag{79}$$

This might seem a natural generalization of the usual rigid body mechanics. However, it is not the case. First of all the above kinetic energy is not invariant either on the left or the right regular translations. The reason is that it depends explicitly on the metric tensors g_{ij}, η_{AB}. In a consequence it is not invariant either on the left or on the right regular translations. Let us try to improve this, initially without discussing its deeper motivation, just on the aesthetical basis. The left and right affine invariance enable one to save the Lie group structure and the possibility to find solutions on the basis of special functions.

First let us introduce the necessary affine concepts. The first of them are non-holonomic affine velocities

$$\Omega = \dot{\varphi} \varphi^{-1} \ , \ \Omega^i{}_j = \dot{\varphi}^i{}_A \varphi^{-1A}{}_j \tag{80}$$

$$\widehat{\Omega} = \varphi^{-1} \dot{\varphi} \ , \ \widehat{\Omega}^A{}_B = \varphi^{-1A}{}_i \dot{\varphi}^i{}_B. \tag{81}$$

Eringen used the term gyration for them. Obviously,

$$\Omega^i{}_j = \varphi^i{}_A \widehat{\Omega}^A{}_B \varphi^{-1B}{}_j, \qquad \widehat{\Omega}^A{}_B = \varphi^{-1A}{}_i \Omega^i{}_j \varphi^j{}_B. \tag{82}$$

Non-holonomic angular velocities are given by skew-symmetric parts

$$\omega^i{}_j = \Omega^i{}_j - \Omega_j{}^i = \Omega^i{}_j - g_{jk}\Omega^k{}_m g^{mi} \tag{83}$$

$$\widehat{\omega}^A{}_B = \widehat{\Omega}^A{}_B - \widehat{\Omega}_B{}^A = \widehat{\Omega}^A{}_B - \eta_{BC}\widehat{\Omega}^C{}_D\eta^{DA}. \tag{84}$$

The affine spins (hyperspins) conjugate to Ω, $\widehat{\Omega}$ are given by [17, 33]:

$$\Sigma = \varphi\pi, \qquad \widehat{\Sigma} = \pi\varphi, \tag{85}$$

i.e.,

$$\Sigma^i{}_j = \varphi^i{}_A\pi^A{}_j, \qquad \widehat{\Sigma}^A{}_B = \pi^A{}_i\varphi^i{}_B. \tag{86}$$

They are Hamiltonian generators, i.e., momentum mappings of the left and right affine transformations

$$\varphi \mapsto A\varphi B, \qquad A \in GL(V), B \in GL(U). \tag{87}$$

Rotational generators, i.e., metrical spin and vorticity are given by:

$$S^i{}_j = \Sigma^i{}_j - \Sigma_j{}^i, \qquad V^A{}_B = \widehat{\Sigma}^A{}_B - \widehat{\Sigma}_B{}^A. \tag{88}$$

Remark: they are not φ-transforms of each other. Poisson brackets are given by:

$$\left\{\Sigma^i{}_j, \Sigma^k{}_l\right\} = \delta^i{}_l\Sigma^k{}_j - \delta^k{}_j\Sigma^i{}_l \tag{89}$$

$$\left\{\widehat{\Sigma}^A{}_B, \widehat{\Sigma}^C{}_D\right\} = \delta^C{}_B\widehat{\Sigma}^A{}_D - \delta^A{}_D\widehat{\Sigma}^C{}_B \tag{90}$$

$$\left\{\Sigma^i{}_j, \widehat{\Sigma}^A{}_B\right\} = 0 \tag{91}$$

$$\left\{\widehat{\Sigma}^A{}_B, \hat{p}_C\right\} = \delta^A{}_C\hat{p}_B \tag{92}$$

$$\left\{I^i{}_j, p_k\right\} = \left\{\Lambda^i{}_j, p_k\right\} = \delta^i{}_k p_j \tag{93}$$

where

$$\hat{v}^A = \varphi^{-1A}{}_i v^i, \qquad \hat{p}_A = p_i\varphi^i{}_A \tag{94}$$

$$\Lambda^i{}_j = x^i p_j, \qquad I^i{}_j = \Lambda^i{}_j + \Sigma^i{}_j. \tag{95}$$

Obviously, $\Lambda^i{}_j$ is the center of mass affine momentum and $I^i{}_j$ is the total affine momentum with respect to the fixed point of the space M [10].

Transformation properties of "sigmas" and "omegas" are reciprocal to those with the roof symbol:

$$A \in \mathrm{GL}(V): \ \Sigma \mapsto A\Sigma A^{-1}, \quad \widehat{\Sigma} \mapsto \widehat{\Sigma}, \quad \Omega \mapsto A\Omega A^{-1}, \quad \widehat{\Omega} \mapsto \widehat{\Omega} \tag{96}$$

$$B \in \mathrm{GL}(U): \ \Sigma \mapsto \Sigma, \quad \widehat{\Sigma} \mapsto B^{-1}\widehat{\Sigma}B, \quad \Omega \mapsto \Omega, \quad \widehat{\Omega} \mapsto B^{-1}\widehat{\Omega}B. \tag{97}$$

Obviously, for any function depending only on the configuration variables we have [10]:

$$\left\{F, \Sigma^i{}_j\right\} = \varphi^i{}_A \frac{\partial F}{\partial \varphi^j{}_A}, \qquad \left\{F, \widehat{\Sigma}^A{}_B\right\} = \varphi^i{}_B \frac{\partial F}{\partial \varphi^i{}_A}, \qquad \left\{F, \Lambda^i{}_j\right\} = x^i \frac{\partial F}{\partial x^j}. \quad (98)$$

Kinematical representations of the affine spin and affine torques are given by:

$$K^{ij} = \int \left(y^i - x^i\right)\left(\dot{y}^j - \dot{x}^j\right) d\mu(a) = \varphi^i{}_A \frac{\mathrm{d}\varphi^j{}_B}{\mathrm{d}t} J^{AB} \quad (99)$$

$$N^{ij} = \int \left(y^i - x^i\right) \mathscr{F}^j(y) d\mu(a), \quad (100)$$

where $\mathscr{F}$ is the material density of forces.

The total system of equations of motion may be written in the following balance form:

$$\frac{\mathrm{d}k^i}{\mathrm{d}t} = F^i, \qquad k^i = g^{ij} p_j = \varphi^i{}_A \hat{k}^A \quad (101)$$

$$\frac{\mathrm{d}K^{ij}}{\mathrm{d}t} = \frac{\mathrm{d}\varphi^i{}_A}{\mathrm{d}t} \frac{\mathrm{d}\varphi^j{}_B}{\mathrm{d}t} J^{AB} + N^{ij} \quad (102)$$

where

$$F^i = \int \mathscr{F}^i(y(a)) d\mu(a) \quad (103)$$

is the total force acting on the center of mass.

In the case of potential forces

$$N^{ij} = -\varphi^i{}_A \frac{\partial \mathscr{V}}{\partial \varphi^k{}_A} g^{kj}. \quad (104)$$

The power of forces is given by:

$$P = P_{\mathrm{tr}} + P_{\mathrm{int}} = F_i v^i + N^{ij} \Omega_{ji}. \quad (105)$$

Let us observe that equation of internal motion may be simply written as follows:

$$\varphi^i{}_A \frac{\mathrm{d}^2 \varphi^j{}_B}{\mathrm{d}t^2} J^{AB} = N^{ij}. \quad (106)$$

Therefore, the equations of additionally constrained affine motion are easily obtained on the basis of the d'Alembert principle.

For example, the metrically rigid motion is described by the skew-symmetric part of the last equation:

$$\varphi^i{}_A \frac{\mathrm{d}^2\varphi^j{}_B}{\mathrm{d}t^2} J^{AB} - \varphi^j{}_A \frac{\mathrm{d}^2\varphi^i{}_B}{\mathrm{d}t^2} = N^{ij} - N^{ji} = \mathcal{N}^{ij}, \tag{107}$$

where $\mathcal{N}^{ij}$, the doubled skew-symmetric part of the affine torque is the usual metrical torque.

Similarly, the incompressible motion is ruled by the trace-less part of the primary equation:

$$\varphi^i{}_A \frac{\mathrm{d}^2\varphi^j{}_B}{\mathrm{d}t^2} J^{AB} - \frac{1}{n} g_{ab}\varphi^a{}_A \frac{\mathrm{d}^2\varphi^b{}_B}{\mathrm{d}t^2} J^{AB} g_{ij} = N^{ij} - \frac{1}{n} g_{ab} N^{ab} g^{ij}. \tag{108}$$

And finally let us quote something really new: equations of rotationless motion. In contrast to the rigid body motion, those equations are given by the symmetric part:

$$\varphi^i{}_A \frac{\mathrm{d}^2\varphi^j{}_B}{\mathrm{d}t^2} J^{AB} + \varphi^j{}_A \frac{\mathrm{d}^2\varphi^i{}_B}{\mathrm{d}t^2} = N^{ij} + N^{ji}, \tag{109}$$

But symmetric matrices do not form either Lie group or Lie algebra. Because of this the constraints

$$\Omega^i{}_j - \Omega_j{}^i = 0 \tag{110}$$

are essentially nonholonomic in contrast to those given by the antisymmetric part (rigid motion)

$$\Omega^i{}_j + \Omega_j{}^i = 0 \tag{111}$$

It is seen that k^a, K^{ij}, p_a, $\Sigma^i{}_j$ are proper quantities corresponding to the balance laws. Nevertheless, in the theory based on the d'Alembert principle, none of the balance law reduces to the conservation laws in the interaction-free case. This is the main drawback of this principle and of the use of metric tensors. Let us summarize with the balance laws in co-moving representation:

$$\frac{\mathrm{d}\hat{k}^A}{\mathrm{d}t} = -\hat{k}^B \widetilde{J}_{BC} \widehat{K}^{CA} + \widehat{F}^A \tag{112}$$

$$\frac{\mathrm{d}\widehat{K}^{AB}}{\mathrm{d}t} = -\widehat{K}^{AC} \widetilde{J}_{CD} \widehat{K}^{DB} + \widehat{N}^{AB} \tag{113}$$

In velocity representation they become:

$$m\frac{\mathrm{d}\hat{v}^A}{\mathrm{d}t} = -m\widehat{\Omega}^A{}_B \hat{v}^B + \widehat{F}^A \tag{114}$$

$$J^{AC}\frac{\mathrm{d}\widehat{\Omega}^B{}_C}{\mathrm{d}t} = -\widehat{\Omega}^B{}_D \widehat{\Omega}^D{}_C \widetilde{J}^{CA} + \widehat{N}^{AB} \tag{115}$$

It is clear that in the interaction-free case they never become conservation laws.

4 Towards Affine Dynamical Models

It follows from the transformation rule that the most general internal kinetic energy invariant on the left is given by:

$$T_{\text{int}} = \frac{1}{2}\mathscr{L}^{B}{}_{A}{}^{D}{}_{C}\widehat{\Omega}^{A}{}_{B}\widehat{\Omega}^{C}{}_{D}. \tag{116}$$

The equations of internal motion are then given by:

$$\frac{\mathrm{d}\Sigma^{i}{}_{j}}{\mathrm{d}t} = N^{i}{}_{j}. \tag{117}$$

Similarly, for the right invariant model we have

$$T_{\text{int}} = \frac{1}{2}\mathscr{R}^{j}{}_{i}{}^{l}{}_{k}\Omega^{i}{}_{j}\Omega^{k}{}_{l}, \qquad \frac{\mathrm{d}\widehat{\Sigma}^{A}{}_{B}}{\mathrm{d}t} = \widehat{N}^{A}{}_{B}, \tag{118}$$

i.e., conservation laws just like in the general models on group theory. Observe that $\mathscr{L}^{B}{}_{A}{}^{D}{}_{C}$, $\mathscr{R}^{j}{}_{i}{}^{l}{}_{k}$ are constant and satisfy the obvious symmetry relationship. Let us observe that in the d'Alembert model we had:

$$T_{\text{int}} = g_{ij}J^{KL}\frac{\mathrm{d}\varphi^{i}{}_{K}}{\mathrm{d}t}\frac{\mathrm{d}\varphi^{j}{}_{L}}{\mathrm{d}t}. \tag{119}$$

The full affine invariance with translational degrees of freedom is impossible. The left-invariant and right-invariant kinetic energies are given respectively as follows:

$$T_{\text{tr}} = \frac{m}{2}C_{ij}\frac{\mathrm{d}x^{i}}{\mathrm{d}t}\frac{\mathrm{d}x^{j}}{\mathrm{d}t} = \frac{m}{2}\eta_{AB}\hat{v}^{A}\hat{v}^{B} \tag{120}$$

$$T_{\text{tr}} = \frac{m}{2}g_{ij}\frac{\mathrm{d}x^{i}}{\mathrm{d}t}\frac{\mathrm{d}x^{j}}{\mathrm{d}t} = \frac{m}{2}G_{AB}\hat{v}^{A}\hat{v}^{B}. \tag{121}$$

For the left-invariant models the explicit form of the balance equations of motion reads:

$$\frac{\mathrm{d}p_{i}}{\mathrm{d}t} = Q_{i}, \qquad \frac{\mathrm{d}\Sigma^{i}{}_{j}}{\mathrm{d}t} = -\frac{1}{m}\widetilde{C}^{ik}p_{k}p_{j} + Q^{i}{}_{j}, \tag{122}$$

where the generalized forces are given by:

$$Q_{i} = -\frac{\partial\mathscr{V}}{\partial x^{i}}, \qquad Q^{i}{}_{j} = -\varphi^{i}{}_{A}\frac{\partial\mathscr{V}}{\partial\varphi^{j}{}_{A}} \tag{123}$$

when forces are derived from the potential. For the total quantities the form is much more suggestive:

$$\frac{\mathrm{d}p_i}{\mathrm{d}t} = Q_i, \qquad \frac{\mathrm{d}I(\mathscr{O})^i{}_j}{\mathrm{d}t} = Q_{\mathrm{tot}}{}^i{}_j, \tag{124}$$

where the following natural definition of the total quantities are accepted:

$$I(\mathscr{O})^i{}_j = \Lambda(\mathscr{O})^i{}_j + \Sigma^i{}_j = x^i p_j + \Sigma^i{}_j \tag{125}$$

$$Q_{\mathrm{tot}}(\mathscr{O})^i{}_j = Q_{\mathrm{tr}}(\mathscr{O})^i{}_j + Q^i{}_j = x^i Q_j + Q^i{}_j. \tag{126}$$

Similarly for the right-invariant models we obtain:

$$\frac{\mathrm{d}\hat{p}_A}{\mathrm{d}t} = \widehat{Q}_A, \quad \text{i.e.,} \quad \frac{\mathrm{d}p_i}{\mathrm{d}t} = Q_i, \qquad \frac{\mathrm{d}\widehat{\Sigma}^A{}_B}{\mathrm{d}t} = \widehat{Q}^A{}_B. \tag{127}$$

Obviously, here we have

$$\widehat{Q}_A = Q_i \varphi^i{}_A, \qquad \widehat{Q}^A{}_B = \varphi^{-1A}{}_i \Sigma^i{}_j \varphi^j{}_B. \tag{128}$$

As mentioned, the total kinetic energy cannot be doubly affine-invariant, just because the affine group fails to be semisimple in a rather unpleasant way. There are however models with the doubly affinely invariant internal kinetic energy. The translational model may be at most one-side affinely invariant, on the left or on the right. The resulting total kinetic energy will be also left-affinely invariant and right affinely-invariant. The opposite invariances will be purely metrical, i.e., orthogonal-invariant. They are respectively given by:

$$\begin{aligned} T^{\mathrm{aff-metr}} &= \frac{m}{2}\eta_{KL}\hat{v}^K\hat{v}^L + \frac{I}{2}\eta_{KL}\widehat{\Omega}^K{}_M\widehat{\Omega}^L{}_N\eta^{MN} \\ &\quad + \frac{A}{2}\widehat{\Omega}^K{}_L\widehat{\Omega}^L{}_K + \frac{B}{2}\widehat{\Omega}^K{}_K\widehat{\Omega}^L{}_L \end{aligned} \tag{129}$$

$$\begin{aligned} T^{\mathrm{metr-aff}} &= \frac{m}{2}g_{ij}v^i v^j + \frac{I}{2}g_{ij}\Omega^i{}_k\Omega^j{}_l g^{kl} \\ &\quad + \frac{A}{2}\Omega^i{}_j\Omega^j{}_i + \frac{B}{2}\Omega^i{}_i\Omega^j{}_j \end{aligned} \tag{130}$$

where m, I, A, B are constants. This expressions are implied by the assumed invariance principles. The two last expressions are identical, although written in a different way. Let us notice that the expression

$$\frac{m}{2}C_{ij}(\varphi)v^i v^j = \frac{m}{2}\eta_{KL}\hat{v}^K\hat{v}^L \tag{131}$$

resembles the tensor of effective mass in physics of the solid state [19, 36]. Because of this $p_i = C_{ij}(\varphi)v^j$ is a constant of motion, but $v^i = \widetilde{C}^{ij}p_j$ fails to be so. Obviously, in $T^{\mathrm{metr-aff}}$ it is constant and the corresponding expression predicts the constant value of the velocity in appropriately chosen potential term. In a sense, $T^{\mathrm{metr-aff}}$ may

be used as a finite-dimensional counterpart of the Arnold description of ideal fluid, obviously in the isochoric motion.

The above models of the kinetic energy are very special and because of this they admit solutions given by exponentials. For example, for the doubly-invariant model without translational motion and without translational force, we have simply:

$$\varphi(t) = \exp(Et)\varphi_0 = \varphi_0 \exp(\widehat{E}t), \qquad \widehat{E} = {\varphi_0}^{-1} E \varphi_0, \tag{132}$$

where φ_0, E and $\widehat{E}$ are quite arbitrary. If we consider the geodetic motion with T left affinely-invariant and T right metrically invariant, then $\varphi(t)$ is given by:

$$\varphi(t) = \varphi_0 \exp(Ft), \tag{133}$$

where φ_0 is arbitrary, and F is η-normal,

$$\left[F, F^{\eta T}\right] = FF^{\eta T} - F^{\eta T}F = 0, \qquad \left(F^{\eta T}\right)^{AB} = \eta_{BD} F^{D}{}_{C} \eta^{CA}, \tag{134}$$

in particular when

$$F^{\eta T} = -F, \qquad \text{or} \qquad F^{\eta T} = F. \tag{135}$$

And conversely, if T is left metrically invariant and right affinely invariant, then

$$\varphi(t) = \exp(Et)\varphi_0, \tag{136}$$

for arbitrary φ_0 and arbitrary g-normal E,

$$\left[E, E^{gT}\right] = EE^{gT} - E^{gT}E = 0, \qquad \left(E^{gT}\right)^{i}{}_{j} = g_{jl} E^{l}{}_{k} g^{ki}. \tag{137}$$

Those "stationary" solutions are similar to the stationary rotations of the anisotropic rigid body. The question appears however concerning the role and the necessity of using the metric tensor. However, let us notice that even the parts of expressions for affinely invariant T are based on some metric tensors in Q, however different then the g_{ij}, η_{AB} and non-derivable from them. One can show that after performing the Legendre transformation the metric T_{int} may be expressed as follows:

$$\mathscr{T}_{\text{int}}^{\text{aff}-\text{metr}} = \frac{1}{2\alpha}\text{Tr}\left(\widehat{\Sigma}^2\right) + \frac{1}{2\beta}\left(\text{Tr}\widehat{\Sigma}\right)^2 - \frac{1}{4\mu}\text{Tr}(V^2) \tag{138}$$

$$\mathscr{T}_{\text{int}}^{\text{metr}-\text{aff}} = \frac{1}{2\alpha}\text{Tr}\left(\Sigma^2\right) + \frac{1}{2\beta}\left(\text{Tr}\Sigma\right)^2 - \frac{1}{4\mu}\text{Tr}(S^2) \tag{139}$$

The constants α, β, μ are given by:

$$\alpha = I + A, \qquad \beta = -\frac{1}{B}(I + A)(I + A + nB), \qquad \mu = \frac{1}{I}(I^2 - A^2). \tag{140}$$

Expressing this by Casimir invariants of V, S, Σ we obtain:

$$\mathscr{T}_{\text{int}}^{\text{aff}-\text{metr}} = \frac{1}{2\alpha}C(2) + \frac{1}{2\beta}C(1)^2 + \frac{1}{2\mu}\|V\|^2 \tag{141}$$

$$\mathscr{T}_{\text{int}}^{\text{metr}-\text{aff}} = \frac{1}{2\alpha}C(2) + \frac{1}{2\beta}C(1)^2 + \frac{1}{2\mu}\|S\|^2 \tag{142}$$

where $\|V\|^2 = -\frac{1}{2}\text{Tr}(V^2)$, $\|S\|^2 = -\frac{1}{2}\text{Tr}(S^2)$, and obviously, the Casimir invariants of Σ, $\widehat{\Sigma}$ are given by:

$$C(k) = \text{Tr}(\widehat{\Sigma}^k) = \text{Tr}(\Sigma^k). \tag{143}$$

The first two expressions in $\mathscr{T}_{\text{int}}^{\text{aff}-\text{metr}}$, $\mathscr{T}_{\text{int}}^{\text{metr}-\text{aff}}$ are identical, the difference is only in the third terms. It is clear that the combination of first two terms is not positively definite. This is in the consequence of the lack of compactness of $\text{GL}(n, \mathbb{R})$, $\text{SL}(n, \mathbb{R})$. The same is true in general for the general forms of T_{int} based on coefficients L and R. Nevertheless in some range of coefficients I, A, B (equivalently α, β, μ) the kinetic energy is positive. Nevertheless, the main terms $C(2)$ of $\mathscr{T}_{\text{int}}^{\text{aff}-\text{metr}}$, $\mathscr{T}_{\text{int}}^{\text{metr}-\text{aff}}$ are non-definite. This fact may make us reluctant to affinely-invariant models of kinetic energy. Nevertheless, it turns out that such models may be useful. First of all, affine models may be considered as approximation to the d'Alembert ones, and at the same time they are endowed with all computational and qualitative advantages of those usual models, even in geodetic, i.e., potential-free dynamical equations. Besides, they are interesting from the point of view of the dynamics of integrable lattices in one dimension. Let us observe also that there are approximately affinely rigid bodies the deformations of which do not have anything to do with the d'Alembert principle. Their kinetic energies seem to be implied by the metric tensors suggested rather by affine invariance then by fixed spatial or material metrics. Let us mention e.g., such objects as atomic nuclei, neutron stars, soap bubbles or fluid droplet inclusions in fluid matrices [17, 22, 23, 29–31].

Let us describe this in terms of two-polar and polar decompositions of linear mappings. Namely, any $\varphi \in LI(U, V)$ may be described as follows:

$$\varphi = LDR^{-1} \tag{144}$$

where $L\colon \mathbb{R}^n \to V$, $R\colon \mathbb{R}^n \to V$ are orthogonal mappings acting respectively between Riemann spaces $(\mathbb{R}^n, \delta)$, (V, g) and $(\mathbb{R}^n, \delta)$, (U, η). The matrix D is a diagonal mapping of $\mathbb{R}^n$ onto itself. The inverse mappings are linear orthonormal co-frames $L^{-1}\colon V \to \mathbb{R}^n$, $R^{-1}\colon U \to \mathbb{R}^n$. Analytically this is the decomposition of the matrix $\varphi^i{}_A$ into the product of two orthogonal matrices L, R and the diagonal matrix D. Similarly as the polar coordinates of $\mathbb{R}^n$, the elements L, D, R are not unique, nevertheless they may be effectively used when some care is applied. They are given by the following eigenequations

$$\widehat{G}R_a = \lambda_a R_a = \exp(2q^a)R_a, \qquad \widehat{C}L_a = \exp(-2q^a)L_a, \tag{145}$$

where L_a, R_a are bases in V, U and q^a are real. Let as notice that L_a, R_a are basis vectors in V, U. The parameters q^a are logarithmic deformation invariants, and

$$D_{\underline{aa}} = \exp(q^a) \tag{146}$$

are the usual eigenvalues deformation invariants.

Let us notice that the usual polar decompositions are given by pairs $(U[\varphi], L[\varphi])$, or $(U[\varphi], \Lambda[\varphi]) = (U[\varphi], U[\varphi]L[\varphi]U[\varphi]^{-1})$ where $U[\varphi]$ is an isometry of (U, η) onto (V, g), and $L[\varphi]\colon U \to U$, $\Lambda[\varphi]\colon V \to V$ are respectively η-symmetric and V-symmetric and positive mappings of U onto U and V onto V. Then

$$\varphi = U[\varphi]L[\varphi] = \Lambda[\varphi]U[\varphi]. \tag{147}$$

Unlike the two-polar decomposition, the polar ones are unique. From this point of view the polar decomposition is natural, nevertheless the two-polar is more natural and easy in calculations. From the formal point of view the internal configuration $\varphi \in LI(U, V)$ is represented as a triple of mutually interacting systems: metrically rigid bodies L and R in V and U and N fictitious material points in the real line $\mathbb{R}$ with positions $q^1, \ldots, q^n$. Their "center of mass" is given by:

$$q = \frac{1}{n}\left(q^1 + \cdots + q^n\right), \tag{148}$$

and the corresponding "canonical momentum"

$$p = p_1 + \cdots + p_n \tag{149}$$

As usual there are two kinds of angular velocities and spin: $\hat{\chi}^a{}_b$, $\hat{\vartheta}^a{}_b$ and $\chi^i{}_j$, $\vartheta^i{}_j$ in the case of angular velocities and $\hat{\rho}^a{}_b$, $\hat{\tau}^a{}_b$ and $\rho^i{}_j$, $\tau^i{}_j$, as measures of spin and vorticity. Let us stress that in our system of notation the first letters of alphabet are used to denote the "internal" components in $\mathbb{R}^n$ and the middle letters denote the "physical" components in V and U. Therefore:

$$\hat{\chi}^a{}_b = L^a{}_i \frac{\mathrm{d}L^i{}_b}{\mathrm{d}t}\,, \qquad \hat{\vartheta}^a{}_b = R^a{}_K \frac{\mathrm{d}R^K{}_b}{\mathrm{d}t} \tag{150}$$

$$\chi^i{}_j = \frac{\mathrm{d}L^i{}_b}{\mathrm{d}t} L^b{}_j\,, \qquad \vartheta^K{}_L = \frac{\mathrm{d}R^K{}_i}{\mathrm{d}t} R^i{}_L \tag{151}$$

Similarly for the spin and vorticity variables: $\hat{\rho}^a{}_b$, $\hat{\tau}^a{}_b$, $\rho^i{}_j$, $\tau^K{}_L$. Let us observe that $\rho^i{}_j = S^i{}_j$, $\tau^K{}_L = V^K{}_L$ are the usual spin and vorticity in terms of V, U, whereas $\hat{\rho}^a{}_b$, $\hat{\tau}^a{}_b$ are their $\mathbb{R}^n$-comoving representations. Let us repeat that $\hat{\rho}^a{}_b$, $\hat{\tau}^a{}_b$ are Hamiltonian-conjugate to $\hat{\chi}^a{}_b$, $\hat{\vartheta}^a{}_b$, while $\rho^i{}_j$, $\tau^K{}_L$ are Hamiltonian-conjugate to $\chi^i{}_j$, $\vartheta^K{}_L$. The advantage of using $\hat{\chi}^a{}_b$, $\hat{\vartheta}^a{}_b$, $\hat{\rho}^a{}_b$, $\hat{\tau}^a{}_b$ is that from the point of view of the kinetic energy the configuration variables of the L- and R-gyroscopes are cyclic coordinates. Let us introduce the quantities:

$$M^a{}_b = -\hat{\rho}^a{}_b - \hat{\tau}^a{}_b, \qquad N^a{}_b = \hat{\rho}^a{}_b - \hat{\tau}^a{}_b. \tag{152}$$

One can show that indeed:

$$C(2) = \sum_a p_a^2 + \frac{1}{16}\sum_{a,b}\frac{(M^a{}_b)^2}{\sinh^2\frac{q^a-q^b}{2}} - \frac{1}{16}\sum_{a,b}\frac{(N^a{}_b)^2}{\cosh^2\frac{q^a-q^b}{2}}. \tag{153}$$

Therefore, the main part of the kinetic energy when $I = 0$, $B = 0$, i.e., one based on $C(2)$ is given by:

$$\mathscr{T}_{\text{latt}} = \frac{1}{2\alpha}\sum_a p_a^2 + \frac{1}{32\alpha}\sum_{a,b}\frac{(M^a{}_b)^2}{\sinh^2\frac{q^a-q^b}{2}} - \frac{1}{32\alpha}\sum_{a,b}\frac{(N^a{}_b)^2}{\cosh^2\frac{q^a-q^b}{2}}. \tag{154}$$

Formally, from the point of view of the dynamics of deformation invariants, this is a kind of the Sutherland lattice. It is interesting that the spin-like variables lead to the terms of the kind of singular centrifugal repulsion (the $M^a{}_b$-term) but also to the rather strange centrifugal attraction at large distances.

Let us quote an interesting reformulation of the last formula for $\mathscr{T}_{\text{int}}$, expressing the model $\mathscr{T}_{\text{int}}^{\text{aff}-\text{aff}}$ in binary terms:

$$\begin{aligned}\mathscr{T}_{\text{int}}^{\text{aff}-\text{aff}} = {} & \frac{1}{4An}\sum_{a,b}(p_a - p_b)^2 + \frac{1}{32A}\sum_{a,b}\frac{(M^a{}_b)^2}{\sinh^2\frac{q^a-q^b}{2}} + \\ & - \frac{1}{32A}\sum_{a,b}\frac{(N^a{}_b)^2}{\cosh^2\frac{q^a-q^b}{2}} + \frac{1}{2n(A+nB)}p^2.\end{aligned} \tag{155}$$

When in addition the I-term in $\mathscr{T}$ is allowed, the corresponding affine-metric expressions become:

$$\mathscr{T}_{\text{int}}^{\text{aff}-\text{metr}} = \mathscr{T}_{\text{int}}^{\text{aff}-\text{aff}}[A \to I + A] + \frac{I}{2\left(I^2 - A^2\right)}\|V\|^2 \tag{156}$$

$$\mathscr{T}_{\text{int}}^{\text{metr}-\text{aff}} = \mathscr{T}_{\text{int}}^{\text{aff}-\text{aff}}[A \to I + A] + \frac{I}{2\left(I^2 - A^2\right)}\|S\|^2. \tag{157}$$

In any case it is seen that even without assuming any potential energy, there is a dissociation threshold and if the isochoric constraints are introduced, the body may perform bounded elastic vibrations. Therefore, just like in the mechanical Maupertuis principle, the dynamics, even in the non-compact configuration space may be described by the appropriately chosen, let us add geometrically motivated way, in purely geodetic terms. This enables one to use special functions of mathematical physics, both on the classical and quantum level.

When speaking about integrable lattices, one should mention also some correspondence with the usual Sutherland lattice. Applying the reasoning similar to the above one, let us mention that replacing the straight line by the circle, we obtain:

$$\mathscr{T}_{\text{int}} = \frac{1}{2A}\sum_a p_a^2 + \frac{1}{32A}\sum_{a,b}\frac{(M^a{}_b)^2}{\sin^2\frac{q^a-q^b}{2}} + \frac{1}{32A}\sum_{a,b}\frac{(N^a{}_b)^2}{\cos^2\frac{q^a-q^b}{2}} - \frac{B}{2A(A+nB)}p^2. \tag{158}$$

This is obtained from the previous expression by the unitary substitution: $D_{\underline{aa}} = \exp(\mathrm{i}q^a)$. Let us observe, there is no problem with the absence of the minus sign in T, because in the compact circular case there is no difference between repulsion and attraction.

Let us also observe the relationship between usual the d'Alembert model and the traditional Calogero–Moser lattice. Namely, the Calogero-like expression is obtained from the d'Alembert model of T by the substitution

$$Q^a = \exp(q^a), \qquad P_a = \exp(-q^a)p_a, \qquad p_a = \exp(\mathrm{i}q^a)P_a \tag{159}$$

to the d'Alembert expression for T:

$$\mathscr{T}_{\text{int}} = \frac{1}{2I}\sum_a P_a^2 + \frac{1}{8I}\sum_{a,b}\frac{(M^a{}_b)^2}{\left(Q^a-Q^b\right)^2} + \frac{1}{8I}\sum_{a,b}\frac{(N^a{}_b)^2}{\left(Q^a-Q^b\right)^2}. \tag{160}$$

But now the two expressions depending on Q^a are repulsive, and the model may be realistic in the sense of admitting bounded vibrations only with the explicit use of some potential term or some boundary conditions restricting the behavior of Q^a.

Let us go back to the affinely invariant model of T. For simplicity let us consider the "Flathland" model $n = 2$ [1]. Then the part of the effective interaction between deformation invariants q^a is ruled by $M^1{}_2 = M$, $N^1{}_2 = N$, and the Hamiltonian becomes:

$$H^{\text{eff}}_{M,N} = \frac{1}{2m}\left(p_1^2+p_2^2\right) + U^{\text{centr}}_{M,N}\left(q^1,q^2\right) + \mathscr{V}\left(q^1,q^2\right). \tag{161}$$

Here, as in the case of general n, we have

$$U^{\text{centr}}_{M,N} = \frac{M^2}{16m\sinh^2\frac{q^a-q^b}{2}} - \frac{N^2}{16m\cosh^2\frac{q^a-q^b}{2}} \tag{162}$$

for the "centrifugal" effective potential. $\mathscr{V}\left(q^1,q^2\right)$ is a possibly existing additional potential. Now it is clear that M, N are constants of motion and there is a dissociation threshold for the motion of q^1, q^2. To be more precise, for $\mathscr{T}^{\text{aff}-\text{aff}}_{\text{int}}$ after introducing the new variables

$$x = q^2 - q^1, \qquad q = \frac{1}{2}(q^1+q^2) \tag{163}$$

$$p_x = \frac{1}{2}(p_2-p_1), \qquad p = p_1+p_2 \tag{164}$$

we obtain

$$\begin{aligned}\mathscr{T}_{\text{int}}^{\text{aff}-\text{aff}} &= \mathscr{T}_{\text{int}}^{\text{aff}-\text{aff}}[x] + U_{M,N}^{\text{centr}}(x) \\ &= \frac{p_x^2}{A} + \frac{M^2}{16A\sinh^2\frac{x}{2}} - \frac{N^2}{16A\cosh^2\frac{x}{2}} + \frac{p^2}{4(A+2B)}\end{aligned} \tag{165}$$

The external potential $\mathscr{V}\left(q^1, q^2\right)$ is assumed in the form

$$\mathscr{V}\left(q^1, q^2\right) = V(x) + W(q), \tag{166}$$

so finally we obtain the following splitting of the Hamiltonian:

$$\mathscr{H} = \frac{p_x^2}{A} + U_{M,N}^{\text{centr}}(x) + V(x) + \frac{p^2}{4(A+2B)} + W(q). \tag{167}$$

The first three terms describe the $\mathrm{SL}(2,\mathbb{R})$-ruled part of the dynamics, whenever the last two separate the purely dilatational motion. This Hamiltonian part describes the dilatational motion, in particular restricting it to small vibrations when W has the form of strongly concentrated in q potential well, e.g., of the oscillatory form, or just the usual rectangular well of very large depth. This will be realization of the approximately isochoric motion on $\mathrm{SL}(2,\mathbb{R})$. Even if $V(x) \equiv 0$, there is a dissociation threshold below which the motion is bounded, and above which it is scattering. The perspective of such bounded motions on the non-compact $\mathrm{SL}(2,\mathbb{R})$, just following from the curvature of $\mathrm{SL}(2,\mathbb{R})$ itself, without the attractive external potential V is very interesting in itself. Apparently it has to do with the fact that M, N are constants of motion when $n = 2$. Nevertheless, even for $n > 2$ this fact is still valid, in spite that M, N are then also variable. This is a consequence of the structure of commutation relations. Of course, again the dilatational motion must be restricted or just constrained by the shape of W. The quantities $(q^a,\ p_b,\ M^a{}_b,\ N^a{}_b)$ are also then "Funktionengruppe" in the sense of Caratheodory.

$$\{\xi^\mu, \xi^\nu\} = C^{\mu\nu}(\xi). \tag{168}$$

Their dynamics is given by Poisson brackets

$$\frac{\mathrm{d}\xi^\mu}{\mathrm{d}t} = \{\xi^\mu, H\}. \tag{169}$$

This enables one to express the functions $\hat{\chi}(t)$, $\hat{\vartheta}(t)$ in terms of special functions and then perhaps to find the vibrating motion of L and R by integrating the time-dependent ordinary differential equations:

$$\frac{\mathrm{d}L}{\mathrm{d}t} = L\hat{\chi}, \qquad \frac{\mathrm{d}R}{\mathrm{d}t} = R\hat{\vartheta}. \tag{170}$$

The explicit time-dependence is one of $\hat{\chi}(t)$, $\hat{\vartheta}(t)$.

This study belongs to the general idea of replacing the metrical invariance in physics by the affine invariance. The metrical concepts are to appear as some byproducts of affine geometry. We remain here on the level of classical elasticity, but similar ideas appeared in gravitation theory and quantum mechanics. Let us mention in particular the papers by Hehl [17], Sijacki [29–31] and Ne'emann [22, 23].

Acknowledgments We are very grateful to Professor Krzysztof Wilmański, the late, for his interest shown to our activity. Our thanks are also due to the chair-persons of CMwM for inviting one of us (Jan Jerzy Sławianowski) to participation in the Conference. Both of us are also grateful to NCN for the grant N N501 049 540 which enabled us to work on the topic.

References

1. Abbott, E.: Flatland: A Romance of Many Dimensions. Seely and Co., London (1884)
2. Abraham, R., Marsden, J.: Foundations of Mechanics, 2nd edn. The Benjamin-Cummings Publishing Company, London (1978)
3. Arnold, V.: Mathematical Methods of Classical Mechanics. Springer, New York (1978)
4. Arnold, V.I., Avez, A.: Ergodic Problems of Classical Mechanics. W. A. Benjamin Inc., New York (1968)
5. Burov, A., Chevallier, D.: On the variational principle of Poincare, the Poincare–Chetayev equations and the dynamics of affinely deformable bodies. Cahier de C.E.R.M.I.C.S. **14** (1996)
6. Burov, A., Chevallier, D.: Dynamics of affinely deformable bodies from the standpoint of theoretical mechanics and differential geometry. Rep. Math. Phys. **62**, 325–363 (2009)
7. Burov, A., Stepanov, S.: On geometry of masses in dynamics of deformable bodies. In: Problems of Investigation on Stability and Stabilization of Motion, pp. 107–130. Vychisl. Tsentr. Ross. Akad. Nauk, Moscow (1995) (in Russian)
8. Capriz, G.: Continua with Microstructure. Springer, New York (1989)
9. Capriz, G., Mariano, P.: Symmetries and hamiltonian formalism in complex material. J. Elast. **72**, 57–70 (2003)
10. Caratheodory, C.: Variationsrechnung und Partielle Differential-Gleichungen Erster Ordnung. B. G. Teubner, Leipzig (1956)
11. Dyson, F.: Dynamics of a spinning gas cloud. J. Math. Mech. **18**, 91 (1968)
12. Eringen, A.: Mechanics of micromorphic continua. In: Krüner, E. (ed.) Proceedings of the IUTAM Symposium on Mechanics of Generalized Continua, pp. 18–33. Springer, Berlin (1968)
13. Eringen, A., Suhubi, E.: Nonlinear theory of simple micro-elastic solids I. Int. J. Eng. Sci. **2**, 189–203 (1964)
14. Gołubowska, B.: Affine models of internal degrees of freedom and their action-angle description. Rep. Math. Phys. **51**, 205–214 (2003)
15. Gołubowska, B.: Action-angle analysis of some geometric models of internal degrees of freedom. J. Nonlinear Math. Phys. **11**(Supplement), 138–144 (2004)
16. Halmos, P.R.: Lectures on Ergodic Theory. Chelsea, New York (1956)
17. Hehl, F., Lord, E., Ne'eman, E.: Hadron dilatation, shear and spin as components of the intrinsic hypermomentum. Current and metric-affine theory of gravitation. Phys. Lett. **71B**, 432–434 (1977)
18. Hellwig, K., Wegner, B.: Mathematik und Theoretische Physik. Bd. 1 und 2, de Gruyter (1992)
19. Kittel, C.: Introduction to Solid State Physics, 8th edn. Wiley, New York (2005)
20. Kobayashi, S., Nomizu, K.: Foundations of Differential Geometry. Interscience Publishers, New York (1963)

21. Marsden, J., Ratiu, T.: Introduction to Mechanics and Symmetry. A Basic Exposition of Classical Mechanical Systems, 2nd edn. Springer, New York (1999)
22. Ne'eman, Y., Sijacki, Dj: $\overline{\mathrm{GL}}(4, \mathbb{R})$ group-topology, covariance and curved-space spinors. Int. J. Mod. Phys. **A2**, 1655–1669 (1987)
23. Ne'eman, Y., Sijacki, Dj: Hadrons in an SL(4, $\mathbb{R}$) classification. Phys. Rev. D **37**, 3267–3284 (1988)
24. Rożko, E.E.: Dynamics of affinely-rigid bodies with degenerate dimension. Rep. Math. Phys. **56**, 311–332 (2005)
25. Rożko, E.E.: Quantization of affinely-rigid bodies with degenerate dimension. Rep. Math. Phys. **65**, 1–15 (2010)
26. Rubin, M.: On the theory of a cosserat point and its application to the numerical solution of continuum problems. J. Appl. Mech. **52**(1985), 368–372 (1985)
27. Rubin, M.: On the numerical solution of one-dimensional continuum problems using the theory of a cosserat point. J. Appl. Mech. **52**, 373–378 (1985)
28. Seiliger, D.: Theory of Motion of a Similarly Variable Body. Typo-Lythography of Kazan Imperial University, Kazan (1892)
29. Sijacki, Dj: The unitary irreducible representations of SL(3, $\mathbb{R}$). J. Math. Phys **16**, 298–311 (1975)
30. Sijacki, Dj: World spinors revisited. Acta Phys. Pol. B **29**, 1089–1097 (1998)
31. Sijacki, Dj, Ne'eman, Y.: Algebra and physics of the unitary multiplicity-free representations of SL(4, $\mathbb{R}$). J. Math. Phys. **26**, 2457–2464 (1985)
32. Sławianowski, J.: The mechanics of an affinely-rigid body. Int. J. Theor. Phys. **12**, 271–296 (1975)
33. Sławianowski, J.: The mechanics of the homogeneously-deformable body. Dynamical models with high symmetries. Zeitschrift für Angewandte Mathematik und Mechanik **62**, 229–240 (1982)
34. Sławianowski, J.: Geodetic systems on linear and affine groups. Classics and quantization. J. Nonlin. Math. Phys. **11**, Supplement 130–137 (2004)
35. Sławianowski, J., Kovalchuk, V.: Invariant geodetic problems on the affine group and related Hamiltonian systems. Rep. Math. Phys. **51**, 371–379 (2003)
36. Sławianowski, J., Kovalchuk, V., Gołubowska, B., Martens, A., Rożko, E.E.: Quantized excitations of internal affine modes and their influence on Raman spectra. Acta Phys. Pol. B **41**, 165–218 (2010)
37. Sławianowski, J., Kovalchuk, V., Sławianowska, A., Gołubowska, B., Martens, A., Rożko, E.E., Zawistowski, Z.: Affine symmetry in mechanics of collective and internal modes. Part I. Classical models. Rep. Math. Phys. **54**, 373–427 (2004)
38. Sławianowski, J., Kovalchuk, V., Sławianowska, A., Gołubowska, B., Martens, A., Rożko, E.E., Zawistowski, Z.: Affine symmetry in mechanics of collective and internal modes. Part II. Quantum models. Rep. Math. Phys. **55**, 1–45 (2005)
39. Suhubi, E., Eringen, A.: Nonlinear theory of simple micro-elastic solids II. Int. J. Eng. Sci. **2**, 389–404 (1964)

Part II
Thermodynamics

An Alternative to the Allen-Cahn Phase Field Model for Interfaces in Solids—Numerical Efficiency

Hans-Dieter Alber

Abstract The derivation of the Allen-Cahn and Cahn-Hilliard equations is based on the Clausius-Duhem inequality. This is not a derivation in the strict sense of the word, since other phase field equations can be fomulated satisfying this inequality. Motivated by the form of sharp interface problems, we formulate such an alternative equation and compare the properties of the models for the evolution of phase interfaces in solids, which consist of the elasticity equations and the Allen-Cahn equation or the alternative equation. We find that numerical simulations of phase interfaces with small interface energy based on the alternative model are more effective then simulations based on the Allen-Cahn model.

1 Introduction

The phase field approach is used to model the evolution of phase interfaces in many different materials and accordingly the resulting models differ widely. However, in spite of all the differences the evolution equations for the order parameter S in the models is almost always formulated by the standard approach to set the time derivative of the order parameter equal to a suitable function of the functional derivative of the Ginzburg-Landau free energy with respect to S, which leads to an Allen-Cahn type equation, or equal to the divergence of a suitable function of the gradient of this functional derivative, which leads to a Cahn-Hilliard type equation. Often this function is chosen to be linear. For a thorough discussion of this approach to formulate material models with the Allen-Cahn und Cahn-Hilliard equation we refer to [8].

The leading idea behind these approaches to formulate the evolution equation is that in both cases for the resulting model the Clausius-Duhem inequality is guaranteed to hold. Yet, there are other possibilities to choose the evolution equation such that

Dedicated to the memory of Krzysztof Wilmański.

H.-D. Alber (✉)
Fachbereich Mathematik, Technische Universität Darmstadt,
Schlossgartenstr. 7, 64289 Darmstadt, Germany
e-mail: alber@mathematik.tu-darmstadt.de

B. Albers and M. Kuczma (eds.), *Continuous Media with Microstructure 2*,
DOI 10.1007/978-3-319-28241-1_8

this inequality holds. Therefore the question arises whether the standard approach is always the best or whether there are situations where other choices of the evolution equation for the order parameter lead to better results.

Of course, this question can only be discussed at a concrete example of an alternative phase field equation in a concrete mathematical material model. We consider here the prototypic model for the evolution of phase interfaces in solids, neglecting temperature effects, which consists of the elasticity equations coupled to an evolution equation for S. For this evolution equation one usually inserts the Allen-Cahn equation. We formulate here an alternative phase field equation and compare the mathematical properties of the two different models, which are obtained when we use the Allen-Cahn equation or the alternative equation as the evolution equation. Our main result is that simulations of phase interfaces in solids, which have small or vanishing interface energy density, are numerically more effective when the alternative equation is used instead of the Allen-Cahn equation.

We stress that the alternative phase field equation can replace the Allen-Cahn equation in other models. The properties of the resulting models have as yet to be investigated.

This paper is based on our investigations of phase field equations in the articles [1–7]. It summarizes in particular the results obtained in [6, 7], but adds also some new considerations.

2 The Clausius-Duhem Inequality and the Allen-Cahn Equation

To formulate the alternative phase field equation, we must know the form of the Ginzburg-Landau free energy, which appears in the Clausius-Duhem inequality. Therefore we first introduce the physical situation and the elasticity equations, from which the form of the Ginzburg-Landau free energy results.

Let $\Omega \subseteq \mathbb{R}^3$ be an open bounded set, which represents a solid body. We assume that the atoms of the material can be arranged in crystal lattices of two different types. The crystal type present at a material point $x \in \Omega$ at time t is indicated by the order parameter. The value $S(t, x) = 0$ means that type one is present, $S(t, x) = 1$ indicates that type two is present. The sets of points

$$\gamma(t) = \{x \in \Omega \mid S(t, x) = 0\}, \qquad \gamma'(t) = \{x \in \Omega \mid S(t, x) = 1\},$$

where crystal type one or crystal type two is present, respectively, are called phase 1 or phase 2 of the material at time t, respectively. Let $u(t, x) \in \mathbb{R}^3$ denote the displacement of the material point x at time t and let

$$\varepsilon(\nabla_x u) = \frac{1}{2}\big(\nabla_x u + (\nabla_x u)^T\big) \in \mathscr{S}^3$$

be the linear strain tensor, where $\mathscr{S}^3$ denotes the set of symmetric 3×3–matrices. We assume that only small displacements occur and we consider a quasistatic model. This means that for every given time t the displacement $x \mapsto u(t,x)$ and the Cauchy stress tensor $x \mapsto T(t,x) \in \mathscr{S}^3$ must solve the boundary value problem of linear elasticity posed in the domain Ω, which is given by

$$-\operatorname{div}_x T = \mathsf{b}, \tag{1}$$

$$T = D\big(\varepsilon(\nabla_x u) - \overline{\varepsilon} S\big), \tag{2}$$

$$u(t,x) = \mathsf{U}(t,x), \qquad x \in \partial\Omega, \tag{3}$$

where $\overline{\varepsilon} \in \mathscr{S}^3$ is the given transformation strain, where $D : \mathscr{S} \to \mathscr{S}$ is the elasticity tensor, a linear, symmetric, positive definite mapping, and where $\mathsf{b}(t,x), \mathsf{U}(t,x) \in \mathbb{R}^3$ denote the given volume force and boundary displacement. By (2), the material is stree free in phase one if $\varepsilon(\nabla_x u)$ is equal to zero, and in phase two if $\varepsilon(\nabla_x u)$ is equal to the transformation strain $\overline{\varepsilon}$.

To close the system of model equations, we need an evolution equation for S. To formulate it, note that according to (2), the stored elastic energy is

$$\mathsf{W}\big(\varepsilon(\nabla_x u), S\big) = \frac{1}{2}\Big(D\big(\varepsilon(\nabla_x u) - \overline{\varepsilon} S\big)\Big) : \big(\varepsilon(\nabla_x u) - \overline{\varepsilon} S\big), \tag{4}$$

which leads to the Ginzburg-Landau free energy

$$\psi^*\big(\varepsilon(\nabla_x u), S, \nabla_x S\big) = \mathsf{W}\big(\varepsilon(\nabla_x u), S\big) + \hat{\psi}(S) + \frac{1}{2}|\nabla_x S|^2. \tag{5}$$

where $\hat{\psi} : \mathbb{R} \to \mathbb{R}$ is a double well potential satisfying

$$\hat{\psi}(0) = \hat{\psi}(1) = 0, \qquad \hat{\psi}(r) > 0, \ \text{for } 0 < r < 1. \tag{6}$$

The second law of thermodynamics requires that there is a flow of the free energy $q\big(u, u_t, \varepsilon(\nabla_x u), S, S_t, \nabla_x S\big)$, such that the Clausius-Duhem inequality

$$\frac{\partial}{\partial t}\psi^* + \operatorname{div}_x q \le \mathsf{b} \cdot u_t \tag{7}$$

holds for all solutions (u, T, S) of the model equations. We use the flow

$$q = -T u_t - S_t \nabla_x S. \tag{8}$$

If we insert (5) and (8) into (7) and note (1) and the equation $\partial_{(\nabla_x u)}\mathsf{W} = T$, which follows from (4), (2), then we obtain by a short computation that

$$0 \geq \frac{\partial}{\partial t}\psi^* + \mathrm{div}_x q - \mathsf{b}\cdot u_t = \partial_{(\nabla_x u)}\mathsf{W} : \nabla_x u_t + \big(\partial_S \mathsf{W} + \hat{\psi}'(S)\big)S_t + \nabla_x S \cdot \nabla_x S_t$$
$$- \mathrm{div}_x(T u_t) - \mathrm{div}_x(S_t \nabla_x S) - \mathsf{b}\cdot u_t = (\partial_S \mathsf{W} + \hat{\psi}'(S) - \Delta_x S)S_t\,. \tag{9}$$

The Clausius-Duhem inequality (7) is therefore satisfied, if the evolution equation for S guarantees that the right hand side of (9) is non-positive. The simplest possibility to obtain this is to set

$$\partial_t S = -f\Big(\partial_S \mathsf{W}\big(\varepsilon(\nabla_x u), S\big) + \hat{\psi}'(S) - \Delta_x S\Big), \tag{10}$$

with a function $f : \mathbb{R} \to \mathbb{R}$ satisfying $r \cdot f(r) \geq 0$. If for f the linear function $f(r) = cr$ is chosen with a positive constant c, then the Allen-Cahn equation results.

Equations (1), (2), (10) form a closed system of partial differential equations. The standard phase field model for the evolution of phase interfaces consists of this system, combined with the boundary condition (3) and an initial condition for S.

3 Formulation of an Alternative Phase Field Equation

By the inequality (9), the expression

$$\mathscr{F} = \partial_S \mathsf{W} + \hat{\psi}'(S) - \Delta_x S \tag{11}$$

and the time derivative S_t must have opposite signs, which means that the value of S_t at (t, x) cannot be independent of the value $\mathscr{F}(t, x)$. Instead, there must be a functional relation between both values. Of course, this does not mean that S_t must depend on $\mathscr{F}$ alone as in the ansatz (10), it can depend on additional variables as well. The question arises, on which other variables S_t should depend.

To discuss this question we start from the usual physical interpretation of the observation, that there must be a functional relation between S_t and $\mathscr{F}$. The interpretation is that $\mathscr{F}$ is a configurational force, which drives the time evolution of the order parameter S. This interpretation is used as an additional justification for the Eq. (10), which we write in the short form

$$S_t(t, x) = -f\big(\mathscr{F}(t, x)\big). \tag{12}$$

What one wants to have is that the variation of the order parameter S is confined to a narrow diffuse interface, which moves with a propagation speed, which is a linear or nonlinear function of the configurational force $\mathscr{F}$. In fact, standard sharp interface models contain an equation, which prescribes the propagation speed of the interface as a function of the configurational driving force. This equation is called kinetic relation. We extend the meaning of this notation also to phase field models.

In a standard sharp interface model the kinetic relation can therefore be explicitly read off from the model equations. It would be of interest to have a phase field model, where the kinetic relation can also be read off directly from the form of the model equations. For the phase field Eq. (12) this is not possible. Instead, the kinetic relation is a hidden property of this equation, which must be determined by a very technical asymptotic analysis of this equation.

Our goal is therefore to formulate a phase field equation, for which the Clausisus-Duhem inequality (7) is satisfied, and which allows to read off the kinetic relation directly from the form of the equation. To formulate such an equation, assume that S is an order parameter, whose transition from 0 to 1 defines a diffuse phase interface moving in time. We say that the speed of the diffuse interface at (t, x_0) is equal to the normal speed $s(t, x_0)$ of the level set $\Gamma_c(t) = \{x \in \Omega \mid S(t, x) = c\}$, which contains x_0. The normal speed of $\Gamma_c(t)$ at $x \in \Gamma_c(t)$ can be defined as follows: If $\tilde{t} \mapsto x(\tilde{t}) \in \mathbb{R}^3$ is a function defined for all $\tilde{t}$ from a neighborhood of t and if $x(\tilde{t}) \in \Gamma_c(\tilde{t})$ holds for all $\tilde{t}$, then the normal speed $s(t, x)$ of $\Gamma_c(t)$ at $x = x(t) \in \Gamma_c(t)$ is the component of the velocoity $x'(t)$ in the direction of the unit normal vector $n(t, x)$ to $\Gamma_c(t)$ at x. Since $n(t, x) = \frac{\nabla_x S(t,x)}{|\nabla_x S(t,x)|}$, we obtain

$$s(t, x(t)) = \frac{\mathrm{d}x(t)}{\mathrm{d}t} \cdot \frac{\nabla_x S(t, x(t))}{|\nabla_x S(t, x(t))|}. \tag{13}$$

The function $t \mapsto x(t)$ satisfies $x(t) \in \Gamma_c(t)$ if and only if $t \mapsto S\big(t, x(t)\big) = c$ holds, and this last equation holds if and only if for a fixed time t_0 the function $x(t)$ satisfies the initial value problem

$$\begin{aligned} 0 = \frac{d}{dt} S\big(t, x(t)\big) &= S_t\big(t, x(t)\big) + \frac{dx(t)}{dt} \cdot \nabla_x S\big(t, x(t)\big) \\ &= S_t\big(t, x(t)\big) + s\big(t, x(t)\big) |\nabla_x S\big(t, x(t)\big)|, \qquad x(t_0) \in \Gamma_c(t_0), \end{aligned}$$

with s defined by (13). From this we conclude that if $t_1 < t_2$ are given times and if $s : [t_1, t_2] \times \Omega \to \mathbb{R}$ is a given function, then S satisfies the partial differential equation

$$S_t + s|\nabla_x S| = 0 \tag{14}$$

in the domain $[t_1, t_2] \times \Omega$, if and only if every level set $\Gamma_c(t)$ moves with normal speed $s(t, x)$ at $x \in \Gamma_c(t)$.

This suggests to combine the Eqs. (1)–(3) with the evolution equation

$$S_t(t, x) = -f\big(\mathscr{F}(t, x)\big)|\nabla_x S(t, x)|, \tag{15}$$

with the driving force $\mathscr{F}$ defined by (11) and with a given linear or nonlinear function $f : \mathbb{R} \to \mathbb{R}$. If we compare (14) and (15), then we see that the propagation speed of the diffuse interface defined by (15) is equal to $s = f\big(\mathscr{F}(t, x)\big)$, whence the kinetic relation is given by f and can be read off directly from the evolution equation (15).

From (9) we immediately see that every solution (u, T, S) of the Eqs. (1), (2), (15) satisfies the Clausius-Duhem inequality (7) if f satisfies $r \cdot f(r) \geq 0$ for all $r \in \mathbb{R}$. The evolution equation (15) has therefore the desired properties.

Equation (15) has the form of a Hamilton-Jacobi equation. However, if one inserts the definition (11) of $\mathscr{F}$ into (15), one obtains the phase field equation

$$S_t = -f\big(\partial_S \mathsf{W} + \hat{\psi}'(S) - \Delta_x S\big)|\nabla_x S|, \tag{16}$$

which is degenerate parabolic. Equation (16) has therefore mixed hyperbolic–parabolic properties. This is why we call (16) hybrid phase field equation.

4 The Allen-Cahn and the Hybrid Models

We have now two different phase field models for the evolution of phase interfaces in solids: If we combine the Eqs. (1), (2) with the phase field Eq. (10) of Allen-Cahn type we obtain the system

$$-\operatorname{div}_x T = \mathsf{b}, \tag{17}$$

$$T = D\big(\varepsilon(\nabla_x u) - \overline{\varepsilon} S\big), \tag{18}$$

$$\partial_t S = -\frac{c}{(\mu\lambda)^{1/2}}\Big(\partial_S \mathsf{W}\big(\varepsilon(\nabla_x u), S\big) + \frac{1}{\mu^{1/2}}\hat{\psi}'(S) - \mu^{1/2}\lambda\Delta_x S\Big), \tag{19}$$

which must be solved in the domain $[0, \infty) \times \Omega$. As boundary and initial conditions we choose, for example,

$$u(t, x) = \mathsf{U}(t, x), \qquad (t, x) \in [0, \infty) \times \partial\Omega, \tag{20}$$

$$\partial_{n_{\partial\Omega}} S(t, x) = 0, \qquad (t, x) \in [0, \infty) \times \partial\Omega, \tag{21}$$

$$S(0, x) = \mathsf{S}(x), \qquad x \in \Omega. \tag{22}$$

To obtain (19) from (10) we specialized the function f in (10) to be $f(r) = cr$ with a positive constant c and we introduced two scaling parameters $\mu > 0$ and $\lambda > 0$, whose meaning will become clear later. To have a short name, we call the system (17)–(19) the Allen-Cahn phase field model.

The second model is obtained by combination of (1), (2) with the hybrid phase field Eq. (16). If we specialize the function f in (16) to be $f(r) = cr$ with a constant $c > 0$ and introduce a scaling parameter $\nu > 0$, the resulting system is

$$-\operatorname{div}_x T = \mathsf{b}, \tag{23}$$

$$T = D\big(\varepsilon(\nabla_x u) - \overline{\varepsilon} S\big), \tag{24}$$

$$\partial_t S = -c\Big(\partial_S \mathsf{W}\big(\varepsilon(\nabla_x u), S\big) + \hat{\psi}'(S) - \nu\Delta_x S\Big)|\nabla_x S|. \tag{25}$$

These equations must be solved in the domain $[0, \infty) \times \Omega$. For the boundary and initial conditions we can again take (20)–(22). We call the system (23)–(25) the hybrid phase field model.

Several questions arise immediately. Equation (25) is a quasilinear, degenerate parabolic equation. Little is known about equations of the form (25). The first question therefore concerns existence and uniqueness of solutions to the system (23)–(25). Moreover, if solutions (u, T, S) exist, does the function S have the properties required from an order parameter? If both questions can be answered positively, what is then the difference between the Allen-Cahn model and the hybrid model? We have studied these questions in recent years. To the first two questions only partial answers can be given, whereas the answer to the third question is quite well known.

In [3] it is proved that weak solutions of the hybrid model (20)–(25) exist in the case of one space dimension. The proof is based on the observation that the one-dimensional version of the evolution equation (25) has some monotonicity properties. In higher space dimensions no rigorous existence proof is available. We must therefore rely on extensive numerical tests and on formal asymptotic analysis. The numerical test computations seem to indicate quite clearly, that solutions (u, T, S) exist and that the function S in these solutions has the properties required from an order parameter. In fact, the test computations converge in higher space dimensions better then in one space dimension. A part of the test computations is documented in [6].

The last question on the difference of the models is answered in the remainder of this paper. Of course, to answer the question we need to have more information on the properties of the models. This information is collected in Sects. 5 and 6. The information is obtained by asymptotic analysis of the models, more precisely by construction of approximate solutions to the Allen-Cahn and the hybrid models. The answer to the comparison question is finally given in Sect. 7.

5 Model Error and Asymptotics

To compare the models we need to define what we understand under the model error. In this section we first give this definition and subsequently state in Theorems 1 and 2 some results on approximate solutions, which have been obtained in [6, 7].

To define the model error we must first specify the type of material interfaces, which we want to model. Of great current interest are phase interfaces in functional materials. Very often such interfaces are thin and consist only of a few atomic layers. A large number of phase field models to simulate the time evolution of such interfaces have been devised and more are developed. It is therefore of interest to study how well the Allen-Cahn and the hybrid models are adapted to the simulation of thin interfaces in solids. More precisely, it is of interest to study how large the difference between the propagation speed of a thin phase interface in the real material and of the interface in the respective phase field model is. This difference is the model error.

To give a precise definition of the model error, we must approximately know the propagation speed of the real phase interface. For very thin interfaces mathematical models with sharp interface are appropriate. We therefore base the following considerations on the hypothesis that the propagation speed of the interface in the sharp interface model is a good approximation to the propagation speed of the interface in the real material. The model error of a phase field model is then the difference of the propagation speed of the sharp interface and the propagation speed of the diffuse interface in the phase field model.

To formulate the sharp interface model to be used we must introduce some notations. The asymptotic solution is constructed in the bounded domain

$$Q = [t_1, t_2] \times \Omega,$$

where $0 \le t_1 < t_2 < \infty$ are given times. $\Gamma(t)$ denotes the sharp interface at time t. We assume that the phase sets $\gamma(t)$, $\gamma'(t)$ introduced in Sect. 2 are open, disjoint subsets of Ω, whose common boundary is $\Gamma(t)$, such that $\Omega = \gamma(t) \cup \gamma'(t) \cup \Gamma(t)$. We set

$$\begin{aligned}
\Gamma &= \{(t,x) \in Q \mid x \in \Gamma(t),\ t_1 \le t \le t_2\},\\
\gamma &= \{(t,x) \in Q \mid x \in \gamma(t),\ t_1 \le t \le t_2\},\\
\gamma' &= \{(t,x) \in Q \mid x \in \gamma'(t),\ t_1 \le t \le t_2\}.
\end{aligned}$$

Let

$$n : \Gamma \to \mathbb{R}^3$$

be the continuous vector field, for which $n(t,x)$ is the unit normal vector to $\Gamma(t)$ at $x \in \Gamma(t)$, which points into the domain $\gamma'(t)$. For a function w defined in a neighborhood of Γ and $(t,x) \in \Gamma$ we set

$$\begin{aligned}
w^{(\pm)}(t,x) &= \lim_{\xi \searrow 0} w\big(t, x \pm n(t,x)\xi\big),\\
[w](t,x) &= w^{(+)}(t,x) - w^{(-)}(t,x),\\
\langle w \rangle(t,x) &= \frac{1}{2}\big(w^{(+)}(t,x) + w^{(-)}(t,x)\big).
\end{aligned}$$

Now we can formulate the sharp interface model. Let $\hat{S} : Q \to \{0,1\}$ be a piecewise constant function, which only takes the values 0 and 1 with a jump across Γ, such that

$$\gamma(t) = \{x \in \Omega \mid \hat{S}(t,x) = 0\}, \quad \gamma'(t) = \{x \in \Omega \mid \hat{S}(t,x) = 1\}.$$

The sharp interface model consists of a transmission problem for the elasticity equations and of a kinetic relation. The transmission problem is given by

$$-\operatorname{div}_x \hat{T} = \mathsf{b}, \tag{26}$$

$$\hat{T} = D\big(\varepsilon(\nabla_x \hat{u}) - \overline{\varepsilon}\hat{S}\big), \tag{27}$$

$$[\hat{u}] = 0, \tag{28}$$

$$[\hat{T}]n = 0, \tag{29}$$

$$\hat{u}(t)|_{\partial\Omega} = \mathsf{U}(t). \tag{30}$$

To determine the kinetic relation we proceed as in Sect. 2. We use the Clausius-Duhem inequality

$$\partial_t \psi_{\text{sharp}} + \operatorname{div}_x q_{\text{sharp}} \le \hat{u}_t \cdot \mathsf{b}, \tag{31}$$

with the free enery and the flux

$$\psi_{\text{sharp}}\big(\varepsilon(\nabla_x \hat{u}), \hat{S}\big) = \mathsf{W}\big(\varepsilon(\nabla_x \hat{u}), \hat{S}\big) + \lambda^{1/2} c_1 \int_{\Gamma(t)} \mathrm{d}\sigma, \tag{32}$$

$$q_{\text{sharp}}(\hat{T}, \hat{S}) = -\hat{T} \cdot \hat{u}_t\,,$$

where $c_1 \ge 0$ is an arbitrarily chosen constant. The last term on the right hand side of (32) is the interface energy, hence $\lambda^{1/2} c_1$ is the interface energy density. It is well known that if $(\hat{u}, \hat{T})$ is a solution of the transmission problem (26)–(30) and if the interface $\Gamma(t)$ in this problem moves with the normal speed $s_{\text{sharp}}(t, x)$ at $x \in \Gamma(t)$, then the Clausius-Duhem inequality (31) holds if and only if the inequality

$$s_{\text{sharp}}(t, x) \cdot \Big(-\overline{\varepsilon} : \langle \hat{T} \rangle(t, x) + \lambda^{1/2} c_1 \kappa_\Gamma(t, x) \Big) \ge 0 \tag{33}$$

is satisfied at every point $x \in \Gamma(t)$. Here $\kappa_\Gamma(t, x)$ denotes twice the mean curvature of the surface $\Gamma(t)$ at $x \in \Gamma(t)$.

A proof of this well known result is given in [1], however only for the case where $c_1 = 0$ in (32). The proof can be readily generalized to the case $c_1 > 0$.

A simple linear kinetic relation, for which (33) obviously holds, is

$$s_{\text{sharp}} = \hat{c}\,\big(-\overline{\varepsilon} : \langle \hat{T} \rangle + \lambda^{1/2} c_1 \kappa_\Gamma \big), \tag{34}$$

with a positive constant $\hat{c}$. The sharp interface problem thus consists of the transmission problem (26)–(30) combined with the kinetic relation (34).

We can now define the model error. To this end note that solutions of the Allen-Cahn model depend on the parameters μ and λ, whereas solutions of the hybrid model depend on the parameter ν. Therefore we record these parameters in the notation. For a solution $(u_{\text{AC}}^{(\mu\lambda)}, T_{\text{AC}}^{(\mu\lambda)}, S_{\text{AC}}^{(\mu\lambda)})$ of the Allen-Cahn model and for a solution $(u_{\text{hyb}}^{(\nu)}, T_{\text{hyb}}^{(\nu)}, S_{\text{hyb}}^{(\nu)})$ of the hybrid model consider the level sets

$$\Gamma_{\text{AC}}^{(\mu\lambda)} = \Big\{ (t, x) \in Q \;\Big|\; S_{\text{AC}}^{(\mu\lambda)}(t, x) = \frac{1}{2} \Big\}. \quad \Gamma_{\text{hyb}}^{(\nu)} = \Big\{ (t, x) \in Q \;\Big|\; S_{\text{hyb}}^{(\nu)}(t, x) = \frac{1}{2} \Big\}.$$

Let $s_{\mathrm{AC}}^{(\mu\lambda)}(t,x)$ denote the normal speed of $\Gamma_{\mathrm{AC}}^{(\mu\lambda)}(t)$ at $x \in \Gamma_{\mathrm{AC}}^{(\mu\lambda)}(t)$, and let $s_{\mathrm{hyb}}^{(\nu)}(t,x)$ denote the normal speed of $\Gamma_{\mathrm{hyb}}^{(\nu)}(t)$ at $x \in \Gamma_{\mathrm{hyb}}^{(\nu)}(t)$. These normal speeds are approximately equal to the propagation speeds of the diffuse phase interfaces defined by the solutions of the Allen-Cahn and hybrid models.

Let $t \in [t_1, t_2]$ be a given, fixed number. As initial conditions for the sharp interface problem we can choose

$$\Gamma(t) = \Gamma_{\mathrm{AC}}^{(\mu\lambda)}(t), \quad \text{or} \quad \Gamma(t) = \Gamma_{\mathrm{hyb}}^{(\nu)}(t).$$

Definition 1 We call the functions $\mathscr{E}^{(\mu\lambda)}(t) : \Gamma(t) \to \mathbb{R}$ and $\mathscr{E}^{(\nu)}(t) : \Gamma(t) \to \mathbb{R}$, respectively, which are defined by

$$\mathscr{E}^{(\mu\lambda)}(t) = s_{\mathrm{AC}}^{(\mu\lambda)}(t) - s_{\mathrm{sharp}}(t), \qquad \text{if } \Gamma(t) = \Gamma_{\mathrm{AC}}^{(\mu\lambda)}(t), \tag{35}$$

$$\mathscr{E}^{(\nu)}(t) = s_{\mathrm{hyb}}^{(\nu)}(t) - s_{\mathrm{sharp}}(t), \qquad \text{if } \Gamma(t) = \Gamma_{\mathrm{hyb}}^{(\nu)}(t), \tag{36}$$

the error of the Allen-Cahn model or the error of the hybrid model at time t, respectively.

We next state some results for the Allen-Cahn and hybrid models obtained by asymptotic analysis.

By $B_{\mathrm{AC}}^{(\mu\lambda)} > 0$ and $B_{\mathrm{hyb}}^{(\nu)} > 0$ we denote the widths of the diffuse interfaces defined by the order parameter in solutions of the Allen-Cahn model and by the order parameter in solutions of the hybrid model. Here we do not define the interface width precisely. If S is an order parameter, one could define the interface width to be the maximal distance between the level surfaces $\{x \in \Omega \mid S(t,x) = 0.1\}$ and $\{x \in \Omega \mid S(t,x) = 0.9\}$, for example. We are interested in the limits $\mu \to 0, \lambda \to 0$, $\nu \to 0$ and assume therefore that $\mu \in (0, \mu_0]$, $\lambda \in (0, \lambda_0]$, $\nu \in (0, \nu_0]$, with suitably chosen fixed constants $\mu_0, \lambda_0, \nu_0 > 0$.

Theorem 1 *Let* $\left(u_{\mathrm{AC}}^{(\mu\lambda)}, T_{\mathrm{AC}}^{(\mu\lambda)}, S_{\mathrm{AC}}^{(\mu\lambda)}\right)$ *be a solution of the Allen-Cahn model (17)–(21), let* $t \in [t_1, t_2]$ *be a given time, and let* $(\hat{u}(t), \hat{T}(t))$ *be the solution of the transmission problem (26)–(30) with the interface given by* $\Gamma(t) = \Gamma_{\mathrm{AC}}^{(\mu\lambda)}(t)$. *Then*

$$s_{\mathrm{AC}}^{(\mu\lambda)}(t,x) = s_0(t,x) + \mu^{1/2}\big(s_{10}(t,x) + \lambda^{1/2} s_{11}(t,x)\big) + \mu^{1/2} R_{\mathrm{AC}}(\mu,\lambda,t,x), \tag{37}$$

where $s_0 = s_0\big(\Gamma_{\mathrm{AC}}^{(\mu\lambda)}(t)\big)$, $s_{10} = s_{10}\big(\Gamma_{\mathrm{AC}}^{(\mu\lambda)}(t)\big)$ *and* $s_{11}\big(\Gamma_{\mathrm{AC}}^{(\mu\lambda)}(t)\big)$ *are nonlocal functions of* $\Gamma_{\mathrm{AC}}^{(\mu\lambda)}(t)$. *In particular, we have*

$$s_0(t,x) = \frac{c}{c_1}\big(-\overline{\varepsilon} : \langle \hat{T} \rangle(t,x) + \lambda^{1/2} c_1 \kappa_\Gamma(t,x)\big), \tag{38}$$

with the constant

$$c_1 = \int_0^1 \sqrt{2\hat{\psi}(r)}\, dr. \tag{39}$$

For the remainder term $R_{\mathrm{AC}}(\mu, \lambda, t, x)$ *there is a function* $\mu \to \mathscr{C}_{\mathscr{E}}(\mu)$ *with the property that* $\lim_{\mu \to 0} \mathscr{C}_{\mathscr{E}}(\mu) = 0$*, such that for all* $0 < \mu \leq \mu_0$, $0 < \lambda \leq \lambda_0$ *and all* $(t, x) \in \Gamma_{\mathrm{AC}}^{(\mu\lambda)}$ *the inequality*

$$|R_{\mathrm{AC}}(\mu, \lambda, t, x)| \leq \mathscr{C}_{\mathscr{E}}(\mu) \tag{40}$$

holds. Moreover, there is a constant $C_1 > 0$ *such that for all* $0 < \mu \leq \mu_0$, $0 < \lambda \leq \lambda_0$

$$B_{\mathrm{AC}}^{(\mu\lambda)} \leq C_1 (\mu\lambda)^{1/2}. \tag{41}$$

These results are contained in [7]. We stress here the fact, that the results are obtained by formal asymptotic analysis. No rigorous mathematical proof of these statements is given in [7]. The asymptotic analysis with respect to $\mu \to 0$ uses mathematical methods, which are standard in the analysis of phase field models. This is different for the estimate (40), which says that the remainder term R_{AC} tends to zero for $\mu \to 0$, uniformly with respect to λ. This uniformity estimate is obtained by a second asymptotic analysis with respect to $\lambda \to 0$. The formal derivation of this estimate is a novelty introduced in [7].

Theorem 2 *Let* $\left(u_{\mathrm{hyb}}^{(\nu)}, T_{\mathrm{hyb}}^{(\nu)}, S_{\mathrm{hyb}}^{(\nu)}\right)$ *be a solution of the hybrid model (20), (21), (23)–(25), let* $t \in [t_1, t_2]$ *be a given time, and let* $(\hat{u}(t), \hat{T}(t))$ *be the solution of the transmission problem (26)–(30) with the interface given by* $\Gamma(t) = \Gamma_{\mathrm{hyb}}^{(\nu)}(t)$*. Then*

$$s_{\mathrm{hyb}}^{(\nu)}(t, x) = c\Big(- \overline{\varepsilon} : \langle \hat{T} \rangle(t, x) + \nu^{1/2} R_{\mathrm{hyb}}(\nu, t, x) \Big), \tag{42}$$

where $c > 0$ *is the constant from (25). For the remainder term* $R_{\mathrm{hyb}}(\nu, t, x)$ *there is a constant* C_2 *such that for all* $0 < \nu \leq \nu_0$ *and all* $(t, x) \in \Gamma_{\mathrm{hyb}}^{(\nu)}$ *the inequality*

$$|R_{\mathrm{hyb}}(\nu, t, x)| \leq C_2 \tag{43}$$

holds. Moreover, there is a constant $C_3 > 0$ *such that for all* $0 < \nu \leq \nu_0$

$$B_{\mathrm{hyb}}^{(\nu)} \leq C_3 \nu^{1/2}. \tag{44}$$

These results are obtained in [6], again by formal asymptotic analysis.

6 Characteristic Equations

From the results on the asymptotic behavior of the models stated in Theorems 1 and 2 we derive in this section for both models some relations between parameters of the models. We call these relations the characteristic relations of the models. The comparison of the models in Sect. 7 is based on these relations.

We first consider the Allen-Cahn model. For c_1 in the free energy (32) we choose the value given by (39), With this value we adapt the interface energy density $\lambda^{1/2}c_1$ to the value in the real material by varying λ. In (19) we choose $c = \hat{c}c_1$. By (34) and (38) we then have

$$s_0 = s_{\text{sharp}}\,,$$

hence (35) and (37) together imply

$$\mathscr{E}^{(\mu\lambda)} = s_{\text{AC}}^{(\mu\lambda)} - s_0 = \mu^{1/2}(s_{10} + \lambda^{1/2}s_{11}) + \mu^{1/2}R_{\text{AC}}\,. \tag{45}$$

This equation and (40) together yield

$$|\mathscr{E}^{(\mu\lambda)}| \le C\mu^{1/2}, \tag{46}$$

with a constant C, which can be chosen independently of λ. By this inequality, $\mu^{1/2}$ controls the model error. Therefore we write $F = \mu^{1/2}$ and call F the error parameter. Moreover, since $\lambda^{1/2}c_1$ is the interface energy density, we call $E = \lambda^{1/2}$ the interface energy parameter. Also, since by (41) the interface width is bounded by a constant, which is proportional to $(\mu\lambda)^{1/2}$, we call $\mathscr{W} = (\mu\lambda)^{1/2}$ the interface width parameter. These three parameters and the propagation speed $s_{\text{AC}} = s_{\text{AC}}^{(\mu\lambda)}$ are connected by the fundamental relations

$$\mathscr{W} = EF, \tag{47}$$

$$s_{\text{AC}} = \hat{c}\,(-\overline{\varepsilon} : \langle\hat{T}\rangle + c_1\kappa_\Gamma E) + \mathscr{E}[E, F], \tag{48}$$

$$|\mathscr{E}[E, F]| \le CF, \tag{49}$$

where we use the notation $\mathscr{E}[E, F] = \mathscr{E}^{(\mu\lambda)}$. The first equation is an immediate consequence of the definition of the parameters, the second is obtained by insertion of (34) into (35), and the last inequality is just a restatement of (46).

Now assume that we want to use a phase field model to numerically simulate the propagation of a phase interface. In such a simulation the numerical effort is proportional to h^{-p}, where h denotes the grid spacing and where the power $p > 1$ depends on whether we want to simulate a problem in 2–d or in 3–d and it depends on the numerical scheme we use. In order for the simulation to be precise, we must guarantee that the model error and the numerical error are small. To make the numerical error small, we must choose the grid spacing h small enough to resolve the transition of the order parameter across the interface, which means that we must choose $h < \mathscr{W}$, hence we have $h^{-p} > \mathscr{W}^{-p}$. Therefore we see that the numerical effort of a simulation based on a phase field model is measured by the number $\mathscr{W}^{-p}$. We call the number

$$e_{\text{num}} = \mathscr{W}^{-p}$$

the parameter of numerical effort. For a simulation based on the Allen-Cahn model we see from (47) that the numerical effort is

$$e_{\text{num}} = (EF)^{-p}. \tag{50}$$

We call the relations (47)–(50) characteristic relations for the Allen-Cahn model.

Next we derive the characteristic relations for the hybrid model. In the free energy (32) we choose $c_1 = 0$, and in (25) we set $c = \hat{c}$. By (34) and (42) we then have

$$s_{\text{hyb}}^{(\nu)} = s_{\text{sharp}} + \nu^{1/2}\hat{c}\, R_{\text{hyb}}. \tag{51}$$

We insert this equation into (36) and obtain for the model error

$$\mathscr{E}^{(\nu)} = \hat{c} R_{\text{hyb}}\, \nu^{1/2}. \tag{52}$$

From this equation and from (43) we infer that

$$|\mathscr{E}^{(\nu)}| = \hat{c}|R_{\text{hyb}}|\nu^{1/2} \leq C\nu^{1/2}. \tag{53}$$

By this equation, $\nu^{1/2}$ controls the model error. In the case of the hybrid model we therefore choose $F = \nu^{1/2}$ as the error parameter. By (44), the interface width is bounded by a constant, which is proportional to $\nu^{1/2}$, whence the interface width parameter is $\mathscr{W} = \nu^{1/2}$. For the hybrid model we therefore have the characteristic relations

$$\mathscr{W} = F, \tag{54}$$

$$s_{\text{hyb}} = -\hat{c}\,\overline{\varepsilon} : \langle \hat{T} \rangle + \mathscr{E}[F], \tag{55}$$

$$|\mathscr{E}[F]| \leq CF, \tag{56}$$

$$e_{\text{num}} = F^{-p}, \tag{57}$$

where we used the notations $s_{\text{hyb}} = s_{\text{hyb}}^{(\nu)}$ and $\mathscr{E}[F] = \mathscr{E}^{(\nu)}$. The first of these relations follows from the definitions of F and $\mathscr{W}$, the second one is obtained by combination of (51) and (52), noting (34), the third one is just a restatement of (53), and the last one follows from the definition $e_{\text{num}} = \mathscr{W}^{-p}$ of the parameter of numerical effort and from (54).

7 Comparison of the Models, Numerical Efficiency

From (48) we see that the Allen-Cahn model can describe the evolution of a phase interface with propagation speed $\hat{c}\,(-\overline{\varepsilon} : \langle \hat{T} \rangle + c_1 \kappa_\Gamma E)$, which by (34) is the propagation speed of an interface with interface energy density $c_1\lambda^{1/2} = c_1 E$. The interface energy density is always positive, since we cannot set $\lambda = 0$ in the Allen-Cahn equation (19). Varying of the parameter E to adjust the interface energy density does not change the model error; this error can be adjusted to a desired value by choosing the parameter $F = \mu^{1/2}$ suitably. Varying of F does not change the interface

energy density. From (50) we see that if the interface energy density parameter E is fixed, then the effort of a numerical simulation grows with F^{-p}, where the power $p > 1$ depends on the numerical method employed and on the space dimension of the problem, which we want to simulate.

From (55) we see that the hybrid model, on the other hand, can describe the evolution of a phase interface with propagation speed $-\hat{c}\,\overline{\varepsilon} : \langle \hat{T} \rangle$, which by (34) is the propagation speed of an interface with interface energy density $c_1\lambda^{1/2} = 0$. The model error can be adjusted to a desired value by choosing the parameter $F = \nu^{1/2}$ suitably. By (57), also for this model the effort of a numerical simulation grows with F^{-p}, where the power $p > 1$ depends on the numerical method employed and on the space dimension of the problem, which we want to simulate.

These observations suggest the following rule:

> Simulations of phase interfaces with positive interface energy density should be based on the Allen-Cahn model, simulations of interfaces with zero or small interface energy density should be based on the hybrid model.

One can object to this rule by arguing that the Allen-Cahn model can also be used to simulate interfaces with zero interface energy density by choosing the interface energy density parameter positive, but very small. However, because of the presence of the factor E^{-p} in the formula (50) the numerical effort will become very large.

To be more specific, we consider an interface with vanishing interface energy density, hence $c_1\lambda^{1/2} = 0$, which by (34) means that the propagation speed of the sharp interface is

$$s_{\text{sharp}} = -\hat{c}\,\overline{\varepsilon} : \langle \hat{T} \rangle.$$

For the Allen-Cahn model it follows from this equation and from (48) that in this case the total model error, which we denote by $\mathscr{E}_{\text{total}}$, is

$$\mathscr{E}_{\text{total}} = s_{\text{AC}} - s_{\text{sharp}} = \hat{c}c_1\kappa_\Gamma E + \mathscr{E}[E, F].$$

This means that the term $\hat{c}c_1\kappa_\Gamma E$ is now part of the total model error.

If we prescribe the maximal value $\mathscr{E}_{\max}$ of the total model error $|\mathscr{E}_{\text{total}}|$, we must therefore choose the parameters E and F such that

$$\hat{c}c_1(\max_\Gamma |\kappa_\Gamma|)E + \max_\Gamma |\mathscr{E}[E, F]| \le \mathscr{E}_{\max}, \tag{58}$$

$$EF \stackrel{!}{=} \max, \tag{59}$$

where the second condition is imposed by the requirement to make the numerical effort $e_{\text{num}} = (EF)^{-p}$ as small as possible. To discuss this optimization problem, we assume first that the term s_{10} in the asymptotic expansion (37) of the propagation speed $s_{\text{AC}}^{(\mu\lambda)}$ is not identically equal to zero. In this case we conclude from (45) and (40) that for sufficiently small $\lambda^{1/2} = E$ and for sufficiently small $\mu^{1/2} = F$ the error $\mathscr{E}[E, F] = \mathscr{E}^{(\mu\lambda)}$ satisfies

$$\max_{\Gamma} |\mathscr{E}[E, F]| \geq \frac{1}{2}(\max_{\Gamma} |s_{10}|)\mu^{1/2} = \frac{1}{2}(\max_{\Gamma} |s_{10}|)F.$$

This inequality and (58) imply that the solution (E, F) of the optimization problem (58), (59) satisfies

$$F \leq \frac{2}{\max\limits_{\Gamma} |s_{10}|} \max_{\Gamma} |\mathscr{E}[E, F]| \leq \frac{2}{\max\limits_{\Gamma} |s_{10}|} \mathscr{E}_{\max} \qquad \text{and} \qquad E \leq \frac{1}{\hat{c}c_1 \max\limits_{\Gamma} |\kappa_\Gamma|} \mathscr{E}_{\max}.$$

From this result we obtain

Corollary 1 *Let $\mathscr{E}_{\max}$ denote the total model error of the Allen-Cahn model in the simulation of an interface without interface energy. If the term s_{10} in the asymptotic expansion (37) of the propagation speed $s_{\mathrm{AC}}^{(\mu\lambda)}$ is not identically equal to zero, then the interface width B_{AC} satisfies*

$$B_{\mathrm{AC}} \leq C_1 EF \leq \frac{2C_1}{\hat{c}c_1(\max\limits_{\Gamma} |s_{10}|)(\max\limits_{\Gamma} |\kappa_\Gamma|)} \mathscr{E}_{\max}^2 . \tag{60}$$

In a numerical simulation of an interface without interface energy based on the Allen-Cahn model the parameter of numerical effort satisfies

$$e_{\mathrm{num}} \geq \left(\frac{\hat{c}c_1(\max\limits_{\Gamma} |s_{10}|)(\max\limits_{\Gamma} |\kappa_\Gamma|)}{2\,\mathscr{E}_{\max}^2} \right)^p , \tag{61}$$

with a power $p > 1$ depending on the space dimension and the numerical method used.

For the hybrid model we have by (55) and (56) that $\mathscr{E}_{\max} = \max_\Gamma |\mathscr{E}[F]| \leq CF$. From (57) and from (61) we thus see that in a simulation of an interface without interface energy or with small interface energy the numerical efforts behave like

$$e_{\mathrm{num}}^{\mathrm{hyb}} \leq C\mathscr{E}_{\max}^{-p} , \qquad e_{\mathrm{num}}^{\mathrm{AC}} \geq C\mathscr{E}_{\max}^{-2p} . \tag{62}$$

Since the time step in a simulation must be decreased when the grid spacing h in x–direction is decreased, the number p can be larger than 4 in a three dimensional simulation. From (62) we thus see that the numerical effort for the Allen-Cahn model grows much faster for the Allen-Cahn model than for the hybrid model when the required accuracy is increased. This confirms the rule stated above for the usage of both models in simulations.

This picture does not change essentially when the term s_{10} vanishes identically. In this case the same considerations show that instead of (60) and (61) we would have $B_{\mathrm{AC}} = O(\mathscr{E}_{\max}^{3/2})$ and $e_{\mathrm{num}}^{\mathrm{AC}} \geq C\mathscr{E}_{\max}^{-\frac{3}{2}p}$, hence the numerical effort for the

Allen-Cahn model would still grow faster than for the hybrid model. However, a close investigation of the terms, which constitute s_{10} and which are computed in [7], shows that only in very exceptional situations one can expect that s_{10} vanishes identically.

References

1. Alber, H.-D.: Evolving microstructure and homogenization. Continum. Mech. Thermodyn. **12**, 235–286 (2000)
2. Alber, H.-D.: Evolution of phase interfaces by configurational forces: a phase field model. Thermodynamische Materialtheorien, Oberwolfach 12.2.2004–18.12.2004. Oberwolfach Rep. **1**(4), 2981–2985 (2004)
3. Alber, H.-D., Zhu, Peicheng: Solutions to a model with nonuniformly parabolic terms for phase evolution driven by configurational forces. SIAM J. Appl. Math. **66**(2), 680–699 (2006)
4. Alber, H.-D., Zhu, Peicheng: Evolution of phase boundaries by configurational forces. Arch. Ration. Mech. Anal. **185**(2), 235–286 (2007)
5. Alber, H.-D., Zhu, Peicheng: Interface motion by interface diffusion driven by bulk energy: justification of a diffusive interface model. Continuum Mech. Thermodyn. **23**(2), 139–176 (2011)
6. Alber, H.-D., Zhu, Peicheng: Comparison of a rapidely converging phase field model for interfaces in solids with the Allen-Cahn model. J. Elast. **111**(2), 153–221 (2013)
7. Alber, H.-D.: Asymptotics and numerical efficiency of the Allen-Cahn model for phase interfaces with low energy in solids. arXiv:1505.05442 (Submitted)
8. Brokate, M., Sprekels, J.: Hysteresis and Phase Transitions. Springer, New York (1996)

Thermoelastic Waves in Microstructured Solids

Arkadi Berezovski and Mihhail Berezovski

Abstract Thermoelastic wave propagation suggests a coupling between elastic deformation and heat conduction in a body. Microstructure of the body influences the both processes. Since energy is conserved in elastic deformation and heat conduction is always dissipative, the generalization of classical elasticity theory and classical heat conduction is performed differently. It is shown in the paper that a hyperbolic evolution equation for microtemperature can be obtained in the framework of the dual internal variables approach keeping the parabolic equation for the macrotemperature. The microtemperature is considered as a macrotemperature fluctuation. Numerical simulations demonstrate the formation and propagation of thermoelastic waves in microstructured solids under thermal loading.

1 Introduction

Microstructure of a body influences both wave propagation and heat conduction. Microstructure-oriented theories of generalized continua [1–4] are, as a rule, isothermal, whereas the generalization of heat conduction to non-Fourier laws [5–8] is usually restricted by the consideration of homogeneous and even rigid conductors. The main problem is, therefore, to elaborate a conjoint framework for the description of coupled conservative and dissipative processes. As shown recently, such an unification is possible on the basis of the dual internal variables approach [9, 10].

In the conventional thermoelasticity, the free energy density is a function of the deformation gradient and temperature only and cannot depend on the temperature gradient. However, the temperature gradient influence on the thermomechanical

A. Berezovski (✉)
Institute of Cybernetics at Tallinn University of Technology, Akadeemia tee 21, 12618 Tallinn, Estonia
e-mail: Arkadi.Berezovski@cs.ioc.ee

M. Berezovski
Embry-Riddle Aeronautical University, 600 S. Clyde Morris Boulevard, Daytona Beach, FL 32114, USA
e-mail: mihhail.berezovski@erau.edu

B. Albers and M. Kuczma (eds.), *Continuous Media with Microstructure 2*,
DOI 10.1007/978-3-319-28241-1_9

response of a microstructured material is expected in the presence of varying temperature fields at the microstructure level [11]. This means that a weakly non-local description should be applied [12]. As a result of the application of the dual internal variables theory, it is possible to obtain a hyperbolic evolution equation for microtemperature keeping the parabolic equation for the macrotemperature [10]. The microtemperature is considered as a macrotemperature fluctuation. Effects of microtemperature gradients exhibit themselves on the macrolevel due to the coupling of equations of macromotion and evolution equations for macro- and microtemperatures. The overall description of thermomechanical processes in microstructured solids includes both direct and indirect couplings of equations of motion and heat conduction at the macrolevel. In addition to the conventional direct coupling, there exists the coupling between macromotion and microtemperature evolution. This means that the macrodeformation induces microtemperature fluctuations due to the heterogeneity in the presence of a microstructure. These fluctuations, propagating with a finite speed, can induce, in turn, corresponding changes in the macrotemperature. Then the appeared changes in the macrotemperature affect macrodeformations again. Numerical simulations demonstrate the formation and propagation of thermoelastic waves in microstructured solids under thermal loading [13].

The purpose of the paper is twofold. First, the difference between the standard single internal variable theory and the dual internal variable approach is emphasized. Next, it is demonstrated how thermal gradients produced by an appropriate microstructure are able to generate fluctuations propagating with a finite speed without introducing a hyperbolic heat conduction equation for the macrotemperature.

2 Internal Variables Formalism

Before the application of the dual internal variable approach to the description of dynamic response of solids with microstructure, it is worth to explain the difference between the single internal variable theory and the dual internal variables approach. We start with the remainder of the single internal variable technique.

2.1 Single Internal Variable in One Dimension

We consider the simplest possible situation, i.e. a "body" or a "system" in one dimension. Suppose that all thermodynamic quantities like temperature, energy, entropy, etc. are defined. Then we assume that the free energy density W is specified as a function of temperature θ and an internal variable φ and its space derivative

$$W = \overline{W}(\theta, \varphi, \varphi_x). \tag{1}$$

Constitutive assumption (1) allows us to write down so-called "equations of state" (just definition of additional quantities)

$$S := -\frac{\partial \overline{W}}{\partial \theta}, \quad \tau := -\frac{\partial \overline{W}}{\partial \varphi}, \quad \eta := -\frac{\partial \overline{W}}{\partial \varphi_x}, \tag{2}$$

where S is the entropy density per unit reference volume.

The balance of internal energy in this case can be represented as

$$E_t + Q_x = 0, \tag{3}$$

where E is the internal energy density and Q is the heat flux, indices denote time and space derivatives. Remembering the connection between internal energy and free energy, i.e., $W = E - S\theta$, we arrive at another form of the energy balance

$$(S\theta)_t + Q_x = h^{int}, \quad h^{int} := -W_t, \tag{4}$$

where the right-hand side of Eq. $(4)_1$ is formally an internal heat source [14].

The energy balance should be accompanied by the second law of thermodynamics here written as

$$S_t + (Q/\theta + K)_x \geq 0, \tag{5}$$

where K is the "extra" entropy flux that vanishes in most cases, but this is not a basic requirement [14].

Multiplying the second law (5) by θ

$$\theta S_t + \theta(Q/\theta + K)_x \geq 0, \tag{6}$$

and taking into account Eq. (4), we obtain

$$-(W_t + S\theta_t) + (\theta K)_x - (Q/\theta + K)\theta_x \geq 0. \tag{7}$$

The internal heat source h^{int} is calculated as follows:

$$h^{int} = -W_t = -\frac{\partial W}{\partial \theta}\theta_t - \frac{\partial W}{\partial \varphi}\varphi_t - \frac{\partial W}{\partial \varphi_x}\varphi_{xt} = S\theta_t + \tau\varphi_t + \eta\varphi_{xt} = h^{th} + h^{intr}. \tag{8}$$

Accounting for Eq. (8), dissipation inequality (7) can be rewritten as

$$\Phi = \tau\varphi_t + \eta\varphi_{xt} - (Q/\theta + K)\theta_x + (\theta K)_x \geq 0. \tag{9}$$

To rearrange the dissipation inequality, we add and subtract the same term $\eta_x\varphi_t$

$$\Phi = \tau\varphi_t + \eta\dot{\varphi}_x - \eta_x\varphi_t + \eta_x\varphi_t - (Q/\theta + K)\theta_x + (\theta K)_x \geq 0, \tag{10}$$

which leads to

$$\Phi = (\tau - \eta_x)\varphi_t - (Q/\theta + K)\theta_x + (\eta\varphi_t + \theta K)_x \geq 0. \tag{11}$$

Following [15], we select the "extra" entropy flux in such a way that the divergence term in Eq. (11) will be eliminated

$$K = -\theta^{-1}\eta\varphi_t. \tag{12}$$

Then dissipation inequality (11) reduces to

$$\Phi = (\tau - \eta_x)\varphi_t - (Q/\theta + K)\theta_x \geq 0. \tag{13}$$

It is remarkable that in the isothermal case ($\theta_x = 0$) the dissipation is determined by the internal variable only.

The simplest choice to satisfy the dissipation inequality (13) in the *isothermal* case

$$\Phi = (\tau - \eta_x)\varphi_t \geq 0, \tag{14}$$

is the following one:

$$\varphi_t = k(\tau - \eta_x), \quad k \geq 0, \tag{15}$$

since dissipation inequality (14) is satisfied automatically in this case

$$\Phi = k\varphi_t^2 \geq 0, \quad \text{if} \quad k \geq 0. \tag{16}$$

It is easy to see that the dissipation is the product of the thermodynamic flux φ_t and the thermodynamic force $(\tau - \eta_x)$. The proportionality between the thermodynamic flux and the conjugated force is the standard choice to satisfy the dissipation inequality.

To see how the obtained evolution equation looks like, we specialize free energy dependence (1) in the isothermal case to a quadratic one

$$\overline{W} = \frac{1}{2}B\varphi^2 + \frac{1}{2}C\varphi_x^2, \tag{17}$$

where B and C are material parameters. It follows from equations of state (2) that

$$\tau := -\frac{\partial \overline{W}}{\partial \varphi} = -B\varphi, \quad \eta := -\frac{\partial \overline{W}}{\partial \varphi_x} = -C\varphi_x, \tag{18}$$

and evolution equation (15) is an equation of reaction-diffusion type

$$\varphi_t = k(C\varphi_{xx} - B\varphi), \quad k \geq 0. \tag{19}$$

The given standard formalism of internal variables of state is sufficient for many cases [16].

2.2 Dual Internal Variables

The dual internal variables approach is the extension of the technique described above. We suppose that the free energy density depends on internal variables φ, ψ and their space derivatives

$$W = \overline{W}(\theta, \varphi, \varphi_x, \psi, \psi_x). \tag{20}$$

The equations of state in the case of two internal variables read

$$S = -\frac{\partial \overline{W}}{\partial \theta}, \quad \tau := -\frac{\partial \overline{W}}{\partial \varphi}, \quad \eta := -\frac{\partial \overline{W}}{\partial \varphi_x}, \quad \xi := -\frac{\partial \overline{W}}{\partial \psi}, \quad \zeta := -\frac{\partial \overline{W}}{\partial \psi_x}. \tag{21}$$

We introduce the non-zero extra entropy flux following the case of a single internal variable and set

$$K = -\theta^{-1}\eta\varphi_t - \theta^{-1}\zeta\psi_t. \tag{22}$$

It can be checked that the intrinsic heat source is determined in the considered case as follows

$$\widetilde{h}^{intr} := (\tau - \eta_x)\varphi_t + (\xi - \zeta_x)\psi_t. \tag{23}$$

The latter means that the dissipation inequality in the isothermal case reduces to

$$\Phi = (\tau - \eta_x)\varphi_t + (\xi - \zeta_x)\psi_t \geq 0. \tag{24}$$

The solution of the dissipation inequality can be represented as [17]

$$\begin{pmatrix} \varphi_t \\ \psi_t \end{pmatrix} = \mathbf{L} \begin{pmatrix} (\tau - \eta_x) \\ (\xi - \zeta_x) \end{pmatrix}, \quad \text{or} \quad \begin{pmatrix} \varphi_t \\ \psi_t \end{pmatrix} = \begin{pmatrix} L_{11} & L_{12} \\ L_{21} & L_{22} \end{pmatrix} \begin{pmatrix} (\tau - \eta_x) \\ (\xi - \zeta_x) \end{pmatrix}. \tag{25}$$

The non-negativity of the entropy production (24) results in the positive semidefiniteness of the conductivity matrix $\mathbf{L}$, which requires

$$L_{11} \geq 0, \quad L_{22} \geq 0, \quad L_{11}L_{22} - \frac{(L_{12} + L_{21})^2}{4} \geq 0. \tag{26}$$

To be more specific, we keep a quadratic free energy density in the isothermal case

$$\overline{W} = \frac{1}{2}B\varphi^2 + \frac{1}{2}C\varphi_x^2 + \frac{1}{2}D\psi^2 + \frac{1}{2}F\psi_x^2. \tag{27}$$

Calculating quantities defined by equations of state

$$\tau := -\frac{\partial \overline{W}}{\partial \varphi} = -B\varphi, \quad \eta := -\frac{\partial \overline{W}}{\partial \varphi_x} = -C\varphi_x, \tag{28}$$

$$\xi := -\frac{\partial \overline{W}}{\partial \psi} = -D\psi, \quad \zeta := -\frac{\partial \overline{W}}{\partial \psi_x} = -F\psi_x, \tag{29}$$

we can represent system of Eqs. (25) in the form

$$\varphi_t = L_{11}(-B\varphi + C\varphi_{xx}) + L_{12}(-D\psi + F\psi_{xx}), \tag{30}$$

$$\psi_t = L_{21}(-B\varphi + C\varphi_{xx}) + L_{22}(-D\psi + F\psi_{xx}). \tag{31}$$

Now we will derive a single equation for the internal variable φ. For this purpose, Eq. (30) is differentiated with respect to time

$$\varphi_{tt} = L_{11}(-B\varphi_t + C\varphi_{xxt}) + L_{12}(-D\psi_t + F\psi_{xxt}). \tag{32}$$

Time derivatives of the internal variable ψ follow from Eq. (31)

$$\psi_t = L_{21}(-B\varphi + C\varphi_{xx}) + L_{22}(-D\psi + F\psi_{xx}), \tag{33}$$

$$\psi_{txx} = L_{21}(-B\varphi_{xx} + C\varphi_{xxxx}) + L_{22}(-D\psi_{xx} + F\psi_{xxxx}). \tag{34}$$

At last, the internal variable ψ can be eliminated using again Eq. (30)

$$(-D\psi + F\psi_{xx}) = \frac{1}{L_{12}}\varphi_t - \frac{L_{11}}{L_{12}}(-B\varphi + C\varphi_{xx}), \tag{35}$$

$$(-D\psi_{xx} + F\psi_{xxxx}) = \frac{1}{L_{12}}\varphi_{txx} - \frac{L_{11}}{L_{12}}(-B\varphi_{xx} + C\varphi_{xxxx}). \tag{36}$$

As a result, time derivatives of the internal variable ψ can be represented in terms of the internal variable φ

$$\begin{aligned}\psi_t &= L_{21}(-B\varphi + C\varphi_{xx}) + L_{22}\left(\frac{1}{L_{12}}\varphi_t - \frac{L_{11}}{L_{12}}(-B\varphi + C\varphi_{xx})\right)\\ &= \frac{L_{22}}{L_{12}}\varphi_t + \frac{L_{12}L_{21} - L_{11}L_{22}}{L_{12}}(-B\varphi + C\varphi_{xx}),\end{aligned} \tag{37}$$

$$\begin{aligned}\psi_{txx} &= L_{21}(-B\varphi_{xx} + C\varphi_{xxxx}) + L_{22}\left(\frac{1}{L_{12}}\varphi_{txx} - \frac{L_{11}}{L_{12}}(-B\varphi_{xx} + C\varphi_{xxxx})\right)\\ &= \frac{L_{22}}{L_{12}}\varphi_{txx} + \frac{L_{12}L_{21} - L_{11}L_{22}}{L_{12}}(-B\varphi_{xx} + C\varphi_{xxxx}),\end{aligned} \tag{38}$$

and the evolution equation for the internal variable φ has the form

$$\begin{aligned}\varphi_{tt} &= L_{11}(-B\varphi_t + C\varphi_{xxt}) + L_{12}(-D\psi_t + F\psi_{xxt})\\ &= L_{11}(-B\varphi_t + C\varphi_{xxt}) - DL_{22}\varphi_t - D(L_{12}L_{21} - L_{11}L_{22})(-B\varphi + C\varphi_{xx})\\ &\quad + FL_{22}\varphi_{txx} + F(L_{12}L_{21} - L_{11}L_{22})(-B\varphi_{xx} + C\varphi_{xxxx}).\end{aligned} \tag{39}$$

After rearranging, we have finally

$$\begin{aligned}\varphi_{tt} &= (CD + BF)(L_{11}L_{22} - L_{12}L_{21})\varphi_{xx} + (L_{12}L_{21} - L_{11}L_{22})(BD\varphi + CF\varphi_{xxxx})\\ &\quad -(BL_{11} + DL_{22})\varphi_t + (CL_{11} + FL_{22})\varphi_{txx}.\end{aligned} \tag{40}$$

The free energy density W is non-negative by default, which results in non-negativity of material parameters B, C, D, and F. This means that Eq. (40) is the hyperbolic wave equation with dispersion and dissipation.

Thus, extending the state space of our thermodynamic system by an additional internal variable and keeping the quadratic form for the free energy density, we arrive at the hyperbolic evolution equation for the primary internal variable.

3 One-dimensional Thermoelasticity in Solids with Microstructure

Now we are ready to apply the dual internal variables approach to thermoelasticity in solids with microstructure. We will keep the one-dimensional setting to be as simple as possible. The 3D tensorial representation of the application of the dual internal variables approach is given in [18, 19].

3.1 Reminder: Classical Linear Thermoelasticity

The one-dimensional motion of the thermoelastic conductors of heat is governed by local balance laws for linear momentum and energy (no body forces)

$$\rho v_t - \sigma_x = 0, \tag{41}$$

$$E_t - \sigma\varepsilon_t + Q_x = 0, \tag{42}$$

and by the second law of thermodynamics

$$S_t + J_x \geq 0. \tag{43}$$

Here σ is the one-dimensional stress, v is the particle velocity, J is the entropy flux, subscripts denote derivatives.

The constitutive relations include the Hooke law

$$\sigma = (\lambda + 2\mu)\varepsilon, \tag{44}$$

and the Fourier law

$$Q = -\kappa^2 \theta_x, \tag{45}$$

where λ and μ are Lamé coefficients, κ^2 is the thermal conductivity. The entropy flux is proportional to the heat flux

$$J = \frac{Q}{\theta}. \tag{46}$$

The combined constitutive relation known as the Duhamel-Neumann equation has the form

$$W(\varepsilon, \theta) = \frac{1}{2}(\lambda + 2\mu) u_x^2 - \frac{\rho c_p}{2\theta_0}(\theta - \theta_0)^2 + m(\theta - \theta_0) u_x, \tag{47}$$

where u is the displacement, c_p is the heat capacity, the thermoelastic coefficient m is related to the dilatation coefficient a and the Lamé coefficients λ and μ by $m = -a(3\lambda + 2\mu)$, θ_0 is the reference temperature.

Correspondingly, the time derivative of internal energy

$$E_t = \theta S_t + \sigma \varepsilon_t, \tag{48}$$

and entropy definition

$$S =: -\frac{\partial W}{\partial \theta} = \frac{\rho c_p}{\theta_0}(\theta - \theta_0) - m u_x, \tag{49}$$

yield in the balance of energy

$$S_t \theta - (k\theta_x)_x = \left(\frac{\rho c_p}{\theta_0}\theta_t - m u_{xt}\right)\theta - (k\theta_x)_x = 0, \tag{50}$$

which can be reduced for small deviations from the reference temperature to

$$\rho c_p \theta_t - (\kappa^2 \theta_x)_x = m\theta_0 u_{xt}. \tag{51}$$

The latter equation together with the balance of linear momentum

$$\rho u_{tt} = (\lambda + 2\mu) u_{xx} + m\theta_x, \tag{52}$$

form the coupled system of equations for linear thermoelasticity.

3.2 Microstructure Influence: Dual Internal Variables

Now we suppose that the free energy density depends on internal variables φ, ψ and their space derivatives $W = \overline{W}(u_x, \theta, \varphi, \varphi_x, \psi, \psi_x)$. We use a quadratic free energy function [9]

$$W = \frac{1}{2}(\lambda + 2\mu)\, u_x^2 - \frac{\rho_0 c_p}{2\theta_0}(\theta - \theta_0)^2 + m(\theta - \theta_0)\, u_x + A\varphi_x u_x + \frac{1}{2} C\varphi_x^2 + \frac{1}{2} D\psi^2. \tag{53}$$

Here A, C, and D are material parameters. This means that state variables include strain, temperature, and two internal variables (and their gradients). For simplicity, only a contribution of the second internal variable itself and the gradient of the primary internal variable are included here. The corresponding equations of state determine macrostress σ

$$\sigma := \frac{\partial \overline{W}}{\partial u_x} = (\lambda + 2\mu)\, u_x + m(\theta - \theta_0) + A\varphi_x, \tag{54}$$

microstress η

$$\eta := -\frac{\partial \overline{W}}{\partial \varphi_x} = -C\varphi_x - Au_x, \tag{55}$$

zero interactive internal force τ

$$\tau := -\frac{\partial \overline{W}}{\partial \varphi} = 0, \tag{56}$$

and auxilary quantities related to the second internal variable

$$\zeta = -\frac{\partial \overline{W}}{\partial \psi_x} = 0, \quad \xi = -\frac{\partial \overline{W}}{\partial \psi} = -D\psi. \tag{57}$$

Accounting for the time derivative of internal energy

$$E_t = \theta S_t + \sigma \varepsilon_t - \tau \varphi_t - \eta \varphi_{xt} - \xi \psi_t - \zeta \psi_{xt}, \tag{58}$$

results in the energy balance in the form

$$\theta S_t - \tau \varphi_t - \eta \varphi_{xt} - \xi \psi_t - \zeta \psi_{xt} + Q_x = 0, \tag{59}$$

which together with the second law of thermodynamics

$$\theta S_t + \theta J_x \geq 0, \tag{60}$$

determines the dissipation inequality

$$(\tau - \eta_x)\varphi_t + (\xi - \zeta_x)\psi_t + (\theta J + \eta\varphi_t + \zeta\psi_t - Q)_x - J\theta_x \geq 0. \tag{61}$$

Including into consideration the non-zero extra entropy flux according to Eq. (22)

$$K = -\theta^{-1}\eta\varphi_t - \theta^{-1}\zeta\psi_t. \tag{62}$$

we reduce the dissipation inequality to the sum of intrinsic and thermal parts

$$\Phi = (\tau - \eta_x)\varphi_t + (\xi - \zeta_x)\psi_t - \left(\frac{Q - \eta\varphi_t - \zeta\psi_t}{\theta}\right)\theta_x \geq 0. \tag{63}$$

Assuming that the intrinsic dissipation is independent of the temperature gradient, we are forced to modify the Fourier law as follows

$$Q - \eta\varphi_t - \zeta\psi_t = -\kappa^2\theta_x, \tag{64}$$

to satisfy the thermal part of the dissipation inequality.

The remaining intrinsic part of dissipation inequality (63) is satisfied by a choice of evolution equations for internal variables. As it is shown in [9], the thermal influence of a microstructure can be taken into account by the following choice

$$\varphi_t = R(\xi - \zeta_x), \quad \psi_t = -R(\tau - \eta_x) + R_2(\xi - \zeta_x), \tag{65}$$

where R and R_2 are certain appropriate constants. This choice means that the intrinsic dissipation is partly canceled and its remaining part is the square with a positive coefficient.

It follows from Eqs. (65) and (57) that

$$\varphi_t = -RD\psi, \tag{66}$$

i.e., the dual internal variable ψ is proportional to the time derivative of the primary internal variable φ_t. Then the evolution equation for the internal variable ψ

$$\psi_t = -R(\tau - \eta_x) + R_2(\xi - \zeta_x), \tag{67}$$

can be represented as

$$-\frac{1}{RD}\varphi_{tt} = -R(C\varphi_{xx} + Au_{xx}) + \frac{R_2}{R}\varphi_t, \tag{68}$$

or in the following form ($I = 1/R^2D$)

$$I\varphi_{tt} + \frac{R_2}{R^2}\varphi_t = C\varphi_{xx} + Au_{xx}, \tag{69}$$

which is a Cattaneo-Vernotte-type hyperbolic equation [5] for the internal variable φ.

Correspondingly, energy balance (59) in this case has the form

$$\rho_0 c_p\, \theta_t - \left(\kappa^2 \theta_x\right)_x = m\theta_0 u_{xt} + \frac{R_2}{R^2}\varphi_t^2. \tag{70}$$

Equation for macrotemperature (70) is influenced by a source term which depends on the internal variable φ. This equation, as well as evolution equation for the internal variable φ (69) is coupled with the equation of motion [9]

$$\rho_0 u_{tt} = (\lambda + 2\mu)\, u_{xx} + m\theta_x + A\varphi_{xx}, \tag{71}$$

which means that the internal variable φ possesses a wave-like behavior induced by the macrodeformation. Identifying the internal variable φ with the microtemperature [9], we see that the microtemperature may induce a wave-like propagation also for the macrotemperature due to the corresponding source term in heat conduction equation (70). Physically, the introduced microtemperature describes fluctuations about the mean temperature due to the presence of a microstructure.

4 Numerical Simulations

Now we will check the influence of microstructure on the thermoelastic wave propagation numerically. The solution of equations (69)–(71) in the case of plane wave motion in a thermoelastic half-space is obtained by means of the wave propagation algorithm explained in detail in [13]. We consider the matrix material as silicon and the microstructure is represented by copper particles embedded randomly in the matrix. Material parameters for silicon are the following [20]: the macroscopic density, ρ_0, is equal to 2390 kg/m^3, the Lamé coefficients $\lambda = 48.3$ GPa, and $\mu = 61.5$ GPa, the heat capacity, $c_p = 800$ J/(kg K), the reference temperature, $\theta_0 = 300$ K, the thermal conductivity, $k = 149$ W/(m K), the thermal expansion coefficient, $\alpha = 2.6 \times 10^{-6}$ 1/K. Correspondingly, material parameters of copper are [21]: the macroscopic density, ρ_0, is equal to 8960 kg/m^3, the Lamé coefficients $\lambda = 101.5$ GPa, and $\mu = 47.75$ GPa, the heat capacity, $c_p = 386$ J/(kg K), the reference temperature, $\theta_0 = 300$ K, the thermal conductivity, $k = 401$ W/(m K), the thermal expansion coefficient, $\alpha = 16.5 \times 10^{-6}$ 1/K.

The problem under consideration is the thermoelastic wave propagation induced by a thermal excitation at the boundary of the half-space. It is assumed that the material is initially at rest. Two consecutive heat pulses are generated at the traction free boundary plane for the first 120 time steps following the rule

$$\theta(0,t) = \frac{1}{2}\left(1 + \cos\left(\frac{\pi(t - 30\Delta t)}{30}\right)\right). \tag{72}$$

The scale of excitation, U_0, is chosen as 6 % of the length of the computational domain, L, so that $U_0/L = 0.06$. The scale of the microstructure, l, is supposed to be even less $l/L = 0.002$. Following [22] coupling parameters used in calculations are chosen as follows:

$$\frac{R_{22}}{R_{12}^2} = \frac{\rho_0 c_0}{l}, \quad A = 0.02\rho_0 c_0^2, \quad C = \rho_0 c_0^2. \tag{73}$$

To exclude the direct influence of stress field on the macrotemperature, it was assumed that the velocity gradient in Eq. (70) is negligible.

All calculations were performed by means of the finite-volume numerical scheme [13] using the value of the Courant number 0.98. This scheme is a modification of the previously reported conservative finite-volume algorithm [23, 24] adapted for microstructure modeling. It belongs to a broad class of finite-volume methods for thermomechanical problems [25, 26].

Results of calculations are presented in Fig. 1. This Figure demonstrates explicitly how the coupling in mathematical model (69)–(71) works. In the case of pure silicon we see only thermal diffusion in the vicinity of the boundary. The double pulse thermal excitation generates the corresponding stress pulses propagating through the material. If microstructure is taken into account, this stress pulses induce

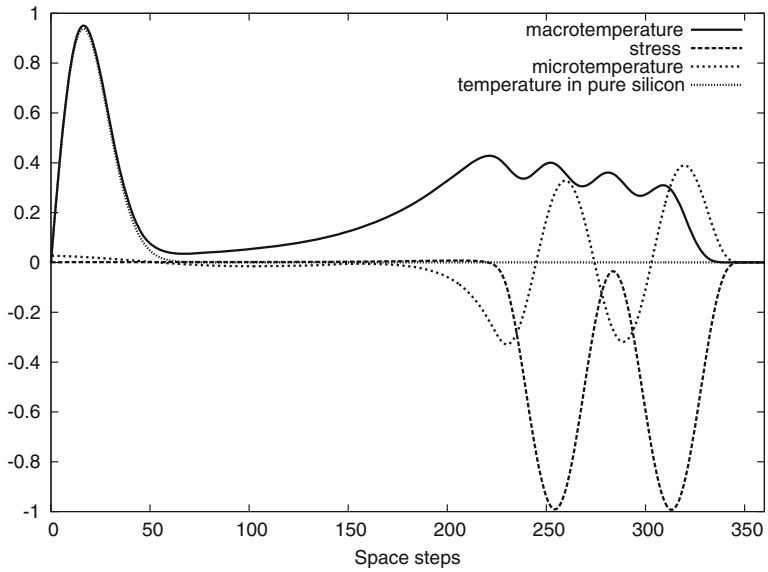

Fig. 1 Normalized temperature, stress, and microtemperature distribution at 350 time steps

the microtemperature waves. The microtemperature affects the macrotemperature resulting in the oscillations of the macrotemperature hump with a fading thermal wake.

It should be noted that the scales for all quantities in Fig. 1 are different and chosen artificially to show all quantities in a single picture. The real effect of the microstructure is sufficiently small and can be made visible only by means of a corresponding zooming.

5 Conclusions

The dual internal variables approach leads naturally to a hyperbolic evolution equation for the primary internal variable. In the case of thermoelasticity, this internal variable can be interpreted as a microtemperature or, in other words, as a temperature fluctuation due to the microstructure. Coupling of the governing equations results in the wave-like temperature behavior.

Although the observed effect of the microstructure is small, it exists in the case of realistic values of material parameters. This effect can be amplified by a choice of suitable materials or even by a design of corresponding artificial materials.

It is remarkable that the governing equation for the macrotemperature remains parabolic. The wave-like temperature behavior appears only due to the influence of microstructure.

Acknowledgments The research was supported by the EU through the European Regional Development Fund and by the Estonian Research Council project PUT 434.

References

1. Mindlin, R.D.: Arch. Ration. Mech. Anal. **16**(1), 51 (1964)
2. Capriz, G.: Continua with Microstructure. Springer, New York (1989)
3. Eringen, A.C.: Microcontinuum Field Theories. Springer (1999)
4. Forest, S.: J. Eng. Mech. **135**(3), 117 (2009)
5. Joseph, D.D., Preziosi, L.: Rev. Mod. Phys. **61**(1), 41 (1989)
6. Chandrasekharaiah, D.: Appl. Mech. Rev. **51**(12), 705 (1998)
7. Ignaczak, J., Ostoja-Starzewski, M.: Thermoelasticity with Finite Wave Speeds. Oxford University Press (2009)
8. Straughan, B.: Heat Waves, vol. 177. Springer Science and Business Media (2011)
9. Berezovski, A., Engelbrecht, J., Maugin, G.A.: Arch. Appl. Mech. **81**(2), 229 (2011)
10. Berezovski, A., Engelbrecht, J., Maugin, G.A.: J. Therm. Stress. **34**(5–6), 413 (2011)
11. Tamma, K.K., Zhou, X.: J. Therm. Stress. **21**(3–4), 405 (1998)
12. Berezovski, A., Engelbrecht, J., Ván, P.: Arch. Appl. Mech. **84**(9–11), 1249 (2014)
13. Berezovski, A., Berezovski, M.: Acta Mech. **224**(11), 2623 (2013)
14. Maugin, G.A.: Arch. Appl. Mech. **75**(10–12), 723 (2006)
15. Maugin, G.: J. Non-Equilib. Thermodyn. **15**(2), 173 (1990)
16. Horstemeyer, M.F., Bammann, D.J.: Int. J. Plast. **26**(9), 1310 (2010)

17. Ván, P., Berezovski, A., Engelbrecht, J.: J. Non-Equilib. Thermodyn. **33**(3), 235 (2008)
18. Berezovski, A., Engelbrecht, J., Maugin, G.A.: Arch. Appl. Mech. **81**(2), 229 (2011a)
19. Berezovski, A., Engelbrecht, J., Maugin, G.A.: J. Therm. Stress. **34**(5–6), 413 (2011b)
20. Hopcroft, M.A., Nix, W.D., Kenny, T.W.: J. Microelectromech. Syst. **19**(2), 229 (2010)
21. Lienhard, J.H.: A Heat Transfer Textbook. Courier Corporation (2011)
22. Berezovski, A., Engelbrecht, J.: J. Coupled Syst. Multiscale Dyn. **1**(1), 112 (2013)
23. Berezovski, A., Engelbrecht, J., Maugin, G.: Arch. Appl. Mech. **70**(10), 694 (2000)
24. Berezovski, A., Maugin, G.: J. Comput. Phys. **168**(1), 249 (2001)
25. LeVeque, R.J.: Finite Volume Methods for Hyperbolic Problems. Cambridge University Press (2002)
26. Guinot, V.: Wave Propagation in Fluids: Models and Numerical Techniques. Wiley (2012)

Unconventional Thermodynamical Model of Processes in Material Structures

Bogdan T. Maruszewski

Abstract Fast development of applied sciences, particularly of the technical ones has resulted in the creation of a complex situation in which independently developing scientific branches such as mathematics, mechanics, physics, chemistry, Earth sciences and even biology began to cover each other. So, a new area called the coupled field theory in mono- and multiphase materials of various internal structures has been created. One of the best ways to model real processes and interactions occuring in any continuous material region within the phenomenological manner taking into consideration a reasonably wide range of effects is the so-called *thermomechanics*. The paper deals with an abbreviated form of this extremely broad area concerning a concise description of physical reality.

Keywords Thermomechanical modelling · Coupled field theory · Materials of internal structure

1 Introduction

Thermomechanical modelling (cf. [1–3]) is able to concern simultaneously many phenomena and interactions thanks its deep fixing in physics (mechanics, thermodynamics, electrodynamics, quantum mechanics, and the like) and necessary mathematical branches (differential and integral equations, group theory, operator calculus, algebra and others). Several parts can be distinguished creating such a model of interactions. But the main condition that should be put on any thermomechanical model is such that it has to be admissible by nonequilibrium irreversible thermodynamics.

B.T. Maruszewski (✉)
Institute of Applied Mechanics, Poznan University of Technology, ul. Jana Pawła II 24, 60-965 Poznan, Poland
e-mail: bogdan.maruszewski@put.poznan.pl

B. Albers and M. Kuczma (eds.), *Continuous Media with Microstructure 2*,
DOI 10.1007/978-3-319-28241-1_10

2 General Structure of Thermomechanical Modelling

THE FIRST PART should concern the set and properties of materials, structures and other elements creating the system, its geometry, scale and fields interacting there, and also properties of physical processes running during transferring the system through a set of states. As a result it is necessary to formulate *a vector of the state (the set of independent variables)* [4–15]:

$$C = \left\{ \mathbf{A}^{\beta}, \mathbf{a}^{\gamma}, \alpha^{\delta} \left| \mathbf{D}^{\lambda}, \mathbf{b}^{x}, \xi^{\mu} \right| \mathbf{B}^{\varepsilon}, \mathbf{j}^{\eta} \right\}. \tag{1}$$

This set consists of three parts: the controllable state variables (tensor, vector and scalar), the noncontrollable state variables (the internal or hidden variables also called order parameters [4] also tensor, vector and scalar) and the fluxes of the fields described by variables from the first and second ones [16] (only of tensor and vector characters). The upper greek letters count particular variables. Each field from (1) reads:

$$C = C(x_k, t). \tag{2}$$

Moreover set (1) can be extended to gradients

$$\mathbf{C} = \left\{ C, C_{,i}, C_{,ij}, \ldots, C_{,ij\ldots s} \right\}, \tag{3}$$

and/or time derivatives of (2)

$$\mathbf{C} = \left\{ C, \dot{C}, \ddot{C}, \ldots, \overset{(n)}{C} \right\} \tag{4}$$

Example 1 Thermoelastic paramagnet in an applied magnetic field [7]

The vector of state reads

$$\mathbf{C} = \{\varepsilon, \mathbf{B}, T, \nabla T\} \tag{5}$$

ε is the strain tensor, $\mathbf{B}$ is the magnetic induction and T is the temperature. All the variables are controllable.

Example 2 Magnetothermoelastic n-type semiconductor defective by dislocations and irradiated by neutrons [5, 8, 13, 17]

The vector of state can be chosen in the form:

$$\mathbf{C} = \{\varepsilon, \mathbf{E}, \mathbf{B}, T, \nabla T \,|\alpha, \tilde{\mu}, n, \nabla\alpha, \nabla\mu, \nabla n\}. \tag{6}$$

$\mathbf{E}$ is the electric field intensity. But α is the dislocation density tensor, $\tilde{\mu}$ is the magnetic moment density vector of neutrons and n is the electron density—they are the internal variables.

Example 3 Thermoelastic body with temperature relaxation [9, 16]

This time the vector of state is the following:

$$\mathbf{C} = \{\varepsilon, T, \nabla T \,|\mathbf{q}\}\,. \tag{7}$$

$\mathbf{q}$ is the heat flux density.

Example 4 Thermo-magneto-visco-elastic field of the magnetic vortices in II-type superconductor with the time relaxation of the thermal and magnetic vortex fields [14]

This time the vector of state is as follows:

$$\mathbf{C} = \left\{\varepsilon, \phi, \mathbf{A}, T, \nabla T \,\middle|\, \Psi, \Psi^*, \nabla\Psi, \nabla\Psi^*, \sigma, \mathbf{q}, \mathbf{j}^s\right\}. \tag{8}$$

ϕ and $\mathbf{A}$ are scalar and vector electromagnetic potentials, Ψ is the wave function of the Cooper pairs (internal variable—order parameter), σ is the stress tensor (momentum flux)—its presence indicates the viscosity of the vortex field (elastic relaxation) and $\mathbf{j}^s$ is the supercurrent density.

SECOND PART deals, naturally, with the formulation of laws necessary to determine space-time distributions of fields from the state vector. Such a set can be proposed in the form of:

- the balances of [1–3]
  - mass
  - momentum
  - moment of momentum
  - internal energy (the I principle of thermodynamics)
- the evolution equations of electromagnetic field (Maxwell's equations) [3]
- the evolution equations of internal variables [4]
- the evolution equations of nonequilibrium fluxes [16].

To ensure the physical meaning of the solutions of the above set

- the entropy inequality (the II principle of thermodynamics) has to be formulated [2].

THE THIRD PART consists of a creation of the constitutive theory. It should be started from the definition of the so-called *constitutive vector (set of dependent variables)*. Then using the Lagrange multipliers method and Liu's theorem [18] to the entropy inequality with the laws formulated within the previous part we arrive at:

- the laws of state
- the affinities
- the laws of the processes
- the residual inequality.

Introducing the scalar and vector thermodynamical potentials the detailed constitutive theory can be formulated. Then the particular analysis of the entropy inequality with the help of the Onsager-Casimir theory [1] leads to the kinetic part of the modelled processes. But sometimes the use of the representation theory of the tensor, vector and scalar functions of the tensor, vector and scalar variables allows to describe all the above considerations in a reasonably more general manner [3, 19]. To complete the created model the solutions of the laws introduced in the previous parts for a particular case need to be obtained. So in **THE FOURTH PART** we have to determine such laws at singular surfaces, lines and other geometrical objects which characterize the considered multiphase physical system [20]. So, to find exact solutions of the field equations resulting from balances, external field evolution equations (electromagnetic, for instance), evolution equations of internal variables and evolution equations of nonequilibrium fluxes in material systems of finite extent, the formulation of the suitable jump conditions of variables forming the vector of state (1) across singular surfaces is necessary. If we deal with a surface whose points move with the same velocities as the material points appearing there, we deal with the so-called material surface.

2.1 Jump Conditions Across a Singular Surface for Balances

- *The balance of mass*

$$n_i \left[\left[\rho(v_i - v_i^s)\right]\right] = f^{\rho}(\rho^s). \tag{9}$$

  v_i^s is the velocity of a point at the singular surface, f^{ρ} is a function of the surface mass concentration, n_i is the unit normal vector positive outward and $[[a]] = a^+ - a^-$ denotes the jump of quantity a across the singular surface. If $v_{\mathrm{i}} = v_i^s$ we deal with the material surface.
- *The balance of momentum*

$$\left[\left[\sigma_{ij}\right]\right] n_j = f_i^{\rho}(\rho^s, \not{\sigma}^s) + \left[\left[\rho(v_k - v_k^s) n_k v_i\right]\right]. \tag{10}$$

  f_i^{ρ} is a function of ρ^s and the surface tension $\not{\sigma}^s$. The surface momentum source in (10) is very often omitted.
- *The balance of moment of momentum*
  We skip here the problem of the jump of the balance of moment of momentum across a singular surface because we deal in the paper only with physical interactions in thermomechanical media of symmetric elastic properties (we exclude Cosserat and other skew-symmetric—like media from the considerations; see Conclusions).
- *The balance of energy*

$$[[q_i - v_k \sigma_{ki}]] n_i = f^E(e^s, \not{\sigma}^s) + \left[\left[\rho\left(e - \frac{v^2}{2}\right)(v_k - v_k^s) n_k\right]\right] - \left[\left[E^c\right]\right] v_i n_i. \tag{11}$$

In (11) the lack of the surface energy flux and the surface sources of mass, momentum and energy has been already assumed. f^E is a function of the surface internal energy e^s and the surface tension. e denotes the internal energy density and E^c deals with other kinds of energies coming from various external fields.

2.2 Jump Conditions for External Fields Influencing the Material System

These conditions depend on a kind of a problem which is taken into considerations. So, it is difficult or almost impossible to present them in any general form. If the external field is an electromagnetic one, such jump conditions come from classical discontinuity conditions for electric and magnetic fields across a singular surface (cf. [3]).

2.3 Jump Conditions for Evolution Equations of Tensor, Vector and Scalar Fields

Based on the ojective Zaremba-Jaumann time derivative definition we have for:

- the arbitrary rank tensor field evolution equation

$$\frac{\partial}{\partial t}\left[\left[W_{k\ldots m}\right]\right] + v_i^s n_i \left(n_j \left[\left[W_{k\ldots m}\right]\right]_{,j} - \left[\left[n_k \frac{\partial W_{k\ldots m}}{\partial x_k}\right]\right]\right) + v_i \left[\left[W_{k\ldots m,i}\right]\right] - w_{kq}\left[\left[W_{q\ldots m}\right]\right] - \cdots - w_{mq}\left[\left[W_{k\ldots q}\right]\right] = \left[\left[\mathbf{W}_{k\ldots m}\right]\right] \quad (12)$$

  where $w_{kl} = \frac{1}{2}(v_{k,l} - v_{l,k})$
- the vector field evolution equation

$$\frac{\partial}{\partial t}\left[\left[W_i\right]\right] + v_k^s n_k \left(n_j \left[\left[W_i\right]\right]_{,j} - \left[\left[n_k \frac{\partial W_i}{\partial x_k}\right]\right]\right) + v_k \left[\left[W_{i,k}\right]\right] - w_{ik}\left[\left[W_k\right]\right] = \left[\left[\mathbf{W}_i\right]\right] \quad (13)$$

- the scalar field evolution equation

$$\frac{\partial}{\partial t}\left[\left[W\right]\right] + v_k^s n_k \left(n_j \left[\left[W\right]\right]_{,j} - \left[\left[n_k \frac{\partial W}{\partial x_k}\right]\right]\right) + v_k \left[\left[W_{,k}\right]\right] = \left[\left[\mathbf{W}\right]\right]. \quad (14)$$

The above presented jump conditions are obviously one of the possibilities leading to particular boundary value problems concerning physical field interactions in mono- and multi-phase materials of finite extent.

3 Application of the Proposed Model

The presented thermomechanical model will be now, as an illustration, applied to describe *reciprocal interactions of the mass diffusion field and dislocation field with an elastic body* [15]. The system consists of two mass components: diffusing mass of density ρ_1 and an elastic body of density ρ_2 (two-component mixture of density $\rho = \rho_1 + \rho_2$, $\rho_1 \ll \rho_2$). Before we use the proposed thermomechanical model let us define the field of mass. The concentration of diffusing mass reads:

$$c = \frac{\rho_1}{\rho}. \tag{15}$$

Then, following the mass conservation principle we have:

$$\dot{\rho} + \rho v_{i,i} = 0, \tag{16}$$

$$\frac{\partial \rho_1}{\partial t} + (\rho_1 v_{1i})_{,i} = r_1, \quad \frac{\partial \rho_2}{\partial t} + (\rho_2 v_{2i})_{,i} = r_2, \quad \text{(we assume } r_1 = r_2 = 0) \tag{17}$$

$$\rho v_i = \rho_1 v_{1i} + \rho_2 v_{2i}, \qquad \text{(barycentric velocity)}, \tag{18}$$

so the flux of mass reads:

$$j_i = \rho_1 (v_{1i} - v_i). \tag{19}$$

THE FIRST PART—the determination of the set of independent variables (the state vector):

$$C = \left\{ \varepsilon_{ij}, c, T, a_{ij}, j_i, q_i, V_{ijk}, c_{,j}, T_{,i}, a_{ij,k} \right\}. \tag{20}$$

Temperature, concentration and dislocation fields are also of the relaxation character and heterogeneous. The viscosity of the body is omitted.

THE SECOND PART—the fundamental laws:

- the evolution equations of the diffusing mass field

$$\rho \dot{c} + j_{i,i} = 0, \tag{21}$$

$$\overset{*}{j}_i - J_i(C) = 0, \tag{22}$$

- the evolution equations of the elastic field

$$\rho \dot{v}_i - \sigma_{ij,j} - f_i = 0, \tag{23}$$

$$\in_{ijk} \sigma_{jk} + g_i = 0, \tag{24}$$

f_i and g_i are the densities of body forces and moments;

- the evolution equations of the temperature field

$$\rho\dot{e} - (\sigma_{ji}v_{i,j} - q_{i,i} + \rho r) = 0, \tag{25}$$

$$\overset{*}{q}_i - Q_i(C) = 0, \tag{26}$$

  e is the internal energy density and r is the heat source distribution;
- the evolution equations of the dislocation field

$$\overset{*}{a}_{ij} + V_{ijk,k} - A_{ij}(C) = 0, \tag{27}$$

$$\overset{*}{V}_{ijk} - \mathscr{V}_{ijk}(C) = 0, \tag{28}$$

  the superimposed star denotes the Zaremba-Jaumann time derivative and $Q_i(C)$, $A_{ij}(C)$ and $\mathscr{V}_{ijk}(C)$ will be determined by the constitutive theory;
- the entropy inequality (the Clausius-Duhem inequality)

$$\rho S + \Phi_{i,i} - \frac{\rho r}{T} \geq 0, \tag{29}$$

  S is the entropy density and Φ_i is the entropy flux, so the solutions of the evolution equations should have now physical meaning.

THE THIRD PART—the constitutive theory:
Let us define now the *set of dependent variables (the constitutive vector)* and propose the general form of the *constitutive laws* in the following form:

$$Z = \left\{\sigma_{ij}, \mu^c, \eta_{ij}, g_i, e, A_{ij}, J_i, Q_i, \mathscr{V}_{ijk}, S, \Phi_i\right\}, \qquad Z = \tilde{Z}(C), \tag{30}$$

Z and C are determined in the same point and time, μ^C is the chemical potential of the mass concentration field and n_{ij} plays the same role for the dislocation density field.

The searched constitutive relations are obtained exploiting the entropy inequality with the help of Liu's theorem. Denoting the left hand sides of the fundamental laws as F^c, F_i^v, F^e, F_{ij}^a, F_i^I, F_i^Q and F_{ijk}^w this inequality reads [18]:

$$\rho\frac{\partial S}{\partial t} + \rho v_k S_{,k} + \Phi_{k,k} - (\Lambda^c F^c + \Lambda_i^v F_i^v + \Lambda^e F^e + \Lambda_{ij}^a F_{ij}^a + \Lambda_i^I F_i^I + \Lambda_i^Q F_i^Q + \Lambda_{ijk}^w F_{ijk}^w) \geq 0. \tag{31}$$

$$\Lambda =: \Lambda^c, \Lambda_i^v, \Lambda^e, \Lambda_{ij}^a, \Lambda_i^I, \Lambda_i^Q, \Lambda_{ijk}^w \tag{32}$$

denotes the set of the indefinite Liu-Langrange multipliers. Introducing now the scalar thermodynamical potential (the free energy density)

$$\Psi = e - TS \tag{33}$$

and the vector thermodynamical (kinetic) potential [7]

$$\kappa_i = \rho\Psi v_i - T\Phi_i, \tag{34}$$

taking the multipliers in the form

$$\begin{aligned} \Lambda^e &= \frac{1}{T}, \qquad \Lambda^c = -\frac{1}{T}\mu^c, \qquad \Lambda^a_{ij} = -\frac{1}{T}\eta_{ij}, \\ \Lambda^I_i &= -\frac{1}{T}\Pi^I_i, \qquad \Lambda^Q_i = -\frac{1}{T}\Pi^Q_i, \qquad \Lambda^w_{ijp} = -\frac{1}{T}\pi_{ijp} \end{aligned} \tag{35}$$

and using the fact that the Clausius-Duhem inequality is linear with respect to higher range derivatives of independent variables C we arrive at

- the laws of state

$$\begin{aligned} \sigma_{ij} &= \rho\frac{\partial\Psi}{\partial\varepsilon_{ij}}, \qquad \mu^c = \frac{\partial\Psi}{\partial c}, \qquad \frac{\partial\Psi}{\partial c_{,i}} = 0, \\ S &= -\frac{\partial\Psi}{\partial T}, \qquad \eta_{ij} = \frac{\partial\Psi}{\partial a_{ij}}, \qquad \frac{\partial\Psi}{\partial T_{,i}} = 0, \qquad \frac{\partial\Psi}{\partial a_{ij,k}} = 0, \end{aligned} \tag{36}$$

- the affinities

$$\Pi^I_i \equiv \rho\frac{\partial\Psi}{\partial j_i}, \qquad \Pi^Q_i \equiv \rho\frac{\partial\Psi}{\partial q_i}, \qquad \pi_{ijp} \equiv \rho\frac{\partial\Psi}{\partial V_{ijp}}, \tag{37}$$

- the laws of the processes

$$\begin{aligned} &\frac{\partial\kappa_k}{\partial\varepsilon_{ij}} = 0, \qquad \frac{\partial\kappa_k}{\partial j_i} = \mu^C\delta_{ik} + v_k\Pi^I_i, \\ &\frac{\partial\kappa_k}{\partial q_i} = -\delta_{ik} + v_k\Pi^Q_i, \qquad \frac{\partial\kappa_k}{\partial V_{ijp}} = \eta_{ij}\delta_{pk} + v_k\pi_{ijp}, \\ &\frac{\partial\kappa_k}{\partial c_{,i}} = 0, \qquad \frac{\partial\kappa_k}{\partial T_{,i}} = 0, \qquad \frac{\partial\kappa_k}{\partial a_{ij,p}} = 0, \end{aligned} \tag{38}$$

- the residual inequality

$$T\frac{\partial\Phi_k}{\partial c}c_{,k} + T\frac{\partial\Phi_k}{\partial T}T_{,k} + T\frac{\partial\Phi_k}{\partial a_{ij}}a_{ij,k} - \eta_{ij}A_{ij} - \Pi^I_i J_i - \Pi^Q_i Q_i - \pi_{ijk}\mathcal{V}_{ijk} \geq 0. \tag{39}$$

Finally, the scalar and vector potentials take the form

$$\Psi = \Psi(\varepsilon_{ij}, c, T, a_{ij}, j_i, q_i, V_{ijk}), \tag{40}$$

$$\kappa_k = -q_k + \mu^c j_k + \eta_{ij}V_{ijk} + \rho v_k\Psi. \tag{41}$$

Then the entropy flux is the following

$$\Phi_k = \frac{1}{T}(q_k - \mu^c j_k - \eta_{ij} V_{ijk}). \tag{42}$$

Using now any method which leads to the linear approximation of Ψ and applying the Onsager-Casimir reciprocity relations to the residual inequality we arrive at the following state and kinetic constitutive relations. We confine them to the isotropic form as

$$\sigma_{ij} = 2\mu\varepsilon_{ij} + (\lambda\varepsilon_{kk} - \lambda^c c - \lambda^a a)\delta_{ij}, \tag{43}$$

$$\frac{\partial a}{\partial t} + V_{k,k} = d_1\varepsilon_{kk} + d_2 c + \frac{1}{\tau^A}a + d_3 j_i + d_4 V_i + d_5 c_{,i} + d_6 a_{,i}, \tag{44}$$

$$\tau^c \frac{\partial j_i}{\partial t} = -j_i + d_7 V_i - \rho D c_{,i} + \xi^I a_{,i}, \tag{45}$$

$$\tau^a \frac{\partial V_i}{\partial t} = d_8 j_i + V_i - D^V c_{,i} + \xi a_{,i}. \tag{46}$$

$\lambda, \mu, \lambda^c, \lambda^a, d_1, \ldots, d_8, \tau^A, \tau^c, \tau^a, D, D^V, \xi^I$ and ξ are the characteristic coefficients of the considered physical problem that have to be determined by experiment. Assuming now that all the processes modelled within the proposed description are isothermal the fundamental laws can be presented as the set of field equations in the following linear form

$$\begin{aligned} &\mu u_{k,ii} + (\lambda + \mu)u_{i,ki} - \rho\ddot{u}_k - \lambda^c c_{,k} - \lambda^a a_{,k} = 0, \\ &\rho D_{c,kk} - \rho\dot{c} - \tau^c\rho\ddot{c} - \xi^I a_{,kk} = 0, \\ &\xi a_{,kk} - \dot{a} - \tau^a\ddot{a} + d_1 u_{k,k} + \tau^a d_1 \dot{u}_{k,k}. \end{aligned} \tag{47}$$

If we deal with the system of finite extent and/or multiphase structure there is the necessity to use ***THE FOURTH PART*** of the modelling in order to determine the proper boundary-value problem for the final field equations if we use Eq. (47) in such a system and structure.

4 Conclusion

The paper shows a concise routine of the thermomechanical modelling of simultaneous interactions of various physical fields in materials of various physical and geometrical properties. The presented proposition should be understood and treated as a kind of fundamental description, one among many others possible which in particular situations may be considerably modified and developed.

Acknowledgments The paper has been supported by 02/21/DSPB/3463—2015 grant.

References

1. Hutter, K.: The foundations of thermodynamics, its basic postulates and implications. A review of modern thermodynamics. Acta Mech. **27**, 1–54 (1977)
2. De Groot, S.R., Mazur, P.: Non-equilibrum Thermodynamics. North-Holland, Amsterdam (1962)
3. Eringen, A.C. (ed.): Continuum Physics. Academic Press, New York, London, vol. I - 1971, vol. - 1975, vol. III - 1976, vol. IV - 1976
4. Maugin, G.A.: Vectorial internal variables in magnetoelasticity. J. Mécanique **18**, 541–563 (1979)
5. Maruszewski, B.: Charge carrier and elastic waves in thin epitaxial film grown on a semiconductor. Wave Motion **13**, 89–106 (1991)
6. Maruszewski B., Termodynamiczne podstawy magnetotermodyfuzji i elektrotermodyfuzji w ośrodku ciągłym, WNPP, Nr 178, Poznań 1986
7. Maruszewski, B.: Evolution equations of thermodiffusion in paramagnets. Int. J. Eng. Sci **26**, 1217–1230 (1988)
8. Maugin, G.A., Maruszewski, B.: Equations of neutron transport through deformable paramagnets. J. Non-Equilibr. Thermodyn. **14**, 385–396 (1989)
9. Restuccia, L., Maruszewski, B.: Nonlinear thermoelasticity of ferroelastics. Mech. Res. Com. **25**, 137–145 (1998)
10. Muschik, W., Papenfuss, C., Ehrentraut, H.: Mesoscopic theory of liquid crystals. J. Non-Equilbr. Thermodyn. **29**, 75–106 (2004)
11. Muschik, W., Papenfuss, C., Ehrentraut, H.: Sketch of the mesoscopic description of nematic liquid crystals. J. Non-Newton. Fluid Mech. **119**, 91–104 (2004)
12. Maruszewski, B.: Dynamical magnetothermoelastic problem in circular cylinders—I. Basic equations. Int. J. Eng. Sci. **19**, 1233–1240 (1981)
13. Restuccia, L., Maruszewski, B.: Interactions between electronic field and dislocations in a deformable semiconductor. Int. J. Appl. Electrom. Mech. **6**, 139–153 (1995)
14. Maruszewski, B.: On a nonclasical thermoviscomechanical stress in a vortex field in the type—II superconductor. Phys. Stat. Sol. (b) **244**, 919–927 (2007)
15. Restuccia, L., Maruszewski, B.: Diffusion and dislocation influences on the dynamics of elastic bodies. Int. J. Eng. Sci. **29**, 1053–1063 (1991)
16. Jou, D., Casas Vázques J., Lebon G.: Extended irreversible thermodynamics. Rep. Prog. Phys. **51**, 1105–1179 (1988)
17. Maruszewski, B.: On a dislocation-core tensor. Phys. Stat. Sol. (b) **168**, 59–66 (1991)
18. Liu, I.S.: Method of Lagrange multipliers for exploitation of the entropy principle. ARMA **46**, 131 (1972)
19. Smith, G.F.: On isotropic functions of symmetric tensors, skew—symetric tensors and vectors. Int. J. Eng. Sci. **9**, 899–916 (1971)
20. Kosiński, W.: Wstęp do teorii osobliwości pola i analizy fal. PWN, Warszawa-Poznań (1981)

A Monatomic Ideal Gas—Prototype of a Continuous Medium with Microstructure

Ingo Müller

Abstract A complete set of equations for the description of the properties of monatomic ideal gases is formed by the balance equations of all moments of the distribution function which satisfies the Boltzmann equation. In a manner of speaking these balance equations describe a continuum and the elements of its microstructure are the moments. There are infinitely many moments and for rapidly changing processes with steep gradients they are all needed. However, for slow and smooth processes the necessary set of balance equations may be cut off at some point and may then still be useful. The most drastic cut-off provides the Euler equations in which no dissipation occurs, so that its applicability is limited to isentropic flows. A less rigorous cut-off leads to the equations of Navier-Stokes and Fourier which permit the mathematical treatment of viscous flow and heat conduction. Those curtailed sets of balance equations have been studied at great length: Their study is the subject of ordinary thermodynamics. A still less drastic cut-off leads to Grad's 13- and 14-moment equations. These provide some improvement upon both Euler and Navier-Stokes-Fourier. Thus they forbid rigid rotation of a gas in the presence of heat conduction. Even so, the Grad theory is not suitable for high frequency sound propagation and high frequency light scattering and for the study of shock structures. The study of Grad's equations and of the balance equations for higher moments is the subject of extended thermodynamics. Mathematically speaking the set of balance equations of moments in the kinetic theory of gases provides a prototype of the hyperbolic balance laws of continuum physics. Indeed, the equations are hyperbolic and the entropy principle makes them symmetric hyperbolic. High frequency light scattering in monatomic gases proves the applicability and usefulness of extended thermodynamics, because it furnishes results that are in full agreementwith experiments at any frequency, while ordinary thermodynamics merely describes the low-frequency limit. In hyperbolic equations there is a competition between non-linearity and dissipation: Non-linearity attempts to steepen a field to a shock while dissipation smoothes it out. And if dissipation is big enough, no shock singularities will appear. In extended thermodynamics singularities can be prevented by adding more equations, hence more dissipative terms. The study of shock structures makes

Ingo Müller (✉)
Technische Universität Berlin, Straße des 17. Juni, 10623 Berlin, Germany
e-mail: ingo.mueller@alumni.tu-berlin.de

B. Albers and M. Kuczma (eds.), *Continuous Media with Microstructure 2*,
DOI 10.1007/978-3-319-28241-1_11

this evident. Hyperbolic equations have as many sound modes as there are equations and all their speeds are different from the ordinary sound speed. Extended thermodynamics proves that the highest sound speed increases monotonically as more equations are added. It is when a shock structure moves more rapidly than the highest sound speed that discontinuities appear in the theory. One may thus say that the flow is truely supersonic only when its speed is quicker than the highest characteristic speed. However, that will generally happen at Mach numbers well beyond Ma equal to 1. It is a clear sign that more equations are needed.

1 Introduction

Few people will think of microstructure in the context of an ideal gas, let alone of a monatomic ideal gas. They may well ask: Do not the five fields of mass density $\rho(x_n, t)$, velocity $v_i(x_n, t)$, energy density $\rho(x_n, t)e(x_n, t)$ or temperature $T(x_n, t)$ fully provide whatever there is to be known about monatomic gases?

Well, definitly not. To be sure these are important fields but they only form the tip of an iceberg. Indeed, the full knowledge of the state of a monatomic gas is furnished by the distribution of atoms of all velocities in all positions of the gas and at all times. That knowledge is embodied in the *distribution function* $f(x_n, c_n, t)$ defined such that

$$f(x_n, c_n, t)\mathrm{d}c \tag{1}$$

is the density of atoms at position x_n and time t with velocities between c_n and $c_n + \mathrm{d}c_n$. ρ, v and e are moments of the distribution function

$$\rho = m\int f\,\mathrm{d}f, \quad \rho v_i = m\int c_i f\,\mathrm{d}c, \quad 2\rho e = \int c^2 f\,\mathrm{d}c \tag{2}$$

so that they provide only minimal knowledge about $f(x_n, c_n, t)$: mean value and first and second moment.

Full knowledge is provided by the full set of moments

$$F_{i1i2\ldots in} = m\int c_{i1}c_{i2}\ldots c_{in} f\ \mathrm{d}c \tag{3}$$

which represent tensors of rank n ($n = 1, 2, \ldots$). Knowledge of the full set of infinitely many moments is equivalent to the knowledge of the distribution function itself.

Thus in a manner of speaking ρ, v_i, and e or T define the macrostructure of a gas while all other moments define its microstructure. It is in that sense that we may speak of a monatomic ideal gas as a prototypical medium with microstructure.

Fortunately macrostructural phenomena—(ρ, v_i, e)-phenomena—dominate in dynamics and thermodynamics of gases. Thus in heat engines, internal combustion

engines and jets microstructural effects may be ignored in very good approximation. Technical thermodynamics and gas dynamics thrive on this fact.

However aerodynamics and heat transfer need to account for friction and heat conduction, where the fluxes of momentum and energy—F_{ij} and F_{iij}—or viscous stress and heat flux play a role and those are—by our definition—microstructural variables. Thermodynamics of irreversible processes accounts for them. Exact solutions are few and far- between but the effects of viscosity and thermal conduction are ubiquitous and commonplace. So we may be tempted to reconsider: We may be tempted,—in contrast to what was said before—, to count the viscous stress and the heat flux among the macrostructural variables.

But what about all the infinitely many other moments? Surely they are truely microstructural variables. Do they matter at all? Do they make themselves felt? If so, where? Those are questions asked and answered by extended thermodynamics, the truely microstructural theory of ideal gases.

2 Microstructural Effects

2.1 Coriolis Effect on the Heat Flux

The differential equation for the distribution function is the Boltzmann equation and the Boltzmann equation implies equations of balance for the moments

$$\frac{\partial F_{i1i2\ldots ip}}{\partial t} + \frac{\partial F_{i1i2\ldots ipn}}{\partial x^n} - \underbrace{pF_{i1\ldots i(p-1)}(g_{ip} + i^v_{ip}) - pF_{n(i1\ldots i(p-1))}2W_{ipn}}_{\text{gravitational and inertial terms}} \quad (4)$$
$$= \Pi_{i1i2\ldots ip} \qquad (p = 0, 1, 2, \ldots, N).$$

$\Pi_{i1i2\ldots ip}$ represents productions in these equations of balance; they are due to collisions between the atoms and they are responsible for dissipation and irreversibility. And W_{ij} is the matrix of angular velocity of the frame of reference; the term with W represents the effect of the Coriolis force on the atomic motion.

The Coriolis effect is typical for a microstructural phenomenon. Therefore we proceed to discuss its significance in a suggestiv form. For that purpose we consider a gas between two co-axial cylinders which are kept at different temperatures T so that a radially outward temperature gradient is created, see Fig. 1. We focus the attention on a small element of the gas of the order or magnitude of a mean free path of the atoms. The atoms flying inwards from the hot outer boundary of the element carry more energy in the mean than the atoms flying outwards from the colder inner boundary. Thus when a pair of atoms has passed the middle plane H-H—one flying inwards and one outwards—an amount of energy has also passed, and that amount is proportional to the gradient of T and opposite to it. At least that is the situation, if the gas is at rest in an inertial frame. If, however, the gas is at rest in a non-inertial

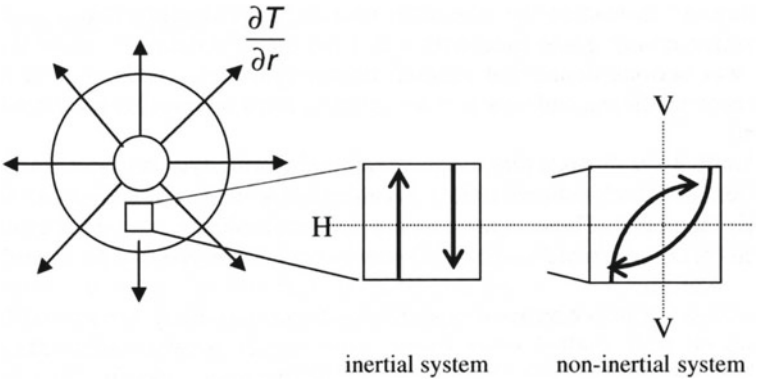

Fig. 1 The Coriolis effect on heat conduction

frame, the free paths of the atoms are bent by the Coriolis force as shown in the figure and now, in addition to a transport of energy through H-H, there is also a transport through the plane V-V, i.e. perpendicular to the gradient T and to the angular velocity ω of the non-inertial frame. The kinetic theory of gases interprets such transports of energy as a heat flux q and thus we conclude that we have

$$\begin{aligned} q &= -\kappa \tfrac{\partial T}{\partial r} && \text{in an inertial frame and} \\ q &= -\kappa \left(\tfrac{\partial T}{\partial r} + \tau\omega \times \tfrac{\partial T}{\partial r}\right) && \text{in a non-inertial frame} \end{aligned} \tag{5}$$

The time τ is of the order of magnitude of a mean free path and κ is the thermal conductivity. Note that there is a qualitative difference between the two formulae: In a non-inertial frame the heat flux is no longer parallel and opposite to the temperature gradien, rather it has a component perpendicular to the temperature gradient.

Nor is this the only qualitative effect of the rotation of the frame. It turns out that the velocity field is also affected. Thus a state of rest of the gas between the two cylinders is impossible in a non-inertial frame, if heat conduction occurs.

It is true though that such phenomena depend on the extent to which the Coriolis force can bend the mean free path. And that can happen to an appreciable extent only if either the gas is strongly rarefied or the angular velocity is impractically large.[1] Therefore the frame dependence of the relation between the heat flux and the temperature gradient has not been observed.

The same is true for the inertial terms of the other equations for all N. In the sequel we shall therefore ignore those terms and concentrate the attention on the differential parts of the equations of balance and on the productions. Thus the equations read in the present synthetic form

[1] I conjecture that the effect of rotation has been observed in HeII, which may be considered—for quantum reasons—as a degenerate ideal gas with large mean free paths. The effect may then be responsible for the observed field of quantum vortices which mimick a rigid rotation.

$$\frac{\partial F_{i1i2\ldots ip}}{\partial t} + \frac{\partial F_{i1i2\ldots ipn}}{\partial x^n} = \Pi_{i1i2\ldots ip}. \qquad (p = 0, 1, 2 \ldots N) \tag{6}$$

The equations of balance are not closed field equations for the moments $F_{i1i2\ldots ip}$ because of the occurrence of the last flux $F_{i1i2\ldots ipn}$ and of the productions $\Pi_{i1i2\ldots ip}$. In thermodynamics we face that situation be adopting constitutive equations for those additional quantities. And in extended thermodynamics we consider the constitutive equations as local and instantaneous, so that $F_{i1i2\ldots ipn}$ and $\Pi_{i1i2\ldots ip}$ at one point and time depend only on the values of $F_{i1i2\ldots ipn}$ at that point and time:

$$F_{i1i2\ldots ipn} = \hat{F}_{i1i2\ldots ipn}(F_{i1i2\ldots ip}), \quad \Pi_{i1i2\ldots ip} = \hat{\Pi}_{i1i2\ldots ip}(F_{i1i2\ldots in}). \tag{7}$$

The entropy principle ensures that the constitutive functions $\hat{F}$ and $\hat{\Pi}$ lead to symmetric hyperbolic field equations,—for the proper fields. And that fact implies well-posedness of the system, i.e. existence, uniqueness of solutions of initial value problems for small times, and finite wave speeds. For larger times though there may be a problem with uniqueness, see below.

2.2 *Explicit Form for $N = 3$. Navier-Stokes-Fourier Equations and Grad 13-Moment Equations*

In order to appreciate the nature of the equations of balance better we shall write them explicitly—and in linearized form—for the case $N = 3$. In that case there are 20 equations and Fig. 2 exhibits them in a panel, where they are repeated four times: Upper left, upper right, lower left, and lower right. For simplicity we have inserted productions appropriate to Maxwellian molecules so that they are all characterized by a single parameter τ, a time of the order of magnitude of the mean time of free flight. Also we have introduced the conventional notation: ρ for mass density, v_i for velocity, T for temperature, $t_{\langle ij\rangle}$ for deviatoric stress, q_i for heat flux. The third rank moment ρ_{ijk} has no conventional name. We emphasize that the 20 equations are fully explicit, except for the single unknown parameter τ which we shall identify shortly. The purpose of the panel with four parts lies in the black frames which differ between the parts:

Upper left: The frame embraces the Euler equations. These represent the conservation laws of mass, momentum and energy in a dissipation-less gas; there is no irreversibility and ρ, v_i and T are the only fields.

Upper right: The equations within the frame represent the Navier-Stokes-Fourier equations. The deviatoric stress is proportional to the deviatoric part of the velocity gradient and the factor of proportionality, containing τ is the viscosity; since the viscosity can be measured, τ is known. The heat flux is proportional to the gradient of temperature.

Lower right: The frame encloses Grad's 13-moment equations. They represent the prototypical equations of extended thermodynamics. Comparison of Grad's

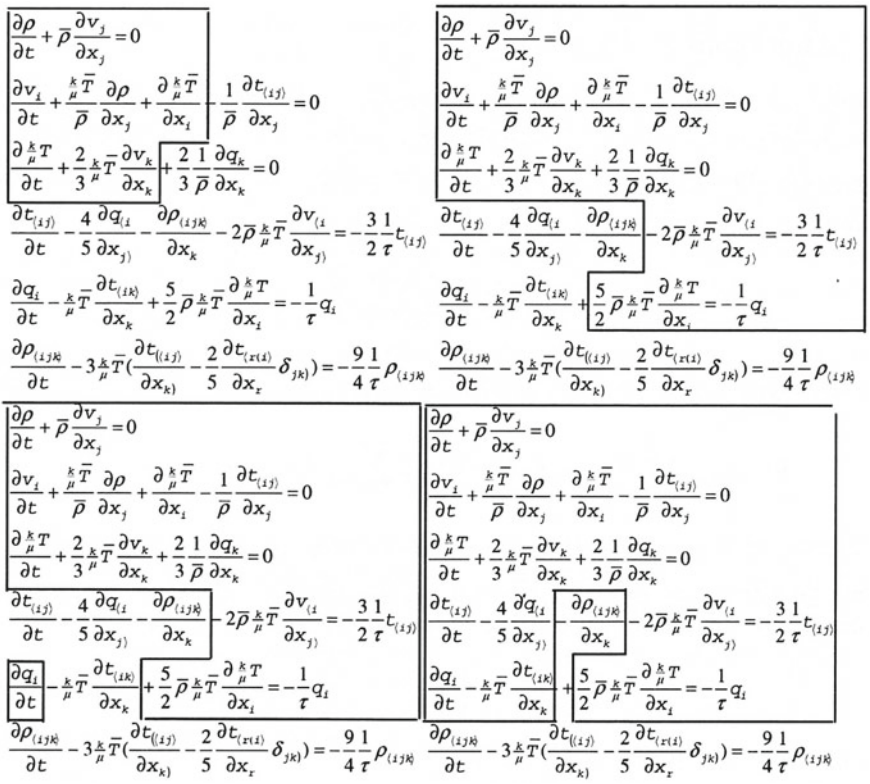

Fig. 2 The twenty equations of balance for $N = 3$. *Upper left* Euler equations. *Upper right* Navier-Stokes-Fourier equations. *Lower left* Cattaneo equations. *Lower right* Grad 13-moment equations

equations with the Navier-Stokes-Fourier equations shows that the latter ones ignore the rates of change and the gradients of $t_{\langle ij\rangle}$ and q_i Since rates of change are measured in terms of mean times of free flight and gradients in terms of mean free paths we conclude that the Navier-Stokes-Fourier equations represent the behaviour of dense gases in slow processes, while extended thermodynamics describes the gases in rapid processes and in rarefied gases.

Lower left: The frames enclose the equations of the Cattaneo theory, the earliest—and incomplete—version of extended thermodynamics. It was invented in an ad hoc manner so as to resolve the *paradox of heat conduction*, by which disturbances in temperature propagate at an infinite speed. There is no such paradox according to Grad's equations.

The twenty equations of Fig. 2 are only here for illustration. It is possible to calculate the explicit full set of balance equations for moments for any N, and this has been done, although the result it too long to print out. So, in a manner of speaking the full set for $N = 40$ (say),—where there are 12341 equations—is only known to

the computer. However, the computer can work with them; thus it can work out the speeds of propagation of acceleration waves implied by the system for any finite N.

2.3 Acceleration Waves

Acceleration waves are singular surfaces across which the fields themselves are continuous, while their gradients and time derivatives are not. Their speeds and their growth and decay can be calculated and the result can be compared with observations at least in principle.

We go back to the synthetic form of our equations for this topic

$$\frac{\partial F_{i1i2\ldots ip}}{\partial t} + \frac{\partial F_{i1i2\ldots ipn}}{\partial x^n} = \Pi_{i1i2\ldots ip}.$$

Using square brackets for the difference between front and back of the wave we can thus write

$$\left[\frac{\partial F_{i1i2\ldots ip}}{\partial x_n}\right] = A_{i1i2\ldots ip} n_n \quad \text{and} \quad \left[\frac{\partial F_{i1i2\ldots ip}}{\partial t}\right] = -V A_{i1i2\ldots ip}, \tag{8}$$

where n_n is the normal to the surface and V is its speed in the normal direction. Because of the constitutive properties of extended thermodynamics we obtain

$$\left(\frac{\partial F_{i1i2\ldots ipn}}{\partial F_{j1j2\ldots jp}} n_n - V \delta_{i1i2\ldots ip\, j1j2\ldots jp}\right) A_{j1j2\ldots jp} = 0. \tag{9}$$

This is called the characteristic equation of the wave, while the $\upsilon \cdot \upsilon$-matrix in braces is called the characteristic matrix.[2] We conclude there are υ speeds to be calculated as eigenvalues of the characteristic matrix, and that the jumps across the wave are determined by the right eigenvector $d_{j1j2\ldots jp}$:

$$A_{j1j2\ldots jp} = A d_{j1j2\ldots jp} \tag{10}$$

A is called the amplitude of the acceleration wave.

Since we know the field equations explicitly we can calculate all speeds and, in particular we can calculate the *pulse speed*, the largest speed of propagation which the gas can accommodate at the level N of extension. The table in Fig. 3 provides some such pulse speeds for $N = 3$ through $N = 40$ referred to the "ordinary" sound speed $\sqrt{\frac{5}{3}\frac{k}{m}T}$ of a monatomic ideal gas.

[2] υ equals $\frac{1}{6}(N+1)(N+2)(N+3)$.

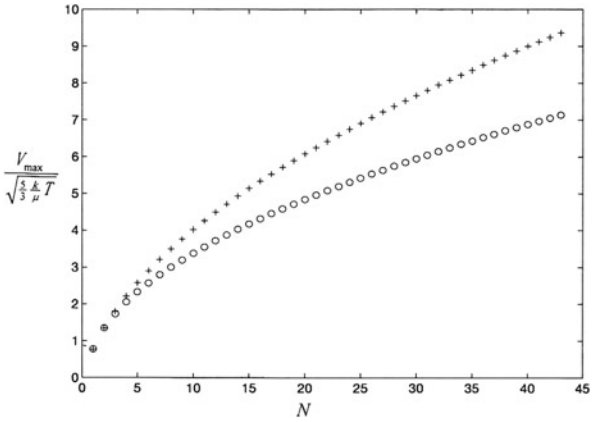

N	υ	$V_{max}/\sqrt{\frac{5}{3}\frac{k}{m}T}$
3	20	1.808
10	286	4.018
20	1771	6.080
30	5456	7.663
40	12341	8.996

Fig. 3 Pulse speeds referred to the normal sound speed. *Crosses* Calculations. *Circles* Lower bound

Clearly the pulse speed grows monotonically for growing N.This conjecture is confirmed by a lower estimate calculated by Boillat and Ruggeri according to which the pulse speed must be greater than $\sqrt{\frac{6}{5}(N-\frac{1}{2})}$.

The obvious question is, of course, whether all these many sound speeds are ever seen, or heard. The answer is obviously negative and the reason for this lies in the fact that the acceleration waves are strongly damped before they reach our ears. So, let us investigate the decay of acceleration waves. It turns out that the field equations allow us to calculate the development of the amplitude A of an acceleration wave as

$$\frac{\partial A}{\partial t} - \underbrace{\frac{\partial V}{\partial F_\alpha} d_\beta}_{a} A^2 - \underbrace{l_\alpha \frac{\partial \Pi_\alpha}{\partial F_\beta} d_\beta}_{b} A = 0. \tag{11}$$

Here we have introduced the multi-index $a \equiv i1i2...ip$ and l_α, d_α denote the left and right eigenvectors of the characteristic matrix. This is a Bernoulli equation with the coefficient a determining the nonlinearity and b determining dissipation. The nonlinearity consists of the velocity dependence on the value of the field and the dissipation is due to collisions between atoms. The solution of the Bernoulli equation reads

$$A(t) = \frac{A(0)e^{-bt}}{1 + A(0)\frac{a}{b}\left(e^{-bt} - 1\right)} \tag{12}$$

so that—without nonlinearity—there is a simple exponential decay of the initial value $A(0)$ due to dissipation. With nonlinearity, however, $A(t)$ will grow and eventually diverge at a time when the denominator of the expression becomes zero. Thus we have a competition between nonlinearity and dissipation. Dissipation makes for smooth solutions and decay of disturbances and non-linearity makes for growth of

the disturbance and the eventual generation of a shock wave from the acceleration wave.

In a gas under normal conditions the situation is such that dissipation prevails and that is the reason that we do not hear the multiple sound waves inherent in the microstructure of the gas.

2.4 Shock Waves

Concerning the foregoing remark about the formation of shocks from acceleration waves there is a basic observation to be made. Indeed, shocks do not exist in nature as experiments have clearly shown: The microstructural nature of a gas prevents shocks. What does exist—and what may appear as a shock—is a *shock structure,* a smooth but steep transition between two relatively flat states of a gas; to be sure, the thickness of the shock structure is of the order of magnitude of a few mean free paths, but still it is smooth. Therefore, if a theory predicts a shock, or allows for a shock, it is not a valid theory and it has to be improved. Extended thermodynamics shows how this has to be done. Let us consider this:

First of all, the Navier-Stokes-Fourier theory does not allow shocks. This would seem to recommend it as a good theory in view of the forgoing remarks. However, the shock structure which the theory permits us to calculate is wrong, see Fig. 4.

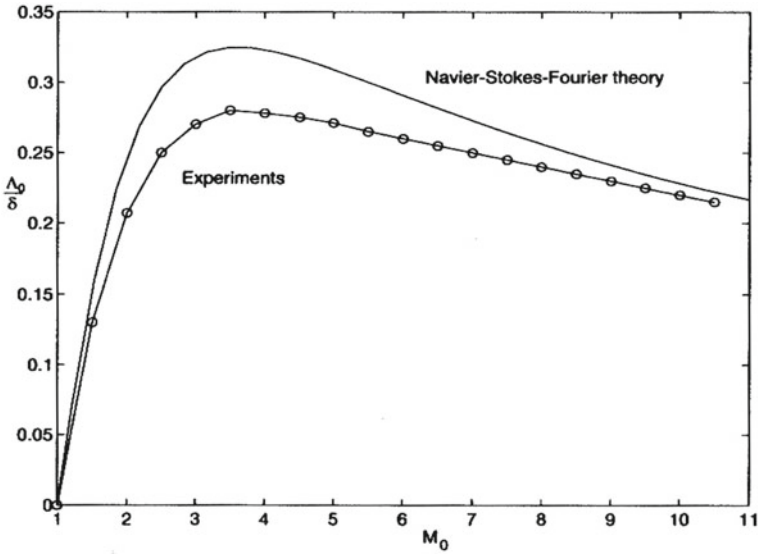

Fig. 4 Thickness δ of a shock structure according to the Navier-Stokes-Fourier theory as a function of the Mach number M_0 of the structure. Λ_0 is the mean free path of the gas before the structure

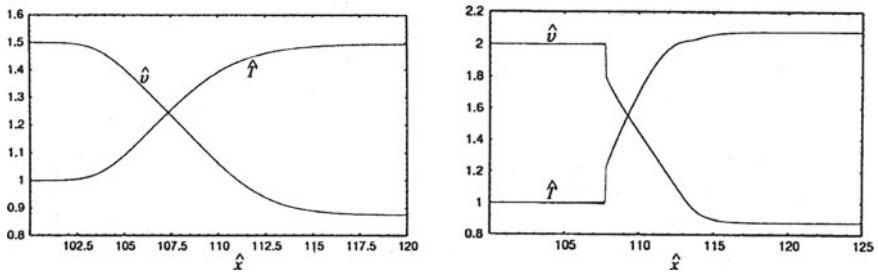

Fig. 5 Shock structures for Grad's 13-moment theory at $M_0 = 1.5$ (*left*) and at $M_0 = 2$ (*right*). The subshock of Fig. 5 (*right*) begins to develop at $M_0 = 1.65$, the pulse speed of the 13-moment theory

Grad knew this when he first derived the 13-moment theory. He tried that theory out on shock structures, hoping, perhaps, to do better than Navier-Stokes-Fourier.

Unfortunatly, however, his calculation came out worse,—much worse! It is true that for $M = 1.5$ Grad did calculate a nice shock structure—see Fig. 5—but for that low Mach number there was a minimal discrepancy between observation and the Navier-Stokes Fourier theory anyhow according to Fig. 4. So that effort was not decisive. Therefore Grad proceeded with $M_0 = 2$ and he had a surprise: A subshock appeared, see Fig. 5b and certainly that was worse than the discrepancy of Fig. 4. Going up in Mach numbers one can show that the subshock is first seen slightly above $M_0 = 1.65$ and then it grows in size. Grad did not appreciate the significance of this Mach number or, at least, he does not comment on it. The significance is that $M_0 = 1.65$ is the pulse speed according to the 13-moment theory and, if the gas rushes forward with more than that speed, its down-stream region cannot move aside in time and a shock must form or, in this case, a subshock. In a manner of speaking it is for $M_0 > 1.65$ that we must speak of a truely supersonic flow in a 13-moment theory.

The recipe for avoiding this subshock is simple: We must abandon the 13-moment theory and adopt an extended theory with more equations and, therefore, a larger pulse speed, see the table of Fig. 3. So, if we adopt a 286-moment theory, the appearance of the subshock is pushed upwards to $M_0 = 4.018$, and if we adopt a 12341-moment theory the appearance of the subshock is pushed to $M_0 = 8.996$. Eventually, if we prefer to have no subshock appear, we need to go to a ∞-moment theory, because its pulse speed is infinite.

3 Light Scattering

The knowledge of the atomic microstructure of a gas makes all the above phenomena plausible and there is no doubt that they exist, • the frame dependence of the heat flux, • the multiple speeds, • the pulse speed, and • the shift of subshocks to high

Mach numbers. Yet, our experimantal tools—thermal and caloric measurements—are too rough to detect such phenomena and to quantify them. More sensitive probes into the microstructure are needed. The measurement of light scattering spectra is such a probe.

Indeed, light scattering is a paradigm for the usefulness and practicality of extended thermodynamics. Let us consider this:
Incoming laser light, i.e. light of a single frequency ω_i—most often green light with the wave length $\lambda_i \approx 0.4 \cdot 10^{-6}$ m—is scattered on the density fluctuations of a gas in equilibrium, see Fig. 6 (top). While most of the scattered light has the same frequency as the incoming light, the scattering spectrum also contains neighbouring frequencies. For dense gases,—typically a gas under the pressure of 4 bar or higher—the spectrum has three well-defined peaks, like the uppermost curve in Fig. 6 (bottom). When the gas pressure is lowered, the peaks become less pronounced; they degenerate into shoulders, until eventually—for pressures less than 1 bar—there is a single bump in the center.

As long as there are peaks, i.e. for dense gases, the distance of the central and lateral peaks determines the sound speed of the gas, or its temperature. From the half-width of the peaks and their relative heights we may read off the viscosity and the thermal conductivity of the gas. That should come as a surprise! Indeed, we may well ask a question: How, if the scattering spectrum represents properties of density fluctuations in equilibrium, can it carry information about macroscopic transport coefficients like the viscosity?

The answer lies in the Onsager hypothesis according to which the mean regression of fluctuations follows the same laws as the macroscopic fields which—in our case—are the moments $F_{i1i2\ldots ip}$. We shall not go here into a discussion of the controversial hypothesis. Let it suffice to say that, without it, the interpretation of light scattering spectra in terms of the moments would be impossible. We accept the hypothesis, since it furnishes good results as we shall see.

If we compare the observed scattering spectra for a *dense* gas with the predictions of the Navier-Stokes equations we obtain an excellent agreement. Moreover the transport coefficients so determined agree well with their values obtained by more conventional means than light scattering, or calculated from the kinetic theory of gases.

However, for a *rarefied* gas the agreement is not good, if we still use the Navier-Stokes-Fourier equations. It is true that the expected gross features do appear: For a stronger degree of rarefaction the three peaks of the spectrum degenerate into shoulders and, eventually, into a bump, even for Navier-Stokes. But the finer details are all wrong. We may well consider this as an opportunity to check out the validity of the equations of extended thermodynamics,—and of the Onsager hypothesis—both at the same time.

A prototypical case for the linearized equations is the 20-moment system shown in Fig. 2 and used there illustratively for the identification of various special cases. Equations like that for any specific number of moments are available, e.g. $\upsilon = 20, 35, 56, 84$, and their scattering spectra are shown in Fig. 7 (left). Not two of them agree among themselves and none of them agrees with with the measured dots.

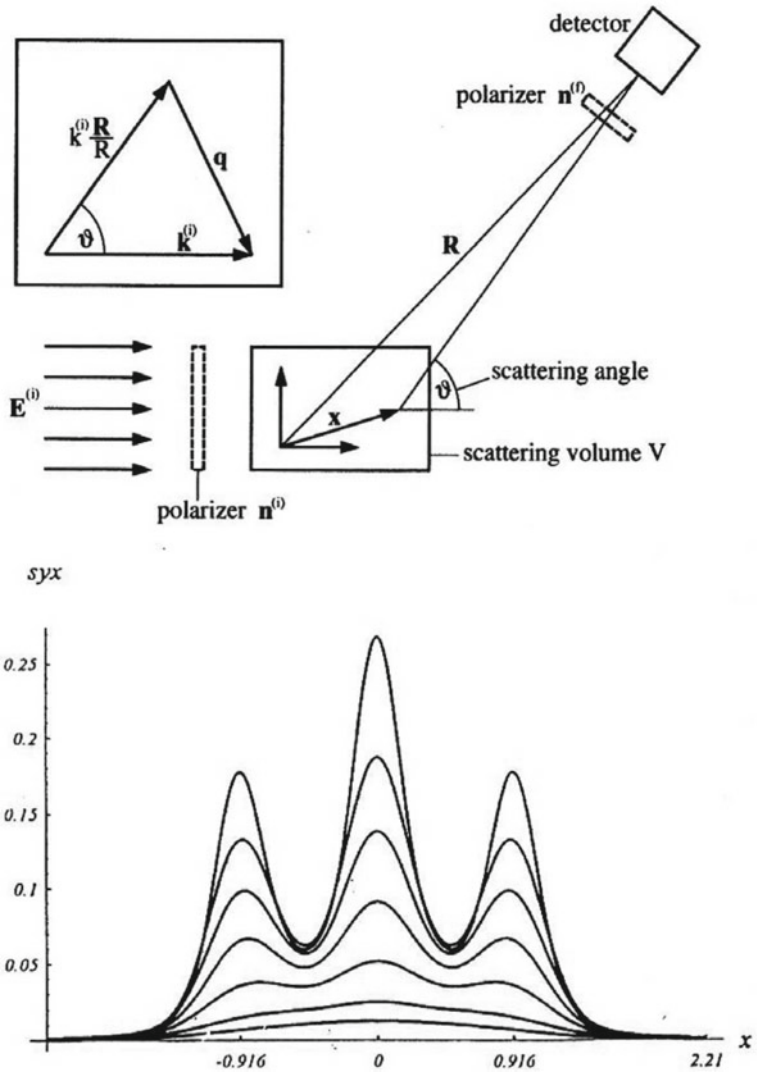

Fig. 6 Light scattering and scattering spectrum. *Top* Schematic experimental set-up, *Bottom* Experimental curves for different pressures (see text)

Ordinarily a situation like this calls for an adjustment of parameters, but that is impossible in the present case, because there are no free parameters, e.g. see Fig. 2. Indeed, extended thermodynamics is a *theory of theories* with only *one* parameter: The number of equations. So, if we push up that number to $\upsilon = 120,\ 165,\ 220,\ 286$ and calculate the scattering spectra, we obtain convergence of results at $\upsilon = 120$ in

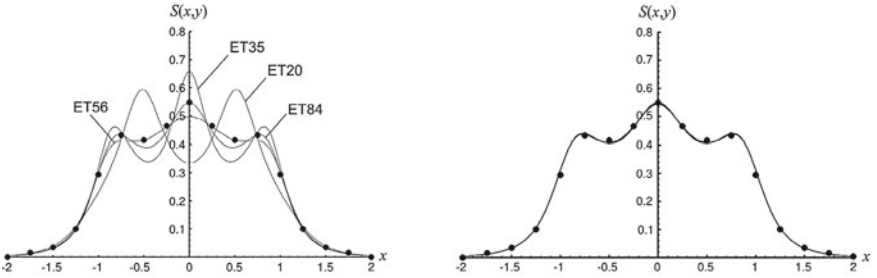

Fig. 7 Scattering spectra for Xenon in extended thermodynamics for a low pressure. *Dots* represent measurements by Clark. *Left* Spectra for 20, 35, 56, 84 moments. *Right* Spectra for 120, 165, 220, 286 moments

the sense that more moments do not change the scattering spectrum and—what is more—they all agree with the measured values, see Fig. 7 (right).
In other words, for a given pressure our *theory of theories* provides the possibility to determine its own range of validity, something that is usually said a theory cannot possibly do. Here, however, if we have two successive theories which provide the same results, the lower one is good enough: and *we can say that without conducting a single experiment.*

All of this is most satisfactory, but there is also disappointment. Indeed, we might have hoped that 13 or 14 moments might bring about a great improvement over the Navier Stokes-Fourier solution and a good representation of experimental results. Instead we need hundreds of moments for even moderately rarefied gases. The microstructure of the gas is deeply hidden indeed.

References

All relevant results of this paper are already described—in more detail—in the book and survey paper listed below. Also the reader may find extensive lists of references there.

1. Müller, I., Ruggeri, T.: Rational Extended Thermodynamics (2nd edn.) Springer Tracts in Natural Philosophy, vol. 37 (1998)
2. Müller, I., Weiss, W.: Thermodynamics of Irreversible Processes—Past and Present. Springer, Heidelberg (2012) (The European Physics Journal H)

From Second Law Violations to Continuum Mechanics

Martin Ostoja-Starzewski

Abstract The violations of the Second Law become relevant as the length and/or time scales become very small. The Second Law then needs to be replaced by the fluctuation theorem and, mathematically, the irreversible entropy evolves as a submartingale. Next, a framework thermomechanics relying on stochastic functionals of energy and entropy is outlined. This allows a study of diffusion-type problems with random field constitutive coefficients not required to satisfy the positive definiteness everywhere. Finally, a formulation of stochastic micropolar fluid mechanics is developed, accounting for the lack of symmetry of stress tensor on molecular scales.

Keywords Continuum mechanics · Second law violations · Fluctuation theorem · Submartingale · Micropolar fluid

1 Motivation

The theory, simulations, and experiments of statistical mechanics over the past two decades indicate that violations of the Second Law of thermodynamics are relevant where/when the length and/or time scales become very small [5, 7, 9, 17, 19]. The Second Law must then be replaced by the *fluctuation theorem* or, strictly speaking, a group of such theorems. In effect, the Second Law holds on average, be it an ensemble average, or a spatial average over a sufficiently large domain, or a temporal average over a sufficiently large time interval. Interestingly, the Second Law violations may occur for up to 3 s (!) in cholesteric liquids. While the focus in statistical mechanics has been on stochastic thermodynamics, our interest is in introducing these results into continuum mechanics, i.e. in formulating stochastic continuum thermomechanics with spontaneous violations of the Second Law [12–14].

M. Ostoja-Starzewski (✉)
Department of Mechanical Science & Engineering, Institute for Condensed Matter Theory and Beckman Institute, University of Illinois at Urbana-Champaign, Urbana, IL 61801, USA
e-mail: martinos@illinois.edu

B. Albers and M. Kuczma (eds.), *Continuous Media with Microstructure 2*,
DOI 10.1007/978-3-319-28241-1_12

So far, we have obtained these results:

- entropy evolution over time is a submartingale;
- classification of thermomechanical processes into four types depending on whether they are conservative or not and/or conventional continuum mechanical;
- stochastic generalizations of thermomechanics in the vein of either thermodynamic orthogonality [20] or primitive thermodynamics [4]; with explicit models formulated for Newtonian fluids with, respectively, parabolic or hyperbolic heat conduction;
- random field models of the martingale component, possibly including spatial fractal and Hurst effects;
- evolution of an acceleration wavefront randomly encountering regions with negative viscosity coefficient;
- Lyapunov function of a diffusion phenomenon where the random field coefficients do not satisfy the positive definiteness everywhere;
- spontaneous random fluctuations of the microrotation field in a viscous micropolar fluid model in the absence of random (turbulence-like) fluctuations of the classical (Cauchy) velocity field.

In this paper, following a brief account of the fluctuation theorem, we review some of the above results.

2 Background: Fluctuation Theorem

It has been established in statistical physics over the past two decades that the entropy production may be negative on short time and space scales, see reviews in [8, 15]. This is described by a so-called *fluctuation theorem* giving, in its basic form, an estimate of the relative probability of observing processes that have positive and negative total dissipation in non-equilibrium systems

$$\frac{\mathsf{P}\left(\phi_t = A\right)}{\mathsf{P}\left(\phi_t = -A\right)} = e^{At}. \tag{1}$$

Here t is the time, while ϕ_t is the dissipation function quantifying the thermodynamic reversibility of a trajectory taken by a thermodynamic system, and A is the value of ϕ_t. To help explain it, in Fig. 1 we reproduce Fig. 1.1 from [8] giving the probability density histogram of fluctuations of the time-averaged shear stress σ_{xy} in Couette flow. Note that (i) the fluctuations are not confined to the negative values of σ_{xy}, and (ii) for any pair of two points symmetrically distributed about 0.00 on the σ_{xy} axis consistent with (1) the probability of a negative fluctuation $[\mathsf{P}\left(\phi_t = A\right)]$ is greater than the probability of a positive fluctuation $[\mathsf{P}\left(\phi_t = -A\right)]$.

That is, the fluctuation theorem compares the probability $\mathsf{P}\left(\phi_t = A \pm dA\right)$ of observing an arbitrary system trajectory having a dissipation total infinitesimally close to A with that of the time reverse of that trajectory (its conjugate anti-trajectory)

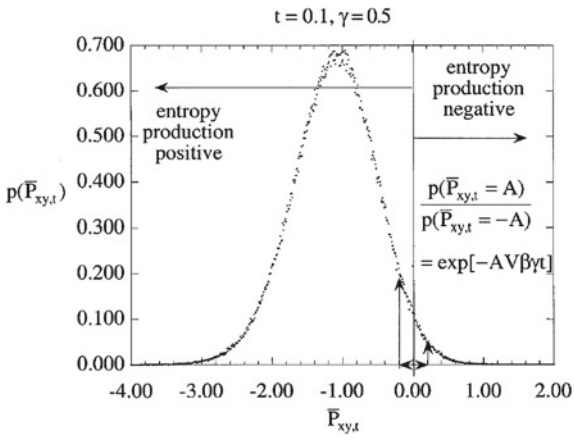

Fig. 1 A histogram showing fluctuations in the time-averaged shear stress for a system undergoing Couette flow; figure taken from [8]

in the ensemble of trajectories:

$$\phi_t\left(\boldsymbol{\Gamma}(0)\right) = \ln \frac{\mathsf{P}\left(\boldsymbol{\Gamma}(0), 0\right)}{\mathsf{P}\left(\boldsymbol{\Gamma}^*(t), 0\right)} \tag{2}$$

More specifically, with $\boldsymbol{\Gamma} = (q_1, p_1, \ldots q_N, p_N)$ being the phase space vector of the system which corresponds to a system trajectory and $\boldsymbol{\Gamma}^*(t)$ being the result of a time reversal map applied to $\boldsymbol{\Gamma}(0)$, $\phi_t\left(\boldsymbol{\Gamma}(0)\right)$ is the total dissipation for a trajectory originating at 0 and evolving for a time t:

$$\phi_t\left(\boldsymbol{\Gamma}(0)\right) = \int_0^t \phi\left(\boldsymbol{\Gamma}(s)\right) ds. \tag{3}$$

This integration involves an instantaneous dissipation function:

$$\phi\left(\boldsymbol{\Gamma}(0)\right) = \frac{d\phi_t\left(\boldsymbol{\Gamma}(0)\right)}{dt}. \tag{4}$$

The fluctuation theorem as expressed by (1) states that (i) positive dissipation is exponentially more likely to be observed than negative dissipation, and (ii) upon ensemble averaging of ϕ_t (with E denoting the mathematical expectation), leading to

$$\mathsf{E}\left[\phi_t | \mathscr{F}_t\right] \geq 0. \tag{5}$$

Here $|\mathscr{F}_n$ indicates the conditioning on the past history and is discussed below. Considering that the time-integrated dissipation function ϕ_t equals the irreversible entropy production in continuum thermomechanics with internal variables (TIV), the inequality (5) is seen as a generalization of the Second Law of thermodynamics (i.e., the entropy production rate is non-negative). Note that ϕ in (3) and (4) is recognized as the irreversible entropy production rate.

3 Entropy Is a Submartingale

In view of the random fluctuations, ϕ_t is a stochastic process with a specific type of memory effect to be examined as follows. First, every stochastic process is defined with reference to a probability space $(\Omega, \mathscr{F}, \mathscr{P})$, where Ω is the sample space, $\mathscr{F}$ is the σ-field, and $\mathscr{P}$ the probability measure, the argument $\omega \in \Omega$ being employed to indicate an elementary event as well as the random character of ϕ_t. We now switch from a continuous (t) to a discrete (n) time parametrization

$$\phi_n := \phi_{t=n}, \tag{6}$$

The point is that the analytical aspects of discrete-time stochastic processes are simpler than those of continuous-time processes; the integral in (3) is replaced by a summation, while the derivative in (4) is understood in a finite-difference sense.

Our growing knowledge of the process ϕ_n at the successive times (i.e., its history) is represented by a so-called *filtration* on Ω: a sequence $\{\mathscr{F}_n : n = 0, 1, 2, \ldots\}$ of sub-sigma fields of $\mathscr{F}$ such that for all time instants t_n, $\mathscr{F}_n \subset \mathscr{F}_{n+1}$. In view of (5), we observe that this inequality is satisfied

$$\mathsf{E}\{\phi_{n+1}|\mathscr{F}_n\} \leq \phi_n, \tag{7}$$

which indicates that ϕ_n is a *submartingale*. On the technical side dictated by the probability theory, (7) has to be accompanied by two more conditions: (i) $\{\mathscr{F}_n; n = 0, 1, 2, \ldots\}$ is a filtration and ϕ_n is adapted to $\mathscr{F}_n$; (ii) for each n, ϕ_n is integrable.

If the $\leq$ sign in (7) were replaced by an equality sign, we would have a so-called *martingale*. In fact, this observation acquires more light in view of the so-called *Doob decomposition* [3] saying that any submartingale is the sum of a martingale (M) and an increasing process (G): Let $\phi = \{\phi_n; n \geq 0\}$ be a submartingale relative to the filtration $(\mathscr{F}_n)$. Then there exists a martingale $M = \{M_n; n \geq 0\}$ and a process $G = \{G_n; n \geq 0\}$ such that

(i) M is a martingale relative to $\mathscr{F}_n$;
(ii) G is an increasing process: $G_n \leq G_{n+1}$ almost everywhere;
(iii) G_n is $\mathscr{F}_{n-1}$-measurable $\forall n$;
(iv) $\phi_n = M_n + G_n$.

In [12] we have employed an analogous (Doob–Meyer decomposition) theorem in continuous time, also giving a unique decomposition of a submartingale into a martingale and a "drift" process. The discrete time case should be sufficient for most continuum physics applications, while allowing a simpler analytical treatment.

4 Violations of Second Law in Diffusion Problems

The partial differential equation of diffusion hinges on a coarse scale and a deterministic continuum approximation of a random medium. If we consider a very fine scale resolution where the violations of the Second Law relative to heat conduction occur [16], we must replace the deterministic picture by a stochastic one. Thus, the internal energy density u (per unit volume) and the entropy s (per unit volume) are random fields over the material ($\mathscr{D}$) and time (T) domains:

$$u : \mathscr{D} \times T \times \Omega \to \mathbb{R}, \quad s : \mathscr{D} \times T \times \Omega \to \mathbb{R}, \tag{8}$$

where we consider the heat conduction problem in a rigid (undeformable) conductor. With reference to Sect. 2, the Second Law of thermodynamics takes the ensemble averaged Clausius–Duhem form

$$\mathsf{E}\{\phi|\mathscr{F}_n\} \geq 0, \quad \phi = T\dot{s}^{(i)} = -q_k \frac{T,_k}{T} \equiv -\mathbf{q} \cdot \frac{\nabla T}{T}. \tag{9}$$

Here we recognize the pair of affinities: vector of velocity $T,_k$ conjugate to the vector of dissipative force $-q_k/T$ and introduce a dissipation function $\phi(q_k)$. Given the medium's randomness, ϕ is a random field

$$\phi : \mathscr{D} \times T \times \Omega \to \mathbb{R}. \tag{10}$$

At any given continuum point $\mathbf{x}$ in $\mathscr{D}$, ϕ is a random functional $\phi(\mathbf{q}, \omega), \omega \in \Omega$. The randomness of ϕ disappears as the time and/or spatial scales become large and then ϕ reverts to a deterministic functional of a homogeneous continuum. According to the model outlined in Sect. 2,

$$\phi(\mathbf{q}, \omega) = \dot{G}(\mathbf{q}) + \dot{M}(\mathbf{q}, \omega), \tag{11}$$

which for the linear Fourier-type conductivity becomes more explicit with

$$\dot{G}(\mathbf{q}) = q_i \lambda_{ij} q_j \;\; \dot{M}(\mathbf{q}, \omega) = q_i \mathscr{M}_{ij}(\omega) q_j. \tag{12}$$

Here $\dot{G}(\mathbf{q})$ involves the thermal resistivity λ_{ij} which is positive definite, and $\dot{M}(\mathbf{q}, \omega) = dM(\mathbf{q}, \omega)/dt$, with M being the martingale modeling the random fluctuation according to (4). Clearly, the randomness residing in $M(\mathbf{d}, \omega)$ allows the total resistivity (and, hence, the total conductivity $\kappa_{ij} = \left(\lambda_{ij} + \mathscr{M}_{ij}\right)^{-1}$) to become negative since $\mathscr{M}_{ij}$ is not required to be positive definite, thus signifying the violations of the Second Law. More specifically, the second-rank tensor $\mathscr{M}_{ij} : \mathscr{V} \to \mathscr{V}$ (where $\mathscr{V}$ is a linear vector space) also is a second-order random field [12], such that

$$\mathscr{M}_{ij} : \mathscr{D} \times \Omega \to \mathscr{V}^2 \tag{13}$$

In view of the Gaussian character of fluctuations in Fig. 1, $\mathscr{M}_{ij}$ is a Gaussian random field.

Next, consider the evolution of energy in a spatial domain $\mathscr{D} \in \mathbb{R}^n$ ($n = 2$ or 3) having a boundary $\partial\mathscr{D} = \partial\mathscr{D}_q \cup \partial\mathscr{D}_T$ with both parts disjoint and such that $\partial\mathscr{D}_q$ is insulated and $\partial\mathscr{D}_T$ has a constant temperature prescribed on it:

$$\begin{array}{l} q_i n_i = 0 \quad \text{on} \quad \partial\mathscr{D}_q, \\ T = T_0 \quad \text{on} \quad \partial\mathscr{D}_T. \end{array} \tag{14}$$

Following [2], we observe from the energy balance that $u = -q_{i,i}$, and from the decomposition of entropy rate $\dot{s} = \dot{s}^{(r)} + \dot{s}^{(i)}$ (having the reversible part $\dot{s}^{(r)} = -\left(q_i/T\right)_{,i}$ and the irreversible part $\dot{s}^{(r)} = -q_i T_{,i}/T^2$) that $\dot{s} = -q_{i,i}/T$. Therefore,

$$\frac{d}{dt}\int_{\mathscr{D}} (u - T_0 s)\, dv = T_0 \int_{\mathscr{D}} \frac{q_i T_{,i}}{T^2} dv, \tag{15}$$

where the boundary conditions (14) have been employed. Noting, according to spontaneous violations of the Second Law mentioned in (11) and (12), that the scalar product $q_i T_{,i}$ takes random and possibly negative values, we cannot conclude that this is a Lyapunov function just like in diffusion systems obeying the Second Law considered in the aforementioned reference. It is upon taking the ensemble average of (15) that

$$\mathsf{E}\left\{\frac{d}{dt}\int_{\mathscr{D}} (u - T_0 s)\, dv\right\} = \mathsf{E}\left\{T_0 \int_{\mathscr{D}} \frac{q_i T_{,i}}{T^2} dv\right\} \leq 0 \tag{16}$$

which yields the Lyapunov function.

Interestingly, the result (17) does not depend on the heat conduction being linear. But, if that actually is the case (with c being the specific heat capacity), the equation governing the temperature field is a stochastic partial differential one

$$\frac{\partial T}{\partial t} = \frac{1}{c}\left(\kappa_{ij}\left(\mathbf{x}, \omega\right) T_{,j}\right)_{,i}. \tag{17}$$

Next, upon ensemble averaging, the Clausius-Duhem inequality reduces to the condition of positive definiteness of the conductivity tensor $\kappa_{ij} = \lambda_{ij}^{-1}$ (with $\mathscr{M}_{ij} \to 0$), the second-order random field κ_{ij} becomes a constant tensor field, and the diffusion equations for anisotropic and then isotropic homogeneous medium are obtained:

$$\frac{\partial T}{\partial t} = \frac{1}{c}\kappa_{ij} T_{,ji} \underset{\kappa_{ij} \to \kappa\delta_{ij}}{\to} \frac{\kappa}{c}\nabla^2 T. \tag{18}$$

5 Micropolar Fluid Model

5.1 Dissipation Functions

As noted in [6], the Cauchy stress tensor (i.e., the negative of the pressure tensor) generally lacks symmetry on length scales where the Second Law violations occur and this is the case with the molecular fluids. Indeed, the complete description of the hydrodynamics of molecular liquids must include angular momentum considerations and this challenge can naturally be met by using, instead of the classical (Cauchy) continuum, a micropolar continuum, Fig. 2a, b.

To have a micropolar model, a couple traction $m_i^{(n)} = \mu_{ji} n_j$ is introduced in addition to the Cauchy traction $t_i^{(n)} = \tau_{ji} n_j$ on a unit surface of the outer normal n_i; the body force and body torque as being unimportant to our considerations. The kinematics of the continuum point is described by the displacement u_i and the microrotation φ_i; their time rates, respectively, are v_i and w_i. Also, the intrinsic angular momentum per unit mass is $l_i = I_{ik} w_k$, where I_{ik} is the microinertia; for an isotropic micropolar fluid $I_{ik} = I\delta_{ik}$, where I is the microintertia of a continuum fluid particle. The balance equations are:

the conservation of mass

$$\frac{D\rho}{Dt} = -\rho v_{i,i} \,, \tag{19}$$

the conservation of linear momentum

$$\rho \frac{Dv_i}{Dt} = \tau_{ji,j} \,, \tag{20}$$

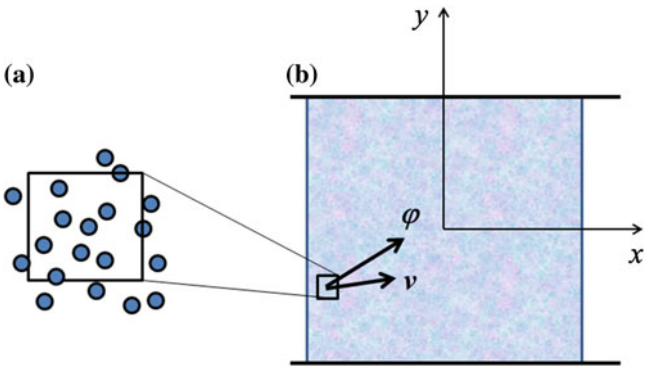

Fig. 2 **a** Molecular fluid in which the stress tensor of continuum approximation is not symmetric; **b** dV element of a micropolar continuum (with the velocity v and microrotation φ degrees of freedom) having spatial (and temporal) random field fluctuations. This is the basis for a study of Couette- or Poiseuille-type stochastic flow of a micropolar fluid in a channel

the conservation of angular momentum

$$\rho \frac{Dl_i}{Dt} = \mu_{ji,j} + e_{ijk}\tau_{jk}, \tag{21}$$

the conservation of internal energy

$$\rho \frac{Du}{Dt} = -q_{i,i} + \tau_{ji}\left(v_{i,j} - e_{kji}w_k\right) + \mu_{ji}w_{i,j} + \rho g_i. \tag{22}$$

For an isotropic micropolar fluid $I_{ik} = I\delta_{ik}$, where I is the microintertia of a continuum fluid particle. The special case of classical continuum mechanics is recovered when $\mu_{ji} = 0$, and $w_k = g_k = 0$.

In the presence of micropolar effects the constitutive equations are [11]

$$\begin{aligned} \tau_{ij} &= (-p + \lambda v_{k,k})\,\delta_{ij} + \mu\left(v_{j,i} + v_{i,j}\right) + \mu_r\left(v_{j,i} - v_{i,j}\right) - 2\mu_r e_{mij}w_m \\ \mu_{ij} &= c_0 w_{k,k}\,\delta_{ij} + c_d\left(w_{j,i} + w_{i,j}\right) + c_a\left(w_{j,i} - w_{i,j}\right), \end{aligned} \tag{23}$$

where λ and μ are the usual viscosity coefficients, μ_r is the dynamic microrotation viscosity, while c_0, c_d, and c_a are the micropolar viscosity coefficients. Now, the governing equations (20)–(22) become

$$\rho \frac{Dv_i}{Dt} = -p_{,i} + (\lambda + \mu - \mu_r)\,v_{j,ji} + (\mu + \mu_r)\,v_{i,kk} + 2\mu_r e_{ijk}w_{k,j}, \tag{24}$$

$$\rho I \frac{Dw_i}{Dt} = 2\mu_r\left(e_{mij}v_{j,i} - 2w_i\right) + (c_0 + c_d - c_a)\,w_{j,ji} + (c_d + c_a)\,w_{i,kk}, \tag{25}$$

$$\rho \frac{Du}{Dt} = -q_{i,i} - pv_{i,i} + \rho\phi_{int}, \tag{26}$$

where ϕ_{int} is the intrinsic (i.e., fluid mechanical part of) dissipation function per unit mass, such that

$$\begin{aligned} \rho\phi_{int} = {} & \lambda\left(v_{i,i}\right)^2 + 2\mu_{ij}d_{ij} + 4\mu_r\left(\frac{1}{2}e_{mij}v_{j,i} - w_i\right)^2 \\ & + c_0\left(w_{i,i}\right)^2 + (c_d + c_a)\,w_{i,k}w_{i,k} + (c_d - c_a)\,w_{i,k}w_{k,i}, \end{aligned} \tag{27}$$

where d_{ij} is the deformation rate tensor. As discussed in [12], the intrinsic mechanical dissipation (ϕ_{int}) is superposed with the thermal (ϕ_{th}) dissipation

$$\phi = \phi_{int}\left[\left(v_{i,j} - e_{kji}w_k\right), w_{i,j}, \omega\right] + \phi_{th}(q_i, \omega). \tag{28}$$

Here the first two arguments of ϕ_{int} indicate its dependence on kinematic fields and its randomness and, similarly, the first argument of ϕ_{th} indicates its dependence on the heat flux. Furthermore, in the vein of probability theory, the ω parametrization

(i.e. the third argument of ϕ_{int} and the second argument of ϕ_{th}) indicate the stochastic character of these functionals. Thus

$$\phi\left(\mathbf{V},\omega\right)=\phi_{int}\left[\mathbf{V}_1,\mathbf{V}_2,\omega\right]+\phi_{th}(\mathbf{V}_3,\omega), \tag{29}$$

in which the velocity vector $\mathbf{V}$ has three components

$$\mathbf{V}_1=\nabla\mathbf{v}-\mathbf{e}_j\times\mathbf{e}_i\cdot\mathbf{w},\quad \mathbf{V}_2=\nabla\mathbf{w},\quad \mathbf{V}_3=\mathbf{q}. \tag{30}$$

Corresponding to $\mathbf{V}$ there is the dissipative force $\mathbf{Y}$:

$$\mathbf{Y}_1=\tau,\quad \mathbf{Y}_2=\mu,\quad \mathbf{Y}_3=-\frac{\nabla T}{T}. \tag{31}$$

Given the randomly occurring violations of the Second Law, just like in (4), the time integral of ϕ evolves as a submartingale: the entropy production inequality holds on average

$$\mathsf{E}\{\rho\,\phi(\mathbf{V},\omega)\}\geq 0. \tag{32}$$

By the Doob decomposition theorem, the submartingale is split into an increasing process and a martingale

$$\int_0^t \phi dt'=G+M \tag{33}$$

or, instantaneously,

$$\phi=\dot{G}+\dot{M}. \tag{34}$$

Clearly, $\dot{M}$ represents the microscale fluctuation, while G represents the conventional (well-known) entropy growth. Thus, $\dot{G}\equiv dG/dt$ is identified with the average of the irreversible entropy rate ($\mathsf{E}\{s^{*(i)}\}$) and $\dot{M}\equiv dM/dt$ with its zero-mean random fluctuations. In terms of the irreversible entropy production, we have

$$\mathsf{E}\{s^{*(i)}\}=\dot{G},\quad s^{*(i)}-\mathsf{E}\{s^{*(i)}\}=\dot{M}. \tag{35}$$

The fluid mechanics (intrinsic) part $\phi_{int}\left[\mathbf{V}_1,\mathbf{V}_2,\omega\right]$ of the random functional $\phi(\mathbf{V},\omega)$ is a superposition of two parts:

$$\phi_{int}(\mathbf{d},\omega)=\dot{G}(\mathbf{d})+\dot{M}(\mathbf{d},\omega), \tag{36}$$

with the randomness residing in $M(\mathbf{d},\omega)$, and the viscosity coefficients assuring the positive-definiteness of G:

$$\begin{gathered}\mu\geq 0,\quad 3\lambda+2\mu\geq 0,\\ c_d+c_a\geq 0,\ c_d+c_a\geq 0,\ 2c_d+3c_0\geq 0,\\ -\left(c_d+c_a\right)\leq c_d-c_a\leq\left(c_d+c_a\right),\ \mu_r\geq 0.\end{gathered} \tag{37}$$

In general, the motion on microscale is turbulent. The micropolar fluid mechanics accounts for turbulence in terms of zero-mean perturbations about the means of both degrees of freedom ($\mathbf{v}$, $\mathbf{w}$) and pressure (p):

$$\begin{aligned} \mathbf{v} &= \overline{\mathbf{v}} + \mathbf{v}', \quad \overline{\mathbf{v}'} = 0, \\ \mathbf{w} &= \overline{\mathbf{w}} + \mathbf{w}', \quad \overline{\mathbf{w}'} = 0, \\ p &= \overline{p} + p', \quad \overline{p'} = 0. \end{aligned} \tag{38}$$

With reference to the analysis of Couette- and Poiseuille-type flows conducted in [10], we ask: Are non-zero microrotational disturbances $\mathbf{w}'$ possible for vanishing classical flow disturbances $\mathbf{v}'$? According to the analysis of steady parallel flows, assuming the conventional Second Law of thermodynamics holds, the answer is in the negative. However, given the spontaneous violations of the Second Law, non-zero fluctuations $\mathbf{w}'$ will also spontaneously appear (!) under imposed zero fluctuation field ($\mathbf{v}' = \mathbf{0}$) of the velocity field $\mathbf{v}$ [14].

5.2 *Upscaling from Stochastic to Deterministic Media*

As the spatial scale increases, the micropolar effects tend to vanish, and the fluid becomes classical Newtonian, so that only the first line of these inequalities remains relevant. As is well known, for incompressible response, the Newtonian fluid simplifies to a Navier–Stokes fluid in the special case of a vanishing bulk viscosity: $\lambda + \frac{2}{3}\mu \to 0$. The upscaling from the molecular level to stochastic and then deterministic continua involves the gradual replacement of field equations (20)–(22) by the equations of conventional continuum mechanics, whereby $\mu_{ji} = 0$ and $w_k = g_k = 0$, so that

$$\begin{aligned} &\text{conservation of linear momentum} && \rho \frac{Dv_i}{Dt} = \sigma_{ji,j}\,, \\ &\text{conservation of angular momentum} && e_{ijk}\sigma_{jk} = 0, \\ &\text{conservation of internal energy} && \rho \frac{Du}{Dt} = -q_{i,i} + \sigma_{ji} d_{ji}. \end{aligned} \tag{39}$$

Note that, since dV is a statistical volume element (SVE), not a representative volume element (RVE), the response depends on the type of loading. To this end, guided by the analogy to upscaling of a spatially random micropolar elastic continuum [18], we set up a homogenization condition of Hill-Mandel type for a micropolar fluid medium [a generalization of the Hill-Mandel condition]:

$$\overline{\sigma_{ij} d_{ij} + \beta_{ij}\alpha_{ij} + \mu_{ij}\dot{\kappa}_{ij}} = \overline{\sigma}_{ij}\,\overline{d}_{ij} + \overline{\beta}_{ij}\,\overline{\alpha}_{ij} + \overline{\mu}_{ij}\,\overline{\kappa}_{ij}\,, \tag{40}$$

where $\overline{f} \equiv \frac{1}{V}\int f\,dV$ denotes the volume average. The quantities appearing here are defined by first introducing decompositions of the generally non-symmetric velocity gradient l_{ij} and the generally non-symmetric Cauchy stress τ_{ij} according to

$$l_{ij} = d_{ij} + \alpha_{ij}, \qquad \tau_{ij} = \sigma_{ij} + \beta_{ij}\,, \tag{41}$$

where d_{ij} is the deformation rate and σ_{ij} is the symmetric Cauchy stress.

$$\begin{aligned} d_{ij} &= \tfrac{1}{2}(v_{i,j} + v_{j,i}), \qquad \alpha_{ji} = \tfrac{1}{2}(v_{i,j} - v_{j,i}) - e_{kij}\dot{\varphi}_k, \\ \sigma_{ij} &= \tfrac{1}{2}(\tau_{ij} + \tau_{ji}), \qquad \beta_{ji} = \tfrac{1}{2}(\tau_{ij} - \tau_{ji}) \end{aligned} \tag{42}$$

Similar to the aforementioned reference, a computational study using molecular dynamics, under boundary conditions consistent with (40), will reveal the quantitative scaling of classical and micropolar viscosities in terms of the SVE size $\sqrt[n]{dV}$ in either $n = 2$ or 3 dimensions.

6 Conclusions

That "*the Second Law is of the nature of strong probability … not an absolute certainty*" was already recognized by J.C. Maxwell. However, it is only in the past two decades that statistical physics has come out in support of that statement. The fundamental fact is that there is a non-zero probability of negative entropy production rate on very small scales and (very) short times. To this end, the fluctuation theorem replaces the Second Law of thermodynamics (and Clausius-Duhem inequality) as a weaker (and stochastic) restriction to be placed on the dependent fields and material properties. In turn, this leads to a generalization of continuum (thermo)mechanics. Next, given the lack of symmetry of stress tensor on molecular scales, a stochastic micropolar fluid is proposed a more appropriate model of hydrodynamics on very small levels; consequences relating to fine scale turbulent motions and upscaling to a deterministic continuous medium are then reviewed. On the history of mechanics side, while finalizing this paper, the author became aware of the study [1], where a microcrack density function was modeled as a submartingale.

Acknowledgments Constructive comments of the reviewers are appreciated. This work was partially supported by the NSF under grants IIP-1362146 and CMMI-1462749.

References

1. Augusti, G., Mariano, P.M.: Stochastic evolution of microcracks in continua. Comp. Meth. Appl. Mech. Eng. **168**, 155–171 (1999)
2. Ball, J.M.: Dynamical Systems and Energy Minimization. http://people.maths.ox.ac.uk/ball/Teaching/dynenergy2013.pdf (2014)
3. Doob, J.L.: Stochastic Processes. Wiley (1953)
4. Edelen, D.G.B.: Primitive thermodynamics: a new look at the Clausius-Duhem inequality. Int. J. Eng. Sci. **12** (1974)

5. Evans, D.J., Cohen, E.G.D., Morriss, G.P.: Probability of second law violations in steady states. Phys. Rev. Lett. **71** (1993)
6. Evans, D.J., Morriss, G.P.: Statistical Mechanics of Nonequilibrium Liquids. Cambridge University Press (2008)
7. Evans, D.J., Searles, D.J.: Equilibrium microstates which generate second law violating steady states. Phys. Rev. E **50**, 1645 (1994)
8. Evans, D.J., Searles, D.J.: The fluctuation theorem. Adv. Phys. **51**(7), 1529–1585 (2002)
9. Jarzynski, C.: Equalities and inequalities: irreversibility and the second law of thermodynamics at the nanoscale. Annu. Rev. Condens. Matter Phys. **2**, 329–351 (2011)
10. Liu, C.Y.: On turbulent flow of micropolar fluids. Int. J. Eng. Sci. **8**, 457–466 (1970)
11. Łukaszewicz, G.: Micropolar Fluids: Theory and Applications. Birkhäuser (1999)
12. Malyarenko, A., Ostoja-Starzewski, M.: Statistically isotropic tensor random fields: correlation structures. Math. Mech. Comp. Syst. (MEMOCS) **2**(2), 209–231 (2014)
13. Ostoja-Starzewski, M., Malyarenko, A.: Continuum mechanics beyond the second law of thermodynamics. Proc. R. Soc. A **470**, 20140531 (2014)
14. Ostoja-Starzewski, M.: Second law violations, continuum mechanics, and permeability, Continuum Mech. Thermodyn., in press (2015)
15. Reid, J.C., Brookes, S.J., Evans, D.J., Searles, D.J.: The dissipation function: its relationship to entropy production, theorems for nonequilibrium systems and observations on its extrema. In: Dewar, R.C., et al. (eds.) Beyond the Second Law, Understanding Complex Systems. Springer, Berlin (2014)
16. Searles, D.J., Evans, D.J.: Fluctuation theorem for heat flow. Int. J. Thermophys. **22**(1), 123–134 (2001)
17. Seifert, D.J.: Stochastic thermodynamics, fluctuation theorems and molecular machines. Rep. Prog. Phys. **75**, 126001 (58pp) (2001)
18. Trovalusci, P., Ostoja-Starzewski, M., de Bellis, M.L., Muralli, A.: Scale-dependent homogenization of random composites as micropolar continua. Europ. J. Mech./A: Solids **49**, 396–407 (2014)
19. Wang, G.M., Sevick, E.M., Mittag, E., Searles, D.J., Evans, D.J.: Experimental demonstraiton of violations of the second law of thermodynamics for small systems and short time scales. Phys. Rev. Lett. **89**, 050601 (2002)
20. Ziegler, H., Wehrli, C.: The derivation of constitutive relations from the free energy and the dissipation functions. Adv. Appl. Mech. **25**, 183–238 (1987)

Phase Change Materials and Thermochemical Materials for Large-Scale Energy Storage

Camilo Rindt, Shuiquan Lan, Mohammadreza Gaeini, Huaichen Zhang, Silvia Nedea and David M.J. Smeulders

Abstract Replacing the use of fossil fuels by renewables is of paramount importance not so much because of declining reserves (fossil fuel reserves are estimated abundant for at least over a century) but because of increasing CO_2 emissions which cause irreversible climate changes. To overcome the mismatch between supply and demand of solar heat and electricity, smart combinations of heat pumps and heat storage are currently investigated. A reliable method for heat storage is to use thermochemical (TCM) and phase change materials (PCM). These materials should be tested for energy density, temperature range, corrosion, toxicity, (dis)charge time and longevity. A prototype TCM reactor is built and tested for hot water generation. Using zeolite 13X as TCM, it is shown that tap water temperatures of 45 °C can be obtained. Using optical microscopy, the hydration and dehydration process of TCM material can be observed, as well as the phase transitions of PCMs. It is also argued that computational molecular modelling methods provide a powerful tool for both TCM and PCM material synthesis.

C. Rindt · S. Lan · M. Gaeini · H. Zhang · S. Nedea · D.M.J. Smeulders (✉)
Eindhoven University of Technology, P.O. Box 513, 5600 MB Eindhoven, The Netherlands
e-mail: D.M.J.Smeulders@tue.nl

S. Lan
e-mail: S.Lan@tue.nl

M. Gaeini
e-mail: M.Gaeini@tue.nl

H. Zhang
e-mail: H.Zhang@tue.nl

S. Nedea
e-mail: S.V.Nedea@tue.nl

C. Rindt
e-mail: C.C.M.Rindt@tue.nl

B. Albers and M. Kuczma (eds.), *Continuous Media with Microstructure 2*,
DOI 10.1007/978-3-319-28241-1_13

1 Introduction

In Europa heat for domestic purposes constitutes 40 % of the total energy demand. In summer, the sun provides more heat than needed to warm residential houses while in winter the heat demand cannot be met by solar energy supply. A solution is to store excess solar energy in a so-called thermal battery which can be discharged to meet the residential heat demand in winter. A reliable method for seasonal solar heat storage is by means of phase change materials (PCMs) or thermochemical materials (TCMs). Both methods can store heat more compactly than by means of the traditional sensible heat system where a liquid (typically water) is heated and stored in an insulated tank. The TCM process is based on a reversible adsorption-desorption reaction, which is exothermic in hydration and endothermic in dehydration [1, 2]. Examples are zeolites and salt hydrates. The PCM process is based on latent heat release upon crystallization for example in sodium acetate which is used in heat packs, and sugar alcohols. This means that for TCMs humid air has to be in contact with the storage material, while for PCMs the material is isolated and large-scale heat transfer is achieved through heat exchangers. In the forthcoming, we will first discuss TCM applications and next focus on PCM computations.

2 Theory

A thermal model is developed for the packed bed during the hydration of the zeolite [3]. The model includes mass and heat transfer in the gas, the packed bed and the reactor wall, as well as the adsorption reaction of water vapor on the zeolite. Equilibrium constants are modeled as a function of temperature. By comparing the temperatures of the experimental investigation with the results of the numerical simulation model, the kinetic parameters for the adsorption in non-isothermal and non-adiabatic conditions are found. We consider constant gas flow (interstitial velocity u_m) through a packed bed. The energy equation of a moving fluid in a packed bed is given by

$$\rho_f c_f \left(\frac{\partial T_f}{\partial t} + u_m \frac{\partial T_f}{\partial x} \right) = -\nabla \cdot \mathbf{q}, \tag{1}$$

where T_f is the fluid temperature, c_f is the heat capacity of the fluid and $\mathbf{q}$ the heat flux from the fluid to the bed (W/m^2). Integrating over a cylindrical pore volume $V_p = \phi \pi R^2 \Delta z$ (ϕ is the porosity) we obtain

$$\rho_f c_f \left(\frac{\partial T_f}{\partial t} + u_m \frac{\partial T_f}{\partial x} \right) \phi \pi R^2 \Delta z = - \int_{V_p} \nabla \cdot \mathbf{q} dV_p. \tag{2}$$

Using Gauß' theorem the right-hand-side of (2) can be written as $- \int \mathbf{q} \cdot \mathbf{n} dA_p$, with A_p the contact area between the fluid and the bed particles. The heat transfer

between the fluid and the bed can be described by Newton's 'Ansatz' in terms of the convective heat transfer coefficient α:

$$-\int \mathbf{q} \cdot \mathbf{n} dA_p = \alpha A_p (T_s - T_f), \tag{3}$$

with T_s the temperatures of the solid. Note that we assume a uniform temperature distribution in the bed particles (lumped-parameter model), which is only true for Biot numbers smaller than 0.1. As the solid volume $V_s = \pi R^2 (1-\phi)\Delta z$, and assuming spherical particles with radius b, the number of spheres is $\frac{3}{4}(1-\phi)R^2\Delta z/b^3$. Multiplying by the individual surface of each sphere, it is straightforward to show that $A_p = 3\pi R^2(1-\phi)\Delta z/b$. Combination of (2) and (3) yields that

$$\rho_f c_f \left(\frac{\partial T_f}{\partial t} + u_m \frac{\partial T_f}{\partial x} \right) \phi \pi R^2 = \alpha S_p (T_s - T_f), \tag{4}$$

where we have introduced the contact surface per length scale $S_p = A_p/\Delta z$. For the bed particles, it holds that

$$\rho_s c_s \left(\frac{\partial T_s}{\partial t} \right) (1-\phi)\pi R^2 = -\alpha S_p (T_s - T_f). \tag{5}$$

The coupled equations (4) and (5) can be solved for temperature profiles $T_f(x,t)$ and $T_s(x,t)$ as was shown by e.g., [3].

3 Experiments

In order to investigate the potential for TCM applications for heat storage, a reactor was designed and built to measure temperature and humidity profiles in a zeolite packed bed. Moreover, on the smaller scale, optical microscopy was applied to study hydration and dehydration in salt hydrates.

3.1 Reactor Design

Following [4], a lab-scale prototype thermochemical heat storage system was tested (see Fig. 1). In the experimental setup, air enters a reactor vessel filled with zeolite 13X. The air can be hot and dry to charge the thermal battery, or cold and moist for discharge. In the latter case, the idea is that the thermal battery generates heat to warm up the air by means of an exothermic adsorption of water to the zeolite (hydration of zeolite and dehydration of the moist air). The temperature profile is measured as a function of time along the flow direction. Input and output temperatures, pressures

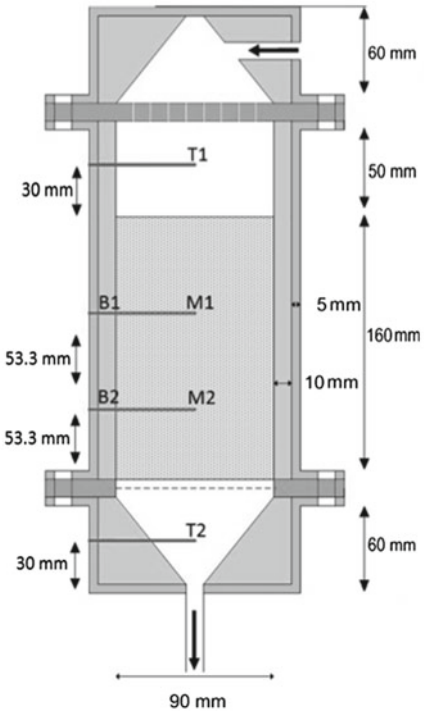

Fig. 1 Reactor filled with zeolite 13X beads. During charging hot air entering from the *top* dehydrates the zeolite beads and leaves the reactor at the *bottom* as cold moist air until the zeolite is fully dehydrated. During discharge, moist cold air hydrates the zeolite and leaves the reactor at the *bottom* as hot dry air. Temperature profiles are measured by themocouples T1, T2, M1 and M2. The humidity is measured at the outflow port

and humidity are measured. In the dehydration (charging) experiment, an electric heater is used to produce dry air of 200 °C which is blown into the reactor. This leads to an increase in temperature from 25 to 160 °C at the inlet of the reactor (T1). The measured temperatures and humidity ratio (gram of water per 100 g of dry air) in a dehydration experiment are shown in Fig. 2. The temperature in the bed starts to increase layer by layer. Two endothermic effects can be determined in the graph; one is around the bed temperature of 35 °C and the other one is around 120 °C. This may be related to the sorption characteristics of the zeolite, but to establish this, additional DTA (Differential Thermal Analysis) measurements need to be done. After almost 2 h the humidity ratio becomes zero which means that the material is dehydrated as far as possible with this dehydration temperature and vapor pressure. The remaining fluctuations in the humidity ratio are due to the limited accuracy of the humidity measurement at high temperatures, since the humidity ratio is calculated from the measured relative humidity.

Next, humid air of 25 °C is blown into the reactor to start the exothermic hydration reaction. In Fig. 3, it can be seen that the temperatures M1 and M2 rapidly rise to more than 55 °C. The inflow temperature T1 is more or less constant. After some 100 min, the temperature M1 drops off, indicating that the reaction has ended in the upper layer of the reactor (above M1). The temperature M2 drops off much later (around 200 min), because this temperature is a measure of the heat produced in

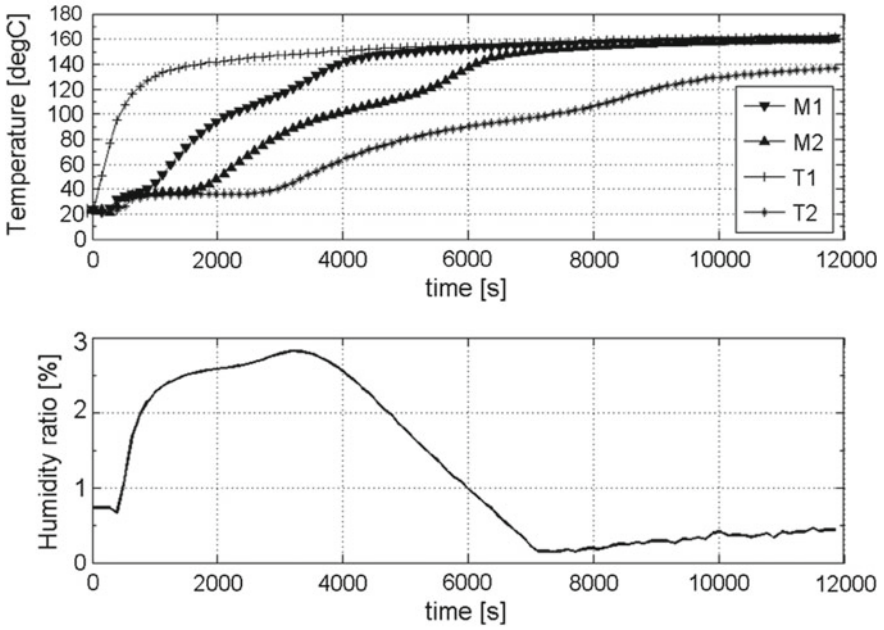

Fig. 2 Dehydration results. The temperatures of the *top panel* are measured at the positions indicated in Fig. 1. The humidity of the effluent air is indicated in the *bottom panel*. From [4]

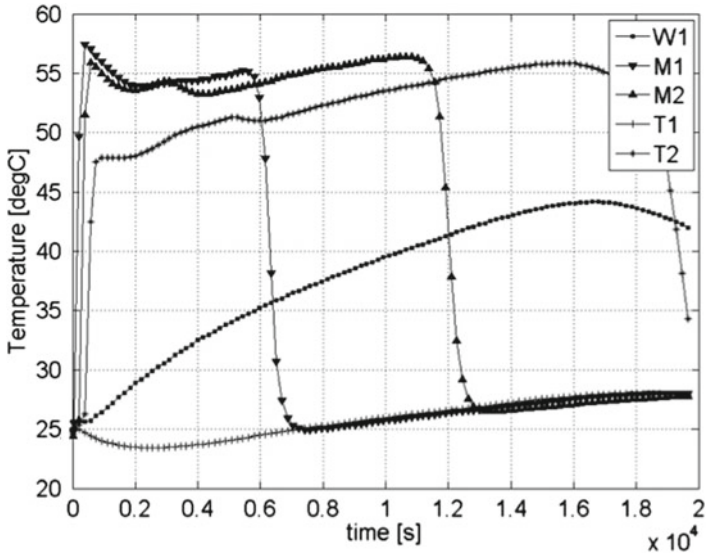

Fig. 3 Hydration results. The temperatures are measured at the positions indicated in Fig. 1. The produced heat in the reactor is used to heat a separate water vessel whose temperature W1 is also plotted in the figure. From [4]

a larger part of the reactor (above M2). Note that the heat is transported through the reactor by air flow. The outflow temperature (T2) also increases suddenly after the experiment is started to the temperature of 48 °C which is somewhat lower than the bed temperature due to heat losses. The outflow temperature still increases until some 4.5 h after the start of the experiment due to the reaction in the lower layers of the bed. The hot outflow is used to heat up water in a separate vessel. The water temperature in this vessel (W1) is also plotted. We notice that a maximum water temperature of 45 °C is reached. Next, for about 1 h (from t= 4.5–5.5 h approximately), the hot hydrated material in the bed transfers its remaining heat to the flow while cooling down. The water temperature (W1) starts to decrease when the outflow temperature starts to decrease indicating that the reaction is now completely finished in the bed.

3.2 *Microscopy*

We also investigate the dehydration reaction on the smaller scale by means of optical microscopy. Following [5, 6], we now use $Li_2SO_4 \cdot H_2O$ as heat storage material. The dehydration reaction is found to proceed through formation and growth of nuclei over time (see Fig. 4). Crystals were embedded at room temperature in a liquid

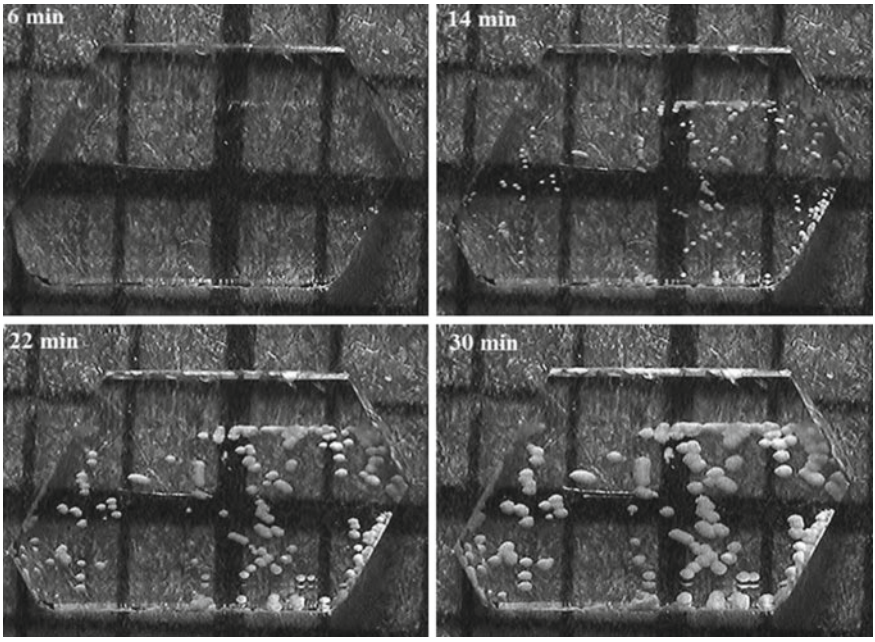

Fig. 4 Surface growth sequence of the anhydrous nuclei formed during the dehydration of a $Li_2SO_4 \cdot H_2O$ crystal at 100 °C and under a water vapor pressure of 13 mbar. From [6]

resin called EpoFix resin, which hardened within 10 h. An important feature of this resin is that it will maintain its transparency at 130 °C up to 5 h, which ensures that the phase change is visible during the entire reaction. Encapsulated crystals were polished using abrasive paper. The resin layer was polished up to a thickness of approximately 1 mm, which is thick enough to impede gaseous product release. There are two reasons to make the resin layer this thin. One is that the resin is a poor thermal conductor. In order to achieve a certain reaction temperature, the resin has to be heated up to a higher temperature if the layer would be too thick. Unfortunately, the transparency diminishes rapidly as the temperature increases. The other reason is that the reaction temperature profile should be close to the resin temperature profile to establish the correct reaction kinetics [7]. Figure 4 shows a typical sequence of the nucleation and nuclei growth processes on the surface of a single crystal. The mesh on the background provides information on the length scale (grid size 1 mm). The reaction proceeds by the conversion of the transparent phase to the opaque white phase indicating the formation of nuclei and nuclei growth. Imperfections of a crystal are potential nucleation sites. Hence, more nuclei are observed at the grain boundaries such as edges and cracks. Apparently, in this case the growth process was dominant over nucleation. It was found that the number of nuclei is more or less constant.

4 Sugar Alcohols as PCMs

Sugar alcohols are a category of organic materials derived from natural sugars. As byproducts of the food industry, sugar alcohols are environmentally friendly and economically competitive. For most common C4–C6 acyclic sugar alcohols, preliminary studies have shown relatively high latent heat of melting ΔH_m and moderate melting points T_m for seasonal heating applications. Figure 5 summarizes T_m and ΔH_m for all C4–C6 acyclic sugar alcohols (for nomenclature of sugar alcohols see [8]). Recent studies suggest the use of eutectic mixtures of sugar alcohols to form molecular alloys, to further increase their latent heat or decrease their melting points. Diarce et al. [9] examined three most promising mixtures and Gunasekara et al. [10] further designed a test protocol for xylitol–erythritol mixture. Their results are also included in Fig. 5.

The commonly seen and produced sugar alcohols, can roughly be divided into two groups. The lower melting point group has melting points ranging from 70 to 105 °C and melting enthalpies ranging from 170 to 260 kJ/kg including xylitol, glucitol, and ribitol. The higher melting point group with melting point ranging from 120 to 200 °C includes erythritol, mannitol, and glactitol. The density of sugar alcohols are in the range of 1.3–1.5 g/cm^3 with around 9 % volumetric expansion upon melting [8]. Sugar alcohols are generally poor thermal conductors. Typical thermal conductivities of sugar alcohols are in the order of 10^{-1} W/(m·K) [11]. Carbon foams are investigated to boost thermal conductivity and the effect is proven to be considerable [12].

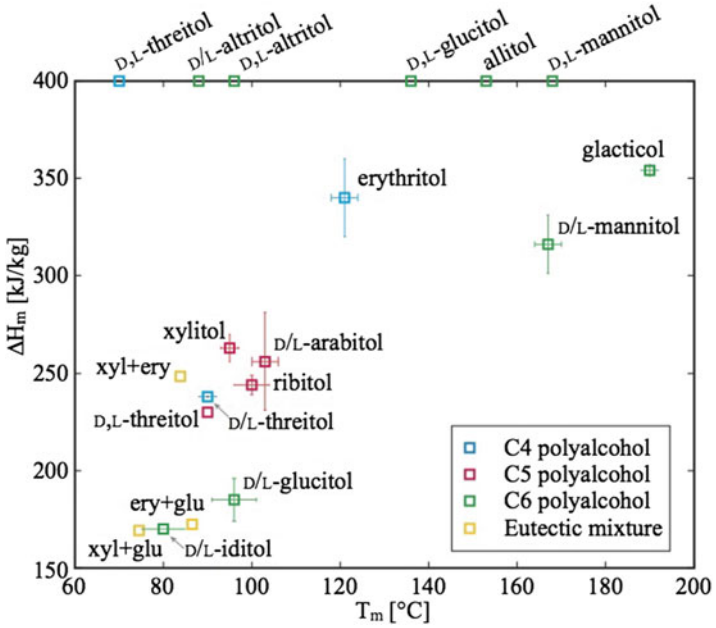

Fig. 5 Melting points and latent heat of C4–C6 acyclic sugar alcohols. The *error bars* cover the data range from various sources. The compounds without latent heat data are plotted on *top* of the figure to show their melting points only. From [8]

The stability and cycling effects of sugar alcohols are studied only for a few sugar alcohol species. In general, sugar alcohols suffer from caramelization, oxidation, and thermal decomposition. For example, D-mannitol reacts with oxygen, forming a non-stable material with a lower storage capacity [13]. Erythritol decomposes at 160 °C [14] but below this temperature it showed good cyclability [15]. Therefore high operating temperatures must be avoided.

Sugar alcohols have evident supercooling effect. This makes sugar alcohols suitable for low-loss heat storage at relatively lower temperatures. However, the shear viscosity of sugar alcohols increases significantly with high degrees of supercooling [16]. This makes the low melting point group of sugar alcohols hard to nucleate and crystallize [17]. For example, the crystal front growth speed of xylitol is at maximum 3 μm/s. Erythritol and D-mannitol have good nucleation and crystallization kinetics. However, this reduces the degree of supercooling they can achieve without spontaneous nucleation [17].

Sugar alcohols can grow with distinct branching morphologies under different temperatures. Figure 6 shows erythritol crystallizing at 90 °C and 1 °C of supercooling respectively. In general, higher degrees of supercooling encourage surface nucleation and branching.

To summarize, sugar alcohols are a promising category of materials suitable for seasonal heat storage applications where the evident supercooling effect can help

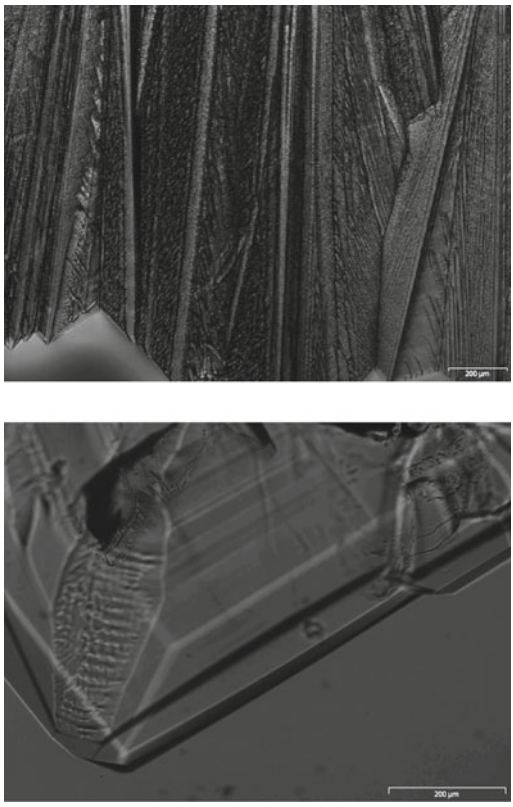

Fig. 6 Microscopic images of Erythritol supercooled crystallization at 28 °C (*top*) and 117 °C (*bottom*) showing different branching morphologies. The melting point T_m of Erythritol is 118 °C. The *scale bars* are 200 μm, in both pictures

significantly reduce insulation costs. In seasonal storages, the cycling effects can be neglected, given the limited number of cycles to be used in this scenario. To work with sugar alcohols, temperatures much higher than their melting points must be avoided. The 9 % volumetric expansion upon melting could reduce applicability for seasonal storage.

5 Molecular Modeling Method for PCMs

The sugar alcohol molecules can be modeled using state-of-the-art force fields, which are derived from density functional theory calculations. Previous works have used a generalized AMBER force field [18] to succesfully evaluate thermodynamic and transport properties of sugar alcohols [16, 19], including enthalpy, heat capacity, shear viscosity, and solid-liquid interfacial free energy. In this force field, all atoms in the molecules are modeled as point masses which interact according to a set of conservative potentials. The total potential energy is expressed as

$$E_{\mathrm{p}}(\mathbf{r}_1, \mathbf{r}_1, \ldots, \mathbf{r}_N,) = E_{\mathrm{bond}} + E_{\mathrm{angle}} + E_{\mathrm{dih}} + E_{\mathrm{LJ}} + E_{\mathrm{el}}, \quad (6)$$

where E_{p} represents the total potential energy, $\mathbf{r}_i$ is the coordinate vector of the ith atom. At the right-hand-side of the equation are the bond stretching energy, angle bending energy, dihedral torsional energy, the van der Waals interaction in the so-called 6–12 Lennard-Jones form, and the electrostatic interaction, respectively.

6 Molecular Modeling Methods for TCMs

Thermochemical heat storage materials can also be modeled using molecular simulation tools. Because of the nature of thermochemical storage, chemical reactions and charge transfers may occur during the hydration and dehydration processes [20]. Therefore, a force field that allows bond breaking and forming is required. In the work of Smeets et al. ReaxFF is parameterized and used in the simulations of $MgCl_2$ hydrates [21, 22]. The dehydration of $MgSO_4$ heptahydrate is studied by Zhang et al. [23] based on a non-reactive force field and no charge transfer assumption [20].

References

1. Shigeishi, R.A., Langford, C.H., Hollebone, B.R.: Solar energy storage using chemical potential changes associated with drying of zeolites. Solar Energy **23**, 489–495 (1979)
2. Zondag, H., Kikkert, B., Smeding, S., de Boer, R., Bakker, M.: Prototype thermochemical heat storage with open reactor system. Appl. Energy **109**, 360–365 (2013)
3. Gaeini, M., Zondag, H.A., Rindt, C.C.M.: Non-isothermal kinetics of zeolite water vapor adsorption into a packed bed lab scale thermochemical reactor. In: Proceedings of 15th International Heat Transfer Conference, IHTC-15, August 10–15, Kyoto, Japan (2014)
4. Gaeini, M., de Jong, E.C.M., Zondag, H.A., Rindt, C.C.M.: Design of a thermochemical heat storage system for tap water heating in the built environment. Adv. Thermal Energy Storage EUROTHERM **99** (2015)
5. Brown, M.E., Galwey, A.K., Li Wan Po, A.: Reliability of kinetic measurements for the thermal dehydration of lithium sulphate monohydrate: part 1. Isothermal measurements of pressure of evolved water vapour. Thermochimica Acta **203**, 221–240 (1992)
6. Lan, S., van Maris, M., Zondag, H., Rindt, C.: In-situ observation of the dehydration of $LiSO_4{\cdot}H_2O$ mono crystals. Adv. Thermal Energy Storage EUROTHERM **99** (2014)
7. Koga, N., Tanaka, H.: Kinetics and mechanisms of the thermal dehydration of Li2SO4.H2O. J. Phys. Chem. **93**, 7793–7798 (1989)
8. Zhang, H., Nedea, S.V., Rindt, C.C.M.: Review and in silico characterization of sugar alcohols as seasonal heat storage materials. In: 13th International Conference on Energy Storage, Greenstock (2015)
9. Diarce, G., Gandarias, I., Campos-Celador, A., García-Romero, A., Griesser, U.J.: Eutectic mixtures of sugar alcohols for thermal energy storage in the 50–90 °C temperature range. Solar Energy Mater. Solar Cells **134**, 215–226 (2015)
10. Gunakunsara, S.N., Chiu, J.N., Victoria, M.: Binary phase equilibrium study of the polyols blend erythritol-xylitol with the T-history method for phase change materials design. In: 13th International Conference on Energy Storage, Greenstock (2015)

11. Gunasekara, S.N., Pan, R., Chiu, J.N., Martin, V.: Polyols as phase change materials for low-grade excess heat storage. Energy Procedia **61**, 664–669 (2014)
12. Jana, P., Fierro, V., Pizzi, A., Celzard, A.: Biomass-derived, thermally conducting, carbon foams for seasonal thermal storage. Biomass Bioenergy **67**, 312–318 (2014)
13. Solé, A., Neumann, H., Niedermaier, S., Martorell, I., Schossig, P., Cabeza, L.F.: Stability of sugar alcohols as PCM for thermal energy storage. Solar Energy Mater. Solar Cells **126**, 125–134 (2014)
14. Kaizawa, A., Maruoka, N., Kawai, A., Kamano, H., Jozuka, T., Senda, T., Akiyama, T.: Thermophysical and heat transfer properties of phase change material candidate for waste heat transportation system. Heat Mass Transf. **44**(7), 763–769 (2008)
15. Shukla, A., Buddhi, D., Sawhney, R.L.: Thermal cycling test of few selected inorganic and organic phase change materials. Renew. Energy **33**(12), 2606–2614 (2008)
16. Zhang, H., van Wissen, R.M.J., Nedea, S.V., Rindt, C.C.M.: Characterization of sugar alcohols as seasonal heat storage media: experimental and theoretical investigations. Adv. Thermal Energy Storage EUROTHERM **99** (2014)
17. van Wissen, R.M.J.: Phase change behavior of sugar alcohol based heat storage materials. MSc Thesis, Eindhoven University of Technology (2013)
18. Wang, J., Wolf, R.M., Caldwell, J.W., Kollman, P.A., Case, D.A.: Development and testing of a general amber force field. J. Comput. Chem. **25**(9) (2004)
19. Zhang, H., Nedea, S.V., Rindt, C.C.M., Zondag, H.A., Smeulders, D.M.J.: Prediction of anisotropic crystal-melt interfacial free energy of sugar alcohols through molecular simulations. In: 15th International Heat Transfer Conference (IHTC-15) (2014)
20. Iype, E., Nedea, S.V., Rindt, C.C.M., van Steenhoven, A.A., Zondag, H.A., Jansen, A.P.J.: DFT study on characterization of hydrogen bonds in the hydrates of $MgSO_4$. J. Phys. Chem. C **116**(35), 18584–18590 (2012)
21. Iype, E., Hütter, M., Jansen, A.P.J., Nedea, S.V., Rindt, C.C.M.: Parameterization of a reactive force field using a Monte Carlo algorithm. J. Comput. Chem. **34**(13), 1143–1154 (2013)
22. Smeets, B., Iype, E., Nedea, S.V., Zondag, H.A., Rindt, C.C.M.: A DFT based equilibrium study on the hydrolysis and the dehydration reactions of $MgCl_2$ hydrates. J. Chem. Phys. **139**(12), 124312 (2013)
23. Zhang, H., Iype, E., Nedea, S.V., Rindt, C.C.M.: Molecular dynamics study on thermal dehydration process of epsomite ($MgSO_4 \cdot 7H_2O$). Mol. Simul. **40**(14), 1157–1166 (2013)

Distribution of Temperature in Multicomponent Multilayered Composites

Monika Wągrowska and Olga Szlachetka

Abstract The object of analysis is a heat conduction problem within the framework of tolerance modelling in multicomponent, multilayered periodic composites. The proposed model equations describe heat conduction in the discussed laminates by means of partial differential equations with constant coefficients. This paper describes the one-dimensional, stationary problems of heat conduction in direction perpendicular to layers.

1 Introduction

The object of the presented investigation is a heat conduction problem in a multicomponent, multilayered periodical material structure (Fig. 1). The problem of heat conduction in multilayered twocomponent periodic composite and composite with functional gradation of material properties (FGM) is well known in the literature. We can mention here papers: [1–27, 31–33, 35–37, 40–44].

The problem of modelling of heat conduction in multicomponent composites based on the tolerance model procedure was presented by [38, 39] and applied by [34] and by [28–30].

By means of a formal limit transition with the length parameter tending to zero it is possible to obtain the equation of the local homogenization model from the tolerance model equations [38]. The process of heat conduction will be discussed within the frames of this model. Examples of heat conduction will be narrowed down to the one-dimensional, stationary problems of heat conduction in direction perpendicular to layers for homogeneous and isotropic components.

M. Wągrowska (✉) · O. Szlachetka
Faculty of Civil and Environmental Engineering, Warsaw University of Life Sciences-SGGW, Nowoursynowska 166, Warsaw, Poland
e-mail: monika_wagrowska@sggw.pl

O. Szlachetka
e-mail: olga_szlachetka@sggw.pl

B. Albers and M. Kuczma (eds.), *Continuous Media with Microstructure 2*,
DOI 10.1007/978-3-319-28241-1_14

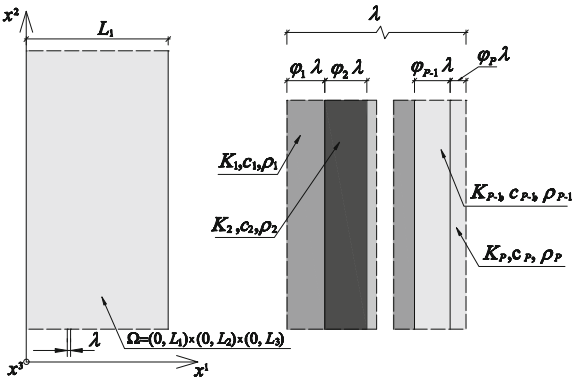

Fig. 1 The scheme of multicomponent multilayered periodic composite

2 Object of Analysis

Let the physical space be parameterized by an orthogonal Cartesian coordinate system $Ox^1x^2x^3$. The object of analysis is a rigid heat conductor that occupies a region $\Omega \equiv (0, L_1) \times (0, L_2) \times (0, L_3)$ in the physical space. The conductor is assumed to be homogeneous in the Ox^2 and Ox^3 direction and multilayered in the Ox^1 direction.

The composite is made of N identical thin layers with constant thickness λ, $\lambda = L_1/N$. Let $L = \max(L_1; L_2; L_3)$ then $\lambda << L$ (L—the characteristic dimension of the composite). Every layer of the periodic composite is assumed to be made of M different orthotropic, homogeneous components with known mass densities, specific heats and thermal conductivities. These components are sublayers of the representative layer and number of them is P, $P \geq M$.

Moreover let $\varphi_m(\cdot)$, $m = 1, \ldots, P$, be positive constant functions, such that $\varphi_1\left(x^1\right) + \cdots + \varphi_P\left(x^1\right) = 1$ for all $x^1 \in [0, L_1]$. The thickness of the mth ($m = 1, \ldots, P$) sublayer in every layer is equal to $\lambda_m = \varphi_m \lambda$.

The heat conduction problem in the discussed composite will be described by the Fourier law:

$$q^{\alpha}(\mathbf{x}, t) = -k^{\alpha\beta}(\mathbf{x})\partial_{\beta}\theta(\mathbf{x}, t) \tag{1}$$

and the heat balance equation in the form:

$$c(\mathbf{x})\partial_t\theta(\mathbf{x}, t) - \partial_{\alpha}\left(k^{\alpha\beta}(\mathbf{x})\partial_{\beta}\theta(\mathbf{x}, t)\right) = 0 \tag{2}$$

where: $\mathbf{x} \equiv (x^1, x^2, x^3) \in \Omega$, $\theta(\cdot, \cdot)$—temperature in the region of Ω for every $t \in [\,0, t_*\,)$, $k^{\alpha\beta}(\cdot)$—components of the thermal conductivity tensor (for orthotropic materials $k^{\alpha\beta}(\mathbf{x}) = 0$ for $\alpha \neq \beta$ and $k^{\alpha\alpha}(\mathbf{x}) \equiv k^{\alpha}(\mathbf{x})$, $c(\cdot)$—specific heat, subscripts and superscripts α and β are equal to 1, 2 and 3 (summation convention holds). $\partial_{\alpha}(\cdot) \equiv \frac{\partial}{\partial x^{\alpha}}$, $\partial_{\beta}(\cdot) \equiv \frac{\partial}{\partial x^{\beta}}$, $\partial_t \equiv \frac{\partial}{\partial t}$.

Let us introduce the decomposition of the ith interval of periodicity into P subintervals Δ_m^i which are defined as:

$$\Delta_m^i \equiv \left(\lambda(i-1) + \sum_{k=1}^{m-1} \varphi_k \lambda_k, \left(\lambda(i-1) + \sum_{k=1}^{m} \varphi_k \lambda_k\right)\right), \quad m = 1, 2, \ldots, P, \quad i = 1, 2, \ldots, N \tag{3}$$

The set which is occupied by the mth component in the discussed composite can be described as follows:

$$\Omega_m = \bigcup_{i=1}^{N} \Delta_m^i \times (0, L_2) \times (0, L_3), \qquad m = 1, 2, \ldots, P \tag{4}$$

Then the components of thermal conductivity tensor $k^{\alpha\beta}(\cdot)$ are equal to $k^{\alpha\beta}(\mathbf{x}) = k_m^{\alpha\beta}$, for $\mathbf{x} \in \Omega_m$, $m = 1, 2, \ldots, P$ and the specific heat $c(\cdot)$ is equal $c(\mathbf{x}) = c_m$, for $\mathbf{x} \in \Omega_m$, $m = 1, 2, \ldots, P$.

The Eq. (2) holds at all points of region Ω and $\forall t \in [0, t_*)$. It is a partial differential equation with discontinuous and highly oscillating coefficients $k^{\alpha\beta}(\cdot)$, $c(\cdot)$ which depend only on the x^1 coordinate. The fact that the coefficients are discontinuous implies that the solution of the heat conduction problem will be considered within the frames of the tolerance modelling in which discontinuous coefficients will be replaced by constant ones.

The model of heat conduction for multicomponent multilayered composites based on the process of tolerance modelling was proposed by [38, 39].

3 Modelling Concepts

In the process of tolerance modelling for periodic composites notion of slowly varying function, tolerance averaging approximation and oscillating micro-shape function are needed.

- Slowly varying functions
  Let Π stand for an arbitrary convex set in the space R^m, and let $f \in C^1(\Pi)$ be an arbitrary real-valued function. Let us define the tolerance parameter $d \equiv (\lambda, \delta_0, \delta_1)$ as a triplet of real positive numbers and use the notation $\partial_j \equiv \frac{\partial}{\partial x_j}$, $j = 1, \ldots, m$.
  We shall deal with two classes of slowly varying functions: weakly slowly varying function (WSV) and slowly varying function (SV) [44].

1. Function $f \in C^1(\Pi)$ is weakly slowly varying function ($f \in \mathrm{WSV}_d^1(\Pi) \subset C^1(\Pi)$) if the condition $||\mathbf{x}-\mathbf{y}|| \leq \lambda$ implies the conditions $|f(\mathbf{x}) - f(\mathbf{y})| \leq \delta_0$ and $\left|\partial_j f(\mathbf{x}) - \partial_j f(\mathbf{y})\right| \leq \delta_1$ for $j = 1, \ldots, m$ for all $(\mathbf{x}-\mathbf{y}) \in \Pi^2$.
2. Function $f \in \mathrm{WSV}_d^1(\Pi)$ is slowly varying function ($f \in \mathrm{SV}_d^1(\Pi)$) if conditions $\lambda \left|\partial_j f(\mathbf{x})\right| \leq \delta_0$ hold for $j = 1, \ldots, m$ for every $\mathbf{x} \in \Pi$.

- Tolerance averaging approximation
  Let us define $\Delta \equiv \left(-\frac{\lambda}{2}, \frac{\lambda}{2}\right)$ and local interval $\Delta(x) \equiv \left(x - \frac{\lambda}{2}, x + \frac{\lambda}{2}\right)$ for every $x \in \left[\frac{\lambda}{2}, L - \frac{\lambda}{2}\right]$. Let $f_x \in L^2((0, L))$. We shall define:

$$\langle f \rangle(x) \equiv \frac{1}{\lambda} \int\limits_{\Delta(x)} f_x(z)\, \mathrm{d}z \tag{5}$$

  Let $f_x \in L^2(\Delta(x))$ and $F \in \mathrm{WSV}_d^1((0, L))$. By the tolerance averaging approximation we shall mean the approximation of functions $\langle f F \rangle_T(x)$, $\langle f \partial_1 F \rangle_T(x)$ by functions $\langle f \rangle(x) F(x)$ and $\langle f \rangle(x) \partial_1 F(x)$, respectively.

$$\begin{aligned} \langle f F \rangle_T(\mathbf{x}) &\equiv \langle f \rangle(\mathbf{x}) F(\mathbf{x}) \\ \langle f \partial_1 F \rangle_T(\mathbf{x}) &\equiv \langle f \rangle(\mathbf{x}) \partial_1 F(\mathbf{x}) \end{aligned} \tag{6}$$

- Oscillating micro-shape function for heat conduction problems
  Function $\gamma(\cdot)$ is oscillating micro-shape function (for heat conduction problems) if [38]:

$$\begin{gathered} \gamma_m = \gamma_{m-1} + \lambda \varphi_m \left(\frac{K^0}{K_m} - 1\right), \qquad m = 1, 2, \ldots, P, \\ \gamma(\cdot) \text{ is piecewise linear}, \\ \langle \rho \gamma \rangle = 0. \end{gathered} \tag{7}$$

  where $\gamma_m, m = 1, 2, \ldots, P$, are values of function $\gamma(\cdot)$ on the interfaces between sublayers of a periodicity layer and

$$K^0 \equiv \left(\frac{\varphi_1}{K_1} + \cdots + \frac{\varphi_P}{K_P}\right)^{-1} \tag{8}$$

  where $K_m \equiv k_m^{11} = k_m^1$.

An example of oscillating micro-shape function for twocomponent structure is presented in Fig. 2.

It is easy to calculate that if $k_1 = k_2$ then $\gamma(x_1) = 0$ and $\tilde{\theta} = \vartheta(\cdot)$. It means that the limit passage exists from twocomponent composite to onecomponent body.

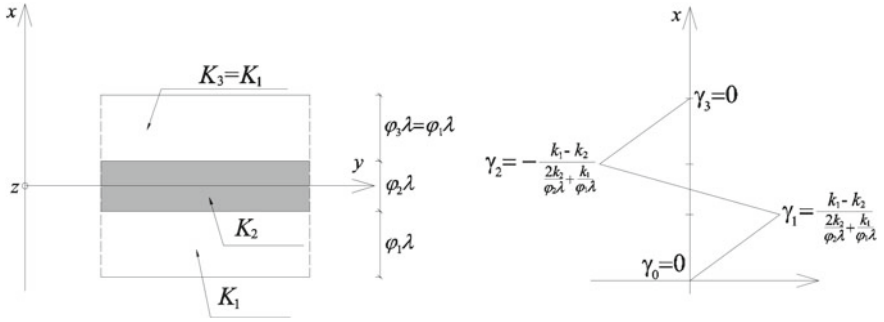

Fig. 2 The oscillating micro-shape function for two component periodic composite where $\left(x^1, x^2, x^3\right) \equiv (x, y, z)$

4 Modelling Procedure

The process of tolerance modelling is based on two assumptions.

4.1 First Assumption

The temperature $\theta(\cdot)$ is approximated by $\tilde{\theta}$ in the form [44]:

$$\tilde{\theta}(\mathbf{x}, t) = \vartheta(\mathbf{x}, t) + \gamma(x_1)\Psi(\mathbf{x}, t), \qquad x \in [0, L], \quad t \in [\in 0, t_*). \tag{9}$$

This formula is the same as micro-macro decomposition of temperature field in two component composites. The fields $\vartheta(\cdot, x_2, x_3), \psi(\cdot, x_2, x_3) \in SV_d^1((0, L_1))$ are unknown functions, which are called macro-temperature and amplitude fluctuation of temperature, $\gamma(\cdot)$is the oscillating micro-shape function, which is given a priori by (7).

Before formulating the second assumption let us define the residual field of $\tilde{\theta}$ in the region Ω for $t \in [0,t_*)$ [43]:

$$r(\mathbf{x}, t) \equiv \partial_\alpha \left(k^{\alpha\beta}(\mathbf{x})\partial_\beta \tilde{\theta}(\mathbf{x}, t)\right) - c\partial_t \tilde{\theta}(\mathbf{x}, t) \tag{10}$$

4.2 Second Assumption

The tolerance averaging approximation of the residual field and the residual field multiplied by the oscillating micro-shape function is equal to zero:

$$\begin{aligned} \langle r \rangle_T &= 0, \\ \langle \gamma r \rangle_T &= 0. \end{aligned} \tag{11}$$

5 Modelling Equations

After implementation both assumptions the system of equations for unknown functions $\theta(\cdot)$, $\psi(\cdot)$ $\left(\vartheta(\cdot, x_2, x_3), \psi(\cdot, x_2, x_3) \in \mathrm{SV}_d^1((0, L_1))\right)$ takes the form:

$$\begin{aligned} &\left\langle k^j \right\rangle \partial_j^2 \vartheta - \langle c \rangle \partial_t \vartheta + \left\langle k^1 \partial_1 \gamma \right\rangle \partial_1 \psi = 0, \\ &\left\langle k^j (\gamma)^2 \right\rangle \partial_j^2 \psi - \left\langle k^1 (\partial_1 \gamma)^2 \right\rangle \psi - \left\langle k^1 \partial_1 \gamma \right\rangle \partial_1 \vartheta - \left\langle c (\gamma)^2 \right\rangle \partial_t \psi = 0. \\ &j = 1, 2, 3 \end{aligned} \tag{12}$$

It has to be emphasized that the above system of partial differential equations, obtained within the frames of tolerance modelling procedure for periodic multicomponent multilayered composites, has constant coefficients.

Subsequently coordinate x_1 be denoted by x, $x \equiv x_1$. For one-dimensional, stationary problem for isotropy, homogeneous components Eq. (12) take the form:

$$\begin{aligned} &\langle k \rangle \frac{\mathrm{d}^2}{\mathrm{d}x^2} \vartheta + \left\langle k \frac{\mathrm{d}}{\mathrm{d}x} \gamma \right\rangle \frac{\mathrm{d}}{\mathrm{d}x} \psi = 0, \\ &\underline{\left\langle k (\gamma)^2 \right\rangle} \frac{\mathrm{d}^2}{\mathrm{d}x^2} \psi - \left\langle k \left(\frac{\mathrm{d}}{\mathrm{d}x} \gamma \right)^2 \right\rangle \psi - \left\langle k \frac{\mathrm{d}}{\mathrm{d}x} \gamma \right\rangle \frac{\mathrm{d}}{\mathrm{d}x} \vartheta = 0. \end{aligned} \tag{13}$$

where $k(\cdot)$ is the thermal conductivity coefficient for isotropic materials.

The underlined component in the Eq. $(13)_2$ depends on the length parameter λ.

If $\lambda \to 0$ then Eq. $(13)_2$ can be written in the form:

$$\psi = -\frac{\left\langle k \frac{\mathrm{d}}{\mathrm{d}x} \gamma \right\rangle}{\left\langle k \left(\frac{\mathrm{d}}{\mathrm{d}x} \gamma \right)^2 \right\rangle} \frac{\mathrm{d}}{\mathrm{d}x} \vartheta. \tag{14}$$

Substituting relation (14) into Eq. $(13)_1$ the equation for unknown temperature field $\vartheta(\cdot)$ takes the form:

$$K_0 \frac{\mathrm{d}^2}{\mathrm{d}x^2} \vartheta = 0 \tag{15}$$

where $K_0 \equiv \left(\frac{\varphi_1}{k_1} + \cdots + \frac{\varphi_P}{k_P} \right)^{-1}$.

Equations (9) and (15) are the base equations for the presented examples.

6 Examples

This section presents the distribution of approximate temperature field $\tilde{\theta}$ for some specific cases ofmulticomponent multilayered periodic composites. All components of the discussed composites are isotropic and homogeneous.

6.1 Periodicity Cell Composed of an Odd Number of Layers

6.1.1 Example 1

Let us assume that composite with a thickness $L = 20\,\text{cm}$ is composed of $P = 20$ layers with constant thicknesses $\lambda = 1\,\text{cm}$. It means that the thickness of the periodicity layer is equal to 1 cm. The periodicity layer consists of seven sublayers made of four different materials. Thicknesses of sublayers "1", "2", "6" and "7" are equal to 0.1 cm, ($l_1 = l_2 = l_6 = l_7 = 0.1\,\text{cm}$) and thicknesses of sublayers "3", "4" and "5" are equal to 0.2 cm ($l_3 = l_4 = l_5 = 0.2\,\text{cm}$).

There will be considered two variants of distribution of components. In the first variant the sublayers made of the same material are distributed symmetrically respect to the midplane of the periodicity layer and in the second one the sublayers made of the same material are not distributed symmetrically respect to this midplane.

The coefficients of thermal conductivity related to the corresponding sublayers in both variants are shown in Table 1.

The graphs of the oscillating micro-shape functions $\gamma(\cdot)$ for considered variants are shown in Fig. 3.

It should be noted that if components are symmetrically distributed respect to the midplane of periodicity layer the graph of the oscillating micro-shape function is antisymmetric with respect to this midplane and that the oscillating micro-shape function is equal 0 on the edges of periodicity layer.

For two considered variants of distribution of components in the periodicity layer, the boundary conditions on the macro-temperature are: $\vartheta(0) = \vartheta_0 = 0\,^\circ\text{C}$, $\vartheta(20) =$

Table 1 Thermal conductivity coefficients (example 1)

Sublayer	1	2	3	4	5	6	7
K (W/mK) in variant 1	160	0.05	0.35	380	0.35	0.05	160
K (W/mK) in variant 2	0.35	0.05	160	380	0.05	0.35	160

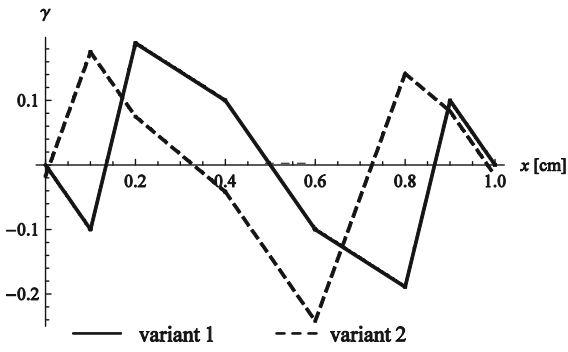

Fig. 3 Graphs of the oscillating micro-shape functions $\gamma(\cdot)$ in periodicity layer (example 1)

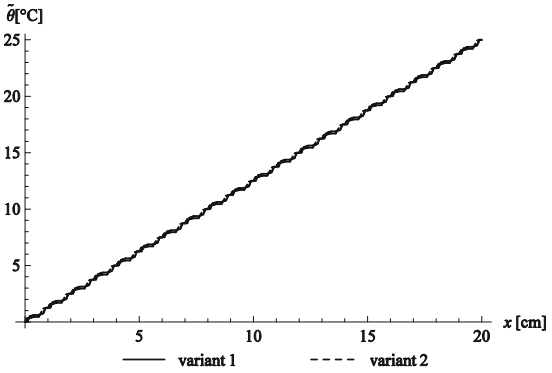

Fig. 4 Distributions of the approximated temperature fields $\tilde{\theta}(\cdot)$ for $x \in (0, 20)$ (example 1)

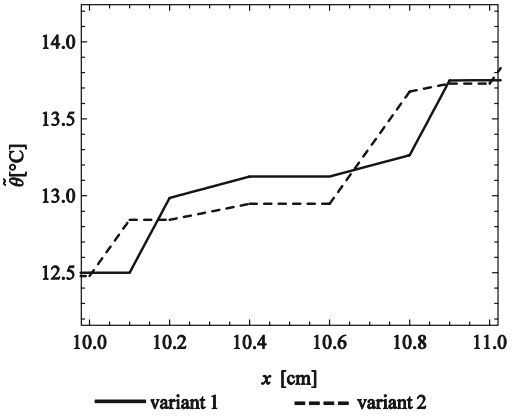

Fig. 5 Distributions of the approximated temperature fields $\tilde{\theta}(\cdot)$ in periodicity layer (example 1)

$\vartheta_L = 25\,^{\circ}\mathrm{C}$. The distribution of the approximated temperature fields $\tilde{\theta}(\cdot)$ for $x \in (0, 20)$ and $x \in (10, 11)$ are shown in Figs. 4 and 5.

6.1.2 Example 2

Let us assume that a composite with a thickness $L = 20\,\mathrm{cm}$ is composed of $P = 20$ layers with constant thicknesses $\lambda = 1\,\mathrm{cm}$ and the periodicity layer consists of seven sublayers made of seven different isotropic materials. Thicknesses of sublayers "1", "2", "6" and "7" are equal to $0.1\,\mathrm{cm}$ ($l_1 = l_2 = l_6 = l_7 = 0.1\,\mathrm{cm}$) and thicknesses of sublayers "3", "4" and "5" are equal to $0.2\,\mathrm{cm}$ ($l_3 = l_4 = l_5 = 0.2\,\mathrm{cm}$). The thermal conductivity coefficients are shown in Table 2.

Table 2 Thermal conductivity coefficients (example 2)

Sublayer	1	2	3	4	5	6	7
K (W/mK) in variant 1	160	0.05	380	0.035	1.7	0.004	0.2

The graph of the oscillating micro-shape function $\gamma(\cdot)$ in periodicity layer for considered composite is shown in Fig. 6. The distribution of the approximated temperature field $\tilde{\theta}(\cdot)$, with boundary conditions on the macro-temperature given as $\vartheta(0) = \vartheta_0 = 0\,^{\circ}\mathrm{C}$, $\vartheta(20) = \vartheta_L = 25\,^{\circ}\mathrm{C}$, for $x \in (0, 20)$ and $x \in (10, 11)$, are shown in Figs. 7 and 8.

6.2 *Periodicity Cell Composed of an Even Number of Layers*

6.2.1 Example 3

Let us assume that a composite with a thickness $L = 20\,\mathrm{cm}$ is composed of $P = 20$ layers with constant thicknesses $\lambda = 1\,\mathrm{cm}$. It means that thickness of periodicity layer is equal $\lambda = 1\,\mathrm{cm}$. The periodicity layer consists of four sublayers made of two different isotropic materials. Thicknesses of sublayers "1" and "4" are equal to $0.3\,\mathrm{cm}$ ($l_1 = l_4 = 0.3\,\mathrm{cm}$) and thicknesses "2" and "3" are equal to $0.2\,\mathrm{cm}$ ($l_2 = l_3 = 0.2\,\mathrm{cm}$).

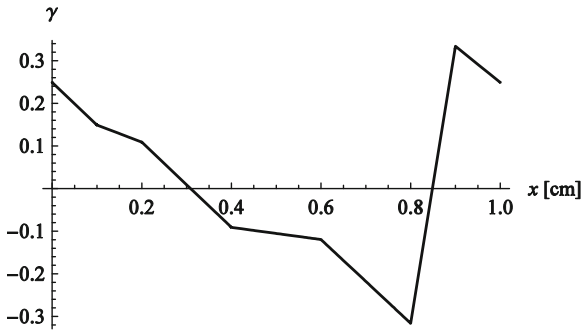

Fig. 6 The graph of the oscillating micro-shape function $\gamma(\cdot)$ in periodicitylayer (example 2)

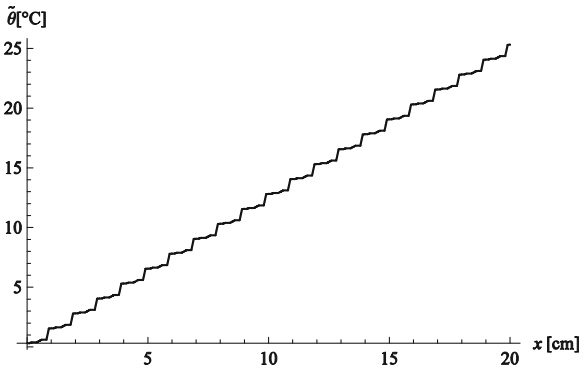

Fig. 7 Distribution of the approximated temperature field $\tilde{\theta}(\cdot)$ for $x \in (0, 20)$ (example 2)

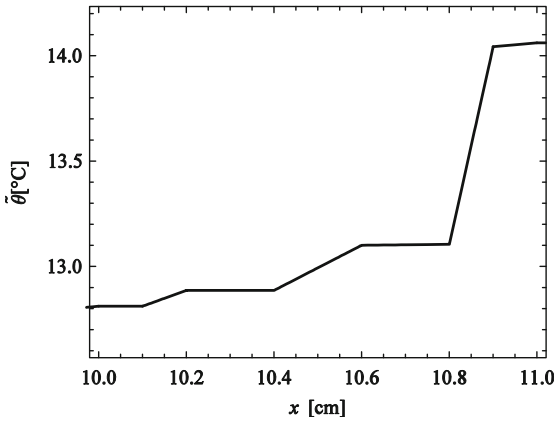

Fig. 8 Distribution of the approximated temperature field $\tilde{\theta}(\cdot)$ in periodicity layer (example 2)

Table 3 Thermal conductivity coefficients (example 3)

Sublayer	1	2	3	4
K (W/mK) in variant 1	100	20	20	100
K (W/mK) in variant 2	20	100	20	100
K (W/mK) in variant 3	100	100	20	20
K (W/mK) in variant 4	100	20	100	20
K (W/mK) in variant 5	20	20	100	100
K (W/mK) in variant 6	20	100	100	20

Six variants of distribution of components will be considered. The coefficients of thermal conductivity related to the corresponding sublayers are shown in Table 3.

In the first and the sixth variant the sublayers made of the same material are symmetrically distributed in the periodicity layer with respect to the midplane. In the second and the forth variant the sublayers made of the same material, are distributed in a such way that the periodicity layer has a periodic structure.

The third and the fifth variant comes down to the case in which the periodicity layer is composed of two sublayers of the same thickness.

Graphs of the oscillating micro-shape functions $\gamma(\cdot)$ for considered variants are shown in Fig. 9.

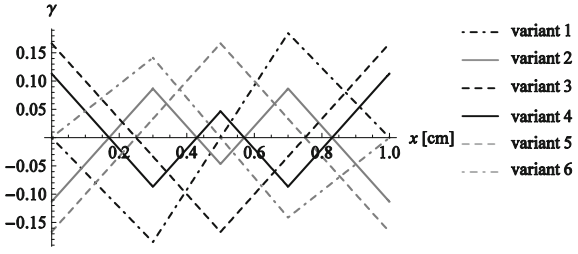

Fig. 9 Graphs of the oscillating micro-shape functions $\gamma(\cdot)$ in periodicity layer(example 3)

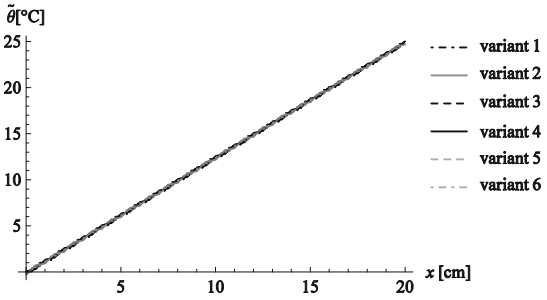

Fig. 10 Distributions of the approximated temperature fields $\tilde{\theta}(\cdot)$ for $x \in (0, 20)$ (example 3)

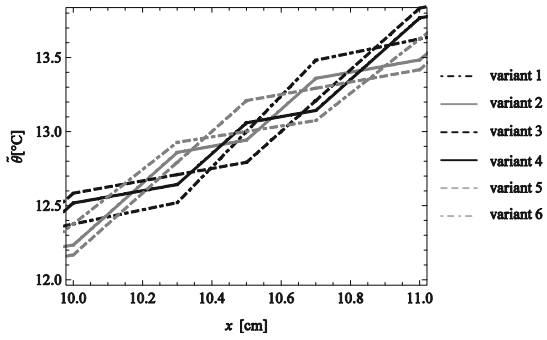

Fig. 11 Distributions of the approximated temperature fields $\tilde{\theta}(\cdot)$ in periodicity layer (example 3)

It should be noted that the oscillating micro-shape function is equal to zero on the edges of periodicity layer only for variants 1 and 6. This is related to the fact that the structure of the periodicity layer is symmetrical with respect to the midplane of the periodic layer. In other variants the oscillating micro-shape functions on the edges of periodicity layer have a value different from zero. In this three variants, for the assumed boundary conditions on the macro-temperature $\vartheta_0 = 0\,^{\circ}\mathrm{C}$, $\vartheta_L = 25\,^{\circ}\mathrm{C}$, the distribution of approximate temperature field $\tilde{\theta}(\cdot)$ for $x \in (0, 20)$ and $x \in (10, 11)$ are shown in Figs. 10 and 11.

6.2.2 Example 4

Let us assume that composite with a thickness $L = 20\,\mathrm{cm}$ is composed of $P = 20$ layers with constant thicknesses $\lambda = 1\,\mathrm{cm}$ and a periodicity layer consists of four sublayers made of four different isotropic materials. Thicknesses of sublayers "1" and "1" are equal to $0.3\,\mathrm{cm}$ ($l_1 = l_4 = 0.3\,\mathrm{cm}$) and thicknesses of sublayers "2" and "3" are equal to $0.2\,\mathrm{cm}$ ($l_2 = l_3 = 0.2\,\mathrm{cm}$). The thermal conductivity coefficients in the sublayers are shown in Table 4.

The graph of the oscillating micro-shape function $\gamma(\cdot)$ in the periodicity layer is shown in Fig. 12.

Table 4 Thermal conductivity coefficients (example 4)

Sublayer	1	2	3	4
K (W/mK) in variant 1	2.8	0.35	1.7	0.05

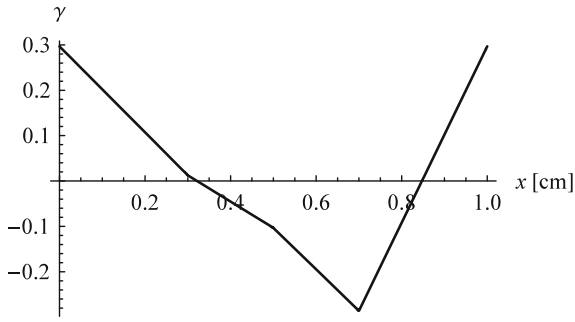

Fig. 12 Graph of the oscillating micro-shape function $\gamma(\cdot)$ in periodicity layer (example 4)

It can be observed that if the periodicity layer consists of four sublayers made of four different materials then the graph of oscillating micro-shape function is not symmetric with respect to midplane of the periodicity layer. The distribution of the approximated temperature field $\tilde{\theta}(\cdot)$, for assumed boundary conditions on the macro-temperature $\vartheta_0 = 0\,^{\circ}\mathrm{C}$, $\vartheta_L = 25\,^{\circ}\mathrm{C}$, for $x \in (0, 20)$ and $x \in (10, 11)$ are shown in Figs. 13 and 14.

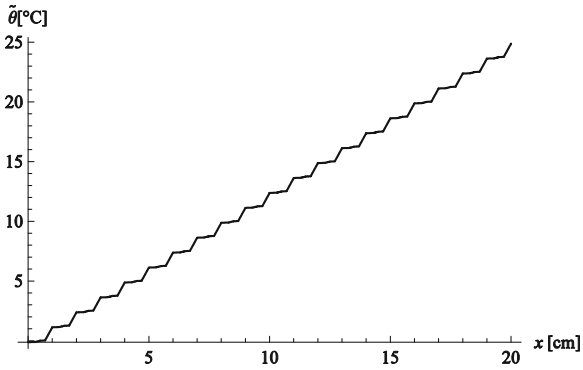

Fig. 13 Distribution of the approximated temperature field $\tilde{\theta}(\cdot)$ for $x \in (0, 20)$ (example 4)

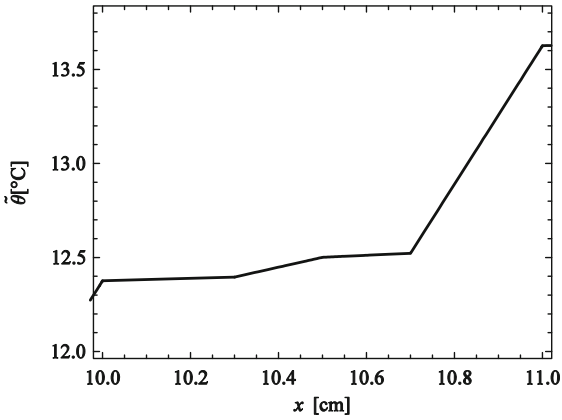

Fig. 14 Distribution of approximated temperature field $\tilde{\theta}(\cdot)$ in periodicity layer (example 4)

7 Conclusions

In the recent papers concerning the tolerance modelling only twocomponent composites were considered. A shape function, occurred there, had the form which was proper only for the structures of such type. It was not possible to limit pass to a onecomponent body within the frames of this model. The term of oscillating microshape function, introduced by [38, 39], enables to describe periodic multilayered composites made of many components, furthermore the definition of this function gives the possibility of the passage from a twocomponent to onecomponent body. It results from the presented example of this function (Fig. 2). If $k_1 = k_2$ then $\gamma = 0$ and the temperature distribution does not show oscillations $-\tilde{\theta}(\cdot) = \vartheta(\cdot)$.

The examples presented in the paper illustrate the form of the oscillating microshape function for various material distributions in periodic multicomponent multilayered composites.

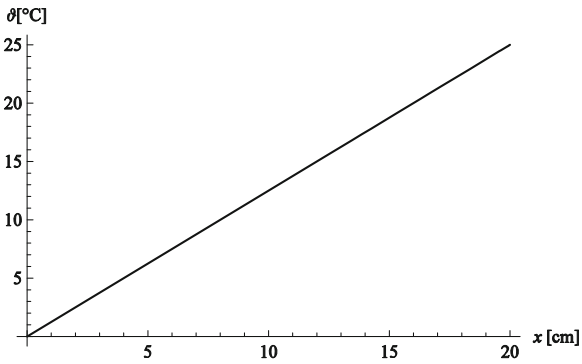

Fig. 15 Distribution of the approximated temperature field $\tilde{\theta}(\cdot) = \vartheta(\cdot)$ for $x \in (0, 20)$

If the same boundary conditions for the temperature are assumed for various multilayered composites having the same size L, then the distribution of the macro-temperature $\vartheta(\cdot)$ is the same linear function (Fig. 15).

The influence of structure of the composites is visible only on the approximated temperature distribution. This is shown in the Figs. 4, 5, 7, 8, 10, 11, 13 and 14. The calculations were performed with the use of MATHEMATICA 8.0 software program.

References

1. Bakhvalov, N.S., Panasenko, G.P.: Homogenization: Averaging Processes in Periodic Media. Nauka, Moscow (1984) (in Russian). English edition: Kluwer, Dordrecht/Boston/Londyn (1989)
2. Bensoussan, A., Lions, J.L., Papanicolaou, G.: Asymptotic Analysis for Periodic Structures. North-Holland Publication Company, Amsterdam (1978)
3. Hornung, D.: Homogenization and porous media. Interdisciplinary Applied Mathematics, 6. Springer (1997)
4. Ignaczak, J., Baczyński, Z.: On a refined heat-conduction theory of micro-periodic layered solids. J. Therm. Stress. **20**, 749–771 (1997)
5. Jędrysiak, J.: Termomechanika laminatów, płyt i powłok o funkcyjnej gradacji własności. Lodz University Press, Łódź (2010)
6. Jędrysiak, J., Radzikowska, A.: On the modelling of heat conduction in a nono-periodically laminated layer. J. Theor. Appl. Mech. **45**(2), 239–257 (2007)
7. Jędrysiak, J., Radzikowska, A.: Some problems of heat conduction for transversally graded laminates with non-uniform distribution of laminas. Arch. Civ. Mech. Eng. **11**(1), 75–87 (2011)
8. Jędrysiak, J., Radzikowska, A.: Tolerance averaging of heat conduction in transversally graded laminates. Meccanica (AIMETA) **47**(1), 95–107 (2012)
9. Jikov, V.V., Kozlov, C.M., Oleinik, O.A.: Homogenization of differential operators and integral functionals. Springer, Berlin (1994)
10. Łaciński, Ł., Woźniak, Cz.: Boundary-layer phenomena in the laminated rigid heat conduction. J. Therm. Stress. **29**, 665–682 (2006)
11. Lewiński, T., Telega, J.: Plates, Laminates and Shells. World Scientific Publishing Company, Singapore (2000)
12. Matysiak, S.J.: On certain problems of heat conduction in periodic composites. J. Appl. Math. Mech. (ZAMM) **71**, 524–528 (1991). doi:10.1002/zamm.19910711218
13. Michalak, B.: Teromechanika ciałz pewną niejednorodną mikrostrukturą. Technika tolerancyjnej aproksymacji, Lodz University Press, Łódź (2011)
14. Michalak, B., Ostrowski, P.: Modelling and analysis of the heat conduction in a certain functionally graded material. In: Pauk, V. (ed.) Mechanics of Solids and Structures, pp. 23–35. Kielce Technical University Press, Kielce (2007)
15. Michalak, B., Woźniak, M.: On the heat conduction in certain functionally graded composites. In: Woźniak, Cz, Świtka, R., Kuczma, M. (eds.) Selected Topics in the Mechanics of Inhomogeneous Media, pp. 229–238. University of Zielona Góra Press (2006)
16. Michalak, B., Woźniak, Cz., Woźniak, M.: Modelling and analysis of certain functionally graded heat conductor. Arch. Appl. Mech. **77**, 823–834 (2007)
17. Nagórko, W., Piwowarski, M.: On the heat conduction in periodically nonhomogeneous solids. In: Woźniak, Cz., Świtka, R., Kuczma, M. (eds.) Selected Topics in the Mechanics of Inhomogeneous Media, pp. 241–254. University of Zielona Góra Press (2006)
18. Nagórko, W., Wągrowska, M.: A contribution to modelling of composite solids. J. Theory Appl. Mech. **40**, 149–158 (2002)

19. Nagórko, W., Zieliński, J.: On heat conduction modelling in plates formed by periodically nonhomogeneous layers. Visnyk Livi Univ. Ser. Mech. Math. **55**, 100–105 (1999)
20. Ostrowski, P.: On the heat transfer in a two-phase hollow cylinder with piecewise continuous boundary conditions. PAMM **9**, 259–260 (2009)
21. Ostrowski, P.: Zagadnienie przewodnictwa ciepła w laminatach z funkcyjną gradacją własności, PhD Thesis, Wydz. BAiIS PŁ (2009)
22. Ostrowski, P., Michalak, B.: Non-stationary heat transfer in a hollow cylinder with functionally graded material properties. J. Theory Appl. Mech. **49**(2), 385–397 (2011)
23. Sanchez-Palencia, E.: Lecture Notes in Physics. Non-Homogeneous Media and Vibration Theory. Springer, Berlin (1980)
24. Suresh, S., Mortensen, A.: Fundamentals of Functionally Graded Materials. The University Press, Cambridge (1998)
25. Szlachetka, O.: Tolerance and asymptotic modelling for functionally graded heat conductors. In: Bzówka, J. (ed.) Badania doświadczalne i teoretyczne w budownictwie, pp. 205–220. Publication House of Silesian University of Technol (2012)
26. Szlachetka, O., Wągrowska, M.: Efekt warstwy brzegowej w warstwowej przegrodzie o poprzecznej gradacji własności. Acta Sci. Polon. Ser. Architectura **9**(4), 15–23 (2010)
27. Szlachetka, O., Wągrowska, M.: Efekt brzegowy w warstwowej przegrodzie o podłużnej gradacji własności. Acta Sci. Polon. Ser. Architectura **10**(3), 27–34 (2011)
28. Szlachetka, O., Wągrowska, M.: Przewodnictwo ciepła w wieloskładnikowych kompozytach warstwowych. In: Paper Presented at the Conference Aktualne Problemy Budownictwa, Warszawa, pp. 65–66 (2014)
29. Szlachetka, O., Wągrowska, M.: Wpływ struktury periodycznych wieloskładnikowych kompozytów warstwowych na rozkład temperatury. In: Paper Presented at the 7th Sympozjon Kompozyty, Konstrukcje Warstwowe, Wrocław, pp. 67–68 (2014)
30. Szlachetka, O., Wągrowska, M.: Przewodnictwo ciepła w wieloskładnikowych kompozytach wielowarstwowych. Materiały Kompozytowe **2**, 27–29 (2015)
31. Szlachetka, O., Wągrowska, M., Woźniak, Cz.: A two-step asymptotic modelling of the heat conduction in a functionally graded stratified layer. Acta Sci. Polon. Ser. Architectura **11**(3), 3–9 (2012)
32. Wągrowska, M.: On the homogenization of elastic-plastic periodic composites by the microlocal parameter approach. Acta Mech. **73**, 45–65 (1988)
33. Wągrowska, M., Witkowska-Dobrev, J.: Wpływ struktury gradientowej na własności sprężyste kompozytów warstwowych. Acta Sci. Polon. Ser. Architectura **9**(4), 5–13 (2010)
34. Wągrowska, M., Woźniak, Cz.: A new 2D-model of the heat conduction in multilayered medium-thickness plates. Acta Sci. Polon. Ser. Architectura **13**(1), 3–44 (2014)
35. Wierzbicki, E., Siedlecka, U.: Isotropic models for a heat transfer in periodic composites. PAMM **4**(1), 502–503 (2004)
36. Woźniak, Cz.: Homogenized thermoelasticity with microlocal parameters. Bull. Polish. Acad. Tech. **35**, 133–141 (1987)
37. Woźniak, Cz.: On the linearized problems of thermoelasticity with microlocal paramiters. Bull. Pol. Ac. Tech. **35**, 143–151 (1987)
38. Woźniak, Cz.: Macroscopic models of the heat conduction in periodically stratified multicomponent composites (1D-models). In: Paper Presented at the 6th Sympozjon Kompozyty. Konstrukcje Warstwowe, Wrocław-Srebrna Góra, pp. 67–68 (2012)
39. Woźniak, Cz.: On elastodynamics of a functionally graded thick layer. In: Paper Presented at the Conference Mechanika Ośrodków Niejednorodnych, Zielona Góra-Łagów, pp. 83–84 (2013)
40. Woźniak, Cz., Wierzbicki, E.: Averaging techniques in thermomechanics of composite solids. Tolerance averaging versus homogenization, Wydaw. PCz, Cząstochowa (2000)
41. Woźniak, Cz., Michalak, B., Jędrysiak, J. (eds.): Thermomechanics of Microheterogeneous Solids and Structures. Tolerance Averaging Approach. Lodz University Press, Łódź (2008)
42. Woźniak, Cz., Wągrowska, M., Szlachetka, O.: Asymptotic modelling and design of some microlayered functionally graded heat conductors. J. Appl. Math. Mech. (ZAMM) **92**(10), 841–848 (2012). doi:10.1002/zamm.201100092

43. Woźniak, Cz., Wągrowska, M., Szlachetka, O.: On the tolerance modeling of heat conduction in functionally graded laminated media. J. Appl. Mech. Tech. Phys. **56**(2), 274–281 (2015)
44. Woźniak, Cz., Wągrowska, M., Nagórko, W. et al. (eds.): Mathematical modelling and analysis in continuum mechanics of microstructured media. Publication House of Silesian University of Technolgy, Gliwice (2010)

Part III
Porous Media

Hysteresis in Unsaturated Porous Media—Two Models for Wave Propagation and Engineering Applications

Bettina Albers and Pavel Krejčí

Abstract Two models for the description of unsaturated porous media flow are revisited. The first is a continuum model suitable for the description of sound wave propagation in elastic media. Even if the model does not contain a hysteresis operator, the effect of hysteresis in the capillary pressure curve is accounted for. The two processes drainage and imbibition are investigated separately and the limit values of material parameters and acoustic properties are determined. The second model is a thermomechanical model capable for the description of flows in elastoplastic porous media. It contains two independent hysteresis operators describing hysteresis phenomena in both the solid and the pore fluids.

1 Introduction

Porous media whose pores are filled by two (or more) immiscible fluids are called unsaturated or partially saturated. The pore fluids possess different partial pressures and the difference is called capillary pressure. Thus, at the interface of the pore-fluids a discontinuity appears which depends on the geometry of the pore space, on the nature of the solids and on the degree of saturation. The latter is the ratio of the volumes occupied by one of the pore fluids and the entire pore space.

Although it is well known that the capillary pressure exhibits two branches depending on the initial state of a sample—and thus hysteresis occurs—(see the left panel of Fig. 1) often only one of them is considered. The connection between capillary

B. Albers (✉)
Department of Soil Mechanics and Geotechnical Engineering, TU Berlin,
Gustav-Meyer-Allee 25, 13355 Berlin, Germany
e-mail: bettina.albers@alumni.tu-berlin.de

P. Krejčí
Institute of Mathematics, Czech Academy of Sciences,
Žitná 25, 11567 Praha 1, Czech Republic
e-mail: krejci@math.cas.cz

B. Albers and M. Kuczma (eds.), *Continuous Media with Microstructure 2*,
DOI 10.1007/978-3-319-28241-1_15

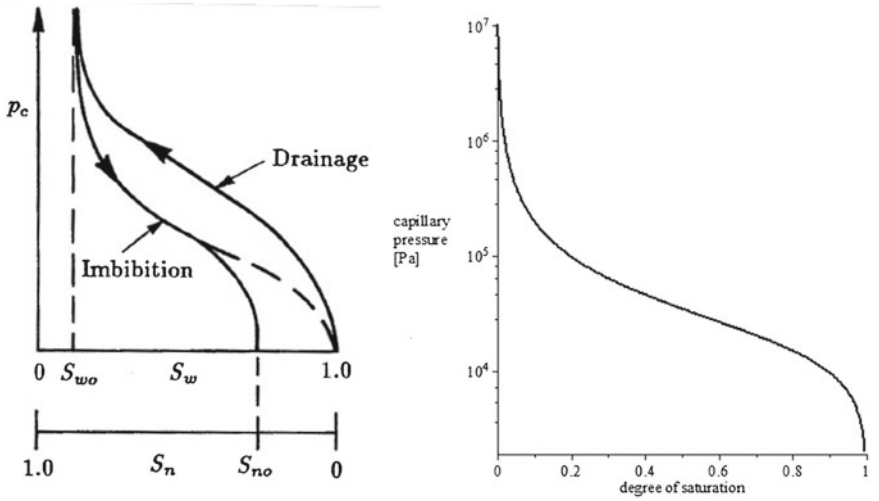

Fig. 1 *Left* Two branches of the capillary pressure curve, from [11]; *right* capillary pressure in dependence on the degree of saturation, calculated by (1)

pressure p_c and degree of saturation S may be described e.g. by the empirical law by van Genuchten [17]

$$p_c = \frac{1}{\alpha_{vG}} \left[S^{(-1/m_{vG})} - 1 \right]^{1/n_{vG}} . \tag{1}$$

This relation contains three parameters m_{vG}, n_{vG} and α_{vG}. The choice of these parameters controls the shape of the curve (m_{vG} and n_{vG}) and its position in the capillary pressure-saturation-diagram (α_{vG}). It is used in the continuum model which was build with the intention to investigate the wave propagation in partially saturated soils [4]. Equation (1) is exemplarily illustrated in the right panel of Fig. 1.

The continuum model is the first model which is revisited in this work. It has been applied to the description of the wave propagation of air-water mixtures in sandstones [7] and other soil types [3, 6]. The aim of further investigations which led to the second model was to find a closed-form description of the propagation of sound waves including the the hysteresis effects of the capillary pressure curve. However, since the continuum model is linear but models containing hysteresis operators are nonlinear, such a model would describe other types of waves. Therefore, instead of a new model, a more engineering approach has been used to incorporate the two branches of the capillary pressure curve, drainage and imbibition, into the model—even if the model does not contain a hysteresis operator. Namely, for the two processes the corresponding values for main drying and main wetting are inserted into the model separately. For two examples of soils, namely for Del Monte sand and for a silt loam both filled by an air-water mixture the procedure is shown in [1].

Another model containing two different hysteresis operators has been proposed in [8]. Both for solid and fluid constituents it includes hysteresis effects, namely the above described hysteresis of the capillary pressure curve and elastoplastic hysteresis. In [8] it is derived from basic thermodynamic principles. In the isothermal case, we have proved the existence of a global strong solution to the resulting system of PDEs with two independent hysteresis operators and a degeneracy under the time derivative. The main argument of the proof is a time discretization scheme and a variant of the Moser iteration technique.

In the following two sections the two above mentioned models are introduced shortly.

2 Continuum Model for Partially Saturated Soils

The linear model for three-component materials with an immiscible mixture of two pore fluids (F and G) in the voids of a solid material (S) has been introduced e.g. in [4]. The fields $\{\mathbf{v}^S, \mathbf{v}^F, \mathbf{v}^G, \mathbf{e}^S, \varepsilon^F, \varepsilon^G\}$, the velocities of the three components, the macroscopic deformation tensor $\mathbf{e}^S$ and the volume changes of fluid and gas, respectively, satisfy the following field equations

$$\begin{aligned}
\rho_0^S \frac{\partial \mathbf{v}^S}{\partial t} &= \operatorname{div}\left\{\lambda^S e\mathbf{1} + 2\mu^S \mathbf{e}^S + Q^F \varepsilon^F \mathbf{1} + Q^G \varepsilon^G \mathbf{1}\right\} \\
&\quad + \pi^{FS}\left(\mathbf{v}^F - \mathbf{v}^S\right) + \pi^{GS}\left(\mathbf{v}^G - \mathbf{v}^S\right), \\
\rho_0^F \frac{\partial \mathbf{v}^F}{\partial t} &= \operatorname{grad}\left\{\rho_0^F \kappa^F \varepsilon^F + Q^F e + Q^{FG}\varepsilon^G\right\} - \pi^{FS}\left(\mathbf{v}^F - \mathbf{v}^S\right), \\
\rho_0^G \frac{\partial \mathbf{v}^G}{\partial t} &= \operatorname{grad}\left\{\rho_0^G \kappa^G \varepsilon^G + Q^G e + Q^{FG}\varepsilon^F\right\} - \pi^{GS}\left(\mathbf{v}^G - \mathbf{v}^S\right), \\
\frac{\partial \mathbf{e}^S}{\partial t} &= \operatorname{sym}\operatorname{grad}\mathbf{v}^S, \quad \frac{\partial \varepsilon^F}{\partial t} = \operatorname{div}\mathbf{v}^F, \quad \frac{\partial \varepsilon^G}{\partial t} = \operatorname{div}\mathbf{v}^G, \quad e \equiv \operatorname{tr}\mathbf{e}^S.
\end{aligned} \tag{2}$$

Instead of the partial mass densities of the components, ρ^S, ρ^F, ρ^G, the equations depend on the volume changes of the components $e, \varepsilon^F, \varepsilon^G$ for which hold

$$e = \frac{\rho_0^S - \rho^S}{\rho_0^S}, \quad \varepsilon^F = \frac{\rho_0^F - \rho^F}{\rho_0^F}, \quad \varepsilon^G = \frac{\rho_0^G - \rho^G}{\rho_0^G}. \tag{3}$$

Quantities with subindex zero are initial values of the corresponding current quantity. Q^F, Q^G and Q^{FG} are coupling parameters between solid-fluid, solid-gas and fluid-gas, respectively. λ^S and μ^S are Lamé parameters. The compressibilities of fluid and gas are denoted by κ^F and κ^G.

In principle, the porosity also is a field and satisfies an own balance equation (see e.g. [18]). However, if we neglect memory effects, the balance equation can be solved and its consideration is no longer necessary to solve the problem.

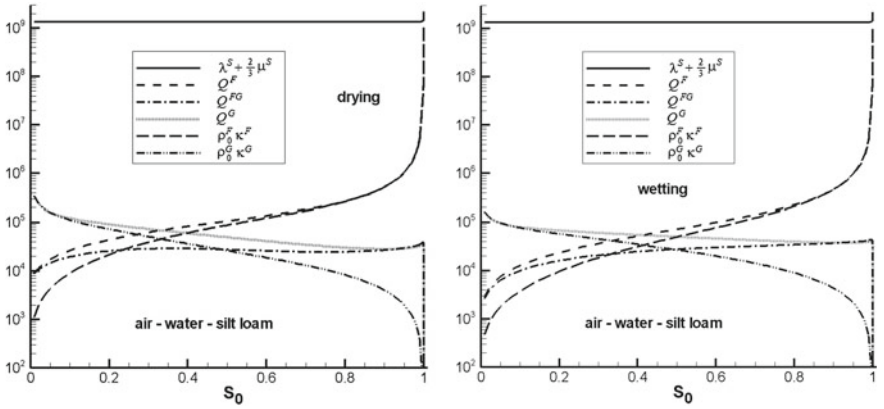

Fig. 2 Macroscopic material parameters appearing in (2) in dependence on the initial saturation for silt loam; for the parameters on the *left hand side* the MDC (main drying curve) data, for those on the *right hand side* the MWC (main wetting curve) data have been used, respectively

The current saturation of the fluid S is not included in the series of fields. Instead, a constitutive law of van Genuchten type is used for this quantity. With this equation, actually only one branch of the capillary pressure curve is described. In order to incorporate the hysteresis into the model, the macroscopic material parameters $\left\{\lambda^S + \frac{2}{3}\mu^S, \kappa^F, \kappa^G, Q^F, Q^G, Q^{FG}\right\}$ appearing in the Cauchy stress tensors in (2) have to be specified for the drying branch and the wetting branch separately. This is done by applying a transition from the micro- to the macro-scale (see e.g. [5]). Consequently, the micro-macro-transition-procedure for the material parameters is applied twice, once to find the macroscopic wetting parameters from the measured microscopic ones for wetting and the same for the drying branch. In Fig. 2 exemplarily for silt loam the two sets of material parameters for drying and wetting are illustrated. For details see [1].

Instead of permeabilities resistances of fluid and gas, π^{FS} and π^{GS}, appear in the model which reflect the resistance of the flow through the channels of the skeleton. These parameters are given by

$$\pi^{FS} = \frac{\pi^F}{k_f}, \qquad \pi^{GS} = \frac{\pi^G}{k_g}. \tag{4}$$

The quantities π^F and π^G account not only for the permeability of the solid but also for the viscosity of the pore fluid. Furthermore, k_f and k_g are relative permeabilities which depend on the degree of saturation. Van Genuchten [17] not only proposed the theoretical relationship between the capillary pressure and the saturation (1) but also formulae for the relative permeabilities

$$k_f = S^{\frac{1}{2}}\left[1 - \left(1 - S^{\frac{1}{m_{vG}}}\right)^{m_{vG}}\right]^2, \qquad k_g = (1-S)^{\frac{1}{3}}\left(1 - S^{\frac{1}{m_{vG}}}\right)^{2m_{vG}}. \tag{5}$$

3 Model with Two Types of Hysteresis

Consider a domain $\Omega \subset \mathbb{R}^3$ filled with a deformable solid matrix material with pores containing a mixture of liquid and gas. We state the balance laws in referential (Lagrangian) coordinates, assume the deformations small, and denote for $x \in \Omega$ and time $t \in [0, T]$

$u(x,t)$	displacement vector of the referential particle x at time t;
$\varepsilon(x,t) = \nabla_s u(x,t)$	linear strain tensor, $(\nabla_s u)_{ij} := \frac{1}{2}\left(\frac{\partial u_i}{\partial x_j} + \frac{\partial u_j}{\partial x_i}\right)$;
$\sigma(x,t)$	stress tensor;
$p(x,t)$	capillary pressure;
$\theta(x,t)$	absolute temperature;
$W(x,t)$	relative liquid content;
$A(x,t)$	relative gas content.

To explain the meaning of W and A, consider an arbitrary control volume $V_0 \subset \Omega$ in the reference state, set

$$V(t) = \{y \in \mathbb{R}^3 : y = x + u(x,t)\,,\ x \in V_0\}\,,$$

and denote by $V_A(t)$, $V_W(t)$, $V_S(t)$ the subdomains of $V(t)$ occupied at time t by gas, liquid, and solid, respectively. Then $V_A(t) \cup V_W(t) \cup V_S(t) = V(t)$, and denoting by $|V|$ the Lebesgue measure of a set V, we assume that the porosity

$$\nu := \frac{|V_A(t) \cup V_W(t)|}{|V(t)|} \in (0,1) \tag{6}$$

remains constant and independent of the choice of V_0 and t. Let $J(x,t)$ be the Jacobian of the transformation $x \mapsto x + u(x,t)$. Under the small deformation hypothesis, we may consider $J(x,t) \approx 1 + \operatorname{div} u(x,t)$, hence $\operatorname{div} u$ represents the relative volume increment. Indeed, we have

$$|V(t)| = \int_{V(t)} \mathrm{d}y = \int_{V_0} J(x,t)\,\mathrm{d}x\,,$$

so that

$$\lim_{|V_0|\to 0,\, x\in V_0} \frac{|V(t)|}{|V_0|} \approx 1 + u(x,t)\,. \tag{7}$$

We now define

$$W(x,t) = \lim_{|V_0|\to 0,\, x\in V_0} \frac{|V_W(t)|}{|V_A(0) \cup V_W(0)|}\,,\ A(x,t) = \lim_{|V_0|\to 0,\, x\in V_0} \frac{|V_A(t)|}{|V_A(0) \cup V_W(0)|}\,.$$

Note that by (6), we have

$$\frac{|V_A(t) \cup V_W(t)|}{|V_A(0) \cup V_W(0)|} = \frac{|V(t)|}{|V(0)|},$$

so that by virtue of (7) under the hypothesis of small deformations, we have

$$W + A = \frac{1 + \operatorname{div} u}{1 + \operatorname{div} u(\cdot, 0)} \approx 1 + \operatorname{div} u - \operatorname{div} u(\cdot, 0). \tag{8}$$

3.1 Constitutive Equations

For the stress σ and gas content A we assume the empirical constitutive relations

$$\sigma = \mathbf{B}\varepsilon_t + P[\varepsilon] + (p - \beta(\theta - \theta_c))\mathbf{1}, \tag{9}$$

$$A = G[p], \tag{10}$$

where P is a hysteresis operator describing the elastoplastic response of the solid, see Sect. 3.4.1, $\mathbf{B}$ is a constant symmetric positive definite fourth order viscosity tensor, $\beta \in \mathbb{R}$ is the relative solid-liquid thermal expansion coefficient, $\theta_c > 0$ is a fixed referential temperature, $\mathbf{1}$ is the Kronecker tensor, and G is of the form as on Fig. 3. We assume that it can be decomposed into the sum $G[p] = G_0[p] + f(p)$, where f is a bounded monotone function, and G_0 is a Preisach hysteresis operator, see Sect. 3.4.2. The use of the Preisach operator for pressure-saturation hysteresis modeling is justified in [12].

3.2 Mass Balance

Consider an arbitrary control volume $V \subset \Omega$. The liquid content in V is given by the integral $\int_V \rho_L W \, dx$, where ρ_L is the liquid mass density. The mass conservation

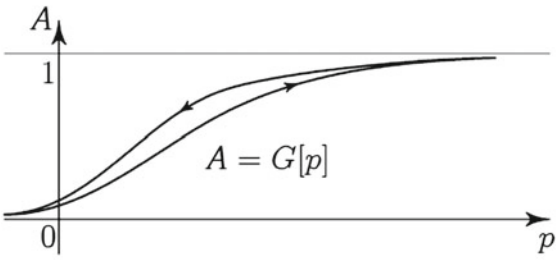

Fig. 3 Pressure-saturation hysteresis diagram

principle then reads

$$\frac{\mathrm{d}}{\mathrm{d}t}\int_V \rho_L W\,\mathrm{d}x + \int_{\partial V} \xi\cdot n\,\mathrm{d}s(x) = 0\,, \tag{11}$$

where ξ is the liquid mass flux vector and n the outward normal vector to ∂V. We assume that there exists a proportionality factor $\mu(p) > 0$ (the permeability coefficient) such that

$$\xi = \mu(p)\nabla p\,. \tag{12}$$

The assumption that the permeability depends only on p is a considerable simplification. However, if μ is allowed to depend also on the liquid content, the problem becomes difficult even if mechanical interaction between solid and fluid is completely neglected. Existence results have been obtained in this case only if additional time or space regularizing operators are involved, see [9, 10].

Using Eqs. (8), (10), and (12), and the Gauss formula, we rewrite (11) as

$$\int_V \left((G[p] - \operatorname{div} u)_t - \frac{1}{\rho_L}\operatorname{div}(\mu(p)\nabla p)\right)\mathrm{d}x = 0 \tag{13}$$

for every control volume $V \subset \Omega$. Hence, in differential form, we have in Ω

$$G[p]_t - \operatorname{div} u_t - \frac{1}{\rho_L}\operatorname{div}(\mu(p)\nabla p) = 0\,. \tag{14}$$

3.3 Momentum, Energy, and Entropy Balance

The momentum balance in the solid phase reads

$$\rho_S u_{tt} = \operatorname{div}\sigma + g\,, \tag{15}$$

where ρ_S is the solid mass density, and $g = g(x,t)$ is a given volume force density (e. g., gravity). Taking (9) into account, we obtain from (15) the equation

$$\rho_S u_{tt} = \operatorname{div}\mathbf{B}\varepsilon_t + \operatorname{div} P[\varepsilon] + \nabla p - \beta\nabla\theta + g\,,\quad \varepsilon = \nabla_s u\,. \tag{16}$$

The operators P and G admit hysteresis potentials V_P (clockwise) and V_G (counterclockwise) and dissipation operators D_P, D_G such that the inequalities

$$P[\varepsilon] : \varepsilon_t - V_P[\varepsilon]_t = \|D_P[\varepsilon]_t\|_*\,,\quad G[p]_t p - V_G[p]_t = |D_G[p]_t| \tag{17}$$

hold a. e. for all absolutely continuous inputs, where $\|\cdot\|_*$ is a seminorm in $\mathbb{R}^{3\times 3}_{\mathrm{sym}}$.

We have to derive formulas for the densities of internal energy U and entropy S such that the energy balance equation and the Clausius-Duhem inequality hold for all processes. Let q be the heat flux vector, and let $V \subset \Omega$ be again an arbitrary control volume. The total internal energy in V is $\int_V U \, \mathrm{d}x$, and the total mechanical power $Q(V)$ supplied to V equals

$$Q(V) = \int_V \sigma : \varepsilon_t \, \mathrm{d}x + \int_{\partial V} \frac{1}{\rho_L} p \, \xi \cdot n \, \mathrm{d}s(x) \,,$$

where ξ is the liquid mass flux (12). We thus have

$$\frac{\mathrm{d}}{\mathrm{d}t} \int_V U \, \mathrm{d}x + \int_{\partial V} q \cdot n \, \mathrm{d}s(x) = \int_V \sigma : \varepsilon_t \, \mathrm{d}x + \int_{\partial V} \frac{1}{\rho_L} p\mu(p) \nabla p \cdot n \, \mathrm{d}s(x) \,. \quad (18)$$

By the Gauss formula, we obtain the energy balance equation in differential form

$$U_t + \operatorname{div} q = \sigma : \varepsilon_t + \frac{1}{\rho_L} \operatorname{div} (p\mu(p) \nabla p) \,. \quad (19)$$

The internal energy and entropy densities U and S as well as the heat flux vector q have to be chosen in order to satisfy for all processes the Clausius-Duhem inequality

$$S_t + \operatorname{div} \left(\frac{q}{\theta} \right) \geq 0 \quad (20)$$

or, taking into account the energy balance (19),

$$U_t - \theta S_t + \frac{q \cdot \nabla \theta}{\theta} \leq \sigma : \varepsilon_t + \frac{1}{\rho_L} \operatorname{div} (p\mu(p) \nabla p) \,. \quad (21)$$

As a consequence of (21), two inequalities have to hold separately for all processes, namely

$$q \cdot \nabla \theta \leq 0 \,, \quad U_t - \theta S_t \leq \sigma : \varepsilon_t + \frac{1}{\rho_L} \operatorname{div} (p\mu(p) \nabla p) \,. \quad (22)$$

For the heat flux, we assume Fourier's law

$$q = -\kappa \nabla \theta \quad (23)$$

with constant heat conductivity $\kappa > 0$. We further introduce the free energy F by the formula $F = U - \theta S$, so that in terms of F, the second inequality in (22) has the form

$$F_t + \theta_t S \leq \sigma : \varepsilon_t + \frac{1}{\rho_L} \operatorname{div} (p\mu(p) \nabla p) \,. \quad (24)$$

We claim that the right choice of F for (24) to hold is

$$F = V_P[\varepsilon] + V_G[p] - \beta(\theta - \theta_c)\,\mathrm{div}\,u + F_0(\theta)\,, \quad S = -\frac{\partial F}{\partial \theta} = \beta\,\mathrm{div}\,u - F_0'(\theta)\,, \tag{25}$$

where $F_0(\theta)$ is a purely caloric component of F. It remains to check that (24) holds for all processes. This is indeed true, since by (14) and (17) we have

$$\begin{aligned} F_t + \theta_t S - \sigma : \varepsilon_t - \frac{1}{\rho_L}\,\mathrm{div}\,(p\mu(p)\nabla p) \\ = -\|D_P[\varepsilon]_t\|_* - |D_G[p]_t| - \mathbf{B}\varepsilon_t : \varepsilon_t - \frac{1}{\rho_L}\mu(p)|\nabla p|^2 \le 0\,. \end{aligned} \tag{26}$$

We have

$$U = F + \theta S = V_P[\varepsilon] + V_G[p] + \beta\theta_c\,\mathrm{div}\,u + F_0(\theta) - \theta F_0'(\theta)\,. \tag{27}$$

The derivative of the purely caloric component $F_0(\theta) - \theta F_0'(\theta)$ is the specific heat capacity $c(\theta) = -\theta F''(\theta)$. Assuming that $c(\theta) = c_0$ is a positive constant, we obtain $F_0(\theta) = -c_0\theta\log(\theta/\theta_c)$ up to a linear function, and

$$U = V_P[\varepsilon] + V_G[p] + \beta\theta_c\,\mathrm{div}\,u + c_0\theta\,. \tag{28}$$

With q given by (23), we can write the energy balance equation (19), using again (14) and (17), in the form

$$c_0\theta_t - \kappa\,\Delta\theta = \|D_P[\varepsilon]_t\|_* + |D_G[p]_t| + \mathbf{B}\varepsilon_t : \varepsilon_t + \frac{1}{\rho_L}\mu(p)|\nabla p|^2 - \beta\theta\,\mathrm{div}\,u_t\,. \tag{29}$$

To summarize, in terms of the unknown functions u, p, θ, our model system of equations has the form

$$\rho_S u_{tt} = \mathrm{div}\,(\mathbf{B}\nabla_s u_t + P[\nabla_s u]) + \nabla p - \beta\nabla\theta + g\,, \tag{30}$$

$$G[p]_t = \mathrm{div}\,u_t + \frac{1}{\rho_L}\,\mathrm{div}\,(\mu(p)\nabla p)\,, \tag{31}$$

$$\begin{aligned} c_0\theta_t = \kappa\,\Delta\theta + \|D_P[\nabla_s u]_t\|_* + |D_G[p]_t| + \mathbf{B}\nabla_s u_t : \nabla_s u_t \\ + \frac{1}{\rho_L}\mu(p)|\nabla p|^2 - \beta\theta\,\mathrm{div}\,u_t\,, \end{aligned} \tag{32}$$

which is to be complemented with boundary and initial conditions.

3.4 Hysteresis Operators

We now recall the basic concepts of hysteresis modeling that are used here.

3.4.1 The Operator *P*

In (9), P stands for the elastoplastic part σ^{ep} of the stress tensor σ. We proceed as in [15] and assume that σ^{ep} can be represented as the sum $\sigma^{ep} = \sigma^e + \sigma^p$ of an elastic component σ^e and plastic component σ^p. While σ^e obeys the classical linear elasticity law

$$\sigma^e = \mathbf{A}^e \varepsilon \tag{33}$$

with a constant symmetric positive definite fourth order elasticity tensor $\mathbf{A}^e$, for the description of the behavior of σ^p, we split also the strain tensor ε into the sum $\varepsilon = \varepsilon^e + \varepsilon^p$ of the elastic strain ε^e and plastic strain ε^p, and assume

$$\sigma^p = \mathbf{A}^p \varepsilon^e \tag{34}$$

again with a constant symmetric positive definite fourth order elasticity tensor $\mathbf{A}^p$, and for a given time evolution $\varepsilon(t)$ of the strain tensor, $t \in [0, T]$, we require σ^p to satisfy the constraint

$$\sigma^p(t) \in Z \quad \forall t \in [0, T]\,, \tag{35}$$

where $Z \subset \mathbb{R}^{3\times 3}_{\rm sym}$ is a convex closed domain containing 0 in its interior representing the domain of admissible stresses. Its boundary ∂Z is the *yield surface*. The time evolution of ε^p is governed by the *flow rule*

$$\varepsilon^p_t : (\sigma^p - \tilde\sigma) \geq 0 \quad \forall \tilde\sigma \in Z\,. \tag{36}$$

We can eliminate the internal variables ε^e, ε^p and write (36) in the form

$$(\varepsilon_t - (\mathbf{A}^p)^{-1}\sigma^p_t) : (\sigma^p - \tilde\sigma) \geq 0 \quad \forall \tilde\sigma \in Z\,. \tag{37}$$

We now define a new scalar product $\langle \cdot, \cdot \rangle_{\mathbf{A}^p}$ in $\mathbb{R}^{3\times 3}_{\rm sym}$ by the formula $\langle \xi, \eta \rangle_{\mathbf{A}^p} = (\mathbf{A}^p)^{-1}\xi : \eta$, and rewrite (37) as

$$\left\langle \mathbf{A}^p \varepsilon_t - \sigma^p_t, \sigma^p - \tilde\sigma \right\rangle_{\mathbf{A}^p} \geq 0 \quad \forall \tilde\sigma \in Z\,. \tag{38}$$

We prescribe a canonical initial condition for σ^p, namely

$$\sigma^p(0) = \mathrm{Proj}_Z(\mathbf{A}^p \varepsilon(0)) \,, \tag{39}$$

where Proj_Z is the orthogonal projection $\mathbb{R}^{3\times3}_{\mathrm{sym}} \to Z$ with respect to the scalar product $\langle \cdot, \cdot \rangle_{\mathbf{A}^p}$ and is characterized by the variational inequality

$$x = \mathrm{Proj}_Z(u) \iff x \in Z \,,\ \langle u - x, x - y \rangle_{\mathbf{A}^p} \geq 0 \quad \forall y \in Z \,. \tag{40}$$

It is shown in [14] that for each given $\varepsilon \in W^{1,1}(0, T; \mathbb{R}^{3\times3}_{\mathrm{sym}})$ there exists a unique solution $\sigma^p \in W^{1,1}(0, T; \mathbb{R}^{3\times3}_{\mathrm{sym}})$ to (38) and (39), so that we may define the solution operator $P_0 : \varepsilon \mapsto \sigma^p = P_0[\varepsilon]$. Combining this relation with (33) we obtain

$$P[\varepsilon] = \mathbf{A}^e \varepsilon + P_0[\varepsilon]. \tag{41}$$

3.4.2 The Preisach Operator G_0

Preisach introduced his model in [16] as a weighted superposition of non-ideal relays, see also [13]. We use here an equivalent definition of the Preisach operator G_0 as in [14], which is also based on a variational inequality of the type (38) and (39). More precisely, for a given input function $p \in W^{1,1}(0, T)$ and a memory parameter $r > 0$, we define the function $\xi_r(t)$ as the solution of the variational inequality

$$\begin{cases} |p(t) - \xi_r(t)| \leq r & \forall t \in [0, T] \,, \\ (\xi_r)_t(t)(p(t) - \xi_r(t) - z) \geq 0 \ \text{ a. e.} & \forall z \in [-r, r] \,, \\ \xi_r(0) = \max\{p(0) - r, \min\{0, p(0) + r\}\} \,. \end{cases} \tag{42}$$

This is indeed, for a fixed value of r, a scalar version of (38) and (39) with Z replaced by the interval $[-r, r]$, ε replaced by p, and σ^p replaced by $p - \xi_r$. Here, we consider the whole continuous family of variational inequalities (42) parameterized by $r > 0$.

The mapping $\mathfrak{p}_r : W^{1,1}(0, T) \to W^{1,1}(0, T)$ which with $p \in W^{1,1}(0, T)$ associates the solution $\xi_r = \mathfrak{p}_r[p] \in W^{1,1}(0, T)$ of (42) is called the *play*, see [13].

Given a nonnegative function $\rho \in L^1((0, \infty) \times \mathbb{R})$ (the *Preisach density*), we define the Preisach operator $G_0 : W^{1,1}(0, T) \to W^{1,1}(0, T)$ by the integral

$$G_0[p](t) = \int_0^\infty \int_0^{\mathfrak{p}_r[p](t)} \rho(r, v) \, \mathrm{d}v \, \mathrm{d}r \,. \tag{43}$$

The construction of the energy potentials V_P, V_G and of the dissipation operators D_P, D_G associated with the operators P, G and satisfying the energy balance equations (17) is discussed in detail in [8].

4 Final Remarks

Two models for the description of unsaturated porous media flow are shown. While the first one was introduced to describe and analyze the propagation of sound waves in poroelastic media, the second one is capable to describe flow processes in deformable elastoplastic media. One practical application of the theoretical analysis of the first model may be the construction of non-destructive testing methods for soils. In [2] three different applications of the theory are described: soil characterization, surface wave analysis and soils with anisotropic permeability. One application of the second model may be a wall which is covered by plaster for protection against humidity, temperature changes, etc. If water droplets penetrate into an outer layer of the plaster by the capillary effect, the pressure difference between the wet and the dry layer produces a deformation and eventually a detachment of the plaster from the wall. Further applications in other branches of Civil Engineering are imaginable, e.g. such in which also phase transitions occur (e.g. freezing and thawing processes). In a forthcoming paper such a problem will be discussed.

Acknowledgments Supported by the Einstein Junior Fellowship of the Einstein Foundation Berlin (BA) and by the GAČR Grant GA15-12227S and RVO: 67985840 (PK).

References

1. Albers, B.: On the influence of the hysteretic behavior of the capillary pressure on the wave propagation in partially saturated soils, accepted for publication. In: Journal of Physics: Conference Series, Proceedings of the 7th International Workshop on Multi-Rate Processes and Hysteresis (2015)
2. Albers, B.: Theoretical basis for non-destructive testing of multi-component media by means of sound wave analysis. Submitted to *Water Science and Engineering* (2015)
3. Albers, B.: Linear elastic wave propagation in unsaturated sands, silts, loams and clays. Transp. Porous Media **86**, 567–587 (2011)
4. Albers, B.: Modeling and Numerical Analysis of Wave Propagation in Saturated and Partially Saturated Porous Media. Habilitation thesis, Veröffentlichungen des Grundbauinstituts der Technischen Universität Berlin, vol. 48. Shaker-Verlag (2010)
5. Albers, B.: On a micro-macro transition for a poroelastic three-component model. Z. Angew. Math. Mech. **90**(12), 929–943 (2010)
6. Albers, B.: Micro-macro transition and linear wave propagation in three-component compacted granular materials. In: Goddard, J.D., Jenkins, J.T., Giovine, P. (eds.) AIP Conference Proceedings of the Joint IUTAM-ISIMM Symposium on Mathematical Modeling and Physical Instances of Granular Flows, vol. 1227, pp. 391–404, Melville, New York (2010)
7. Albers, B.: On the influence of saturation and frequency on monochromatic plane waves in unsaturated soils. In: Schanz, I. (eds.) Coupled site and soil-structure interaction effects with application to seismic risk mitigation. NATO Science Series, pp. 65–76. Springer, Netherlands (2009)
8. Albers, B., Krejčí, P.: Unsaturated porous media flow with thermomechanical interaction. Accepted for publication in *Mathematical Methods in the Applied Sciences* (2015)
9. Bagagiolo, F., Visintin, A.: Hysteresis in filtration through porous media. Z. Anal. Anwendungen **19**(4), 977–997 (2000)

10. Bagagiolo, F., Visintin, A.: Porous media filtration with hysteresis. Adv. Math. Sci. Appl. **14**(2), 379–403 (2004)
11. Bear, J., Bachmat, Y.: Introduction to Modeling of Transport Phenomena in Porous Media. Kluwer, Dordrecht (1991)
12. Flynn, D., McNamara, H., O'Kane, J.P., Pokrovskiĭ, A.V.: The Science of Hysteresis. In: Bertotti, G., Mayergoyz, I. (eds.) Application of the Preisach model to soil-moisture hysteresis, pp. 689–744. Academic Press, Oxford (2006)
13. Krasnosel'skiĭ M.A., Pokrovskiĭ A.V.: Systems with Hysteresis. Springer, Berlin (1989). Russian edition: Nauka, Moscow (1983)
14. Krejčí P.: Hysteresis, Convexity and Dissipation in Hyperbolic Equations. Gakuto Intern. Ser. Math. Sci. Appl. vol. **8**, Gakkotōsho, Tokyo (1996)
15. Lemaitre, J., Chaboche, J.-L.: Mechanics of Solid Materials. Cambridge University Press, Cambridge (1990)
16. Preisach, F.: Über die magnetische Nachwirkung. Z. Phys. **94**, 277–302 (1935) (in German)
17. Van Genuchten, M.T.: A closed-form equation for predicting the hydraulic conductivity of unsaturated soils. Soil Sci. Soc. Am. J. **44**, 892–898 (1980)
18. Wilmański K.: Macroscopic Modeling of Porous Materials. In: Awrejcewicz, J. et al (eds.) Mathematical Modelling and Analysis in Continuum Mechanics of Microstructured Media: Professor Margaret Woźniak pro memoria: sapiens mortem non timet, pp. 167–195. Wydawnictwo Politechniki Śląskiej, Gliwice (2010)

Simulation of the Influence of Grain Damage on the Evolution of Shear Strain Localization

Erich Bauer

Abstract The influence of grain damage on shear strain localization in a lateral infinite granular layer under monotonic plane shearing is simulated using a micro-polar continuum description. The change of the grading of the grain sizes caused by grain damage is taken into account in a simplified manner by a reduction of the mean grain diameter, which is embedded in the constitutive model as an internal length. It is assumed that a reduction of the mean grain diameter caused by grain breakage and grain abrasion is related to an increase in the pressure, the micro-rotation and the micro-curvature. A reduction of the grain sizes is accompanied by a reduction of the limit void ratios and a reduction of the material against compaction. In the constitutive model the decrease of the mean grain diameter is linked to the so-called solid hardness, which is defined within a continuum description. The proposed concept of reduction of the mean grain diameter and the solid hardness is embedded in a micro-polar hypoplastic model. The results of the numerical simulations show that the reduction of the mean grain diameter has a significant effect on the evolution of the void ratio within the zone of shear strain localization.

1 Introduction

The focus of the present paper is on constitutive modeling of the influence of grain damage on the mechanical response of cohesionless granular materials like sand, gravel or broken rock. The results of experimental investigations reveal that the amount of grain damage in form of grain abrasion and grain fragmentation strongly depends on the grain strength, the morphology of the granular material and the loading path [36, 37]. Grain damage causes a change of the grading of the grain sizes, the grain shape, the limit void ratios and the critical void ratio [3, 29, 38]. It can also be accompanied by a change of the course of force chains and a reorientation of the grain skeleton into a denser state. Grain damage becomes dominant within the localized zone while outside of the shear band the material remains almost undamaged

E. Bauer (✉)
Institute of Applied Mechanics, Graz University of Technology, 8010 Graz, Austria
e-mail: erich.bauer@tugraz.at

B. Albers and M. Kuczma (eds.), *Continuous Media with Microstructure 2*,
DOI 10.1007/978-3-319-28241-1_16

under continuous shearing [2]. Moreover grain damage in shear zones can already be detected under low pressures. Thus the occurrence of grain crushing is not only a question of the stress level, but it is also influenced by different factors related to the grading of the grain sizes, the angularity of the grains and the loading history. The amount of grain damage under shearing can be rather different to the one under predominant isotropic loading.

Only little experimental data is available in the literature, so that numerical simulations are a possibility to gain deeper insight into the mechanisms of grain damage under shearing [15, 39]. In this context the question arises as to what state quantities are appropriate for constitutive modeling of the influence of grain damage on the incremental stiffness. As the shear stress inside and outside the localized zone is the same, the pronounced grain damage observed within the localized zone cannot only be explained by an interaction between the shear stress and the evolution of grain damage. On the other hand experiments reveal progressive grain damage under constant shear stress, a non-linear displacement field and particle rotations within the localized zone e.g. [19, 35]. Such properties of granular materials, however, cannot be modeled appropriately using a classical continuum. The influence of the grain size, particle rotation and a non-linear displacement field within shear zones can be taken into account for instance with a micro-polar continuum description. Furthermore, micro-polar constitutive equations are endowed with an internal length, so that the problem described is regularized and the thickness of zones of shear localization predicted by finite element calculations is independent of the size of the finite elements provided that the elements are small enough. For shear strain localization in granular bodies without grain damage the performance of micro-polar constitutive models was demonstrated by several authors, e.g. [16, 17, 23, 26, 27, 32, 40, 41, 44]. The hypoplastic modelling of the influence of grain crushing on the change of the mean grain size was first discussed by Tejchman [42] and Tejchman et al. [43] using formulae from breakage mechanics described by Nguyen and Einav [33] . In a recent paper by Bauer et al. [14] a new concept has been presented, which is embedded in a micro-polar hypoplastic description. The micro-polar hypoplasticity of the Karlsruhe type is an extension of the constitutive concept originally developed within the framework of a classical, non-polar continuum [28]. It differs fundamentally from the concept of elasto-plasticity, as no decomposition of the rate of deformation into reversible and irreversible parts is needed. Inelastic material properties are modeled in hypoplasticity with inherently nonlinear evolution equations. Various extensions and applications of the basic concept are proposed, e.g. [4–7, 10, 12, 13, 20, 22, 24, 30, 34, 45–47]. For modeling the influence of grain damage the micro-polar hypoplastic concept by Bauer et al. [14] is based on evolution equations proposed for the void ratio, the mean grain diameter, the solid hardness, the stress tensor and the couple stress tensor. As a measure of the packing density of the grains the void ratio is used, which is defined as the ratio of the volume of the voids to the volume of the solid grains. In soil mechanics it is common to represent the gradation of the grain sizes in the so-called grain size distribution curve. A characteristic quantity of the grain size distribution is the mean grain diameter, d_{50}, which is embedded in the proposed micro-polar hypoplastic continuum model as the internal length. A

change of the grain size distribution caused by grain damage is also reflected by a reduction of d_{50}. In this paper grain damage is assumed to depend mainly on the pressure level, particle rotation and curvature. In the constitutive model the effect of change of the grain size distribution is included by a reduction of d_{50}. It can be noted that with a reduction of d_{50} the thickness of the localized zone reduces and the effect of the micro-polar quantities on the mechanical behavior dims, i.e. for $d_{50} \to 0$ the response of the micro-polar constitutive model tends towards the classical, non-polar continuum description [27]. But also for pronounced grain damage the state $d_{50} = 0$ has no physical relevance for granular materials, so that only states with $d_{50} > 0$ are considered in the following. In contrast to the paper by Bauer et al. [14] a more enhanced description of the influence of grain damage on the pressure dependent limit void ratios and the critical void ratio is proposed in the present paper, i.e. the maximum, minimum and critical void ratio decrease with a reduction of d_{50}. The reduction of d_{50} usually leads to a reorientation of the grain skeleton into a denser state. The additional compaction is modeled by a reduction of the incremental stiffness which is related to a change of the solid hardness, h_s. The state parameter h_s is defined within a continuum description and should not be confused with the hardness of a single grain [5]. In the constitutive model the reduction of the critical void ratio, the limit void ratios and of h_s is linked to the evolution equation for the reduction of d_{50}.

The present paper is organized as follows: In Sect. 2 of this paper the micro-polar hypoplastic constitutive model with respect to grain damage is outlined. In Sect. 3 the proposed constitutive model and the finite element method is used to investigate different mechanisms of grain damage for the case of monotonic plane shearing of a lateral infinite granular layer under a constant vertical load. In order to illustrate the reduction of d_{50} depending on particle rotation and on the curvature these two effects are investigated separately. Particular attention is paid to the influence of the reduction of the mean grain diameter on the evolution of the shear deformation and the void ratio. The main results are summarized and discussed in Sect. 4.

Throughout the paper, bold letters denote vectors and tensors in symbolic notation. Indices on vector and tensor components refer to an orthonormal Cartesian basis. The symbol δ_{ik} denotes the Kronecker delta and ε_{ijk} denotes the permutation symbol. The summation convention over repeated indices is employed. A superimposed dot indicates the material time derivative, and the symbol $||.||$ the Euclidian norm of a tensor, i.e. $||\mathbf{A}|| = \sqrt{A_{ij}\, A_{ij}}$. Compressive stress and strain and their rates are negative as in the sign convention of continuum mechanics.

2 Micro-Polar Hypoplastic Model

The kinematics of a micro-polar continuum is characterized by the macro-displacements u_i and micro-rotations ω_i^c $(i = 1, 2, 3)$ [18]. The components of the rate of the macro-spin tensor, $\mathbf{W}$, and the rate of the micro-spin tensor, $\mathbf{W}^c$, are defined as:

$$\dot{W}_{ij} = \frac{1}{2}\left(\frac{\partial \dot{u}_i}{\partial x_j} - \frac{\partial \dot{u}_j}{\partial x_i}\right) = -\varepsilon_{kij}\,\dot{\omega}_k \qquad \text{and} \qquad \dot{W}^c_{ij} = -\varepsilon_{kij}\,\dot{\omega}^c_k \tag{1}$$

respectively, where x_i $(i = 1, 2, 3)$ denote the spatial coordinates of the state in the current configuration. The components of the corresponding macro-spin vector, $\boldsymbol{\omega}$, and micro-spin vector, $\boldsymbol{\omega}^c$, are related to the skew tensors $\mathbf{W}$ and $\mathbf{W}^c$ according to:

$$\omega_k = -\frac{1}{2}\varepsilon_{ijk}\,W_{ij} \qquad \text{and} \qquad \omega^c_k = -\frac{1}{2}\varepsilon_{ijk}\,W^c_{ij}. \tag{2}$$

The components of the rate of the deformation tensor, $\dot{\boldsymbol{\varepsilon}}$, and the rate of curvature tensor, $\dot{\boldsymbol{\kappa}}$, can be written as:

$$\dot{\varepsilon}_{ij} = \frac{\partial \dot{u}_i}{\partial x_j} + \varepsilon_{kij}\,\dot{\omega}^c_k \qquad \text{and} \qquad \dot{\kappa}_{ij} = \frac{\partial \dot{\omega}^c_i}{\partial x_j}. \tag{3}$$

It is obvious that the tensor of the rate of deformation is usually non-symmetric and only becomes symmetric for cases where the macro-spin is equal to the micro-spin [11]. For quasi-static processes and with respect to the stress tensor $\boldsymbol{\sigma}$ and the couple stress tensor $\boldsymbol{\mu}$ defined for the current configuration the components of the local equilibrium equations read:

$$\frac{\partial \sigma_{ij}}{\partial x_j} + \rho\,\tilde{b}_i = 0, \tag{4}$$

$$\frac{\partial \mu_{ij}}{\partial x_j} - \varepsilon_{ikl}\,\sigma_{kl} + \rho\,\tilde{c}_i = 0. \tag{5}$$

Here ρ denotes the bulk density of the material and the vectors $\tilde{\mathbf{b}}$ and $\tilde{\mathbf{c}}$ represent the body force and body couple, respectively. Equation 5 indicates that the stress tensor in a micro-polar continuum is usually non-symmetric with the exception of states with $\mathrm{div}\boldsymbol{\mu} = \mathbf{0}$ and $\tilde{\mathbf{c}} = \mathbf{0}$. In order to have objective measures for the stress rate and couple stress rate the time derivative given by Green and Naghdi [21] is used, i.e.

$$\mathring{\sigma}_{ij} = \dot{\sigma}_{ij} - \Omega_{ik}\,\sigma_{kj} + \sigma_{ik}\,\Omega_{kj}, \tag{6}$$

$$\mathring{\mu}_{ij} = \dot{\mu}_{ij} - \Omega_{ik}\,\mu_{kj} + \mu_{ik}\,\Omega_{kj}. \tag{7}$$

Here the angular velocity tensor, $\boldsymbol{\Omega}$, is related to the rotation tensor, $\mathbf{R}$, and to the rate of the rotation tensor, $\dot{\mathbf{R}}$, as $\boldsymbol{\Omega} = \dot{\mathbf{R}}\,\mathbf{R}^T$. In order to model inelastic material properties based on the concept of hypoplasticity the objective stress rate tensor, $\mathring{\boldsymbol{\sigma}}$, and couple stress tensor, $\mathring{\boldsymbol{\mu}}$, are described by incrementally non-linear tensor-valued functions, which depend on the current void ratio e, the mean grain diameter d_{50}, the solid hardness h_s, the non-symmetric stress tensor $\boldsymbol{\sigma}$, the couple stress tensor $\boldsymbol{\mu}$, the rate of deformation tensor $\dot{\boldsymbol{\varepsilon}}$, the rate of curvature tensor $\dot{\boldsymbol{\kappa}}$ and the pressure

dependent density factor f_d and stiffness factor f_s. The components of these rate type equations read [26]:

$$\mathring{\sigma}_{ij} = f_s \left[\hat{a}^2 \, \dot{\varepsilon}_{ij} + (\hat{\sigma}_{kl} \, \dot{\varepsilon}_{kl} + \hat{\mu}_{kl} \, \dot{\overline{\kappa}}_{kl}) \, \hat{\sigma}_{ij} + f_d \, (\hat{\sigma}_{ij} + \hat{\sigma}^d_{ij}) \sqrt{\hat{a}^2 \dot{\varepsilon}_{kl} \, \dot{\varepsilon}_{kl} + a_m^2 \dot{\overline{\kappa}}_{kl} \, \dot{\overline{\kappa}}_{kl}} \right] \tag{8}$$

$$\mathring{\mu}_{ij} = f_s \, d_{50} \left[a_m^2 \, \dot{\overline{\kappa}}_{ij} + \hat{\mu}_{ij} \, (\hat{\sigma}_{kl} \, \dot{\varepsilon}_{kl} + \hat{\mu}_{kl} \, \dot{\overline{\kappa}}_{kl} + 2 \, f_d \sqrt{\hat{a}^2 \dot{\varepsilon}_{kl} \, \dot{\varepsilon}_{kl} + a_m^2 \dot{\overline{\kappa}}_{kl} \, \dot{\overline{\kappa}}_{kl}} \,) \right]. \tag{9}$$

With respect to a constant density of the solid grains the evolution equation for the void ratio can be derived from the balance equation of mass to:

$$\dot{e} = (1 + e) \, \dot{\varepsilon}_{kk}. \tag{10}$$

In Eqs. 8 and 9 $\hat{\sigma}_{ij}$, $\hat{\sigma}^d_{ij}$, $\hat{\mu}_{ij}$ and $\dot{\overline{\kappa}}_{ij}$ denote the components of the normalized quantities of the stress tensor, the deviatoric part of the stress tensor, the couple stress tensor and the rate of curvature tensor, respectively, which are defined as:

$$\hat{\sigma}_{ij} = \frac{\sigma_{ij}}{\sigma_{kk}} \, , \qquad \hat{\sigma}^d_{ij} = \hat{\sigma}_{ij} - \frac{1}{3} \, \delta_{ij} \, , \qquad \hat{\mu}_{ij} = \frac{\mu_{ij}}{d_{50} \, \sigma_{kk}} \qquad \text{and} \qquad \dot{\overline{\kappa}}_{ij} = d_{50} \, \dot{\kappa}_{ij}.$$

Factors $\hat{a}$ and a_m in Eqs. 8 and 9 are related to critical states, i.e. a_m is assumed to be a constant and $\hat{a}$ is related to the limit condition given by Matsuoka and Nakai [31]. Function $\hat{a}$ depends on the so-called critical friction angle, φ_c, and the symmetric part of the normalized stress deviator, $\hat{\sigma}^{ds} = (\hat{\sigma}^d_{kl} + \hat{\sigma}^d_{lk})/2$, which can be represented as [11]:

$$\hat{a} = \frac{\sin \varphi_c}{3 + \sin \varphi_c} \left[\sqrt{\frac{8/3 - 3 \, (\hat{\sigma}^{ds}_{kl} \, \hat{\sigma}^{ds}_{kl}) + g \, \sqrt{3/2} \, (\hat{\sigma}^{ds}_{kl} \, \hat{\sigma}^{ds}_{kl})^{3/2}}{1 + g \, \sqrt{3/2} \, (\hat{\sigma}^{ds}_{kl} \, \hat{\sigma}^{ds}_{kl})^{1/2}}} + \sqrt{\hat{\sigma}^{ds}_{kl} \hat{\sigma}^{ds}_{kl}} \right] \tag{11}$$

$$\text{with:} \qquad g = -\frac{\sqrt{6} \, \hat{\sigma}^{ds}_{kl} \, \hat{\sigma}^{ds}_{lm} \, \hat{\sigma}^{ds}_{mk}}{(\hat{\sigma}^{ds}_{pq} \, \hat{\sigma}^{ds}_{pq})^{3/2}}.$$

The influence of the current void ratio, e, and the mean pressure on the incremental stiffness, the peak friction angle and dilatancy behavior is modeled with the stiffness factor f_s and the density factor f_d, i.e.

$$f_s = \frac{\left(\frac{e_i}{e}\right)^{\beta} \, \frac{h_s \, (1 + e_i)}{n \, (\hat{\sigma}_{pq} \hat{\sigma}_{pq}) \, e_i} \left(-\frac{\sigma_{kk}}{h_s}\right)^{1-n}}{\frac{8 \, \sin^2 \varphi_c}{(3 + \sin \varphi_c)^2} + 1 - \frac{2 \sqrt{2} \, \sin \varphi_c}{3 + \sin \varphi_c} \left(\frac{e_{io} - e_{do}}{e_{co} - e_{do}}\right)^{\alpha}} \tag{12}$$

and

$$f_d = \left(\frac{e - e_d}{e_c - e_d} \right)^{\alpha} . \tag{13}$$

In Eqs. (12) and (13) α , β and n are constitutive constants, e_i , e_d and e_c denote the maximum void ratio, minimum void ratio and critical void ratio, respectively. In order to take into account the influence of grain damage the quantities e_i , e_d and e_c are related to the mean pressure $p = -\sigma_{kk}/3$, the current value of the mean grain diameter d_{50} and the solid hardness h_s, i.e.

$$e_i = e_{i0} \left(\frac{d_{50}}{d_{50_0}} \right)^{b_e} \exp\left[- \left(\frac{3p}{h_s} \right)^{n} \right], \tag{14}$$

$$e_d = e_{d0} \left(\frac{d_{50}}{d_{50_0}} \right)^{b_e} \exp\left[- \left(\frac{3p}{h_s} \right)^{n} \right], \tag{15}$$

$$e_c = e_{c0} \left(\frac{d_{50}}{d_{50_0}} \right)^{b_e} \exp\left[- \left(\frac{3p}{h_s} \right)^{n} \right], \tag{16}$$

where e_{i0}, e_{d0}, e_{c0} are the corresponding initial values for $\sigma_{kk} = 0$. d_{50_0} is the initial mean grain diameter and b_e is a constitutive constant. The solid hardness h_s is defined in the sense of a continuum description and it is a key parameter to reflect the stiffness of the granular material under isotropic compression.

The influence of grain damage on the change of the grading of the grain sizes of the granular material is taken into account by a reduction of the mean grain diameter d_{50}. For monotonic shearing the reduction of d_{50} is modeled by the following evolution equation [14]:

$$\dot{d}_{50} = - d_{50} \left[b_k \, ||\dot{\overline{\boldsymbol{\kappa}}}|| + b_\omega \, ||\dot{\boldsymbol{\omega}}^c - \dot{\boldsymbol{\omega}}|| + b_p \, f_p(\dot{p} > 0) + b_\eta \, f_\eta(\dot{\eta}, \, \dots) \right]. \tag{17}$$

In Eq. (17) $||\dot{\overline{\boldsymbol{\kappa}}}||$ denotes the norm of the normalized rate of curvature, $||\dot{\boldsymbol{\omega}}^c - \dot{\boldsymbol{\omega}}||$ denotes the norm of the difference of the rate of the micro- and macro-rotations, $f_p(\dot{p})$ is a function depending on the rate of the mean stress and $f_\eta(\dot{\eta})$ is a function depending on other state quantities not yet specified. The scalar factors b_k, b_ω, b_p and b_η can also depend on the current state variables, but are assumed to be constant for the present paper. The rate of the solid hardness, $\dot{h}_s$, is linked to the rate of d_{50} by the differential equation:

$$\dot{h}_s = b_s \, h_s \, \frac{\dot{d}_{50}}{d_{50}} , \tag{18}$$

where b_s is a constitutive constant.

3 Numerical Investigation of the Influence of Grain Damage on Plane Shearing

Experiments with the plane simple shear apparatus of the Cambridge type show size effects and a nonuniform evolution of stress and strain distributions within the specimen [8], Similar size effects were also detected from numerical simulations [27]. Thus, the simple shear deformation of a granular material does not represent a homogeneous element test. In order to prevent size effects, shearing of a lateral infinite granular strip under constant vertical pressure will be considered for the present numerical simulations as illustrated in Fig. 1a. For a micro-polar continuum and for the case of plane strain the relevant kinematic and static quantities are shown in Fig. 1b and c, respectively. With respect to the Cartesian co-ordinate system u_1 and u_2 are the two displacement degrees of freedom and ω_3 is the micro-rotation degree of freedom. The non-zero stress components are σ_{11}, σ_{22}, σ_{33}, σ_{12} and σ_{21}, and the couple stress components are μ_{31} and μ_{32}. With the assumption of an initially homogeneous specimen the evolution of any state quantity $\psi(x_2)$ is independent of the coordinate x_1 in the direction of shearing, i.e. $\partial\psi(x_2)/\partial x_1 = 0$ [11]. If body forces and body couples are neglected, i.e. in Eqs. 4 and 5 the quantities $\boldsymbol{b_i}$ and $\boldsymbol{c_i}$ are set to zero, the equilibrium condition requires that the vertical stress σ_{22} and the horizontal shear stress σ_{12} is independent of the coordinate x_2. For plane strain conditions the field quantities are also independent of the co-ordinate x_3. Very rough surfaces of the bounding structures at the bottom and top surface are assumed, so that no relative displacements and particle rotations can take place along the interfaces.

For numerical simulation a four-node Cosserat element for plane strain conditions is used which was implemented into the finite element program ABAQUS [1] by Huang [25]. Linear shape functions for displacements and the micro-polar rotation are used. With an updated Lagrange formulation large deformations can be taken into account. The condition of a lateral infinite layer is modeled by applying constraint conditions to the side nodes of the finite element mesh, i.e., each node on the left boundary is controlled to have the same displacements and Cosserat rotation as the corresponding node with the same vertical coordinate on the right boundary [9].

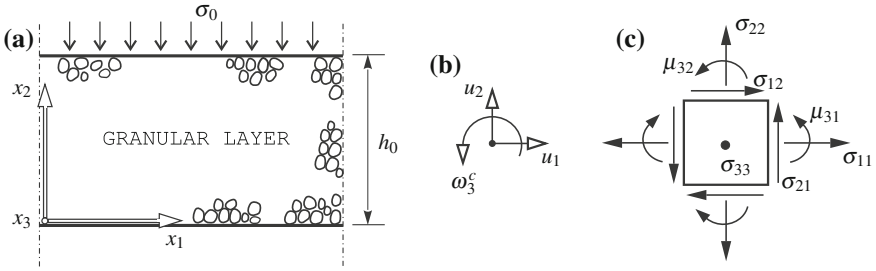

Fig. 1 Modeling of plane shearing under constant vertical pressure: **a** Section of the lateral infinite granular layer; **b** Kinematic quantities; **c** Stress components and couple stress components

Particularly, a granular layer with an initial height of $h_0 = 4\,\text{cm}$ is discretized by Cosserat elements with an initial size of $1.25\,\text{mm} \times 1.25\text{mm}$. For the initial state, a homogeneous distribution of the initial void ratio of $e_0 = 0.62$ is assumed. A constant vertical stress of $\sigma_{22} = -1000$ kPa is applied at the top surface. With the assumption of a constant vertical stress the height of the layer can decrease or increase as a result of compaction or dilation of the granular material under shearing. A monotonic shear deformation up to 4 cm is initiated at the top surface of the granular layer, i.e. same horizontal displacements are prescribed for all nodes along the top surface. In order to study separately the influence of the individual factors in Eq. (17) on the reduction of the mean grain diameter, numerical simulations are carried out for three different cases:

Case A: In Eq. (17) only the term $b_k\,||\dot{\boldsymbol{\kappa}}||$ is active.
Case B: In Eq. (17) only the term $b_\omega\,||\dot{\boldsymbol{\omega}}^c - \dot{\boldsymbol{\omega}}||$ is active.
Case C: No grain damage is considered, i.e. $d_{50_0} = const.$ and $h_{s0} = const.$

Because of the constant vertical stress σ_0 the increase of the mean pressure in the specimen during shearing is small, so that the influence of the third term in Eq. (17) is neglected. For the present investigations the values assumed for the constitutive parameters in the constitutive relations in Sect. 2 are summarized in Table 1. For different state quantities the results obtained from the numerical simulations are shown for Case A and Case B in Figs. 2 and 3, respectively. The dashed curves represent the results for the Case C where no grain damage is taken into account. The evolution of the horizontal shear stress and the distribution of the horizontal displacements across the shear layer indicate that the influence of grain damage becomes dominant after the stress peak. At the beginning of shearing the displacement field is almost linear as it is in the non-polar continuum. After the stress peak the reduction of the shear stress is more pronounced for the case of grain damage than for $d_{50} = const.$ From Figs. 2b and 3b it is clearly visible that for larger shear displacements of the top surface the shear deformation localizes and the displacement filed becomes non-linear. Because of the symmetric boundary conditions for the rough surfaces at the top and at the bottom shear strain localization occurs in the middle of the shear layer. Within the localized zone, called shear band, pronounced micro-rotations and an increase of the void ratio can be observed also for the case without grain damage. The extreme values for ω_3^c and e arise in the middle of the shear band, while the distribution of the curvature κ_{32} shows extreme values at the boundary of the localized zone. With respect to grain damage some differences can be detected between Case A and Case B. In particular, for Case A the maximum reduction of the mean grain diameter occurs at the boundary of the localized zone, while for Case B the reduction is dominant in the middle of the localized zone. Similar results can also be observed under large shearing in a ring shear device, where grain breakage is concentrated in the shear band and almost no grain damage occurs outside the shear band. Grain damage is accompanied with an additional compaction of the granular material which is also

Table 1 Constitutive parameters used for the numerical simulations

Case	$\varphi_c[\circ]$	e_{i0}	e_{d0}	e_{c0}	$h_{s0}[MPa]$	n	α	β	a_m	$d_{50_0}[mm]$	b_k	b_ω	b_x	b_e
A	30	1.02	0.51	0.82	10^4	0.35	0.14	1.05	0.8	0.5	4.0	0	5.0	0.15
B	30	1.02	0.51	0.82	10^4	0.35	0.14	1.05	0.8	0.5	0	4.0	5.0	0.15
C	30	1.02	0.51	0.82	10^4	0.35	0.14	1.05	0.8	0.5	0	0	0	0

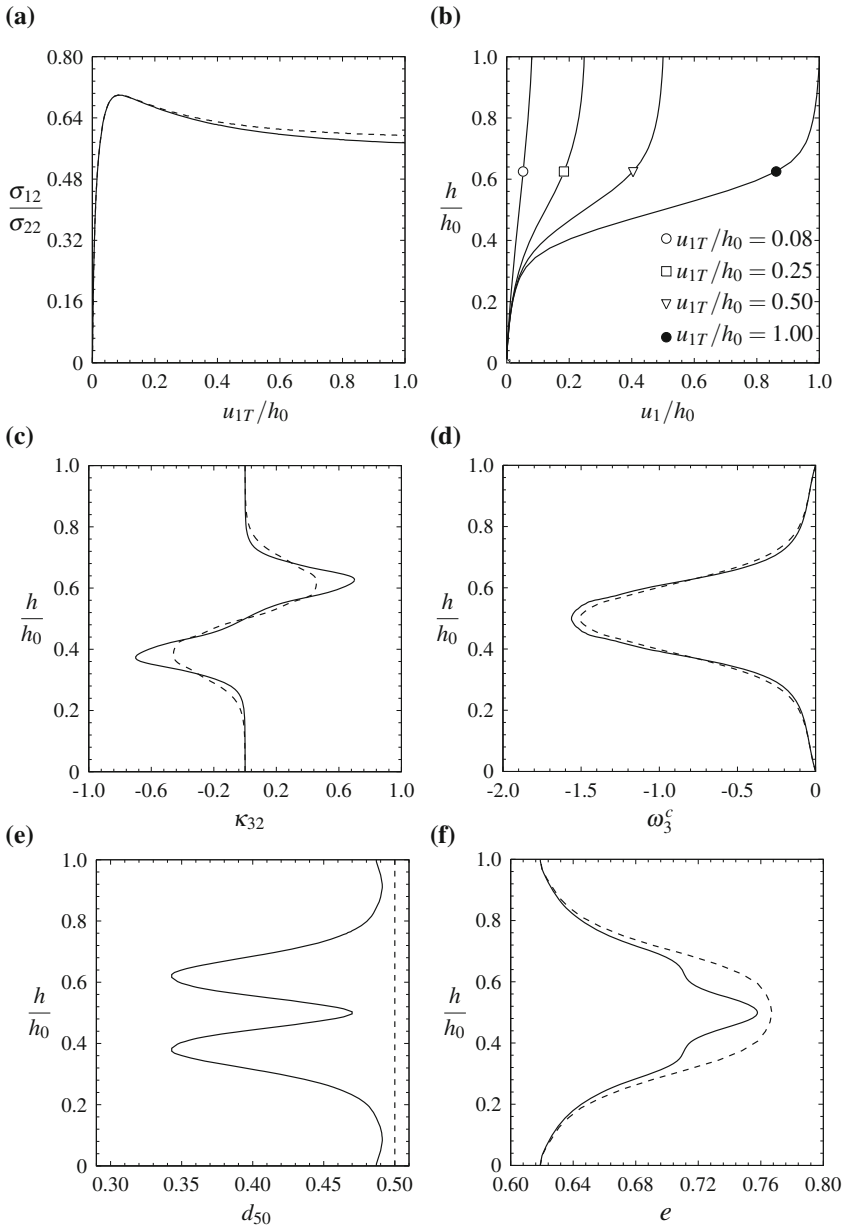

Fig. 2 Case A: Influence of the curvature κ_{32} on the reduction of the mean grain diameter d_{50} according to Eq. (17). The *solid curves* and *dashed curves* represent the numerical results obtained with grain damage and without grain damage, respectively. **a** Normalized shear stress, σ_{12}/σ_{22}, versus normalized horizontal displacement, u_{1T}/h_0, of the top boundary, **b** evolution of the normalized horizontal displacement, u_1/h_0, across the normalized height, h/h_0, of the shear layer for four states, **c** distribution of the curvature κ_{32}, **d** distribution of the micro-rotation ω_3^c, **e** distribution of the mean grain diameter d_{50}, **f** distribution of the void ratio e

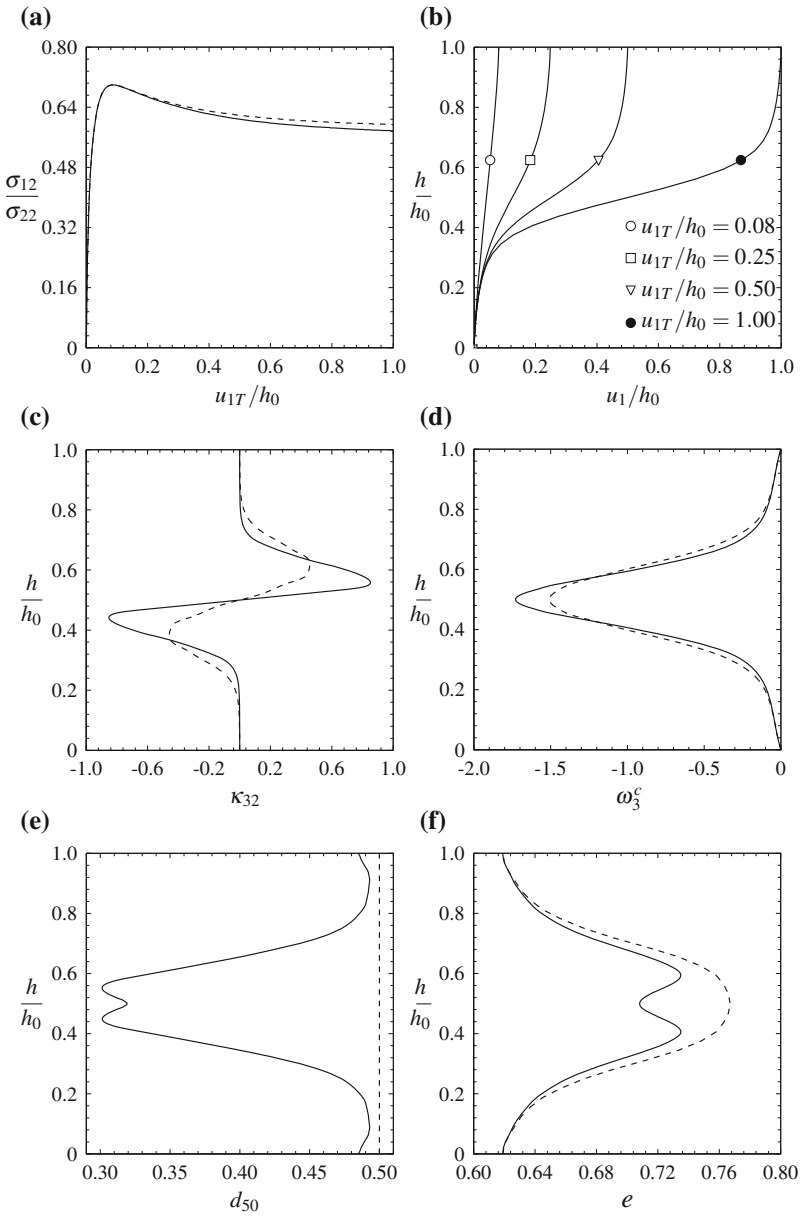

Fig. 3 Case B: Influence of the micro-rotation ω_3^c on the reduction of the mean grain diameter d_{50} according to Eq. (17). The *solid curves* and *dashed curves* represent the numerical results obtained with grain damage and without grain damage, respectively. **a** Normalized shear stress, σ_{12}/σ_{22}, versus normalized horizontal displacement, u_{1T}/h_0, of the top boundary, **b** evolution of the normalized horizontal displacement, u_1/h_0, across the normalized height, h/h_0, of the shear layer for four states, **c** distribution of the curvature κ_{32}, **d** distribution of the micro-rotation ω_3^c, **e** distribution of the mean grain diameter d_{50}, **f** distribution of the void ratio e

reflected by a reduction of the void ratio e. A comparison of Figs. 2f and 3f shows that for Case A the reduction of the void ratio is more pronounced close to the boundaries of the shear band, while for Case B the maximum reduction arises in the middle.

4 Conclusions

In this paper a new concept is proposed for the constitutive modeling of the influence of grain damage in granular materials based on the framework of micro-polar hypoplasticity. The effect of grain abrasion and grain fragmentation on the change of the grain size distribution is taken into account by the corresponding change of the mean grain diameter, which is embedded in the constitutive model as an internal length. In particular, it is assumed that a decrease in the mean grain diameter is influenced by an increase in the mean stress, the norm of the rate of the curvature and the norm of the difference of the rate of the micro- and macro-rotations. The reduction of the mean grain diameter is linked to the reduction of the limit void ratios and the critical void ratio and takes into account an additional compaction of the material as a result of grain damage. Particular attention is paid to modeling the effect of particle rotation and curvature on the process of particle damage. It is demonstrated that for monotonic plane shearing under constant vertical stress grain damage becomes dominant within the localized zone. In particular, grain damage in the middle of the localized zone is mainly related to the particle rotation while the effect of large curvature on grain damage is pronounced close to the boundaries of the localized zone. Under shearing grain damage also leads to a reduction of the dilatancy behavior of the material. The proposed concept of a reduction of the mean grain diameter and of the limit void ratios is mathematically simple, but for practical application it needs further experimental and physical clarifications.

Acknowledgments The assistance of Mr. Linke Li in calibrating the model and running the numerical simulations presented in the paper is gratefully acknowledged.

References

1. ABAQUS User's Manual Version 6.3. Hibbitt, Karlsson and Sorensen Inc.: Pawtucket, RI, USA (2002)
2. Alikarami, R., Andò, E., Gkiousas-Kapnisis, M., Torabi, A., Viggiani, G.: Strain localisation and grain breakage in sand under shearing at high mean stress: insights from in situ X-ray tomography. Acta Geotechnica **10**, 15–30 (2015)
3. Ando, E., Hall, S.A., Viggiani, G., Desrues, J., Besuelle, P.: Grain-scale experimental investigation of localised deformation in sand: a discrete particle tracking approach. Acta Geotechnica **7**, 1–13 (2012)
4. Bauer, E., Wu, W.: A hypoplastic constitutive model for cohesive powders. Powder Technology **85**, 1–9 (1995)

5. Bauer, E.: Calibration of a comprehensive hypoplastic model for granular materials. Soils and Foundations **36**(1), 13–26 (1996)
6. Bauer, E.: Analysis of shear band bifurcation with a hypoplastic model for a pressure and density sensitive granular material. Mechanics of Materials **31**, 597–609 (1999)
7. Bauer, E.: Conditions for embedding Casagrande's critical states into hypoplasticity. Mechanics of Cohesive-Frictional Materials **5**, 125–148 (2000)
8. Budhu, M.: Nonuniformities imposed by simple shear apparatus. Canadian Geotechnical Journal **21**(1), 125–137 (1984)
9. Bauer, E., Huang, W.: Evolution of polar quantities in a granular Cosserat material under shearing. In: Mühlhaus, H.B., Dyskin, A.V., Pasternak, E. (eds.) Proceedings of the 5th International Workshop on Bifurcation and Localization Theory in Geomechanics, Balkema press, pp. 227–38 (2001)
10. Bauer, E., Huang, W., Wu, W.: Investigation of shear banding in an anisotropic hypoplastic material. Solids and Structures **41**, 5903–5919 (2004)
11. Bauer, E.: Initial response of a micro-polar hypoplastic material under plane shearing. J. Engin. Mathematics **52**, 35–51 (2005)
12. Bauer, E.: Hypoplastic modelling of moisture-sensitive weathered rockfill materials. Acta Geotechnica **4**, 261–72 (2009)
13. Bauer, E.: Analysis of shear banding with a hypoplastic constitutive model for a dry and cohesionless granular material. In: Albers, B. Continuous Media with Microstructure, pp. 335–350. Springer Publisher (2010)
14. Bauer, E., Li, L., Huang, W.: Hypoplastic constitutive modelling of grain damage under plane shearing. In: Bifurcation and Degradation of Geomaterials in the New Millennium, pp. 181–187 (2015)
15. Daouadji, A., Hicher, P.Y., Rahma, A.: An elastoplastic model for granular materials taking into account grain breakage. Eur. J. Mech. A/Solids **20**, 113–137 (2001)
16. Ebrahimian, B., Bauer, E.: Numerical simulation of the effect of interface friction of a bounding structure on shear deformation in a granular soil. International Journal for Numerical and Analytical Methods in Geomechanics **36**, 1486–1506 (2012)
17. Ehlers, W., Wenz, S.: From particle ensembles to Cosserat continua: definition of the macroscopic variables. In: Vermeer, P.A., Ehlers, W., Herrmann, H.J., Ramm, E. (eds.) Modelling of Cohesive-Frictional Materials, pp. 149–159. Balkema at Taylor & Francis, Lisse (2004)
18. Eringen, A.C.: Polar and nonlocal field theories. IV, Academic Press, New York, San Francisco, London, Continuum Physics (1976)
19. Garga, V.K.: Infante Sedano, J. A.: Steady state strength of sands in a constant volume ring shear apparatus. Geotechnical Testing Journal **25**, 414–421 (2002)
20. Goddard, J.D.: Parametric hypoplasticity as continuum model for granular media - from Stokesium to Mohr - Coulombium and beyond. Granular Mat. **12**, 145–150 (2010)
21. Green, A.E., Naghdi, P.M.: A general Theory of an elastic-plastic continuum. Arch. Rat. Mech. Anal. **18**, 251–281 (1965)
22. Gudehus, G.: A comprehensive constitutive equation for granular materials. Soils and Foundations **36**(1), 1–12 (1996)
23. Gudehus, G.: Shear localization in simple grain skeleton with polar effect. In: Adachi, T., Oka, F., Yashima, A. (eds.) Proceedings of the 4th International Workshop on Localization and Bifurcation Theory for Soils and Rocks. pp. 3–10. Balkema press (1998)
24. Gudehus, G., Jiang, Y.M., Liu, M.: Seismo - and thermodynamics of granular solids. Granular Matter **13**, 319–340 (2011)
25. Huang, W.: Hypoplastic modelling of shear localisation in granular materials, Ph.D. thesis, Graz University of Technology, Austria (2000)
26. Huang, W., Nübel, K., Bauer, E.: A polar extension of hypoplastic model for granular material with shear localization. Mechanics of Materials **34**, 563–576 (2002)
27. Huang, W., Bauer, E.: Numerical investigations of shear localization in a micro-polar hypoplastic material. Int. J. Numer. Anal. Methods Geomech. **27**, 325–352 (2003)
28. Kolymbas, D.: An outline of hypoplasticity. Archive of Applied Mechanics **61**, 143–151 (1991)

29. Luzzani, L., Coop, M.R.: On the relationship between particle breakage and the critical state of sand. Soils and Foundation **42**(2), 71–82 (2002)
30. Masin, D., Herle, I.: Improvement of a hypoplastic model to predict clay behaviour under undrained conditions. Acta Geotechnica **2**, 261–268 (2007)
31. Matsuoka, H., Nakai, T.: Stress-strain relationship of soil based on the 'SMP'. In: Proceedings of the Speciality Session 9, IX International Conference on Soil Mechanics and Foundation Engineering, pp. 153–162. Tokyo (1977)
32. Mühlhaus, H.B.: Application of Cosserat theory in numerical solutions of limit load problems. Archive of Applied Mechanics **59**(2), 124–137 (1989)
33. Nguyen, G.D., Einav, I.: Numerical regularization of a model based on breakage mechanics for granular materials. International Journal for Solids and Structures **47**(10), 1350–1360 (2010)
34. Niemunis, A., Herle, I.: Hypoplastic model for cohesionless soils with elastic strain range. Mechanics of Cohesive-Frictional Materials **2**(4), 279–299 (1997)
35. Oda, M.: Micro-fabric and couple stress in shear bands of granular materials. In: Thornton, C. (ed.) Powders and Grains, Vol. 3, pp. 161–167 (1993)
36. Ovalle, C., Frossard, E., Dano, C., Hu, W., Maiolino, S., Hicher, P.-Y.: The effect of size on the strength of coarse rock aggregates and large rockfill samples through experimental data. Acta Mechanica **225**(8), 2199–2216 (2014)
37. Ovalle, C., Dano, C., Hicher, P.Y., Cisternas, M.: An experimental framework for evaluating the mechanical behavior of dry and wet crushable granular materials based on the particle breakage ratio. Canadian Geotechnical Journal **52**, 1–12 (2015)
38. Sadrekarimi, A., Olson, S.M.: Critical state friction angle of sands. Géotechnique **61**(9), 771–783 (2011)
39. Salim, W., Indraratna, B.: A new elastoplastic constitutive model for coarse granular aggregates incorporating particle breakage. Canadian Geotechnical Journal **41**, 657–671 (2004)
40. Tejchman, J., Bauer, E.: Numerical simulation of shear band formation with a polar hypoplastic constitutive model. Comput. Geotech. **19**, 221–44 (1996)
41. Tejchman, J., Bauer, E.: Fe-simulations of a direct and a true simple shear test within a polar hypoplasticity. Computers and Geotechnics **32**(1), 1–16 (2005)
42. Tejchman, J.: Effect of grain crushing on shear localization in granular bodies within micro-polar hypoplasticity. Arch. Hydro-Engineering Environ. Mech. **57**, (1–2), 3–30 (2010)
43. Tejchman, J., Górski, J., Einav, I.: Effect of grain crushing on shear localization in granular bodies during plane strain compression. Int. J. Numer. Anal. Meth. Geomech. **36**, 1909–1931 (2012)
44. Vardoulakis, I.: Shear banding and liquefaction in granular materials on the basis of a Cosserat continuum theory. Ingenieur Archiv **59**, 106–113 (1989)
45. Wu, W., Bauer, E., Kolymbas, D.: Hypoplastic constitutive model with critical state for granular materials. Mech. Mat. **23**, 45–69 (1996)
46. Wu, W., Kolymbas, D.: Hypoplasticity then and now. In: Kolymbas (ed.) Constitutive Modelling of Granular Materials, pp. 57–105, Springer press (2000)
47. Wu, W., Niemunis, A.: Failure criterion, flow rule and dissipation function derived from hypoplasticity. Mechanics of Cohesive-Frictional Materials **1**, 145–163 (1996)

Non-hydrostatic Free Surface Flows: Saint Venant Versus Boussinesq Depth Integrated Dynamic Equations for River and Granular Flows

Kolumban Hutter and Oscar Castro-Orgaz

Abstract Nineteenth and early twentieth century channel flow hydraulics is dominated by depth averaged equations. Saint Venant and Boussinesq present approximations with and without the imposition of the shallowness approximation, respectively. In the former approximation the vertical momentum equation is replaced by the so-called hydrostatic equation, in which the vertical pressure gradient and the gravity force balance, but the vertical acceleration and the horizontal shear stress gradients are dropped. In the classical Boussinesq-type amendments to the Saint Venant approach the acceleration terms are accounted for, but the shear stress gradients are generally ignored. For non-ideal fluids this is questionable. We derive the unabridged depth integrated equations and demonstrate the subtleties of this problem using as examples the potential, Navier-Stokes and granular fluid with earth-pressure constitutive structure.

1 Introduction

Understanding granular mass flow is a basic step in the prediction and control of natural or manmade disasters due to avalanches on Earth. Savage and Hutter [19] pioneered the mathematical modeling of these geophysical flows; numerous follow-up papers were subsequently published, for a summary, see Pudasaini and Hutter [18], and are still being published to this date. Most of these papers are based on a shallowness assumption in curvilinear coordinates following terrain, in which the length scale tangential to the main flow directions, $[L]$, is significantly larger than the corresponding length scale, $[H]$, orthogonal to this two-dimensional tangential manifold, so that $\varepsilon = [H/L] \ll 1$. Thus, the shallowness parameter is small, suggesting

K. Hutter (✉)
ETH Zürich, HIA D58, Hönggerberg-Ring 26, 8093 Zuerich, Switzerland
e-mail: hutter@vaw.baug.ethz.ch

O. Castro-Orgaz
University of Córdoba, Hydraulic Area, Campus Rabanales,
Leonardo da Vinci Building, Madrid Road, Km 396, E-14071 Córdoba, Spain
e-mail: oscarcastro@ias.csic.es

B. Albers and M. Kuczma (eds.), *Continuous Media with Microstructure 2*,
DOI 10.1007/978-3-319-28241-1_17

approximations of the governing equations in the spirit of perturbation expansions. Its lowest order approximation for rapid granular flows is known as Savage-Hutter (SH)-equations. In the context of classical fluid mechanics corresponding depth averaged mass and momentum balance equations are attributed to Barré de Saint-Venant [1]; they are all characterized by the fact that the bed-normal momentum equation reduces to a hydrostatic force balance, in which the bed-normal pressure gradient balances the corresponding gravity force, assuming a small channel slope.

This class of governing equations is intimately related to the stretching transformation, expressed by the shallowness assumption $\varepsilon \ll 1$. Topographic variations often occur with a spectrum of wavelengths, in which significant amplitudes arise at wavelengths comparable to the depth of the moving avalanches, implying that necessarily $\varepsilon = O(1)$, if the topographic protuberances are to execute an effect in rapid geophysical flows over such bumpy beds. In a Cartesian horizontal-vertical coordinate system the dynamical equations of rapid granular flows were formulated by Denlinger and Iverson [8] to essentially abandon the hydrostatic pressure assumption, but they expressed it differently: In the words of Castro-Orgaz et al. [6] they "found that vertical accelerations in granular mass flows are of the same order as the gravity acceleration, requiring the consideration of non-hydrostatic modeling of granular mass flows".

Free surface water flow simulations based on non-hydrostatic depth-averaged models are well known in hydraulic modeling ever since Boussinesq [4, 5] introduced his famous equations about 140 years ago; existing literature based on the Boussinesq-type equations is overwhelming. The derivation of these equations is equally based on a stretch-free scaling of the hydrodynamic equations, but the cause of the non-negligible vertical acceleration term in Cartesian coordinates is not necessarily the bumpiness of the bed but rather the non-linear large amplitude of the free surface in gravity driven surface waves and possibly undular hydraulic jumps, etc., on rather flat bottom topography. Denlinger and Iverson [8] did not seem to have been aware of the connection of their non-hydrostatic granular modeling approach with the Boussinesq approach. Moreover, they employed an unnecessary linearization of the vertical normal stress in the depth integration, which can be amended. The equivalence in the mathematical handling suggests the question, *whether Boussinesq-type gravity waves would also be formed in rapid granular mass flows,* perhaps even when the topography is smooth. Furthermore, *certain forms in the basal topography give rise to enhanced or damped free surface profiles*.

These questions call for answers and their positive solution is likely, given the potential to apply the approach of the Boussinesq-type procedure to channel flow or to undular flow of two-dimensional and three-dimensional terrain. This will be initiated in this memoir by employing the Boussinesq-type analysis to an arbitrary granular mass flow using the depth integrated balance equations of mass and momentum.

The simplest geometric situation of a granular avalanching mass on a flat horizontal bed will be used to isolate the salient physical features. Using simple academic test cases, it will be demonstrated that the above question can be answered in an affirmative way. This will open a new framework for the physical and mathematical

modeling of granular mass flow in geo- and environmental physics in a consistent way in this simple example. However, a wealth of additional detailed problems lie ahead of us to generalize the mathematical approach to arbitrarily curved basal topographies.

2 Vertically Integrated Balance Laws of Mass and Horizontal Momentum

2.1 Governing Equations

Consider a horizontal-vertical Cartesian coordinate setting in Euclidean 3-space, in which the balance laws of mass and momentum of a density preserving continuum take the forms

$$\frac{\partial u}{\partial x}+\frac{\partial v}{\partial y}+\frac{\partial w}{\partial z} = 0 \tag{1}$$

$$\frac{\partial u}{\partial t}+u\frac{\partial u}{\partial x}+v\frac{\partial u}{\partial y}+w\frac{\partial u}{\partial z} = -\frac{1}{\rho}\left(\frac{\partial \tau_{xx}}{\partial x}+\frac{\partial \tau_{xy}}{\partial y}+\frac{\partial \tau_{xz}}{\partial z}\right), \tag{2}$$

$$\frac{\partial v}{\partial t}+u\frac{\partial v}{\partial x}+v\frac{\partial v}{\partial y}+w\frac{\partial v}{\partial z} = -\frac{1}{\rho}\left(\frac{\partial \tau_{xy}}{\partial x}+\frac{\partial \tau_{yy}}{\partial y}+\frac{\partial \tau_{yz}}{\partial z}\right), \tag{3}$$

$$\frac{\partial w}{\partial t}+u\frac{\partial w}{\partial x}+v\frac{\partial w}{\partial y}+w\frac{\partial w}{\partial z} = -\frac{1}{\rho}\left(\frac{\partial \tau_{xz}}{\partial x}+\frac{\partial \tau_{yz}}{\partial y}+\frac{\partial \tau_{zz}}{\partial z}\right)-g. \tag{4}$$

In these equations, (x, y) are the horizontal coordinates and z is the vertical coordinate; (u, v, w) are the corresponding velocity components. Moreover, the stress tensor is introduced as a pressure tensor, the negative of the usual notation, ρ is the constant density and g the gravity constant. The above equations are considered in this contribution to be applied to free surface flows of water on a rigid impermeable bed in channels or of debris, mud or snow avalanches. The process to obtain vertically-integrated equations is identical to that used for river flow over 3D terrain in hydraulics (Fig. 1). For simplicity, boundary conditions are formulated for a movable material bed (subscript b) and a movable material stress-free upper surface (subscript s)

$$\left(\frac{\partial z}{\partial t}+u\frac{\partial z}{\partial x}+v\frac{\partial z}{\partial y}-w\right)_{b,s} = 0, \tag{5}$$

and the free surface is considered stress free, whilst the traction at the bed follows a given sliding law

$$\boldsymbol{\tau}_s\mathbf{n} = \mathbf{0}, \quad \boldsymbol{\tau}_b = C\mathbf{u}_b. \tag{6}$$

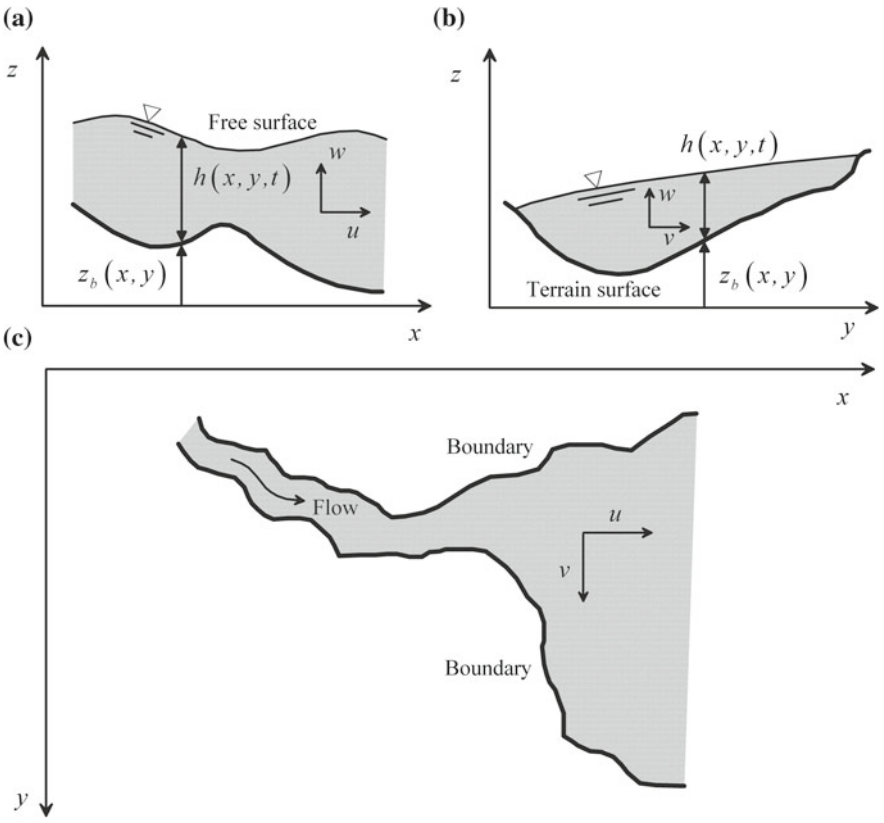

Fig. 1 Definition sketch for flow over 3D terrain. **a** Profile, **b** section, **c** plan

$C = 0$ corresponds to perfect sliding and $C \to \infty$ to the no-slip condition. In applications C will be specified. Alternatively, a Coulomb sliding law could also be used,

$$\boldsymbol{\tau}_s \mathbf{n}_s = \mathbf{0}, \quad \boldsymbol{\tau}_b \mathbf{n}_b - \mathbf{n}_b(\mathbf{n}_b \cdot \boldsymbol{\tau}_b \mathbf{n}_b) = \frac{\mathbf{u}_b}{|\mathbf{u}|_b}(\mathbf{n}_b \cdot \boldsymbol{\tau}_b \mathbf{n}_b)\tan(\phi_{bed}), \tag{7}$$

in which ϕ_{bed} is the basal friction angle. An additive combination of the two sliding laws corresponds to the Voellmy law.

Saint Venant [1] and Boussinesq initiated approximate transformations of equations (1)–(4) to depth integrated form. Saint Venant did this by imposing a shallowness assumption, which implied reduction of the vertical momentum balance equation to the hydrostatic pressure balance. Boussinesq did not assume this, allowed the field quantities to vary in all space directions with comparable magnitude and, thus accounted for vertical acceleration and non-hydrostatic stress contributions in the dynamic processes. Here this process will be performed and scrutinized by integrating equations (1)–(4) in the z-direction. In this process the differentiation and

integration operations are interchanged using the Leibniz rule, and the free and basal surface boundary conditions are used to simplify the emerging mathematical expressions. This mathematical procedure is standard, albeit somewhat complicated and has for rapid surface flows explicitly been demonstrated by Castro-Orgaz et al. [6]. These authors also provide a detailed review of precursory literature. This justifies to be brief here. In what follows, we shall employ the notation $(p_{xx}, p_{yy}, p_{zz}) = (\tau_{xx}, \tau_{yy}, \tau_{zz})$ in order to emphasize that these normal stresses are actually pressures.

2.2 Depth Integrated Balance Law of Mass

For the balance law of mass with vanishing entrainment or deposition from above and below, this process yields

$$\frac{\partial h}{\partial t} + \frac{\partial Q_x}{\partial x} + \frac{\partial Q_y}{\partial x} = 0, \quad \text{where} \quad Q_x = \int_{z_b}^{z_s} u \, \mathrm{d}\zeta, \quad Q_y = \int_{z_b}^{z_s} v \, \mathrm{d}\zeta. \tag{8}$$

Here, Q_x and Q_y are the volume fluxes in the x- and y-directions, respectively. The derivation can be found in almost any book on fluid mechanics.

2.3 Depth Integrated Momentum Equations in the Horizontal Plane

The process of transformations, analogous to that described above for the mass balance equation yields for the momentum equations in the horizontal plane

$$\begin{aligned} &\frac{\partial}{\partial t}\int_{z_b}^{z_s} u \, \mathrm{d}\zeta + \frac{\partial}{\partial x}\int_{z_b}^{z_s} u^2 \, \mathrm{d}\zeta + \frac{\partial}{\partial y}\int_{z_b}^{z_s} uv \, \mathrm{d}\zeta \\ &= -\frac{1}{\rho}\left\{\frac{\partial}{\partial x}\int_{z_b}^{z_s} p_{xx} \, \mathrm{d}\zeta + \frac{\partial}{\partial y}\int_{z_b}^{z_s} \tau_{xy} \, \mathrm{d}\zeta\right\} + (p_{xx})_b\frac{\partial z_b}{\partial x} + (\tau_{xy})_b\frac{\partial z_b}{\partial y} - (\tau_{xz})_b, \end{aligned} \tag{9}$$

$$\begin{aligned} &\frac{\partial}{\partial t}\int_{z_b}^{z_s} v \, \mathrm{d}\zeta + \frac{\partial}{\partial x}\int_{z_b}^{z_s} v^2 \, \mathrm{d}\zeta + \frac{\partial}{\partial y}\int_{z_b}^{z_s} uv \, \mathrm{d}\zeta \\ &= -\frac{1}{\rho}\left\{\frac{\partial}{\partial x}\int_{z_b}^{z_s} \tau_{xy} \, \mathrm{d}\zeta + \frac{\partial}{\partial y}\int_{z_b}^{z_s} p_{yy} \, \mathrm{d}\zeta\right\} + (\tau_{xy})_b\frac{\partial z_b}{\partial x} + (p_{yy})_b\frac{\partial z_b}{\partial y} - (\tau_{yz})_b. \end{aligned} \tag{10}$$

These equations do not involve any free surface stress terms, because stress free upper boundary conditions have been assumed. The Eqs. (8), (9) and (10) describe flows as referred to the (x,y)-plane. They allow for several approximations to the kinematic fields u, v, w and parameterizations of the stress tensor $\boldsymbol{T}$ (with the components τ_{ij}, with $i, j = 1, 2, 3$) to produce a family of depth-averaged equations. The local flow depth is

$$h = z_s - z_b. \tag{11}$$

3 Depth Integrated Momentum Equation in the z-Direction

The integration in the z-direction of the vertical momentum equation differs from those in the horizontal directions by the fact that it is performed from an arbitrary z to z_s rather than from z_s to z_b. This is the crucial difference which led Boussinesq to equations different from those of Saint Venant. We now apply this integration to Eq. (4). Because the lower limit z of the vertical integral is now an independent variable, application of the Leibniz rule only involves the upper limit $z = z_s$, so that the equation analogous to (9) and (10) and solved for $\tau_{zz}(z)$ takes the form

$$\begin{aligned} p_{zz}(z) = {} & \rho g(h-\eta) - \rho w^2 \\ & + \rho \frac{\partial}{\partial t} \int_z^{z_s} w \, \mathrm{d}\zeta + \rho \frac{\partial}{\partial x} \int_z^{z_s} wu \, \mathrm{d}\zeta \\ & + \rho \frac{\partial}{\partial y} \int_z^{z_s} wv \, \mathrm{d}\zeta + \rho \int_z^{z_s} \left(\frac{\partial \tau_{xz}}{\partial x} + \frac{\partial \tau_{yz}}{\partial y} \right) \mathrm{d}\zeta, \end{aligned} \tag{12}$$

where the local elevation above the terrain is

$$\eta = z - z_b. \tag{13}$$

The above Eq. (12) is being viewed as an equation for $p_{zz}(z)$ as a function of the overburden pressure (first term on the right-hand side), the vertical velocity terms (the terms at the 2nd, 3rd, 4th and 5th position) and the integrated shear stress divergence (last term on the right-hand side). If $[H]$ and $[L]$ are vertical and horizontal length scales and $\varepsilon = [H/L]$ is small, only the first term on the right hand side survives—the hydrostatic pressure equation emerges. However, for $\varepsilon = O(1)$, Eq. (12) tells us that more than just the vertical acceleration terms (2, 3, 4, 5) on the right-hand side survive; the horizontal integrated stress divergence equally contributes to the vertical overburden pressure.

Equation (12) was not presented by Denlinger and Iverson [8] or Iverson [12], and it was first derived by Castro-Orgaz et al. [6]. Further, Denlinger and Iverson [8] neglected to derive an evolution equation for w to complete the depth- integrated

model, involving only u and v as variables, but not w. This was, however, done in water wave modeling by Nwogu [16] and Kim et al. [13]. The crucial idea is to vertically integrate the continuity equation (1) from z_b to an arbitrary elevation z, using the Leibniz rule and imposing the kinematic boundary condition at the basal surface, Eq. (5). This process yields, if $\partial z_b/\partial t = 0$,

$$w(z) = -\left\{ \frac{\partial}{\partial x} \int_{z_b}^{z} u \, \mathrm{d}\zeta + \frac{\partial}{\partial y} \int_{z_b}^{z} v \, \mathrm{d}\zeta \right\} \tag{14}$$

It states that once any functional representations for u and v are given, $w(z)$ is determined via the conservation of mass. Thus, w is linked to u and v; so, we may in Eq. (14) assume that $u = \bar{u}$ and $v = \bar{v}$, in which an overbar means depth averaging which later will be replaced by U and V, respectively. Alternatively, if we assume that (u, v) are independent of the $z-$coordinate, one easily deduces, with $\mathbf{u} = (\bar{u}, \bar{v})$, from relation (14) that

$$\begin{aligned} w(z) &= -\mathrm{Div}\left[\mathbf{u}(z - z_b)\right] \\ &= \left\{ (\bar{u}, \bar{v}) \cdot \left(\frac{\partial z_b}{\partial x}, \frac{\partial z_b}{\partial y} \right) \right\} - \left\{ \left(\frac{\partial \bar{u}}{\partial x} + \frac{\partial \bar{v}}{\partial y} \right) (z - z_b) \right\}. \end{aligned} \tag{15}$$

At $z = z_b$, one deduces from this relation the kinematic boundary condition of a rigid basal surface (the second term on the rhs in (15) vanishes in this case) and finds at $z = z_s$

$$w(z_s) = \left\{ (\bar{u}, \bar{v})_s \cdot \left(\frac{\partial z_b}{\partial x}, \frac{\partial z_b}{\partial y} \right) \right\} - \mathrm{Div}(\mathbf{u})h. \tag{16}$$

The reduced equation with the first term in braces on the right-hand side of (15) represents the influence of the kinematic boundary condition at z_b on $w(z)$; only the basal boundary condition is involved; the second term in braces says that the local horizontal velocity divergence reduces the basal vertical velocity by an amount which is proportional to the local material depth. Whether this contribution leads to growing w or decreasing w depends on the sign of Div$\mathbf{u}$. A qualitatively analogous behavior can also be inferred from (14) and (15) within the moving mass.

The plug flow assumption, for which u and v are depth independent, can also be implemented into Eqs. (8)–(10). This was done by Savage and Hutter [19] and many others (for a fairly complete literature review see Pudasaini and Hutter [18]) in the context of the shallow flow model, and by Iverson [12] in his more general context, in which no stretching of the coordinates was introduced. If we denote the depth averaged u- and v-velocity components by U and V and replace u and v everywhere by U and V, apply in the computations the property that they have no z-dependence, then the resulting equations can be expressed as a system of partial differential equations in general conservative form as

$$\frac{\partial \mathbf{U}}{\partial t} + \frac{\partial \mathbf{F}}{\partial x} + \frac{\partial \mathbf{G}}{\partial y} = \mathbf{S}, \tag{17a}$$

$$\mathbf{U} = \begin{pmatrix} h \\ Uh \\ Vh \end{pmatrix}, \quad \mathbf{F} = \begin{pmatrix} Uh \\ U^2h + \frac{1}{\rho}\int\limits_{z_b}^{z_s} p_{xx}\,\mathrm{d}\zeta \\ UVh + \frac{1}{\rho}\int\limits_{z_b}^{z_s} \tau_{xy}\,\mathrm{d}\zeta \end{pmatrix}, \quad \mathbf{G} = \begin{pmatrix} Vh \\ VUh + \frac{1}{\rho}\int\limits_{z_b}^{z_s} \tau_{xy}\,\mathrm{d}\zeta \\ V^2h + \frac{1}{\rho}\int\limits_{z_b}^{z_s} p_{yy}\,\mathrm{d}\zeta \end{pmatrix} \tag{17b}$$

$$\mathbf{S} = -\frac{1}{\rho}\begin{pmatrix} 0 \\ (\tau_{xx})_b \frac{\partial z_b}{\partial x} + (\tau_{xy})_b \frac{\partial z_b}{\partial y} - (\tau_{xz})_b \\ (\tau_{yy})_b \frac{\partial z_b}{\partial y} + (\tau_{xy})_b \frac{\partial z_b}{\partial x} - (\tau_{yz})_b \end{pmatrix}. \tag{17c}$$

In these equations, $\mathbf{U}$ is the dependent variable vector, a column matrix with three components; $\mathbf{F}$ and $\mathbf{G}$ are the fluxes in the x- and y-directions, respectively, and $\mathbf{S}$ is a source involving only basal stress terms. We also record Eq. (12) for the special case that the horizontal velocity components are independent of the z- coordinate

$$p_{zz} = \rho g\,(h-\eta) - \rho w^2 + \rho \frac{\partial}{\partial t}\int\limits_z^{z_s} w\,\mathrm{d}\zeta + \rho \frac{\partial}{\partial x}\left[U\int\limits_z^{z_s} w\,\mathrm{d}\zeta\right] + \rho \frac{\partial}{\partial y}\left[V\int\limits_z^{z_s} w\,\mathrm{d}\zeta\right] + \int\limits_z^{z_s}\left(\frac{\partial \tau_{zx}}{\partial x} + \frac{\partial \tau_{zy}}{\partial y}\right)\mathrm{d}\zeta. \tag{18}$$

Introducing the new quantities [13, 17]

$$\begin{aligned} I(z) &= \int\limits_z^{z_s} w(x,y,z)\,\mathrm{d}\zeta \\ &= -\int\limits_z^{z_s} \mathrm{Div}[\mathbf{u}(z-z_b)]\,\mathrm{d}\zeta = -\mathrm{Div}\left(\mathbf{u}\int\limits_z^{z_s}(z-z_b)\,\mathrm{d}\zeta\right) + \mathbf{u}h\cdot\mathrm{Grad}h \\ &= -\mathrm{Div}\left(\mathbf{u}\frac{h^2-\eta^2}{2}\right) + \mathbf{u}h\cdot\mathrm{Grad}h = -\mathrm{Div}(\mathbf{u})\frac{h^2-\eta^2}{2}, \end{aligned} \tag{19}$$

where $\mathbf{u} = (U, V)$. Equation (19) is a scalar quantity, and it may be shown with the aid of Eq. (15) that for z-independent U, V and when the shear stress divergence term in (18) is ignored,

$$p_{zz} = \rho g\,(h-\eta) + \rho\frac{\partial I}{\partial t} + \rho\mathrm{Div}\,(I\mathbf{u}) - \rho w^2, \tag{20}$$

in which Div and Grad are the two-dimensional horizontal divergence and gradient operators, already used in (15) and (16). Equations (19) and (20) together determine the overburden pressure at the vertical position z whenever the horizontal depth-averaged velocity components are known.

4 Boussinesq-Type Development for Water Flows

4.1 Water Waves on a Horizontal Bottom Surface Treated as an Ideal Fluid

An inviscid density preserving fluid (ρ = const.) does not support shear stresses; consequently, the last term in Eq. (18) drops out of the equation. Moreover, with $w(z)$ given by (14) and I by (19), we may deduce

$$w(z) = \mathrm{Div}(\mathbf{u})\eta, \qquad I(z) = -[\mathrm{Div}(\mathbf{u})]\frac{h^2-\eta^2}{2}, \tag{21}$$

from which we may obtain

$$I\mathbf{u} = -\mathrm{Div}(\mathbf{u})\mathbf{u}\frac{h^2-\eta^2}{2}, \tag{22}$$

and

$$\begin{aligned}\mathrm{Div}(I\mathbf{u}) &= -\mathrm{Div}\left[\mathbf{u}\mathrm{Div}(\mathbf{u})\frac{h^2-\eta^2}{2}\right] \\ &= [\mathrm{Div}(\mathbf{u})]^2\frac{h^2-\eta^2}{2} - \mathbf{u}\cdot\mathrm{Div}(\mathbf{u})h\mathrm{Grad}h - \mathbf{u}\mathrm{Grad}[\mathrm{Div}(\mathbf{u})]\frac{h^2-\eta^2}{2};\end{aligned} \tag{23}$$

so, we can compute

$$\begin{aligned}\frac{\partial I}{\partial t} &= -\mathrm{Div}\left(\frac{\partial \mathbf{u}}{\partial t}\right)\frac{h^2-\eta^2}{2} - \mathrm{Div}(\mathbf{u})h\frac{\partial h}{\partial t} \\ &= -\mathrm{Div}\left(\frac{\partial \mathbf{u}}{\partial t}\right)\frac{h^2-\eta^2}{2} + (\mathrm{Div}(\mathbf{u}))^2 h^2 + \mathrm{Div}(\mathbf{u})\mathbf{u}\cdot h\mathrm{Grad}h,\end{aligned} \tag{24}$$

in which $\partial h/\partial t$ has been replaced by $-\mathrm{Div}(\mathbf{u}h)$ via the mass balance (8).

The vertical normal stress p_{zz}, equivalent to the vertical pressure, can be evaluated using Eq. (20) and relations (22)–(24). This computation yields

$$\frac{p}{\rho} = \frac{p_{zz}}{\rho} = g(h-\eta) + \left\{ [\mathrm{Div}(\mathbf{u})]^2 - \mathrm{Div}\left(\frac{\partial \mathbf{u}}{\partial t}\right) - \mathbf{u}\cdot \mathrm{Grad}\,[\mathrm{Div}(\mathbf{u})] \right\} \frac{h^2-\eta^2}{2}, \tag{25}$$

or, since $\mathrm{Grad}\,[\mathrm{Div}(\mathbf{u})] = \mathrm{Div}\,[\mathbf{u}\mathrm{Div}(\mathbf{u})] - [\mathrm{Div}(\mathbf{u})]^2$,

$$\frac{p}{\rho} = g(h-\eta) + \left\{ 2\,[\mathrm{Div}(\mathbf{u})]^2 - \mathrm{Div}\left(\frac{\partial \mathbf{u}}{\partial t}\right) - \mathrm{Div}\,[\mathbf{u}\mathrm{Div}(\mathbf{u})] \right\} \frac{h^2-\eta^2}{2}. \tag{26}$$

For plane, one-dimensional waves both formulae reduce to

$$\left(\frac{p}{\rho}\right)_{\text{1-dim}} = g(h-\eta) + \left\{ \left(\frac{\partial U}{\partial x}\right)^2 - \frac{\partial^2 U}{\partial x \partial t} - U\frac{\partial^2 U}{\partial x^2} \right\} \frac{h^2-\eta^2}{2}, \tag{27}$$

given by Castro-Orgaz et al. [6], but first essentially presented by Serre [20].

To present the complete two-dimensional water wave model, let us explore equations (17) for an ideal fluid. Setting $\tau_{xy} = 0$ in those expressions and identifying $p_{xx} = p_{yy} = p_{zz} = p$, where p is given either in (25) or (26), we readily find

$$\mathbf{F} = \begin{pmatrix} Uh \\ g\frac{h^2}{2} + U^2 h + D \\ UVh \end{pmatrix}, \quad \mathbf{G} = \begin{pmatrix} Vh \\ VUh \\ V^2 h + g\frac{h^2}{2} + D \end{pmatrix}, \tag{28}$$

with

$$D = \left\{ [\mathrm{Div}(\mathbf{u})]^2 - \mathrm{Div}\left(\frac{\partial \mathbf{u}}{\partial t}\right) - \mathbf{u}\cdot \mathrm{Grad}\,[\mathrm{Div}(\mathbf{u})] \right\} \frac{h^3}{3}. \tag{29}$$

D as defined in (28) and (29) describes the dispersion. For $D = 0$ the partial differential equations reduce to the de Saint Venant equations. So, $D \neq 0$ accounts for the alterations of the Boussinesq model over the de Saint Venant model. Moreover, the source term in (17c) does not vanish when $z = z_b(x, y) \neq$ const. In addition, basal shear tractions could be accounted for if a boundary layer friction model is implemented. In that case one has

$$\mathbf{S} = -\frac{1}{\rho}\begin{pmatrix} 0 \\ (p)_b \frac{\partial z_b}{\partial x} + (\tau_{xy})_b \frac{\partial z_b}{\partial y} - (\tau_{xz})_b \\ (p)_b \frac{\partial z_b}{\partial y} + (\tau_{xy})_b \frac{\partial z_b}{\partial x} - (\tau_{yz})_b \end{pmatrix}, \tag{30}$$

where $(\tau_{xz}, \tau_{yz})_b = C(U, V)$, in which C is a drag coefficient. Here, the thin boundary layer dynamics is replaced by a viscous sliding law. The equations, which are based on Eqs. (28)–(30) are apt for use in estuarine and general lake dynamics. They

can optimally be used in numerical schemes, in which shock-capturing procedures are applied. Their one-dimensional version has originally been derived by Serre [20] and was further explored in hydraulic engineering e.g. by Basco [2], Soares-Frazao and Zech [21], Mohapatra and Chaudhry [15], and Chaudhry [7], among others.

4.2 Water Waves on a Horizontal Bottom Treated as a Newtonian Fluid

In wave problems of a viscous fluid, the shear stresses in Eqs. (17) and (18) cannot be dropped; so, strictly speaking, Eqs. (27)–(30) are invalid and the shear stress terms in (17) and (18) need to be parameterized. For a Newtonian fluid,

$$\tau_{ij} = \rho\nu(u_{i,j} + u_{j,i}) \quad \Rightarrow \quad \tau_{xy} = \tau_{yx} = \rho\nu\left(\frac{\partial u}{\partial y} + \frac{\partial v}{\partial x}\right). \tag{31}$$

Here, ν is the viscosity. When using a viscous linear sliding law, as in Eq. (6), then

$$(\tau_{xz})_b = Cu_b, \qquad (\tau_{yz})_b = Cv_b. \tag{32}$$

C is the drag coefficient of a viscous sliding law, see (6). The flux terms in (17) are, for a viscous fluid, chosen as

$$\frac{1}{\rho}\int_{z_b}^{z_b}(p_{xx}, p_{yy})(\zeta)\,\mathrm{d}\zeta = \frac{1}{\rho}\int_{z_b}^{z_s} p(\zeta)\,\mathrm{d}\zeta \tag{33}$$

$$\frac{1}{\rho}\int_{z_b}^{z_s}\tau_{xy}\,\mathrm{d}\zeta = \nu\int_{z_b}^{z_s}\left(\frac{\partial u}{\partial y} + \frac{\partial v}{\partial x}\right)(\zeta)\,\mathrm{d}\zeta = \nu\left\{\frac{\partial}{\partial y}\int_{z_b}^{z_s} u(\zeta)\,\mathrm{d}\zeta + \frac{\partial}{\partial x}\int_{z_b}^{z_s} v(\zeta)\,\mathrm{d}\zeta\right\}$$
$$-\left[u_s\frac{\partial z_s}{\partial y} - v_s\frac{\partial z_s}{\partial x}\right]_s + \left[u_b\frac{\partial z_b}{\partial y} - v_b\frac{\partial z_b}{\partial x}\right]_b, \tag{34a}$$

$$T_{xy}(z) = \frac{1}{\rho}\int_{z_b}^{z_s}\tau_{xy}\,\mathrm{d}\zeta = \nu\left\{\frac{\partial}{\partial y}(Uh) + \frac{\partial}{\partial x}(Vh) + V\frac{\partial h}{\partial x} - U\frac{\partial h}{\partial y}\right\}, \tag{34b}$$

in which the terms in brackets are due to the application of the Leibniz rule. For flow along a horizontal bed, $z_b = 0$, the last bracket in (34a) vanishes, and $z_s = h$. Moreover, for depth independent horizontal velocity components, (34a) takes the form (34b). In this formula we have also set $u_s = U$ and $v_s = V$ and ignored that the velocity in the basal boundary layer varies with depth. That contribution is accounted

for in the viscous sliding law by adjusting the drag coefficent C accordingly. Newtonian fluids do not exhibit any stress anisotropies, so that $p_{xx} = p_{yy} = p_{zz} = p$. This implies that p_{zz} is given by Eq. (18). Alternatively, this equally implies that the computations performed in Sect. 4.1 down to Eq. (24) remain valid, except that in the expression of p/ρ in Eq. (25) the term

$$\int_z^{z_s} \left(\frac{\partial \tau_{zx}}{\partial x} + \frac{\partial \tau_{zy}}{\partial y} \right) \mathrm{d}\zeta = \frac{\partial}{\partial x} \int_z^{z_s} \tau_{zx} \, \mathrm{d}\zeta + \frac{\partial}{\partial y} \int_z^{z_s} \tau_{zy} \, \mathrm{d}\zeta \tag{35}$$

must be added to Eq. (25). In obtaining the right-hand side of Eq. (35), the Leibniz rule was used and the zero surface traction condition was applied. Employing the sliding law (6), one may write

$$\tau_{zx}(0) = CU, \qquad \tau_{zy}(0) = CV, \tag{36}$$

where U and V are the z-independent horizontal velocity components outside the boundary layer; Eq. (36) are used to approximately model the shear stress distribution in the basal boundary layer. This distribution is modeled as

$$\tau_{zx}(z) = CUf(z), \qquad \tau_{zy}(z) = CVf(z), \tag{37}$$

in which the function $f(z)$ satisfies the conditions

$$f(z = 0) = 1, \quad f(z = \delta) = 0, \quad f'(z = \delta) = 0, \quad \text{and} \quad \delta = \alpha h, \tag{38}$$

with $0 \leq \alpha < 1$ and δ as the boundary layer thickness. A popular choice is $\alpha = 1$ and $f(z) = z/h$, but this is not in conformity with the boundary layer structure of the shear stresses, and violates $f'(h) = 0$, which is less severe, however. A better choice is proposed below. Adequate choices for $f(z)$ and C should deliver a model for the boundary layer transition from the base, $z_b = 0$, to the outer edge of the boundary layer. For $z > \delta$ we set $\tau_{zx} = \tau_{zy} = 0$, in conformity with the z-independence of the (x, y)-velocity. Formula (35) now yields

$$\int_z^{z_s} \tau_{zx}(\zeta) \, \mathrm{d}\zeta = \begin{cases} 0, & z > \delta, \\ \int_z^{\delta} CUf(\zeta) \, \mathrm{d}\zeta = CU \int_z^{\delta} f(\zeta) \, \mathrm{d}\zeta, & 0 < z \leq \delta, \end{cases} \tag{39a}$$

$$\int_z^{z_s} \tau_{zy}(\zeta) \, \mathrm{d}\zeta = \begin{cases} 0, & z > \delta, \\ \int_z^{\delta} CVf(\zeta) \, \mathrm{d}\zeta = CV \int_z^{\delta} f(\zeta) \, \mathrm{d}\zeta, & 0 < z \leq \delta. \end{cases} \tag{39b}$$

With the notation

$$\mathbf{T} = (T_x, T_y) = \int_z^{z_s} (\tau_{zx}, \tau_{zy})\, \mathrm{d}\zeta, \tag{40}$$

Equations (39a), (39b) imply

$$\mathrm{Div}\mathbf{T}(z) = \begin{cases} 0, & z > \delta, \\ \mathrm{Div}\left[C\mathbf{u} \int_z^{\delta} f(\zeta)\, \mathrm{d}\zeta \right], & 0 \le z < \delta. \end{cases} \tag{41}$$

With these results the normal stress Eq. (18) can now be composed by resort to Eqs. (26) and (41). The result is

$$\begin{aligned} p(z) &= p_{zz}(z) \\ &= \rho g(h-\eta) + \left\{ 2\left[\mathrm{Div}(\mathbf{u})\right]^2 - \mathrm{Div}\left(\frac{\partial \mathbf{u}}{\partial t}\right) - \frac{1}{2}\mathrm{Div}\left[\mathbf{u}\mathrm{Div}(\mathbf{u})\right] \right\} (h^2 - \eta^2) \\ &\quad + \begin{cases} 0, & z > 0, \\ \mathrm{Div}\left[C\mathbf{u} \int_z^{\delta} f(\zeta) \mathrm{d}\zeta \right], & 0 \le z < \delta. \end{cases} \end{aligned} \tag{42}$$

With the above results one obtains for the conservative system of partial differential equations (17) when the bottom is flat, $z_b = 0$,

$$\mathbf{F} = \begin{pmatrix} Uh \\ g\frac{h^2}{2} + U^2 h + D^v \\ UVh + T_{xy}^v \end{pmatrix}, \mathbf{G} = \begin{pmatrix} Vh \\ VUh + T_{xy}^v \\ V^2 h + g\frac{h^2}{2} + D^v \end{pmatrix}, \mathbf{S} = \mathbf{S}^v = \frac{1}{\rho} \begin{pmatrix} 0 \\ CU \\ CV \end{pmatrix}, \tag{43}$$

in which the source term reduces to the viscous component $\mathbf{S}^v$, and the term D^v is made of the dispersion term plus a viscous contribution

$$\begin{aligned} D^v &= D + \int_{z_b}^{z_s} \left[\mathrm{Div}\mathbf{T}(z)\right]\, \mathrm{d}\xi = D + \int_0^{z_s} \left(\mathrm{Div}(C\mathbf{u}) \int_z^{z_s} f(\zeta)\, \mathrm{d}\zeta \right)\, \mathrm{d}\xi \\ &= D + \mathrm{Div}(C\mathbf{u}) \int_0^h \int_z^{\delta} f(\zeta)\, \mathrm{d}\zeta\, \mathrm{d}\xi, \end{aligned} \tag{44}$$

with D as given in (29).

The first and second terms in the second row of **F** and the first term in the third row of **F** in expression (43) (and similar terms in **G** but with rows interchanged) are the x- and y-momentum fluxes of an ideal fluid in the approximation of de Saint Venant. D^{ν}consists of two contributions as shown in (44). The first part, D amends the equations to the Boussinesq equations for an ideal fluid and the second term depends on the shear stress (boundary layer) profile $f(z)$ and vanishes if $C = 0$ or/and $f(z) = 0$. Therefore, this term is responsible for the viscous effect of the fluid and the frictional sliding effects as expressed in the deviation of the vertical pressure distribution from that of an ideal fluid. Moreover, T^{ν}_{xy} accounts for the viscous in-plane shear stress τ_{xy} as given in Eq. (34b). The superscript ν is a label for viscous effects. The above notation, therefore, clearly identifies the various sources of the individual terms. When $D^{\nu} = 0$, $T^{\nu}_{xy} = 0$ and $\mathbf{S} = \mathbf{0}$, Eq. (17) with the thus reduced expressions (43) describe the two-dimensional Saint Venant equations for an inviscid fluid. When $D^{\nu} = 0$, $T^{\nu}_{xy} = 0$ and $\mathbf{S} = \mathbf{0}$, the emerging equations are the two-dimensional Boussinesq-type equations for the wave-like motion of an inviscid density preserving fluid; and the remaining terms are of Newtonian viscous origin. To complete this mode, an explicit expression for the boundary layer function $f(z)$ is needed. The choice

$$f(z) = (1 - z/\delta)^n, \quad n > 1, \quad \delta = \alpha h \tag{45}$$

satisfies the boundary conditions (38) and yields

$$\int_z^{\delta} f(\zeta)\,\mathrm{d}\zeta = \int_z^{\delta} \left(1 - \frac{\zeta}{\delta}\right)^n \mathrm{d}\zeta = \frac{\delta}{n+1}\left(1 - \frac{z}{\delta}\right)^{n+1} = \frac{\alpha h}{n+1}\left(1 - \frac{z}{\alpha h}\right)^{n+1}, \tag{46}$$

$$\int_0^h \int_z^{\delta} f(\zeta)\,\mathrm{d}\zeta\,\mathrm{d}z = \frac{\delta^2}{(n+1)(n+2)}. \tag{47}$$

Accordingly, two parameters suffice to model the boundary layer profile.

5 Boussinesq-Type Extension of the Savage-Hutter Equations

5.1 The Savage-Hutter (S-H) Theory

The fundamental equations for a non-hydrostatic dry granular model with enhanced gravity are Eqs. (8), (9) and (10); moreover, when the horizontal velocity components

$(u, v) = (U, V)$ are z-independent, Eqs. (17) and (18) hold in that form, as long as the basal and free surfaces are material. The decisive assumption is that the integral

$$\int_{z_b}^{z_s} \tau_{xy}\, \mathrm{d}\zeta$$

is ignored in the flux and source terms of equations (17b), (17c) in comparison to the remaining terms. It then follows that closure relations have to be postulated only for p_{xx} and p_{yy}. This means physically that τ_{xy} is small in comparison to p_{xx} and p_{yy}. Greve et al. [9] and Koch et al. [14] demonstrate that p_{yy} is close to a principal stress on planes orthogonal to the basal topography. Alternatively, this says also that the flow is nearly unidirectional in the principal flow direction. Within the context of the Mohr-Coulomb earth pressure theory, it is customary to introduce the earth pressure coefficients

$$K_x = \frac{p_{xx}}{p_{zz}}, \qquad K_y = \frac{p_{yy}}{p_{zz}} \tag{48}$$

to account for the normal stress anisotropy, typical for soil mass behavior. The pressure $p_{zz}(z)(= \tau_{zz}(z))$ is given by Eq. (12), in which, in a first approximation, the shear stress integral has been ignored in the one-dimensional treatment by Denlinger and Iverson [8] as well as the otherwise exact ensuing one- dimensional analysis by Castro-Orgaz et al. [6].

The closure procedure of the SH-avalanche model is intimately related to an assumed hydrostatic pressure assumption and cannot rationally be extended to a Boussinesq-type generalization as already seen by Castro-Orgaz et al. [6]. In this paper we shall confine attention to the spatially one-dimensional plane flow. The idea is that the integrated shear divergence term in Eq. (12) should be accounted for. Equation (12) expresses the fact that in a Boussinesq-type extension of the SH-model the hydrostatic (vertical) pressure distribution $p_{zz} = \rho g(h - \eta)$ is corrected according to Eq. (12) by the $z-$integrated vertical acceleration *plus* the integrated stress divergence, which both are considered important in such extensions.

5.2 One-Dimensional Non-hydrostatic Granular Flow Model

The difficulties outlined in the above paragraphs become already evident in steady plane waves of a granular material. This case was analyzed by Castro-Orgaz et al. [6]—though in an approximate manner only. These authors account in their analysis for the vertical acceleration term, but ignore the contribution by the shear stress term τ_{zx}. Specifically, on a flat horizontal plate, $z_b = 0$, $\eta = z$, Eqs. (15), (19), (22) and (20) [in (20) the last stress divergence term in (18) is not dropped] transform in one-dimensional flow into

$$
\begin{aligned}
w &= -U_x z \quad \Rightarrow \quad w^2 = U_x^2 z^2, \quad \text{from(15)},\\
I &= -U_x \frac{h^2 - z^2}{2}, \qquad\qquad\quad \text{from(19)},\\
IU &= -U U_x \frac{h^2 - z^2}{2}, \qquad\qquad\quad \text{from(22)},\\
\tau_{zz} &= p_{zz} = \rho g(h - z) + \rho \frac{\partial I}{\partial t} + \rho (IU)_x - \rho w^2 + \int\limits_z^h \frac{\partial \tau_{zx}}{\partial x}(\zeta)\, \mathrm{d}\zeta, \qquad \text{from(20)},
\end{aligned}
\tag{49}
$$

in which the subscript x, ν denotes differentiation with respect to x, ν. Applying the Leibniz rule in the fourth of Eqs. (49) for the shear stress integral, and imposing the zero traction condition at $z = h$ yields

$$
\int\limits_z^h \frac{\partial \tau_{zx}}{\partial x}(\zeta)\, \mathrm{d}\zeta = \frac{\partial}{\partial x} \int\limits_z^h \tau_{zx}(\zeta)\, \mathrm{d}\zeta. \tag{50}
$$

Moreover, let us now search for a permanent (form preserving) wave in a co-moving coordinate system (Galilei transformation!); then in this new coordinate system we get

$$
\frac{\partial(\cdot)}{\partial t} = 0, \quad \left(\frac{\partial I}{\partial t} = 0\right) \text{ and } q = Uh = \text{const.}, \tag{51}
$$

so that

$$
U = \frac{q}{h}, \quad U_x = -q \frac{h_x}{h^2}, \quad U_{xx} = -q \left\{ \frac{h_{xx}}{h^2} - \frac{2h_x^2}{h^3} \right\}. \tag{52}
$$

From the fourth of Eqs. (49) on may deduce

$$
\frac{\tau_{zz}}{\rho} = \frac{p_{zz}}{\rho} = g(h - z) + (IU)_x - w^2 + \frac{1}{\rho} \frac{\partial}{\partial x} \left(\int\limits_z^h \tau_{zx}(\zeta)\, \mathrm{d}\zeta \right). \tag{53}
$$

With IU as given by the third of Eq. (49) and with expressions (52)

$$
\begin{aligned}
(IU)_x &= -\left[U U_x^2 + U U_{xx} \right] \frac{h^2 - z^2}{2} - U U_x h h_x\\
&= -\left[\frac{q^2}{h^2} h_x^2 - \frac{q^2}{h} \left(\frac{h_{xx}}{h^2} - \frac{2h_x^2}{h^3} \right) \right] \frac{h^2 - z^2}{2} + \frac{q^2}{h^2} h_x^2.
\end{aligned}
\tag{54}
$$

Substituting this and the first of Eq. (48) into Eq. (53) and integrating the resulting expression from $z = 0$ to $z = h$ merges into

$$\int_0^h \frac{p_{zz}}{\rho}\,\mathrm{d}z = \left\{\frac{gh^2}{2} + \frac{q^2}{2}\frac{hh_{xx} - h_x^2}{3}\right\} + \frac{1}{\rho}\frac{\partial}{\partial x}\int_0^h z\tau_{zx}(z)\,\mathrm{d}z. \tag{55}$$

The last term in this expression is obtained as follows

$$\begin{aligned}
&\frac{1}{\rho}\int_z^h \frac{\partial}{\partial x}\left(\int_z^h \tau_{zx}(\zeta)\,\mathrm{d}\zeta\right)\mathrm{d}z = \frac{1}{\rho}\frac{\partial}{\partial x}\int_0^h \mathrm{d}z\int_z^h \tau_{zx}(\zeta)\,\mathrm{d}\zeta - \left(\int_z^h \tau_{zx}(\zeta)\,\mathrm{d}\zeta|^{z=h}\right)\frac{\partial h}{\partial x}\\
&= \frac{1}{\rho}\frac{\partial}{\partial x}\int_0^h \left(\int_z^h \tau_{zx}(\zeta)\,\mathrm{d}\zeta\right)\mathrm{d}z = \frac{1}{\rho}\frac{\partial}{\partial x}\left\{\left[z\int_z^h \tau_{zx}(\zeta)\,\mathrm{d}\zeta\right]\Bigg|_{z=0}^{z=h} - \left[\int_0^h z(-\tau_{zx}(z))\,\mathrm{d}z\right]\right\}\\
&= \frac{1}{\rho}\frac{\partial}{\partial x}\int_0^h z\tau_{zx}(z)\,\mathrm{d}z.
\end{aligned} \tag{56}$$

In the first line the Leibniz rule for the integration of a differentiated function is employed and boundary conditions are then implemented, whilst in the second line integration by parts is used. The first term of Eq. (55) in braces has also been obtained by Castro-Orgaz et al. [6] and is due to the vertical acceleration, originally motivated by Denlinger and Iverson [8] [but these authors have the factor 1/4 instead of 1/3 in the second term of Eq. (55), because of an approximate parameterization of $w(z)$, see Castro-Orgaz et al. [6] for a more detailed discussion]. The last term on the right-hand side of Eq. (55) is missing by both Denlinger and Iverson [8] and Castro-Orgaz et al. [6]. It is due to the stress divergence term in Eq. (18).

The crucial statements are Eqs. (53) and (55) and the x-component of the momentum equation (17), which reduces here for 1D steady flow to

$$\frac{\partial}{\partial x}(U^2 h) + \frac{\partial}{\partial x}\int_0^h \frac{p_{xx}(z)}{\rho}\,\mathrm{d}z = \frac{(\tau_{zx})_b}{\rho}. \tag{57}$$

With the Coulomb anisotropic earth pressure postulate

$$p_{xx}(z) = K p_{zz}(z), \tag{58}$$

where K = const., and the Mohr-Coulomb basal sliding law of the Savage-Hutter model

$$\frac{(\tau_{zx})_b}{\rho} = -\frac{(p_{zz})_b}{\rho}\mathrm{sgn}(U)\tan(\phi_{bed}), \tag{59}$$

in which ϕ_{bed} is the bed friction angle, Eq. (57) assumes the form

$$\frac{\partial}{\partial x}(U^2 h) + K\frac{\partial}{\partial x}\int_0^h \frac{p_{zz}(z)}{\rho}\,\mathrm{d}z = -\frac{(p_{zz})_b}{\rho}\mathrm{sgn}(U)\tan(\phi_{bed}), \tag{60}$$

or

$$\frac{\partial}{\partial x}(U^2 h) + K\frac{\partial}{\partial x}\left\{\left(\frac{gh^2}{2}\right) + \frac{q^2}{2}\frac{hh_{xx}-h_x^2}{3} + \frac{\partial}{\partial x}\int_0^h z\frac{\tau_{zx}}{\rho}(z)\,\mathrm{d}z\right\}$$
$$= \left\{-gh + \left[\frac{q^2}{h^2}h_x^2 - \frac{q^2}{h}\left(\frac{h_{xx}}{h^2} - \frac{2h_x^2}{h^3}\right)\right]\frac{h^2}{2} + \frac{q^2}{h^2}h_x^2 - \frac{1}{\rho}\frac{\partial}{\partial x}\left(\int_0^h \tau_{zx}(z)\,\mathrm{d}z\right)\right\} K\,\mathrm{sgn}(U)\tan(\phi_{bed}). \tag{61}$$

Savage and Hutter [19] have shown that for plane flow

$$K = K_{\text{pas.act.}} = 2\sec^2(\phi_{int})\left\{1 \pm \left[1 - (\cos^2\phi_{int})(\sec(\phi_{bed}))^{\frac{1}{2}}\right]\right\} - 1, \tag{62}$$

in which ϕ_{int} is the constant angle of internal friction.

Equation (61) describes a steady unilateral granular flow along a horizontal bed, when vertical accelerations and the frictional shear stresses τ_{zx} as well as basal frictional resistance are accounted for. The shear stress τ_{zx} as a function of z and the bed friction in the source term were omitted by Castro-Orgaz et al. [6]. Equation (61), subjected to the condition that q = const., then implies if shear stresses are neglected too (source term neglected)

$$Kg\frac{h^2}{2} + \frac{q^2}{h}\left(1 + K\frac{hh_{xx}-h_x^2}{3}\right) = \text{const}, \tag{63}$$

which agrees with the result of Castro-Orgaz et al., in their Eq. (56). For $K = 1$ this statement reduces to the result of potential fluid cnoidal waves, see e.g. Hager and Hutter [10, 11]. Momentum flux is not conserved in Eq. (61) as it is in Eq. (63). This conservation is destroyed by diffusion (last term in braces on the left-hand side) and annihilated by the source term on the right-hand side. To see whether permanent solutions exist in this case, the vertical shear stress integrals must be evaluated by parametrizing the shear stress τ_{zx}. In a first attempt a linear distribution with z may be postulated

$$\tau_{zx}(z) = (\tau_{zx})_b\left(1 - \frac{z}{h}\right) \tag{64}$$

implying

$$\int_0^h \tau_{zx}(z)\,\mathrm{d}z = (\tau_{zx})_b \frac{h}{2}, \qquad \int_0^h z\tau_{zx}(z)\,\mathrm{d}z = (\tau_{zx})_b \frac{h^2}{6}, \tag{65}$$

with $(\tau_{zx})_b$ given in (59).

An alternative closure relation for τ_{zx} can be motivated by imposing a boundary layer profile as suggested previously.

6 Discussion and Conclusion

In this paper the simplest possible dynamic problems for ideal and viscous fluids and rapid granular flows have been looked at, which mathematically emerge, when channelized or avalanching flows are scrutinized with depth averaged balance laws of mass and momentum without imposition of the shallowness assumption. This means that horizontal and vertical length scales may be of comparable size. This corresponds in fluid dynamics to a replacement of the De Saint Venant equations by Boussinesq-type equations, as stated here in Eq. (17). Physically, to surrender the shallowness assumption implies that vertical convective acceleration terms *and* the horizontal divergence of the shear stresses as shown in Eq. (12) compete with the vertical gravity gradient.

In the work of the pioneers, Barré de Saint Venant [1], Serre [20], Benjamin and Lighthill [3], as well as Hager and Hutter [10, 11] and Castro-Orgaz et al. [6], and in granular flow problems by Denlinger and Iverson [8], these stress divergence terms were ignored both in situations of laminar viscous flows and in turbulent modeling attempts where such omissions are a bit doubtful.

In this paper, the above mentioned simplification was not made *ab initio*. In Sect. 4 it was demonstrated that in an inviscid potential flow the stress divergence term is absent in the Boussinesq-type equations and Saint Venant equations would be corrected in the Boussinesq-type extension by the vertical acceleration terms alone. Here, the only simplifying assumption that is generally implemented is the z-independence of the horizontal velocity components. In the emerging terms one may—and we have done so—incorporate a basal friction law even though this is conceptually in violation with the assumption of a potential flow.

In our attempt of applying the depth integrated dynamical equations to a Newtonian fluid it turned out, see Eq. (43), that the contribution to the flux of the two-dimensional depth averaged motion is expressed in two different terms: (i) D^{ν}, which comprises of a contribution due to the vertical acceleration and a stress divergence of diffusive nature due to the boundary layer close to the base and (ii) a sliding source term at the base. The choice of our sliding law does not allow imposition of the no-slip boundary condition. This is only approximately possible in the limit as C in Eq. (6) becomes large.

The implementation of the frictional stress components in the dynamical Savage-Hutter equations is more difficult. We thus, restricted attention to the one-dimensional case, and also were only looking at the situation of a steady state wave situation. Its extension under inclusion of the stress divergence term culminates in the longitudinal momentum equation (61) and shows that, when applying the Coulomb normal stress anisotropy postulation paired with the Mohr-Coulomb basal sliding law, the vertical shear stress component must still be assumed in an *ad-hoc* assumption. With it, a complete model for a permanent non-linear wave follows from Eqs. (58), (59), (60) and $q = \text{const}$. Existence of solutions to this set of equations has so far not been demonstrated. This demonstration is, however, important, because the reduced model of Castro-Orgaz et al. [6] demonstrated this existence for the reduced model.

It turns out that the time dependent one-dimensional and two-dimensional Boussinesq-type models are yet more difficult in terms of the complexity of their governing equations. They will likely be the subject of a further study.

Acknowledgments This work is based in parts on a detailed report by Castro-Orgaz et al. [6]. K. H. thanks PD Dr.-Ing. Bettina Albers at the Technical University Berlin for support in November 2014. He also thanks Dr. David Vetsch, at the Laboratory of Hydraulics, Hydrology and Glaciology, at ETHZ for constructive help in the generation of the final text. We also thank an unknown referee for his/her work and Benedikt Preugschat for translating our Word file into LaTeX. K. H. dedicates this research article to the memory of his friend Prof. Krzyzstof Wilmanski (1940–2012). We knew each other for nearly 40 years since 1974 and had many challenging professional interactions through 4 decades.

References

1. Barré de Saint Venant, A.J.C.: Théorie du mouvement non permanent des eaux, avec application aux crues des riviéres et á l'introduction des marrées dans leur lit. (Theory of unsteady water movement, applied to floods in rivers and the effect of tidal flows). Comptes Rendus de l'Académie des Sciences 73, 147–154; 73, 237–240 (1871) [in French]
2. Basco, D.R.: Computation of rapidly varied unsteady, free surface flows. U.S. geological survey, Water-Resources Investigation Report 83–4284, Reston Virginia, 1–64 (1983)
3. Benjamin, T.B., Lighthill, M.J.: On cnoidal waves and bores. Proc. Roy. Soc. Lond. Ser. A **224**, 448–460 (1954)
4. Boussinesq, J.: Théorie des ondes et des remous qui se propagent le long d'un canal rectangulaire horizontal, en communiquant au liquide contenu dans ce canal des vitesses sensiblement pareilles de la surface au fond (Theory of waves and disturbances propagating along a rectangular horizontal channel, generating nearly uniform velocities from the surface to the bottom). J. Mathématique Pures et Appliqués, Série 2, 17, 55–108 (1872) [in French]
5. Boussinesq, J.: Essai sur la théorie des eaux courantes. Mémoires présentés par divers savants á l'Académie des Sciences, Paris **23**, 1–680 (1877). [in French]
6. Castro-Orgaz, O., Hutter, K., Giráldez, J.V., Hager, W.H.: Non-hydrostatic granular flow over 3D terrain: new Boussinesq-type gravity waves? J. Geophys. Res.-Earth Surf. 120(1), 1–28 (2015)
7. Chaudhry, M.H.: Open-Channel Flow, 2nd edn. Springer, Berlin (2008)
8. Denlinger, R.P., Iverson, R.M.: Granular avalanches across irregular three-dimensional terrain: 1. Theory and computation. J. Geophys. Res. **109**(F1), F01014 (2004). doi:10.1029/2003JF000085

9. Greve, R., Koch, Th, Hutter, K.: Unconfined flow of granular avalanches along partly curved surfaces. I: Theory. Proc. R. Soc. Lond., A 445, 399–413 (1994)
10. Hager, W.H., Hutter, K.: Approximate treatment of plane channel flow. Acta Mech. **51**(3–4), 31–48 (1984)
11. Hager, W.H., Hutter, K.: On pseudo-uniform flow in open channel hydraulics. Acta Mech. **53**(3–4), 183–200 (1984)
12. Iverson, R.M.: Debris-flow mechanics. In: Jakob, M., Hungr, O. (eds.) Debris Flow Hazards and Related Phenomena, pp. 105–134. Springer-Praxis, Heidelberg (2005)
13. Kim, D.-H., Lynett, P.J., Socolofsky, S.: A depth-integrated model for weakly dispersive, turbulent, and rotational fluid flows. Oc. Model. **27**(3–4), 198–214 (2009)
14. Koch, Th, Greve, R., Hutter, K.: Unconfined flow of granular avalanches along partly curved surfaces. II: experiments and numerical computations. Proc. R. Soc. Lond., A 445, 415–435 (1994)
15. Mohapatra, P.K., Chaudhry, M.H.: Numerical solution of Boussinesq equations to simulate dam-break flows. J. Hydraul. Engng. **130**(2), 156–159 (2004)
16. Nwogu, O.: Alternative form of Boussinesq equations for nearshore wave propagation. J. Waterw., Port., Coast. Oc. Engng. 119(6), 618–638 (1993)
17. Peregrine, D.H.: Long waves on a beach. J. Fluid Mech. **27**(5), 815–827 (1967)
18. Pudasaini, S.P., Hutter, K.: Avalanche Dynamics. Springer, Berlin (2007)
19. Savage, S.B., Hutter, K.: The motion of a finite mass of granular material down a rough incline. J. Fluid Mech. **199**, 177–215 (1989)
20. Serre, F.: Contribution á l'étude des écoulements permanents et variables dans les canaux (Contribution to the study of steady and unsteady channel flows). La Houille Blanche 8(6–7), 374–388; 8(12), 830–887 (1953) [in French]
21. Soares-Frazão, S., Zech, Y.: Undular bores and secondary waves: experiments and hybrid finite-volume modelling. J. Hydraul. Res. **40**(1), 33–43 (2002)

A Mixture Theory of Porous Media and Some Problems of Poroelasticity

I-Shih Liu

Abstract Based on the theory of an elastic solid-fluid mixture and the concept of volume fraction, a theory of porous media can be formulated consistent with basic characteristics in soil mechanics, such as Darcy's law, uplift force, and the effective stress principle. Boundary value problem for different models of poroelasticity can be considered depending on the assumptions of incompressibility of solid or fluid constituents. From the consideration of acceleration waves, there are two longitudinal waves in general, except for the model with both incompressible solid and fluid constituents, which admit only one longitudinal wave as known in the literature.

1 An Elastic Solid-Fluid Mixture

For a continuum theory of mixture, all constituents are supposed to be able to occupy the same region of space simultaneously. Let $\mathscr{B}_\alpha$ denote the constituent α and κ_α be its reference configuration and denote $B_\alpha = \kappa_\alpha(\mathscr{B}_\alpha)$. The motion of $\mathscr{B}_\alpha$ is a smooth mapping,

$$\chi_\alpha : B_\alpha \times \mathbb{R} \to \mathbb{E}, \qquad x = \chi_\alpha(X_\alpha, t), \quad X_\alpha \in B_\alpha.$$

It states that for different motion of each constituent, at the instant t, there is a material point $X_\alpha \in \mathscr{B}_\alpha$ in each constituent, $X_\alpha = \kappa_\alpha(X_\alpha)$, that occupies the same spatial position x in the Euclidean space $\mathbb{E}$. The velocity and the deformation gradient of each constituent are defined as

$$v_\alpha = \frac{\partial}{\partial t}\chi_\alpha(X_\alpha, t), \qquad F_\alpha = \nabla_{X_\alpha}\chi_\alpha(X_\alpha, t).$$

In memory of Professor Krzysztof Wilmanski

I.-S. Liu (✉)
Instituto de Matemática, Universidade Federal do Rio de Janeiro, Rio de Janeiro, Brazil
e-mail: liu@im.ufrj.br

B. Albers and M. Kuczma (eds.), *Continuous Media with Microstructure 2*,
DOI 10.1007/978-3-319-28241-1_18

We consider a non-reacting solid-fluid mixture (α = s,f) with the following balance equations of the partial mass and the partial linear momentum of each constituent, and the energy equation of the mixture:

$$\begin{aligned}
&\overset{\cdot}{\rho}_s + \rho_s \operatorname{div} v_s = 0,\\
&\overset{\cdot}{\rho}_f + \rho_f \operatorname{div} v_f = 0,\\
&\rho_s \overset{\cdot}{v}_s - \operatorname{div} T_s + m_f = \rho_s b_s,\\
&\rho_f \overset{\cdot}{v}_f - \operatorname{div} T_f - m_f = \rho_f b_f,\\
&\rho \dot{\varepsilon} + \operatorname{div} q - \operatorname{tr}(T \operatorname{grad} v) = \rho r,
\end{aligned} \tag{1}$$

where ρ_s, ρ_f are the partial mass densities; T_s, T_f are the partial Cauchy stresses; m_f is the interactive force on the fluid constituent; ε, q are the internal energy density and the heat flux of the mixture. The material derivatives with respect to the constituent and the mixture have been used,

$$\overset{\cdot}{y}_\alpha = \frac{\partial y_\alpha}{\partial t} + (\operatorname{grad} y_\alpha) v_\alpha, \qquad \dot{y} = \frac{\partial y}{\partial t} + (\operatorname{grad} y) v.$$

To establish field equations of the basic field variables, $\{\rho_s, \rho_f, \chi_s, \chi_f, \theta\}$, constitutive equations for the quantities in the balance equations,

$$f = \{T_s, T_f, \varepsilon, q, m_f\}, \tag{2}$$

must be specified. For an elastic solid-fluid mixture, we consider the constitutive equations of the form:

$$f = \mathscr{F}(\theta, \rho_f, F_s, \operatorname{grad}\theta, \operatorname{grad}\rho_f, \operatorname{grad} F_s, V). \tag{3}$$

where θ is the temperature and $V = v_f - v_s$ is referred to as the relative velocity.

Thermodynamic considerations of such a mixture theory has been considered by Bowen [1] in which consequences of the entropy principle have been analyzed with Coleman-Noll procedure to obtain general restrictions on the constitutive equations. These results have been confirmed from the analysis with the use of Lagrange multipliers by Liu in [7], and can be summarized in the following constitutive equations:

$$\begin{aligned}
T_f &= \rho_f \psi_f I - \frac{\partial \rho \psi_I}{\partial \rho_f} \rho_f I + \rho_f \frac{\partial \psi_f}{\partial V} \otimes V,\\
T_s &= \rho_s \psi_s I + \frac{\partial \rho \psi_I}{\partial F_s} F_s^T + \rho_s \frac{\partial \psi_s}{\partial V} \otimes V,
\end{aligned}$$

$$\begin{aligned}\varepsilon &= \psi_I - \theta\frac{\partial\psi_I}{\partial\theta} + \frac{1}{2}\frac{\rho_f\rho_s}{\rho^2}V\cdot V,\\ m_f^0 &= \frac{\partial\rho_s\psi_s^0}{\partial\rho_f}\,\text{grad}\;\rho_f - \frac{\partial\rho_f\psi_f^0}{\partial F_s}\cdot\,\text{grad}\,F_s, \qquad q^0 = 0.\end{aligned} \tag{4}$$

where $_0$, denotes the equilibrium value at the state with $V = 0$ and grad $\theta = 0$.

These constitutive equations depend solely on the constitutive functions of the free energy,

$$\begin{aligned}&\psi_f = \psi_f(\theta, \rho_f, F_s, V), \qquad \psi_s = \psi_s(\theta, \rho_f, F_s, V),\\ &\psi_I = \psi_I(\theta, \rho_f, F_s).\end{aligned} \tag{5}$$

Note that although the partial free energies ψ_f and ψ_s may depend on the relative velocity V, the (inner) free energy ψ_I,

$$\rho\psi_I = \rho_f\psi_f + \rho_s\psi_s,$$

does not depend on V.

Moreover, from (4) and (5), the sum of partial stresses becomes

$$\begin{aligned}T_I &= \rho\psi_I I - \frac{\partial\rho\psi_I}{\partial\rho_f}\rho_f I + \frac{\partial\rho\psi_I}{\partial F_s}F_s^T,\\ T &= T_I(\theta, \rho_f, F_s) - \frac{1}{2}\frac{\rho_s\rho_f}{\rho}V\otimes V.\end{aligned} \tag{6}$$

Similarly, although the partial stresses T_f and T_s may depend on V, the sum of partial stress, $T_I = T_f + T_s$, does not depend on V.

If we define the equilibrium partial fluid pressure as

$$p_f = \rho_f\Big(\frac{\partial\rho\psi_I}{\partial\rho_f} - \psi_f^0\Big), \tag{7}$$

then the equilibrium fluid stress reduces to the pressure, $T_f^0 = -p_f I$, and

$$T_f = -p_f\, I + \rho_f(\psi_f - \psi_f^0)I + \rho_f\frac{\partial\psi_f}{\partial V}\otimes V, \tag{8}$$

and from $(4)_4$ and (7), the interaction force can be written as

$$m_f^0 = \frac{p_f}{\rho_f}\,\text{grad}\;\rho_f - \rho_f(\text{grad}\;\psi_f^0)\Big|_0. \tag{9}$$

Note that the definition of equilibrium fluid pressure in (7) implies the usual relation for a pure fluid,

$$p = \rho^2 \frac{\partial \psi}{\partial \rho}. \tag{10}$$

2 Saturated Porous Media

The solid-fluid mixture considered in the previous section can be regarded as a model for saturated porous media provided that the concept of porosity is introduced. For mixture theory of porous media, a material point is regarded as a representative volume element dV which contains pores through them fluid constituent can flow. Physically, it is assumed that a representative volume element is large enough compare to solid grains (connected or not), yet at the same time small enough compare to the characteristic length of the material body.

Let the volume fraction of pores be denoted by ϕ, then for a saturated porous medium, the volume fractions of the fluid and the solid are

$$dV_f = \phi\, dV, \qquad dV_s = (1-\phi) dV.$$

Remember that in the mixture theory, the mass densities are defined relative to the mixture volume, so that the fluid and solid mass in the representative volume element are given by

$$dM_f = \rho_f\, dV = d_f\, dV_f, \qquad dM_s = \rho_s\, dV = d_s\, dV_s,$$

and hence,

$$\rho_f = \phi\, d_f, \qquad \rho_s = (1-\phi) d_s, \tag{11}$$

where d_f and d_s are the true mass densities of fluid and solid constituents respectively.

2.1 Pore Fluid Pressure

We shall also regard the partial fluid pressure p_f in the mixture theory as the outcome of a "microscopic" pressure acting over the area fraction of surface actually occupied by the fluid in the pore, i.e.,

$$p_f\, dA = P\, dA_f, \qquad \text{hence,} \qquad p_f = \phi_a P,$$

where P will be called the *pore fluid pressure* and $\phi_a = dA_f/dA$ is the area fraction of the pores.

In general, the volume fraction ϕ and the area fraction ϕ_a may be different, yet for practical applications, we shall adopt a reasonable assumption that they are the same for simplicity, so that the *pore fluid pressure* is defined as

$$P = \frac{p_f}{\phi}. \tag{12}$$

The pore pressure is an important concept in soil mechanics [3, 6].

Let us write the stresses in the following form,

$$\begin{aligned} T_f &= -\phi PI + \bar{T}_f, \\ T_s &= -(1-\phi)PI + \bar{T}_s. \end{aligned} \tag{13}$$

We call $\bar{T}_f$ the *extra fluid stress* and $\bar{T}_s$ the *effective solid stress*.

2.2 Equations of Motion

The equations of motion $(1)_{3,4}$ for the fluid and the solid constituents can now be written as

$$\begin{aligned} \phi d_f \dot{\hat{v}}_f &= -\phi \text{ grad } P - P \text{ grad } \phi + \text{div } \bar{T}_f + m_f + \phi d_f g, \\ (1-\phi) d_s \dot{\hat{v}}_s &= -(1-\phi) \text{ grad } P + P \text{ grad } \phi + \text{ div } \bar{T}_s - m_f + (1-\phi) d_s g, \end{aligned} \tag{14}$$

where the body force is the gravitational force g.

On the other hand, from (9), the interactive force m_f in equilibrium becomes

$$m_f^0 = P \text{ grad } \phi - \phi r^0, \qquad r^0 = -\frac{P}{d_f} \text{ grad } d_f + d_f (\text{grad } \psi_f^0)\Big|_0. \tag{15}$$

By canceling out the term P grad ϕ in (14) from the interactive force (15) leads to the following equations of motion for porous media,

$$\begin{aligned} \phi d_f \dot{\hat{v}}_f &= -\phi \text{ grad } P + \text{ div } \bar{T}_f + (m_f - m_f^0) - \phi r^0 + \phi d_f g, \\ (1-\phi) d_s \dot{\hat{v}}_s &= -(1-\phi) \text{ grad } P + \text{ div } \bar{T}_s - (m_f - m_f^0) + \phi r^0 + (1-\phi) d_s g, \end{aligned} \tag{16}$$

2.3 Linear Theory

Since equilibrium is characterized by the conditions, grad $\theta = 0$ and $V = 0$, in a linear theory, we shall assume that $|\text{ grad } \theta|$ and $|V|$ are small quantities, and that $o(2)$ stands for higher order terms in these quantities.

From (8) and (13), the extra fluid stress,

$$\bar{T}_f = \phi d_f(\psi_f - \psi_f^0)I + \phi d_f \frac{\partial \psi_f}{\partial V} \otimes V \approx o(2), \tag{17}$$

is a second order quantity because the free energy of fluid constituent must be a scalar-valued isotropic function of the vector variable $(V \cdot V)$.

Moreover, we can define the resistive force as

$$r = r^0 - \frac{1}{\phi}(m_f - m_f^0).$$

It is the force against the flow of the fluid through the medium. Since the non-equilibrium part of the interactive force, $(m_f - m_f^0)$, vanishes in equilibrium, we can represent the resistive force as

$$r = R\,V + G\,\text{grad}\,\theta + r^0 + o(2). \tag{18}$$

The parameter R is called the *resistivity tensor*, and its inverse R^{-1} is called the *permeability tensor*.

2.3.1 Darcy's Law, Uplift, and Effective Stress Principle

The equations of motion (16) in the linear theory becomes

$$\begin{aligned} d_f \grave{v}_f &= -\,\text{grad}\,P - r + d_f g, \\ (1-\phi)d_s \grave{v}_s &= -(1-\phi)\,\text{grad}\,P + \text{div}\,\bar{T}_s + \phi\, r + (1-\phi)d_s g. \end{aligned} \tag{19}$$

The Eq. $(19)_1$ for the motion of the fluid is a generalized Darcy's law. Indeed, for stationary case, and only $r = RV$ is taken into account from (18), it reduces to the classical Darcy's law,

$$v_f - v_s = -R^{-1}(\text{grad}\,P - d_f g)$$

We can obtain an interesting equation for the solid constituent if we multiply the Eq. $(19)_1$ by $(1-\phi)$ and subtract it from the Eq. $(19)_2$,

$$(1-\phi)d_s \grave{v}_s - \text{div}\,\bar{T}_s = r + (1-\phi)(d_s - d_f)g + (1-\phi)d_f \grave{v}_f. \tag{20}$$

From this equation, we notice that the effective stress is not affected by the pore fluid pressure—this is known as the *effective stress principle* in soil mechanics (see [3]).

Note that there are three terms of forces on the right-hand side of the Eq. (20). The first one is the usual resistive force r of diffusive motion. The second term, $(1-\phi)(d_s - d_f)g$, is the weight of solid reduced by the uplift (or buoyancy) from the fluid corresponding to the principle of Archimedes. The importance of uplift in soil

structures had been one of the major concern in the development of soil mechanics (see [2]).

The third term, $(1-\phi)d_f\grave{v}_f$, is the inertia force against the displacement of fluid in the motion of the solid through it. In the theory of Biot (see [11]), the relative acceleration was introduced as a part of interactive force between solid and fluid constituents to account for the apparent added mass effect he expected in the diffusive processes. The inertia force considered here seems to correspond to such an effect. However, from the derivation above, it is clear that it is not a part of interactive force, since there is no inertia effect on the motion of fluid $(19)_1$.

3 Problems in Poroelasticity

Hereafter we shall restrict our attention to mechanical problems (isothermal case) of the theory of elastic porous media,also known as poroelasticity. The governing equations are based on the balance equations of partial mass $(1)_{1,2}$ and partial momentum of fluid and solid constituents (19):

$$\begin{cases} (\phi d_f\grave{)} + \phi d_f \text{ div } v_f = 0, \\ ((1-\phi)d_s\grave{)} + (1-\phi)d_s \text{ div } v_s = 0, \\ \phi\, d_f\grave{v}_f + \phi \text{ grad } P - \text{div } \bar{T}_f + \phi\, r = \phi\, d_f g, \\ (1-\phi)d_s\grave{v}_s + (1-\phi) \text{ grad } P - \text{div } \bar{T}_s - \phi\, r = (1-\phi)d_s g. \end{cases} \tag{21}$$

For this system of equations, from (13), (15), (17), and (18), we have the following constitutive relations:

$$\begin{aligned} \bar{T}_f &= \phi d_f(\psi_f - \psi_f^0)I + \phi d_f \frac{\partial \psi_f}{\partial V} \otimes V \approx o(2), \\ \bar{T}_s &= T_I + PI - \bar{T}_f = T_I + PI + o(2), \\ r &= R\,V - \frac{P}{d_f} \text{ grad } d_f + d_f(\text{grad } \psi_f^0) + o(2). \end{aligned} \tag{22}$$

where $o(2)$ stands for higher order terms in $|V|$, and

$$\psi_f = \psi_f(\phi, d_f, F_s, V), \qquad P = P(\phi, d_f, F_s), \qquad T_I = T_I(\phi, d_f, F_s).$$

3.1 Some Models of Porous Media

The governing system (21) consists of two scalar and two vector equations, while besides the two vector variables of the motions of fluid and solid constituents, there are three scalar variables, namely, the two true densities, d_f and d_s, and the porosity

ϕ. Therefore, the system is under-determinate, namely, there are less number of equations than the number of independent variables.

Porosity is a microstructural variable of the porous media. To deal with this additional variable, without postulating an additional (evolution or balance) equation for porosity, as proposed in some mixture theories in the literature [9, 10], there remain some possibilities to formulate deterministic theories from the present theory of porous media. We may consider following models:

1. Firstly, we can regard the porosity as a constitutive quantity, given by a constitutive relation.
   Independent variables: $(d_f, d_s, \chi_f, \chi_s)$.
   Constitutive variables:

$$P = P(d_f, F_s), \qquad \phi = \phi(d_f, F_s),$$
$$r = r(d_f, F_s, V), \quad \bar{T}_f = \bar{T}_f(d_f, F_s, V), \qquad \bar{T}_s = \bar{T}_s(d_f, F_s, V).$$

   Secondly, we can make some assumption of incompressibility of solid or fluid constituent to reduce the number of scalar variables.
2. Incompressible solid constituent: constant d_s.
   Independent variables: $(\phi, d_f, \chi_f, \chi_s)$.
   Constitutive variables:

$$P = P(\phi, d_f, F_s), \qquad r = r(\phi, d_f, F_s, V),$$
$$\bar{T}_f = \bar{T}_f(\phi, d_f, F_s, V), \qquad \bar{T}_s = \bar{T}_s(\phi, d_f, F_s, V).$$

3. Incompressible fluid constituent: constant d_f.
   Independent variables: $(\phi, d_s, \chi_f, \chi_s)$.
   Constitutive variables:

$$P = P(\phi, F_s), \quad r = r(\phi, F_s, V), \quad \bar{T}_f = \bar{T}_f(\phi, F_s, V), \quad \bar{T}_s = \bar{T}_s(\phi, F_s, V).$$

4. Incompressible porous medium: constant d_s and d_f.
   Note that even composed with incompressible constituents, the porous body is not necessarily incompressible because the porosity may vary. Moreover, we can regard the pore pressure P as an indeterminate pressure so that the system is deterministic.
   Independent variables: $(\phi, P, \chi_f, \chi_s)$.
   Constitutive variables:

$$\bar{T}_f = \bar{T}_f(\phi, F_s, V), \qquad \bar{T}_s = \bar{T}_s(\phi, F_s, V) \qquad r = r(\phi, F_s, V).$$

3.2 Boundary Conditions

Regarding the boundary as a singular surface between the porous body and the external medium, we have the following jump conditions for the mixture as a single body,

$$\begin{aligned} &\left[\rho(v-u^*)\right]\cdot n = 0,\\ &\left[\rho v\otimes(v-u^*)-T\right]n = 0, \end{aligned} \tag{23}$$

where u^* is the surface velocity of the boundary. Therefore, at the boundary of a solid-fluid mixture body, we have $v_s = u^*$ and the jump conditions (23) becomes,

$$\begin{aligned} &[\![\rho_f V]\!]\cdot n = 0,\\ &\left[\!\!\left[v\otimes\rho_f V-(T_f+T_s)+\frac{1}{2}\frac{\rho_f\rho_s}{\rho}V\otimes V\right]\!\!\right]n = 0, \end{aligned} \tag{24}$$

Furthermore, the boundary of a porous body can also be regarded as a semipermeable singular surface for the fluid constituent, in other words, the fluid can flow across the boundary and the solid cannot. In a semipermeable boundary, it has been proved that the jump condition of energy is given by (see [5]),

$$\left[\!\!\left[\mu_f+\tfrac{1}{2}V^2-V\cdot\frac{\partial\psi_f}{\partial V}\right]\!\!\right]=0,$$

where $\mu_f = \dfrac{\partial\rho\psi_I}{\partial\rho_f}$ is the fluid chemical potential. From (7), $p_f = \rho_f(\mu_f-\phi_f^0)$, it implies the jump condition for the pore fluid pressure in a porous body,

$$[\![P]\!]+d_f\left[\!\!\left[\psi_f^0+\frac{1}{2}V^2-V\cdot\frac{\partial\psi_f}{\partial V}\right]\!\!\right]=0. \tag{25}$$

Based on the above jump conditions, we can formulate the boundary condition for the system of partial differential equations. For well-posedness of the problem, two boundary conditions are needed at any point on the boundary, in addition to the proper initial conditions. There are two type of boundary conditions, namely, prescription of the motion of the boundary or the force acting on the free boundary described in the following, where the subindex $_w$ denotes the corresponding prescribed value at the exterior side of the boundary.

3.2.1 Dirichlet Conditions

These are displacement (velocity) boundary conditions. From $(24)_1$, one can prescribe the solid displacement u_{w} and the fluid mass flow m_{w},

$$u_s = u_{\mathrm{w}}, \qquad \phi\, d_f (v_f - v_s) \cdot n = m_{\mathrm{w}},$$

where u_s is the displacement vector of the solid constituent.

3.2.2 Neumann Conditions

Traction boundary conditions must be prescribed according to the relations $(24)_2$ and (25). Provided that the fluid mass flux is small enough, one can prescribe the total surface traction t_{w},

$$Tn = (T_s + T_f)n = t_{\mathrm{w}}$$

If in addition, the equilibrium free energy ψ_f^0 is a function of d_f only, then the second condition implies the continuity of the pore pressure across the boundary,

$$Pn = p_{\mathrm{w}} n,$$

where p_{w} is the pressure of the adjacent fluid acting on the boundary.

3.2.3 Remarks on Boundary Conditions on a Free Boundary

Since there are two equations of motion in the systems of governing equations, for a free boundary, two traction boundary conditions are needed. However, unlike the continuity of total traction, the continuity of pore pressure has been mostly ignored in the literature, and an additional boundary condition is often postulated for the closure of the problem. It is proposed by Rajagobal and Tao [8] a "method of splitting the total traction" into parts acting on the fluid and the solid constituents according to the proportion of volume fraction (or surface fraction more exactly). Therefore, suppose that the boundary separates the porous body and the external fluid with pressure p_w, then the method requires that

$$T_f n \approx -p_f n = -\frac{\rho_f}{d_f}\, p_{\mathrm{w}} n.$$

Since the pore fluid pressure is defined as $P = p_f/\phi$ and $\rho_f = \phi d_f$, the proposed splitting method is consistent with the continuity of pore fluid pressure at the semi-permeable surface.

Another condition was suggested by Deresiewicz and Skalak [4], Wilmanski [11]; in which an interfacial version of Darcy's law simulates the fluid flow across the boundary,

$$\rho_f(v_f - v_s)\cdot n = \alpha\left(p_f - \frac{\rho_f}{d_f}p_{\mathrm{w}}\right),$$

where α is referred to as the interface permeability. For $\alpha = 0$ the condition reduces to $v_f = v_s$, i.e., the boundary is impermeable, while for $\alpha = \infty$, it reduces to the continuity of pore fluid pressure. For the value in between, the boundary is not an ideal singular surface as proposed in the usual mixture theories, instead, the interface has its physical property. To include such an effect, a more sophisticated mixture theory containing interfacial membrane must be considered. Such a theory is beyond the present consideration. However, with of the jump condition (25), which relates the mass flux and the pore pressure across the boundary, it seems that the postulate of an additional condition, such as Deresiewicz condition, is superfluous in the framework of the usual mixture theories of porous media.

4 Acceleration Waves

It is known in a theory of binary fluid mixture, there are two longitudinal waves, usually referred to as the first and the second sound (see [9] Appendix 5B). For porous media, the existence of two longitudinal waves, referred to as P1 and P2 waves, was predicted in Biot's theory [11]. From this observation, mathematically, the existence of two longitudinal wave in a well formulated theory of two component system seems beyond doubt in general. Nevertheless, the non- existence of second longitudinal wave in incompressible porous media has been pointed out in the literature (see [11]). Therefore, we would like to consider wave propagations in the porous models formulated from the present theory under some incompressibility assumption and show that indeed, in the model with both incompressible solid and fluid constituents, the second longitudinal wave does not exist. In other models with only one incompressible constituent two longitudinal waves may exist in general.

4.1 Wave Front Propagation

A propagating wave can be regarded as a moving singular surface through a material region, across which some physical quantities may suffer jump discontinuity. Let

$$[\![A]\!] = A^- - A^+,$$

be the jump of the quantity A, where A^- and A^+ denote its limiting value ahead and behind of the surface respectively. Let n be the unit normal vector pointing in the

propagating direction and U be the normal speed of the moving singular surface in the present configuration. According to Hadamard lemma, if $[\![A]\!] = 0$, we have the following geometric and kinematic compatibility conditions:

$$[\![\operatorname{grad} A]\!] = [\![\operatorname{grad} A \cdot n]\!]\, n, \qquad [\![\tfrac{\partial A}{\partial t}]\!] = -U\,[\![\operatorname{grad} A \cdot n]\!]\,. \tag{26}$$

We shall consider a wave front propagating into a homogeneous region of porous body in equilibrium, in which $v_f = v_s = 0$. For a weak discontinuity wave, i.e., on the singular surface, we assume that

$$\begin{aligned} &[\![v_f]\!] = 0, \qquad [\![v_s]\!] = 0, \qquad [\![F_s]\!] = 0, \\ &[\![d_f]\!] = 0, \qquad [\![d_s]\!] = 0, \qquad [\![\phi]\!] = 0, \end{aligned}$$

and let

$$a_f = \left[\!\!\left[\frac{\partial v_f}{\partial t} \right]\!\!\right], \quad a_s = \left[\!\!\left[\frac{\partial v_s}{\partial t} \right]\!\!\right], \quad \delta_f = \left[\!\!\left[\frac{\partial d_f}{\partial t} \right]\!\!\right], \quad \delta_s = \left[\!\!\left[\frac{\partial d_s}{\partial t} \right]\!\!\right], \quad \varphi = \left[\!\!\left[\frac{\partial \phi}{\partial t} \right]\!\!\right].$$

The amplitude vectors a_f and a_s are the jumps of acceleration of fluid and solid constituents and such a weak wave is called an acceleration wave.

By repeated use of the compatibility conditions (26), the following jump conditions at the wave front hold:

$$\begin{aligned} &[\![\operatorname{grad} v_f]\!] = -\tfrac{1}{U}\, a_f \otimes n, && [\![\operatorname{grad} v_s]\!] = -\tfrac{1}{U}\, a_s \otimes n, \\ &[\![\operatorname{grad} d_f]\!] = -\tfrac{1}{U}\, \delta_f\, n, && [\![\operatorname{grad} d_s]\!] = -\tfrac{1}{U}\, \delta_s\, n, \\ &[\![\operatorname{grad} \phi]\!] = -\tfrac{1}{U}\, \varphi\, n, && [\![\operatorname{grad} F_s]\!] = \tfrac{1}{U^2}\, a_s \otimes F^T n \otimes n. \end{aligned} \tag{27}$$

Since the relative velocity $V = v_f - v_s = 0$ vanishes at the wave front, we can replace the equations of motion in $(21)_{3,4}$ by the equations $(19)_1$ and (20) of the linear theory,

$$\begin{aligned} d_f \dot{v}_f &= -\operatorname{grad} P - r + d_f g, \\ (1-\phi)(d_s \dot{v}_s - d_f \dot{v}_f) &= \operatorname{div} \bar{T}_s + r + (1-\phi)(d_s - d_f) g, \end{aligned} \tag{28}$$

in the systems of the governing equations, without loss of generality.

4.2 Porous Media with Incompressible Solid Constituent

We consider the porous media model of incompressible solid constituent ($d_s =$ constant) governed by the system (21). With the following abbreviations for partial derivatives,

$$P_A = \frac{\partial P}{\partial A}, \qquad H_A = \frac{\partial \bar{T}_s}{\partial A},$$

and

$$r = RV - \frac{P}{d_f} \text{ grad } d_f + d_f \text{ grad } \psi_f^0 = RV + R_{d_f} \text{ grad } d_f + R_\phi \text{ grad } \phi + R_{F_s} \cdot \text{ grad } F_s,$$

the jumps of the governing equations at the wave front become

$$\begin{aligned}
&U d_f \varphi + U\phi\, \delta_f - \phi d_f (a_f \cdot n) = 0,\\
&U\varphi + (1-\phi)(a_s \cdot n) = 0,\\
&U^2 d_f a_f - U(P_\phi + R_\phi)\varphi\, n - U(P_{d_f} + R_{d_f})\delta_f n + \Big((R_{F_s} + P_{F_s}) \cdot a_s \otimes F_s^T n\Big) n = 0,\\
&U^2(1-\phi)(d_s a_s - d_f a_f) + U(R_\phi I + H_\phi)\varphi\, n\\
&\quad + U(R_{d_f} I + H_{d_f})\delta_f n - \Big((I \otimes R_{F_s} + H_{F_s}) \cdot a_s \otimes F_s^T n\Big) n = 0.
\end{aligned}$$

For clarity, the last two equations in (Cartesian) component forms are

$$\begin{aligned}
&U^2 d_f a_f^i - U(P_\phi + R_\phi)\varphi\, n_i - U(P_{d_f} + R_{d_f})\delta_f n_i + \Big((R_{F_s} + P_{F_s})_{ka} a_s^k F_s^{ja} n_j\Big) n_i = 0,\\
&U^2(1-\phi)(d_s a_s^i - d_f a_f^i) + U(R_\phi I + H_\phi)_{ij}\varphi\, n_j\\
&\quad + U(R_{d_f} I + H_{d_f})_{ij}\delta_f n_j - \Big((\delta_{ij}(R_{F_s})_{ka} + (H_{F_s})_{ijka}) a_s^k F_s^{la} n_l\Big) n_j = 0.
\end{aligned}$$

If we define

$$\widehat{\Pi}_{ik} = (R_{F_s} + P_{F_s})_{ka} F_s^{ja} n_j\, n_i, \qquad \widehat{Q}_{ik} = (\delta_{ij}(R_{F_s})_{ka} + (H_{F_s})_{ijka}) F_s^{la} n_l n_j, \tag{29}$$

then the system can be written as

$$\begin{aligned}
&U d_f \varphi + U\phi\, \delta_f - \phi d_f (a_f \cdot n) = 0,\\
&U\varphi + (1-\phi)(a_s \cdot n) = 0,\\
&U(P_\phi + R_\phi)\varphi\, n + U(P_{d_f} + R_{d_f})\delta_f n - U^2 d_f a_f - \widehat{\Pi}\, a_s = 0,\\
&U(R_\phi I + H_\phi)\varphi\, n + U(R_{d_f} I + H_{d_f})\delta_f n - U^2(1-\phi)(d_f a_f - d_s a_s) - \widehat{Q}\, a_s = 0.
\end{aligned} \tag{30}$$

4.2.1 Longitudinal Acceleration Waves

For longitudinal waves, let

$$a_f = \hat{a}_f n, \qquad a_s = \hat{a}_s n,$$

i.e., the amplitude vectors of accelerations of fluid and solid constituents are in the direction of the propagation direction, and let

$$\widehat{P}_\phi = P_\phi + R_\phi, \quad \widehat{P}_{d_f} = P_{d_f} + R_{d_f}, \quad \widehat{H}_\phi = R_\phi + n \cdot H_\phi n, \quad \widehat{H}_{d_f} = R_{d_f} + n \cdot H_{d_f} n.$$

The system (30) then can be written as

$$\begin{bmatrix} Ud_f & U\phi & -\phi d_f & 0 \\ U & 0 & 0 & (1-\phi) \\ U\widehat{P}_\phi & U\widehat{P}_{d_f} & -U^2 d_f & -n \cdot \widehat{\Pi} n \\ U\widehat{H}_\phi & U\widehat{H}_{d_f} & -U^2(1-\phi)d_f & U^2(1-\phi)d_s - n \cdot \widehat{Q} n \end{bmatrix} \begin{bmatrix} \varphi \\ \delta_f \\ \hat{a}_f \\ \hat{a}_s \end{bmatrix} = \begin{bmatrix} 0 \\ 0 \\ 0 \\ 0 \end{bmatrix}.$$

The propagation condition requires the determinant of the coefficient matrix be vanish.

Obviously, if $U = 0$, the determinant is identically zero, as well as $\hat{a}_f = \hat{a}_s = 0$, which is an uninteresting case. Therefore we are looking for moving longitudinal wave with $U \neq 0$. The vanishing of the determinant can be simplified to

$$\det \begin{bmatrix} d_f & \phi & -\phi & 0 \\ 1 & 0 & 0 & (1-\phi) \\ \widehat{P}_\phi & \widehat{P}_{d_f} & -U^2 & -n \cdot \widehat{\Pi} n \\ \widehat{H}_\phi & \widehat{H}_{d_f} & -U^2(1-\phi) & U^2(1-\phi)d_s - n \cdot \widehat{Q} n \end{bmatrix} = 0, \tag{31}$$

which is a quadratic equation in U^2, say

$$aU^4 + bU^2 + c = 0,$$

with the coefficients given by

$$\begin{aligned} a &= \phi(1-\phi)d_s, \\ b &= -\phi(n \cdot \widehat{Q} n) + (1-\phi)\phi(n \cdot \widehat{\Pi} n) \\ &\quad + (1-\phi)^2 \phi \widehat{P}_\phi - (1-\phi)(\phi d_s + (1-\phi)d_f)\widehat{P}_{d_f} + (1-\phi)(d_f \widehat{H}_{d_f} - \phi \widehat{H}_\phi), \\ c &= \phi \widehat{P}_{d_f}(n \cdot \widehat{Q} n) - \phi \widehat{H}_{d_f}(n \cdot \widehat{\Pi} n) - (1-\phi)\phi(\widehat{P}_\phi \widehat{H}_{d_f} - \widehat{P}_{d_f} \widehat{H}_\phi). \end{aligned}$$

In case there are two positive real roots of this quadratic equation, there will be two longitudinal waves propagating in the porous body. Obviously, this possibility depends on the constitutive parameters in the above coefficients.

To be more specific, we shall consider a simple case with constitutive relations,

$$\psi_f^0 = \psi_f^0(d_f), \qquad \bar{T}_s = \bar{T}_s(F_s), \tag{32}$$

so that

$$H_\phi = 0, \qquad H_{d_f} = 0, \qquad R_\phi = 0, \qquad R_{F_s} = 0.$$

Moreover, if we assume the free energy $\psi_f^0(d_f)$ is the same as that of the pure fluid in the pore and the relation (10) holds, i.e.,

$$P = d_f^2 \frac{\partial \psi_f^0}{\partial d_f}, \qquad \text{hance} \qquad P_\phi = 0, \qquad P_{F_s} = 0,$$

and, from (22), we have

$$R_{d_f} = -\Big(\frac{P}{d_f} - d_f \frac{\partial \psi_f^0}{\partial d_f}\Big) = 0.$$

In this simple case, we have, from (29),

$$\begin{aligned} &\widehat{P}_\phi = 0, \qquad \widehat{\Pi} = 0, \qquad \widehat{H}_\phi = 0, \qquad \widehat{H}_{d_f} = 0, \\ &\widehat{Q}_{ik} = (H_{F_s})_{ijka} F_s^{la} n_l n_j = L_{ijkl}\, n_j n_l, \end{aligned} \tag{33}$$

where, from (13),

$$L_{ijkl} = \frac{\partial T_s^{ij}}{\partial F_s^{ka}} F_s^{la}$$

is the elasticity tensor of the solid constituent. It is usually assumed that the elasticity tensor is strong elliptic and the compressibility is positive, i.e.,

$$P_{d_f} = \frac{\partial P}{\partial d_f} > 0, \qquad L_{ijkl}\, u_i v_j u_k v_l > 0 \quad \forall\, u, v \neq 0. \tag{34}$$

The quadratic equation of the propagation condition can then be written as

$$(U^2 - c_1^2)(U^2 - c_2^2) - \Big(\frac{d_f}{d_s} \frac{1-\phi}{\phi} c_2^2\Big) U^2 = 0, \tag{35}$$

where, by (34),

$$c_1 = \sqrt{\frac{n \cdot \widehat{Q} n}{(1-\phi) d_s}}, \qquad c_2 = \sqrt{\frac{\partial P}{\partial d_f}},$$

are the well-known speeds of longitudinal wave in an elastic solid and an elastic fluid respectively. In the present case, from the roots of (35), these two speeds are modified by the presence of the last term in the Eq. (35).

From this simple case, it seems reasonable to expect two longitudinal wave speeds, known as P1 and P2 wave, in the present theory of porous media with incompressible solid constituent, from the propagation condition (31) in general.

4.2.2 Transversal Acceleration Wave

For transversal wave, $a_f \cdot n = 0$ and $a_s \cdot n = 0$, from the the first three equations of (30), it follows that

$$\varphi = 0, \qquad \delta_f = 0, \qquad d_f a_f = -\frac{1}{U^2}\widehat{\Pi} a_s,$$

and the last equation becomes

$$\big((\widehat{Q} - (1-\phi)\widehat{\Pi}) - (1-\phi)d_s U^2 I\big)a_s = 0 \tag{36}$$

Let $a_s = \hat{a}_s m$ where m is a unit vector normal to the propagation direction, i.e., $m \cdot n = 0$. Then from (36), there is a transversal wave with propagation speed given in the following relation,

$$(1-\phi)d_s U^2 = m \cdot \big(\widehat{Q} - (1-\phi)\widehat{\Pi}\big)m.$$

In particular, for the simple case given by (32), the velocity of propagation reduces to the well-known speed of shear wave in an elastic body,

$$U = c_s = \sqrt{\frac{m \cdot \widehat{Q} m}{(1-\phi)d_s}}.$$

4.3 Porous Media with Incompressible Fluid Constituent

Similarly, for the model of incompressible fluid constituent ($d_f =$ constant) governed by the system (21), we have

$$\begin{aligned}
&U\varphi - \phi(a_f \cdot n) = 0,\\
&Ud_s\varphi - U(1-\phi)\delta_s + (1-\phi)d_s(a_s \cdot n) = 0,\\
&U\widehat{P}_\phi \varphi\, n - U^2 d_f a_f - \widehat{\Pi}\, a_s = 0,\\
&U(R_\phi I + H_\phi)\varphi\, n - U^2(1-\phi)(d_f a_f - d_s a_s) - \widehat{Q}\, a_s = 0.
\end{aligned} \tag{37}$$

For longitudinal waves, we have

$$\begin{bmatrix} U & 0 & -\phi & 0 \\ Ud_s & -U(1-\phi) & 0 & (1-\phi)d_s \\ U\widehat{P}_\phi & 0 & -U^2 d_f & -n \cdot \widehat{\Pi} n \\ U\widehat{H}_\phi & 0 & -U^2(1-\phi)d_f & U^2(1-\phi)d_s - n \cdot \widehat{Q} n \end{bmatrix} \begin{bmatrix} \varphi \\ \delta_s \\ \hat{a}_f \\ \hat{a}_s \end{bmatrix} = \begin{bmatrix} 0 \\ 0 \\ 0 \\ 0 \end{bmatrix}.$$

and the determinant of the coefficient matrix reduces to

$$\det \begin{bmatrix} 1 & -\phi & 0 \\ \widehat{P}_\phi & -U^2 d_f & -n \cdot \widehat{\Pi} n \\ \widehat{H}_\phi & -U^2(1-\phi)d_f & U^2(1-\phi)d_s - n \cdot \widehat{Q} n \end{bmatrix} = 0, \tag{38}$$

which lead to the quadratic equation in U^2,

$$\big(U^2(1-\phi)d_s - n \cdot \widehat{Q} n\big)\big(U^2 d_f - \phi \widehat{P}_\phi\big) + (n \cdot \widehat{\Pi} n)\big(U^2(1-\phi)d_f - \phi \widehat{H}_\phi\big) = 0.$$

Therefore, there may also exist two longitudinal wave in the incompressible fluid model.

We may also consider a simple case that the pore pressure and the fluid free energy are independent of F_s, so that $\widehat{\Pi} = 0$. In this case, there are two longitudinal waves (P1 and P2 waves),

$$U_1 = \sqrt{\frac{n \cdot \widehat{Q} n}{(1-\phi)d_s}}, \qquad U_2 = \sqrt{\frac{\phi}{d_f} \widehat{P}_\phi}.$$

The first wave is the same as the longitudinal wave in the elastic body, while the second wave is essentially the compressive wave of pore fluid.

For transversal wave, from (37), one can easily check that the propagation condition is exactly the same as the relation (36) for the incompressible solid model.

4.4 Incompressible Porous Media

For an incompressible porous medium, we assume that both the solid and the fluid true densities are constant. In this model the pore pressure is regarded as an indeterminate pressure, and for acceleration waves, we have, in addition,

$$[\![P]\!] = 0, \qquad [\![\operatorname{grad} P]\!] = \pi\, n,$$

where $\pi = [\![\operatorname{grad} P \cdot n]\!]$. By taking the jump of the system of equations (21) at the wave front, we obtain

$$\begin{aligned} &U\varphi - \phi(a_f \cdot n) = 0, \\ &U\varphi + (1-\phi)(a_s \cdot n) = 0, \\ &UR_\phi \varphi\, n - U^2 \pi\, n - U^2 d_f a_f - \widehat{\Pi}\, a_s = 0, \\ &U(R_\phi I + H_\phi)\varphi\, n - U^2(1-\phi)(d_f a_f - d_s a_s) - \widehat{Q}\, a_s = 0. \end{aligned} \tag{39}$$

The abbreviations are the same as before except

$$\widehat{\Pi}_{ik} = (R_{F_s})_{ka} F_s^{ja} n_j n_i.$$

For longitudinal wave, the system can be written as

$$\begin{bmatrix} U & 0 & -\phi & 0 \\ U & 0 & 0 & (1-\phi) \\ UR_\phi & -U^2\pi & -U^2 d_f & -n\cdot\widehat{\Pi}n \\ U\widehat{H}_\phi & 0 & -U^2(1-\phi)d_f & U^2(1-\phi)d_s - n\cdot\widehat{Q}n \end{bmatrix} \begin{bmatrix} \varphi \\ \pi \\ \hat{a}_f \\ \hat{a}_s \end{bmatrix} = \begin{bmatrix} 0 \\ 0 \\ 0 \\ 0 \end{bmatrix},$$

and the determinant of the coefficient matrix reduces to

$$\det \begin{bmatrix} 1 & -\phi & 0 \\ 1 & 0 & (1-\phi) \\ \widehat{H}_\phi & -U^2(1-\phi)d_f & U^2(1-\phi)d_s - n\cdot\widehat{Q}n \end{bmatrix} = 0,$$

which gives only one propagation speed,

$$U^2 = \frac{\phi\, n\cdot\widehat{Q}n + \phi(1-\phi)\widehat{H}_\phi}{\phi(1-\phi)d_s + (1-\phi)^2 d_f}.$$

Therefore, there is no second longitudinal wave in this model as pointed out in the literature. As for the transversal wave, the propagation speed is the same as before.

Acknowledgments This research is partially the results of a research project supported by Brazilian Petroleum Company (PETROBRAS).

References

1. Bowen, R.M.: In: Eringen, A.C. (ed.) The Theory of Mixtures in Continuum Mechanics, vol. III. Academic Press (1976)
2. De Boer, R., Ehlers, W.: Uplift, friction and capillarity: three fundamental effects for liquid-saturated porous solids. Int. J. Solids Struct. **26**, 43–57 (1990)
3. De Boer, R.: Development of porous media theories—a brief historical review. Transp. Porous Media **9**, 155–164 (1992)
4. Deresiewicz, H., Skalak, R.: On uniqueness in dynamic poroelasticity. Bull. Seismol. Soc. Am. **53**, 783–788 (1963)
5. Liu, I.-S.: On chemical potential and incompressible porous media. Journal de Mécanique **19**, 327–342 (1980)
6. Liu, I.-S.: On pore fluid pressure and effective solid stress in the mixture theory of porous media. In: Albers, B. (ed.) Continuous Media with Microstructure. Springer (2010)
7. Liu, I.-S.: A solid-fluid mixture theory of porous media. Int. J. Eng. Sci. **84**, 133–146 (2014)
8. Rajagopal, K.R., Tao, L.: Mechanics of Mixtures. World Scientific Singapore (1995)

9. Truesdell, C.: Rational Thermodynamics, 2nd edn. Springer, New York (1984)
10. Wilmanski, K.: A thermodynamic model of compressible porous materials with the balance equation of porosity. Transp. Porous Media **32**, 21–47 (1998)
11. Wilmanski, K.: A few remarks on Biot's model and linear acoustics of poroelastic saturated materials. Soil Dyn. Earthq. Eng. **26**, 509–536 (2006)

Plane Waves, Uniqueness Theorems and Existence of Eigenfrequencies in the Theory of Rigid Bodies with a Double Porosity Structure

Merab Svanadze

Abstract The present paper concerns the linear theory of rigid bodies with a double porosity structure. Some basic properties of plane harmonic waves are treated. The internal boundary value problems (BVPs) of steady vibrations are formulated. The uniqueness theorems for regular (classical) solutions of these problems are proved. The existence and asymptotic distribution of eigenfrequencies of the internal BVPs of steady vibrations are established. Finally, the connection between plane harmonic waves, uniqueness of solutions and existence of eigenfrequencies are presented.

1 Introduction

The mathematical models of double porosity media, as originally developed for the mechanics of naturally fractured reservoirs, have found applications in many branches of civil engineering, geotechnical engineering, technology and, in recent years, biomechanics.

On the basis of Darcy's law the general 3D theory of consolidation for materials with single porosity was formulated by Biot [4]. The mathematical model of porous media with double porosity is proposed by Barenblatt et al. [2]. The theory of consolidation for elastic materials with double porosity is presented by Aifantis and coauthors [3, 21, 51]. This theory unifies the earlier proposed models for porous media with double [2] and single porosities [4]. More general models of double porosity materials (the cross-coupled terms are included in the equations of conservation of mass for the pore and fissure fluid) are introduced by several authors [16, 17, 22–25, 52]. The linear theory of viscoelasticity for Kelvin-Voigt materials with double porosity is presented and fundamental solution of equations of steady vibrations is constructed by Svanadze [43]. The double porosity concept was extended to media with multiple porosity by Bai et al. [1] and Moutsopoulos et al. [28].

M. Svanadze (✉)
Ilia State University, K. Cholokashvili Ave., 3/5, 0162 Tbilisi, Georgia
e-mail: svanadze@gmail.com

B. Albers and M. Kuczma (eds.), *Continuous Media with Microstructure 2*,
DOI 10.1007/978-3-319-28241-1_19

In the last decade there has been interest in investigation of problems of the theories of elasticity and thermoelasticity for solids with double porosity. In this connection, the linear theory of elastodynamics for anisotropic nonhomogeneous materials with double porosity is studied by Straughan [34]. The properties acceleration waves in the nonlinear double porosity elasticity are established by Gentile and Straughan [18]. The fundamental solutions in the theories of elasticity and thermoelasticity for materials with double porosity are constructed by Scarpetta et al. [33], Svanadze [37, 42], Svanadze and De Cicco [47]. The basic properties of plane harmonic waves in the coupled linear theory of elasticity for solid with double porosity are established by Ciarletta et al. [10] and Svanadze [41]. The three-dimensional BVPs and initial-BVPs of the theory of elasticity for materials with double porosity are investigated by potential method and the theory of singular integral equation by Scarpetta and Svanadze [32] and Svanadze [39, 40, 44].

The double porosity model represents a new possibility for the study of important problems concerning the civil engineering. The intended applications of the theories of elasticity and thermoelasticity for materials with a double porosity structure are to geological materials such as rocks and soils, manufactured porous materials such as ceramics and pressed powders, and biomaterials such as bone. The double porosity model would consider the bone fluid pressure in the vascular porosity and the bone fluid pressure in the lacunar-canalicular porosity. The mathematical problems of the theory of bone poroelasticity are studied by Svanadze and Scalia [48, 49]. An extensive review of the results of this theory, along with references to various pertinent contributions, may be found in the survey papers by Cowin [12], Cowin et al. [13] and Rohan et al. [30].

Recently, on the basis of balance of equilibrated force the theories of elasticity and thermoelasticity for materials with a double porosity structure are presented by Ieşan and Quintanilla [20]. In this paper the Cowin-Nunziato theory of materials with voids [14, 29] is generalized to derive a theory of thermoelastic solids, which have a double porosity structure. The basic equations for elastic materials with a double porosity structure involve the displacement vector field and the volume fraction fields associated with the pores and the fissures. The basic three-dimensional BVPs of the equilibrium theory of elasticity for materials with a double porosity structure are investigated by potential method and the theory of singular integral equations by Ieşan [19]. The uniqueness and existence theorems for external BVPs of steady vibrations in the linear theory of rigid bodies with a double porosity structure are proved by Svanadze [45].

In the present paper, we shall consider the 3D linear theory of rigid bodies with a double porosity structure [20]. This work is articulated as follows. Section 2 is based on the dynamical equations for rigid bodies with a double porosity structure. In Sect. 3 some basic properties of plane harmonic waves are treated. In Sect. 4 the basic internal BVPs of steady vibrations are formulated. In Sect. 5 the uniqueness theorems for regular (classical) solutions of these problems are proved, the existence and asymptotic distribution of eigenfrequencies of the internal BVPs of steady vibrations are established. Finally, in Sect. 6 the connection between plane harmonic waves, uniqueness of solutions and existence of eigenfrequencies are presented.

2 Basic Equations

Let $\mathbf{x} = (x_1, x_2, x_3)$ be a point of the Euclidean three-dimensional space R^3, let t denote the time variable, $t \geq 0$. In what follows we consider a rigid body with a double porosity structure that occupies the region Ω of R^3. $\tilde{\varphi}(\mathbf{x}, t)$ and $\tilde{\psi}(\mathbf{x}, t)$ denote the changes of volume fractions from the reference configuration corresponding to pores and fissures, respectively.

We assume that subscripts preceded by a comma denote partial differentiation with respect to the corresponding Cartesian coordinate, repeated indices are summed over the range (1, 2, 3), and the dot denotes differentiation with respect to t.

The governing field equations in the linear dynamical theory of rigid bodies with a double porosity structure are as follows [20]:

(1) *The constitutive equations*

$$\tilde{\sigma}_j = \alpha\tilde{\varphi}_{,j} + \beta\tilde{\psi}_{,j}, \qquad \tilde{\tau}_j = \beta\tilde{\varphi}_{,j} + \gamma\tilde{\psi}_{,j}, \tag{1}$$

where $\tilde{\sigma}_j$ and $\tilde{\tau}_j$ are the components of equilibrated stress vectors, $j = 1, 2$.

(2) *The balance of equilibrated forces*

$$\tilde{\sigma}_{j,j} + \tilde{\xi} + \tilde{F}_1 = \rho_1\ddot{\tilde{\varphi}}, \qquad \tilde{\tau}_{j,j} + \tilde{\zeta} + \tilde{F}_2 = \rho_2\ddot{\tilde{\psi}}, \tag{2}$$

where

$$\tilde{\xi} = -\alpha_1\tilde{\varphi} - \alpha_3\tilde{\psi}, \qquad \tilde{\zeta} = -\alpha_3\tilde{\varphi} - \alpha_2\tilde{\psi}, \tag{3}$$

$\alpha, \beta, \gamma, \alpha_1, \alpha_2, \alpha_3$ are constitutive coefficients, $\tilde{\xi}$, $\tilde{\zeta}$ and $\tilde{F}_1$, $\tilde{F}_2$ are the intrinsic and extrinsic equilibrated body forces, respectively, ρ_1 and ρ_2 are the coefficients of the equilibrated inertia, $\rho_1 > 0$, $\rho_2 > 0$.

Substituting Eqs. (1) and (3) into (2), we obtain the following system of equations of motion in the linear theory of rigid bodies with a double porosity structure expressed in terms of the volume fraction fields $\tilde{\varphi}$ and $\tilde{\psi}$:

$$\begin{aligned} \alpha\,\Delta\,\tilde{\varphi} + \beta\,\Delta\,\tilde{\psi} - \alpha_1\,\tilde{\varphi} - \alpha_3\,\tilde{\psi} &= \rho_1\ddot{\tilde{\varphi}} - \tilde{F}_1, \\ \beta\,\Delta\,\tilde{\varphi} + \gamma\,\Delta\,\tilde{\psi} - \alpha_3\,\tilde{\varphi} - \alpha_2\,\tilde{\psi} &= \rho_2\ddot{\tilde{\psi}} - \tilde{F}_2, \end{aligned} \tag{4}$$

where Δ is the Laplacian operator.

Neglecting the extrinsic equilibrated body forces in (4), we obtain the following system of homogeneous equations of motion in the considered theory:

$$\begin{aligned} \alpha\,\Delta\,\tilde{\varphi} + \beta\,\Delta\,\tilde{\psi} - \alpha_1\,\tilde{\varphi} - \alpha_3\,\tilde{\psi} - \rho_1\ddot{\tilde{\varphi}} &= 0, \\ \beta\,\Delta\,\tilde{\varphi} + \gamma\,\Delta\,\tilde{\psi} - \alpha_3\,\tilde{\varphi} - \alpha_2\,\tilde{\psi} - \rho_2\ddot{\tilde{\psi}} &= 0. \end{aligned} \tag{5}$$

We will suppose that the following assumptions on the constitutive coefficients hold true [20]

$$\alpha > 0, \qquad \alpha\gamma - \beta^2 > 0, \qquad \alpha_1 > 0, \qquad \alpha_1\alpha_2 - \alpha_3^2 > 0. \tag{6}$$

3 Plane Harmonic Waves

Let us suppose that plane harmonic waves corresponding to a wave number τ and to an angular frequency ω propagate in the x_1-direction through the rigid solid with a double porosity structure. Then

$$\tilde{\varphi}(\mathbf{x}, t) = C_1\, e^{i(\tau x_1 - \omega t)}, \qquad \tilde{\psi}(\mathbf{x}, t) = C_2\, e^{i(\tau x_1 - \omega t)}, \tag{7}$$

where C_1 and C_2 are constant values, $\omega > 0$.

It is obvious that if $\tau > 0$, then the corresponding plane wave has the constant amplitude, and if τ is complex with $\operatorname{Im}\tau > 0$, then the plane wave is attenuated as $x_1 \to +\infty$.

Keeping in mind the condition (7), from (5) it follows that

$$\begin{aligned} \left(\alpha\tau^2 - \eta_1\right) C_1 + \left(\beta\tau^2 + \alpha_3\right) C_2 = 0, \\ \left(\beta\tau^2 + \alpha_3\right) C_1 + \left(\gamma\tau^2 - \eta_2\right) C_2 = 0, \end{aligned} \tag{8}$$

where $\eta_j = \rho_j\omega^2 - \alpha_j$, $j = 1, 2$.

We introduce the notation

$$\begin{aligned} &\alpha_0 = \alpha\gamma - \beta^2, \qquad \beta_0 = \alpha_1\alpha_2 - \alpha_3^2, \\ &\zeta_0 = \alpha\eta_2 + \gamma\eta_1 + 2\beta\alpha_3, \qquad \eta_0 = \eta_1\eta_2 - \alpha_3^2. \end{aligned} \tag{9}$$

Obviously, from (6) it follows that $\alpha_0 > 0$, $\beta_0 > 0$.

If τ is a solution of the biquadratic equation

$$\alpha_0\tau^4 - \zeta_0\tau^2 + \eta_0 = 0, \tag{10}$$

then (8) has non-trivial solutions (C_1, C_2). The relation (10) is the dispersion equation of longitudinal plane harmonic waves. In this section, we will establish the basic properties of solutions of (10).

It is easy to see that

$$\eta_0 = \rho_1\rho_2\omega^4 - (\rho_1\alpha_2 + \rho_2\alpha_1)\omega^2 + \beta_0 \tag{11}$$

with the discriminant $\mathscr{D}^* = (\rho_1\alpha_2 - \rho_2\alpha_1)^2 + 4\rho_1\rho_2\alpha_3^2 \geq 0$. On the basis of (6) the equation

$$\rho_1\rho_2\omega^4 - (\rho_1\alpha_2 + \rho_2\alpha_1)\omega^2 + \beta_0 = 0$$

with respect to ω has two positive roots ω_1 and ω_2 called the *cutoff frequencies* in the considered theory. Obviously, if $\mathscr{D}^* > 0$, then $\omega_1 \neq \omega_2$ (in this case we assume that $\omega_1 < \omega_2$) and if $\mathscr{D}^* = 0$, then $\omega_1 = \omega_2$.

Let $\tilde{\omega}_1 = \sqrt{\frac{\alpha_1}{\rho_1}}$ and $\tilde{\omega}_2 = \sqrt{\frac{\alpha_2}{\rho_2}}$. Assume without loss of generality that $\tilde{\omega}_1 \leq \tilde{\omega}_2$, that is

$$\frac{\alpha_1}{\alpha_2} \leq \frac{\rho_1}{\rho_2}. \tag{12}$$

Clearly,

$$\omega_1 \leq \tilde{\omega}_1 \leq \tilde{\omega}_2 \leq \omega_2. \tag{13}$$

Remark 1 The cutoff frequency is the critical frequency between wave propagation with the constant amplitude and attenuation, which corresponds to the frequency at which the longitudinal wave number is zero. The wave propagation in the single porosity materials is studied by Biot [5], where the existence of one cutoff frequency (called as "the certain frequency") is established. In addition, in [5, 6], the frequency intervals below and above the cutoff frequency are called as "low-frequency range" and "higher frequency range", respectively.

Remark 2 The dispersion equation (10) is also valid below the cutoff frequency, where the longitudinal wave number is imaginary.

Obviously, If $\mathscr{D}^* = 0$, then $\omega_1 = \omega_2$ and there are two frequency ranges in the considered theory:

1. *Low-frequency range* $LF' = \{\omega : 0 < \omega < \omega_1\}$,
2. *Higher frequency range* $HF' = \{\omega : \omega > \omega_1\}$.

If $\mathscr{D}^* > 0$, then there are three frequency ranges in the linear theory of rigid bodies with a double porosity structure:

1. *Low-frequency range* $LF = \{\omega : 0 < \omega < \omega_1\}$,
2. *Medium frequency range* $MF = \{\omega : \omega_1 < \omega < \omega_2\}$,
3. *Higher frequency range* $HF = \{\omega : \omega > \omega_2\}$.

The Eq. (10) may be written in the form

$$\alpha_0\xi^2 - \zeta_0\xi + \eta_0 = 0, \tag{14}$$

where $\xi = \tau^2$. Let $\mathscr{D} = \zeta_0^2 - 4\alpha_0\eta_0$.

We will consider separately the cases: (a) $\mathscr{D}^* = 0$ and (b) $\mathscr{D}^* > 0$.

(a) Let $\mathscr{D}^* = 0$. On the basis of (9), (11)–(13) we have the following results.

Lemma 1 *If* $\mathscr{D}^* = 0$, *then*

(i) $\dfrac{\alpha_1}{\alpha_2} = \dfrac{\rho_1}{\rho_2}, \quad \alpha_3 = 0,$

(ii) $\omega_1 = \tilde{\omega}_1 = \tilde{\omega}_2 = \omega_2 = \sqrt{\frac{\alpha_1}{\rho_1}}$ *is the cutoff frequency,*

(iii) $\eta_0 = \eta_1\eta_2 = \rho_1\rho_2\left(\omega^2 - \omega_1^2\right)^2, \quad \zeta_0 = (\rho_1\gamma + \rho_2\alpha)\left(\omega^2 - \omega_1^2\right),$

(iv) the dispersion equation (10) has the form

$$\alpha_0\xi^2 - (\rho_1\gamma + \rho_2\alpha)\left(\omega^2 - \omega_1^2\right)\xi + \rho_1\rho_2\left(\omega^2 - \omega_1^2\right)^2 = 0, \tag{15}$$

(v)

$$\mathscr{D} = \left[(\rho_1\gamma - \rho_2\alpha)^2 + 4\beta^2\rho_1\rho_2\right]\left(\omega^2 - \omega_1^2\right)^2 \geq 0$$

and (15) has two real roots ξ_1 *and* ξ_2.

Lemma 2 *If* $\mathscr{D}^* = 0$, *then*

(i) $\xi_j < 0$ *for* $\omega \in LF'$,

(ii) $\xi_j = 0$ *for* $\omega = \omega_1$,

(iii) $\xi_j > 0$ *for* $\omega \in HF'$,

where $j = 1, 2$.

Lemma 3 *Let* $\omega \in LF' \cup HF'$ *and* $\mathscr{D}^* = 0$. *The equation* $\mathscr{D} = 0$ *implies:*

(i)

$$\frac{\alpha}{\gamma} = \frac{\rho_1}{\rho_2}, \qquad \beta = 0,$$

(ii) the dispersion equation (15) has the double root

$$\xi_1 = \xi_2 = \frac{\rho_1}{\alpha}\left(\omega^2 - \omega_1^2\right),$$

(iii) the system (8) has the following form

$$\left(\tau^2 - \xi_1\right)C_l = 0, \qquad l = 1, 2.$$

Let $\tau_j = \sqrt{\xi_j}$ for $\xi_j \geq 0$ and $\tau_j = i\sqrt{-\xi_j}$ for $\xi_j < 0$, $j = 1, 2$, where ξ_1 and ξ_2 are the solutions of (14). Obviously, τ_1 and τ_2 be roots of (10) with respect to τ, i.e. τ_1 and τ_2 are the wave numbers of longitudinal plane harmonic waves. If τ_j is represented by complex value, then the amplitude change of a decaying plane wave can be expressed as

$$C_l' = C_l\, e^{-\mathrm{Im}\tau_j x_1}, \qquad j, l = 1, 2.$$

In this expression the amplitude C_l' is the reduced amplitude after the wave has traveled a distance x_1 from the initial location, C_l is the unattenuated amplitude of the propagating wave at the same location, the quantity $\operatorname{Im}\tau_j$ is the attenuation coefficient of the wave traveling in the x_1-direction.

Lemmas 1–3 lead the following theorems.

Theorem 1 *If $\mathscr{D}^* = \mathscr{D} = 0$ and $\omega \in LF' \cup HF'$, then through a rigid body with a double porosity structure one longitudinal plane wave P_1 propagates with wave number τ_1. This is attenuated wave for $\omega \in LF'$ and has the constant amplitude for $\omega \in HF'$ as $x_1 \to +\infty$.*

Theorem 2 *If $\mathscr{D}^* = 0$, $\mathscr{D} > 0$ and $\omega \in LF' \cup HF'$, then through a rigid body with a double porosity structure two longitudinal plane waves P_1 and P_2 propagate with wave numbers τ_1 and τ_2, respectively. These are attenuated waves for $\omega \in LF'$ and have the constant amplitudes for $\omega \in HF'$ as $x_1 \to +\infty$.*

(b) Let $\mathscr{D}^* > 0$. In what follows we use the following results.

Lemma 4 *If $\mathscr{D}^* > 0$ and $\omega \in LF \cup HF$, then*

(i) $\eta_0 > 0$,
(ii) $\eta_1 < 0,\ \eta_2 < 0,\ \zeta_0 < 0$ *for* $\omega \in LF$,
(iii) $\eta_1 > 0,\ \eta_2 > 0,\ \zeta_0 > 0$ *for* $\omega \in HF$.

Proof (i) On the basis of relations $\omega \in LF \cup HF$ and (13) from (11) we have $\eta_0 > 0$.

(ii) Let $0 < \omega < \omega_1$. Then $\eta_1 = \rho_1(\omega^2 - \omega_1^2) < 0$ and $\eta_2 = \rho_2(\omega^2 - \omega_2^2) < \rho_2(\omega^2 - \omega_1^2) < 0$. However, from (6) and inequality $\eta_0 > 0$ it follows that $|\beta| < \sqrt{\alpha\gamma}$ and $|\alpha_3| < \sqrt{\eta_1\eta_2}$. Therefore,

$$|\beta\alpha_3| < \sqrt{\alpha\gamma}\sqrt{(-\eta_1)(-\eta_2)} = \sqrt{-\alpha\eta_2}\sqrt{-\gamma\eta_1} \le -\frac{1}{2}(\alpha\eta_2 + \gamma\eta_1)$$

and $\alpha\eta_2 + \gamma\eta_1 - 2|\beta\alpha_3| < 0$. Hence, $\zeta_0 < 0$.

(iii) Let $\omega > \omega_2$. Then $\eta_1 = \rho_1(\omega^2 - \omega_1^2) > \rho_1(\omega^2 - \omega_2^2) > 0$ and $\eta_2 = \rho_2(\omega^2 - \omega_2^2) > 0$. However,

$$|\beta\alpha_3| < \sqrt{\alpha\gamma}\sqrt{\eta_1\eta_2} = \sqrt{\alpha\eta_2}\sqrt{\gamma\eta_1} \le \frac{1}{2}(\alpha\eta_2 + \gamma\eta_1)$$

and $\alpha\eta_2 + \gamma\eta_1 - 2|\beta\alpha_3| > 0$. Hence, $\zeta_0 > 0$. □

Quite similarly we can proved the following result.

Lemma 5 *If $\mathscr{D}^* > 0$ and $\eta_0 = 0$, then*

(i) $\eta_1 \le 0,\ \eta_2 < 0,\ \zeta_0 < 0$ *for* $\omega = \omega_1$,
(ii) $\eta_1 > 0,\ \eta_2 \ge 0,\ \zeta_0 > 0$ *for* $\omega = \omega_2$.

We introduce the notation

$$a = \eta_1\gamma - \eta_2\alpha, \qquad b_1 = \eta_2\beta + \alpha_3\gamma, \qquad b_2 = \eta_1\gamma + \alpha_3\alpha. \tag{16}$$

Obviously,

$$\eta_1 b_1 = \eta_2 b_2 + \alpha_3 a. \tag{17}$$

Lemma 6 *If $\eta_1\eta_2 \neq 0$, then*

$$\mathscr{D} = \frac{1}{\eta_1\eta_2}\left[(\eta_1 b_1 + \eta_2 b_2)^2 + \eta_0 a^2\right]. \tag{18}$$

Proof Taking into account (9) and (16) we have

$$\begin{aligned}\mathscr{D} &= (\alpha\eta_2 + \gamma\eta_1 + 2\beta\alpha_3)^2 - 4(\alpha\gamma - \beta^2)(\eta_1\eta_2 - \alpha_3^2) \\ &= (\alpha\eta_2 - \gamma\eta_1)^2 + 4\left[\beta^2\eta_1\eta_2 + \beta\alpha_3(\alpha\eta_2 + \gamma\eta_1) + \alpha\gamma\alpha_3^2\right] = a^2 + 4b_1b_2.\end{aligned} \tag{19}$$

By virtue (17) from (19) it follows that

$$\begin{aligned}\mathscr{D} &= a^2 + \frac{4}{\eta_1}(\eta_2 b_2 + \alpha_3 a)b_2 = \frac{1}{\eta_1}\left(\eta_1 a^2 + 4\alpha_3 a b_2 + 4\eta_2 b_2^2\right) \\ &= \frac{1}{\eta_1\eta_2}\left(4\eta_2^2 b_2^2 + 4\eta_2 b_2 a\alpha_3 + \alpha_3^2 a^2 + \eta_0 a^2\right) \\ &= \frac{1}{\eta_1\eta_2}\left[(2\eta_2 b_2 + a\alpha_3)^2 + \eta_0 a^2\right] = \frac{1}{\eta_1\eta_2}\left[(\eta_1 b_1 + \eta_2 b_2)^2 + \eta_0 a^2\right].\end{aligned}$$

□

Lemma 7 *If $\mathscr{D}^* > 0$, then the Eq. (14) has real roots ξ_1 and ξ_2 with respect to ξ. In addition*

(i) $\xi_1 < 0$ *and* $\xi_2 < 0$ *for* $\omega \in LF$,
(ii) $\xi_1 = 0$ *and* $\xi_2 < 0$ *for* $\omega = \omega_1$,
(iii) $\xi_1 > 0$ *and* $\xi_2 < 0$ *for* $\omega \in MF$,
(iv) $\xi_1 > 0$ *and* $\xi_2 = 0$ *for* $\omega = \omega_2$,
(v) $\xi_1 > 0$ *and* $\xi_2 > 0$ *for* $\omega \in HF$.

Proof If $\omega \in MF$, then $\eta_0 < 0$ and $\mathscr{D} = \zeta_0^2 - 4\alpha_0\eta_0 > 0$. If ω is a cutoff frequency, then $\eta_0 = 0$, $\zeta_0 \neq 0$ and from (18) we get $\mathscr{D} > 0$. However, if $\omega \in LF \cup HF$, then by Lemma 1 we have $\eta_0 > 0$ and from (18) it follows that $\mathscr{D} \geq 0$. Hence, $\mathscr{D} \geq 0$ for arbitrary positive ω and consequently, the Eq. (14) has real roots with respect to ξ.

On account of Lemmas 4 and 5 it is simple to establish the sings of the roots of Eq. (14). □

Lemma 7 leads to the following results.

Theorem 3 *If $\mathscr{D} > 0$, $\mathscr{D}^* > 0$ and ω is not the cutoff frequencies, then through a rigid body with a double porosity structure two longitudinal plane waves P_1 and P_2 propagate with wave numbers τ_1 and τ_2, respectively:*

(i) *these are attenuated waves as* $x_1 \to +\infty$ *for* $\omega \in LF$,
(ii) P_1 *has the constant amplitude and* P_2 *is attenuated wave as* $x_1 \to +\infty$ *for* $\omega \in MF$,
(iii) *these waves have the constant amplitudes for* $\omega \in HF$.

Theorem 4 *If* $\mathscr{D} > 0$, $\mathscr{D}^* > 0$ *and* ω *is the cutoff frequencies, then through a rigid body with a double porosity structure one longitudinal plane wave propagates:*

(i) *this is attenuated wave as* $x_1 \to +\infty$ *for* $\omega = \omega_1$,
(ii) *this wave has the constant amplitude for* $\omega = \omega_2$.

It is easy to see that the system (8) can be written as

$$\begin{aligned} \left(\alpha_0\tau^2 - a_1\right) C_1 + b_1 C_2 = 0, \\ b_2 C_1 + \left(\alpha_0\tau^2 - a_2\right) C_2 = 0, \end{aligned} \tag{20}$$

where $a_1 = \eta_1\gamma + \alpha_3\beta$, $a_2 = \eta_2\alpha + \alpha_3\beta$, b_1 and b_2 given by (16). Obviously, $a_1 + a_2 = \zeta_0$ and $a_1 - a_2 = a$.

In addition, the inequality $\mathscr{D}^* > 0$ implies

$$\frac{\alpha_1}{\alpha_2} < \frac{\rho_1}{\rho_2} \tag{21}$$

or

$$\frac{\alpha_1}{\alpha_2} = \frac{\rho_1}{\rho_2}, \qquad \alpha_3 \neq 0. \tag{22}$$

Now we study the case $\mathscr{D} = 0$ and we will establish the values of the frequency ω from $LF \cup HF$, when the Eq. (14) has a double root. Clearly, on the basis of (18), if $\eta_0 > 0$, then the Eq. (14) has a double root for some frequencies from $LF \cup HF$.

We have the following results.

Lemma 8 *If* $\mathscr{D} = 0$ *and the condition (21) is satisfied, then*

(i)
$$\frac{\alpha}{\gamma} \in \left]0; \frac{\alpha_1}{\alpha_2}\right[\cup \left]\frac{\rho_1}{\rho_2}; +\infty\right[, \qquad (\alpha_1\gamma - \alpha_2\alpha)(\rho_1\gamma - \rho_2\alpha) > 0,$$

(ii)
$$\begin{aligned} &\omega_1 = \tilde{\omega}_1 < \tilde{\omega}_2 = \omega_2, \qquad \beta = 0 \ \ \textit{for} \ \ \alpha_3 = 0 \ \ \textit{and} \\ &\omega_1 < \tilde{\omega}_1 < \tilde{\omega}_2 < \omega_2, \qquad \beta \neq 0 \ \ \textit{for} \ \ \alpha_3 \neq 0, \end{aligned}$$

(iii)
$$\beta(\alpha_1\rho_2 - \alpha_2\rho_1) = \alpha_3(\alpha\rho_2 - \gamma\rho_1),$$

(iv)
$$\zeta_0 = \frac{2\alpha_0(\alpha_1\rho_2 - \alpha_2\rho_1)}{\rho_1\gamma - \rho_2\alpha},$$

(v)

$$\begin{aligned} &\alpha_3\beta > 0 \quad for \quad \tfrac{\alpha}{\gamma} \in \left]0; \tfrac{\alpha_1}{\alpha_2}\right[, \qquad \alpha_3 \neq 0 \quad and \\ &\alpha_3\beta < 0 \quad for \quad \tfrac{\alpha}{\gamma} \in \left]\tfrac{\rho_1}{\rho_2}; +\infty\right[, \qquad \alpha_3 \neq 0. \end{aligned}$$

Lemma 9 *If $\mathscr{D} = 0$ and the condition (21) is satisfied, then*

(i) $\omega = \omega_0$, *where*

$$\omega_0 = \sqrt{\frac{\alpha_1\gamma - \alpha_2\alpha}{\rho_1\gamma - \rho_2\alpha}}, \tag{23}$$

(ii)

$$\xi_1 = \xi_2 = \frac{\alpha_1\rho_2 - \alpha_2\rho_1}{\rho_1\gamma - \rho_2\alpha},$$

(iii)

$$\begin{aligned} &\omega_0 \in LF, \qquad \xi_1 = \xi_2 < 0 \quad for \quad \tfrac{\alpha}{\gamma} \in \left]0; \tfrac{\alpha_1}{\alpha_2}\right[\quad and \\ &\omega_0 \in HF, \qquad \xi_1 = \xi_2 > 0 \quad for \quad \tfrac{\alpha}{\gamma} \in \left]\tfrac{\rho_1}{\rho_2}; +\infty\right[. \end{aligned}$$

Lemma 10 *If $\mathscr{D} = 0$ and the condition (22) is satisfied, then*

(i)

$$\frac{\alpha}{\gamma} = \frac{\alpha_1}{\alpha_2},$$

(ii)

$$\omega_1 < \tilde{\omega}_1 = \tilde{\omega}_2 < \omega_2, \qquad \beta \neq 0,$$

(iii)

$$\frac{\alpha_3}{\beta} < \frac{\alpha_1}{\alpha},$$

(iv)

$$\zeta_0 = -\frac{2\alpha_0\alpha_3}{\beta}.$$

Lemma 11 *If $\mathscr{D} = 0$ and the condition (22) is satisfied, then*

(i) $\omega = \tilde{\omega}_0$, *where*

$$\tilde{\omega}_0 = \sqrt{\frac{\alpha_1\beta - \alpha\alpha_3}{\rho_1\beta}}, \tag{24}$$

(ii)

$$\xi_1 = \xi_2 = -\frac{\alpha_3}{\beta},$$

(iii)

$$\begin{aligned} &\tilde{\omega}_0 \in LF, \qquad \xi_1 = \xi_2 < 0 \quad \textit{for} \quad 0 < \tfrac{\alpha_3}{\beta} < \tfrac{\alpha_1}{\alpha} \quad \textit{and} \\ &\tilde{\omega}_0 \in HF, \qquad \xi_1 = \xi_2 > 0 \quad \textit{for} \quad \tfrac{\alpha_3}{\beta} < 0. \end{aligned}$$

Let $\mathscr{D} = 0$ and $\omega \in LF \cup HF$. Then from (18) we have $a = 0,\ \eta_1 b_1 + \eta_2 b_2 = 0$. By virtue of (21) we get $a_1 = a_2,\ b_1 = b_2 = 0$ and from (20) it follows that

$$\left(\alpha_0 \tau^2 - a_1\right) C_1 = 0, \qquad \left(\alpha_0 \tau^2 - a_1\right) C_2 = 0.$$

Hence,

$$\tau_1^2 = \tau_2^2 = \frac{a_1}{\alpha_0}.$$

In addition, $a_1 = \frac{1}{2}\zeta_0$. By Lemma 4 we obtain $a_1 < 0$ for $\omega \in LF$ and $a_1 > 0$ for $\omega \in HF$.

We have thereby proved.

Theorem 5 *If $\mathscr{D} = 0$ and the condition (21) is satisfied, then $\omega = \omega_0$ and through a rigid body with a double porosity structure one longitudinal plane wave propagates;*

(i) this is attenuated wave as $x_1 \to +\infty$ for $\omega_0 \in LF$,
(ii) this wave has the constant amplitude for $\omega_0 \in HF$, where ω_0 given by (23).

Theorem 6 *If $\mathscr{D} = 0$ and the condition (22) is satisfied, then $\omega = \tilde{\omega}_0$ and through a rigid body with a double porosity structure one longitudinal plane wave propagates;*

(i) this is attenuated wave as $x_1 \to +\infty$ for $\tilde{\omega}_0 \in LF$,
(ii) this wave has the constant amplitude for $\tilde{\omega}_0 \in HF$, where $\tilde{\omega}_0$ given by (24).

Remark 3 It is obvious that if plane harmonic waves propagate in an arbitrary direction $\mathbf{d} = (d_1, d_2, d_3)$ through a rigid body with a double porosity structure, then we obtain the same result given in Theorems 1–6.

4 Internal Boundary Value Problems of Steady Vibrations

If the volume fractions fields $\tilde{\varphi},\ \tilde{\psi}$ and the extrinsic equilibrated body forces $\tilde{F}_1,\ \tilde{F}_2$ are postulated to have a harmonic time variation, that is,

$$\left\{\tilde{\varphi}, \tilde{\psi}, \tilde{F}_1, \tilde{F}_2\right\}(\mathbf{x}, t) = \mathrm{Re}\left[\{\varphi, \psi, F_1, F_2\}(\mathbf{x})\, e^{-i\omega t}\right],$$

then from the system of equations of motion (4) we obtain the following system of nonhomogeneous equations of steady vibrations in the linear theory of rigid bodies with a double porosity structure

$$\begin{aligned}(\alpha\,\Delta+\eta_1)\,\varphi+(\beta\,\Delta-\alpha_3)\,\psi&=-F_1,\\(\beta\,\Delta-\alpha_3)\,\varphi+(\gamma\,\Delta+\eta_2)\,\psi&=-F_2.\end{aligned}\tag{25}$$

The corresponding system of homogeneous equations of steady vibrations in this theory can be written as

$$\begin{aligned}(\alpha\,\Delta+\eta_1)\,\varphi+(\beta\,\Delta-\alpha_3)\,\psi&=0,\\(\beta\,\Delta-\alpha_3)\,\varphi+(\gamma\,\Delta+\eta_2)\,\psi&=0.\end{aligned}\tag{26}$$

We introduce the matrix differential operator

$$\mathbf{A}(\mathbf{D_x})=\left(A_{lj}(\mathbf{D_x})\right)_{2\times 2},$$

where

$$\begin{aligned}&A_{11}(\mathbf{D_x})=\alpha\,\Delta+\eta_1, \qquad A_{12}(\mathbf{D_x})=A_{21}(\mathbf{D_x})=\beta\,\Delta-\alpha_3,\\&A_{22}(\mathbf{D_x})=\gamma\,\Delta+\eta_2, \qquad \mathbf{D_x}=\left(\tfrac{\partial}{\partial x_1},\tfrac{\partial}{\partial x_2},\tfrac{\partial}{\partial x_3}\right).\end{aligned}$$

The system (25) can be written as

$$\mathbf{A}(\mathbf{D_x})\mathbf{u}(\mathbf{x})=\mathbf{F}(\mathbf{x}),\tag{27}$$

where $\mathbf{u}=(\varphi,\psi)$ and $\mathbf{F}=(-F_1,-F_2)$ are two-component vector functions.

Let S be the closed surface surrounding the finite domain Ω^+ in R^3, $S\in C^{1,\nu}$, $0<\nu\le 1$, $\overline{\Omega^+}=\Omega^+\cup S$. The scalar product of two vectors $\mathbf{u}=(u_1,u_2)$ and $\mathbf{v}=(v_1,v_2)$ is denoted by $\mathbf{u}\cdot\mathbf{v}=\sum\limits_{j=1}^{2}u_j\bar{v}_j$, where $\bar{v}_j$ is the complex conjugate of v_j.

Definition 1 A vector function $\mathbf{u}=(\varphi,\psi)$ is called *regular* in Ω^+ if $\varphi,\ \psi\in C^2(\Omega^+)\cap C^1(\overline{\Omega^+})$.

In the sequel, we use the matrix differential operator

$$\mathbf{P}(\mathbf{D_x},\mathbf{n})=(P_{lj}(\mathbf{D_x},\mathbf{n}))_{2\times 2},$$

where

$$P_{11}(\mathbf{D_x},\mathbf{n})=\alpha\tfrac{\partial}{\partial\mathbf{n}}, \qquad P_{12}(\mathbf{D_x},\mathbf{n})=P_{21}(\mathbf{D_x},\mathbf{n})=\beta\tfrac{\partial}{\partial\mathbf{n}}, \qquad P_{22}(\mathbf{D_x},\mathbf{n})=\gamma\tfrac{\partial}{\partial\mathbf{n}},$$

$\mathbf{n}=(n_1,n_2,n_3)$ is the unit vector, $\frac{\partial}{\partial\mathbf{n}}$ is the derivative along the vector $\mathbf{n}$.

The basic internal BVPs of steady vibrations in the linear theory of rigid bodies with a double porosity structure are formulated as follows.

Find in Ω^+ a regular (classical) solution $\mathbf{u}=(\varphi,\ \psi)$ to system (27) satisfying the boundary condition

$$\lim_{\Omega^+ \ni \mathbf{x} \to \mathbf{z} \in S} \mathbf{u}(\mathbf{x}) \equiv \{\mathbf{u}(\mathbf{z})\}^+ = \mathbf{f}(\mathbf{z})$$

in the internal *Problem* $(I)^+_{\mathbf{F},\mathbf{f}}$,

$$\lim_{\Omega^+ \ni \mathbf{x} \to \ \mathbf{z} \in S} \mathbf{P}(\mathbf{D}_\mathbf{x}, \mathbf{n}(\mathbf{z}))\mathbf{u}(\mathbf{x}) \equiv \{\mathbf{P}(\mathbf{D}_\mathbf{z}, \mathbf{n}(\mathbf{z}))\mathbf{u}(\mathbf{z})\}^+ = \mathbf{f}(\mathbf{z})$$

in the internal *Problem* $(II)^+_{\mathbf{F},\mathbf{f}}$, where $\mathbf{F}$ and $\mathbf{f}$ are known two-component smooth vector functions, $\mathbf{n}(\mathbf{z})$ is the external unit normal vector to S at $\mathbf{z}$.

In the next section, the uniqueness of regular solutions of the BVPs $(I)^+_{\mathbf{F},\mathbf{f}}$ and $(II)^+_{\mathbf{F},\mathbf{f}}$ will be studied.

5 Uniqueness Theorems

On the basis of the Green's first identity [26, 27]

$$\int_{\Omega^+} \left[\Delta\varphi(\mathbf{x})\overline{\psi}(\mathbf{x}) + \nabla\varphi(\mathbf{x}) \cdot \nabla\psi(\mathbf{x})\right] d\mathbf{x} = \int_S \frac{\partial\varphi(\mathbf{z})}{\partial\mathbf{n}(\mathbf{z})}\overline{\psi}(\mathbf{z}) d_\mathbf{z} S$$

we have

$$\begin{aligned} &\int_{\Omega^+} \left[(\alpha\Delta + \eta_1)\varphi\overline{\varphi} + \alpha|\nabla\varphi|^2 - \eta_1|\varphi|^2\right] d\mathbf{x} = \alpha \int_S \frac{\partial\varphi}{\partial\mathbf{n}}\overline{\varphi} d_\mathbf{z} S, \\ &\int_{\Omega^+} [(\beta\Delta - \alpha_3)\psi\overline{\varphi} + \beta\nabla\psi \cdot \nabla\varphi + \alpha_3\psi\overline{\varphi}] d\mathbf{x} = \beta \int_S \frac{\partial\psi}{\partial\mathbf{n}}\overline{\varphi} d_\mathbf{z} S. \end{aligned} \tag{28}$$

Taking into account (28) we obtain

$$\int_{\Omega^+} \{[(\alpha\Delta + \eta_1)\varphi + (\beta\Delta - \alpha_3)\psi]\overline{\varphi} + W_1\} d\mathbf{x} = \int_S \left(\alpha\frac{\partial\varphi}{\partial\mathbf{n}} + \beta\frac{\partial\psi}{\partial\mathbf{n}}\right)\overline{\varphi} d_\mathbf{z} S, \tag{29}$$

where $W_1 = \alpha|\nabla\varphi|^2 + \beta\nabla\psi \cdot \nabla\varphi - \eta_1|\varphi|^2 + \alpha_3\psi\overline{\varphi}$.

Quite similarly we get

$$\int_{\Omega^+} \left\{[(\beta\Delta - \alpha_3)\varphi + (\gamma\Delta + \eta_2)\psi]\overline{\psi} + W_2\right\} d\mathbf{x} = \int_S \left(\beta\frac{\partial\varphi}{\partial\mathbf{n}} + \gamma\frac{\partial\psi}{\partial\mathbf{n}}\right)\overline{\varphi} d_\mathbf{z} S, \tag{30}$$

where $W_2 = \beta\nabla\varphi \cdot \nabla\psi + \gamma|\nabla\psi|^2 - \eta_2|\psi|^2 + \alpha_3\varphi\overline{\psi}$.

From (29) and (30) it follows that

$$\int_{\Omega^+} [\mathbf{A}(\mathbf{D}_\mathbf{x})\mathbf{u}(\mathbf{x}) \cdot \mathbf{u}(\mathbf{x}) + W(\mathbf{x})] d\mathbf{x} = \int_S \mathbf{P}(\mathbf{D}_\mathbf{z}, \mathbf{n}(\mathbf{z}))\mathbf{u}(\mathbf{z}) \cdot \mathbf{u}(\mathbf{z}) d_\mathbf{z} S, \tag{31}$$

where

$$W = W_0 + W_3, \qquad W_0 = \alpha|\nabla\varphi|^2 + 2\beta\mathrm{Re}\,(\nabla\varphi\cdot\nabla\psi) + \gamma|\nabla\psi|^2,$$
$$W_3 = -\eta_1|\varphi|^2 + 2\alpha_3\mathrm{Re}\,(\varphi\overline{\psi}) - \eta_2|\psi|^2. \tag{32}$$

Taking into account (6) from (32) we have

$$W_0 \geq 0. \tag{33}$$

Theorem 7 *If $\mathscr{D}^* > 0$ and $\omega \in LF$, then the internal BVP $(K)^+_{\mathbf{F},\mathbf{f}}$ has one regular solution, where $K = I, II$.*

Proof Suppose that there are two regular solutions of problem $(K)^+_{\mathbf{F},\mathbf{f}}$, where $K = I, II$. Then their difference $\mathbf{u} = (\varphi, \psi)$ is a regular solution of the internal homogeneous BVP $(K)^+_{\mathbf{0},\mathbf{0}}$. Hence, the vector $\mathbf{u}$ is a regular solution of the system (26), i.e.

$$\mathbf{A}(\mathbf{D}_\mathbf{x})\mathbf{u}(\mathbf{x}) = \mathbf{0}, \qquad \text{for} \quad \mathbf{x} \in \Omega^+ \tag{34}$$

and satisfies the boundary condition

$$\{\mathbf{P}(\mathbf{D}_\mathbf{z}, \mathbf{n}(\mathbf{z}))\mathbf{u}(\mathbf{z})\cdot\mathbf{u}(\mathbf{z})\}^+ = 0 \qquad \text{for} \quad \mathbf{x} \in \Omega^+. \tag{35}$$

Taking into account (34) and (35) from the equality (31) we obtain

$$\int_{\Omega^+} W(\mathbf{x})d\mathbf{x} = 0. \tag{36}$$

By virtue of Lemma 4 and the condition $\omega \in LF$ it follows that $\eta_0 > 0$, $\eta_1 < 0$, $\eta_2 < 0$ and we have $W_3 \geq 0$. On the basis of (32) and (33) from (36) we get $\mathrm{W}(\mathbf{x}) = 0$, and this relation implies $W_3(\mathbf{x}) = 0$. By inequality $\eta_0 > 0$ from (32) we obtain $\mathbf{u}(\mathbf{x}) = \mathbf{0}$ for $\mathbf{x} \in \Omega^+$. □

Theorem 8 *If $\mathscr{D}^* = 0$ and $\omega \in LF'$, then the internal BVP $(K)^+_{\mathbf{F},\mathbf{f}}$ has one regular solution, where $K = I, II$.*

Theorem 8 can be proved similarly to Theorem 7.

Theorem 9 *If $\mathscr{D}^* > 0$ and $\omega = \omega_1$, then*

(i) the internal BVP $(I)^+_{\mathbf{F},\mathbf{f}}$ has one regular solution,

(ii) any two regular solutions of the internal BVP $(II)^+_{\mathbf{F},\mathbf{f}}$ may differ only for an additive vector $\mathbf{u}(\mathbf{x}) = (\varphi(\mathbf{x}), \psi(\mathbf{x}))$, where

$$\varphi(\mathbf{x}) = c_1 = \mathrm{const}, \qquad \psi(\mathbf{x}) = c_2 = \mathrm{const} \qquad \text{for} \quad \mathbf{x} \in \Omega^+, \tag{37}$$

c_1 and c_2 are arbitrary complex numbers satisfy the equation

$$\alpha_3 c_1 = \eta_2 \bar{c}_2. \tag{38}$$

Proof Clearly, the difference $\mathbf{u} = (\varphi, \psi)$ of two regular solutions of the BVP $(K)^+_{\mathbf{F},\mathbf{f}}$ is a regular solution of the homogeneous BVP $(K)^+_{\mathbf{0},\mathbf{0}}$, where $K = I, II$. The vector $\mathbf{u}$ satisfies the system of homogeneous equations (34) and boundary condition (35). Hence, we have (36).

On the other hand, by Lemma 5 we have $\eta_1 \le 0$, $\eta_2 < 0$, $\eta_1\eta_2 = \alpha_3^2$ and

$$W_3 = -\frac{1}{\eta_2}\left[\alpha_3^2|\varphi|^2 - 2\alpha_3\eta_2 \mathrm{Re}(\varphi\tilde{\psi}) + \eta_2^2|\psi|^2\right] = -\frac{1}{\eta_2}|\alpha_3\varphi - \eta_2\tilde{\psi}|^2 \ge 0. \tag{39}$$

By virtue of (33) and (39) from (36) it follows that $W_0(\mathbf{x}) = 0$ and $W_3(\mathbf{x}) = 0$ for $\mathbf{x} \in \Omega^+$. The last two equations imply the Eqs. (37) and (38).

In the case of BVP $(I)^+_{\mathbf{0},\mathbf{0}}$, in view of homogeneous boundary condition $\{\mathbf{u}(\mathbf{z})\}^+ = 0$ from (37) we get $c_1 = c_2 = 0$ and hence, $\mathbf{u}(\mathbf{x}) = 0$ for $\mathbf{x} \in \Omega^+$.

In addition, in the case of BVP $(II)^+_{\mathbf{0},\mathbf{0}}$, if $\alpha_3 = 0$, then from (38) it follows that $c_2 = 0$ and consequently, we obtain $\mathbf{u}(\mathbf{x}) = (c_1, 0)$. □

Theorem 10 *If $\mathscr{D}^* = 0$ and $\omega = \omega_1$, then*

(i) the internal BVP $(I)^+_{\mathbf{F},\mathbf{f}}$ has one regular solution;

(ii) any two regular solutions of the internal BVP $(II)^+_{\mathbf{F},\mathbf{f}}$ may differ only for an additive vector $\mathbf{u}(\mathbf{x}) = (\varphi(\mathbf{x}), \psi(\mathbf{x}))$, where φ and ψ satisfy the condition (37), c_1 and c_2 are arbitrary complex numbers.

Proof Quite similarly, as in the previous theorem, the difference $\mathbf{u} = (\varphi, \psi)$ of two regular solutions of the BVP $(K)^+_{\mathbf{F},\mathbf{f}}$ is a regular solution of the homogeneous BVP $(K)^+_{\mathbf{0},\mathbf{0}}$, where $K = I, II$. Hence, we have (36).

On the other hand, by Lemma 1 from equations $\mathscr{D}^* = 0$ and $\omega = \omega_1$ we have $\eta_1 = \eta_2 = \alpha_3 = 0$. These equations imply $W_3(\mathbf{x}) = 0$. By virtue of (32) and (33) from (36) it follows that $W_0(\mathbf{x}) = 0$. From the last equation we obtain the condition (37).

In addition, in the case of BVP $(I)^+_{\mathbf{0},\mathbf{0}}$, in view of homogeneous boundary condition $\{\mathbf{u}(\mathbf{z})\}^+ = 0$ from (37) we get $c_1 = c_2 = 0$ and hence, $\mathbf{u}(\mathbf{x}) = 0$ for $\mathbf{x} \in \Omega^+$. □

Now we begin to study uniqueness of regular solution of BVP $(K)^+_{\mathbf{F},\mathbf{f}}$ for $\omega > \omega_1$, where $K = I, II$. Let $\mathbf{u} = (\varphi, \psi)$ be a regular solution of the first internal homogeneous BVP $(I)^+_{\mathbf{0},\mathbf{0}}$. As in classical theory of elasticity (see [26, 27]), this problem is reduced to the equivalent Fredholm's homogeneous integral equation

$$\mathbf{v}(\mathbf{x}) - \omega^2 \int_{\Omega^+} \mathbf{G}(\mathbf{x}, \mathbf{y})\mathbf{v}(\mathbf{y}) d_{\mathbf{y}} S = \mathbf{0}, \tag{40}$$

with the symmetrical kernel $\mathbf{G}(\mathbf{x},\mathbf{y}) = \overline{\mathbf{G}^{\top}(\mathbf{y},\mathbf{x})}$ of class L_2, where $\mathbf{G}^{\top}$ is the transpose of matrix $\mathbf{G}$, $\mathbf{v}(\mathbf{x}) = \mathbf{E}\mathbf{u}(\mathbf{x})$ and

$$\mathbf{E} = \begin{pmatrix} \sqrt{\rho_1} & 0 \\ 0 & \sqrt{\rho_2} \end{pmatrix}_{2\times 2}.$$

This is proved in the conventional manner, applying Green's formula of the considered theory. Hence, in agreement with the Hilbert-Schmidt theorem follows the existence of a discrete spectrum of real eigenvalues of the parameter ω^2 for which integral equation (40) has solutions different from zero. These values ω are called the eigenfrequencies of the internal homogeneous BVP $(I)^{+}_{\mathbf{0},\mathbf{0}}$.

Let $\{\omega_{(j)}\}_{j=1}^{\infty}$ is the complete system of the eigenfrequencies of BVP $(I)^{+}_{\mathbf{0},\mathbf{0}}$, where $\omega_{(1)} \leq \omega_{(2)} \leq \cdots$. On the basis of Theorems 7–10 it follows that

$$\omega_1 < \omega_{(1)} \leq \omega_{(2)} \leq \cdots, \qquad \omega_{(j)} \to +\infty \quad \text{for} \quad j \to +\infty. \tag{41}$$

Therefore the following theorem is valid.

Theorem 11 *The first internal homogeneous BVP $(I)^{+}_{\mathbf{0},\mathbf{0}}$ has a discrete spectrum of eigenfrequencies $\{\omega_{(j)}\}_{j=1}^{\infty}$, where $\left\{\omega^2_{(j)}\right\}_{j=1}^{\infty}$ is the complete system eigenvalues of the integral equation (40). These eigenfrequencies satisfy the condition (41).*

Keeping in mind Theorems 7–10 the following theorem is proved quite similarly.

Theorem 12 *The second internal homogeneous BVP $(II)^{+}_{\mathbf{0},\mathbf{0}}$ has a discrete spectrum of eigenfrequencies $\{\tilde{\omega}_{(j)}\}_{j=1}^{\infty}$, where $\left\{\tilde{\omega}^2_{(j)}\right\}_{j=1}^{\infty}$ is the complete system eigenvalues of Fredholm's integral equation*

$$\mathbf{v}(\mathbf{x}) - \omega^2 \int_{\Omega^+} \tilde{\mathbf{H}}(\mathbf{x},\mathbf{y})\mathbf{v}(\mathbf{y})d_{\mathbf{y}}S = \mathbf{0}$$

with the symmetrical kernel $\tilde{\mathbf{H}}(\mathbf{x},\mathbf{y}) = \overline{\tilde{\mathbf{H}}^{\top}(\mathbf{y},\mathbf{x})}$. These eigenfrequencies satisfy the conditions $\omega_1 = \tilde{\omega}_{(1)} \leq \tilde{\omega}_{(2)} \leq \cdots$ and $\tilde{\omega}_{(j)} \to +\infty$ for $j \to +\infty$.

Now we establish the asymptotic distribution of eigenfrequencies $\{\omega_{(j)}\}_{j=1}^{\infty}$ and $\{\tilde{\omega}_{(j)}\}_{j=1}^{\infty}$. Let us denote by $N(r)$ the number of eigenvalues $\omega_{(j)}$ (or $\tilde{\omega}_{(j)}$) not exceeding r, where $r > 0$, $j = 1, 2, \ldots$:

$$N(r) = \sum_{\omega_j \leq r} 1 \qquad \left(\text{or} \quad N(r) = \sum_{\tilde{\omega}_j \leq r} 1\right).$$

Let v_1 and v_2 be the positive roots of equation (with respect to v)

$$\rho_1\rho_2 v^4 - (\rho_1\gamma + \rho_2\alpha)v^2 + \alpha_0 = 0,$$

i.e.

$$\begin{aligned} v_1 &= \sqrt{\tfrac{1}{2\rho_1\rho_2}\left[\rho_1\gamma + \rho_2\alpha - \sqrt{(\rho_1\gamma - \rho_2\alpha)^2 + 4\rho_1\rho_2\beta^2}\right]}, \\ v_2 &= \sqrt{\tfrac{1}{2\rho_1\rho_2}\left[\rho_1\gamma + \rho_2\alpha + \sqrt{(\rho_1\gamma - \rho_2\alpha)^2 + 4\rho_1\rho_2\beta^2}\right]}. \end{aligned} \tag{42}$$

Obviously, v_1 and v_2 are the velocities of the longitudinal plane waves in the linear theory of rigid bodies with a double porosity structure for $\alpha_1 = \alpha_2 = \alpha_3 = 0$. Clearly, if $\beta = 0$, then from (42) it follows that

$$v_1 = \sqrt{\frac{\alpha}{\rho_1}}, \qquad v_2 = \sqrt{\frac{\gamma}{\rho_2}}.$$

Quite similarly as in the theory of elasticity of binary mixtures [35], by using the same technique of Tauberian theorems due to Carleman [9] we obtain the following theorem.

Theorem 13 *The asymptotic behavior of eigenfrequencies of the internal homogeneous BVP* $(K)^{+}_{\mathbf{0},\mathbf{0}}$ *is independent of the shape of the rigid body with a double porosity structure, is simply proportional to its volume and expressed by formula*

$$N(r) = \frac{|\Omega^+|}{6\pi^2} M r^3 + O(r^2)$$

for $r \to +\infty$, *where* $|\Omega^+|$ *is the volume of* Ω^+, $M = v_1^{-3} + v_2^{-3}$, v_1 *and* v_2 *are given by (42),* $K = I, II$.

Remark 4 Using the theory of integral equations, the earliest results on the asymptotic form of distribution of eigenfrequencies were obtained by Weyl [50] for the case of the Laplacian Δ operator in two dimensions.

6 Connection Between Plane Waves and Uniqueness of Solutions

By virtue of our Theorems 1–12 we have the following connection between plane waves and the uniqueness of solutions (or existence of eigenfrequencies) of the internal BVPs of steady vibrations in the linear theory of rigid bodies with a double porosity structure:

1. If ω is in the low-frequency range, then the longitudinal plane harmonic waves propagating through a rigid body with a double porosity structure are attenuated and the interior BVP of steady vibrations $(K)^{+}_{\mathbf{F},\mathbf{f}}$ has one regular solution, where $K = I, II$.
2. If ω is not in the low-frequency range, then at least one longitudinal plane harmonic wave always propagate with constant amplitude throughout a rigid body with a double porosity structure and the internal homogeneous BVP $(K)^{+}_{\mathbf{0},\mathbf{0}}$ has a discrete spectrum of eigenfrequencies, where $K = I, II$.

Remark 5 The connection between plane harmonic waves and the uniqueness of solutions (or existence of eigenfrequencies) of the internal BVPs of steady vibrations in the linear theories of elasticity and thermoelasticity of binary mixtures is established by Svanadze [36, 38], in the coupled theory of elasticity for solids with double porosity and the theory of micropolar thermoelasticity for materials with voids by Ciarletta et al. [10, 11].

Remark 6 On the basis of uniqueness Theorems 7–10 it is possible to prove existence theorems in the linear theory of rigid bodies with a double porosity structure by means of the potential method (boundary integral equations method) and the theory of singular integral equations. This method is developed in the books [7, 26, 27] and papers [8, 19, 31, 46]. For an extensive review of works on the potential method, see [15].

References

1. Bai, M., Elsworth, D., Roegiers, J.C.: Multiporosity/multipermeability approach to the simulation of naturally fractured reservoirs. Water Resour. Res. **29**, 1621–1633 (1993)
2. Barenblatt, G.I., Zheltov, I.P., Kochina, I.N.: Basic concept in the theory of seepage of homogeneous liquids in fissured rocks (strata). J. Appl. Math. Mech. **24**, 1286–1303 (1960)
3. Beskos, D.E., Aifantis, E.C.: On the theory of consolidation with double porosity-II. Int. J. Eng. Sci. **24**, 1697–1716 (1986)
4. Biot, M.A.: General theory of three-dimensional consolidation. J. Appl. Phys. **12**, 155–164 (1941)
5. Biot, M.A.: Theory of propagation of elastic waves in a fluid-saturated porous solid. I. Low-frequency range. J. Acoust. Soc. Am. **28**, 168–178 (1956)
6. Biot, M.A.: Theory of propagation of elastic waves in a fluid-saturated porous solid. II. Higher frequency range. J. Acoust. Soc. Am. **28**, 179–191 (1956)
7. Burchuladze, T.V., Gegelia, T.G.: The Development of the Potential Methods in the Elasticity Theory. Metsniereba, Tbilisi (1985)
8. Burchuladze, T., Svanadze, M.: Potential method in the linear theory of binary mixtures for thermoelastic solids. J. Therm. Stress. **23**, 601–626 (2000)
9. Carleman, T.: Über die asymptotische Verteilung der Eigenwerte partieller Differentialgleichungen. Ber. der Sachs. Akad. d. Wiss. Leipzig **88**, 119–132 (1936)
10. Ciarletta, M., Passarella, F., Svanadze, M.: Plane waves and uniqueness theorems in the coupled linear theory of elasticity for solids with double porosity. J. Elast. **114**, 55–68 (2014)
11. Ciarletta, M., Svanadze, M., Buonanno, L.: Plane waves and vibrations in the theory of micropolar thermoelasticity for materials with voids. Eur. J. Mech. A Solids **28**, 897–903 (2009)

12. Cowin, S.C.: Bone poroelasticity. J. Biomech. **32**, 217–238 (1999)
13. Cowin, S.C., Gailani, G., Benalla, M.: Hierarchical poroelasticity: movement of interstitial fluid between levels in bones. Phil. Trans. Roy. Soc. A **367**, 3401–3444 (2009)
14. Cowin, S.C., Nunziato, J.W.: Linear elastic materials with voids. J. Elast. **13**, 125–147 (1983)
15. Gegelia, T., Jentsch, L.: Potential methods in continuum mechanics. Georgian Math. J. **1**, 599–640 (1994)
16. Gelet, R., Loret, B., Khalili, N.: A thermo-hydro-mechanical coupled model in local thermal non-equilibrium for fractured HDR reservoir with double porosity. J. Geophys. Res.: Solid. Earth **117**, B07205 (2012). doi:10.1029/2012JB009161
17. Gelet, R., Loret, B., Khalili, N.: Borehole stability analysis in a thermoporoelastic dual-porosity medium. Int. J. Rock Mech. Min. Sci. **50**, 65–76 (2012)
18. Gentile, M., Straughan, B.: Acceleration waves in nonlinear double porosity elasticity. Int. J. Eng. Sci. **73**, 10–16 (2013)
19. Ieşan, D.: Method of potentials in elastostatics of solids with double porosity. Int. J. Eng. Sci. **88**, 118–127 (2015)
20. Ieşan, D., Quintanilla, R.: On a theory of thermoelastic materials with a double porosity structure. J. Therm. Stress **37**, 1017–1036 (2014)
21. Khaled, M.Y., Beskos, D.E., Aifantis, E.C.: On the theory of consolidation with double porosity III. Int. J. Numer. Anal. Methods Geomech. **8**, 101–123 (1984)
22. Khalili, N.: Coupling effects in double porosity media with deformable matrix. Geophys. Res. Lett. **30**, 2153 (2003)
23. Khalili, N., Habte, M.A., Zargarbashi, S.: A fully coupled flow deformation model for cyclic analysis of unsaturated soils including hydraulic and mechanical hysteresis. Comp. Geotech. **35**, 872–889 (2008)
24. Khalili, N., Selvadurai, A.P.S.: A fully coupled constitutive model for thermo-hydro-mechanical analysis in elastic media with double porosity. Geophys. Res. Lett. **30**, 2268 (2003)
25. Khalili, N., Valliappan, S.: Unified theory of flow and deformation in double porous media. Eur. J. Mech. A Solids **15**, 321–336 (1996)
26. Kupradze, V.D.: Potential methods in the theory of elasticity. Israel Program Science Translation, Jerusalem (1965)
27. Kupradze, V.D., Gegelia, T.G., Basheleishvili, M.O., Burchuladze, T.V.: Three-Dimensional Problems of the Mathematical Theory of Elasticity and Thermoelasticity, North-Holland, Amsterdam, New York, Oxford (1979)
28. Moutsopoulos, K.N., Konstantinidis, A.A., Meladiotis, I., Tzimopoulos, ChD, Aifantis, E.C.: Hydraulic behavior and contaminant transport in multiple porosity media. Trans. Porous Med. **42**, 265–292 (2001)
29. Nunziato, J.W., Cowin, S.C.: A nonlinear theory of elastic materials with voids. Arch. Rat. Mech. Anal. **72**, 175–201 (1979)
30. Rohan, E., Naili, S., Cimrman, R., Lemaire, T.: Multiscale modeling of a fluid saturated medium with double porosity: relevance to the compact bone. J. Mech. Phys. Solids **60**, 857–881 (2012)
31. Scalia, A., Svanadze, M.: Potential method in the linear theory of thermoelasticity with microtemperatures. J. Therm. Stress **32**, 1024–1042 (2009)
32. Scarpetta, E., Svanadze, M.: Uniqueness theorems in the quasi-static theory of thermoelasticity for solids with double porosity. J. Elast. **120**, 67–86 (2015)
33. Scarpetta, E., Svanadze, M., Zampoli, V.: Fundamental solutions in the theory of thermoelasticity for solids with double porosity. J. Therm. Stress **37**, 727–748 (2014)
34. Straughan, B.: Stability and uniqueness in double porosity elasticity. Int. J. Eng. Sci. **65**, 1–8 (2013)
35. Svanadze, M.: Asymptotic distribution of eigenfunctions and eigenvalues of the boundary value problems of linear theory of elastic mixtures. Georgian Math. J. **3**, 177–200 (1996)
36. Svanadze, M.: On existence of eigenfrequencies in the theory of two-component elastic mixtures. Q. J. Mech. Appl. Math. **51**, 427–437 (1998)
37. Svanadze, M.: Fundamental solution in the theory of consolidation with double porosity. J. Mech. Behav. Mater. **16**, 123–130 (2005)

38. Svanadze, M.: Plane waves and eigenfrequencies in the linear theory of binary mixtures of thermoelastic solids. J. Elast. **92**, 195–207 (2008)
39. Svanadze, M.: Dynamical problems of the theory of elasticity for solids with double porosity. Proc. Appl. Math. Mech. **10**, 309–310 (2010)
40. Svanadze, M.: The boundary value problems of the full coupled theory of poroelasticity for materials with double porosity. Proc. Appl. Math. Mech. **12**, 279–282 (2012)
41. Svanadze, M.: Plane waves and boundary value problems in the theory of elasticity for solids with double porosity. Acta Appl. Math. **122**, 461–471 (2012)
42. Svanadze, M.: Fundamental solution in the linear theory of consolidation for elastic solids with double porosity. J. Math. Sci. **195**, 258–268 (2013)
43. Svanadze, M.: On the theory of viscoelasticity for materials with double porosity. Discr. Contin. Dynam. Syst. B **19**, 2335–2352 (2014)
44. Svanadze, M.: Uniqueness theorems in the theory of thermoelasticity for solids with double porosity. Mecanicca **49**, 2099–2108 (2014)
45. Svanadze, M.: External boundary value problems of steady vibrations in the theory of rigid bodies with a double porosity structure. Proc. Appl. Math. Mech. **15**(1), 365–366 (2015)
46. Svanadze, M.M.: Potential method in the linear theory of viscoelastic materials with voids. J. Elast. **114**, 101–126 (2014)
47. Svanadze, M., De Cicco, S.: Fundamental solutions in the full coupled linear theory of elasticity for solid with double porosity. Arch. Mech. **65**, 367–390 (2013)
48. Svanadze, M., Scalia, A.: Mathematical problems in the theory of bone poroelasticity. Int. J. Math. Meth. Models Biosci. **1**(1211225), 1–4 (2012)
49. Svanadze, M., Scalia, A.: Mathematical problems in the coupled linear theory of bone poroelasticity. Comp. Math. Appl. **66**, 1554–1566 (2013)
50. Weyl, H.: Über die asymptotische Verteilung der Eigenwerte. Nachr. Ges. Wiss. Göttingen 110–117 (1911)
51. Wilson, R.K., Aifantis, E.C.: On the theory of consolidation with double porosity-I. Int. J. Eng. Sci. **20**, 1009–1035 (1982)
52. Zhao, Y., Chen, M.: Fully coupled dual-porosity model for anisotropic formations. Int. J. Rock Mech. Min. Sci. **43**, 1128–1133 (2006)

Seismic Response of Poroelastic Graded Geological Region with Underground Structures by BIEM

Frank Wuttke, Ioanna-Kleoniki Fontara and Petia Dineva

Abstract This work addresses horizontally polarized shear *SH* seismic wave radiated from an embedded seismic source in a continuously inhomogeneous poroelastic half-plane with cavities presenting underground structures as unlined tunnels and pipelines. The mechanical model and corresponding computational tool are: (1) viscoelastic approximation (isomorphism) to Biot's equations of dynamic poroelasticity and (2) boundary integral equation method (BIEM) using frequency-dependent fundamental solution of the governing wave equation for continuously inhomogeneous media. The problem is formulated under anti-plane strain conditions and time-harmonic motions are assumed. Two different mechanical models for inhomogeneous in depth poroelastic half-plane are presented: (a) *Model A*: the density and shear modulus vary proportionally as quadratic functions of depth, but the wave velocity remains constant. In this case is used BIEM based on an analytically derived Green's function for graded half-plane; (b) *Model B*: the material properties vary with respect to the spatial coordinates in a different manner, so that the wave velocity is both frequency and position-dependent. The formulation of the considered problem by boundary integral equations (BIE) is realized via fundamental solution of equation of motion for viscoelastic full-plane with position-dependent wave speed profiles. The parametric study reveals the dependence of the seismic signals along the free surface and inside the geological region on the following key factors: (a) type and properties of the material gradient; (b) characteristics of the applied load; (c) position and number of cavities; (d) dynamic cavities interaction; (e) cavity-free surface interaction; (f) poroelastic soil properties.

Keywords Anti-plane elastodynamic problem · Poroelasticity · Inhomogeneity · Underground structure · BIEM · Seismic response

F. Wuttke (✉) · I.-K. Fontara
Chair of Geomechanics and Geotechnics, Christian-Albrechts University, Kiel, Germany
e-mail: fw@gpi.uni-kiel.de

I.-K. Fontara
e-mail: fontara@gpi.uni-kiel.de

P. Dineva
Institute of Mechanics, BAS, Sofia, Bulgaria
e-mail: petia@imbm.bas

B. Albers and M. Kuczma (eds.), *Continuous Media with Microstructure 2*,
DOI 10.1007/978-3-319-28241-1_20

1 Introduction

The BIEM has proven to be a most efficient and accurate numerical tool for elastodynamics of infinite or semi-infinite regions, see Beskos [2], Dominguez [8]. This method is based on a recasting of the governing partial differential equations of a given problem in mechanics, with its prescribed boundary conditions, into integral equations defined along the problem surfaces, so that all field variables become boundary quantities. The main reason for using the BIEM in computational geomechanics is the presence of the free surface of the earth, whereby large categories of problems involve continua with a small surface to volume ratio. At the same time this technique requires surface discretization only. Due to this BIEM feature substantial savings can be realized in terms of the size of the mesh resulting from the discretization procedure as compared to domain-type numerical methods as finite element methods and finite difference ones. In the evaluation of the state of the art we will concentrate mainly on the BIEM results for seismic wave propagation in poroelastic geological media. The key role played by the fundamental solution is to reduce a given boundary-value problem (BVP) into a system of boundary integral equations through the use of reciprocal theorems. For this reason the recovery of fundamental solutions in analytical form, or at least in an easy to calculate numerical form, is so important. A lot of research work has been directed towards the derivation of fundamental solutions for the governing partial differential equations of Biot's poroelasticity [4–7, 17, 21, 23, 24]. These include derivations in either the time domain or in transform domains, and under both 2D and 3D conditions. To summarize, the comprehensive state-of-the-art reviews by Gatmiri and Kamalian [11], Gatmiri and Nguyen [12], Seyrafian et al. [25] and Gatmiri and Eslami [10] contain abundant information on the dynamic fundamental solutions derived for the porous media and their subsequent incorporation within coupled integral equation statements. 2D dynamic response of unlined and lined tunnels in poroelastic soil to harmonic body waves is studied in Kattis and Beskos [14]. So far, BIE- based methods have seen limited application to seismic wave propagation in saturated geological media due to difficulties in accounting for the multi-phase nature of the problem. There is, however, a marked similarity between poroelastic and viscoelastic materials in terms of their dynamic response. This fact suggests the possibility to use a single phase model with special, augmented properties in lieu of the multiphase one. This idea was promulgated by Bardet [1] and Morochnik and Bardet [20], who proposed an equivalent viscoelastic solid to model saturated poroelastic materials governed by Biot's theory. The main conclusion from the short review of the obtained BIEM results shows that there is a lack of models and efficient computational tools able to consider simultaneously the geological profile as continuously inhomogeneous (graded), heterogeneous and poroelastic for synthesis of seismic signals.

The main aim of this work is to solve 2D elastodynamic problem for graded poroelastic by Bardet model and heterogeneous with multiple cavities geological profile via BIEM.

The rest of the paper is structured as follows. In Sect. 2 the problem statement is presented, while Sect. 3 deals with its reformulation via BIEs and simulation results, while conclusions are discussed in Sect. 4.

2 Problem Statement

Consider graded in respect to the depth viscoelastic half-plane Ω_0 with free surface S_f containing N cylindrical unlined tunnels (or pipelines) with common boundary $\Gamma_t = \bigcup_{k=1}^{N} \Gamma_k$, k = 1, 2, ... N, subjected to seismic SH wave radiated from a line seismic source acting as a time-harmonic body force with magnitude f_{03}, frequency ω and located at a prescribed point $\mathbf{x_0} = \mathbf{x_0}(x_{01}, x_{02})$, see Fig. 1. For the state of anti-plane wave motion, the only non-zero field quantities are displacement component u_3, stresses $\sigma_{i3} = \mu(x_2)u_{3,i}$, $i = 1, 2$, and traction $t_3 = \sigma_{i3}n_i$, where n_i are the components of the outward pointing normal vector, all depending on the coordinates (x_1, x_2). The viscoelastic shear modulus is complex-valued with the same real part as in its elastic counterpart, while its imaginary part is due to the dissipative processes developed during wave propagation in soils. For a Kelvin-Voigt model the wave number is $k_S^2 = \frac{\omega^2}{C_S(1-i\omega\xi_S)}$, where $C_S(x_2) = \sqrt{\frac{\mu(x_2)}{\rho(x_2)}}$ is the real part of the SH wave velocity, while ξ_S is the corresponding attenuation coefficient representing a small amount of hysteretic damping. In the low frequency range, i.e. $\omega\xi_S \ll 1$, the wave number reduces to, see [1]:

$$k_S \approx \frac{\omega\,(1 + 0.5\omega\xi_S)}{C_S}. \tag{1}$$

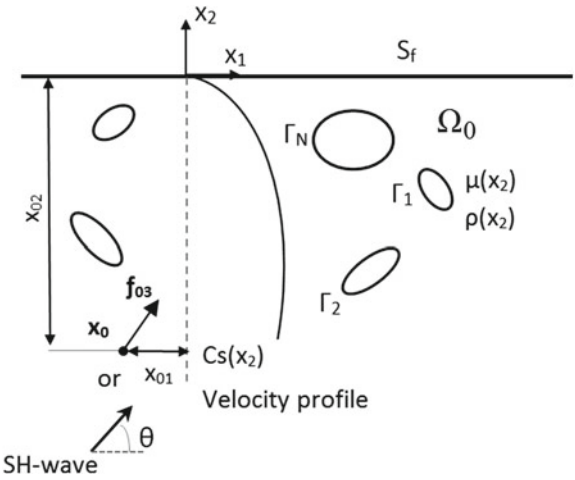

Fig. 1 Soil-tunnel interaction in poroelastic graded half-plane

The material properties of the graded half-plane are depth dependent shear module $\mu(x_2)$ and density $\rho(x_2)$. Assume that attenuation coefficient ξ_S is constant.

The governing equation of motion is as follows:

$$\nabla.\{\mu(\mathbf{x})\nabla u_3(\mathbf{x},\omega)\} = -\rho(\mathbf{x})\omega^2 u_3(\mathbf{x},\omega) - f_{03}\delta(\mathbf{x},\mathbf{x}_0); \qquad \mathbf{x} \in \boldsymbol{\Omega}_0. \tag{2}$$

The corresponding boundary conditions are:

$$t_3(x_1,x_2,\omega) = \sigma_{i3}(x_1,x_2,\omega)\,\mathrm{n}_i(x_1,x_2) = 0; \qquad (x_1,x_2) \in \Gamma = S_f \cup \Gamma_t. \tag{3}$$

In addition, the Sommerfeld radiation condition holds for waves at infinity. In the above equations, n_i are the components of the outward pointing normal vector, the summation convention over repeated indices is implied, ∇ is the gradient operator and (.) is the inner product.

Two different mechanical models for the material gradient are considered:

1. *Type A*, where the density and the shear modulus vary proportionally in a quadratic way in respect to the depth, and in this case the phase velocity is not position-dependent:

$$\mu(x_1,x_2) = \mu^0 h(x_2), \qquad \rho(x_1,x_2) = \rho^0 h(x_2), \qquad h(x_2) = (bx_2+1)^2, \tag{4}$$

   where $h(x)$ is the inhomogeneity function, $b \leq 0$ is the inhomogeneity magnitude, and $\mu^0 = \mu(x_1,0)$, $\rho^0 = \rho(x_1,0)$ are the reference viscoelastic constants.
2. *Type B*, where shear modulus and density vary in respect to depth in different way, phase velocity is both frequency and position-dependent. The material profiles follows the inhomogeneous model proposed in Manolis and Shaw [18, 19] and in Karakostas and Manolis [13], where the shear module and density are the following functions of depth and frequency:

$$\mu^{1/2}(x_2) = (\mu^\infty)^{1/2} + H_1 exp(-\gamma x_2) + H_2 exp(ik_S^\infty x_2), \tag{5}$$

$$\rho(x_2) = \frac{1}{\omega^2}\mu^{1/2}(x_2)\left[(k_S^\infty)^2(\mu^\infty)^{1/2} + \left((k_S^0)^2(\mu^0)^{1/2} - (k_S^\infty)^2(\mu^\infty)^{1/2} exp(-\gamma x_2)\right)\right], \tag{6}$$

$$H_1 = \frac{\left((k_S^0)^2(\mu^0)^{1/2} - (k_S^\infty)^2(\mu^\infty)^{1/2}\right)}{\gamma^2 + (k_S^\infty)^2}, \tag{7a}$$

$$H_2 = \left((\mu^0)^{1/2} - (\mu^\infty)^{1/2} - \frac{\left((k_S^0)^2(\mu^0)^{1/2} - (k_S^\infty)^2(\mu^\infty)^{1/2}\right)}{\gamma^2 + (k_S^\infty)^2}\right), \tag{7b}$$

where: $C_S^0 = \sqrt{\mu^0/\rho^0}$ and $k_S^0 = \omega/C_S^0$ are wave velocity and wave number respectively at the free surface $x_2 = 0$, while $C_S^\infty = \sqrt{\mu^\infty/\rho^\infty}$ and $k_S^\infty = \omega/C_S^\infty$ are their counterparts at great depth $x_2 \to \infty$, where the material becomes homogeneous. Coefficient γ is a small number taken as equal to 0.1, see Karakostas and Manolis [13]. Let's define the inhomogeneity magnitude in this model as the ratio $c = \frac{C_S^\infty}{C_S^0}$.

The aim of this work is to evaluate stress-strain state at any point of the graded poroelastic half-plane with cavities of arbitrary number, shape and geometrical configuration by solution of the formulated above BVP presented by Eq. (2), boundary condition (3) and using the viscoelastic isomorphism of Bardet [1] to Biot's equations of dynamic poroelasticity.

First Biot [3] derived the frequency dependent equations of motion for fluid-saturated materials considered as two-phase ones. A characteristic equation for the wave numbers in the frame of the Biot's model was obtained in Bardet [1] and Lin et al. [15]. Three solutions to Biot's wave equation have been identified, corresponding to shear wave S transmitted through the solid skeleton, fast dilatational P wave and slow dilatational P wave. The corresponding wave velocities are complex and frequency dependent, hence they correspond to dissipative and dispersive waves. Finally, the solid and fluid dilatations are in phase for the first arriving P wave, and in reverse phase for the slower P wave, which damps out quickly. In a series of publications, Bardet [1] discussed the applicability of the viscoelastic behavior equivalent to Biot's model [3] of dynamic poroelasticity in the low frequency range. As a matter of fact, Bardet [1] proposed a single-phase viscoelastic material representation for saturated soils. At first, the viscoelastic material constants are complex-valued with the same real part expressed via Biot's coefficients P, Q, R basing on the viscoelastic isomorphism. The same holds true for the governing viscoelastic wave equation, with wave numbers which are complex-valued, frequency dependent functions that satisfy causality conditions. A poroelastic-viscoelastic isomorphism proposed in Bardet [1] is based on the equating of the wave numbers in Biot's poroelastic model with those in viscoelastic Kelvin-Voigt model.

We briefly will define the terminology used for description of solid-fluid continuum in poroelasticity. A representative volume V for the solid-fluid continuum comprises an elastic, isotropic solid skeleton (matrix) with porosity $n = V_P/V$, where V_P is the pore volume. The "dry rock" approximation is the case of an air-filled solid skeleton, while the "solid grain" characteristics are the properties of the skeleton material. The elastic bulk modulus and density are denoted as follows for dry rock K_{dry}, $\rho_{dry} = (1-n)\rho_g$, solid grain K_g; ρ_g and fluid K_f; ρ_f.

The solid-fluid system density is $\rho_{sat} = \rho_{dry} + n\rho_f = (1-n)\rho_g + n\rho_f$. The shear strength of the porous material is provided by the solid skeleton and is not affected by the fluid, since fluids sustain dilatational deformations only. Thus, both dry and saturated soils are described by the same shear modulus, i.e. $\mu = \mu_{sat} = \mu_{dry} = \frac{3(1-2\nu)}{2(1+\nu)}K_{dry}$, where ν is the Poisson's ratio for the dry skeleton. A poroelastic-viscoelastic isomorphism proposed in Bardet [1] is based on equating the wave numbers in Biot's poroelastic model with those in viscoelastic Kelvin-Voigt model.

The following expressions were obtained for complex-valued phase velocities of viscoelastic materials that provide the equivalence between the dynamic responses of the poroelastic and viscoelastic solids:

$$C_P = \sqrt{\frac{P+2Q+R}{\rho_{sat}}}; \qquad C_S = \sqrt{\frac{\mu}{\rho_{sat}}} \tag{8}$$

$$\xi_P = \frac{\rho_{sat}}{b}\left(\frac{Q+R}{P+2Q+R}\cdot\frac{n\rho_f}{\rho_{sat}}\right)^2; \qquad \xi_S = \frac{\rho_{sat}}{b}\left(\frac{n\rho_f}{\rho_{sat}}\right)^2 \tag{9}$$

$$P = \frac{3(1-\nu)}{1+\nu}K_{dry} + \frac{Q^2}{R}; \qquad Q = \frac{n(1-n-K_{dry}/K_g)}{(1-n-K_{dry}/K_g+nK_g/K_f)}K_g \tag{10}$$

$$R = \frac{n^2K_g}{1-n-K_{dry}/K_g+nK_g/K_f}; \quad N = \frac{3}{2}\frac{1-2\nu}{1+\nu}K_{dry}; \quad K_{dry} = \frac{2}{3}\frac{\mu(1+\nu)}{1-2\nu} \tag{11}$$

$$\lambda_{sat} = \lambda_{dry} + \frac{Q^2}{R}; \qquad b = \frac{n^2 g\rho_f}{\hat{k}} \tag{12}$$

where g is the acceleration of gravity and $\hat{k}$ is the soil permeability with values in the interval 10^{-10}–10^{-2} m/sec. The above approximate expressions are correct when the following condition is satisfied: $(\omega\rho_{sat}/b) \ll 1$. It is always satisfied in earthquake engineering field since permeability values for most soils is small. Figure 2 shows the sensitivity of the SH phase velocity for dry and saturated sandstone to the porosity. It is used the sandstone with the following characteristics:

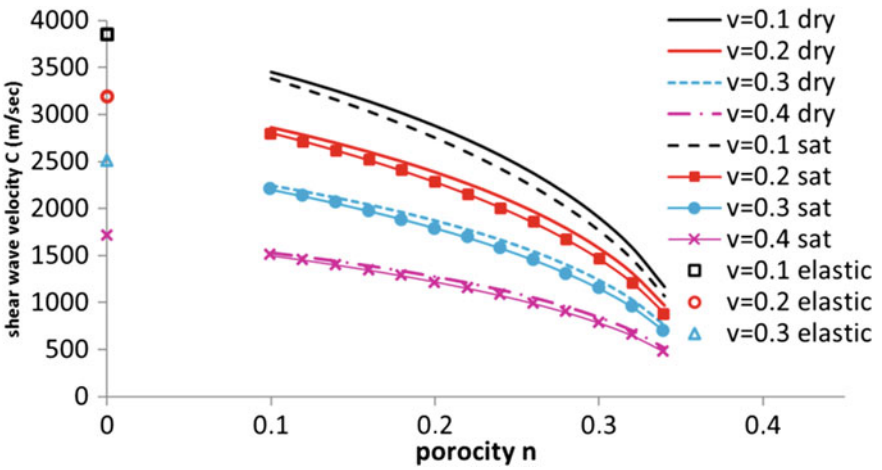

Fig. 2 SH-wave velocity variation with porosity for homogeneous dry, saturated and pure elastic soil by Bardet [1] model

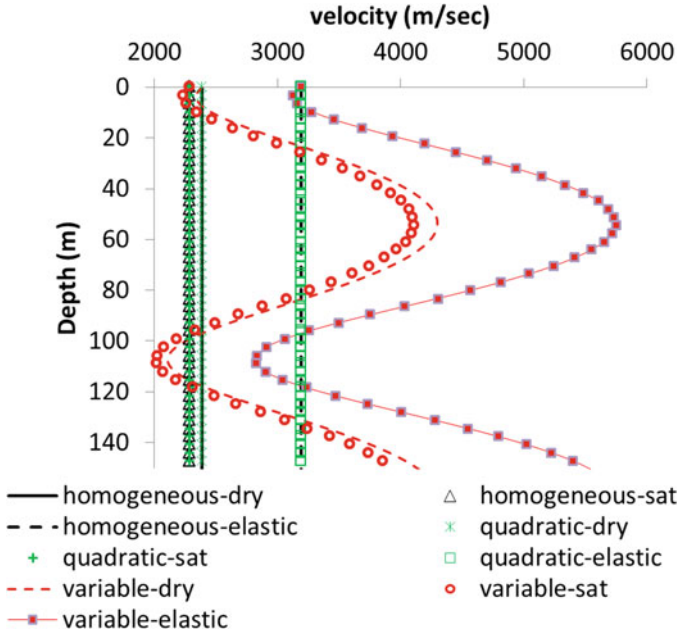

Fig. 3 Velocity profile along the depth for elastic and poroelastic (with porosity n = 0.2) material

$$K_g = 36000\,\text{MPa}; \quad \rho_g = 2650\,\text{kg/m}^3; \quad K_f = 2000\,\text{MPa}; \rho_f = 1000\,\text{kg/m}^3$$
$$K_{dry} = K_{cr} + (1 - n/n_{cr})(K_g - K_{cr}), \quad n_{cr} = 0.36; \quad K_{cr} = 200\,\text{MPa},$$

see Lin et al. [15]. All numerical results further are obtained for this type of soil.

Velocity profile along the depth for homogeneous and inhomogeneous (type A and type B at a fixed non-dimensional frequency $\eta = 0.25$ defined below), pure elastic, dry and saturated (with porosity n = 0.2) half-plane is given in Fig. 3. For the inhomogeneous model of type B the velocity profile depends also on the frequency.

3 BEM Solution and Numerical Results

The defined above boundary-value problem (BVP) can be reformulated via a set of boundary integral equations (13) along the boundary Γ based on the frequency-dependent fundamental solution of partial differential equation (2), see Dominguez [8]:

$$cu_3(\mathbf{x}, \omega) = \int_\Gamma U_3^*(\mathbf{x}, \mathbf{y}, \omega)\mathbf{t}_3(\mathbf{y}, \omega)\mathrm{d}\Gamma + \int_\Gamma P_3^*(\mathbf{x}, \mathbf{y}, \omega)u_3(\mathbf{y}, \omega)\,\mathrm{d}\Gamma + f_{03}U_3^*(\mathbf{x}, \mathbf{x}_0, \omega); \quad \mathbf{x} \in \Gamma \tag{13}$$

In the above, c is the jump term dependent on the local geometry at the collocation point $\mathbf{x}(x_1, x_2)$, U_{ij}^* is the displacement fundamental solution of the governing equation (2) derived analytically in Manolis and Shaw [18, 19] for the inhomogeneous viscoelastic mechanical model of *type B* (see the Appendix), $P_3^*(\mathbf{x}, \mathbf{y}, \omega) = \mu(\mathbf{x}_2) U_{3,i}^*(\mathbf{x}, \mathbf{y}, \omega) n_i(\mathbf{x})$ is the corresponding traction fundamental solution. The displacements and stresses at any point inside the solid can be obtained from the well-known integral representation formulas using the solutions of Eq. (13).

The BIEM formulation of *type A* mechanical model is as follows:

$$cu_3(\mathbf{x}, \omega) = -\int_\Gamma t_3^{g^*}(\mathbf{x}, \boldsymbol{\xi}, \omega)\mathbf{u}_3(\xi, \omega)\, \mathrm{d}S_1 + \int_\Gamma g_3^*(\mathbf{x}, \boldsymbol{\xi}, \omega) t_3(\boldsymbol{\xi}, \omega)\, \mathrm{d}S_1 + f_{03} g_3^*(\mathbf{x}, \mathbf{x}_0, \omega); \qquad \mathbf{x} \in \Gamma \quad (14)$$

Here: c is the jump term depending on the surface geometry at the collocation point, $\mathbf{x}$ and $\boldsymbol{\xi}$ are the vector-positions of the source and field points respectively, $g_3^*(\mathbf{x}, \boldsymbol{\xi}, \omega)$ is the frequency-dependent Green's function for quadratically inhomogeneous in depth half-plane derived analytically in Rangelov and Manolis [22], $t_3^{g^*}(\mathbf{x}, \boldsymbol{\xi}, \omega) = \sigma_{3i}^*(\mathbf{x}, \boldsymbol{\xi}, \omega) n_i(\xi) = \mu(\xi) g_{3,i}^*(\mathbf{x}, \boldsymbol{\xi}, \omega) n_i(\xi)$ is its corresponding traction, where derivatives are in respect to the field point. For the completeness of the text, the Green's function and the corresponding traction are given in the Appendix. BIEs (13) and (14) are solved numerically via discretization and collocation techniques, see Fontara et al. [9] and Wuttke et al. [26] respectively.

To the authors' best knowledge there are no results in the literature for even the case of a single cavity in graded half-plane following the material profiles of *type A* and *B*. This is the reason we verify our numerical schemes by test example for homogeneous case, using the codes developed for inhomogeneous material. In what follows we present a validation test that consists of a single circular cavity with radius a and center coordinates $(0, -h)$ located in a homogeneous half-plane where normally incident time-harmonic SH wave is propagating, see Fig. 4. It is introduced the non-dimensional frequency defined as $\eta = \frac{2a}{\lambda_S^0}$, where $\lambda_S^0 = \frac{2\pi}{\omega}\sqrt{\frac{\mu^0}{\rho^0}}$. Figure 4 demonstrates the accuracy of the developed numerical schemes by comparison of the authors' solutions with those of Luco and de Barros [16] for the absolute values of the normalized displacements $\left|\frac{u_3}{u_{30}}\right|$ along the free surface due to normal incident SH wave with frequency $\eta = 0.5$ and $\eta = 1$. The following values of cavity depth defined by the ratio $\frac{h}{a} = 1.5$ and $\frac{h}{a} = 5$, for shallow and deep burial, respectively, are used.

For the BEM based on fundamental solution the mesh consists of 124 constant boundary elements along the free surface and 44 constant boundary elements along the cavity, while the size of the discretized flat free surface is $\pm 22a$. For the BEM based on Green's function the mesh consists of 22 constant boundary elements along the circular cavity.

Displacement amplitudes along free surface of elastic inhomogeneous graded poroelastic half-plane with an embedded single circular cavity subjected to concen-

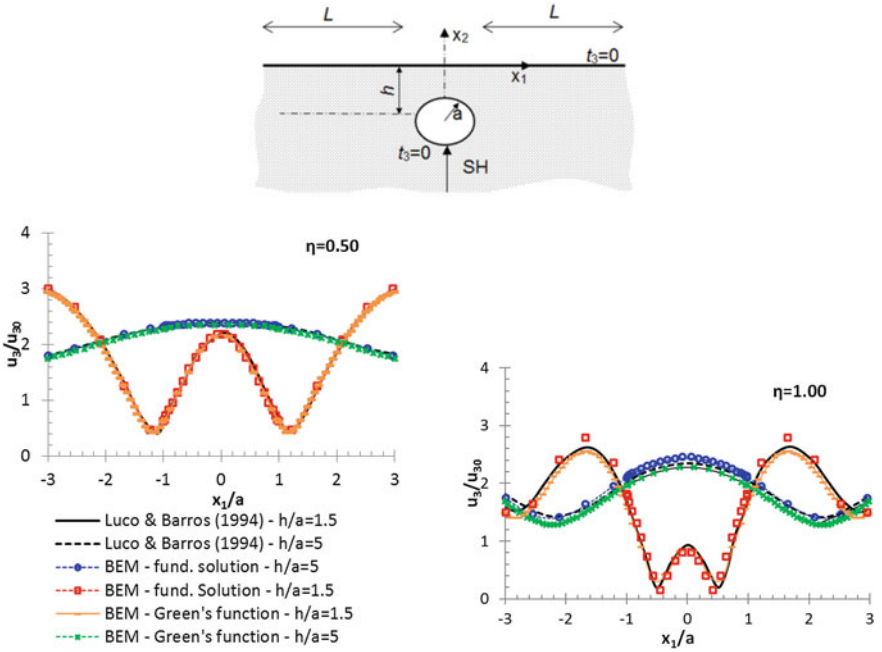

Fig. 4 Displacement amplitude variation along the free surface of an elastic homogeneous half-plane with an embedded circular cavity of radius a under a normally incident SH wave with dimensionless frequency $\eta = 0.5$ and $\eta = 1.0$

trated at point $\mathbf{x_0}$ $(0, -15a)$ body force with frequency $\eta = 0.25$ are drawn in Fig. 5. The presented results are obtained for homogeneous case and for inhomogeneous one considering two different material profiles of *type A* (quadratic variation of stiffness and density, but the phase velocity is constant) and *B* (variable velocity). The porosity is n = 0.2, the Poisson ration is 0.25 and $\frac{\mu^0(0)}{\mu^\infty} = \frac{1}{2}$.

Figure 5 demonstrates how sensitive the wave field is to the following parameters: (i) the type of the inhomogeneity model, (ii) the type of the material gradient and (iii) the poroelasticity of the material. The difference between the dry and saturated case is insignificant because the porosity is not great, however the difference increases at higher porosity values. It can be seen that the response of the *Type B* material profile diverges the most from the response of the homogeneous case. The difference in terms of displacements between *Type A* and the homogeneous case is smaller and even negligible at higher frequency, because macroscopically the wave speeds are the same for these two materials.

Figure 6 draws the normalized displacement amplitude $\left|\frac{u_{3poroelastic}}{u_{3elastic}}\right|$ along the free surface of continuously inhomogeneous poroelastic half plane of *type B* with inhomogeneity coefficient in the interval $c = 0.25 \div 4$ due to SH-wave propagating from an embedded seismic source located at (0, −15a) with frequency $\eta = 0.25$ in the case of a single and two cavities with radius a. The obtained results are for pure

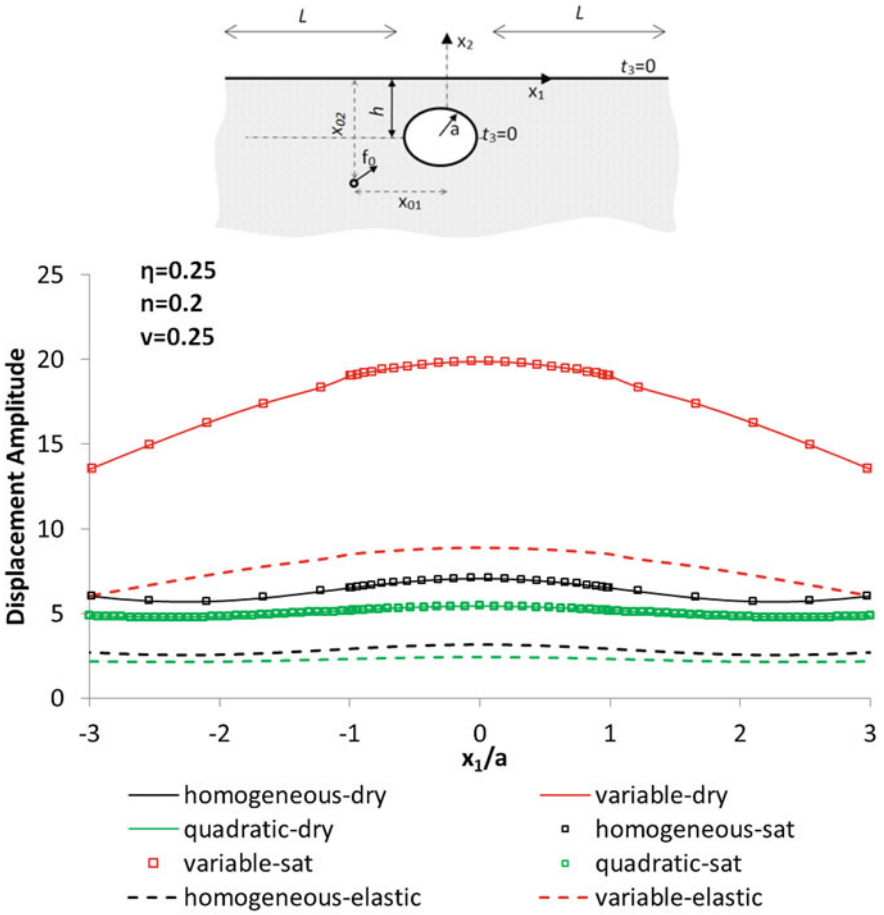

Fig. 5 Displacement amplitude along the free surface of an elastic and poroelastic (n = 0.2) graded half-plane with a single circular tunnel due to waves radiating from an embedded at point (0, −15a) seismic source at frequency value $\eta = 0.25$. Comparison is between results obtained by homogeneous and inhomogeneous models of type A (constant velocity profile) and B (variable velocity profile)

elastic and poroelastic case with porosity n = 0.3 and n = 0.35. The normalization is done with respect to the maximal displacement along the free surface of the same geological profile with pure elastic material. With increasing the porosity the displacement along the free surface increases significantly in respect to the displacement in the elastic case. Additionally with increasing the inhomogeneity coefficient the displacement also increases and attains its maximum value at inhomogeneity coefficient c = 0.3. Observe that when the poroelasticity and the inhomogeneity effect are combined the material response may lead to 30 times greater value than the pure elastic homogeneous case.

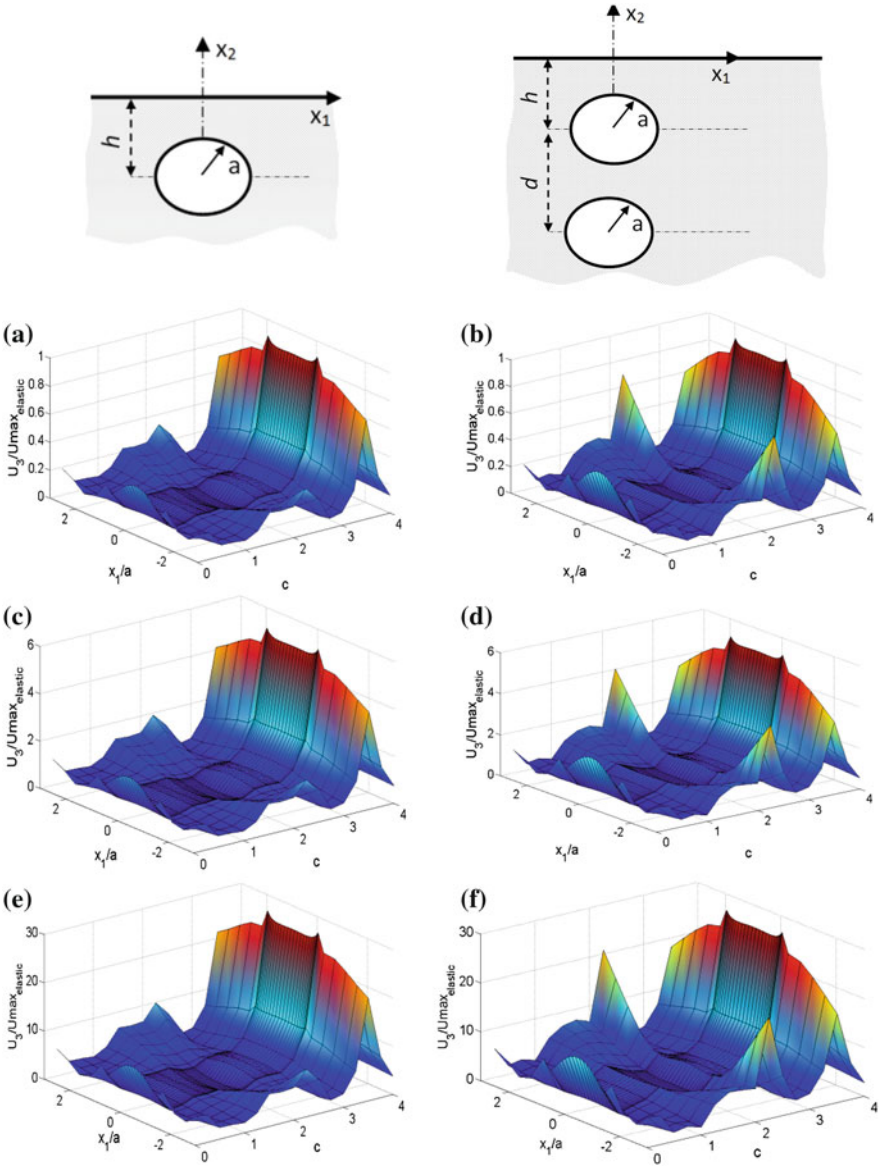

Fig. 6 Normalized displacement amplitude along the free surface of continuously inhomogeneous of type B half plane with inhomogeneity coefficient c = 0.25-4 due to SH-wave propagating from embedded seismic source located at (0, −15a) with frequency $\eta = 0.5$ in the case of a single and two tunnels. The obtained results are for pure elastic (**a**) and (**b**) and poroelastic cases with n = 0.3 (**c**) and (**d**) and n = 0.35 (**e**) and (**f**)

The obtained results reveal that the seismic wave field is a complex result due to a hybrid influence of different key factors like poroelasticity and inhomogeneity of the material, existence of multiple heterogeneities (cavities) at arbitrary geometrical configuration. Furthermore, dynamic interactions between the heterogeneity free surface and among heterogeneities play an important role in the kinematic field along the free surface. Finally, the type of external load and its frequency content are also important parameters in this mechanical problem. Note here, that although the cavities in all numerical results are of circular shape, the developed numerical scheme allows consideration of arbitrary geometry.

4 Conclusion

In the present work wave propagation problems in graded poroelastic half-plane containing multiple cavities are investigated. The geological region is poroelastic, inhomogeneous and heterogeneous. The poroelasticity is taken into consideration by the Bardet model. The two-phase poroelastic dynamic behavior described by the Biot's model is approximated by the dynamic response of one-phase viscoelastic material. The main advantage of the proposed viscoelastic isomorphism is that due to its mechanical (one-phase instead two-phase material) and mathematical simplicity (the wave equation and its fundamental solution are much simpler in this case than in Biot's model), it gives the possibility to obtain approximate solutions for complex boundary-value problems related to seismic wave propagation in continuously inhomogeneous with material gradient fluid-saturated geological region. The equivalent model can deal with the changes of the stiffness and the damping mechanism in the poroelastic material. Two different mechanical models for material gradient are presented and inserted in numerical simulations. Application of BIEM to problems in elastodynamics for inhomogeneous continua runs into serious difficulties, because the method pre-supposes the existence of fundamental solutions for the corresponding governing wave equation with variable coefficients. In general, partial differential equations with variable coefficients do not possess explicit fundamental solutions that can easily be implemented within existing BIEM numerical codes. This in turn prevents reduction of a given BVP to a system of boundary integral equations that can be evaluated by numerical quadrature. The authors used frequency-dependent Green's function for quadratically inhomogeneous half-plane and fundamental solution for infinite domain with position dependent phase velocity. Additionally the half-plane is heterogeneous with multiple heterogeneities like cavities. The developed computational tool is an efficient mesh-reduced BIEM numerical scheme. Research software is developed, verified and used for extensive parametric studies. The numerical simulations demonstrate the potential of the BIEM to produce highly accurate results regarding the seismic response of underground structures in graded saturated geological regions.

Acknowledgments The authors acknowledge the support of the DFG Grant No. DFG-Wu 496/5-1.

Appendix

Green's Function for Quadratically Inhomogeneous Half-plane

Green's function g_3^* is the solution of the following boundary value problem in frequency domain:

$$\begin{aligned} &\sigma_{i3,i}(\mathbf{x},\omega) + \rho(\mathbf{x})\omega^2 g_3^*(\mathbf{x},\omega) = -\delta(\mathbf{x}-\boldsymbol{\xi}) \\ &t_3^*(\mathbf{x},\omega) = \mu(\mathbf{x}) g_{3,i}^*(\mathbf{x},\boldsymbol{\xi},\omega) n_i(x) = 0 \qquad \text{for} \qquad x_2 = 0 \end{aligned} \tag{A.1}$$

In Rangelov and Manolis [22] this Green's function was derived in a closed form by the usage of the smooth transformation of the type $g_3^*(\mathbf{x},\boldsymbol{\xi},\omega) = h^{-1/2}(\mathbf{x})$ $G_3^*(\mathbf{x},\xi,\omega)$ and thus reducing the boundary-value problem with variable coefficients presented by Eq. (2) to one with constant coefficients with respect to the transformed Green's function $G_3^*(\mathbf{x},\boldsymbol{\xi},\omega)$ available for analytical derivation by the usage of a suitable integral, see details in Rangelov and Manolis [22].

Here for the completeness of the text we give the Green's function and the corresponding traction below:

$$\begin{aligned} &g_3^*(\mathbf{x},\boldsymbol{\xi},\omega) \\ &= h^{-1/2}(\boldsymbol{\xi}) h^{-1/2}(\mathbf{x}) \left[\frac{i}{4\mu_0} H_0^{(1)}(kr) + \frac{1}{4\pi\mu_0} \int_{-\infty}^{+\infty} \frac{\gamma+b}{\gamma(\gamma-b)} e^{\gamma(x_2+\xi_2)} e^{i\eta(x_1+\xi_1)} \, \mathrm{d}\eta \right] \end{aligned} \tag{A.2}$$

where: $\gamma = \sqrt{\eta^2 - \mathbf{k}^2}$; $\mathbf{k} = \mathbf{k}_1 + i\mathbf{k}_2$; $\mathbf{k}_1^2 = \frac{\rho_0}{\mu_0}\omega^2$; $k_1^2 > 0$; $k_2 > 0$, $r = \sqrt{(x_1-\xi_1)^2 + (x_2-\xi_1)^2}$, $H_0^{(1)}(z)$ and $H_1^{(1)}(z)$ is 1st Hankel function of 0 and 1 order.

Fundamental Solution of Equation of Motion for Inhomogeneous Material of Type B

Fundamental solution is derived in Manolis and Shaw [18, 19]. It is solution of Eq. (2) for a right-hand-side (RHS) in the form of a unit point force (i.e., Dirac delta function). The methodology is based on an algebraic transformation of the displacement of the type $u_3^*(\mathbf{x},\omega) = \mu^{-1/2}(\mathbf{x},\omega) U_3^*(\mathbf{x},\omega)$, which also modifies the RHS as $\mu^{-1/2}(\mathbf{x},\omega)\delta(\mathbf{x}-\boldsymbol{\xi})$, where $\mathbf{x}, \boldsymbol{\xi}$ is the source-receiver pair. This procedure transforms the partial differential equation with variable coefficients for displacement $u_3(\mathbf{x},\omega)$ to one with constant coefficients for the transformed displacement $U_3(\mathbf{x},\omega)$. Solution of the latter type of equations defined for an "equivalent" homogeneous medium are readily available, see Dominguez [8]:

$$U_3^{*hom}(R,\omega) = \frac{1}{2\pi\mu^{\infty}} K_0\left(\frac{i\omega R}{C_S^{\infty}}\right); \qquad R = \sqrt{(x_1-\xi_1)^2+(x_2-\xi_2)^2}. \tag{A.3}$$

In the above, K_0 is the modified Bessel function of second kind and zero order. Thus, the fundamental solution of Eq. (2) attains the following final form:

$$u_3^*(\mathbf{x},\boldsymbol{\xi},\omega) = \mu^{\infty}\mu^{-1/2}(x_2)\mu^{-1/2}(\xi_2)U_3^{*hom}(R,\omega). \tag{A.4}$$

The above form is conditional on the shear modulus and the density satisfying the following constraint equation, which dictates acceptable depth profiles for material parameters $\mu(x_2)$, $\rho(x_2)$ and wave number $k(x_2)$:

$$\frac{1}{4}\mu^{-1}\left(\frac{\mathrm{d}\mu}{\mathrm{d}x_2}\right)^2 - \frac{1}{2}\frac{\mathrm{d}^2\mu}{\mathrm{d}x_2^2} + \omega^2\rho = \mu k^2. \tag{A.5}$$

References

1. Bardet, J.P.: A viscoelastic model for the dynamic behaviour of saturated poroelastic soils. Trans. ASME **59**, 128–135 (1992)
2. Beskos, D.E.: Boundary element methods in dynamic analysis: Part II (1986–1996). Appl. Mech. Rev. **50**(3), 149–197 (1997)
3. Biot, M.: Theory of propagation of elastic waves in a fluid-saturated porous solid. J. Acoust. Soc. Am. **4**, 168–191 (1956)
4. Burridge, R., Vargas, C.A.: The fundamental solution in dynamic poroelasticity. Geophys. J. R. Astron. Soc. **58**(1), 61–90 (1979)
5. Cheng, A.H.D.: Heterogeneities in flows through porous media by boundary element method. Topics in boundary element research. Appl. Geomech. **4**, 1291–1344 (1987)
6. Chen, J.: Time domain fundamental solution to Biot's complete equations of dynamic poroelasticity. Part I: Two-dimensional solution. Int. J. Solids Struct. **31**(10), 1447–1490 (1994a)
7. Chen, J.: Time domain fundamental solution to Biot's complete equations of dynamic poroelasticity. Part II: Three-dimensional solution. Int. J. Solids Struct. **31**(2), 169–202 (1994b)
8. Dominguez, J.: Boundary Elements in Dynamics. Computational Mechanics Publications, Southampton (1993)
9. Fontara, I.-K., Dineva, P., Manolis, G., Wuttke, F.: BEM modeling of elastic waves in a graded half-plane with position-dependent velocity containing cavities. In: EUROMECH-Colloquia Micromechanics of Metal Ceramic Composites, Stuttgart, Germany (2015)
10. Gatmiri, B., Eslami, H.: Scattering of harmonic waves by a circular cavity in a porous medium: complex functions theory approach. Int. J. Geomech. **7**(5), 371–381 (2007)
11. Gatmiri, B., Kamalian, M.: On the fundamental solution of dynamic poroelastic boundary integral equations in time domain. Int. J. Geomech. **2**(4), 381–398 (2002)
12. Gatmiri, B., Nguyen, K.V.: Time 2D fundamental solution for saturated porous media with incompressible fluid. Commun. Numer. Methods Eng. **21**(3), 119–132 (2005)
13. Karakostas, C.Z., Manolis, G.D.: Transient signal simulation due to explosion in heterogeneous soil media. Int. J. BEM Commun. **8**, 160–167 (1997)
14. Kattis, S.E., Beskos, D.E., Cheng, A.H.D.: 2D dynamic response of unlined and lined tunnels in poroelastic soil to harmonic body waves. Earthq. Eng. Struct. Dyn. **32**(1), 97–110 (2003)
15. Lin, C.H., Lee, V.W., Trifunac, M.D.: The reflection of plane waves in a poroelastic half-space saturated with inviscid fluid. Soil Dyn. Earthq. Eng. **25**, 205–223 (2005)

16. Luco, J.E., de Barros, C.P.: Dynamic displacements and stresses in the vicinity of a cylindrical cavity embedded in a half- space. Earthq. Eng. Struct. Dyn. **23**, 321–340 (1994)
17. Manolis, G.D., Beskos, D.E.: Integral formulation and fundamental solutions of dynamic poroelasticity and thermoelasticity. Acta Mecanica **83**, 223–226 (1990)
18. Manolis, G.D., Shaw, R.: Harmonic wave propagation through viscoelastic heterogeneous media exhibiting mild stochasticity-I. Fundamental solutions. Soil Dyn. Earthq. Eng. **15**, 119–127 (1996a)
19. Manolis, G.D., Shaw, R.P.: Harmonic wave propagation through viscoelastic heterogeneous media exhibiting mild stochasticity-II. Applications. Soil Dyn. Earthq. Eng. **15**, 129–139 (1996b)
20. Morochnik, V., Bardet, J.P.: Viscoelastic approximation of poroelastic media for wave scattering problems. Soil Dyn. Earthq. Eng. **15**(5), 337–346 (1996)
21. Norris, A.N.: Radiation from a point source and scattering theory in a fluid-saturated porous solid. J. Acoust. Soc. Am. **77**, 2012–2023 (1985)
22. Rangelov, T.V., Manolis, G.D.: Point force and dipole solutions in the inhomogeneous half-plane under time-harmonic conditions. Mech. Res. Commun. **56**, 90–97 (2014)
23. Schanz, M.: Wave propagation in viscoelastic and poroelastic continua: a boundary element approach. In: Pfeiffer, F. (ed.) Lecture Notes in Applied Mechanics, vol. 2. Berlin, Springer (2001)
24. Schanz, M.: Application of 3D time-domain boundary element formulation to wave propagation in poroelastic solids. Eng. Anal. Bound. Elem. **25**, 363–376 (2001)
25. Seyrafian, S., Gatmiri, B., Nourzad, A.: Green functions for a continuously nonhomogenous saturated media. Int. J. Comput. Methods Eng. Sci. **15**(2), 115–125 (2006)
26. Wuttke, Fr., Fontara, I.-K., Dineva, P., Rangelov, Ts.: SH-wave propagation in a continuously inhomogeneous half-plane with free-surface relief by BIEM. ZAMM Z. Angew. Math. Mech. 1–16 (2014). doi:10.1002/zamm.201300198

Part IV
Engineering Applications

Determination of Foundation Coefficients for a 2-Parameter Model on the Basis of Railway Sleeper Deflection

Włodzimierz Andrzej Bednarek

Abstract In the paper foundation coefficients for a 2-parameter model on the basis of the railway sleeper deflection are determined. The railway sleeper is assumed as an Euler-Bernoulli beam of finite length resting on a two-parameter elastic foundation. During the analysis two types of railway sleepers are considered (wooden and concrete). The railway sleeper in FEM is divided into 80 elements. The parameters connected with the railway sleeper are: the sleeper's width, length and stiffness, variable value of the force transferred from the rail to the railway sleeper. The foundation parameters (k_1 i k_2) are determined based on a modified Vlasov soil model [12, 16]. The parameters connected with the foundation are modulus of elasticity (usually measured by a VSS plate)—E_s, the Poisson's ratio (ν_S) of the foundation. In the Vlasov two-parameter foundation model, the foundation is treated as an elastic layer, and the constraints are imposed by restricting the deflection within the foundation to an appropriate mode shape described as $\varphi(z)$. The Vlasov model accounts for the effect of the neglected shear strain energy in the soil and shear forces that come from the surrounding soil by introducing an arbitrary parameter γ. This parameter characterises the vertical distribution of the deformation in the foundation. The parameter γ is determined as a function of the characteristic of the beam and foundation soil using an iterative procedure (modified Vlasov foundation) [16]. Because the γ value needs to be known before the function $\varphi(z)$ can be solved, an iterative approach is used to evaluate γ. The initial value of γ is first arbitrarily assumed to evaluate the k_1 and k_2 parameters. Next, the value of γ is calculated from an equation using beam displacements, which is calculated in the previous step. With a corrected value of γ, the values of k_1 and k_2 are again evaluated. The iteration process is continued until the change in γ between the two successive iterations is less than the assumed tolerance.

W.A. Bednarek (✉)
Division of Bridge Building and Railway Tracks, Institute of Civil Engineering, Poznan University of Technology, Poznan, Poland
e-mail: wlodzimierz.bednarek@put.poznan.pl

B. Albers and M. Kuczma (eds.), *Continuous Media with Microstructure 2*,
DOI 10.1007/978-3-319-28241-1_21

1 Introduction

The general job of a railway sleeper is to sustain rail forces and transfer them to the ballast bed [4, 5, 7, 14]. Sleepers also preserve track gauge corresponding to formal railway track width. Sleeper displacements under action of longitudinal and horizontal forces are countered by ballast resistance and friction arising between ballast and sleepers. The vertical loads transferred from the rail to the sleeper cause ballast reaction. In order to preserve the rail on the sleeper in one plane one should provide correct sleeper packing. A proper grain-size distribution should be within borders shown in Fig. 1.

2 Types of Railway Sleepers

In railway tracks we distinguish concrete, wooden and steel sleepers (i.e. Ypsylon sleepers—*Y* type) shown in Fig. 2. Concrete sleepers are made with reinforced concrete by strings or steel bars. The wooden sleepers are made by softwood (pine) and hardwood (oak, beech, azobe). This type of sleeper is most popular around the world. The wooden sleepers have a beam shape at rectangular cross-section or close to them. In order to extend their life (up to 25 years) they are impregnated by creosote oil.

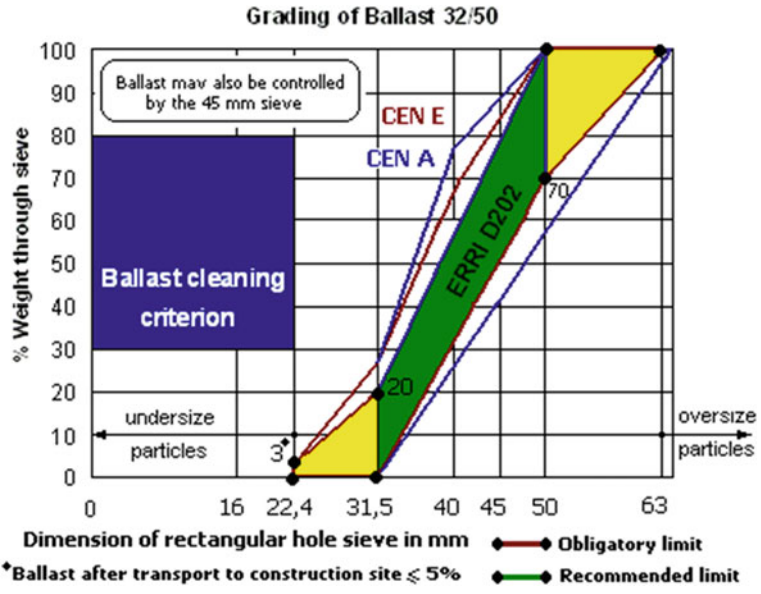

Fig. 1 Ballast bed specification [4, 5, 14]

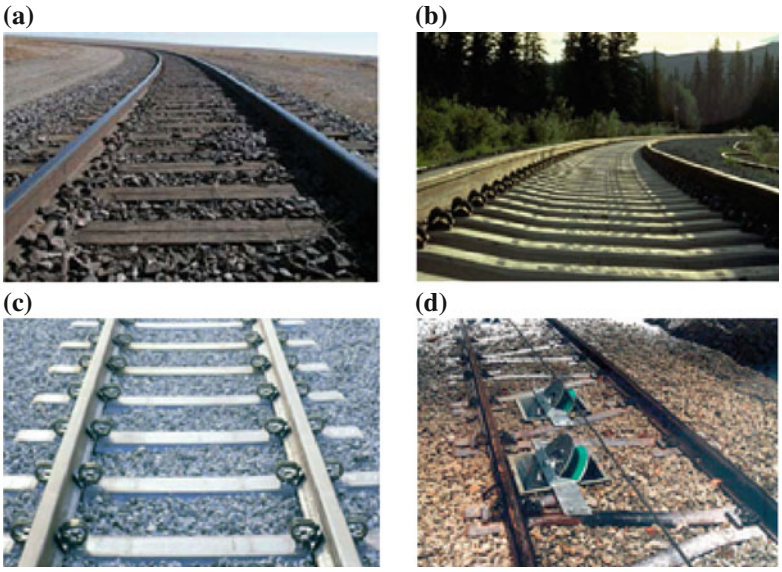

Fig. 2 Examples of railway sleeper types. **a** Wooden sleepers; **b** concrete sleepers; **c** steel sleepers; **d** *Y* sleepers [8, 18]

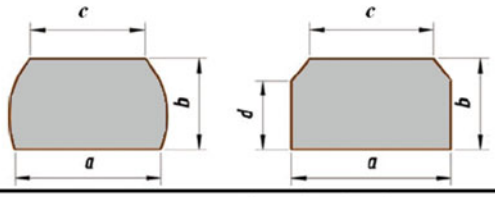

sleeper type	dimensions [mm]				
	a	*b*	*c*	*d*	length
I B	260	150	160	110	2600
II B	240	150	160	110	2600
III B	240	140	160	100	2500
II O	240	150	160	–	2600
III O	240	140	160	–	2500
IV O	220	140	160	–	2500

Fig. 3 Dimensions of wooden sleepers produced and mainly used in Poland

Typical characteristics of wooden sleepers are shown in Fig. 3. The reinforced concrete sleepers (further denoted as concrete sleepers) are made in beam shape from prestressed concrete. For the railway track structure mainly concrete sleepers (Fig. 4) PS-83 and PS-94 are used with SB fastening for 49E1 or 60E1 types of the rails (Table 1). PS-83 type concrete sleeper is delivered also with *K* type fastening

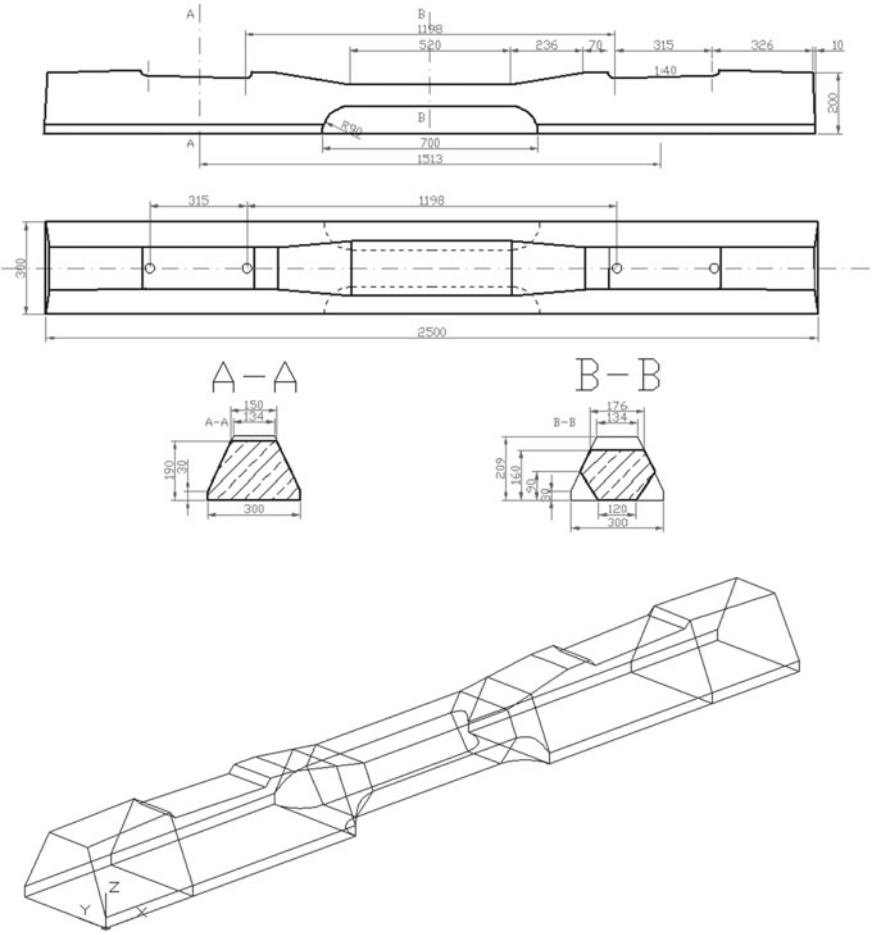

Fig. 4 Schematics of concrete railway sleepers (e.g. INBK-7) and their dimensions

previously installed in a finned sole-plate or only with dowels. Nowadays in railway tracks often steel sleepers of Ypsylon type are used. These sleepers revealed their usefulness, excellent properties in track stability and minimal requirements connected with subgrade maintenance during railway operation. Adaptation of *Y* steel sleepers decreases the quantity needed for 1 km track from 1666 beam sleepers to 803 Ypsylon steel sleepers [8]. It also decreases the height and width of the railway track and consequently reduces the quantity of ballast by 30–40 % in comparison with typical track structures with standard beam sleepers.

Table 1 Where a—anchors clearance; b—width between external anchors; d—length; h—height; p—width of sleeper bottom area

Type	Mass (kg)	Support area (m^2)	Dimensions (mm)				
			a	b	d	h	p
1	2	3	4	5	6	7	8
INBK-3	226	0.5335	285	1803	2500	202	265
INBK-4	210	0.4466	285	1803	2300	192	286
INBK-7	250	0.6310	315	1828	2500	190	300
INBK-8	240	0.5818	285	1795	2500	195	286
PBS-1	250	0.5400	285	1795	2500	193	300
PS-83	250	0.6843	173	1687	2500	210	300
PS-93	286	0.6805	173	1687	2600	227	300
PS-94	294	0.6805	173	1687	2600	229	300

3 Influence of Dynamical Factors Due to Train Velocity and Track State (k_v^J Coefficient)

The dynamical character of the reaction of running trains on the track structure is described by the dynamical coefficient k_v (which is dependent on the velocity of the rail-vehicle). For Polish National Railways for the calculation of this dynamical coefficient a cubic multinomial is applied in the following form [2, 4, 5]

$$k_v = 1 + 5 \cdot 10^{-4} \cdot V + 4 \cdot 10^{-5} \cdot V^2 - 1.3 \cdot 10^{-7} \cdot V^3, \tag{1}$$

where V is the train speed (km/h). The behavior of the coefficient k_v is illustrated in Fig. 5. It does not depend only on train speed but, above all, on the track structure state and also on the types and the state of the rail-vehicles [2]. Thus, it is recommended to calculate it according to a synthetic indicator of the railway track quality J, using

$$k_v^J = 1 + \frac{J}{1.5} \cdot (k_v - 1), \quad \Psi_J = k_v^J \cdot (1 + 0.2 \cdot J \cdot t), \tag{2}$$

where k_v^J is a dynamical coefficient due to track state and motion velocity [-], k_v is a dynamical coefficient considering only motion velocity [-], J is a synthetic coefficient of track quality (mm) and t a value denoting a confidence level. The parameter t depends on the line category for which a dynamical coefficient is calculated. The higher the category the higher the operational reliability required. Common values of the parameter t are

t = 3.00 for 0 track class, t = 1.50 for 3 track class,
t = 2.50 for 1 track class, t = 1.00 for 4 track class,
t = 2.00 for 2 track class, t = 0.75 for 5 track class

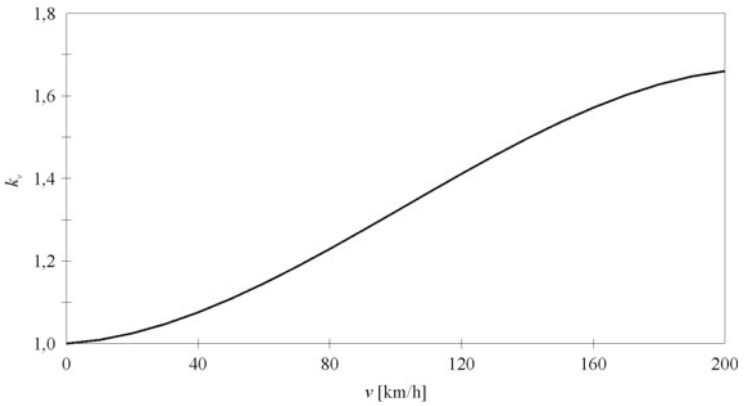

Fig. 5 Diagram showing the dynamical coefficient depending on the speed

4 Beam on Elastic Foundation

4.1 Introduction

The problem of a beam resting on an elastic and visco-elastic foundation has been widely investigated in the literature [1, 3, 9–11, 17]. The first soil model was proposed by Winkler, in which the foundation is described by a series of closely-spaced independent elastic springs. Furthermore, the reacting pressure at each point of the soil surface is directly proportional to the deflection of the beam through a material constant called the Winkler modulus. However, many alternative soil models have been proposed to obtain more accurate descriptions of the soil-beam interaction and to avoid the limits of the Winkler assumption:

- a model in which the soil is modelled as a homogeneous isotropic elastic half space;
- the Wieghardt model, which proposed an integral dependence of the soil displacement at a point upon the contact pressure on the whole contact region through an exponential kernel (this model introduces a material constant k_G in addition to the typical Winkler modulus, and the model belongs to the class of two-parameter foundations);
- the Pasternak model, which describes the foundation as an elastic spring layer covered by an elastic incompressible membrane that is shear deformable;
- the Reissner model, a proposed generalisation of the Pasternak model that introduces the second order derivative of the reacting pressure in the deflection-pressure relationship (in this case, the soil model can be viewed as a reduced three-parameter soil model consisting of an embedded shear layer between two layers of elastic springs that have a specific ratio between the spring layer stiffness);

- the Vlasov model, which adopted the simplified-continuum approach based on the variational principle and derived from a two-parameter foundation model (in this model, the foundation is treated as an elastic layer, and the constraints are imposed by restricting the deflection within the foundation to an appropriate mode shape—an arbitrary parameter γ);
- a model with a modified Vlasov foundation, in which the parameter γ is treated as a function of the beam and the foundation soil (using an iterative procedure). The unilateral nature of the beam-soil contact results in a nonlinear feature.

4.2 A BE-Beam on a Two-Parameter Vlasov Foundation (Finite Element Formulation)

For a further analysis, in order to avoid Winkler's assumption, here, the foundation of a sleeper is mainly treated as a two-parameter Vlasov foundation. Therefore, an analysis of static forces in a railway sleeper as an Euler-Bernoulli (E-B) elastic beam resting on a two-parameter modified Vlasov foundation (defined by k_1 (MPa) and k_2 (MN) coefficients) is done (shown in Fig. 6). Specifically, the concentrated static forces causing the deflection of the railway sleeper are investigated. The differential equation for a BE-beam resting on a two-parameter soil has the following form [16]

$$EI \cdot z(x)^{IV} + k_1(x) \cdot z(x) - k_2(x) \cdot z(x)'' = q(x), \tag{3}$$

where z is the beam deflection; k_1 the first subsoil parameter (MPa), k_2 the second subsoil parameter (MN) and $q(x)$ the distributed load on beam.

Using Galerkin's Residual Method (GRM) for the two-parameter foundation we obtain [16]

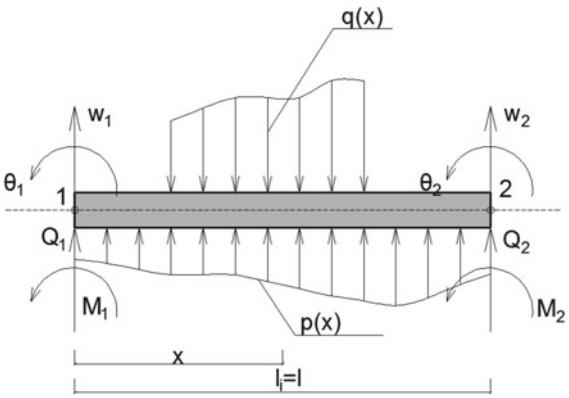

Fig. 6 General scheme of a single element of a beam. w_i, θ_i—two degrees of freedom: deflection and slope; M_i, Q_i—bending moment and transverse force of beam

$$EI \cdot \int_0^l N_i(x) \cdot z_e^{IV}(x)dx - \int_0^l N_i(x) \cdot k_2(x) \cdot z_e^{II}(x)dx + \int_0^l N_i(x) \cdot k_1(x) \cdot z_e(x)dx - \int_0^l N_i(x) \cdot q(x)dx = 0. \quad (4)$$

In matrix notation: $([k_{EI}] + [k_V] + [k_H]) \cdot \{u_e\} = \{S_e\} - \{R_e\}$, where $[k_{EI}]$ is the bending stiffness matrix of the beam element, $[k_V]$ the matrix for the elastic foundation under an the influence of its first parameter, $[k_H]$ the matrix for the elastic foundation under an influence of its second parameter, $[S_e]$ the vector of reaction to concentrated forces applied to the beam (forces were applied in the beam's nodes), $[R_e]$ the vector of reaction to the evenly distributed load on the beam.

The solutions of Eq. (4) are given as matrices [16]

$$k_{EI} = \frac{EI}{l^3} \cdot \begin{bmatrix} 12 & 6 \cdot l & -12 & 6 \cdot l \\ 6 \cdot l & 4 \cdot l^2 & -6 \cdot l & 2 \cdot l^2 \\ -12 & -6 \cdot l & 12 & -6 \cdot l \\ 6 \cdot l & 2 \cdot l^2 & -6 \cdot l & 4 \cdot l^2 \end{bmatrix}, \quad (5)$$

$$k_V = \frac{l}{840} \cdot \begin{bmatrix} 240 \cdot k_1^1 + 72 \cdot k_1^2 & 2 \cdot l \cdot \left(15 \cdot k_1^1 + 7 \cdot k_1^2\right) & 54 \cdot \left(k_1^1 + k_1^2\right) & -2 \cdot l \cdot \left(7 \cdot k_1^1 + 6 \cdot k_1^2\right) \\ 2 \cdot l \cdot \left(15 \cdot k_1^1 + 7 \cdot k_1^2\right) & l2 \cdot \left(5 \cdot k_1^1 + 3 \cdot k_1^2\right) & 2 \cdot l \cdot \left(6 \cdot k_1^1 + 7 \cdot k_1^2\right) & -3 \cdot l2 \cdot \left(k_1^1 + k_1^2\right) \\ 54 \cdot \left(k_1^1 + k_1^2\right) & 2 \cdot l \cdot \left(6 \cdot k_1^1 + 7 \cdot k_1^2\right) & 24 \cdot \left(3 \cdot k_1^1 + 10 \cdot k_1^2\right) & -2 \cdot l \cdot \left(7 \cdot k_1^1 + 15 \cdot k_1^2\right) \\ -2 \cdot l \cdot \left(7 \cdot k_1^1 + 6 \cdot k_1^2\right) & -3 \cdot l2 \cdot \left(k_1^1 + k_1^2\right) & -2 \cdot l \cdot \left(7 \cdot k_1^1 + 15 \cdot k_1^2\right) & l2 \cdot \left(3 \cdot k_1^1 + 5 \cdot k_1^2\right) \end{bmatrix}, \quad (6)$$

for $k_1^1 = k_1^2 = k_1$

$$k_V = \frac{k_1 \cdot l}{420} \cdot \begin{bmatrix} 156 & 22 \cdot l & 54 & -13 \cdot l \\ 22 \cdot l & 4 \cdot l^2 & 13 \cdot l & -3 \cdot l^2 \\ 54 & 13 \cdot l & 156 & -22 \cdot l \\ -13 \cdot l & -3 \cdot l^2 & -22 \cdot l & 4 \cdot l^2 \end{bmatrix}, \quad (7)$$

$$k_H = \frac{1}{30 \cdot l} \cdot \begin{bmatrix} 3 \cdot \left(11 \cdot k_2^1 + k_2^2\right) & -3 \cdot l \cdot \left(k_2^1 - 2 \cdot k_2^2\right) & -3 \cdot \left(11 \cdot k_2^1 + k_2^2\right) & 3 \cdot l \cdot \left(2 \cdot k_2^1 - k_2^2\right) \\ 3 \cdot l \cdot k_2^1 & l^2 \cdot \left(3 \cdot k_2^1 + k_2^2\right) & -3 \cdot l \cdot k_2^1 & -l^2 \cdot k_2^2 \\ -3 \cdot \left(k_2^1 + 11 \cdot k_2^2\right) & 3 \cdot l \cdot \left(k_2^1 - 2 \cdot k_2^2\right) & 3 \cdot \left(k_2^1 + 11 \cdot k_2^2\right) & -3 \cdot l \cdot \left(2 \cdot k_2^1 - k_2^2\right) \\ 3 \cdot l \cdot k_2^2 & -l2 \cdot k_2^1 & -3 \cdot l \cdot k_2^2 & l2 \cdot \left(k_2^1 + 3 \cdot k_2^2\right) \end{bmatrix}, \quad (8)$$

for $k_2^1 = k_2^2 = k_2$

$$k_{Hj} = \frac{k_2}{30 \cdot l} \cdot \begin{bmatrix} 36 & 3 \cdot l & -36 & 3 \cdot l \\ 3 \cdot l & 4 \cdot l2 & -3 \cdot l_1 & -l2 \\ -36 & -3 \cdot l & 36 & -3 \cdot l \\ 3 \cdot l & -l2 & -3 \cdot l & 4 \cdot l2 \end{bmatrix}, \quad (9)$$

where EI is the element stiffness (MNm^2), l the element length (m), k_1^1 and k_1^2 the subsoil coefficient at the beginning and end of the element for the first subsoil parameter (MPa), k_2^1 and k_2^2 the subsoil coefficient at the beginning and end of the element for the second subsoil parameter (MN).

For $q(x) = q = \text{const}$. The result for the vector of reaction $\{R_e\}$ can be written in a well-known form

$$\{R_e\} = \left\{ -\frac{q \cdot l}{2} \; -\frac{q \cdot l^2}{12} \; -\frac{q \cdot l}{2} \; \frac{q \cdot l^2}{12} \right\}^T .$$

4.3 *Identification of the Parameters for Theoretical Calculations*

The characteristics and parameters of the track (i.e. rail and sleeper stiffness, foundation parameters) in the vertical plane (Fig. 6) can be found in earlier publications [4–7, 14].

In point Sect. 4.2 of this paper the foundation parameters for the theoretical analysis were assumed "in advance". In the Vlasov two-parameter foundation model [12, 16], the foundation is treated as an elastic layer, and the constraints are imposed by restricting the deflection within the foundation to an appropriate mode shape described as $\varphi(z)$. The method of determining these parameters is as follows. The two-parameter Vlasov model (shown in Fig. 7) accounts for the effect of the neglected shear strain energy in the soil and shear forces that come from the surrounding soil by introducing an arbitrary parameter γ. This parameter characterises the vertical distribution of the deformation in the foundation [12]. The proper mechanism for the calculation of γ is given in publications [12, 16]. The parameter γ is determined as a function of the characteristic of the beam (e.g. Figs. 3 and 4) and foundation soil using an iterative procedure (*modified Vlasov foundation*). Because the γ value needs to be known before the function $\varphi(z)$ can be solved, an iterative approach is used to evaluate γ [12, 16]. The initial value of γ is first arbitrarily assumed to evaluate the k_1 and k_2 parameters using Eqs. (11) and (12). Next, the value of γ is calculated from Eq. (13) using beam displacements. With a corrected value of γ, the values of k_1 and k_2 are again evaluated from Eqs. (11) and (12). The iteration process is continued until the change in γ between the two successive iterations is less than the assumed tolerance.

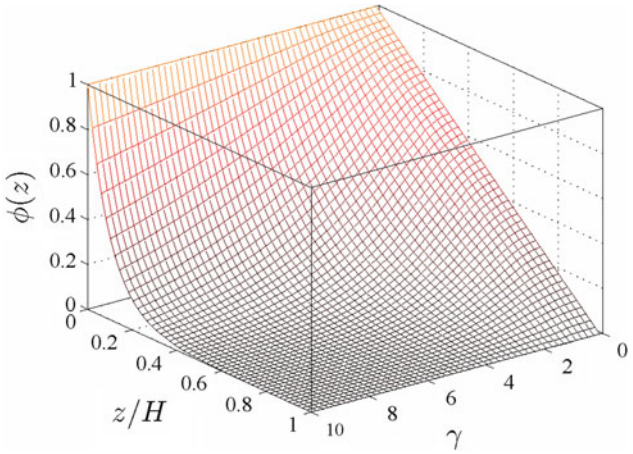

Fig. 7 Form function $\varphi(z)$ in relation to parameters γ and z/H [16]

$$\phi(z) = \frac{\sinh\gamma \cdot \left(1 - \frac{\gamma}{H}\right)}{\sinh\gamma}\gamma^2 = H \cdot \frac{1 - 2 \cdot \nu_s}{2 \cdot (1 - \nu_s)} \cdot \frac{\int_{-\infty}^{\infty} \left(\frac{dv}{dx}\right)^2 dx}{\int_{-\infty}^{\infty} v^2 dx}, \tag{10}$$

$$k_1 = \frac{(1 - \nu_s) \cdot E_s \cdot b}{(1 + \nu_s) \cdot (1 - 2 \cdot \nu_s) \cdot H} \cdot \gamma \cdot \left(\frac{\sinh\gamma \cdot \cosh\gamma + \gamma}{2 \cdot \sinh^2\gamma}\right), \tag{11}$$

$$k_2 = \frac{E_s \cdot b \cdot H}{2 \cdot (1 + \nu_s)} \cdot \frac{1}{\gamma} \cdot \left(\frac{\sinh\gamma \cdot \cosh\gamma - \gamma}{2 \cdot \sinh^2\gamma}\right), \tag{12}$$

$$\left(\frac{\gamma}{H}\right)^2 = \frac{(1 - 2 \cdot \nu_s)}{2 \cdot (1 - \nu_s)} \cdot \frac{\int_0^L \left(\frac{dv}{dx}\right)^2 dx + 0.5 \cdot \sqrt{\frac{k_1}{k_2}} \cdot v^2(0) + v^2(L)}{\int_0^L v^2(x) dx + 0.5 \cdot \sqrt{\frac{k_2}{k_1}} \cdot v^2(0) + v^2(L)}, \tag{13}$$

where k_1 and k_2 are foundation parameters, ν_s is the Poisson ratio of the soil, E_s the modulus of elasticity (usually measured by a VSS plate), γ an arbitrary parameter, *í(z)* the beam deflection, H the assumed depth of co-operated foundation, b the beam width and ϕ (z) an additional parameter.

The subgrade modulus of elasticity (E_s) is a product of elementary load increment proportion to deformation growth of the measured subsoil in a fixed range of elementary loads and multiplied by three quarters of the loading plate diameter. Then [15],

$$E_s = 0.75 \cdot \frac{\Delta p}{\Delta y}\,(\text{MPa}) \cdot D \tag{14}$$

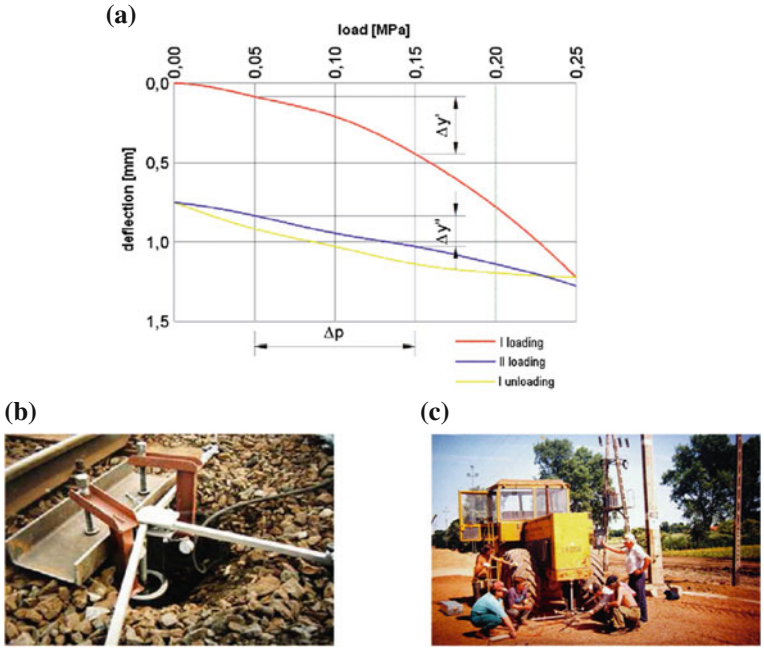

Fig. 8 Measurement of the subgrade modulus of elasticity. **a** Measurement notation; **b** testing equipment in track (author's method); **c** support method

where Δp is the load difference (MPa), Δy the settlement increment corresponding to the load difference (mm), D the loading plate diameter (mm).

A measurement is mainly made by VSS plates [15] at diameter D = 300 (mm), see Fig. 8.

4.4 Numerical Investigations

Using the finite element introduced in Sect. 4.2 and the numerical iteration described in Sect. 4.3, a computer calculation is developed and used in the identification of the 2-parameter foundation. To investigate the foundation response, a beam (sleeper) with the following geometry (Fig. 9) and material data is used: ν_s from 0.20 to 0.35 [-]; E_s from 40 to 80 (MPa), where ν_s denotes Poisson's ratio and E_s denotes the modulus of elasticity. The force Q acting on the sleeper is taken between 100–200 (kN). Figures 10, 11 and 12 show the results of the calculations.

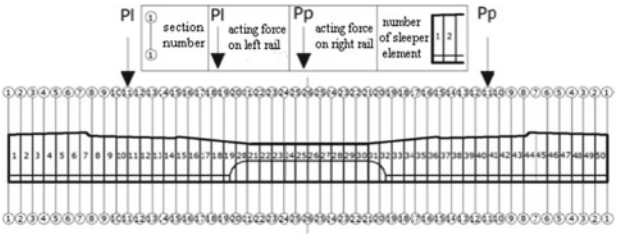

Fig. 9 Beam (sleeper) for numerical investigation

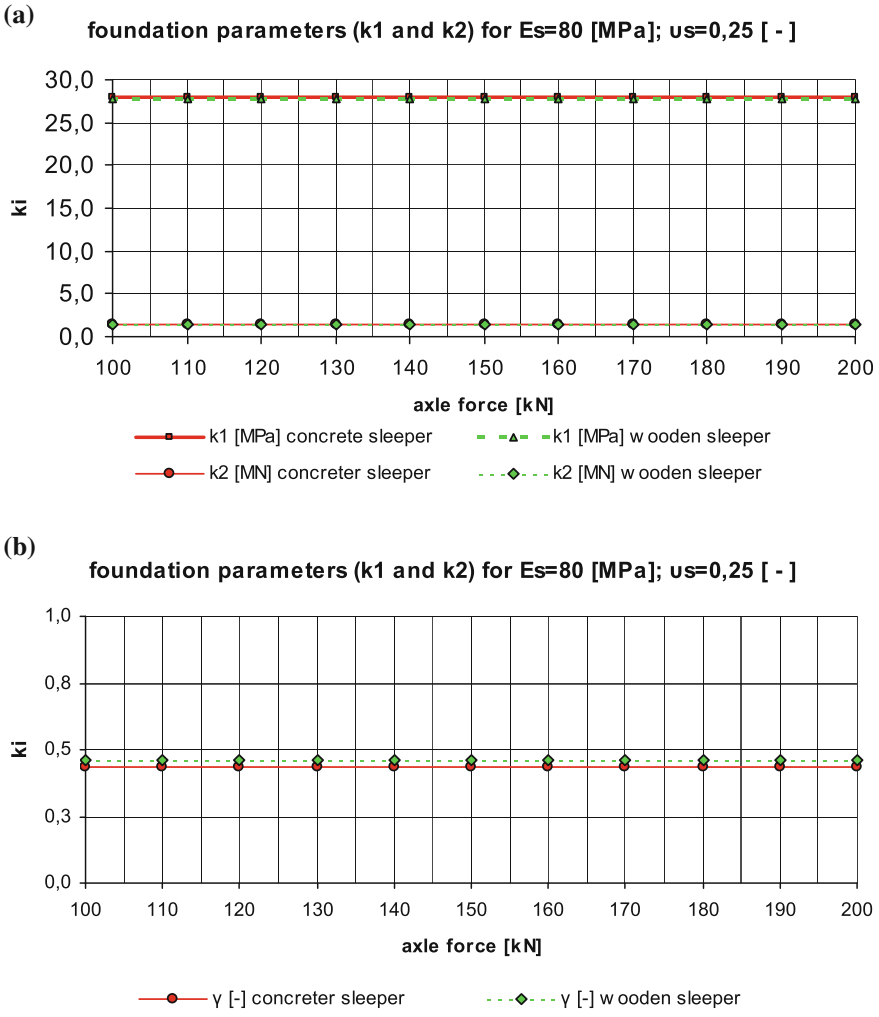

Fig. 10 Influence of force Q acting on the sleeper on k_1 and k_2-parameters

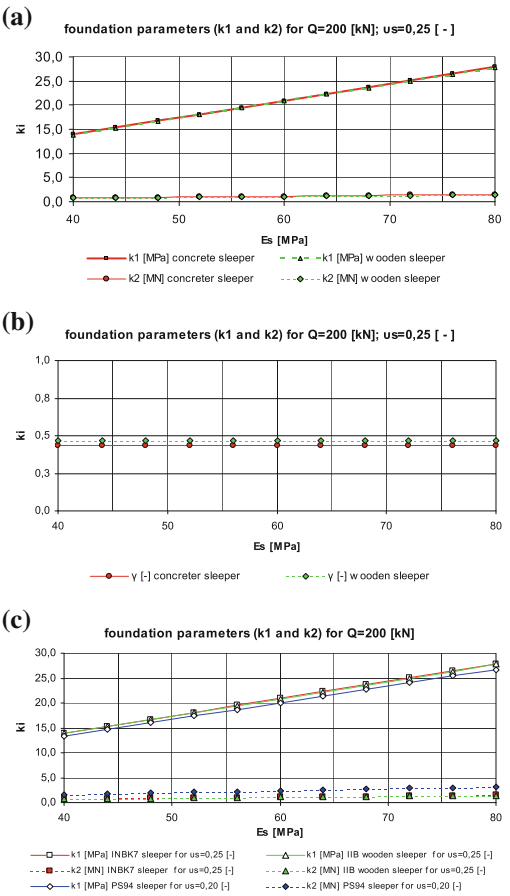

$$k_1(E_s)_{\nu_s=0,25} = 0,34856 \cdot E_s^{1,00003} + 5,1559 \cdot 10^{-4} \text{ [MPa]} \quad \text{for INBK7 sleeper}$$

$$k_2(E_s)_{\nu_s=0,25} = 0,01841 \cdot E_s^{1,0002} + 2,32547 \cdot 10^{-4} \text{ [MN]} \quad \text{for INBK7 sleeper}$$

$$k_1(E_s)_{\nu_s=0,25} = 0,34696 \cdot E_s^{0,99999} - 2,66534 \cdot 10^{-4} \text{ [MPa]} \quad \text{for IIB wooden sleeper}$$

$$k_2(E_s)_{\nu_s=0,25} = 0,01817 \cdot E_s^{1,00042} + 4,52851 \cdot 10^{-4} \text{ [MN]} \quad \text{for IIB wooden sleeper}$$

$$k_1(E_s)_{\nu_s=0,20} = 0,3343 \cdot E_s - 1,9048 \cdot 10^{-4} \text{ [MPa]} \quad \text{for PS94 sleeper}$$

$$k_2(E_s)_{\nu_s=0,20} = 0,0397 \cdot E_s + 1,047610^{-3} \text{ [MN]} \quad \text{for PS94 sleeper}$$

Fig. 11 Influence of the modulus of elasticity E_S on k_1 and k_2 parameters

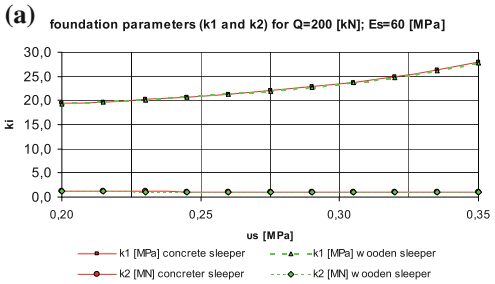

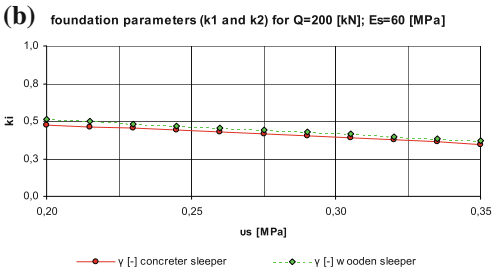

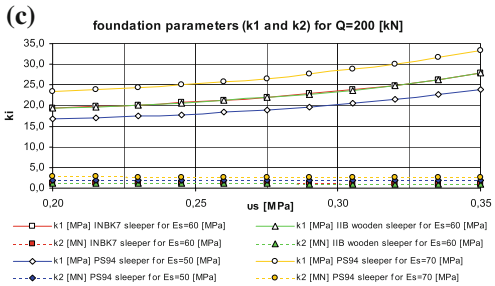

$$k_1(\nu_s)_{E_s=60} = 696{,}41014 \cdot \nu_s^{4{,}09994} + 18{,}4923\ [\text{MPa}] \quad \text{for INBK7 sleeper}$$

$$k_2(\nu_s)_{E_s=60} = -0{,}853 \cdot \nu_s^{0{,}57171} + 1{,}49179\ [\text{MN}] \quad \text{for INBK7 sleeper}$$

$$k_1(\nu_s)_{E_s=60} = 693{,}08586 \cdot \nu_s^{4{,}09997} + 18{,}40355\ [\text{MPa}] \quad \text{for IIB wooden sleeper}$$

$$k_2(\nu_s)_{E_s=60} = -0{,}8405 \cdot \nu_s^{0{,}57826} + 1{,}46956\ [\text{MN}] \quad \text{for IIB wooden sleeper}$$

$$k_1(\nu_s)_{E_s=50} = 454{,}02444 \cdot \nu_s^{3{,}83649} + 15{,}79299\ [\text{MPa}] \quad \text{for PS94 sleeper}$$

$$k_2(\nu_s)_{E_s=50} = 3{,}38838 \cdot \nu_s^{-0{,}09065} - 1{,}9328\ [\text{MN}] \quad \text{for PS94 sleeper}$$

$$k_1(\nu_s)_{E_s=70} = 635{,}48039 \cdot \nu_s^{-0{,}09065} - 22{,}10998\ [\text{MN}] \quad \text{for PS94 sleeper}$$

$$k_2(\nu_s)_{E_s=70} = 4{,}75032 \cdot \nu_s^{-0{,}09093} - 2{,}71145\ [\text{MN}] \quad \text{for PS94 sleeper}$$

Fig. 12 Influence of Poisson's ratio ν_s on k_1 and k_2 parameters

4.5 Experimental Investigations for INBK-7 Sleeper

4.5.1 Details of the Author's Field Investigation

The load was a locomotive with 4 axles at 90 kN per wheel load (180 kN/axle)—see Fig. 13.

The force transferred from the rail to the railway sleeper and the deflections of the railway sleeper were measured and analysed. The field investigation on an actual CWR track is shown in Fig. 14. A static ride (speed below 10 (km/h)) of succeeding SM-42 locomotive axles is analysed. Considering a small speed of the moving locomotive, the problem is treated as static.

To analyse deflections, an optical measurement system by GOM mbh (*Gesellschaft für Optische Messtechnik, Technische Universität, Braunschweig*) was used. The main purpose of this system is to produce 3D digitisation (e.g., in coordinate measurements). The PONTOS system is used for the dynamic analysis of deflections in 3D, making precise (at an accuracy of 0.001 mm), non-contact measurements of position, motion and deformations at short time intervals (in the order of 0.005 s). The PONTOS Viewer version v6.3.0-5 (by GOM mbH) and catmanEasy version 2.1 (by HBM GmbH programs were used.

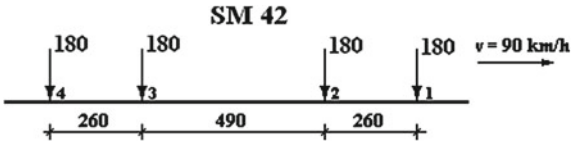

Fig. 13 Applied track load from locomotive during field investigation (kN)

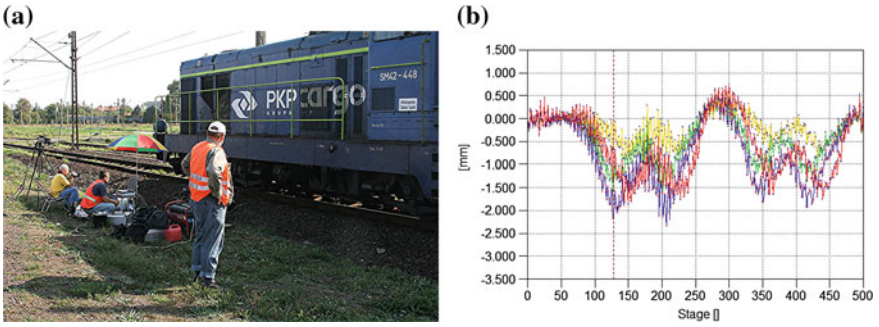

Fig. 14 Field investigations at the Poznan-Franowo station **a** the locomotive acting as a load and the measuring crew during site surveys **b** measured sleeper deflection of succeeding SM-42 locomotive axles (PONTOS viewer)

Table 2 The railway sleeper deflection z_s under the 2nd axle load from Fig. 12

experimental measurement	one-parameter foundation $k_1 = 22,8362$ $[MPa]$ and $k_2 = 0$ $[MN]$	two-parameter foundation $k_1 = 22,8362$ $[MPa]$ and $k_2 = 2,7262$ $[MN]$
z_s = **1,4373** $[mm]$	z_s^{1-par} = **1,5283** $[mm]$	z_s^{2-par} = **1,5051** $[mm]$

where z_s is the measured deflection (sleeper's beginning), z_s^{1-par} the theoretical calculation for a 1-parameter foundation and z_s^{2-par} the theoretical calculation for a 2-parameter foundation

4.5.2 Identification of the Parameters for Theoretical Calculations

The characteristics and parameters of the track (i.e. rail and sleeper stiffness, foundation parameters) in the vertical plane (Fig. 3) can be found in earlier publications [2, 4–7, 14]. For a further analysis presented in this work, exact parameters of the sleeper foundation were determined using results of a test-driving of the locomotive without irregularities; the parameters were also determined by methods described in Sect. 4.3 of this work.

A significant change in the vertical stress in the subgrade (representing an impact on the strain) caused by loaded substructure VSS was calculated to have a vertical range from 3.87 to 4.91 plate diameters D [13]. Therefore the assumed depth was $H = 1.0$ (m).

For $E_s = 68.3478$ (MPa) and $\nu_s = 0.2$, $\gamma = 0.57949$ as determined by the iterative process. The values for k_1 and k_1 were $k_1 = 22.8362$ (MPa) and $k_2 = 2.7262$ (MN) as determined by Eqs. (11) and (12), respectively.

The experimental measurement was compared to theoretical calculations (*FEM*), and the experimental and theoretical results are shown in Table 2. For comparison a 1-parameter foundation is considered (while the second parameter k_2 is assumed to be zero).

5 Final Remarks

To sum up:

1. In the paper a method for the determination of foundation coefficients for a 2-parameter model on the basis of the railway sleeper deflection has been shown.
2. An influence of the parameters Q (sleeper load) (kN), E_S (modulus of elasticity) (MPa) and ν_s (Poisson's ratio) [-] are considered and shown in Figs. 10, 11 and 12.
3. It is noticed that the sleeper load (Q) (kN) is of little importance on the values of k_1 (MPa) and k_2 (MN). The foundation parameters are mainly connected with subsoil properties.
4. On the other hand the foundation parameters such as E_s (modulus of elasticity) (MPa) and ν_s (Poisson's ratio) [-] are of importance (as can be clearly seen in Figs. 11 and 12).

As can be seen from Table 2 containing theoretical results, the best fit to field investigations appears for the sleeper treated as *BE*-beam resting on the 2-parameter elastic foundation.

References

1. Al-Azzawi, A.A., Shaker, A.S.: Finite difference analysis of curved deep beams on Winkler foundation. J. Eng. Appl. Sci. **6**(3), 42–48 (2011)
2. Bałuch, M.: *Ustalanie dopuszczalnych nacisków osi i maksymalnych prędkości na liniach PKP*. Prace Centrum Naukowo-Technicznego Kolejnictwa, z. 139, Warszawa (2003) (in Polish)
3. Beaufait, F.W., Hoadley, P.W.: Analysis of elastic beams on nonlinear foundations. Comput. Struct. **12**(5), 669–676 (1980)
4. Bednarek, Wł.: The analysis of the influence of variable roadbed stiffness and support of railway sleeper on its work. Found. Civil Environ. Eng. (FCEE) 13 (2010)
5. Bednarek, Wł.: Analiza wpł ywu podłoża i sposobu podparcia na pracę podkł adu kolejowego. Archiwum Instytutu Inżynierii Lądowej (Archives of Institute of Civil Engineering). Pozna ń University of Technology, Nr 9 (2011) (in Polish). ISSN 1897-4007
6. Bednarek, Wł.: *Analiza wpływu współczynnikw sprężystego podłoża dwuparametrowego na ugięcia podkładu kolejowego*. Zeszyty Naukowo-Techniczne Stowarzyszenia Inżynierw i Techniknw Komunikacji w Krakowie, Seria: Materiały Konferencyjne (2013) (in Polish). ISSN 1231-9171
7. Czyczuła, W.: *Tor bezstykowy*, Krakw (2002) (in Polish)
8. Czyczyła, Wł., Majerczak, J., Chudyba, Ł.: *Podkłady stalowe typu Y*. Infrastruktura Transportu **6** (2010) (in Polish)
9. Eisenberger, M., Yankelevsky, D.Z.: Exact stiffness matrix for beams on elastic foundation. Comput. Struct. **21**(6), 1355–1359 (1985)
10. Eisenberger, M., Bielak, J.: Finite beams on infinite two-parameter elastic foundations. Comput. Struct. **42**(4), 661–664 (1992)
11. Morfidis, K.: Exact matrices for beams on three-parameter elastic foundation. Comput. Struct. **85**(15–16), 1243–1256 (2007)
12. Mullapudi, R., Ayoub, A.: Nonlinear finite element modelling of beams on two-parameter foundations. Comput. Geotech. **37**, 334–342 (2010)
13. Pawłowski, M.: *Zależność wskaźnika zageszczenia od wskaźnika odkształcenia kruszyw na podstawie próbnych obciążeń płytą statyczną* (doctor's thesis). Poznań (2011) (in Polish)
14. PKP PLK S.A.: *Warunki techniczne utrzymania nawierzchni na liniach kolejowych* (Id-1). Warszawa (2005) (in Polish)
15. PKP PLK S.A.: *Warunki techniczne utrzymania podtorza kolejowego* (Id-3). Warszawa (2009) (in Polish)
16. Teodoru, I.-B., Muşat, V.: The modified Vlasov foundation model: an attractive approach for beams resting on elastic supports. EJGE 15 (2010)
17. Ting, B.Y.: Finite beams on elastic foundation with restraints. J. Struct. Div. **108**, 611–621 (1982)
18. www.thyssenkruppgft.pl (Katalog ThyssenKrupp GfT Polska sp. z o.o.)

Orthotropic Parameters of PU Foam Used in Sandwich Panels

Monika Chuda-Kowalska and Mariusz Urbaniak

Abstract Polyurethane foam used as a core material in sandwich panels is considered in the paper. In this class of structures foam-filled material is treated as an isotropic, elastic material very often. Then, only two independent material parameters are needed to describe this material. Usually, they are chosen from the Young's modulus E, the shear modulus G or the Poisson's ratio ν. In fact, when the material under consideration is a porous structure like a polyurethane foam, the identification of the mechanical properties of this material (even for the isotropic model) is an intricate task. Additionally, as will be shown in the paper, the foam stress-strain response is a function of the applied load. Therefore, the orthotropic behavior of the PU foam is analyzed. To determine mechanical parameters standard tests and a Digital Image Correlation (DIC) technique (named Aramis) are applied. The experimental results are discussed in detail.

1 Introduction

Sandwich panels made up of two, external thin and stiff metal skins separated by a thick, lightweight core are widely used in many areas of engineering. That is caused mainly by their several attractive features like high load-bearing capacity coupled with small weight, good thermal insulation, cost of production and easy assembling. There is strong tendency to apply these panels of larger span lengths and thinner skins. Therefore, a number of papers have been devoted to design and optimization of sandwich plates [9, 17]. The most common core materials used in these layered panels are different kind of cellular solids like metallic, glass, ceramic and polymer foams.

M. Chuda-Kowalska (✉)
Poznan University of Technology, Institute of Structural Engineering,
pl. Sklodowskiej-Curie 5, 60-965 Poznan, Poland
e-mail: monika.chuda-kowalska@put.poznan.pl

M. Urbaniak
Department of Strength of Materials, Lodz University of Technology,
ul. Żeromskiego 116, 90-924 Lodz, Poland
e-mail: mariusz.urbaniak@p.lodz.pl

B. Albers and M. Kuczma (eds.), *Continuous Media with Microstructure 2*,
DOI 10.1007/978-3-319-28241-1_22

For engineering purposes, foams represent an attractive set of features such as high energy absorption capacity, acoustic and thermal insulating properties which make these materials very popular in aircraft industry, automobile, buildings or packing [5]. On the other hand, using porous materials in structural applications, the knowledge of their integrity and mechanical behavior on both micro- and macro-scale is required [13]. In the literature, it is possible to find papers considering different approaches for modeling and can be roughly divided into two categories: micro-mechanical models and phenomenological models. The first group of models is based on the analysis of micro-cell structure [8, 10, 18]. The second group of models based on the best fitting to experimental mechanical behavior without direct relationship to physics the phenomenon. Such models were commonly used and developed by many authors [1, 12] and adopted in this paper. The authors analyzed the behavior of the low density and closed-cell foam used as a core material in sandwich panels. Common application of this kind of panels in civil engineering implies specific computational and testing methods accounting for the influence of the soft core on the behavior of the layered structure [4, 16, 19]. The assumption of isotropy and linear elasticity is very convenient from engineering point of view and frequently used [7]. Then, the shear modulus of the core material and establishment of reliable experimental methods for its determination play a crucial role for structural performance of a sandwich panel [11, 14]. Unfortunately, manufacturing process of the panel produced for civil engineering can have vast influence on the microstructure and behavior of the core material because steel facings limit the growth of foam in the thickness direction. Therefore, isotropy assumption can lead to significant errors and the estimation of the mechanical properties of porous core material needs an extra attention [2, 15].

In this paper the main aim is focused on two aspects: the determination of material anisotropy of PU foam used in sandwich panels and accurate estimation of its elastic parameters such as Young's modulus E and Poisson's ratio ν. In order to obtain more precise results from tension and compression tests a Digital Image Correlation system (Aramis) was used.

2 Standard Approach and Testing Procedure

The closed-cell polyurethane rigid foam used as a core material in sandwich panels is adopted as a material to be investigated in this work. It is manufactured during polymerization reaction from ingredients such as: polyol, isocyanates, catalysts and blowing gases. Microstructure of this foam is presented in Fig. 1. Its relative density R is equal 0.033 (the density of the cellular material divided by that of the solid from which the cell walls are made: $R = 40/1200 = 0.033$). According to Gibson and Ashby [8] for relative densities below 0.3, the material is classified as a cellular structure. To identify and determine material properties of porous materials, standards and experimental methods for solid homogenous materials can be applied. Foams are specific material. Although tensile tests are the most common for other materials, they are rarely used for foams because they are weak in tension, fracture easily and

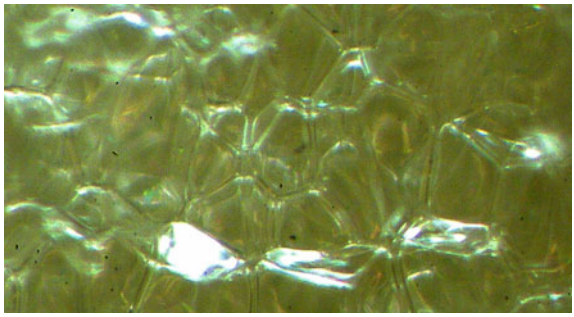

Fig. 1 The microstructure of analyzed PU foam

difficulty to grip to apply tensile loads. In contrast, compressive and shear loading are more common compared to the others.

For analyzed foam used as a core material in sandwich panels the standard experimental methods adopted to estimate material parameters of the core are described in code EN 14509 [6]. They are based on the assumption that the materials of steel facings and the core are isotropic, homogeneous and linearly elastic. For the PU foam only two parameters are mentioned: G_C and E_C—because the relation (1) must be obligatory hold in this classical model.

$$G = \frac{E}{2(1+\nu)} \tag{1}$$

According to EN 14509, the shear modulus of the core G_C should be identified from the four-point bending test based on the Sandwich Beam Theory. The total displacement f of the mid-point of the span of the panel can be decomposed into a flexural component w_B due to the bending moment and a shear component w_S due to the shear force. The second one can be assessed and used to estimate of the desired parameter G_C. This parameter plays significant role in structural response of sandwich panels and should be identified in reliable way.

The next material parameter of the core mentioned in EN 14509 is Young's modulus. It can be determined in tension/compression tests on cubic samples containing the core material and facings. Therefore, the cross-section of the sample depends on the thickness of the plate.

In the present case, the PU foam has a density of 40 kg/m^3. The dimensions of the samples had 100 × 100 × 100 mm. For each tension/compression test 7 samples were used. For bending test 5 samples were analyzed. Obtained mean values are shown in Table 1. In detail, these tests and results were presented by Chuda-Kowalska in [3].

Table 1 Elastic parameters of tested PU foam

	E_{Ct} (tension)	E_{Cc} (compression)	G_C (bending)
[MPa]	3.59	3.82	3.33

It appears that when we introduce E_C and G_C identified from tests described above, then Eq. (1) is not satisfied, because it provides negative values of the Poisson's ratio $\nu = -0.46$. Therefore, the another series of tests were carried out in order to determine this parameter and to study the homogeneity and anisotropy of the PU foam.

3 Orthotropic Analysis—Experimental Setup

The main aim of this paper is to show the foam orthotropy and the discrepancy between mechanical parameters obtained from standard tests compared to Digital Image Correlation system, named Aramis.

The material directions adopted in the paper are chosen based on the plate's format and shown in Fig. 2a. So, mechanical properties shown in Table 1 and available in manufacturer's specifications correspond to "out-of-plane" properties (thickness direction Z). In order to assess experimentally the anisotropy uniaxial tension and compression tests in three orthogonal directions X, Y and Z were carried out. Three Young's moduli E_x, E_y and E_z were calculated from Eq. (2):

$$E_i = \frac{F_{(i)}}{A\varepsilon_i^{(i)}}, \tag{2}$$

where ε_i and A denote axial (vertical) strain according to Fig. 2b and cross-section of the sample, respectively.

The second mentioned parameter is the negative ratio of transverse to axial strain according to Eq. (3)

$$\nu_{ij} = -\frac{\varepsilon_j}{\varepsilon_i}, \tag{3}$$

where ε_j denotes transverse (horizontal) strain and ε_i is axial (vertical) strain (Fig. 2b).

Due to the porous structure of the foam the classical strain measurement using strain gauges is incorrect because of the heterogeneity and voids of tested material. Therefore, only contactless methods should be used.

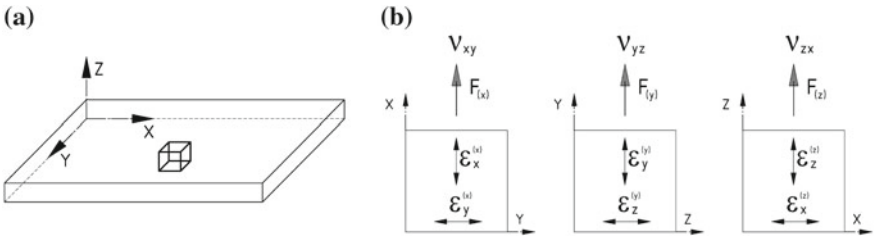

Fig. 2 **a** Adopted material directions, **b** Index system

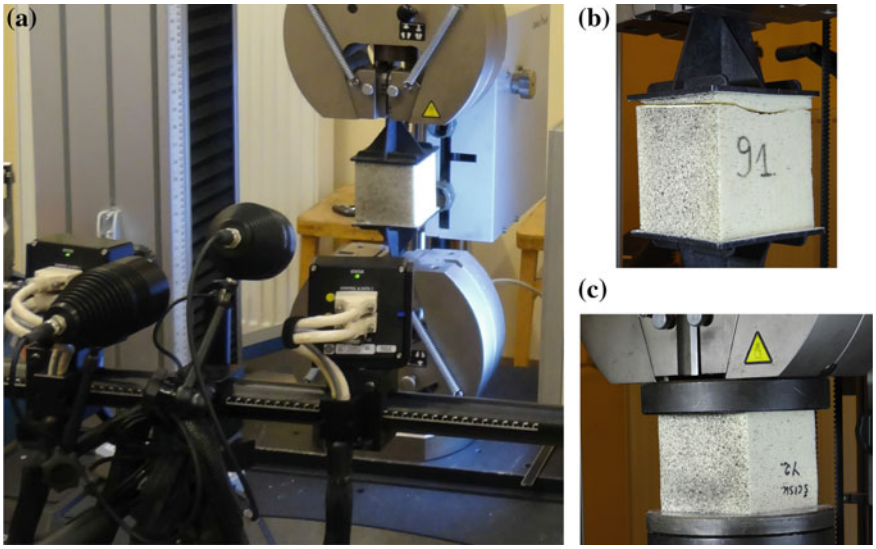

Fig. 3 Experimental setup: **a** Aramis system, **b** extended sample, **c** compressed sample

In the present work a Digital Image Correlation technique (named Aramis) was used. The system was prepared in 3D measurement setup where two cameras were used with focal length 50 mm and 4 MP resolution (Fig. 3a).

In order to recognize the surface of the specimen it was covered with stochastic pattern what is shown in Fig. 3b, c. DIC system compute deformation of the specimen through the images by means of square image details with given size of 15×15 pixels (facets—Fig. 4). Using photogrammetric methods system finds the same facet on image captured by left and right camera and allocate local coordinates to image

Fig. 4 Illustration of facets

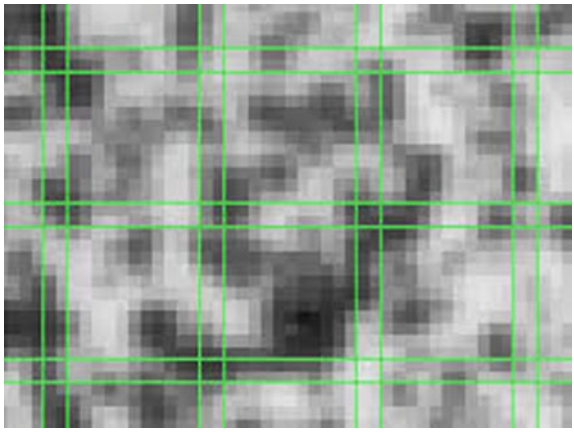

pixels. First captured image represents undeformed specimen. During loading further images were recorded with frequency of 4 fps for tension test and 2 fps for compression test. Then the system compares digital images and calculates displacements and deformation of facets on the surface of specimen. Strain is computed based on deformation of small field (3 × 3 facets) for center point of this field.

According to the appropriate procedure described in [6] the quasi-static loading velocity is controlled by the strain rate, in this case 10 mm/min. The tests were carried out in the Instron testing machine, which was modernized by Zwick/Roell with a 200 kN load cell.

4 Results and Discussion

The PU foam analyzed in this section has a density of 38 kg/m^3—slightly lower density than samples presented in Sect. 2. 18 cubic foam samples 90 × 90 × 90 mm were properly cut out from the panel. In order to identify mechanical properties in three orthogonal directions X, Y and Z steel facings were removed. Nine of the prepared samples devoted to tension test (three samples in each direction). They were positioned between composite handles and glued to them by a two-component polyurethane adhesive Macroplast U.K. 8309 and Macropur U.R. 521 (hardener)—Fig. 3b. The nine of compressed samples were placed directly between two parallel stiff loading plates of a testing machine what is shown in Fig. 3c.

4.1 Tension Test

Tension test was carried out until the ultimate load was reached and the failure of the sample was occurred. During these tests the analyzed PU foam presents quasi-brittle response. The samples destroy by overall rupture of the structure for a various range of forces what is presented in Fig. 5. The tensile strength f_{Ct} and corresponding

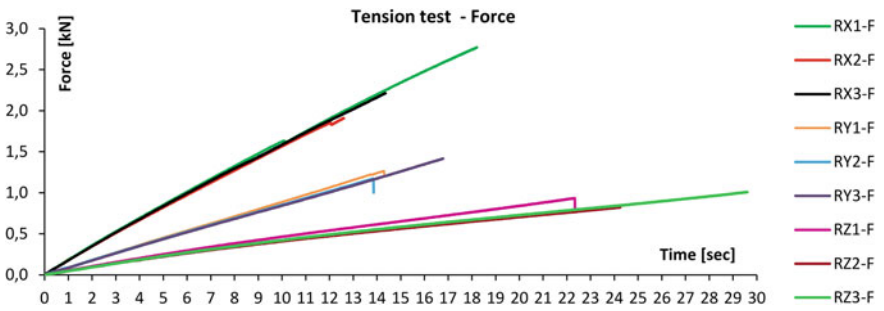

Fig. 5 Force/Time curves under uniaxial tension test

Table 2 Uniaxial tension test in X, Y and Z directions—strength parameters

	f_{Ct}^{X} [kPa]	ε_{max}^{X} [%]	f_{Ct}^{Y} [kPa]	ε_{max}^{Y} [%]	f_{Ct}^{Z} [kPa]	ε_{max}^{Z} [%]
1	311.82	3.34	136.40	2.64	105.06	4.12
2	215.31	2.33	128.88	2.55	101.21	4.25
3	249.12	2.64	151.02	3.08	114.32	5.55
$\bar{k}$*	258.75	2.77	138.77	2.76	106.86	4.64
δ*	48.97	0.52	11.26	0.28	6.74	0.79

*$\bar{k}$ and δ denote mean value and standard deviation, respectively

strain ε_{max} obtained from these tests were presented in Table 2. The behavior of tested samples significantly depended on the stress direction. Rapid failure is usually initiated at the weakest point of the microstructure of the sample and therefore, large differences in ultimate load for various samples were appeared, especially in X direction where the highest forces occurred.

The next analyzing parameter is Poisson' ratio. The relationship between horizontal ($\varepsilon < 0$) and vertical ($\varepsilon > 0$) strains is almost linear for the entire range of the force as presented in Fig. 6. Therefore, very small discrepancy of Poisson's ratio in time has been observed. Table 3 shows a summarization of the obtained results of Poisson's ratios and Young's moduli.

In Table 3 the notation was used: E_i^S—Young's modulus in i direction obtained from standard test according to [6], E_i^A—Young's modulus in i direction obtained from DIC system. The difference between obtained results Δ was evaluated from Eq. (4).

$$\delta = \frac{A - S}{S} \cdot 100 \tag{4}$$

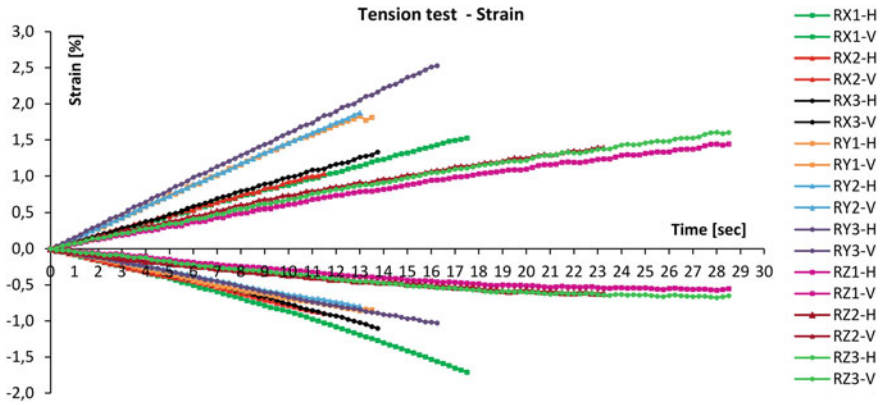

Fig. 6 Tension test—relationship between vertical/horizontal strains

Table 3 Young's moduli and Poisson's ratios of PU foam—tension test

	E_X^S	E_X^A	ν_{xy}	E_Y^S	E_Y^A	ν_{yz}	E_Z^S	E_Z^A	ν_{zx}
	[MPa]		[−]	[MPa]		[−]	[MPa]		[−]
1	10.91	20.94	0.89	5.74	7.19	0.43	3.08	6.26	0.48
2	10.71	21.64	0.85	5.67	7.13	0.42	2.82	6.49	0.50
3	10.94	20.63	0.74	5.56	6.53	0.40	2.75	6.50	0.50
$\bar{k}$	10.85	21.07	0.83	5.66	6.95	0.42	2.88	6.43	0.49
Δ (%)	94.19		–	22.79		–	123.26		–

The Young's moduli obtained directly from the testing machine (according to EN 14509) are much lower than the one obtained from Aramis system. It can be related with the flexibility of the machine, experimental setup e.g. glued handles and the effects of friction at the ends of the samples. Therefore, the properties determined by DIC technique should be considered more accuracy.

4.2 Compression Test

In accordance with EN 14509 for specimens which do not exhibit a well-defined ultimate load, such a polyurethane foam, compression test should be done until the strain reach the level of 10 %. The authors conducted tests far beyond of this level to observe the behavior of analyzed material.

Under uniaxial compression loading PU foam exhibits a linear elastic phase in all three analyzed directions. This range is very short (below 4 %) as shown in Fig. 7a. Past the yield stress, the material behaves similarly to plastic regular materials up to a point where almost all cells have buckled in what is known as crushing due to compression (Fig. 7b). Then, the densification process occurs. For all directions this process begins after exceeding 50 % of strain.

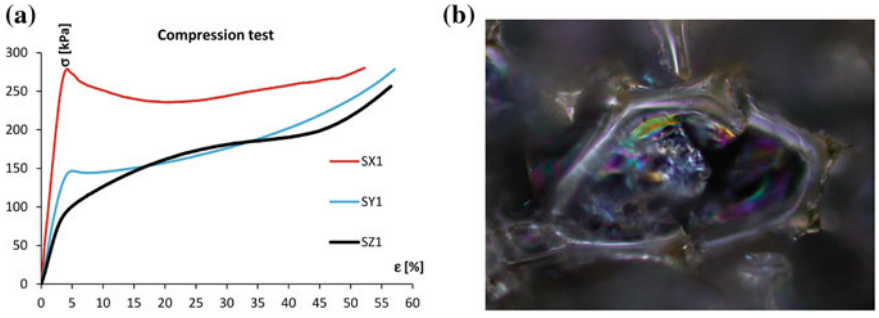

Fig. 7 Compression test: **a** $\sigma - \varepsilon$ plot for X, Y and Z directions, **b** failure of the cell

Table 4 The compressive strength parameters

	X		Y		Z	
	$f_{Cc}^{0.02}$ [kPa]	$f_{Cc}^{0.1}$ [kPa]	$f_{Cc}^{0.02}$ [kPa]	$f_{Cc}^{0.1}$ [kPa]	$f_{Cc}^{0.02}$ [kPa]	$f_{Cc}^{0.1}$ [kPa]
1	215.3	226.1	98.8	159.6	70.8	139.6
2	226.6	268.9	94.6	146.9	69.2	129.3
3	224.0	270.0	97.0	148.7	68.6	127.5
$\bar{k}$*	222.0	255.0	96.8	151.7	69.5	132.1
δ*	5.9	25.0	2.1	6.9	1.1	6.5

The behavior of tested samples significantly depended on the stress direction as for uniaxial tension test. Contrariwise, in compression test the specimens did not exhibit a well-defined ultimate load and thus the compressive strength of the core material shown in Table 4 were calculated for the strain levels $\varepsilon = 2\,\%$ and $10\,\%$ ($f_{Cc}^{0.02}$, $f_{Cc}^{0.1}$), respectively.

In compression tests the relationship between horizontal ($\varepsilon > 0$) and vertical ($\varepsilon < 0$) strains is very sensitive on time and not so obvious and linear compared to tension test what is shown in Fig. 8. All samples demonstrated rapid and irregular distribution of the strain in the initial time range. Even the change of the sign is observed. This phenomenon is associated with the closed-cell microstructure of the PU foam. Therefore, the authors identified elastic parameters for the time range between 11–14 s to skip the initial irregular behavior of the microstructure and do not exceed the elastic range (for 14 s $\longrightarrow \varepsilon = 2.6\,\%$). Obtained values are presented in Table 5.

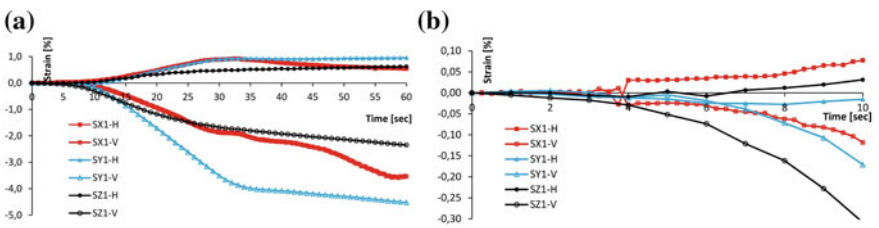

Fig. 8 Compression test: **a** horizontal/vertical strain/time plots, **b** close-up of initial

Table 5 Young's moduli and Poisson's ratios of PU foam—compression test

	E_X^S	E_X^A	ν_{xy}	E_Y^S	E_Y^A	ν_{yz}	E_Z^S	E_Z^A	ν_{zx}
	[MPa]		[−]	[MPa]		[−]	[MPa]		[−]
1	10.57	19.32	0.52	4.34	4.83	0.18	3.08	5.46	0.23
2	11.82	20.74	0.53	4.33	4.60	0.17	2.96	5.17	0.24
3	11.81	20.06	0.54	4.43	4.71	0.16	2.95	5.16	0.25
$\bar{k}$	11.40	20.04	0.53	4.37	4.71	0.17	3.00	5.26	0.24
Δ (%)	75.79		–	7.78		–	75.33		–

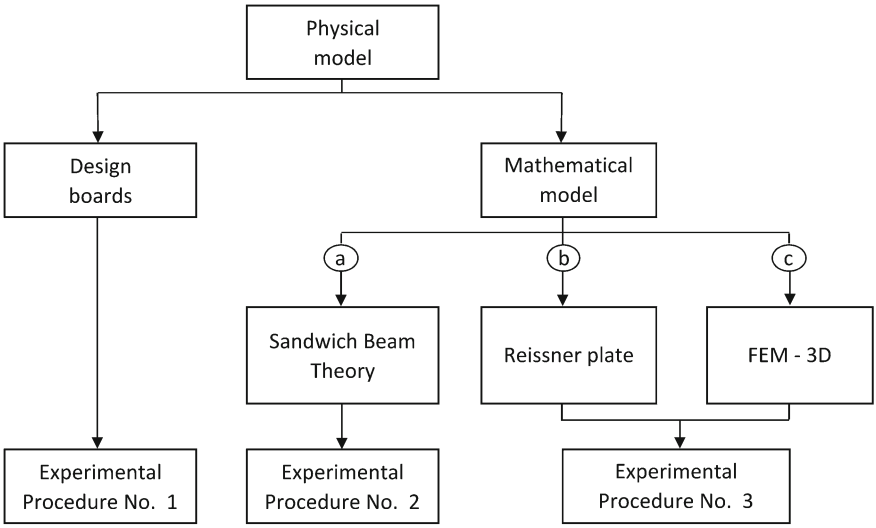

Fig. 9 Scheme of approaches to the analysis of the sandwich plates

4.3 Sandwich Plates—Approaches

In summary, the sandwich panels can be analyzed at different levels of accuracy, what is presented in Fig. 9. The decision to use a particular approach imposes further proceedings relating to the proper identification of mechanical parameters of all sandwich panel and its particular materials.

Experimental procedure No. 1 is connected with standards and regulations used by manufacturers and designers. For layered plates with soft core this procedure is based on Sandwich Beam Model (No. 2) and assumption about isotropy. Then, the shear modulus of the soft core plays crucial role in structural response.

On the other hand, if we want to analyze sandwich plates in more accuracy way we have to use advanced model. Then, there is the possibility to take into account the orthotropy of analyzed material (experimental procedure No. 3).

5 Conclusions

In case of isotropic material model of PU foam the most important parameter is shear modulus what should be taken into account in FE analysis, where only E and ν can be introduced.

Obtained results demonstrate that the assumption about isotropy has to be used with limited confidence. For sandwich panels the most common failure modes occurred in metal facings by their wrinkling. Because the Young's modulus of the steel is 60,000 times bigger than foam modulus the strain occurring in the PU foam

are very small and does not exceed the elastic range. Therefore, orthotropic model seems to be accurate in that particular case. Then, use of the Aramis system (DIC technique) was very strategy to identify the mechanical parameters of the porous material as demonstrated in this paper.

Future works can focus on the study of the structural sensitivity of sandwich plates with PU foam core with respect to material models and boundary conditions.

Acknowledgments Financial support by Poznan University of Technology 01/11/DSPB/0304 is kindly acknowledged.

References

1. Avalle, M., Belingardi, G., Ibba, A.: Mechanical models of cellular solids: parameters identification from experimental tests. Int. J. Impact Eng. **34**, 3–27 (2007)
2. Caliri Júnior, M.F., Soares, G.P., Angélico, R.A., Bresciani Canto, R., Tita, V.: Study of anisotropic polymeric cellular material under compression loading. J. Mater. Res. **15**(3), 359–364 (2012)
3. Chuda-Kowalska, M.: Methodology of Experimental Tests of Three-layered Panels with Thin Facings. Printed by Poznan University of Technology, Poznan, Poland (in Polish) (2013)
4. Chuda-Kowalska, M., Gajewski, T., Garbowski, T.: Mechanical characterization of orthotropic elastic parameters of a foam by the mixed experimental-numerical analysis. J. Theor. Appl. Mech. **53**(2), 383–394 (2015)
5. Davies, J.M. (ed.): Lightweight Sandwich Constructions. Blackwell Science Ltd. (2001)
6. EN 14509 Self-supporting double skin metal faced insulating panels—Factory made products—Specifications (2013)
7. Gibson, R.: A simplified analysis of deflections in shear deformable composite sandwich beams. J. Sandwich Struct. Mater. **13**(5), 579–588 (2011)
8. Gibson, L., Ashby, M.: Cellular Solids: Structure and Properties. Cambridge University Press (1997)
9. Gosowski, B., Gosowski, M.: Exact solution of bending problem for continuous sandwich panels with profiled facings. J. Constr. Steel Res. **101**, 53–60 (2014)
10. Janus-Michalska, M., Pecherski, R.B.: Macroscopic properties of open-cell foams based on micromechanical modelling. Technische Mechanik **23**(2/4), 221–231 (2003)
11. Juntikka, R., Hallstorm, S.: Shear characterization of sandwich core materials using four-point bending. J. Sandwich Struct. Mater. **9**(1), 67–94 (2007)
12. Liu, Q., Subhash, G.: A phenomenological constitutive model for foams under large deformations. Polym. Eng. Sci. **44**(3), 463–473 (2004)
13. Mills, N.J.: Polymer Foams Handbook. Engineering and Biomechanics Applications and Design Guide, Butterworth - Heinemann (2007)
14. Mostafa, A., Shanker, K., Mrozov, E.V.: Insight into the shear behavior of composite sandwich panels with foam core. Mat. Des. **50**, 92–101 (2013)
15. Roux, S., Hild, F., Viot, P., Bernard, D.: Three-dimensional image correlation from X-ray computed tomography of solid foam. Compos. A **39**, 1253–1265 (2008)
16. Stamm, K., Witte, H.: Sandwichkonstruktioneni, Berechnung. Fertigung. Springer, Wien (1974)
17. Studziñski, R., Pozorski, Z., Garstecki, A.: Sensitivity analysis of sandwich beams and plates accounting for variable support conditions. Bull. Pol. Acad. Sci.—Tech. Sci. **61**(1), 201–210 (2013)
18. Subramanian, N., Sankar, B.V.: Evaluation of micromechanical methods to determine stiffness and strength properties of foams. J. Sandwich Struct. Mater. **14**(4), 431–447 (2012)
19. Zenkert, D.: An Introduction to Sandwich Construction. EAMS (1995)

Numerical Elastic-Plastic Model of RPC in the Plane Stress State

Arkadiusz Denisiewicz and Mieczysław Kuczma

Abstract The work is concerned with the determination of effective material parameters of reactive powder concrete (RPC) in the range of its nonlinear response. We have used a two-scale modelling technique and carried out a series of experimental tests which allow us to validate the proposed numerical model of the considered RPC concrete. The behavior of a RPC concrete on a macro scale is described on the basis of phenomena occurring in the microstructure of material. The material microstructure is taken into account by means of a representative volume element (RVE), the structure of which is generated in a stochastic way with data from the designed recipes of RPC. It is assumed that the microstructure of RPC is composed of isotropic linear elastic—(perfectly) brittle constituents and at the macro scale the material is homogenized. This approach is a good basis for a simple modelling of microcracks that cause the nonlinear behaviour of the material at the macro level. The numerical analysis is carried out here for the plane stress state problem, and at each level of analysis the finite element method is applied.

1 Introduction

Reactive powder concrete (RPC) is currently one of the most modern building materials produced on the basis of cement, and belongs to the class of Ultra-High Performance Concrete (UHPC) with its strength and high ductility comparable to steel [7]. Reactive powder concretes are also classified as cement matrix composites with ultrahigh resistance properties and are often called the low-temperature ceramics. Thanks to the ultra high-strength and ductility of RPC, the weight and dimensions of

A. Denisiewicz
Division of Structural Mechanics, University of Zielona Góra,
ul. Prof. Z. Szafrana 1, 65-246 Zielona Góra, Poland
e-mail: a.denisiewicz@ib.uz.zgora.pl

M. Kuczma (✉)
Division of Structural Mechanics, Poznan University of Technology,
ul. Piotrowo 5, 61-965 Poznań, Poland
e-mail: mieczyslaw.kuczma@put.poznan.pl

B. Albers and M. Kuczma (eds.), *Continuous Media with Microstructure 2*,
DOI 10.1007/978-3-319-28241-1_23

cross-sections of structures built from RPC can be significantly reduced. Owing to its physical and mechanical properties, reactive powder concrete finds a wide interest not only as the construction material but also as a cladding one and even as a material for furniture.

We present here a computational method that is capable of taking into account the influence of the composition of RPC concrete on its macro mechanical properties. The model can be used in a structural analysis of buildings and engineering constructions made of RPC. Concrete is a structural composite material with complex hierarchical structure that may be analysed in a multiscale approach, starting from the molecular dynamics simulation of hydrated cement solid nanoparticles [11]. In this paper, we consider reactive powder concrete on two scales and make use of the numerical homogenization technique, schematically illustrated in Fig. 1. In this method, the response of the medium on a macroscale to external loads is determined on the basis of structural analysis on a microscale [4–6, 8]. On the micro-scale level the distributions of micro-strains and microstresses are determined, which by the way of homogenization provide information about the macroquantities. The whole micro-analysis is carried out on the so called representative volume element (RVE). This is a volume assigned to a material point which is representative for a small vicinity of the point. When the characteristic microscopic length is one order smaller than characteristic macroscopic length, we are able to take into consideration only effects

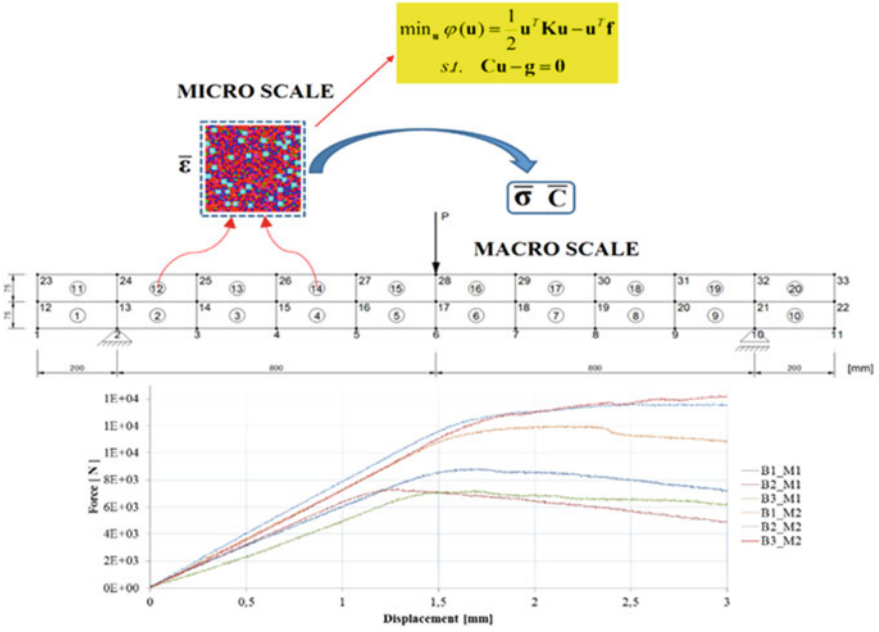

Fig. 1 The idea of two-scale modelling technique applied to beams made of two concrete mixtures, M1 and M2

of the first order. In the case of the RPC concrete, this condition is fulfilled. We shall assume that the characteristic dimension on the microscale corresponds to the size of ground quartz sand, 0.2 mm, while on the macroscale to the size of the cross-section of a structural element, e.g. 0.2 × 0.2 m.

2 Two-Scale Elastic-Plastic Model of RPC

Creating the RVE structure of size 10 × 10 mm consists in the random selection of an element (from a 50 × 50 grid) and also the random assignment of the RCP component (pores, crushed quartz, sand, cement matrix) to the selected position (Fig. 2, [3]). The concept of the RVE is a delicate one, especially for concrete with cracks. The issue of approximation of the random microstructures is discussed in depth in [9]. The boundary value problem of mechanics for the specified RVE after FEM discretization is obtained as the minimization of the energy function with additional constraints

$$\min_{\mathbf{u}} \varphi(\mathbf{u}) = \frac{1}{2}\mathbf{u}^T\mathbf{K}\mathbf{u} - \mathbf{u}^T\mathbf{f} \qquad \text{s.t.} \quad \mathbf{C}\mathbf{u} - \mathbf{g} = \mathbf{0} \tag{1}$$

The problem of homogenization over the RVE of volume V is to find a displacement field $\mathbf{u}(X)$ such that $\mathrm{div}\boldsymbol{\sigma} = \mathbf{0}$ in V, while satisfying the boundary conditions on the boundary Γ so that the Hill energy criterion is fulfilled:

$$\bar{\boldsymbol{\sigma}} \cdot \bar{\boldsymbol{\varepsilon}} = \langle \boldsymbol{\sigma} \cdot \boldsymbol{\varepsilon} \rangle \tag{2}$$

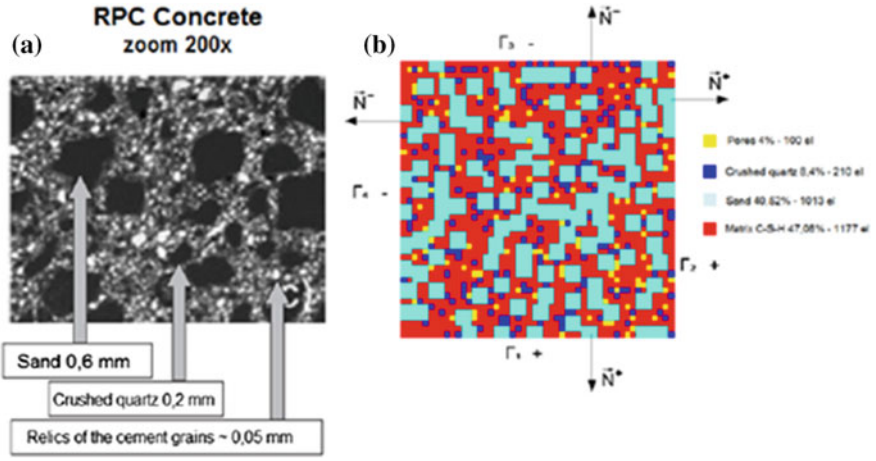

Fig. 2 Representative volume element of RPC: **a** microstructure [12], **b** finite element discretization of RVE

A detailed description of the solution procedure can be found in [1–3].

In solving the system of equations resulting from the optimization problem (1), we can use one of the three types of boundary conditions:

- displacement (Dirichlet) boundary conditions

$$\bar{\mathbf{u}} \equiv \mathbf{x} \cdot \bar{\boldsymbol{\varepsilon}} \qquad \forall \mathbf{x} \in \boldsymbol{\Gamma} \tag{3}$$

- traction (Neumann) boundary conditions

$$\mathbf{t} \equiv \bar{\boldsymbol{\sigma}} \cdot \mathbf{n} \qquad \forall \mathbf{x} \in \boldsymbol{\Gamma} \tag{4}$$

- periodic boundary conditions

$$\delta\mathbf{u}^{+} - \delta\mathbf{u}^{-} \equiv (\mathbf{x}^{+} - \mathbf{x}^{-}) \cdot \delta\bar{\boldsymbol{\varepsilon}} \qquad \forall \mathbf{x} \in \boldsymbol{\Gamma} \tag{5}$$

where the edge Γ consists of two parts $\Gamma = \Gamma^{+} \cup \Gamma^{-}$ of the normal vectors $\mathbf{n}^{+} = -\mathbf{n}^{-}$ and points $\mathbf{x}^{+} \in \Gamma^{+}$ and $\mathbf{x}^{-} \in \Gamma^{-}$. An illustration of the influence of the boundary conditions on the value of a selected constitutive parameter as a function of the size of the RVE (Fig. 2b) is shown in (Fig. 3).

The nonlinear material behaviour is modeled by taking into account degradation of the RCP microstructure (RVE). Calculations between the micro- and macro- scales are carried out iteratively (Fig. 1). At each load increment a reduced stress condition by the Burzyński hypothesis

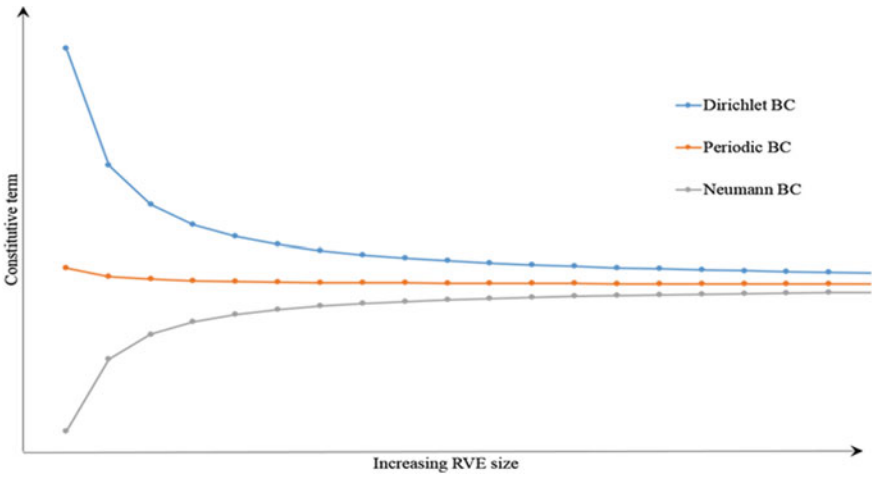

Fig. 3 The influence of boundary conditions on the solution

$$\sigma_{red} = \sqrt{\frac{R_t}{R_c}(\sigma_x + \sigma_y)^2 - \left(\frac{R_t}{R_s}\right)^2 (\sigma_x \sigma_y - \tau_{xy}^2) + R_t \left(1 - \frac{R_t}{R_c}\right)(\sigma_x + \sigma_y)} \quad (6)$$

where:
R_t—tensile strength of a microstructural component,
R_c—compressive strength of a microstructural component,
R_s—shear strength of a microstructural component,
is checked in each element of the RVE. If the reduced stress exceeds a limit value, then the element is treated as destroyed.

It is assumed that the microstructure of RPC is composed of isotropic linear elastic—(perfectly) brittle constituents and at the macro scale the material is homogenized. This approach allows for a simple modelling of microcracks that cause the non-linear behaviour of the material at the macro level. The numerical analysis is done here within the assumption of the plane stress state, and at each level of analysis the rectangular four-noded finite element with bilinear shape functions and eight degrees of freedom is applied.

3 Experimental Tests

During the laboratory tests a large amount of data was collected, including also a non-linear working range of the tested beams. The gathered information will be used to validate the proposed elastic—plastic numerical model of RPC. The tests were conducted on beams B1-M1 ÷ B3-M1 and B1-M2 ÷ B3-M2 made from two RPC mixtures: mixture I (M1) and mixture II (M2), see Table 1. During the conducted tests displacements and deformations of the beams were enforced and measured by the machine Instron 8804 and also strain gauges while the destruction zone was monitored with the system Aramis (Fig. 4). For detailed results of the tests, see [1].

Figure 5 shows the field of deformation measured by the system Aramis 3D, and Fig. 6 presents the force-displacement diagrams for the tested beams obtained from the testing machine Instron. Failure in all the beams was caused by propagation of cracks, but the behaviours of beams before failure were different for mixtures M1 and M2. For the beams of a series M1 at the end of linear elastic range the stress concentration was created at the most strenuous cross-section (Fig. 7), resulting in micro-cracks which finally propagated as one macro-crack (Fig. 8). A different scenario was observed in the case of beams made of a mixture M2, which contains micro-fibers (length 6 mm, thickness 0.17 mm) and macro-fibers (length 38 mm, thickness 1.0 mm). The stress concentrations were observed in the vicinity of the most strenuous cross-section (Fig. 9) resulting in micro-cracks. After the formation of macro-cracks the destruction process proceeded as in the case of beams of a series M1 (Fig. 10). During the tests, there could be heard crackles caused by the pulling out of macro fibers from the concrete matrix.

Table 1 Recipes of RPC

Component	Mixture I M1 $\left(kg/m^3\right)$	Percent amount (%)	Mixture II M2 $\left(kg/m^3\right)$	Percent amount (%)
Cement CEM I 42,5R	905	34.2	905	33.2
Silica fume	230	8.7	230	8.4
Quartz sand 0.063–0.4 mm OS 36	702	26.6	330	12.1
Quartz sand 0.04–0.125 mm OS 38	285	10.8	285	10.5
Quartz sand 0.2–0.8 mm OS 30	–	–	335	12.3
Water	260	9.8	260	9.5
Superplasticizer Woerment FM 787 BASF®	29.6	1.1	29.6	1.1
Micro steel fibres DM 6/0.17 KrampeHarex®	233	8.8	233	8.6
Steel fibres DW 38/1.0 N KrampeHarex®	–	–	117	4.3
Densities	2645	–	2725	–

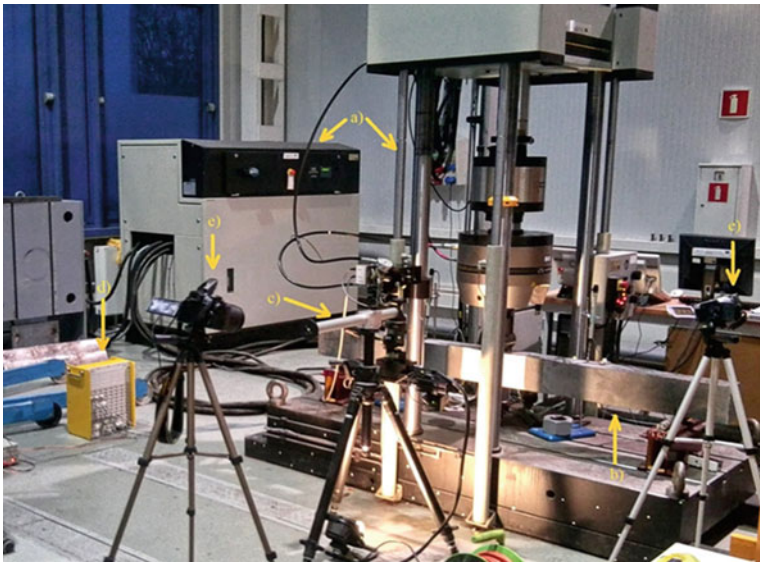

Fig. 4 The test stand for testing beams B1-M1 ÷ B3-M1 and B1-M2 ÷ B3-M2, **a** testing machine Instron 8804, **b** beam subjected to tests, **c** cameras of the deformation measuring system Aramis 3D, **d** strain gauge bridge, **e** cameras recording the tests

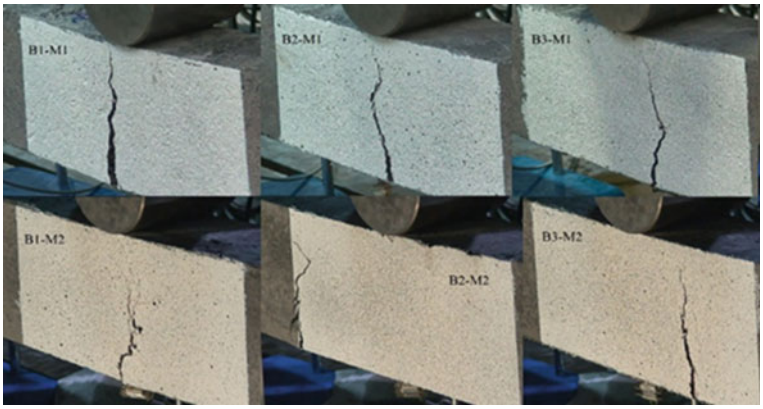

Fig. 5 Destruction zone and measuring field of ARAMIS 3D

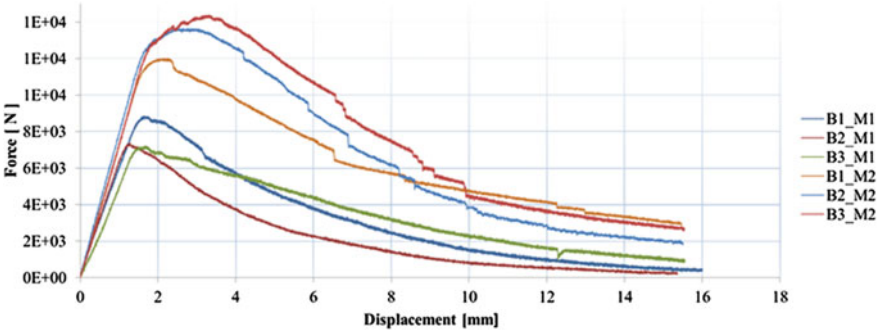

Fig. 6 Force-displacement diagrams for the tested beams

Analyzing the diagrams displayed in (Fig. 6), we can see that RPC made from mixture II is stronger that that made from mixture I. In both the cases, a clearly defined linear elastic range can be observed, followed by nonlinear softening of the RPC material due to the development of damage leading eventually to failure (rapture).

4 Numerical Example

This part of the paper presents the results of numerical simulations of beams of dimensions $10 \times 15 \times 200$ cm made from two RPC mixtures, which were subjected to laboratory tests. For the purpose of the two-scale analysis, RVEs were generated for each mixture by means of the stochastic generator of microstructure geometry [1, 2] (Fig. 12a, b). The amounts of particular components precisely reflect the proposed RPC recipes (Table 1).

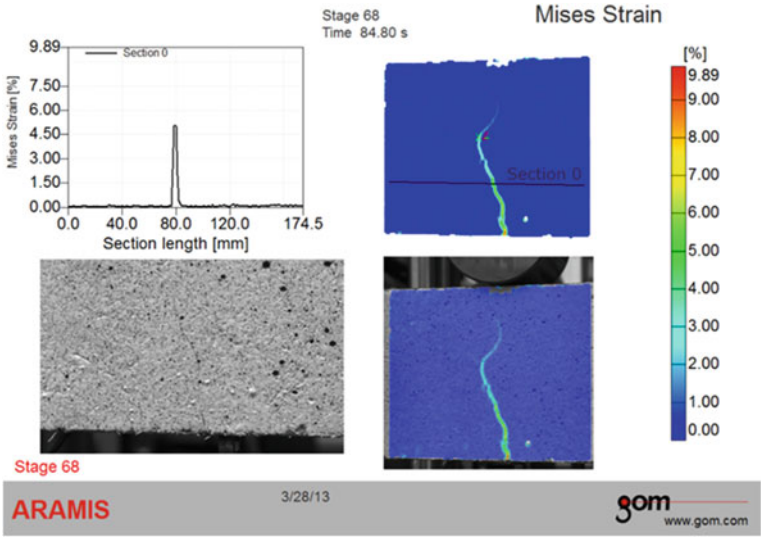

Fig. 7 Beginning of damage phase: beam B2-M1

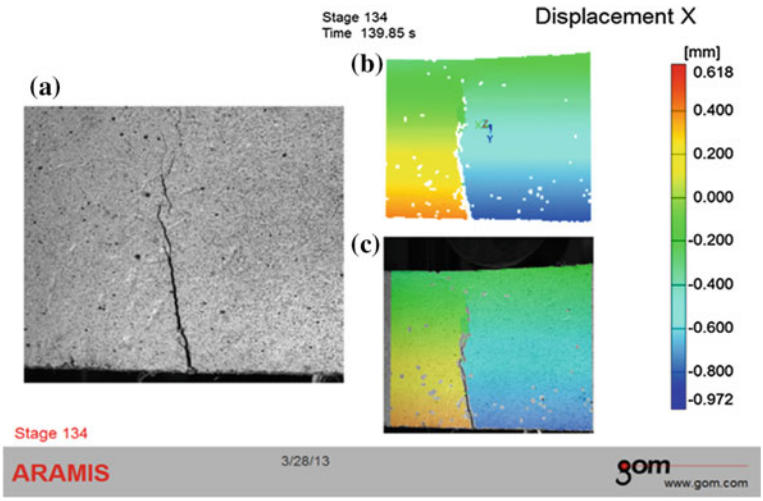

Fig. 8 Damage phase: beam B2-M1

The cement matrix, which consisted of: cement, silica powder, water and superplasticizer, was treated as a single component in numerical simulations. The material parameters of the components were adopted from the paper [10]. The beams were divided at the macro scale into twenty rectangular finite elements (Fig. 11).

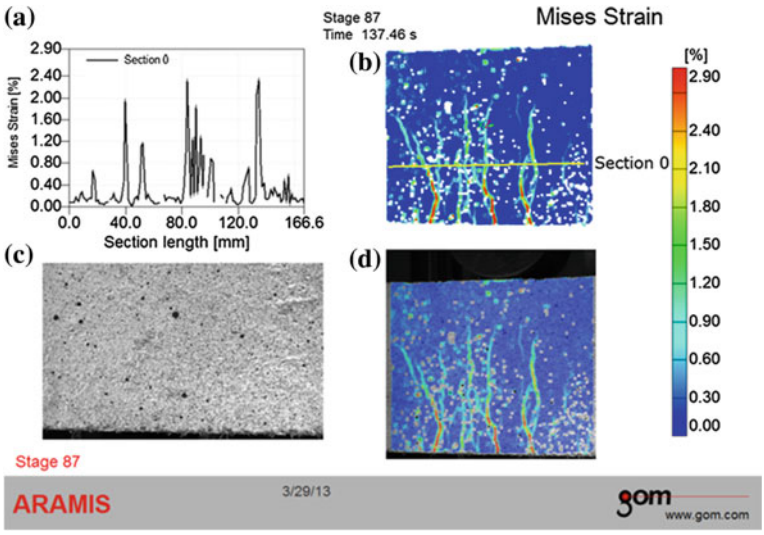

Fig. 9 Beginning of damage phase: beam B3-M2

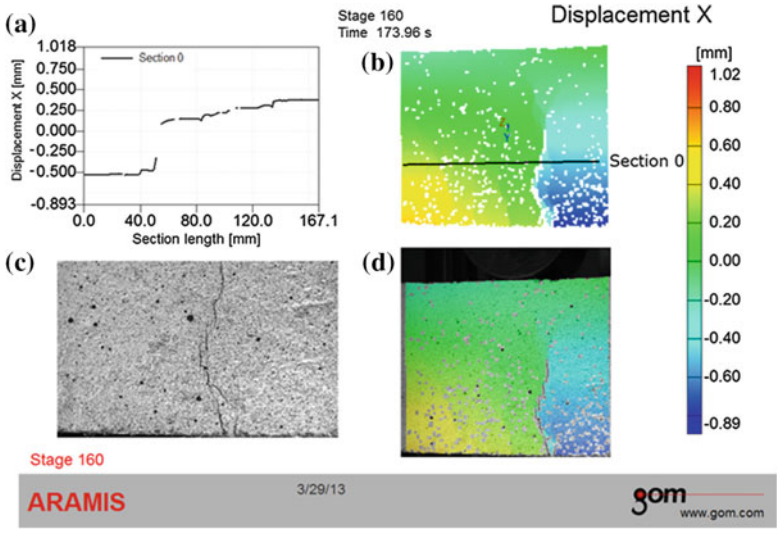

Fig. 10 Damage phase: beam B3-M2

4.1 Mixture I

The following designations have been adopted for components of mixture I (Fig. 12a):

- Red colour represents the cement matrix—percent amount 49.8 %,
- Dark blue colour represents fine quartz sand—percent amount 37.4 %,

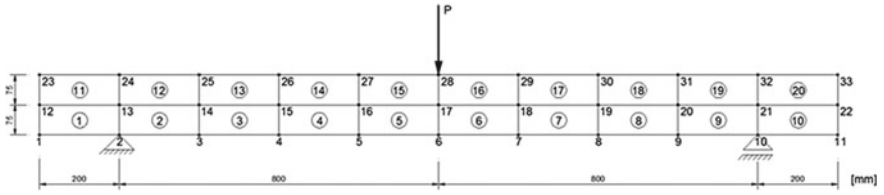

Fig. 11 The discretization of the beam on macro level

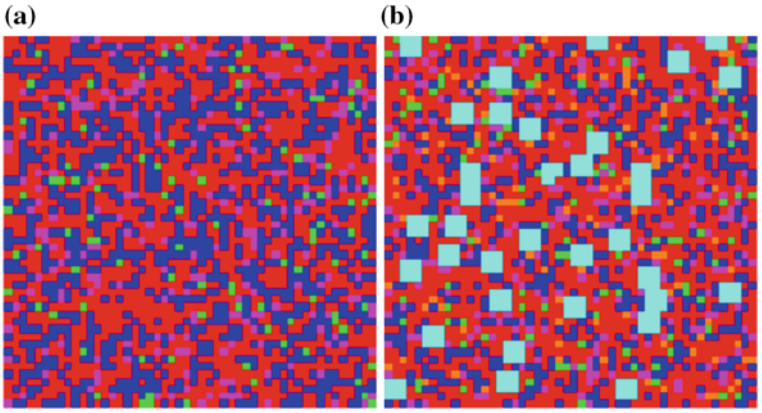

Fig. 12 RVE for **a** Mixture I, **b** Mixture II

- Pink colour represents steel micro fibres—percent amount 8.8 %,
- Yellow colour represents air voids—percent amount 4%.

The parameters of micro-components:

- Cement matrix E = 29900 MPa, $\nu = 0.24$,
- Fine quartz sand E = 48200 MPa, $\nu = 0.20$,
- Steel micro fibres E = 205000 MPa, $\nu = 0.30$,
- Air voids—empty space, no finite elements.

4.2 Mixture II

The following designations have been adopted for components of mixture II (Fig. 12b):

- Red colour represents the cement matrix—percent amount 48.2 %,
- Sky blue colour represents thick quartz sand—percent amount 12.3 %,
- Dark blue colour represents fine quartz sand—percent amount 22.6 %,

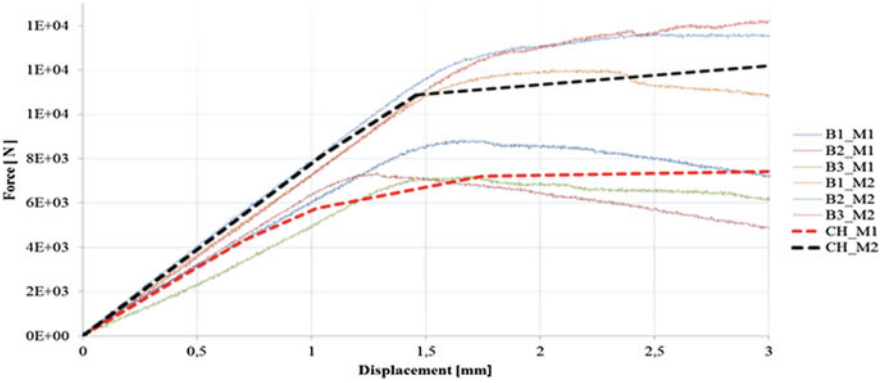

Fig. 13 Experimental and simulated (*broken lines*) responses of tested beams in the three-point bending test

- Pink colour represents steel micro fibres—percent amount 8.6 %,
- Orange colour represents steel fibres—percent amount 4.3 %,
- Yellow colour represents air voids—percent amount 4 %.

The parameters of micro-components:

- Cement matrix E = 29900 MPa, $\nu = 0.24$,
- Thick quartz sand E = 73200 MPa, $\nu = 0.20$,
- Fine quartz sand E = 48200 MPa, $\nu = 0.20$,
- Steel micro fibres E = 205000 MPa, $\nu = 0.30$,
- Steel fibres E = 205000 MPa, $\nu = 0.30$,
- Air voids—empty space, No finite element.

Using our own computer code, with the material deterioration process controlled by the criterion (6) and imposed boundary conditions (3), we have simulated the response of the RPC concrete at the macro level during the three point bending test on beams B1_M1 ÷ B3_M1 and B1_M2 ÷ B3_M2 made from two RPC mixtures M1 and M2 (Table 1). Figure 13 shows both the obtained experimental results and results of numerical simulations (broken lines) obtained with the use of computational homogenization (CH).

5 Conclusions

The results of own experimental testing and numerical simulations of beams made of reactive powder concrete (RPC) have been presented. Some noticeable dispersion of experimental results for both the series of beams can be observed. The proposed numerical elastic-plastic model makes use of computational homogenization and can

simulate effectively the elastic behaviour of RPC. The model's predictions exhibit lesser accuracy in the nonlinear range, and we intend to extend the model to the 3D case and to enrich it with mechanisms of gradual softening behavior instead of brittle fracture as well as an improved stochastic description of 3D placement of fibres.

References

1. Denisiewicz, A.: Two-scale modelling of constitutive relations for reactive powder concrete and their experimental validation (in Polish), PhD thesis, University of Zielona Góra, 2013
2. Denisiewicz, A., Kuczma, M.: Two-scale modelling of reactive powder concrete. Part I: representative volume element and solution of the corresponding boundary value problem. Civil Environ. Eng. Rep. **10**, 41–61 (2013)
3. Denisiewicz, A., Kuczma, M.: Two-scale numerical homogenization of the constitutive parameters of reactive powder concrete. Int. J. Multiscale Comput. Eng. **12**(5), 361–374 (2014)
4. Feyel, F., Chaboche, J.-L.: FE^2 multiscale approach for modelling the elastoviscoplastic behaviour of long fibre SiC/Ti composite materials Comput. Methods Appl. Mech. Engrg. **183**, 309–330 (2000)
5. Geers, M.G.D., Kouznetsova, V.G., Brekelmans, W.A.M.: Multi-scale computational homogenization: trends and challenges. J. Comput. Appl. Math. **234**, 2175–2182 (2010)
6. Ghosh, S., Lee, K., Moorthy, S.: Two scale analysis of heterogeneous elastic-plastic materials with asymptotic homogenization and Voronoi cell finite element model. Comput. Methods Appl. Mech. Engrg. **132**, 63–116 (1996)
7. Jasiczak, J., Wdowska, A., and Rudnicki, T.: Ultra-High Performance Concretes. Properties, technology, applications (in Polish), Association of Cement Producers (Stowarzysz. Producent. Cementu), Cracow, Poland, 2008
8. Miehe, C., Schröder, J., Schotte, J.: Computational homogenization analysis in finite plasticity. Simulation of texture development in polycrystalline materials. Comput. Methods Appl. Mech. Engrg. **171**, 387–418 (1999)
9. Schröder, J., Balzani, D., Brands, D.: Approximation of random microstructures by periodic statistically similar representative volume elements based on lineal-path functions. Arch. Appl. Mech. **81**, 975–997 (2011)
10. Sorelli, L., Constantinides, G., Ulm, F.J., Toutlemonde, F.: The nano-mechanical signature of Ultra High Performance Concrete by statistical nanoindentation techniques. Cem. Concr. Res. **38**, 1447–1456 (2008)
11. Wu, W., Al-Ostaz, A., Cheng, A.H.-D., Song, C.R.: Concrete as a hierarchical structural composite material. J. Multiscale Comput. Eng. **8**, 585–595 (2010)
12. Zdeb, T., Śliwiński, J.: Reactive powder concrete: mechanical properties and microstructure (in Polish). Budownictwo Technologie Architektura **51**, 51–55 (2010)

Causal Damping Ratio Spectra and Dispersion Functions in Geomaterials from the Exact Solution of Kramers-Kronig Equations of Viscoelasticity

Carlo G. Lai and Ali G. Özcebe

Abstract The constitutive parameters controlling the response of geomaterials to low-strain dynamic loading are important in a variety of situations in *Earthquake Geotechnical Engineering* (e.g. ground response analysis) and *Soil Dynamics* (e.g. propagation of ground-borne vibrations). Linear viscoelasticity is the simplest constitutive theory able to satisfactory capture the mechanical response of soils and rocks undergoing small-amplitude oscillations. An important result predicted by this theory is the functional dependence of the speed of propagation V_P and V_S of mechanical P and S waves from the corresponding material damping ratios D_P and D_S. Yet, in the current practice of experimental *Soil Mechanics*, these parameters are measured independently using different and inconsistent procedures. Furthermore, the frequency-dependence of V_P, V_S and D_P, D_S is disregarded in most practical applications. This study thoroughly investigates the *causal* relationship existing in soils between damping ratio spectra and dispersion functions by exploiting a recently obtained, exact solution of the Kramers-Kronig equations. A number of cases associated to realistic damping ratio spectra for geomaterials have been analyzed, from which the corresponding dispersion functions have been rigorously calculated.

1 Introduction

When soils and in general geomaterials are strained below the *linear cyclic threshold shear strain*, they tend to exhibit a linear response under both static-monotonic and dynamic loading when the phenomenon of energy dissipation, although small in magnitude, cannot be neglected. Despite the existence of a cyclic threshold shear

C.G. Lai (✉)
Department of Civil Engineering and Architecture, University of Pavia, Pavia, Italy
e-mail: carlo.lai@unipv.it

A.G. Özcebe
Department of Civil and Environmental Engineering, Politecnico di Milano, Milan, Italy
e-mail: aliguney.ozcebe@polimi.it

B. Albers and M. Kuczma (eds.), *Continuous Media with Microstructure 2*,
DOI 10.1007/978-3-319-28241-1_24

strain has been experimentally proved only for uniaxial stress conditions [23], this notion can in principle be generalized also to multi-axial loading by introducing the *linear cyclic threshold strain boundary surface* in the principal strain space [8].

Several are the practical situations in which geomaterials exhibit a linear response when subjected to dynamic loading. Examples from *Earthquake Geotechnical Engineering* include ground response analysis at stable sites where the low-strain parameters of soil dynamic behavior control the amplification or deamplification of ground motion both in 1D modeling and when analyzing complex geological structures such as deep valleys and alluvial basins (Fig. 1).

The transmission of ground-borne vibrations generated by the passage of a train in an underground tunnel (the source) may be modeled using a linear soil constitutive model due to the low-strain level induced in the medium by the passage of mechanical waves (Fig. 2). An analogue situation occurs when modeling the vibrational impact induced by a surface train or roadway traffic.

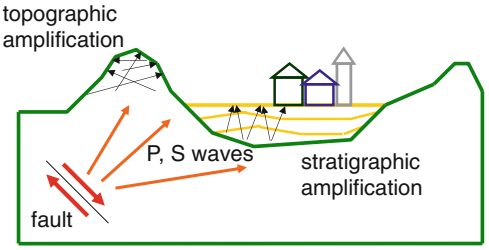

Fig. 1 Schematic illustration of site effects due to local geological and geotechnical conditions

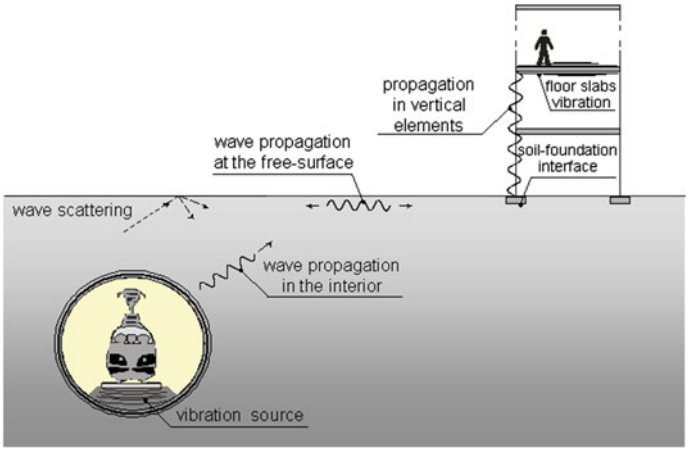

Fig. 2 Sketch of ground-borne vibrations generated by the passage of a train in an underground tunnel and transmission paths along the propagation chain [14]

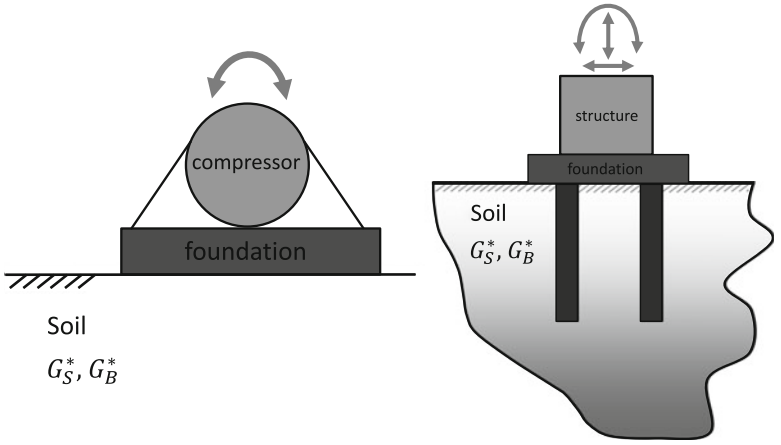

Fig. 3 Examples of soil-foundation-structure interaction problems. (*Left*) Shallow foundation of a compressor. (*Right*) Degrees of freedom of a piled foundation. The dynamic response of the soil-foundation system depends on low-strain complex shear G_S^* and bulk G_B^* moduli of the ground

Other examples where soil linear response is relevant is represented by the foundations of wind turbines, radio antennas, structures exposed to sea wave motion (e.g. wharves, off-shore platforms) and vibrating machines (e.g. compressors, turbo- generators, etc.). In the solution of these contact problems of *Soil Dynamics*, the response of the soil-structural system can be evaluated by assuming a linear viscoelastic soil constitutive model (Fig. 3).

Given the relevance of the response of geomaterials to low amplitude, multi-axial dynamic loading, it is of interest to investigate methods to measure the low-strain constitutive parameters of soil dynamic behavior. However to best discuss this subject, it is useful to first review some peculiar facts of linear viscoelasticity, the simplest formal theory able to satisfactorily capture the most salient aspects of the mechanical response of geomaterials undergoing low-amplitude, dynamic oscillations.

2 Some Relevant Facts on Viscoelasticity Theory

2.1 Review of Constitutive Equations

From a mechanical viewpoint, a viscoelastic material subjected to dynamic loading or involved in phenomena of wave propagation exhibits both the ability to store strain energy and to dissipate strain energy over a finite period of time. Now, experimental evidence shows that soils and rocks, strained at low strain levels, below the linear cyclic threshold shear strain, display exactly this type of behavior, which can then

be satisfactory captured by the theory of linear viscoelasticity [2, 11]. The latter is based on the following four assumptions:

1. validity of *small strain theory*, i.e. $||\boldsymbol{\varepsilon}|| = \max\left\{\left|\lambda^{(1)}\right|, \left|\lambda^{(2)}\right|, \left|\lambda^{(3)}\right|\right\} \ll 1$[1];
2. validity of the *inheritance postulate* stating that at any point of the material, the current value of the Cauchy stress tensor $\boldsymbol{\sigma}(t)$ is only a function of the current value of the strain tensor $\boldsymbol{\varepsilon}(t)$ and of its past strain history;
3. validity of the *time-translation invariance postulate* which states that material response is independent of any time shift (*non-aging* material);
4. validity of the *fading memory hypothesis*, stating that the current state of stress depends more strongly on the recent rather than on the distant strain history.

Under these assumptions, the *Riesz representation theorem* of functional analysis [6] guarantee the existence of a unique relationship between the Cauchy stress tensor $\boldsymbol{\sigma}(t)$ and the strain tensor function $\boldsymbol{\varepsilon}(t)$ via the following convolution integral:

$$\boldsymbol{\sigma}(t) = \int_{-\infty}^{t} \mathbf{G}(t-\tau) : \frac{\mathrm{d}\boldsymbol{\varepsilon}(\tau)}{\mathrm{d}\tau}\mathrm{d}\tau, \tag{1}$$

where $\mathbf{G}(t)$ is a fourth order tensor-valued function named the *relaxation tensor* function. In Eq. (1) the strain history tensor $\boldsymbol{\varepsilon}(\tau)$ is assumed represented by a smooth continuous function however, discontinuities in the strain history functions may be handled if the integral above is intended in the *Stieltjes sense*. Equation (1) is also known as the *Boltzmann's equation* since it can also be obtained by applying the Boltzmann's superposition principle [4].

The relaxation tensor function $\mathbf{G}(t)$ is a *material function* and it has 81 components, however in a general viscoelastic anisotropic material only 21 are independent due to the symmetry of the stress and strain history tensors and after invoking the *Onsager's relations* [5]. They represent the stress response of a material subjected to a strain history specified as a Heaviside function. Boltzmann's equation can be "inverted" to give the current strain tensor $\boldsymbol{\varepsilon}(t)$ as a function of the stress history $\boldsymbol{\sigma}(t)$. In this case the response of the viscoelastic material is specified by the *creep tensor function* $\mathbf{J}(t)$ whose components represent the strain response of a material subjected to a stress history specified as a Heaviside function.

For an isotropic, linear, viscoelastic material, the relaxation tensor function has only *two* independent components. They can be the shear $G_S(t)$ and bulk $G_B(t)$ relaxation functions. As shown by Eq. (1), in the time domain the constitutive relation of a viscoelastic material is an *integral-differential equation*. Thus, the solution of a viscoelastic initial-boundary value problem may not be trivial to obtain. However if Eq. (1) is Fourier transformed, the viscoelastic constitutive relationship becomes:

$$\hat{\boldsymbol{\sigma}}(\omega) = \mathbf{G}^{*}(\omega) : \hat{\boldsymbol{\varepsilon}}(\omega) \tag{2}$$

[1] In this relation $\boldsymbol{\varepsilon}$ is the small-strain tensor and $\lambda^{(j)}(j = 1, 2, 3)$ are the *principal stretches*.

where $\hat{\boldsymbol{\sigma}}(\omega)$ denotes the Fourier transform of $\boldsymbol{\sigma}(t)$. An analogous interpretation holds for $\hat{\boldsymbol{\varepsilon}}(\omega)$. Finally $\mathbf{G}^*(\omega)$ is the *fourth order complex-valued tensor modulus* and it is nothing but the Fourier transform of the relaxation tensor function $\mathbf{G}(t)$ multiplied by $i\omega$. In *isotropic* viscoelastic materials, the mechanical response in the frequency domain is completely defined by the shear $G_S^*(\omega)$ and bulk $G_B^*(\omega)$ complex moduli.

2.2 Velocity and Attenuation of Viscoelastic Waves

As Eq. (2) shows, in the frequency domain the constitutive relation of a linear viscoelastic material is represented by a simple algebraic equation, which resembles Hooke's law of linear elasticity. This resemblance is more profound and it is the result of the "*elastic-viscoelastic correspondence principle*" [19] according to which elastic solutions to steady state boundary-value problems can be converted into viscoelastic solutions for identical boundary conditions by replacing the elastic shear and bulk moduli with the corresponding complex moduli $G_S^*(\omega)$ and $G_B^*(\omega)$. An analogous result can also be obtained by using the Laplace's transform. Although the validity of the correspondence principle is restricted to problems where the prescribed boundary conditions (i.e. displacements and tractions prescribed along the boundary of the domain of interest) are *time-invariant*, its exploitation in elastodynamics turns out to be rather fruitful.

Application of the elastic-viscoelastic correspondence principle to the *Navier's equations of motion* of linear elasticity with no body forces coupled with the *Helmholtz's decomposition theorem* [1] yields a pair of wave equations governing the propagation of viscoelastic body waves. The speed of propagation of these waves is linked to the constitutive parameters $G_S^*(\omega)$ and $G_B^*(\omega)$ of the homogeneous, isotropic medium by the following relations:

$$V_P^*(\omega) = \sqrt{\frac{G_B^*(\omega) + \frac{4}{3}G_S^*(\omega)}{\rho}}, \qquad V_S^*(\omega) = \sqrt{\frac{G_S^*(\omega)}{\rho}} \tag{3}$$

where ρ is the *mass density* of the medium. Equation (3) shows that distortional and volume deformations in isotropic viscoelastic materials are uncoupled modes of deformation just as occurring in linear elasticity. Furthermore, the speed of propagation of P and S waves is complex-valued and frequency-dependent. Both characteristics are inherited by the constitutive parameters $G_S^*(\omega)$ and $G_B^*(\omega)$. The physical interpretation of this fact is that Eq. (3) simultaneously define *phase velocity* and *damping* of monochromatic, viscoelastic body waves as shown, for S waves, by the following relations [17]:

$$V_S(\omega) = \frac{Re^2(V_S^*) + Im^2(V_S^*)}{Re(V_S^*)}, \qquad D_S(\omega) = \frac{Re(V_S^*) \cdot Im(V_S^*)}{Re^2(V_S^*) - Im^2(V_S^*)} \tag{4}$$

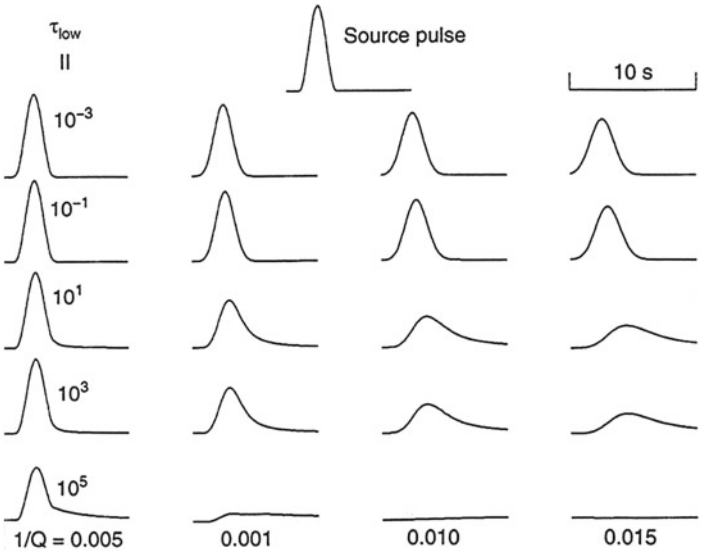

Fig. 4 Pulse spreading in a viscoelastic medium caused by material dispersion for different values of damping ratio here denoted as the inverse of quality factor $Q = 1/2D$ [10]

where $V_S(\omega)$ and $D_S(\omega)$ are respectively *phase velocity* and *damping ratio* of S waves. The terms $Re(V_S^*)$ and $Im(V_S^*)$ denote respectively the *real* and *imaginary* part of the complex-valued shear wave velocity defined by Eq. (3). A relation analogous to Eq. (4) holds also for longitudinal P waves. These equations shows that viscoelastic media are inherently dispersive since the speed of propagation of monochromatic waves varies with frequency [9]. Also damping ratio $D_S(\omega)$, a dimensionless measure of energy dissipation per unit volume of a material undergoing a cycle of harmonic oscillation, is in general frequency-dependent [8]. As a result, in viscoelastic media a localized, narrow-band pulse disperses, and changes its shape as it propagates through the medium (Fig. 4).

Typically, in viscoelastic media high frequencies travel faster than low frequencies (material response gets "stiffer" for high loading rates) and this has consequences on the methods used to measure the speed of propagation of mechanical disturbances. In fact, in exploration geophysics travel time measurements are carried out by picking the first arrivals of P and S phases. These correspond to the speed of propagation of the wave front whose energy is carried mostly by high frequencies.

2.3 Kramers-Kronig Relations

As discussed in the previous section, in linear viscoelastic materials the mechanics of wave propagation is completely defined, in the frequency domain, by either the com-

plex shear $G_S^*(\omega)$ and bulk $G_B^*(\omega)$ moduli or by the complex-valued phase velocities $V_P^*(\omega)$ and $V_S^*(\omega)$. Specifying the viscoelastic constitutive equations in the time or frequency domain would seem to be equivalent however, a preliminary inspection of the corresponding constitutive functions would seem to overturn this statement, at least apparently. Whereas for each mode of deformation, say *shear*, only one material function is required in the time domain, say the *shear* relaxation function $G_S(t)$, to completely specify the mechanical response in the frequency domain two materials functions are needed which are the real and the imaginary parts of either the complex shear modulus $G_S^*(\omega)$ or the complex-valued shear wave velocity $V_S^*(\omega)$. Obviously, the real and imaginary parts of the complex shear modulus (or the complex-valued shear wave velocity) cannot be independent since in the time domain, the shear relaxation function is *real-valued* and it would not be acceptable that more information would be required in the frequency domain, to fully describe the mechanical response of a viscoelastic material, than in the time domain. Indeed, such a relationship exists [6] and can be easily derived from the application of the Fourier integral theorem to Boltzmann's equation (1). The obtained result is the *Kramers-Kronig relation*, a mathematical statement connecting the real and imaginary parts of any complex-valued function, G_S^* or V_S^*, which is *analytic* (or holomorphic) in the upper half of the complex plane for complex-valued frequencies. Equivalently, it can be shown that the real and the imaginary part of the complex shear modulus G_S^* are *Hilbert transforms* pairs [22].

The Kramers-Kronig relation is named in honor of Kronig and Kramers [12, 13] and it is well-known also in other disciplines including physics and electrical engineering. It has an important physical meaning because it represents the necessary and sufficient condition for a response function of a dispersive physical system to satisfy the *principle of causality*. In our case, this means that a disturbance originated at a point of a viscoelastic medium (*source*) is not allowed to arrive at a different point of the same medium (*observer*) before the time d/c has elapsed where d is the distance between the source and the observer and c is the speed of propagation of the disturbance in the medium (V_P or V_S). Inverting Eq. (4) yields [17]:

$$V_S^*(\omega) = \frac{V_S(\omega)}{\sqrt{\left[1 + 4D_S^2(\omega)\right]}} \cdot \left[\frac{1 + \sqrt{\left[1 + 4D_S^2(\omega)\right]}}{2} + i \cdot D_S \right] \tag{5}$$

Therefore, based on the aforementioned discussion on the Kramers-Kronig relation, from Eq. (5) some kind of relationship is also expected to exist between the two real-valued functions $V_S(\omega)$ and $D_S(\omega)$ for exactly the same reason that the real and imaginary parts of the complex modulus are related. Indeed, this relation does exist and it represents another form of the Kramers-Kronig equation, perhaps the most important for applications in *Soil Dynamics* [18]:

$$V_S^2(\omega) + \omega^2 \cdot \int_0^\infty \frac{4}{\pi} \cdot \left[\frac{D_S(\tau)}{\tau \cdot (\tau^2 - \omega^2)} \right] \cdot V_S^2(\tau) \mathrm{d}\tau = G_{S(e)} \cdot \frac{2 \cdot (1 + 4D_S^2)}{1 + \sqrt{1 + 4D_S^2}} \quad (6)$$

where $G_{S(e)} = G_S(t \to \infty)$ is known as the *equilibrium response* of the shear relaxation function $G_S(t)$. Equation (6) is a *Fredholm singular integral equation of 2nd kind with Cauchy kernel*. It is linear in V_S^2 and it establishes a link between material functions $V_S(\omega)$ and $D_S(\omega)$ which cannot be assigned independently despite in the usual practice they are determined separately, using different experimental procedures and often ignoring rate-dependence effects [16].

Meza-Fajardo and Lai [18] using the theory of singular integral equations, obtained an explicit, closed-form solution of Equation (6) for the case when $V_S(\omega)$ is prescribed and also when the specified material function is the damping ratio spectrum $D_S(\omega)$. For the latter case the result is:

$$V_S(\omega) = V_S(0) \cdot \sqrt{\frac{2 \cdot \sqrt{1 + 4D_S^2(\omega)}}{1 + \sqrt{1 + 4D_S^2(\omega)}}} \cdot \exp\left[\frac{1}{\pi} \int_0^\infty \frac{\omega^2 \operatorname{atan}(2D_S(\tau))}{\tau(\omega^2 - \tau^2)} \mathrm{d}\tau \right] \quad (7)$$

where $V_S(0) = \lim_{\omega \to 0} V_S(\omega)$. Equation (7) represents an explicit dispersion relation for low- strain, mechanical disturbances propagating in arbitrary dissipative, linear viscoelastic materials like soils and rocks. By specifying the frequency-dependence of shear damping ratio $D_S(\omega)$, this equation allows to calculate the velocity dispersion function $V_S(\omega)$. The reverse process is also possible and actually, it is even more appealing from a practical point of view since it allows determining the damping ratio spectrum $D_S(\omega)$ entirely from measurements of $V_S(\omega)$ as proposed by Lai and Özcebe [15] in connection with in-situ geophysical prospecting.

A well-known, particular solution of Equation (6), is that obtained under the assumption that $D_S(\omega)$ is frequency-independent (i.e. *hysteretic*) over the seismic band [0.001–10] Hz. This solution is widely used in *Seismology* and is given by the following expression [2, 3]:

$$V_S(\omega) = \frac{V_S(\omega_{ref})}{\left[1 + \frac{2D_S}{\pi} \ln\left(\frac{\omega_{ref}}{\omega} \right) \right]} \quad (8)$$

where ω_{ref} denotes a *reference angular frequency* usually assumed equal to 2π. This dispersion relation predicts values of $V_S(\omega)$ that increase monotonically with material damping ratio for a given frequency. Conversely, for a particular value of damping ratio, Eq. (8) predicts an asymptotic increase of the shear wave velocity with frequency. Equation (8) is also adopted to simulate the dispersion of P waves after replacing D_S with D_P. This type of dispersion relation is often invoked not only in *Seismology* but also in *Soil Dynamics* in light of the fact that experimental

tests in soils and rocks at low strain seem to support the assumption of frequency-independence of damping ratio over the seismic band, as it will be further discussed in the next section.

3 Examples of Causal Dispersion Functions and Damping Ratio Spectra Pairs

In the frequency domain, the Kramers-Kronig relation shows that to completely characterize the mechanical response of viscoelastic materials in a given mode of deformation (say *shear*), only one material function, is required for instance the shear damping ratio $D_S(\omega)$ or, alternatively, the shear wave velocity dispersion function $V_S(\omega)$. If choosing the former, Eq. (7) could be used to set up a parametric study aimed to investigate the dependence of the dispersion function $V_S(\omega)$ on the assumed damping ratio spectrum $D_S(\omega)$. Indeed, this is the objective of this section. Overall, *six cases* were examined. Of these, four refer to variants of a *hysteretic* damping ratio spectrum. This corresponds to a relevant situation since, as mentioned above, frequency independent damping is often postulated a-priori both in *Seismology* and *Soil Dynamics* owing to the rate-independence of energy dissipation exhibited by many soils and rocks in the seismic band [2, 20, 21]. However it can be demonstrated that a *constant* damping ratio over the entire frequency domain $\omega \in]-\infty, +\infty[$ would imply a frequency independent shear (or compression) wave velocity and this violates the principle of causality since no Hilbert transform pair may satisfy the Kramers-Kronig Equation (6) with a constant damping ratio [2]. Thus, some type of frequency-dependence should be admitted outside the seismic band even for an otherwise hysteretic damping ratio spectrum. Another important constraint imposed by viscoelasticity theory over the damping ratio spectrum is the vanishing of damping as the frequency approaches very low and very large values. This is a consequence of the fact that for $\omega \to 0$ and $\omega \to \infty$ it can be shown that a viscoelastic material behaves as an elastic solid [6]. Thus, the spectrum of damping ratio is nonzero and positive definite over a closed set of frequencies (*compact support*) and as a consequence the integral of damping ratio spectrum, over the real axis, is necessarily bounded.

With these premises, the six cases of the parametric study designed to investigate the influence of the assigned damping ratio spectrum $D_S(\omega)$ onto the calculated dispersion function $V_S(\omega)$, are now presented and the results discussed. The numerical integration of Eq. (7) was performed using a robust quadrature scheme given the singularity of the integrand. To increase the accuracy and stability of the algorithm, the domain of integration was split into small sub- domains using an adaptive logarithmic frequency scale.

Figure 5 shows the results of *Case 1* where the goal is to investigate the influence on the shape of the dispersion curve of assuming a hysteretic damping ratio spectrum over a *fixed* frequency bandwidth of $[10^{-2}–10^{2}]$ Hz with different magnitude. The

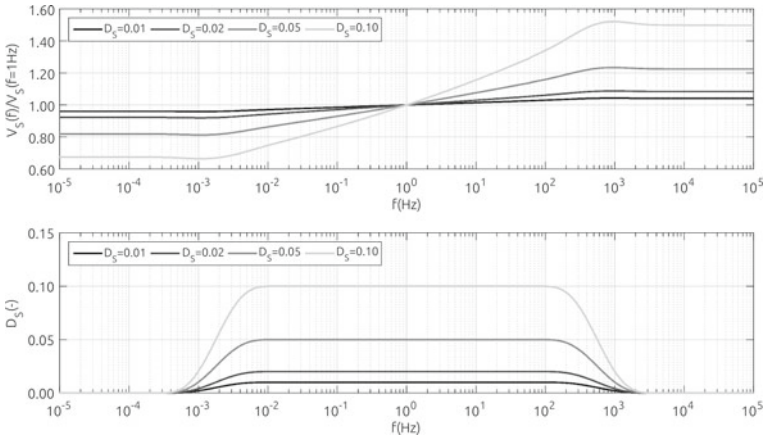

Fig. 5 Dispersion functions and damping ratio spectra pairs satisfying the Kramers-Kronig relations. (*Top*) Calculated dispersion curves. (*Bottom*) Assumed damping ratio spectra. Influence of magnitude of hysteretic damping ratio (over *fixed* bandwidth) on calculated dispersion curves

resulting dispersion curves are *linear* in the portion of the spectrum where damping is rate-independent and slightly beyond, which is a direct consequence of the functional form assumed for the decaying branches.

The major outcome from Fig. 5 is that the larger the damping, the steeper is the slope of the dispersion curve and also the bigger is the difference between the speed of propagation at very low and very large frequencies. For a damping ratio of 2 % (a typical value for many soils at low strain), this difference is on the order of 10 %. The dispersion curves of Fig. 5 have been normalized to the value of V_S specified at a frequency of 1 Hz.

Figure 6 refers to *Case 2* where the objective is to assess the influence on the shape of dispersion curves of assuming hysteretic damping ratio spectra with *constant* magnitude but defined over variable *cut-off frequencies*. The effect is rather apparent: the broader is the frequency band where damping is hysteretic, the larger is the difference in phase velocity at very low and very large frequencies.

In the same way as for *Case 1*, also in *Case 2* the frequency band in which the phase velocity dispersion exhibit a linear behavior is broader than the frequency band wherein damping is assumed rate-independent. In the current example, the linearity of the dispersion function extends to frequencies that are about *one* order of magnitude (at each side) greater and smaller than the corresponding cut-off frequencies where the damping spectrum ceases to be hysteretic.

Overlapped in Fig. 6 is also the dispersion curve (dashed line) calculated using Eq. (8). This is the standard dispersion model adopted in *Seismology*, which is approximate and it corresponds to assuming a *rate- independent* damping ratio spectrum over the frequency range [0.001–10] Hz (seismic bandwidth). The figure shows that in the seismic band the approximate model is actually able to reproduce the exact dispersion function very accurately. Outside this range, the approximate model is still

satisfactory if compared with the exact dispersion curve calculated for frequencies cut-off equal to 10^{-3}, 10^{3} Hz.

Figure 7 illustrates the results of *Case 3* which corresponds to assuming a *Shibuya-like* damping ratio spectrum [21]. This is assumed to represent the frequency-dependence law of *fine-grained soils* and it is characterized by a spectrum having a symmetrical shape (in semi-logarithmic scale) with damping being hysteretic in the frequency range [0.1–10] Hz. Outside this range damping increases monotonically up till *unspecified* cut-off frequencies. Scope of *Case 3* is to investigate the influence on the shape of dispersion curves, of assuming different rates of the rising branches of damping spectra. As shown in Fig. 7, the larger the frequency range outside the hysteretic regime where damping grows, the bigger is the difference of phase velocity at very low and very large frequencies. Also, the smaller is the portion of the dispersion curve, at the two ends of the spectrum, where phase velocity is frequency-independent.

Case 4 explores the effects on the dispersion curve of considering a damping ratio spectrum that is hysteretic in the seismic band, yet, it has a non-symmetrical shape. From the plot, it appears that a "*bulge*" on the damping spectrum yields an extension of the variability of phase velocity on the side of the dispersion curve where the bulge is located. As expected, the dispersion curve is linear in the frequency range where damping ratio is hysteretic (Fig. 8).

It is further observed that the effect of the "*bulge*" vanishes nearly an order of magnitude beyond the frequency at which the damping ratio spectrum reaches its peak. Figure 9 shows the dispersion curves corresponding to assuming a *linear* damping ratio spectrum over a fixed frequency band with a *non*-symmetrical shape (Case 5).

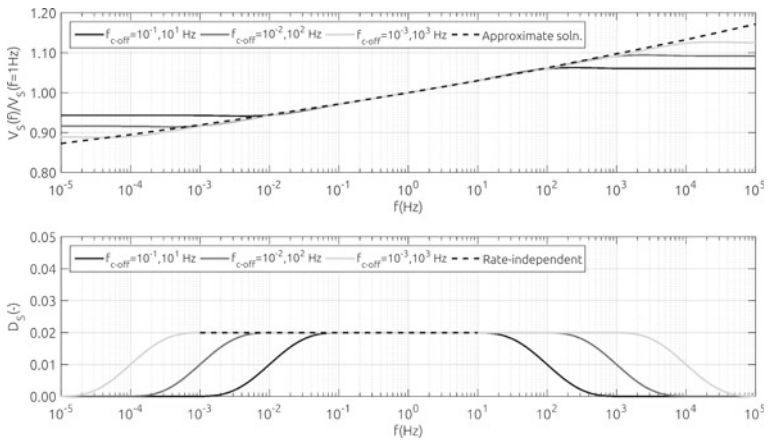

Fig. 6 Dispersion functions and damping ratio spectra pairs satisfying the Kramers-Kronig relations. (*Top*) Calculated dispersion curves. (*Bottom*) Assumed damping ratio spectra. Influence of cut-off frequencies of hysteretic damping (*variable* bandwidth) on computed dispersion curves

The calculated dispersion curves are characterized by a smooth variation with frequency and have either an upward or a downward concavity, depending on the sign of the slope of the linear portion of the damping ratio spectrum.

The last examined case (*Case 6*) is that of a damping ratio spectrum having a *parabolic-like* shape (Fig. 10). The spectrum with an upward concavity corresponds to the so-called *Rayleigh damping ratio*. This is a popular model in earth-quake engineering and it is characterized by the following frequency-dependence law:

$$D_S(\omega) = a \cdot \frac{1}{\omega} + b \cdot \omega \tag{9}$$

where a and b are properly defined constant coefficients [7]. When Eq. (9) is plotted in semi-logarithmic scale, the graph exhibits the parabolic-like shape shown in Fig. 10. Externally to a predefined bandwidth of [0.1–10] Hz, the Rayleigh damping spectrum is first smoothly extrapolated using rising branches with a continuously decreasing slope, then, extended with the usual decaying trend as the frequency approach very low and very large values. The corresponding dispersion curve is anti-symmetric and characterized by an almost rate-independent phase velocity in the frequency interval [0.1–10] Hz. This is occurring since in this band the damping ratio spectrum exhibits rather small values, particularly in the neighborhood of the minimum at 1 Hz. Damping models with larger minima would naturally yield an increase of the slope of the dispersion curve in the frequency range under consideration.

Figure 10 also shows the dispersion curve corresponding to a *Gaussian damping ratio* spectrum. It has also an anti-symmetrical shape however, it is smoother if compared to the dispersion curve of the Rayleigh damping case. Furthermore, the difference in phase velocity, at very low and very large frequency, is limited to

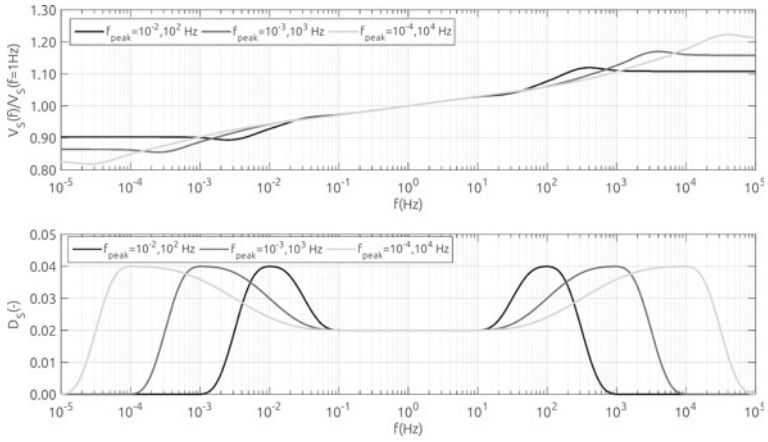

Fig. 7 Dispersion functions and damping ratio spectra pairs satisfying the Kramers-Kronig relations. (*Top*) Calculated dispersion curves. (*Bottom*) Assumed damping ratio spectra (*Shibuya-like model*). Influence of the rate of rising branches' extensions on the computed dispersion curves

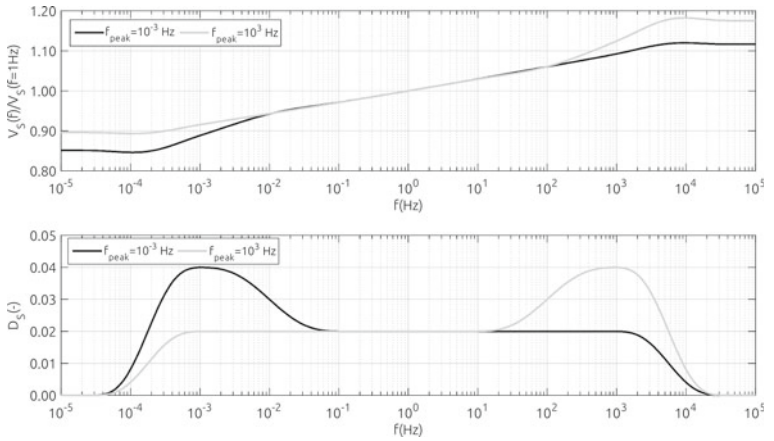

Fig. 8 Dispersion functions and damping ratio spectra pairs satisfying the Kramers-Kronig relations. (*Top*) Calculated dispersion curves. (*Bottom*) Assumed damping ratio spectra (*non-symmetrical hysteretic model*). Influence of damping ratio shape on the computed dispersion curves

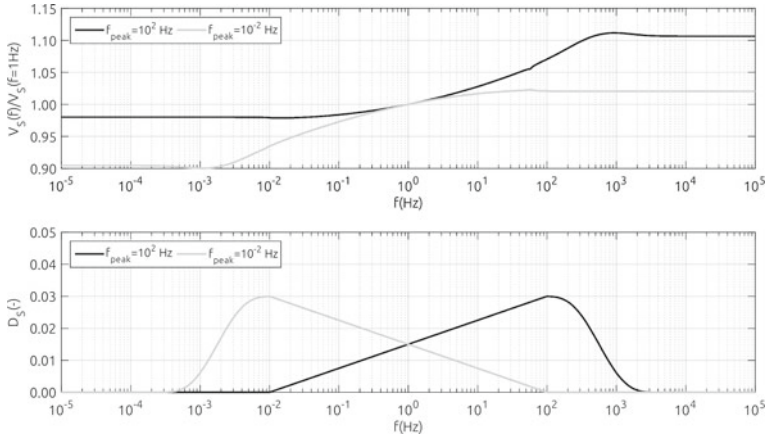

Fig. 9 Dispersion functions and damping ratio spectra pairs satisfying the Kramers-Kronig relations. (*Top*) Calculated dispersion curves. (*Bottom*) Assumed damping ratio spectra (*non-symmetrical linear model*). Influence of damping ratio shape on the computed dispersion curves

approximately 5 % whereas for the Rayleigh damping case it reaches about 10 %. This despite the peak value of damping ratio is the same (about 4 %) for both the Gaussian and the Rayleigh spectrum. Indeed, such result does not appear odd, if one considers that the Rayleigh damping model can be viewed as the superposition of two independent Gaussian-damping models centered at the frequencies corresponding to the peaks of the Rayleigh spectrum.

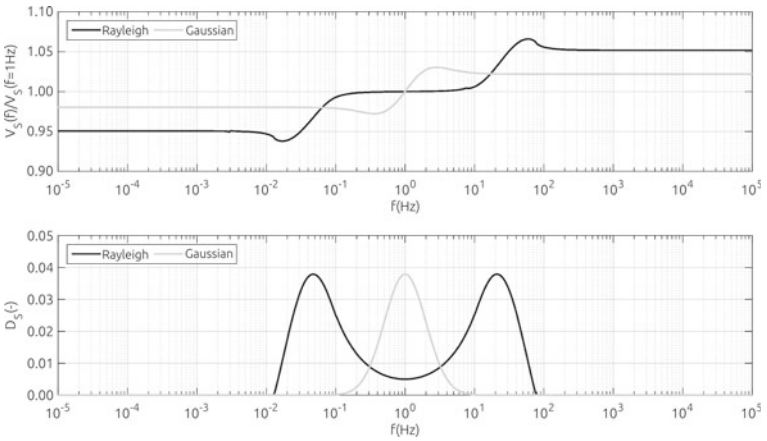

Fig. 10 Dispersion functions and damping ratio spectra pairs satisfying the Kramers-Kronig relations. (*Top*) Calculated dispersion curves. (*Bottom*) Assumed damping ratio spectra (*Rayleigh* and *Gaussian*). Influence of concavity of damping spectrum on the computed dispersion curves

4 Conclusions

Linear viscoelasticity is the simplest constitutive model able to satisfactorily describe the mechanical response of geomaterials subjected to low-amplitude vibrations. An important result predicted by this theory of material behavior is that phase velocities of body waves and material damping ratio are not independent quantities. They are linked by the Kramers-Kronig relations, which can be interpreted as a mathematical statement of the principle of physical causality. The functional coupling between the speed of propagation and damping ratio of viscoelastic waves also involves frequency-dependence of these response functions. This is at the origin of *material dispersion*, a phenomenon by which a spatially localized disturbance changes its shape as it propagates through a dissipative medium.

A distinctive feature of the Kramers-Kronig relations is that they establish a link between two fundamental parameters of a viscoelastic material allowing the computation of one, say the shear wave velocity, as a function of the other, say the shear-damping ratio. This can be very useful since both these material functions are of fundamental importance in the solution of boundary value problems in *Earthquake Geotechnical Engineering* and *Soil Dynamics*. Yet, in the current practice, they are determined separately using different procedures and often ignoring their frequency-dependence.

From a mathematical point of view, the Kramers-Kronig relations are linear, singular, *Fredholm integral equations of* 2*nd kind*. An approximate solution of these equations has long been proposed by seismologists by assuming rate- independent (i.e. hysteretic) damping ratio over the seismic band [0.001–10] Hz. Exact, closed-form solutions of these equations have recently been obtained for the material func-

tions of interest in *Soil Dynamics*, namely phase velocity of body waves and material damping ratio.

This paper illustrated the results of a parametric study aimed to explore the functional dependence of the dispersion function of shear waves on the assumed shear-damping ratio spectrum. For the shear mode of deformation, this is the only material function that needs to be specified to fully describe the mechanical response of the medium (in the frequency domain). Several cases were analyzed which were either suggested by well-known *signatures* of soil response (e.g. hysteretic or Rayleigh damping) or inspired by realistic speculations of soil mechanical behavior. Efforts are underway to apply this procedure to real data. The ultimate goal is to develop a procedure for determining damping ratio spectra of geomaterials from measurement of the dispersion functions of P and S waves through geophysical seismic methods. In fact, the latter are ideal to determine V_P and V_S in soil deposits since the level of strain induced by the artificially generated mechanical waves is very low, certainly below the *linear cyclic threshold shear strain*. Thus, linear response can be assumed without approximation. With ambient noise (if using passive seismic methods), this condition is fulfilled even better. However, in conventional geophysical prospecting, the frequency-dependence of V_P and V_S is usually disregarded. Furthermore, damping ratio is rarely determined from the measurement of body waves owing to the difficulties of separating geometric and intrinsic attenuation. Thus, calculation of damping ratio spectra from phase velocity measurements of P and S waves using geophysical seismic methods seems to be a particularly attractive prospective in experimental *Soil Dynamics*.

References

1. Achenbach, J.D.: Wave Propagation in Elastic Soils. North-Holland, Amsterdam (1984)
2. Aki, K., Richards, P.G.: Quantitative Seismology. University Science Books, Sausalito (2002)
3. Ben-Menahem, A., Singh, S.J.: Seismic Waves and Sources. Dover Publications, Mineola (2000)
4. Boltzmann, L.: Zur Theorie der elastischen Nachwirkung. Poggendorff's Annalen der Physik und Chemie **7**, 624–654 (1876)
5. Carcione, J.M.: Wave Fields in Real Media : Wave Propagation in Anisotropic, Anelastic, Porous and Electromagnetic Media. Elsevier, Amsterdam (2007)
6. Christensen, R.M.: Theory of Viscoelasticity. Dover Publications (2010)
7. Clough, R.W., Penzien, J.: Dynamics of Structures. McGraw-Hill, New York (1993)
8. Foti, S., Lai, C.G., Rix, G.J., Strobbia, C.: Surface Wave Methods for Near-Surface Site Characterization. CRS Press - Taylor & Francis Group (2014)
9. Futterman, W.I.: Dispersive body waves. J. Geophys. Res. **67**(13), 5279–5291 (1962)
10. Gupta, H.K.: Encyclopedia of Solid Earth Geophysics. Encyclopedia of Earth Sciences Series, p. 1539. Springer (2011)
11. Ishihara, K.: Soil Behaviour in Earthquake Geotechnics. Oxford Science Publications, Oxford (1996)
12. Kramers, H.A.: La diffusion de la lumiere par les atomes. Atti Cong. Intern. Fisici, (Transactions of Volta Centenary Congress) Como, Italy, vol. 2, pp. 545–557 (1927)
13. Kronig, R.D.L.: On the theory of dispersion of X-rays. J. Opt. Soc. Am. **12**(6), 547–556 (1926)

14. Lai, C.G., Callerio, A., Faccioli, E., Morelli, V., Romani, P.: Prediction of railway-induced ground vibrations in tunnels. J. Vib. Acoust. **127**(5), 503–514 (2005)
15. Lai, C.G., Özcebe, A.G.: In-Situ measurement of damping ratio spectra from the inversion of phase velocities of P and S waves in cross-hole seismic testing. In: Second International Conference on Transportation Geotechnics. S. M. e. al. Hokkaido-Japan, pp. 578–582 (2012)
16. Lai, C.G., Özcebe, A.G.: Non-conventional methods for measuring dynamic properties of geomaterials. In: 6th International Conference on Earthquake Geotechnical Engineering. Christchurch, New Zealand (2015)
17. Lai, C.G., Rix, G.J.: Solution of the Rayleigh eigenproblem in viscoelastic media. Bull. Seismol. Soc. Am. **92**(6), 2297–2309 (2002)
18. Meza-Fajardo, K.C., Lai, C.G.: Explicit causal relations between material damping ratio and phase velocity from exact solutions of the dispersion equations of linear viscoelasticity. Geophys. J. Int. **171**, 1247–1257 (2007)
19. Read, W.T.: Stress analysis for compressible viscoelastic materials. J. Appl. Phys. **21** (1950)
20. Santamarina, J.C., Klein, K.A., Fam, M.A.: Soils and Waves. Wiley, Chichester (2001)
21. Shibuya, S., Mitachi, T., Fukuda, F., Degoshi, T.: Strain rate effects on shear modulus and damping of normally consolidated clay. Geotech. Test. J. **18**(3), 365–375 (1995)
22. Tschoegl, N.W.: The Phenomenological Theory of Linear Viscoelastic Behavior—An Introduction. Springer, Berlin (1989)
23. Vucetic, M.: Cyclic threshold shear strains in soils. J. Geotech. Eng. **120**(12), 2208–2228 (1994)

A Study of Deformation and Failure of Unidirectional Fiber-Reinforced Polymers Under Transverse Loading by Means of Computational Micromechanics

Marek Romanowicz

Abstract A method for determining the in-situ strength of fiber-reinforced laminas for three types of transverse loading including compression, tension and shear is presented. In the framework of this method, an analysis of local stresses that are responsible for the coalescence of matrix cracks is carried out by using a multi-fiber unit cell model and finite element method. The random distribution of fibers, fiber-matrix decohesion and matrix plastic deformations are taken into account in the micromechanical simulations. The present study also shows that the nonlinear hardening behavior of matrix reflects more realistically the influence of plastic deformations on the in-situ transverse strength of lamina than the perfectly plastic behavior of matrix. The prediction of the in-situ transverse strength is verified against the experimental data for a cross ply laminate subjected to uniaxial tension.

1 Introduction

When a fiber-reinforced polymer-matrix composite lamina is subjected to transverse loading, it fails due to matrix cracking. For an isolated lamina, the initiation of the first matrix crack indicates fracture of the lamina. This process happens differently when the lamina is embedded in a laminate. Since other laminas in a laminate retard the propagation of the matrix cracks, the stiffness of cracked lamina does not drop suddenly but declines gradually with increasing load. In this case, the strains to failure are larger than those of an isolated lamina. The transverse failure mechanism depends on many factors, among which the most important are properties of the fiber-matrix interface, the local fiber distribution and the non-linearity of matrix. In order to predict the life of the lamina in a laminate, it is necessary to use accurate micromechanical models which involve these factors.

The reduction of lamina stiffness due to transverse matrix cracking can be determined by using computational micromechanics. Most of the literature on this subject,

M. Romanowicz (✉)
Department of Mechanical Engineering, Bialystok University of Technology, Bialystok, Poland
m.romanowicz@pb.edu.pl

B. Albers and M. Kuczma (eds.), *Continuous Media with Microstructure 2*,
DOI 10.1007/978-3-319-28241-1_25

such as papers by Llorca and co-workers [1, 2], Vaughan and McCarthy [3, 4] focuses on the study of the influence of matrix and interface properties on the macroscopic response of lamina. In these papers, the authors have proved the utility of unit cell models with random fiber arrangement in determining the transverse strength of isolated laminas. However, they have provided no prediction of the critical damage threshold in polymer matrices. Further development of this approach is to be found in papers by Melro et al. [5], Yang et al. [6], who have applied more complex constitutive laws of the matrices to trace the damage evolution in isolated laminas up to final failure. Although these studies have substantially contributed to our understanding of the failure behavior of unidirectional laminas under transverse loading, the constraining effects of other laminas have been less recognized. Modeling matrix cracking in cross ply composite laminates subjected to in-plane shear through multi-fiber unit cells has recently been presented by Totry et al. [7], Wei et al. [8], Soni et al. [9]. In these papers, the authors found the in-plane shear stress-strain response of laminates by averaging the shear responses of plies. Although they have successfully established methodology for modeling cross ply composite laminates, they have not considered the coalescence of matrix cracks that corresponds to the first ply failure.

The main objective of this paper is to present a simple procedure based on the use of the unit cell with random fiber arrangement and the finite element method to predict the load at which the first lamina embedded in a laminate fails. For this purpose, an analysis of the hoop stresses that are responsible for the coalescence of the matrix cracks is carried out in the present paper. To find the in-situ strength of lamina, the criterion of maximum hoop stress in matrix is used locally for the most loaded fiber. The first ply failure load predicted from proposed method is verified against the experimental data for a cross ply laminate subjected to uniaxial tension.

Another objective of this paper is to assess whether, and to what extent, the transverse failure behavior of lamina is sensitive to the hardening of matrix due to plastic deformation. Most of numerical simulations on the mechanical behavior of composites under transverse loading are based on an assumption that polymer matrices can be represented by an elastic- perfectly plastic solid following the one of the pressure-sensitive yield criterions. Although this simple model of plasticity is able to reproduce the localization of damage along a narrow fracture path, it leads to the overestimation of the plastic deformation because, in reality, a polymer matrix hardens and its ductility decreases. An alternative approach is to consider in-situ properties of the matrix that are back-calculated from experimental data of the lamina. The role of the in-situ properties of matrix in modeling the matrix cracking failure mode remains unexplored and therefore is also undertaken in this paper.

2 Micromechanical Models

Numerical simulations using a concept of the unit cell with random fiber arrangement are a current trend of work in computational micromechanics. The benefit of the use of such unit cells is that the effect of fiber array irregularities on transverse responses of composite can be accurately taken into account. In this paper, the unit

Table 1 Mechanical properties of the unidirectional lamina and its constituents

E-glass fiber		MY750 epoxy matrix			
E_f (GPa)	ν_f	E_m (GPa)	ν_m	k (MPa)	μ
74	0.2	4	0.35	43.35	0
Fiber-matrix interface					
k_n (GPa/m)	k_t (GPa/m)	G_n^c (J/m^2)	G_t^c (J/m^2)	σ_n^c (MPa)	τ_t^c (MPa)
$0.1 \cdot 10^9$	$0.1 \cdot 10^9$	15	30	30	60
Lamina					
ε_{2T} (%)	ε_{2C} (%)	σ_{2T} (%)	σ_{2TC} (%)	V_f (%)	
0.246	1.2	40	145	60	

cell models of randomly distributed fiber composite are generated using Wongsto and Li's algorithm [10]. Analyses were made on models that contained 39 fibers. The data required for the simulation study were taken from the world wide failure exercise WWFE [11] for an example case of E-glass/MY750/HY917/DY063 lamina with the fiber volume content of 60 %. The properties of this material and its constituents are listed in Table 1. Two-dimensional finite element meshes that mainly consisted of plane strain elements with four nodes (PLANE182) were constructed by using ANSYS finite element code [12]. To ensure accurate displacement and stress field representation within each unit cell, sufficiently dense meshes comprising of approximately 45,000 elements were used. A cohesive layer consisted of contact elements with four nodes (CONTA172, TARGE169) was introduced between the fibers and the matrix to reproduce the fiber-matrix debonding. Each fiber/matrix interface contained 100 contact elements equally spaced around the circumference.

2.1 Numerical Homogenization Technique

In this paper, the effect of the matrix ductility has been studied for the selected lamina subjected to three types of transverse loading including compression, tension and shear. For each loading type, periodic boundary conditions were imposed on the unit cell to reflect the repeatability of the microstructure and to ensure the compatibility of the displacement fields. By the assumption of periodicity, each displacement field u_i may be decomposed in a part associated with the applied strain ε_{ij} and a periodic one u_i^p [13]

$$u_i(x_1, x_2) = \varepsilon_{ij} x_j + u_i^p(x_1, x_2). \tag{1}$$

These relations are implemented at each periodic pair of nodes to link the displacements of the top and the bottom boundaries and the displacements of the right and left boundaries of the unit cell. Because of a huge number of nodes at the opposite boundary edges, a Ansys APDL macro has been used to generate automatically all

required constraint conditions (1). The normal σ_2 and shear τ_{23} stresses corresponding to the applied strains ε_2 and $2\varepsilon_{23}$ were computed from the resultant normal and tangential forces acting on the edges divided by the actual cross-section.

2.2 Constitutive Equations of Matrix and Interface

Although the extension of plastic strain zones in polymer matrices is inhibited by the nearest fibers, they can exhibit considerable plastic deformation at the microscopic level [14, 15]. This is because the probability of occurrence of defects in a small volume of material is much lower than in large one and the failure behavior of polymers changes from brittle to ductile when the size scale is decreased. The epoxy matrix is therefore modeled within the framework of the finite deformations as a elasto-plastic solid which hardens isotropically. It is widely accepted, nowadays, that the deformation of polymeric materials is highly sensitive to the hydrostatic pressure and plastic flow of these materials can exhibit plastic dilatancy. To address this requirement, the Drucker-Prager plasticity model [16], which incorporates the linear dependence on the hydrostatic stress, is used. In terms of the first invariant of stress I_1 and the second invariant of the deviatoric part of stress J_2, the yield function is given as

$$f = \left(\frac{\mu I_3}{3}\right) + \sqrt{J_2} - k, \tag{2}$$

where μ is the pressure sensitivity factor, k is the flow stress of the material under pure shear. Experiments showed that the pressure-sensitivity factor μ ranges from 0.10 to 0.25 for polymers [17, 18]. Note, that if $\mu = 0$, Eq. (2) reduces to the von Mises yield function. The Drucker-Prager plasticity model with $\mu = 0.1$ and $k = 43.30$ MPa was used to study the role of the matrix ductility in the matrix cracking failure mode. An associative flow rule is used to compute the direction of plastic flow. The dilatancy factor μ^* describing the volume change during plastic deformation was equal to μ.

For the fiber/matrix interface failure, the cohesive zone model is employed, in which the constitutive equations of the interface relate the normal σ_n and tangential τ_t cohesive tractions to the normal u_n and tangential u_t opening displacement jumps and a scalar damage variable d, through [19]

$$\sigma_n = k_n u_n (1 - d), \qquad t_t = k_t u_t (1 - d), \tag{3}$$

where $_n$, k_t are initial contact stiffnesses in the normal and tangential direction, respectively. The variable d represents the loss of stiffness and it is a function of both opening displacement jumps. The variable d takes values from 0 to 1. Relationships (3) demonstrate linear elastic loading region followed by linear softening region. When $d = 0$, the cohesive elements are closed and the tractions increase linearly up to their maximum values σ_n^c, τ_t^c in the normal and tangential direction, respectively.

When $0 < d < 1$, these elements begin to open and the tractions decrease linearly. When $d = 1$, the tractions are zero and the cohesive elements are completely broken. To define the completion of fracture in the cohesive zone model, a power law based energy criterion is used [19]

$$\left(\frac{G_n}{G_n^c}\right) + \left(\frac{G_t}{G_t^c}\right) = 1, \tag{4}$$

where G_n, G_t denote energy release rates for mode I fracture and mode II fracture, respectively and G_n^c and G_t^c correspond to the interfacial fracture energies.

2.3 Calibration of the Drucker-Prager Plasticity Model

It is well known that polymer matrices cannot behave the same as unreinforced polymers, see, for example [20]. Thus, micromechanical models require in-situ properties of matrices that are different from bulk properties. In this paper, the hardening curve of epoxy matrix is extracted from a micromechanical model subjected to in-plane shear loading. The non-linearity of epoxy matrix is identified such that the unit cell prediction matches the measured in-plane shear response reported by Soden et al. [11]. Figure 1a shows a comparison of the measured shear response and that from the unit cell model. Agreement with experimental data is quite good. It can be seen from this figure that the unit cell model with perfectly-plastic matrix is unable to reproduce the in-plane shear response of composite. To illustrate the difference between the in-situ and bulk properties, the non-linear strain-stress curve established for epoxy matrix from the micromechanical model is compared with results of tensile tests of unreinforced epoxy performed by Fiedler et al. [14] on specimens with very small

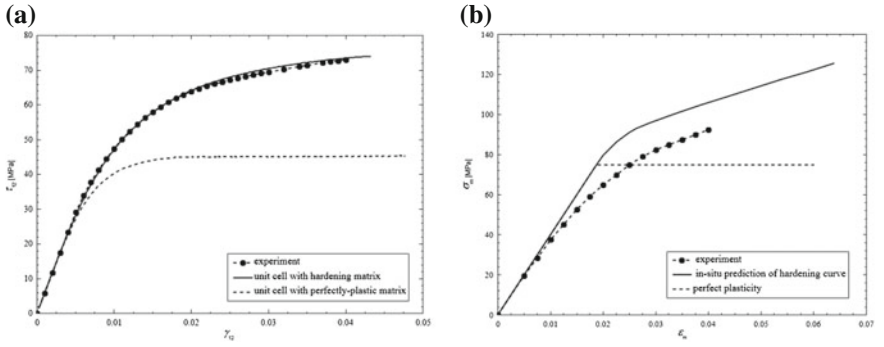

Fig. 1 Identification of the plasticity model. **a** Comparison of experimental in-plane shear response of the E-glass/MY750 epoxy composite [11] with two numerical simulations, **b** comparison of in-situ tensile response of epoxy matrix with experimental data [14]

thickness (t = 0.4 mm). It can be seen in Fig. 1b that the epoxy matrix in the composite is considerably stiffer and stronger than the unreinforced epoxy. The difference between the in-situ and bulk properties would be more evident in the case of standard specimens. Unfortunately, for the matrix system under consideration, only the tensile strength, $\sigma_m^c = 80$ MPa, and the tensile failure strain, $\varepsilon_m^c = 0.05$, are available in the literature [11].

2.4 Calibration of the Interface Model

Computational simulations of interfacial debonding in fiber-reinforced composites require input data such as the interfacial cohesive strength and the interfacial fracture energy. Unfortunately, these data are not precisely known because they are difficult to obtain from simple laboratory experiments, see, for example [21, 22]. In order to ascertain the cohesive properties for the interface of a composite lamina made of E-glass fibers and MY750 epoxy matrix, an analysis of matrix cracking under transverse compression was carried out for various interfacial cohesive strengths and fracture energies. It was assumed that the ratio of the tensile interfacial strength to the shear interfacial strength, σ_n^c/τ_t^c and the ratio of the opening component to the

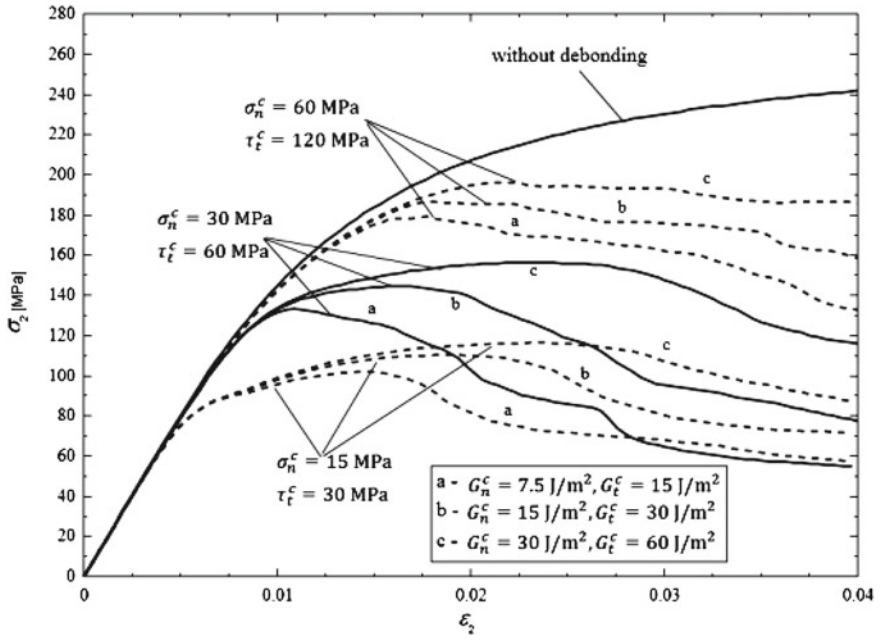

Fig. 2 Influence of the interfacial cohesive strength and the interfacial fracture energy on the mechanical response of the unit cell model under transverse compression

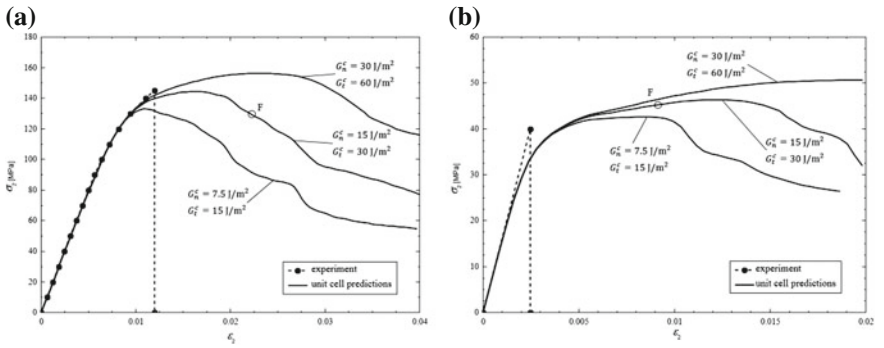

Fig. 3 Comparison of experimental responses of the E-glass/MY750 epoxy composite [11] with numerical simulations for $\sigma_n^c = 30$ MPa and $\tau_n^c = 60$ MPa. Results for **a** transverse compression, **b** transverse tension

sliding component of the interfacial fracture energy, G_n^c / G_t^c are 0.5. The macroscopic compressive stress-strain curves calculated for four different levels of interfacial strength and three different levels of interfacial fracture energy are shown in Fig. 2. It can be observed from this figure that an increase of the interfacial strength produces an increase in the transverse compressive strength of composite and, in turn, a drop of the interfacial fracture energy leads to a larger drop-off in macroscopic stress at the post critical stage. The strength of the interface was calibrated such that the unit cell predictions match transverse compression data, reported by Soden et al. [11]. It was found that the micromechanical models with $\sigma_n^c = 30$ MPa and $\tau_t^c = 60$ MPa produce reasonable results. Figure 3a shows a comparison of the measured compressive response and those obtained from the unit cell models for the above-mentioned cohesive parameters. Figure 3b shows a similar comparison in the case of transverse tension.

3 Results

Two models of matrix plasticity were applied in order to evaluate their utility for predicting the in-situ transverse strengths of lamina and to analyze the impact of the matrix ductility on the overall macroscopic responses of lamina under transverse loading. Figure 4a–c compare the macroscopic stress-strain curves obtained from unit cell models with hardening and perfectly plastic matrix for three types of transverse loading including compression, tension and shear, respectively. It can be seen from these figures that the application of the perfect plasticity theory in modeling transverse shear (Fig. 4c) and transverse compression (Fig. 4a) reduces the strength of lamina. Only for transverse tension (Fig. 4b), the strength of lamina is insensitive to the choice of the plasticity model. This finding suggests that the localization of plastic deformation occurs in this case after the maximum of the macroscopic stress has been

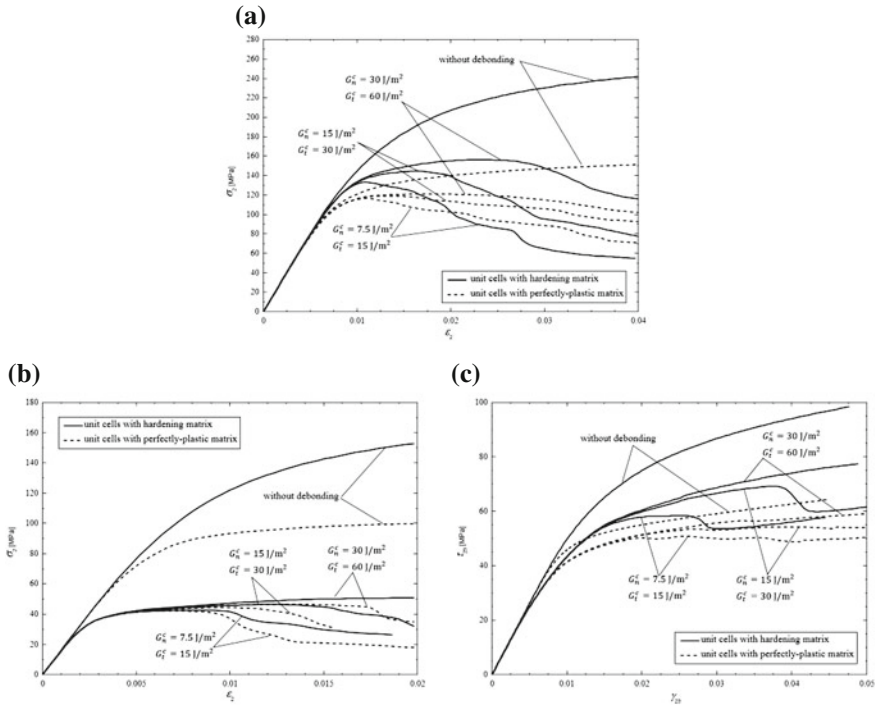

Fig. 4 Influence of the ductility of matrix on the mechanical response of the unit cell model under **a** transverse compression, **b** transverse tension, **c** transverse shear

attained. When a unidirectional lamina is subjected to transverse shear or transverse compression, the development of shear bands in matrix interact with fiber-matrix debonding. In contrast to these cases, the non-linear behavior of lamina for transverse tension is mainly caused by interfacial debonding. Thus, when the mode of failure is shear, matrix hardening plays an equally important role as interfacial properties in predicting the mechanical behavior of composite lamina.

To see whether the micromechanical models with hardening matrix predict correctly the formation of critical planes, three contour plots of effective plastic strain in matrix obtained at the post-critical stage of deformation are presented in Fig. 5a–c. It is interesting to note that extensive plastic deformation of matrix takes place only in the vicinity of interfacial cracks. Furthermore, there is one clearly defined critical plane in these models. Theoretically, the inclination of critical planes depends on the internal friction angle Φ. For the pressure sensitivity factor $\mu = 0.1$, the internal friction angle $\tan \Phi = \mu\sqrt{3}$ is approximately to be 10°. Coulomb type yield criterions predict that plastic yielding occurs in the case of transverse compression along a plane which is inclined at an angle $\alpha_c = 45° + \Phi/2$ with respect to the plane perpendicular to the loading axis, and in the case of transverse shear, at an angle $\alpha_c = \Phi/2$. In the case of transverse tension, the critical plane angle α_c is equal to 0°. It can be

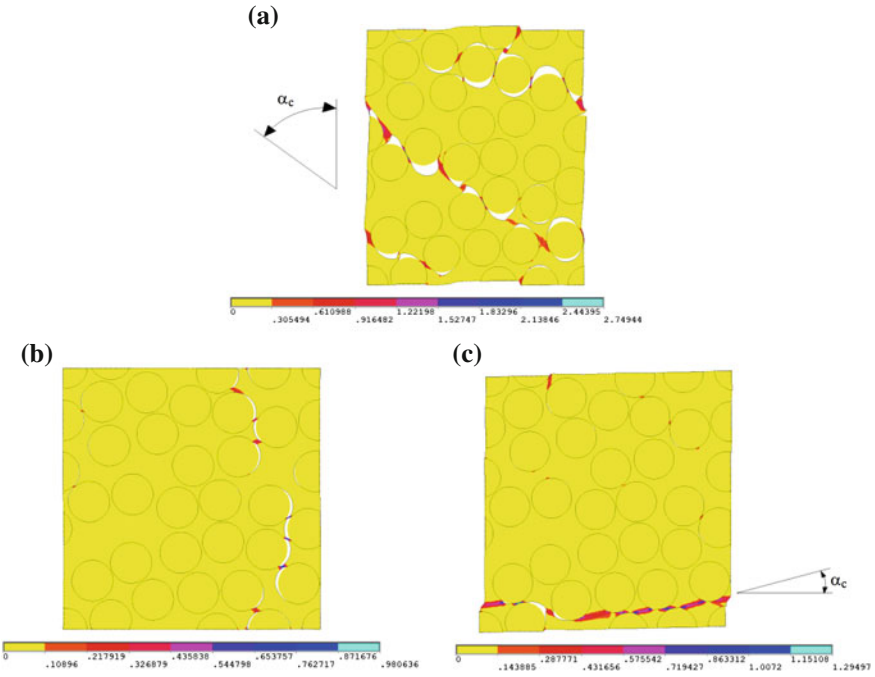

Fig. 5 Contour plots of the effective plastic strain in hardening matrix in the unit cell model subjected to **a** transverse compression at $\varepsilon_2 = 4\,\%$, **b** transverse tension $\varepsilon_2 = 2\,\%$, **c** transverse shear at $2\varepsilon_{23} = 5\,\%$

seen from these figures that the proposed models produce the critical plane angles which are consistent with those obtained from theoretical predictions.

Figure 6 shows the plastic shear bands obtained from the unit cell model with perfectly plastic matrix in the case of transverse compression at the same stage of deformation. From the graph above we can see that there are several possibilities for developing a critical plane across the model. Furthermore, the shear bands occur in the unit cell model with perfectly plastic matrix also in regions without significant interfacial debonding. Comparing Fig. 6 with Fig. 5a, it can be seen that the development of damage by plastic deformation of matrix is now more severe than it was in the corresponding model with hardening matrix. It is interesting to note that both models have the same properties of the fiber-matrix interface. This finding clearly demonstrates that there is an interaction between the two failure mechanisms and that the extension of the plastic deformation in matrix depends on the hardening curve. A similar effect was observed in the existing studies, see, for example [1, 2] in which the development of the plastic deformation in matrix was controlled by changing the interfacial properties.

It is well known that fracture of matrix occurs within regions of tensile stress concentrations. Thus, a unidirectional lamina cannot fail unless the matrix tensile

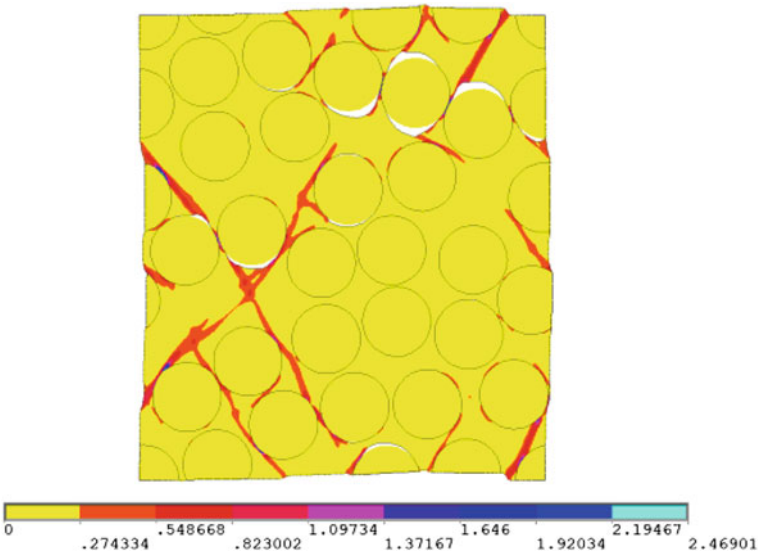

Fig. 6 Contour plot of the effective plastic strain in perfectly-plastic matrix in the unit cell model subjected to transverse compression at $\varepsilon_2 = 4\,\%$

stress exceeds the tensile strength of matrix. Figure 7a–c show how the matrix hoop stress $\sigma_{\theta\theta}$ varies with increasing macroscopic strain in dependence on the polar angle θ for three types of transverse loading including, compression, tension and shear, respectively. For purpose of this analysis, only the most loaded fiber was considered (different for each type of transverse loading). In all cases, such a fiber lies on the critical plane. The evolution of the matrix hoop stress reveals, that the formation of the interfacial crack magnify locally the tensile stress in matrix, as well as that the maximum of this stress locates at the interfacial crack tips. It is interesting to note that even for compressive loading, the tensile stress in matrix appears (Fig. 7a). Experimental tests carried out on microscopic specimens indicate that the tensile strength of epoxy polymers can exceed 100 MPa [14, 15]. Therefore, this value was taken as the reasonable reference level for computing the ultimate failure. When the tensile stress in matrix goes beyond this limit, the existing microcracks have the potential to kink out the interfaces and join into a large macroscopic crack. The values of critical macroscopic strain for all cases considered here were identified on the basis of the evolution of the matrix hoop stress. It was found that the E-glass/MY750 unidirectional lamina fails when its strain exceeds a limit $\varepsilon_c = 0.0220$, 0.0092 and 0.0520 for transverse compression, tension and shear, respectively. The points corresponding to the coalescence of matrix cracks were marked with the letter F in Fig. 3a, b. The results of computing the ultimate failure show that the strains to failure of unidirectional lamina obtained from strain-controlled predictions are much larger than those measured in load-controlled tests. The ratio of the strain to failure from strain-controlled predictions to that from load-controlled tests is $\varepsilon_c/\varepsilon_c^* = 4$ for transverse

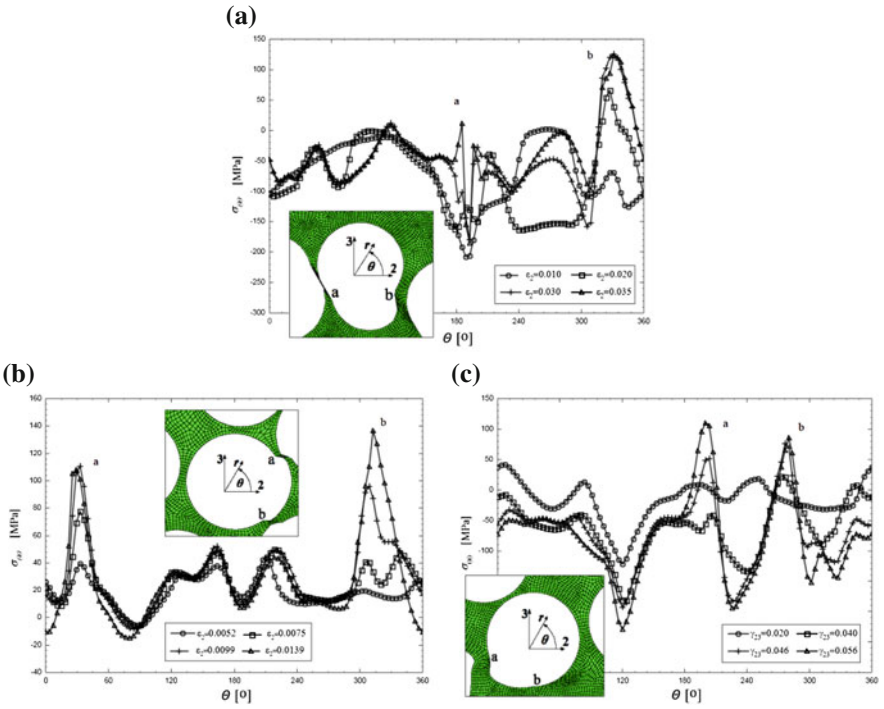

Fig. 7 Angular distribution of the matrix hoop stress $\sigma_{\theta\theta}$ at the interface between matrix and the most loaded fiber for **a** transverse compression, **b** transverse tension, **c** transverse shear

tension, and $\varepsilon_c/\varepsilon_c^* = 2$ for transverse compression. It is hard to determine this ratio for transverse shear because there are no experimental data.

In order to demonstrate the potential of micromechanical simulations in practice, the predicted strain to failure of unidirectional lamina under transverse tension (Fig. 3b) was used to compute the load at which the first lamina failure occurs in a symmetric cross ply $(90°/0)_s$ laminate subjected to uniaxial tension along the 0° direction. In this type of laminate, it is easy to investigate the constraining effects of other laminas because computation of the first ply failure load requires tracking the degradation only in the 90° plies. It is reasonable to assume, that the tensile behavior of a cross ply $(90°/0)_s$ laminate is given by the averaged contribution of the laminas parallel and perpendicular to the loading direction. Since the axial tensile response of the 0° plies remain linear, the stress-strain curve of unidirectional lamina for axial tension is calculated from the known modulus of the constituents by using the rule of mixtures. Figure 8 compares the tensile stress-strain curves of the laminate obtained from experiments and predicted through micromechanical simulations. The experimental stress-strain curve for cross ply laminate made of E-glass/MY750 epoxy material was taken from the world wide failure exercise WWFE [22]. It can be seen from this figure that, although, the experimental response of laminate is linear at

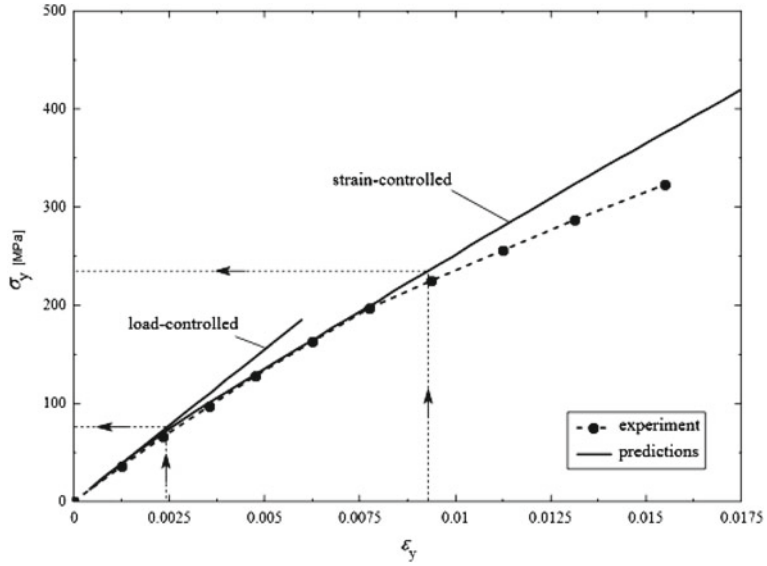

Fig. 8 Comparison of the tensile stress-strain curve of the symmetric cross ply $(90°/0°)_s$ laminate obtained from micromechanical simulations with experimental data [23]

low strain levels, it shows significant softening that begins at a strain level of about 0.0075 and a stress level of about 190 MPa. One possible explanation of this is that the initiation of transverse cracks in the 90° plies results in a change in the slope of the stress-strain curve. The simple averaging procedure outlined here reproduces the initial linear response of the laminate very well. The limit of the applicability of this procedure is defined at the critical point when the matrix tensile stress exceeds the tensile strength of matrix. For the strain to failure of the 90° plies, $\varepsilon_c = 0.00916$, obtained from the strain- controlled predictions (Fig. 3b), the tensile stress in the laminate is 232 MPa. For the strain to failure, $\varepsilon_c = 0.00246$, obtained from the load-controlled tests (Fig. 3b), the tensile stress in the laminate is only 76 MPa. Taking above into account, computational micromechanics provides a better estimate for the first ply failure load than that obtained from the load controlled tests.

4 Conclusions

The present study was designed to determine the in-situ strength of lamina in a symmetric cross ply laminate subjected to uniaxial tension as well as to investigate the effect of matrix ductility on the transverse failure behavior. The results of this investigation showed that regardless of type of transverse loading, a large tensile stress develops in matrix in the vicinity of interfacial crack tips. An analysis of the

matrix hoop stress around the most loaded fiber can be used to predict the in-situ transverse strength of lamina. It was shown that the first ply failure load obtained from micromechanical simulations agrees better with the experimental results than that computed by using data of isolated laminas measured in load-controlled tests. The present study also showed that the application of the unit cell models in which matrix hardens with increasing load predicts realistically the location of plastic zone only in regions with significant debonding. On the contrary, the use of the unit cell models with perfectly plastic matrix leads to the overestimation of the plastic deformation and the reduction in the strength of lamina.

Acknowledgments The financial support of the National Science Centre of Poland under contract DEC-2011/03/D/ST8/04817 is thankfully acknowledged.

References

1. Gonzalez, C., LLorca, J.: Mechanical behavior of unidirectional fiber-reinforced polymersunder transverse compression: microscopic mechanisms and modeling. Compos. Sci. Technol. **67**, 2795–2806 (2007)
2. Totry, E., Gonzalez, C., LLorca, J.: Failure locus of fiber-reinforced composites undertransverse compression and out-of-plane shear. Compos. Sci. Technol. **68**, 829–839 (2008)
3. Vaughan T.J., McCarthy C.T., 2011. A micromechanical study on the effect of intra-ply properties on transverse shear fracture in fibre reinforced composites. Compos.: Part A 42, 1217-1228
4. Vaughan, T.J., McCarthy, C.T.: Micromechanical modelling of the transverse damage behaviour in fibre reinforced composites. Compos. Sci. Technol. **71**, 388–396 (2011)
5. Melro, A.R., Camanho, P.P., Andrade Pires, F.M., Pinho, S.T.: Micromechanical analysis of polymer composites reinforced by unidirectional fibres: part II—micromechanical analyses. Int. J. Solids Struct. **50**, 1906–1915 (2013)
6. Yang, L., Yan, Y., Liu, Y., Ran, Z.: Microscopic failure mechanisms of fiber-reinforced polymer composites under transverse tension and compression. Compos. Sci. Technol. **72**, 1818–1825 (2012)
7. Totry, E., Gonzalez, C., Llorca, J., Molina-Aldareguía, J.: Mechanisms of shear deformation in fibre-reinforced polymers: experiments and simulations. Int. J. Fract. **158**, 197–209 (2009)
8. Ng, W.H., Salvi, A.G., Waas, A.M.: Characterization of the in-situ non-linear shear response of laminated fiber-reinforced composites. Compos. Sci. Technol. **70**, 1126–1134 (2010)
9. Soni, G., Singh, R., Mitra, M., Falzon, B.G.: Modelling matrix damage and fibre-matrix interfacial decohesion in composite laminates via a multi-fibre multi-layer representative volume element (M2RVE). Int. J. Solids Struct. **51**, 449–461 (2014)
10. Wongsto, A., Li, S.: Micromechanical FE analysis of UD fibre-reinforced composites with fibres distributed at random over the transverse cross section. Compos.: Part A **36**, 1246–1266 (2005)
11. Soden, P.D., Hinton, M.J., Kaddour, A.S.: Lamina properties, lay-up configurations and loading conditions for a range of fibre-reinforced composite laminates. Compos. Sci. Technol. **58**, 1011–1022 (1998)
12. ANSYS, Inc.: Theory reference for the mechanical APDL and mechanical applications, release 14.1. Canonsburg PA: ANSYS, Inc, 2012
13. Barbero, E.J.: Finite Element Analysis of Composite Materials. CRC Press (2008)
14. Fiedler, B., Hojo, M., Ochiai, S., Schulte, K., Ando, M.: Failure behavior of an epoxy matrix under different kindsof static loading. Compos. Sci. Technol. **61**, 1615–1624 (2001)

15. Hobbiebrunken, T., Fiedler, B., Hojo, M., Tanaka, M.: Experimental determination of the true epoxy resin strengthusing micro-scaled specimens. Compos.: Part A **38**, 814–818 (2007)
16. Drucker, D.C., Prager, W.: Soil mechanics and plastic analysis for limit design. Q. Appl. Math. **10**, 157–165 (1952)
17. Kinloch, A.J., Young, R.J.: Fracture Behavior of Polymers. Elsevier, Netherlands (1983)
18. Quinson, R., Perez, J., Rink, M., et al.: Yield criteria for amorphous glassy polymers. J. Mater. Sci. **32**, 1371–1379 (1997)
19. Alfano, G., Crisfield, M.A.: Finite element interface models for the delamination analysis of laminated composites: mechanical and computational issues. Int. J. Numer. Method. Eng. **50**, 1701–36 (2001)
20. Gregory, J.R., Spearing, S.M.: Nanoindentation of neat and in situ polymers in polymer-matrix composites. Compos. Sci. Technol. **65**, 595–607 (2005)
21. Zhou, X.F., Wagner, H.D., Nutt, S.R.: Interfacial properties of polymer composites measured by push-out and fragmentation tests. Compos.: Part A **32**, 1543–1551 (2001)
22. Ogihara, S., Koyanagi, J.: Investigation of combined stress state failure criterion for glass-fiber/epoxy interface by the cruciform specimen method. Compos. Sci. Technol. **70**, 143–50 (2010)
23. Soden, P.D., Hinton, M.J., Kaddour, A.S.: Biaxial test results for strength and deformation of a range of E-glass and carbon fibre reinforced composite laminates: failure exercise benchmark data. Compos. Sci. Technol. **62**, 1489–1514 (2002)

The Dynamic Modelling of Thin Skeletonal Annular Plates

Artur Wirowski, Bohdan Michalak and Martyna Rabenda

Abstract The subject of this paper is to derive and apply a macroscopic model for an annular plate with a dense system of ribs in radial and angular directions. The main feature of the proposed mathematical model is that the size of the microstructure (the distance between the ribs) is comparable to the thickness of the plate. The formulation of an approximate mathematical model of those plates is based on the tolerance averaging approach by Wozniak et al. [12, 13]. The general results of the contribution will be illustrated by the analysis of natural vibrations of the plate. It will be carried out by validation of averaged equations of motion and comparison to the results from finite element method (Abaqus program).

1 Introduction

The considered skeletonal plate is made of two families of thin beams with axes intersecting under the right angle. The regions situated between the beams are fills a homogeneous matrix material (Fig. 1a). It is assumed that midplane of the plate represents a certain plane microheterogeneous structure which is a periodic along angular ξ^2—coordinate but have slowly varying apparent properties in the radial direction. The generalized period $\lambda = \sqrt{\lambda_1 \lambda_2}$ of inhomogeneity is assumed to be sufficiently small when compared to the measure of the domain of coordinates ξ^α. At the same time it is assumed that the microstructure length parameter λ is similar compared to thickness h of the plate. It is assumed that the beams have a constant width. Thus we deal with composite plate having what can be called space-varying periodic microstructure. From a formal point of view, the structure under consideration can be described in the framework of the well-known theories for thin elastic plates. However, due to the inhomogeneous microstructure of the plate, this direct description of the structure leads to plate equations with discontinuous and highly oscillating coefficients.

A. Wirowski · B. Michalak · M. Rabenda (✉)
Department of Structural Mechanics, Lodz University of Technology,
Al. Politechniki 6, 90-924 Łódź, Poland
e-mail: martynarabenda@gmail.com

B. Albers and M. Kuczma (eds.), *Continuous Media with Microstructure 2*,
DOI 10.1007/978-3-319-28241-1_26

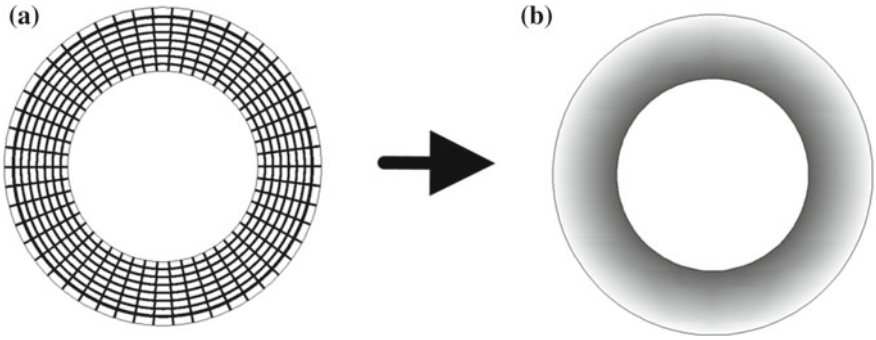

Fig. 1 Considered composite plate **a** at microscopic level **b** at macroscopic level

The aim of the contribution is to derive and apply a macroscopic model describing the dynamic behaviour of the thin plate with the deterministic microstructure that has functional but smooth and slowly varying effective properties (Fig. 1b).

The formulation of averaged mathematical model of the skeletonal plate will be based on the tolerance averaging approach. This modelling technique describes the effect of the microstructure size on the overall response of a composite structure. The general modelling procedures of this technique are given by Wozniak et al. in books [12, 13]. The application of this technique for the modelling and the analysis of dynamic problems of periodic composites and structures are presented in a series of papers. Some of the following papers can be mentioned here as examples: Baron [1] analyzed dynamic behaviour of medium thickness plates with uniperiodic structure. The higher order vibrations caused by microheterogeneous structure of thin periodic plates were analyzed by Jędrysiak [2]. The wave propagation in periodically laminated composites was analyzed by Matysiak and Nagórko [5]. The dynamic modelling of elastic wavy plates was presented in the paper of Michalak et al. [7]. In the paper of Wągrowska and Woźniak [9] the dynamic modelling of visco-elastic composites was discussed. Wierzbicki and Woźniak [10] studied the dynamic behaviour of honeycomb based composite solids.

The approach, based on the tolerance averaging technique, to formulate averaged models for functionally graded stratified solids can be found in the in the following papers. Kaźmierczak and Jędrysiak [3] presented the asymptotic-tolerance model of vibrations of thin transversally graded plates which is based on the tolerance averaging approach. In the paper of Michalak and Wirowski [6] the dynamic modelling of thin plate made of certain functionally graded materials was discussed. The obtained averaged equations of motion were verified by the comparison of the results obtained from the tolerance model and asymptotic model equations with the results from finite element method (Abaqus code). Rychlewska and Woźniak [8] analyzed a boundary layer phenomena in elastodynamics of functionally graded laminates. Wirowski [11] studied natural vibrations of thin plate band with non-linear functionally graded material.

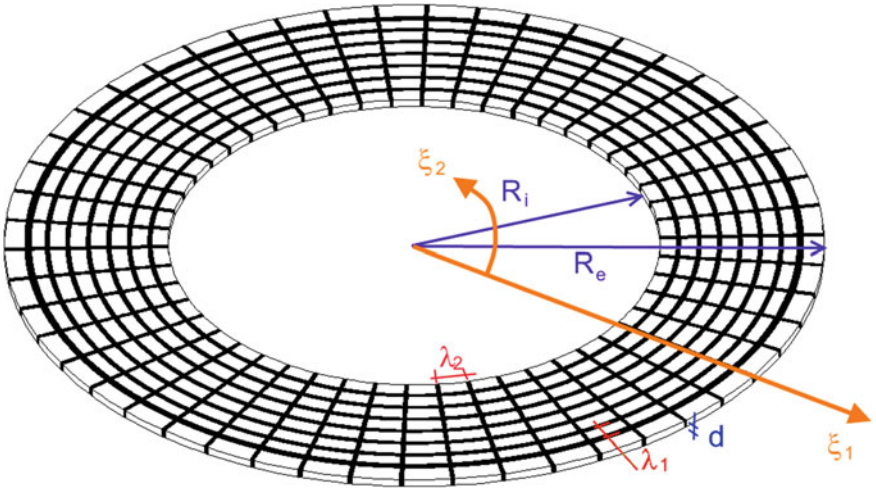

Fig. 2 Skeletonal annular plate

In the above mentioned papers dimension of cells should be much bigger than a thickness of plate. In opposite to these papers, in the presented contribution we deal with plates where the microstructure length parameter λ is similar compared to thickness h of the plate ($\lambda \cong h$) (Fig. 2). The majority of the mentioned papers deal with natural vibrations of a rectangular plate only. In the presented paper, like Michalak and Wirowski, will be analyzed natural vibrations of annular composite plates. These plates have skeletonal microstructure with constant width of the ribs. Hence, the effective properties are graded in space and we deal here with a special case of the functionally graded materials.

2 Direct Description

The object of our considerations are annular plates with microstructure given on Fig. 2. It is introduced the orthogonal curvilinear coordinate system $O\xi^1\xi^2\xi^3$ in the physical space occupied by a composite plate under consideration. The time coordinate will be denoted by t. Sub- and super-scripts i, k, l run over 1, 2, 3 and α, β, δ run over 1, 2. Setting $\mathbf{x} \equiv (\xi^1, \xi^2)$ and $z = \xi^3$ it is assumed that the undeformed plate occupies the region $\Omega \equiv (\mathbf{x}, z) : -h/2 \leq z \leq h/2$, $\mathbf{x} \in \Pi$, where Π is the plate midplane and h is the plate thickness. The starting point of this contribution is the direct description of the structure in the framework of the well known theory of thin plates. The displacement field of the arbitrary point of the plate we write in form:

$$w_3(x, z) = w_3(x) \qquad w_\alpha(x, z) = w_\alpha^0(x) - \partial_\alpha w_3(x) z \tag{1}$$

Denoting by $\mathbf{p}(\mathbf{x}, t)$ the external forces, by ρ the mass density, by $g_{\alpha\beta}$ the metric tensor, by $\in_{\alpha\beta}$ a Ricci tensor, setting $\partial_k = \partial/\partial x^k$ we also introduce gradient operators $\nabla \equiv (\partial_1, \partial_2)$, in the framework of the linear approximated theory for thin plates we obtain the following system of equations

i strain-displacement relations

$$\varepsilon_{\alpha\beta}(x, z) = \kappa_{\alpha\beta}(x)z, \qquad \kappa_{\alpha\beta} = -\nabla_{\alpha\beta}w_3 \tag{2}$$

ii strain energy

$$E_z(x, z) = \frac{1}{2}C^{\alpha\beta\gamma\delta}\varepsilon_{\alpha\beta}\varepsilon_{\gamma\delta} \tag{3}$$

iii kinetic energy

$$K_z(x, z) = \frac{1}{2}\rho(\dot{w}_3\dot{w}_3 + \dot{w}_\alpha\dot{w}_\beta\delta^{\alpha\beta}) \tag{4}$$

for $z \in (-h/2, h/2)$.

The strain energy average over the shell thickness is given by

$$E(x) = \frac{1}{2}B^{\alpha\beta\gamma\delta}\nabla_{\alpha\beta}w_3\nabla_{\gamma\delta}w_3 \tag{5}$$

where $B^{\alpha\beta\gamma\delta} = 0.5\frac{Eh^3}{12(1-\nu^2)}\left[g^{\alpha\mu}g^{\beta\gamma} + g^{\alpha\gamma}g^{\beta\mu} + \nu(\in^{\alpha\gamma}\in^{\beta\mu} + \in^{\alpha\mu}\in^{\beta\gamma})\right]$. It can be seen that the coefficients in the above equations are discontinuous and highly oscillating. The above equations will be used as a starting point of the modelling procedure.

3 Modelling Technique

Let us introduce in the undeformed midplane of the plate the polar coordinates system $O\xi^1\xi^2$. The midplane of annular plate occupies the region $\Pi \equiv [0, \varphi] \times [R_1, R_2]$ (Fig. 2). Denote Π_Δ as a subset of Π for points with coordinates determined by conditions $(\xi^1, \xi^2) \in (\lambda_2/2, \varphi - \lambda_2/2) \times (R_1 + \lambda_1/2, R_2 - \lambda_1/2)$. An arbitrary cell with a center situated on the radial coordinate at point $(\xi^1)_j = \lambda_1/2 + (j-1)\lambda_1$, $j = 1, \ldots, n$ will be determined by $\Delta(\xi^\alpha) \equiv (-\lambda_2/2, -\lambda_2/2) \times ((\xi^1)_j - \lambda_1/2, (\xi^1)_j + \lambda_1/2)$.

In order to derive averaged model equations for skeletonal plate under consideration we applied tolerance averaging approach [12]. We mention some basic concepts of this technique, as an averaging operator, a tolerance parameter, a tolerance periodic function, a slowly varying function, a highly oscillating function.

The fundamental concept of the modelling technique is the averaging operation

$$\langle f\rangle(\xi^\alpha) = \frac{1}{|\Delta|}\int_{\Delta(\xi^\alpha)} f(y,\xi^\alpha)\,\mathrm{d}y, \quad \xi^\alpha \in \bar{\Pi} \tag{6}$$

We shall refer (6) to as averaging of arbitrary integrable function $f(\cdot)$ for an arbitrary $\xi^\alpha \in \bar{\Pi}$. The main concept of the tolerance averaging technique is that values of functions belonging to region Π can be determined only within to certain accuracy δ. Let δ stand for an arbitrary positive number and X be a linear normed space. Tolerance relation $\approx$ for a certain δ is defined by

$$(\forall (x_1,x_2)\in X^2)\,[x_1 \approx x_2 \Leftrightarrow ||x_1 - x_2||_X \le \delta] \tag{7}$$

where δ is said to be *the tolerance parameter*.

Let $\partial^k f$ be the kth gradient of function $f = f(\xi^\alpha)$, $\xi^\alpha \in \Pi$, $k = 0, 1, \ldots, \alpha$, $(\alpha \ge 0)$, where we denote $\partial^0 f \equiv f$. Function $f \in H^\alpha(\Pi)$ is called *the tolerance periodic function* (with respect to cell $\Delta(\xi^\alpha)$ and tolerance parameter δ), $f \in TP^\alpha_\delta(\Pi,\Delta)$, if for $k = 0, 1, \ldots, \alpha$, the following conditions hold

$$\begin{aligned}
&(\forall \xi^\alpha \in \Pi)(\exists \tilde{f}^{(k)})(\xi^\alpha,\cdot)\in H^0(\Delta))\\
&\left[||\partial^k f\,|_{\Pi_{\xi^\alpha}}(\cdot)\tilde{f}^{(k)}(\xi^\alpha,\cdot)||_{H^0(\Pi_{\xi^\alpha})} \le \delta\right]\\
&\int_{\Delta(\cdot)} \tilde{f}^{(k)}(\cdot,y)\,\mathrm{d}y \in C^0(\bar{\Pi})
\end{aligned} \tag{8}$$

Function $\tilde{f}^{(k)}(\xi^\alpha,\cdot)$ is referred to as *the periodic approximation of* $\partial^k f$ in $\Delta(\xi^\alpha)$, $\xi^\alpha \in \Pi$, $k = 0, 1, \ldots, \alpha$.

Function $F \in H^\alpha(\Pi)$ is called *the slowly varying function* (with respect to the cell $\Delta(\xi^\alpha)$ and tolerance parameter δ), $F \in SV^\alpha_\delta(\Pi,\Delta)$, if

$$\begin{aligned}
&F \in TP^\alpha_\delta(\Pi,\Delta),\\
&(\forall \xi^\alpha \in \Pi)\left[\tilde{F}^{(k)}(xi^\alpha,\cdot)|_{\Delta(\xi^\alpha)} = \partial^k F(xi^\alpha), \quad k = 0,\ldots,\alpha\right]
\end{aligned} \tag{9}$$

It can be observed that periodic approximation $\tilde{F}$ of $\partial^k F(\cdot)$ in $\Delta(\xi^\alpha)$ is a constant function for every $\xi^\alpha \in \Pi$. If $F \in SV^\alpha_\delta(\Pi,\Delta)$ then

$$(\forall \xi^\alpha \in \Pi)\left(||\partial^k F(\cdot) - \partial^k F(\xi^\alpha)||_{H^0(\Delta(\xi^\alpha))} \le \delta, \quad k = 0,1,\ldots,\alpha\right).$$

Function $\phi \in H^\alpha(\Pi)$ is called *the highly oscillating function* (with respect to the cell $\Delta(\xi^\alpha)$ and tolerance parameter δ), $\phi \in HO^\alpha_\delta(\Pi,\Delta)$, if

$$\begin{aligned}
&\phi \in TP^\alpha_\delta(\Pi,\Delta)\\
&\forall \mathbf{F} \in SV^\alpha_\delta(\Pi,\Delta)(f \equiv \phi F \in TP^\alpha_\delta(\Pi,\Delta))
\end{aligned} \tag{10}$$

and for $k = 1, \ldots, \alpha$ these functions satisfy conditions

$$\begin{aligned} &(\forall \xi^\alpha \in \Pi)\left[\tilde{\phi}^{(k)}(\xi^\alpha, \cdot)\mid_{\Delta(\xi^\alpha)} = \partial^k \tilde{\phi}(\xi^\alpha)\right], \\ &\tilde{f}^{(k)}(\xi^\alpha, \cdot)\mid_{\Delta(\xi^\alpha)} = F(\xi^\alpha)\partial^k \tilde{\phi}(\xi^\alpha)\mid_{\Delta(\xi^\alpha)} \end{aligned} \tag{11}$$

For $\alpha = 0$ we denote $\tilde{f} \equiv \tilde{f}^{(0)}$.

Let by $\varphi(\cdot)$ denote a highly oscillating function, $\varphi \in HO^2_\delta(\Pi, \Delta)$, defined on $\bar{\Pi}$, continuous together with gradient $\partial^1\varphi$. Its gradient $\partial^2\varphi$ is a piecewise continuous and bounded. Function $\varphi(\cdot)$ is called *the fluctuation shape function* of the 2-nd kind, if it depends on λ as a parameter and satisfies conditions:

$$\begin{aligned} &1^\circ \quad \partial^k\varphi \in O(\lambda^{\alpha-k}) \quad \text{for}\, k = 1, \ldots, \alpha,\ \alpha = 2, \\ &2^\circ \quad \langle\varphi\rangle(\xi^\alpha) \approx 0 \qquad \text{for every}\, \xi^\alpha \in \Pi_\Delta. \end{aligned}$$

Set of all fluctuation shape functions of the 2-nd kind is denoted by $FS^2_\delta(\Pi, \Delta)$. Condition (2°) can be replaced by $\langle\rho\varphi\rangle(\xi^\alpha) \approx 0$ for every $\xi^\alpha \in \Pi_\Delta$, where $\rho > 0$ is a certain tolerance periodic function.

The starting point of the modeling procedure is a decomposition of displacement fields. The modeling procedure will be based on the tolerance averaging approach and on the restriction of the displacement field under consideration given by

$$\begin{aligned} w_3(\xi^\alpha, z, t) &= V_3(\xi^\alpha, t) \\ w_\alpha(\xi^\alpha, z, t) &= (-\partial_\alpha V_3(\xi^\alpha, t) + h^A(\xi^\alpha)u^A_\alpha(\xi^\alpha, t))z \end{aligned} \tag{12}$$

or $\xi^\alpha = \Pi$, $z \in (-h/2, h/2)$, $A = I, II$ and every time t.

The basic modeling assumption, related to the above decomposition, states that $V_3(\cdot, t)$, $u^A_\alpha(\cdot, t)$ are slowly varying functions together with all partial derivatives. Functions $V_3(\cdot, t) \in SV^2_\delta(\Omega, \Delta)$, $u^A_\alpha(\cdot, t) \in SV^1_\delta(\Omega, \Delta)$ are the basic unknowns of the modelling problem. Functions $h^A(\cdot)$ are known, dependent on the microstructure length parameter λ, fluctuation shape functions.

Let $\tilde{h}^A(\cdot)$, $\partial_\alpha\tilde{h}(\cdot)$ stand for periodic approximation of $h^A(\cdot)$, $\partial_\alpha h^A(\cdot)$ in Δ, respectively. Due to the fact that $w_3(\cdot, t)$, $w_\alpha(\cdot, t)$ are tolerance periodic functions, it can be observed that the periodic approximation of $w_{3h}(\cdot, t)$, $w_{\alpha h}(\cdot, t)$ and their derivatives in $\Delta(\xi^\alpha)$, $\xi^\alpha \in \Pi$ have the form

$$\begin{aligned} &w_{3h}(y, \xi^\beta, z, t) = V_3(\xi^\beta, t), \\ &\partial_\alpha w_{3h}(y, \xi^\beta, z, t) = \partial_\alpha V_A(\xi^\beta, t), \\ &\dot{w}_{3h}(y, \xi^\beta, z, t) = \dot{V}_3(\xi^\beta, t), \\ &w_{\alpha h}(y, \xi^{beta}, z, t) = (-\partial_\alpha V_3(\xi^\beta, t) + h^A(y, \xi^\beta)u^A_\alpha(\xi^\beta, t))z \\ &\partial_y w_{\alpha h}(y, \xi^\beta, z, t) = (-\partial_{\alpha\gamma} V_3(\xi^\beta, t) + \partial_y h^A(y, \xi^\beta)u^A_\alpha(\xi^\beta, t))z \\ &\dot{w}_{\alpha h}(y, \xi^\beta, z, t) = (-\partial_\alpha \dot{V}_3(\xi^\beta, t) + h^A(y, \xi^\beta)\dot{u}^A_\alpha(\xi^\beta, t))z \end{aligned} \tag{13}$$

for every $\xi^\alpha \in \Pi$, almost every $y \in \Delta(\xi^\alpha)$ and every $t \in (t_0, t_1)$.

4 Averaging Description

The starting point of the tolerance averaging technique are Eqs. (2)–(5) and decomposition of displacement fields $w_3(\xi^\alpha, z, t)$, $w_\alpha(\xi_\alpha, z, t)$. Substituting the right-hand sides of Eqs. (12) into (5), on the basis of tolerance averaging approximation, we finally arrive the strain energy averaged over the cell $\Delta(\xi^\alpha)$

$$\langle E\rangle = \frac{1}{2}\tilde{B}^{\alpha\beta\gamma\delta}\nabla_{\alpha\beta}V\nabla_{\gamma\delta}V_3 - \tilde{B}^{\alpha A\gamma\delta}u^A_\alpha\nabla_{\gamma\delta}V_3 + \frac{1}{2}\tilde{B}^{\alpha A\gamma B}u^A_\alpha u^B_\gamma \tag{14}$$

where we have denoted

$$\begin{aligned}&\tilde{B}^{\alpha\beta\gamma\delta} = \langle B^{\alpha\beta\gamma\delta}\rangle, \qquad \tilde{B}^{\alpha A\gamma\delta} = \langle B^{\alpha\beta\gamma\delta}\partial_\beta h^A\rangle,\\ &\tilde{B}^{\alpha A\gamma B} = \langle B^{\alpha\beta\gamma\delta}\partial_\beta h^A\partial_\delta h^B\rangle\end{aligned} \tag{15}$$

Substituting displacement field given by decomposition (12) into formula for kinetic energy (4) we obtain for an arbitrary point of the plate

$$\begin{aligned}K_z(\xi^\beta, z, t) = \tfrac{1}{2}\rho\big[&\dot{V}_3(\xi^\beta, t)\dot{V}_3(\xi^\beta, t)\\ &+\big((-\partial_\alpha\dot{V}_3(\xi^\beta, t) + h^A(\xi^\beta)\dot{u}^A_\alpha(\xi^\beta, t))z\big)\\ &\Big((-\partial_\beta\dot{V}_3(\xi^\beta, t) + h^B(\xi^\beta\dot{u}^B_\beta(x)(\xi^\beta, t))z)\Big)\,\delta^{\alpha\beta}\big]\end{aligned} \tag{16}$$

After averaging over the plate thickness and neglecting for thin plates the terms describing rotation inertia (subscripted terms in Eq. (16)) we obtain formula for kinetic energy averaged over cell $\Delta(\xi^\alpha)$

$$\langle K\rangle(\xi^\alpha, t) = \frac{1}{2}\langle\rho h\rangle\dot{V}_3(\xi^\alpha, t)\dot{V}_3(\xi^\alpha, t) \tag{17}$$

Energy external load averaged over the cell $\Delta(\xi^\alpha)$

$$\langle F\rangle(xi^\alpha, t) = \langle f^3\rangle V_3 \tag{18}$$

In order to derive the equations of motion we shall introduce tolerance averaged Lagrangian $\langle L\rangle$

$$\begin{aligned}&\langle L\rangle = \langle K\rangle - \langle E\rangle + \langle F\rangle\\ &\langle L\rangle = \langle L\rangle(xi^\alpha, \nabla_{\alpha\beta}V_3, V_3, u^A_\alpha, \dot{V}_3)\end{aligned} \tag{19}$$

The governing equations derived from stationary action principle of the averaged Lagragian $\langle L\rangle = \langle K\rangle - \langle E\rangle + \langle F\rangle$ have the form

$$\nabla_{\alpha\beta}(\tilde{B}^{\alpha\beta\gamma\delta}\nabla_{\gamma\delta}V_3 - \tilde{B}^{\gamma A\alpha\beta}u_\gamma^A) + \langle\tilde{p}\rangle\ddot{V}_3 - \langle f^3\rangle = 0$$
$$\tilde{B}^{\alpha A\gamma\delta}\nabla_{\gamma\delta}V_3 - \tilde{B}^{\alpha A\gamma B}u_\gamma^B = 0 \tag{20}$$

We can observe that u_γ^B can be eliminated from above equations

$$u_\mu^B = K^{\mu B\alpha A}\tilde{B}^{\alpha A\gamma\delta}\nabla_{\gamma\delta}V_3 \tag{21}$$

where $K^{\mu B\alpha A}$ determine the linear transformation, inverse to that given by $\tilde{B}^{\mu B\alpha A}$ ($K^{\mu B\alpha A}\tilde{B}^{\alpha A\gamma C} = \delta_{\mu\gamma}^{BC}$).

Denoting

$$F^{\alpha\beta\gamma\delta} = \tilde{B}^{\alpha\beta\gamma\delta} - \tilde{B}^{\mu B\alpha\beta}K^{\mu B\tau A}\tilde{B}^{\tau A\gamma\delta} \tag{22}$$

and $\tilde{\rho}$ (mass density related to plate midplane), after simple manipulations we obtain finally the following equation for the averaged displacements $V_3(\xi^\alpha, t)$,

$$\nabla_{\alpha\beta}(F^{\alpha\beta\gamma\delta}\nabla_{\gamma\delta}V_3) + \langle\tilde{\rho}\rangle\ddot{V}_3 = \langle f^3\rangle \tag{23}$$

Coefficients in the above equation are smooth and functional in contrast to equations in direct description with the discontinuous and highly oscillating coefficients. The above equation has an identical form as equation of motion for thin plate with functional coefficients.

5 Applications

5.1 Tolerance Model

In order to illustrate an exemplary application of the above equation, the analysis of free vibrations of the composite annular plates will be shown. Equation (23) represent partial differential equation for the averaged deflection $V_3(\xi^\alpha, t)$. Let us introduce the polar coordinate system $O\xi^1\xi^2$, where ξ^2 represents the angular coordinate and $\xi \equiv \xi^1$ the radial coordinate. We look for a solution to the equations (23) in the form of a function with separable variables

$$V_3(\xi^\alpha, t) = \tilde{V}(\xi^\alpha)e^{i\omega t} \tag{24}$$

Substituting the Eqs. (24) into (23) after rather complicated calculations we obtain the equation for $\tilde{V}(\cdot)$ describing free vibrations of the composite annular plate.

$$
\begin{aligned}
&\tilde{V}_{,1111}\langle F^{1111}\rangle + \tilde{V}_{,1111}\left(\frac{2}{\xi}\langle F^{1111}\rangle + 2\langle F^{1111}\rangle_{,1}\right)\\
&+\tilde{V}_{,11}\left(\langle F^{1111}\rangle_{,11} + \frac{2}{\xi}\langle F^{1111}\rangle_{,1} + \frac{1}{\xi}\langle F^{1122}\rangle_{,1} - \frac{1}{\xi^2}\langle F^{2222}\rangle\right)\\
&+\tilde{V}_{,1}\left(\frac{1}{\xi}\langle F^{1122}\rangle_{,11} + \frac{1}{\xi^3}\langle F^{2222}\rangle - \frac{1}{\xi^2}\langle F^{2222}\rangle_{,1}\right)\\
&+\tilde{V}_{,122}\left(-\frac{4}{\xi^3}\langle F^{1212}\rangle + \frac{4}{\xi^2}\langle F^{1212}\rangle_{,1} - \frac{2}{\xi^3}\langle F^{1122}\rangle + \frac{2}{\xi^2}\langle F^{1122}\rangle_{,1}\right)\\
&+\tilde{V}_{,1122}\left(\frac{4}{\xi^2}\langle F^{1212}\rangle + \frac{2}{\xi^2}\langle F^{1122}\rangle\right)\\
&+\tilde{V}_{,22}\left(\frac{4}{\xi^4}\langle F^{1212}\rangle + \frac{2}{\xi^4}\langle F^{1122}\rangle - \frac{2}{\xi^3}\langle F^{1122}\rangle_{,1}\right.\\
&\qquad\left.\frac{2}{\xi^4}\langle F^{2222}\rangle - \frac{1}{\xi^4}\langle F^{2222}\rangle_{,1} + \frac{1}{+}\xi^3\langle F^{1122}\rangle_{,11}\right)\\
&+\tilde{V}_{,222}\left(\frac{2}{\xi^4}\langle F^{2222}\rangle_{,2}\right) + V_{,2222}\left(\frac{1}{\xi^4}\langle F^{2222}\rangle\right) + \langle\tilde{p}\rangle\omega^2 = 0
\end{aligned}
\tag{25}
$$

The Eq. (25) contain smooth and slowly varying coefficients and can be solved using well known numerical methods. The averaged coefficients $F^{\alpha\beta\gamma\delta}$ together with its derivatives were calculated automatically by symbolic computation programs. Whereby:

$$
\begin{aligned}
F^{1111} &= B^{1111} - B^{\mu B11}K^{\mu B\tau A}B^{\tau A11},\\
F^{1122} &= B^{1122} - B^{\mu B11}K^{\mu B\tau A}B^{\tau A22},\\
F^{1212} &= B^{1212} - B^{\mu B12}K^{\mu B\tau A}B^{\tau A12},\\
F^{2222} &= B^{2222} - B^{\mu B22}K^{\mu B\tau A}B^{\tau A22}
\end{aligned}
\tag{26}
$$

where $K^{\mu B\tau A}$ determine the linear transform inverse to that given by $B^{\mu B\tau A}$.

Formulas for averaged modulus are given below.

$$
B^{1111} = \langle B^{1111}\rangle \tag{27}
$$

$$
\begin{aligned}
&= \frac{1}{l_1\Delta\varphi}\left[\int_{-\frac{1}{2}b_1}^{\frac{1}{2}b_1}\left(\int_{-\frac{1}{2}b_1}^{-\frac{1}{2}b_1} B_r\,\mathrm{d}y_2 + \int_{-\frac{1}{2}b_1}^{\frac{1}{2}b_1}\alpha B_r\,\mathrm{d}y_2 + \int_{-\frac{1}{2}b_1}^{\frac{1}{2}\Delta} B_r\mathrm{d}y_2\right)\mathrm{d}y_1\right.\\
&\qquad\left.+\int_{-\frac{1}{2}\Delta\varphi}^{\frac{1}{2}\Delta\varphi}\int_{\frac{1}{2}b_1}^{-\frac{1}{2}l_1} B_r\,\mathrm{d}y_1\,\mathrm{d}y_2 + \int_{-\frac{1}{2}\Delta\varphi}^{\frac{1}{2}\Delta\varphi}\int_{\frac{1}{2}l_1}^{-\frac{1}{2}b_1} B_r\,\mathrm{d}y_1\,y_2\right]
\end{aligned}
\tag{28}
$$

$$
B^{1111} = \frac{B_r(\Delta\varphi d\xi + dl_1 - d^2 + \alpha\Delta\varphi\xi l_1 - \alpha\Delta\varphi d\xi - \alpha dl_1 + \alpha d^2)}{\Delta\varphi\xi l_1} \tag{29}
$$

$$B^{1I11} = -\frac{2(-1+\alpha)d(\Delta\varphi - d)B_r}{3\xi l_1 \Delta\varphi} \tag{30}$$

$$B^{1I22} = -\frac{2(-1+\alpha\beta)d(\Delta\phi - d)B_r v}{3\xi l_1 \Delta\varphi} \tag{31}$$

$$B^{1I11} = -\frac{8(l_1 - d + d\alpha)d(\Delta\varphi - d)B_r}{15\xi(d-l_1)\Delta\varphi l_1} \tag{32}$$

$$B^{1I2II} = \frac{4d^2\alpha B_r \nu_r \beta}{9\xi\,\Delta\varphi l_1} \tag{33}$$

$$B^{1II12} = -\frac{(d + d\alpha\beta\nu_r - d\nu_r - d\alpha - l_1 - \alpha\beta\nu_r l_1 + \nu_r l_1 + \alpha l_1)B_r d}{3\xi\,\Delta\varphi l_1} \tag{34}$$

$$B^{1II2I} = B^{2I1II} = \frac{2(\beta\nu_r - 1)d^2\alpha B_r}{9\xi\,\Delta\varphi l_1} \tag{35}$$

$$\begin{aligned} B^{1II1II} = -\frac{1}{15\xi(d-\Delta\varphi\xi)\Delta\varphi l_1}\big[4\,\big(d^2 &+ d^2\alpha\beta\nu_r - d^2\alpha - d^2\nu_r \\ &+ d\nu_r\Delta\varphi\xi + d\alpha l_1 - d\Delta\varphi\xi - l_1 d \\ &+ d\nu_r l_1 - d\alpha\beta\nu_r l_1 + l_1\Delta\varphi\xi \\ &- \nu_r l_1\Delta\varphi\xi\ \big)\,B_r d\big] \end{aligned} \tag{36}$$

$$B^{2I12} = \frac{(1 - \nu_r - \alpha + \alpha\nu_r\beta)d(\Delta\varphi - d)B_r}{3\xi l_1 \Delta\varphi} \tag{37}$$

$$B^{2I2I} = -\frac{4(-l_1 + d + \nu_r l_1 - \nu_r d - d\alpha + d\alpha\beta\nu_r)d(\Delta\varphi - d)B_r}{15\xi(d-l_1)\Delta\varphi l_1} \tag{38}$$

$$B^{2II11} = -\frac{2(-d + \beta\alpha d + l_1 - \alpha\beta l_1)d B_r \nu_r}{3\xi\,\Delta\varphi l_1} \tag{39}$$

$$B^{2II22} = -\frac{2(-d + \alpha d + l_1 - \alpha l_1)d B_r}{3\xi\,\Delta\phi l_1} \tag{40}$$

$$B^{2II2II} = -\frac{8(-l_1 d\alpha - l_1 d + l_1\Delta\varphi\xi - d^2\alpha + d^2 - d\Delta\varphi\xi)d B_r}{15\xi(d-l_1)\Delta\varphi l_1} \tag{41}$$

where:

$$b_1 = l_1 - d, b_2 = \Delta\phi - \frac{d}{\xi}, B_m = \alpha B_r, \nu_m = \beta\nu_r$$

$$B^{1I12} = B^{1I21} = B^{1I1II} = B^{1III1} = B^{1II22} = B^{1III1} = B^{1III2II} = B^{2II11}$$

$$B^{2I22} = B^{2I1I} = B^{2I2II} = B^{2II12} = B^{2II2I} = B^{2II1II} = 0 \tag{42}$$

5.2 Shape Functions

The important point of the tolerance modelling approach is to determine the fluctuation shape functions (FSF). In dynamic problems, the system of FSF can be taken to represent the principal modes of free vibrations of the cell $\Delta(\xi^\alpha)$ or a physically reasonable approximation of these modes. In our work, we proposed shape functions that reflect material properties of the plate.

$$\begin{aligned} h^1(y^\alpha, \xi^1) &= S_1(y^1)T_2(y^2, b_2), \\ h^2(y^\alpha, \xi^2) &= S_2(y^2)T_1(y^1, b_1), \end{aligned} \tag{43}$$

where:

$$S_1(y_1) = \begin{cases} -\left(y_1 + \frac{l_1}{2}\right) & \text{for } y_1 \in \langle -\frac{l_1}{2}, \frac{b_1}{2}\rangle, \\ \frac{d}{l_1 - d} & \text{for } y_1 \in \langle -\frac{b_1}{2}, \frac{b_1}{2}\rangle, \\ -\left(y_1 - \frac{l_1}{2}\right) & \text{for } y_1 \in \langle -\frac{b_1}{2}, \frac{l_1}{2}, \rangle, \end{cases}$$

$$S_2(y_2, \xi^1) = \begin{cases} -\left(y_2 + \frac{\Delta\varphi}{2}\right) & \text{for } y_2 \in \langle -\frac{\Delta\varphi}{2}, -\frac{b_2}{2}\rangle, \\ \frac{d}{(+y_1)b_2} y_2 & \text{for } y_2 \in \langle -\frac{b_2}{2}, \frac{b_2}{2}\rangle, \\ -\left(y_2 - \frac{\Delta\varphi}{2}\right) & \text{for } y_2 \in \langle \frac{b_2}{2}, \frac{\Delta\varphi}{2}\rangle, \end{cases}$$

$$T_1(y^1, b_1) = \left[1 - \left(\frac{2y^1}{b_1}\right)^2\right], \qquad T_2(y^2, b_2) = \left[1 - \left(\frac{2y^2}{b_2(xi^1 y^1)}\right)^2\right]$$

Shape functions (43) are presented on the graphs drawn on a cell (Fig. 3).

5.3 Shape Functions

5.3.1 Boundary Conditions

In order to find a particular solution of the equation Eq. (25) we shall investigate the natural vibrations of annular plates for the following boundary conditions:

- for the mutually clamped plate:

$$\begin{aligned} \frac{\partial \tilde{V}(\xi^1\xi^2)}{\partial \xi^1}_{|\,\xi^1 = R_e} &= 0, \qquad \tilde{V}(\xi^1\xi^2)_{|\,\xi^1 = R_e} = 0, \\ \frac{\partial \tilde{V}(\xi^1\xi^2)}{\partial \xi^1}_{|\,\xi^1 = R_i} &= 0, \qquad \tilde{V}(\xi^1\xi^2)_{|\,\xi^1 = R_i} = 0, \end{aligned} \tag{44}$$

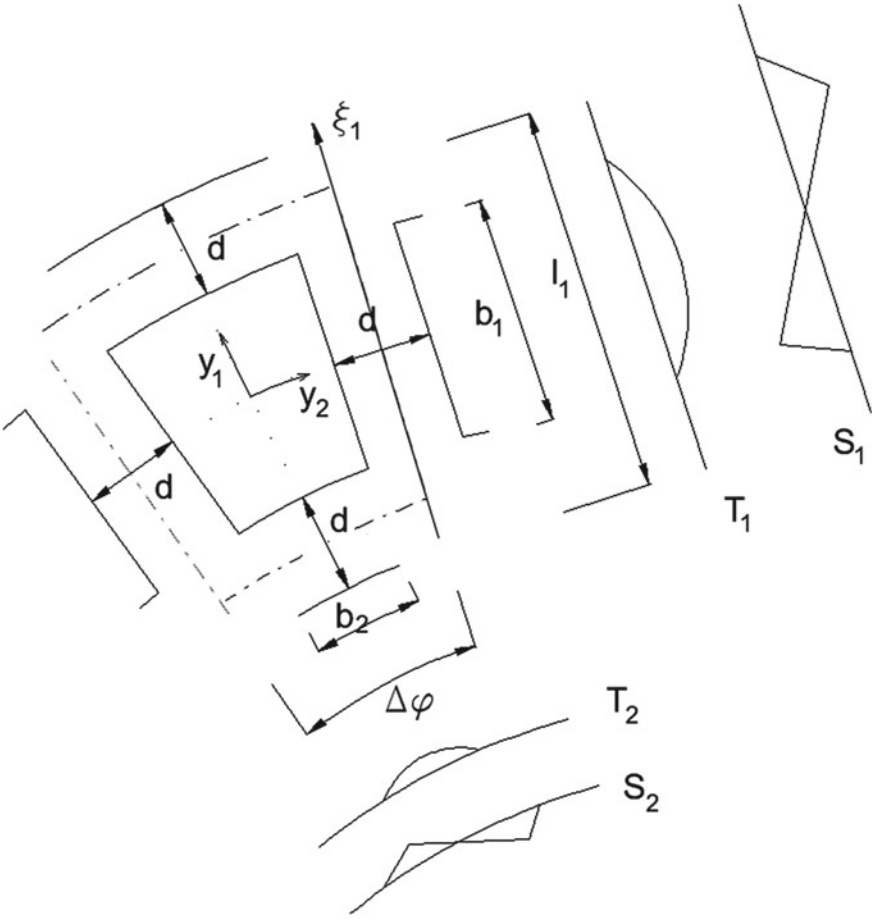

Fig. 3 The cell with shape functions

- for the mutually simply supported plate:

$$\frac{\partial^2 \tilde{V}(\xi^1\xi^2)}{\partial\xi^1\partial\xi^1}_{|\,\xi^1=R_e} + \frac{1}{R_e}\frac{\partial \tilde{V}(xi^1,\xi^2)}{\partial\xi^1}_{|\,\xi^1=R_e} = 0, \qquad \tilde{V}(\xi^1\xi^2)_{|\,\xi^1=R_e} = 0,$$
$$\frac{\partial^2 \tilde{V}(\xi^1\xi^2)}{\partial\xi^1\partial\xi^1}_{|\,\xi^1=R_i} + \frac{1}{R_i}\frac{\partial \tilde{V}(xi^1,\xi^2)}{\partial\xi^1}_{|\,\xi^1=R_i} = 0, \qquad \tilde{V}(\xi^1\xi^2)_{|\,\xi^1=R_i} = 0 \quad (45)$$

5.3.2 Finite Difference Method

The Eq. (25) has smooth and slowly varying coefficients. Hence, to solve it well known numerical methods are needed. The solution of the equation (25) and

obtainment of natural frequencies were made by finite differential method. This method through discretization of the Eq. (25) and consideration of appropriate boundary conditions (44) or (45) lets obtain frequencies from the solution of eigenvalue problem. The solution of eigenvalue problem, obtainment of the natural frequencies and modes were done by using finite difference method.

Numerical problem indicated above was implemented by using MS Visual Studio C++ environment. It let to create fully object- oriented structure of the program simultaneously providing elasticity and expansibility of the solution. The program made in this environment can be applied on any hardware platform based on Windows (XP, Vista, Win7, Win8) both in 32-bit and 63-bit systems. What is more, chosen environment enable to create interface convenient for a user in which the user has possibilities to change many geometric and physical parameters.

The Eq. (25) represents partial differential equation of fourth order with varying coefficients relative to the two variables described in polar coordinate system. For that reason, the discretization based on FDM differs significantly from the classical approach grounded on cartesian coordinate system.

The area of the plate was divided into $\boldsymbol{n}$ equal parts (the rings of equal width) in a radial direction and into $\boldsymbol{m}$ equal parts (sections based on the same angle) in angular direction (Fig. 4a).

According to that, FDM mesh was formed with varying dimensions of mesh opening, whereby

$$dy_i = \xi_i \Psi, \qquad \xi_{j+1}^2 - \xi_j^i = \Delta\xi^2 = \Psi = const,$$
$$\xi_{i+1}^1 - \xi_i^1 = \Delta\xi = const. \tag{46}$$

where $dy, dx = \Delta\xi$ are dimensions of the mesh opening, ξ is a distance from the origin of the coordinate system (a radius).

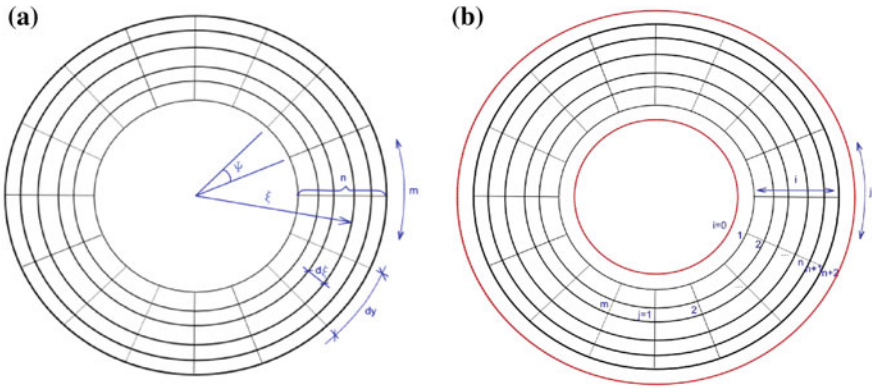

Fig. 4 **a** Partition of a plate area by FDM mesh, **b** The numbering of nodes of the mesh. *Red line* signifies additional virtual nodes

The partial derivatives appearing in the Eq. (25) are drawn closer by central difference method as following [4]:

- the first derivative:

$$\frac{\partial \tilde{V}(\xi^1, \xi^2)}{\partial \xi^1} = \frac{\tilde{V}_{i+1.j} - \tilde{V}_{i-1.j}}{2\Delta\xi} \tag{47}$$

$$\frac{1}{\xi^1}\frac{\partial \tilde{V}(\xi^1, \xi^2)}{\partial \xi^2} = \frac{\tilde{V}_{i.j+1} - \tilde{V}_{i.j-1}}{2\xi_i \Psi} \tag{48}$$

- the second derivative:

$$\frac{\partial^2 \tilde{V}(\xi^1\xi^2)}{\partial \xi^1 \partial \xi^2} = \frac{\tilde{V}_{i+1.j} - 2\tilde{V}_{i,j} + \tilde{V}_{i-1,j}}{\Delta\xi^2} \tag{49}$$

$$\frac{\partial^2 \tilde{V}(\xi^1\xi^2)}{\partial \xi^2 \partial \xi^2} = \frac{\tilde{V}_{i+1.j+1} - \tilde{V}_{i+1,j-1} - \tilde{V}_{i-1,j+1} + \tilde{V}_{i-1,j-1}}{4\xi_i \Psi \Delta\xi} \tag{50}$$

$$\frac{\partial^2 \tilde{V}(\xi^1\xi^2)}{\partial \xi^2 \partial \xi^2} = \frac{\tilde{V}_{i.j+1} - 2\tilde{V}_{i,j} + \tilde{V}_{i.j-1}}{(\xi_i \Psi)^2} \tag{51}$$

- the third derivative:

$$\frac{\partial^3 \tilde{V}(\xi^1\xi^2)}{(\partial \xi^1)^3} = \frac{\tilde{V}_{i+2.j} - 2\tilde{V}_{i+1,j} + 2\tilde{V}_{i-1,j} - \tilde{V}_{i-2.j}}{2\Delta\xi^3} \tag{52}$$

$$\frac{\partial^3 \tilde{V}(\xi^1\xi^2)}{(\partial \xi^1)^2 \partial \xi^2} = \frac{\tilde{V}_{i+1.j+1} - 2\tilde{V}_{i,j+1} + \tilde{V}_{i-1,j+1} - \tilde{V}_{i+1.j-1} + 2\tilde{V}_{i,j-1} - \tilde{V}_i}{2\Delta\xi^2(\xi_i \Psi)} \tag{53}$$

$$\frac{\partial^3 \tilde{V}(\xi^1\xi^2)}{\partial \xi^1 (\partial \xi^2)^2} = \frac{\tilde{V}_{i+1.j+1} - 2\tilde{V}_{i+1,j} + \tilde{V}_{i+1,j-1} - \tilde{V}_{i-1.j+1} + 2\tilde{V}_{i-1,j} - \tilde{V}_{i-1,j}}{2\Delta\xi(\xi_i \Psi)^2} \tag{54}$$

$$\frac{\partial^3 \tilde{V}(\xi^1\xi^2)}{(\partial \xi^2)^3} = \frac{\tilde{V}_{i.j+2} - 2\tilde{V}_{i,j+1} + 2\tilde{V}_{i,j-1} - \tilde{V}_{i.j-2}}{2(\xi_i \Psi)^3} \tag{55}$$

- the fourth derivative:

$$\frac{\partial^4 \tilde{V}(\xi^1\xi^2)}{(\partial \xi^1)^4} = \frac{\tilde{V}_{i+2.j} - 4\tilde{V}_{i+1,j} + 6\tilde{V}_{i,j} - 4\tilde{V}_{i-1,j} - \tilde{V}_{i-2.j}}{\Delta\xi^4} \tag{56}$$

$$\frac{\partial^4 \tilde{V}(\xi^1\xi^2)}{(\partial\xi^1)^3\partial\xi^2} = \frac{\begin{array}{c}\tilde{V}_{i+2.j+1} - 2\tilde{V}_{i+1,j+1} + 2\tilde{V}_{i-1,j+1} - \tilde{V}_{i-2.j+1} \\ -\tilde{V}_{i+2.j-1} + 2\tilde{V}_{i+1,j-1} - 2\tilde{V}_{i-1,j-1} + \tilde{V}_{i-2.j-1}\end{array}}{4\Delta\xi^3\xi_i\Psi} \tag{57}$$

$$\frac{\partial^4 \tilde{V}(\xi^1\xi^2)}{(\partial\xi^1)^2(\partial\xi^2)^2} = \frac{\begin{array}{c}\tilde{V}_{i+1.j+1} - 2\tilde{V}_{i,j+1} + \tilde{V}_{i-1,j+1} - 2\tilde{V}_{i+1.j} + 4\tilde{V}_{i,j} \\ -2\tilde{V}_{i-1,j} + \tilde{V}_{i+1.j-1} - 2\tilde{V}_{i,j-1} + \tilde{V}_{i-1,j-1}\end{array}}{\Delta\xi^2(\xi_i\Psi)^2} \tag{58}$$

$$\frac{\partial^4 \tilde{V}(\xi^1\xi^2)}{\partial\xi^1(\partial\xi^2)^3} = \frac{\begin{array}{c}\tilde{V}_{i+1.j+2} - 2\tilde{V}_{i+1,j+1} + 2\tilde{V}_{i+1,j-1} - \tilde{V}_{i+1.j-2} \\ -\tilde{V}_{i-1,j+2} + 2\tilde{V}_{i-1,j+1} - 2\tilde{V}_{i-1,j-1}\end{array}}{4\Delta\xi(\xi_i\Psi)^3} \tag{59}$$

$$\frac{\partial^4 \tilde{V}(\xi^1\xi^2)}{(\partial\xi^2)^4} = \frac{\tilde{V}_{i.j+2} - 4\tilde{V}_{i,j+1} + 6\tilde{V}_{i,j} - 4\tilde{V}_{i,j-1} + \tilde{V}_{i,j-2}}{(\xi_i\Psi)^4} \tag{60}$$

The discretization of varying coefficients of simultaneous equations was made by taking the values of coefficients in each node of FDM mesh. For this to work, the derivatives of varying coefficients of the system had been previously calculated symbolically (see Sect. 5.1).

Subsequently, the discretization of the boundary conditions needs to be done (see Sect. 5.3.1). Correspondingly to FDM classical approach, we add virtual non-existent nodes and we make the value of the function in those nodes conditional on values of function in appropriate "physical" nodes. The calculations have been made for two types of annular plates according to its boundary conditions—clamped and simply supported. In the case of clamped edges of the plate:

- for the inner edge:

$$\tilde{V}_{0,j} = 0, \qquad \tilde{V}_{-1,j} = \tilde{V}_{1,j} \tag{61}$$

- for the outer edge:

$$\tilde{V}_{N,j} = 0, \qquad \tilde{V}_{N-1,j} = \tilde{V}_{N+1,j} \tag{62}$$

In the case of simply supported plate:

- for the inner edge:

$$\tilde{V}_{0,j} = 0, \qquad \frac{\tilde{V}_{-1,j} + \tilde{V}_{1,j}}{\Delta\xi^2} + \frac{1}{R_i}\frac{\tilde{V}_{-1,j} - \tilde{V}_{1,j}}{2\Delta\xi} = 0 \tag{63}$$

- for the outer edge:

$$\tilde{V}_{N,j} = 0, \qquad \frac{\tilde{V}_{N-1,j} + \tilde{V}_{N+1,j}}{\Delta\xi^2} + \frac{1}{R_e}\frac{\tilde{V}_{N-1,j} - \tilde{V}_{N+1,j}}{2\Delta\xi} = 0 \tag{64}$$

where R_i and R_e are respectively inner and outer radius of skeletonal annular plate.

Using formulas (47)–(64), from the Eq. (25) we obtain system of $(n-1)\cdot(m-1)$ algebraic equations. The solution of the eigenvalue problem of mentioned system gives requested modes and frequencies of natural mode.

5.3.3 The Comparison with Abaqus Program Results

In order to verify the correctness of the derived tolerance model equations, the comparison of the results obtained from the Eq. (25) with the results from Abaqus program (finite element method) for a test task has been made. The following material and geometric parameters have been assumed for the test tasks:

- matrix (aluminum): modulus of elasticity $E_m = 69$ GPa, Poisson's ratio $\nu_m = 0,33$, mass density $\rho_m = 2720\,\text{kg/m}^3$,
- beams (steel): modulus of elasticity $E_r = 210$ GPa, Poisson's ratio $\nu_r = 0,3$, mass density $\rho_r = 7800\ \text{kg/m}^3$,
- thickness of plate h = 10 cm,
- ring width L = 2 m,
- internal radius $R_1 = 3$ m,
- external radius $R_2 = 5$ m,
- thickness of beams d = 0.05 m,
- boundary conditions for the side clamped plate (43),

Mode shape functions for the calculated natural frequencies have the same form for the tolerant model and for Abaqus program. The forms corresponding to the first four frequencies of the free vibrations have been calculated and shown in Fig. 5. The calculations have been performed with the use of two methods:

- finite element method in Abaqus program,
- by solving the tolerance model Eq. (25) by using the finite difference method.

Calculations made by Abaqus program were provided for the linear perturbation (frequency). It is crucial to find the adequate element for the mesh. It was assumed **S4R element** as a 4-node doubly curved thin (or thick) shell which provides reduced integration, hourglass control and finite membrane strains. Hourglass control was adopted as "Stiffness". The rest of the parameters were assumed as default. The mesh was added to the matrix and ribs separately. The size of one element of the mesh is equal to 0.025 m with curvature control. It was generated 45.800 elements on the matrix and 35.595 elements on the ribs (Table 1).

Build a computational model for the annular plate that has many ribs with constant width ($1/n \ll 1$, n-number of the ribs) is very labor-intensive in Abaqus program. Any change of the width of the ribs requires the construction of a new model of

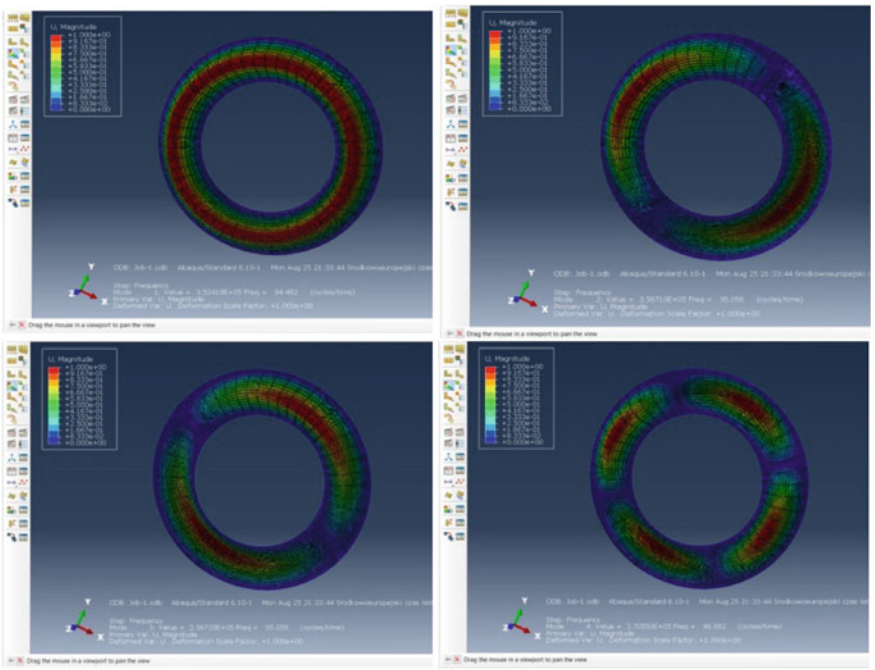

Fig. 5 First four modes of natural frequencies of the annular skeletonal plate

Table 1 First four free frequencies for a microheterogeneous plate

	Abaqus	TTA	Abaqus/TTA
Number of free frequency	Aluminium matrix with steel ribs (Hz)	Aluminium matrix with steel ribs (Hz)	Differences between Abaqus/TTA (%)
1st	121.15	125.65	3.58
2nd	123.25	125.82	2.04
3rd	123.37	125.82	1.95
4th	129.69	126.10	−2.85

this plate. That approach is pretty elaborate to be used in the analysis of engineering problems. In direct description of the plate with microstructure we have dealt with highly oscillating function describing material properties. Averaged model is described by equations with smooth and slowly varying coefficients. Application of FEM for the direct model requires a very dense distribution of the elements which is not necessary in the case of averaged models.

5.3.4 Numerical Examples

The subject of the analysis in this subsection are the composite plates with matrix made of concrete or aluminum and reinforced by steel ribs. The aim of the numerical calculations is to investigate the influence of the material properties of the plate on the natural frequencies of the plate under consideration.

We assume the following geometrical data in the next examples:

- thickness of plate h = 10 cm,
- ring width L = 2 m,
- internal radius R_1 = 3 m,
- external radius R_2 = 5 m,

and material parameters:

- aluminum: modulus of elasticity E = 69 GPa, Poisson's ratio $\nu = 0,33$, mass density $\rho = 2720\,\text{kg/m}^3$,
- steel: modulus of elasticity E = 210 GPa, Poisson's ratio $\nu = 0,3$, mass density $\rho = 7800\,\text{kg/m}^3$,
- concrete: modulus of elasticity E = 30 GPa, Poisson's ratio $\nu = 0,2$, mass density $\rho = 2800\,\text{kg/m}^3$,

Other material and geometrical parameters were variable at the time of the numerical experiment and they are individually described on the charts.

In the Fig. 6 it is presented the natural frequencies versus parametr d/λ (d—width of ribs, λ—size of the cell in its radial direction). If $d/\lambda = 1$ we receive homogeneous plate. We can see that, when the width of ribs is equal to zero, natural frequencies of composite plate aims to natural frequencies of homogeneous plate made of the material of matrix. Further, in the case of increasing the width of the ribs natural frequencies of composite plate seeks to natural frequencies of homogeneous plate made of the material of the rib. In the following example matrix and rib are made properly of concrete and steel.

Consequently, for the graph below, matrix made of aluminum and ribs made of steel were assumed. The dependence of natural frequency from the number of periodic cell was calculated. By changing the width of the ribs, the constant proportions of material between the quantity of the material of the matrix and ribs were maintained. Figure 7 presents almost linear dependence of natural frequencies on the number of the cells (ribs) in the angular direction (on the horizontal axis) for different series of the number of the cells in the radial direction. In all cases, the same proportions of the quantity of the material for the matrix and for the ribs were maintained by controlling the width of the ribs.

In the next figures there is presented the dependence of natural frequencies of the composite on different material proportions. In the first case (Fig. 8), we consider

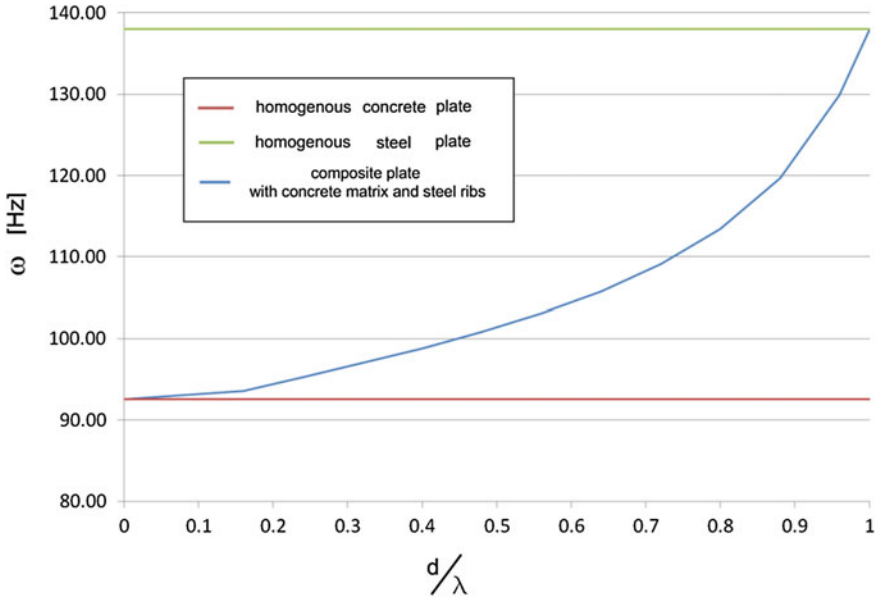

Fig. 6 The dependence of the first natural frequency on the width of the ribs

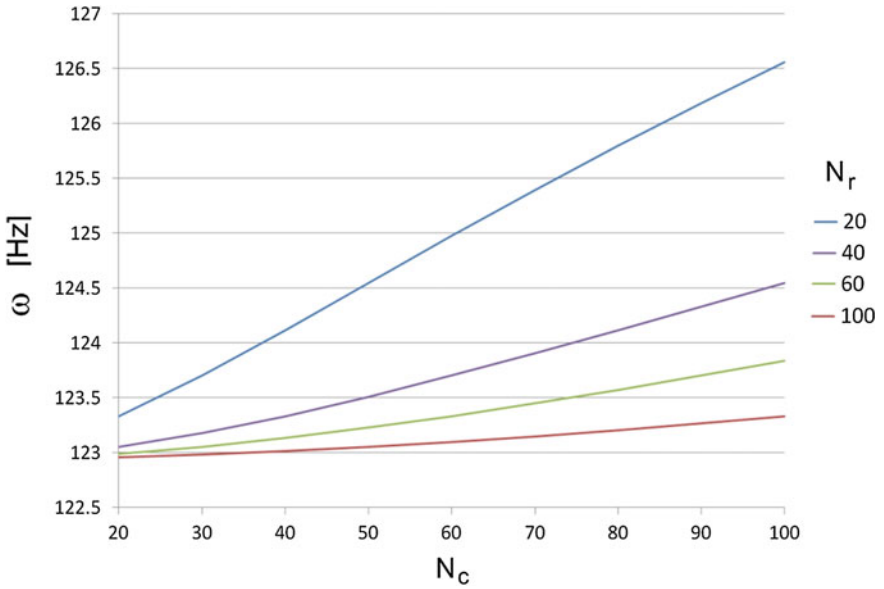

Fig. 7 The dependence of natural frequencies on the number of the ribs in the angular direction (on the horizontal axis) for different numbers of the ribs in the radial direction

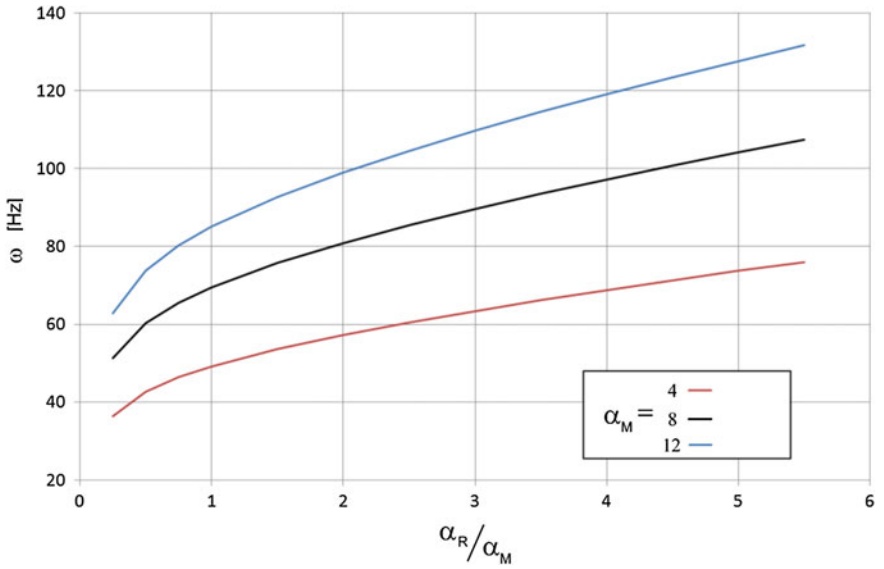

Fig. 8 The dependence of natural frequency on material parameters

variability of Young modulus of the ribs ratio to the density of the ribs for different series of analogical ratio for the matrix, which is defined as:

$$\alpha_i = \frac{E_i}{\rho_i}$$

In the second case (Fig. 9), it is shown the dependence of natural frequencies on Young modulus of the ribs ratio to Young modulus of the matrix for different series of density ratio. A homogenous plate made of the material of the rib was considered as a reference level. Modification of Young modulus ratios for both materials was done by adjustment of material parameters of the matrix. In either case was assumed the width of the ribs equal to 5 cm. The results obtained for different width of the ribs had analogous character and let us draw the same conclusions.

In both cases we see that by controlling the material properties we can obtain desired natural frequencies of the plate. What is more, the relationships between them are nonlinear.

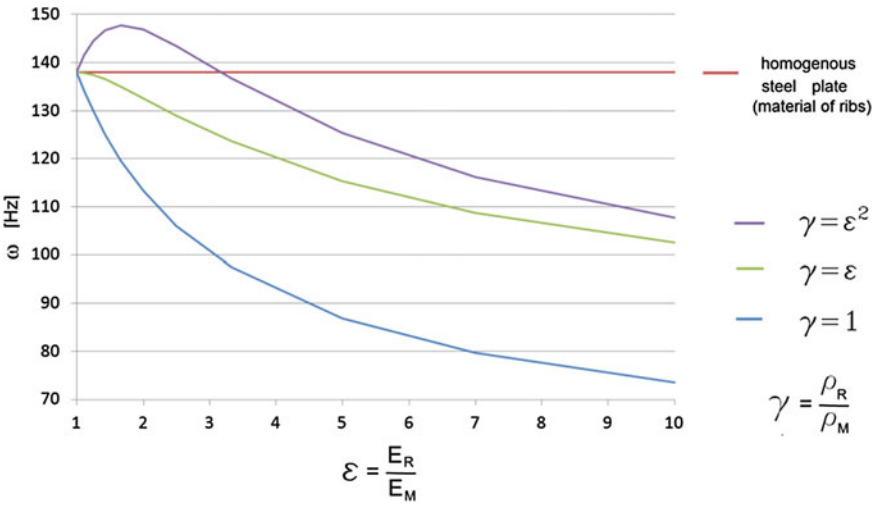

Fig. 9 The dependence of natural frequency on Young modulus of the ribs ratio to Young modulus of the matrix for different series of ribs density to matrix density ratio

5.4 Conclusions

The composite skeletonal plate is described by the tolerance model equations that involves only smooth coefficients. Since the proposed model equations have smooth coefficients, the solution of specific boundary problem can be obtained using well known numerical methods. The obtainment of this average solution is much easier than using FEM for direct description of the plate with microstructure.

The validation of gained averaged model by comparing the results from the TAA model with results from ABAQUS program was performed. For the analyzed plate we have obtained a good consistency of the results (less than 4 % of the difference).

We can see in the Figs. 6, 7, 8 and 9 that by controlling the geometrical and material properties of the ribs and the matrix we can obtain desired natural frequencies of the plate.

In the Fig. 9 we observe that for the composite plate with specific geometric structure we can obtain depending on the value $\varepsilon = E_R/E_M$ both lower and higher vibration frequency than those for homogenous plate made of material of the rib. That occurrence exists in the case where density of the ribs ratio to matrix $\gamma = \rho_R/\rho_M$ increases faster than elastic modulus of the ribs ratio to elastic modulus of the matrix $\varepsilon = E_R/E_M$.

References

1. Baron, E.: On dynamic behaviour of medium thickness plates with uniperiodic structure. Arch. Appl. Mech. **73**, 505–516 (2003)
2. Jędrysiak, J.: Higher order vibrations of thin periodic plates. Thin-Walled Struct. **47**, 890–901 (2009)
3. Kaźmierczak, M., Jędrysiak, J.: A new combined asymptotic-tolerance model of vibrations of thin transversally graded plates. Eng. Struct. **46**, 322–331 (2013)
4. Kączkowski, Płyty, Obliczenia statyczne, Arkady (2000)
5. Matysiak, S.J., Nagórko, W.: On the wave propagation in periodically laminated composites. Bulletin de l'Académie Polonais des Sciences, Série des Sciences Techniques **43**, 1–12 (1995)
6. Michalak, B., Wirowski, A.: Dynamic modeling of thin plate made of certain functionally graded materials. Meccanica **47**, 1487–1498 (2012)
7. Michalak, B., Woźniak, Cz, Woźniak, M.: The dynamic modelling of elastic wavy plates. Arch. Appl. Mech. **66**, 177–186 (1996)
8. Rychlewska, J., Woźniak, Cz: Boundary layer phenomena in elastodynamics of functionally graded laminates. Arch. Mech. **58**, 1–14 (2006)
9. Wągrowska, M., Woźniak, Cz: On the modelling of dynamic problems for visco-elastic composites. Int. J. Eng. Sci. **35**, 923–932 (1996)
10. Wierzbicki, E., Woźniak, Cz: On the dynamic behavior of honeycomb based composite solids. Acta Mech. **141**, 161–172 (2000)
11. Wirowski, A: Self-vibration of thin plate band with non-linear functionally graded material. Arch. Mech. **64**, 603–615 (2012)
12. Woźniak, C. et al. (eds.): Mathematical modeling and analysis in continuum mechanics of microstructured media, Wydawnictwo Politechniki Śląskiej, Gliwice (2010)
13. Woźniak, C., Michalak, B., Jędrysiak, J. (eds.): Thermomechanics of Heterogeneous Solids and Structures, Wydawnictwo Politechniki Łódzkiej, Łódź (2008)